School of Pharmacy and Biomedical Sciences

Curtin Health Innovation Research Institute

Evaluation of Novel Resveratrol Conjugate and Nanoparticle Formulations for Enhanced Anticancer Activity

Yan Jing Yee

This thesis is presented for the Degree of

Doctor of Philosophy

of

Curtin University

September 2018

DECLARATION

To the best of my knowledge and belief this thesis contains no material previously published by any other person except where due acknowledgment has been made. This thesis contains no material which has been accepted for the award of any other degree or diploma in any university.

The research presented and reported in this thesis was conducted in compliance with the National Health and Medical Research Council Australian code for the care and use of animals for scientific purposes 8th edition (2013). The proposed research study received animal ethics approval from the Curtin University Animal Ethics Committee, Approval Number AEC_2016_28.

Signature: 

Date: 17 September 2018

ACKNOWLEDGMENT

First and foremost, I would like to thank God for this journey and privilege of experiencing His great love and care during this 8-year joyous ride. I would not have been able to complete this season of my life without Him and His providence in my and family's lives.

I would like to acknowledge my dearest husband, Lawrence, for being the most patient, loving and encouraging man any woman can have in her life. You lifted me up when I was down and gave me the necessary pushes to get me over the hills. Charis would not have been in our lives and part of this journey without you and your countless days and hours of taking over her care has been tremendous help to me. She is a beautiful and secure little girl because of you. I dedicate this thesis to both of you closest to my heart. My family has been tremendously supportive and patient being babysitters, chefs, cheerleaders, housekeepers, chauffeurs and shoulders to cry on. Thank you for being there and being part of this season of my life.

Special thanks to my main supervisor, Dr Yan Chen, for being so understanding and encouraging through these years. Thank you for standing by me and for me. My other supervisors (Associate Professor Heather Benson, Professor Crispin Dass, Dr Simon Fox and Dr David Brown) have also been my academic and emotional support throughout my PhD. Their time, effort and ideas have been very helpful and useful in preparing this deceivingly uncomplicated document. The times spent discussing my thesis (or everyday life!) and doing research experiments together have been little nuggets of gold which I will carry through not just my academic life but also my personal life. I would like to acknowledge the financial support from the Australian Postgraduate Award and Curtin University Postgraduate Scholarship for allowing me to carry on with my research with a peace of mind. Also, special mention to Basavaraj for kindly synthesising and providing me with his methodology, guidance and material for my project.

My PhD journey would not have been complete without the presence, help and conversations of my research colleagues (peers and senior), administrative staff and technical staff of the School of Pharmacy and Biomedical Sciences and the Curtin

Health Innovation Research Institute. They have made my research life as a PhD student richer and more fulfilling and at some points in time, bearable. I thoroughly appreciate what they have done and wish them all the best in their future undertakings.

Lastly, I would like to appreciate the time and efforts of my examiners for reviewing my thesis. Thank you for your input and your appraisals. It only makes this thesis more worthwhile and credible.

TABLE OF CONTENTS

LIST OF FIGURES

LIST OF TABLES

LIST OF ABBREVIATIONS

Abbreviations and symbols are listed in alphabetical order. Initial use of abbreviations and symbols in the thesis will be elaborated.

Abbreviation or symbol	**Definition**
% *w/v*	Percentage weight-per-volume
% *w/w*	Percentage weight-per-weight
4CL	*p*-coumarate-CoA ligase
ACN	Acetonitrile
AEC	Animal Ethics Committee
AMPK	AMP-activated protein kinase
ANOVA	Analysis of variance
AOX	Antioxidant
ARC	Animal Resource Centre
ATCC®	American Type Culture Collection®
AUC	Area under curve
Aβ	Amyloid-β
BCP	Bicyclo[1.1.1]-pentane
BDNF	Brain-derived neurotrophic factor
BME	Basement membrane extract
C4H	Cinnamate-4-hydroxylase
cat#	Catalogue number
$CDCl_3$	Deuterated chloroform
CGM	Complete growth media
CHIRI	Curtin Health and Innovation Research Institute
CO_2	Carbon dioxide
COX	Cyclooxygenase
d_6-DMSO	Deuterated dimethyl sulfoxide
Da	Dalton (unit)

DAD	Diode-array detector
DCM	Dichloromethane
DDS	Drug delivery system
DL	Drug loading
DMEM	Dulbecco's Modified Eagle's Medium
DMSO	Dimethyl sulfoxide
DNA	Deoxyribonucleic acid
DOX	Doxorubicin
DPPH	2,2-diphenyl-1-picrylhydrazyl
DSPE	Distearoylphosphatidyl ethanolamine
EDC.HCl	*N*-(3-dimethylaminopropyl)-N'-ethylcarbodiimide hydrochloride
EE	Encapsulation efficiency
em	Emission
EPR	Enhanced permeation and retention
ER	Estrogen receptor
EtOH	Ethanol
ex	Excitation
FBS	Foetal bovine serum
FITC	Fluorescein isothiocyanate
FL	Fluorescence
FLD	Fluorescence detector
FSC	Forward scatter (in flow cytometry)
glu	Glutarate
GPC	Gel permeation chromatography
HBSS	Hanks’ balanced salt solution
HEPES	4-(2-Hydroxyethyl)piperazine-1-ethanesulfonic acid
HLM	Human liver microsomes
HPCD	(2-hydroxyl)-β-cyclodextrin or hydroxypropyl-β-cyclodextran
HPLC	High-performance liquid chromatography

IC_{50}	Half-maximal inhibitory concentration
ICH	International Conference on Harmonization
IG	Intragastric or intragastrically
IP	Intraperitoneal or intraperitoneally
IT	Intratumoral or intratumorally
IV	Intravenous or intravenously
LA	Lactide
LC	Loading capacity
LLC	Lewis lung carcinoma or cancer
LOD	Limits of detection
LOQ	Limits of quantitation
MeOH	Methanol
$MgCl_2$	Magnesium chloride
M_n	Number-average molecular weight
mOEG	Methoxy-oligo(ethylene glycol)
M_p	Molecular weight at peak maxima
mPEG	Methoxy-poly(ethylene glycol)
mPEG-PCL	Methoxy-poly(ethylene glycol)-poly-(ε-caprolactone)
mPEG-PLA	Methoxy-poly(ethylene glycol)-polylactic acid
mPEG-PLGA	Methoxy-poly(ethylene glycol)-poly(lactic acid)-(glycolic acid)
MPS	Mononuclear phagocyte system
MQ	Milli-Q ultrapure water
MS	Mass spectrometer
mTOR	Mammalian target of rapamycin
MTT	Thiazolyl blue tetrazolium bromide
MW	Molecular weight
M_w	Weight-average molecular weight
MWCO	Molecular weight cut-off
MWD	Multi-wavelength detector
M_z	*Z*-average molecular weight

M_{z+1}	*Z*+1-average molecular weight
n (from Chapter 3)	Sample size or replicates
n/a	Not applicable
NAFLD	Non-alcoholic fatty liver disease
ND	Not determined
NF-κB	Nuclear factor kappa-light-chain-enhancer
NMR	Nuclear magnetic resonance
NP	Nanoparticle
NR	Not relevant
NSCLC	Non-small-cell lung cancer
PAL	Phenylalanine ammonia-lyase
PBS	Phosphate buffered saline
PC2	Physical Containment II
PC3	Physical Containment III
PCL	Poly-(ε-caprolactone)
PD	Pharmacodynamics
PDH	Pyruvate dehydrogenase
PDI	Polydispersity index
PEG	Poly(ethylene glycol)
PGA	Poly(glycolic acid)
PHBV	Poly(3-hydroxybutyrate-co-3-hydro-xyvalerate)
PI	Propidium iodide
PK	Pharmacokinetic
PKC	Protein kinase C
PLA	Polylactic acid
PLGA	Poly(lactic acid)-(glycolic acid)
PTX	Paclitaxel
PVA	Polyvinyl alcohol
PVDF	Polyvinylidene fluoride
R^2	R-square or linear correlation coefficient

RGD	Arginine–glycine–aspartate
RID	Refractive index detector
RM	Reaction mixture
ROS	Reactive oxygen species
rpm	Revolutions per minute (unit)
RSD	Relative standard deviation
RSV	Resveratrol
RT	Room temperature
RTA	Tri-acetate resveratrol
SD	Standard deviation
SEDS	Solution Enhanced Dispersion by Supercritical Fluids
SEM	Standard error of the mean
SLNs	Solid lipid nanoparticles
SME	Self-emulsifying
SOD	Superoxide dismutase
SSC	Side scatter (in flow cytometry)
STS	Stilbene synthase
succ	Succinate
$t_{1/2}$	Half-life
THF	Tetrahydrofuran
t_{max}	Time point to maximum % cumulative amounts of RSV or RSV conjugate released
TPGS	d-α-tocopherol polyethylene glycol
t_R	Retention time
TSP1	Thrombospondin-1
UD	Undetermined
UDPGA	Uridine 5’-diphosphoglucuronic acid trisodium salt
UPLC-MS/MS	Ultra-performance liquid chromatography-tandem mass spectrometry/mass spectrometry
UV	Ultraviolet

UVD	Ultraviolet detector
UVR	Ultraviolet radiation
UV-Vis	Ultraviolet-visible
v/v	Volume-per-volume
VEGF	Vascular endothelial growth factor
VWD	Variable wavelength detection or detector
w/v	Weight-per-volume
w/w	Weight-per-weight
δ	Chemical shift or peak position in NMR spectra
ε-CL or CL	*ε*-caprolactone

ABSTRACT

Resveratrol (RSV) is a natural product with multiple biological benefits including anticancer properties. Unfortunately, its biological benefits are limited by its low bioavailability and rapid hepatic metabolism and degradation in the body which instigated high oral doses of up to 100mg/kg to be used for significant therapeutic effects in pre-clinical and clinical studies. Several strategies including chemical modification and nano-formulation have been used to overcome the limitations of RSV, however, most research published focused on improved *in vitro* or *in vivo* stability of RSV without assessing on the improvement of *in vivo* anticancer or other biological effects of RSV by various formulation strategies. This did not allow for a holistic understanding of the impact of modified or formulated RSV on its biological effects. As the purpose of the strategies were to improve the pharmacokinetic (PK) profile of RSV to increase its availability at the disease sites, it would be logical to evaluate the application of the enhanced properties of RSV.

The aim of this project was to enhance the plasmatic stability and decrease the metabolism rate of RSV through a dual strategy of chemical modification and nano-sized formulation for the application of RSV anticancer treatment in a mouse cancer model. In this study, RSV was conjugated to an array of low molecular weight (MW) PEGylated amphiphilic copolymers and formulated into nano-sized particles together with unconjugated RSV, henceforth known as conjugated RSV nanoparticles (NPs). As a comparison, native RSV was encapsulated in the same amphiphilic copolymers, henceforth known as encapsulated RSV NPs.

Conjugation of RSV to low MW methoxy-poly(ethylene glycol)-poly(L-lactic acid) (mPEG-PLA) and methoxy-poly(ethylene glycol)-poly-(ε-caprolactone) (mPEG-PCL) was achieved using a carbodiimide coupling reaction *via* an ester bond with either of two linkers, that is a two-carbon succinate (succ) and a three-carbon glutarate (glu). Previous *in vivo* PK and *in vitro* metabolism studies within the research group found that NPs of mPEG750-PLA1000-succ-RSV (RSV conjugated to mPEG-PLA with 750Da and 1000Da, respectively, *via* a succinate linker) was stable against plasmatic and hepatic enzymes *in vitro* and produced more bioavailability *in vivo*. Here, we have

used different MW of mPEG, that is 750Da and 2000Da, to assess the effect of hydrophilic chain on RSV conjugate and different types of hydrophobic polymers (PLA or PCL) on stability of polymeric conjugates. The different linker chain lengths were used to investigate the stability difference between succ and glu. Synthesis of polymers, activated polymers and RSV conjugates were characterised by gel permeation chromatography (GPC) for polymers and nuclear magnetic resonance (NMR) for all syntheses. Yields of copolymers were close to 100% whereas yields for activated copolymers ranged from 40% to 90%. Yields for RSV conjugates were between 16% to 55% with varying content of RSV conjugate and unconjugated RSV (55%-99% *w/w* RSV conjugate in final synthesised product). Further purification of final conjugated RSV products was not carried out to utilise the unconjugated RSV to increase drug loading (DL) of conjugated RSV NPs.

A simple high-performance liquid chromatography (HPLC) gradient method with ultraviolet (UV) and fluorescence (FL) detection was developed with good selectivity to concurrently quantify unconjugated RSV and RSV conjugates, respectively, in conjugated RSV NPs. Separation between unconjugated RSV and RSV conjugates were in the range of 5 to 10 minutes which allowed a better resolution between analytes. A rapid HPLC isocratic method was also optimised to quantify unconjugated RSV in encapsulated RSV NPs with high selectivity and sensitivity. Both methods were validated in non-biological and biological matrices for linearity, limitations, accuracy, precision and storage stability during HPLC analyses.

Selected conjugated RSV NPs (mPEG750-PLA1000-succ-RSV, mPEG750-PLA1000-glu-RSV, mPEG750-PCL1000-succ-RSV and mPEG2000-PLA1000-succ-RSV) were formulated together with unconjugated RSV using simple nanotechnology techniques of solvent diffusion, solvent evaporation and thin film hydration. All NPs had particle sizes ranging from 28nm to 360nm with low to high polydispersity index (PDI) values (0.2 to 0.7) and RSV loading of 10%-48% (*w/w*). In addition, PEG5000-O-RSV (RSV conjugated to PEG 5000Da with an ether bond) synthesised previously in the research group was developed into NPs (particle size 580nm; PDI 0.5) using self-assembly method with RSV loading of 4% (*w/w*). All NPs were negatively charged (-9mV to -35mV) with NPs of mPEG750-PLA1000-succ-RSV and PEG5000-O-RSV having

zeta potential values of -3mV and 0mV, respectively. As a comparison, encapsulated RSV NPs was prepared using solvent diffusion and solvent evaporation methods by encapsulating RSV in amphiphilic copolymers mPEG750-PLA1000, mPEG750-PCL1000 and mPEG2000-PLA1000. All NPs ranged between 160nm to 350nm in size with excellent PDI values (<0.1) and negatively charged particles (-11mV and -20mV) except RSV encapsulated in mPEG2000-PLA1000 NPs where zeta potential was close to 0mV. Encapsulated efficiency (EE) was between 72% to 97% whereas DL of encapsulated RSV NPs ranged between 3%-9% (*w/w*). Conjugated RSV NPs were found to have significantly higher DL when compared to encapsulated RSV NPs while maintaining nano-sized particles due to the presence of unconjugated RSV in the conjugated RSV NPs and contributed to the much slower release of total RSV equivalent than its encapsulated RSV NPs counterpart. Release profiles of conjugated RSV NPs were dependent on the hydrolysis rate of RSV-polymer bond and release kinetics of unconjugated RSV and cleaved RSV from RSV conjugate in NP core. Release profiles of encapsulated RSV NPs were obtained and found to be influenced by the hydrolysis rate of copolymers surrounding the NP shell and NP size.

Based on *in vitro* assays with rat plasma, we concluded that conjugated RSV NPs containing mPEG750-PLA1000-succ-RSV, mPEG2000-PLA1000-succ-RSV and PEG5000-O-RSV and all encapsulated RSV NPs were capable of protecting RSV from degradation in rat plasma. Conjugated RSV NPs containing mPEG750-PLA1000-succ-RSV and PEG5000-O-RSV were the only stable formulations (conjugated and encapsulated) *in vitro* against phase II metabolism when tested using human liver microsomes (HLM) with microsomal $t_{1/2}$ of 2.8h and 17.7h, respectively. Remaining NPs had microsomal $t_{1/2}$ below 2.5h with encapsulated RSV NPs having microsomal $t_{1/2}$ on par or worse than free RSV control (0.5h). We then subjected the NPs to anti-proliferative assays in B16-F10 cells for 48 hours with thiazolyl blue tetrazolium bromide (MTT). At 20μg/mL total RSV equivalent, conjugated RSV NPs did not show significant anti-proliferative effect compared to free RSV whereas encapsulated RSV NPs had similar anti-proliferative effect as free RSV. However, compared to the untreated cells, conjugated RSV NPs containing mPEG750-PCL1000-succ-RSV and all encapsulated RSV NPs significantly reduced the viability of B16-F10 cells. These data

implied that RSV needed to be converted to its native form (that is, unconjugated) to elicit its anticancer effect on B16-F10 cells.

Based on *in vitro* stability and anti-proliferative data, we selected one conjugated RSV NPs (mPEG750-PLA1000-succ-RSV NPs) for its excellent plasma and microsome stability profiles and a comparable encapsulated RSV NPs (RSV in mPEG750-PLA1000 NPs) for further *in vitro* cytotoxicity (using NIH/3T3 cells) and apoptosis assays (using B16-F10 cells) and *in vivo* evaluation. As expected, the apoptotic activity of conjugated RSV NPs and encapsulated RSV NPs were similar to what was observed in anti-proliferative assays, however, the cytotoxicity assay using NIH/3T3 cells showed a slight cytotoxic effect due to the existent cytotoxicity effect of RSV. Apoptosis assays using B16-F10 cells showed that RSV and encapsulated RSV NPs followed the apoptotic pathway in cell death. Despite the lack of anti-proliferative effect on B16-F10 cells, we deemed it necessary to assess the NPs in a mouse model containing a subcutaneous B16-F10 tumour to study the full impact of conjugation and encapsulation against the metabolism and degradation of RSV *in vivo* on their therapeutic effect compared to RSV alone. In our animal study using C57BL6/J mice subcutaneously implanted with B16-F10 tumour, we firstly used the intratumoral (IT) route to assess the precise dose of a formulation at a lower dose. Using knowledge obtained from the IT cohort, we improved our animal study design using intraperitoneal (IP) route to administer the NPs to study the effectiveness of conjugated RSV NPs in producing anticancer effect in subcutaneous tumours in mice.

Through the IT cohort, we discovered that B16-F10 tumours were highly aggressive and tumour growth was uncontrollable after approximately 14 days old which required earlier termination due to overly large tumour size and onset of necrosis. IT injections were also unsuitable due to development of necrosis from multiple dosing and thus, another administration route, for example IP, would be more suitable and advantageous in differentiating the therapeutic effects between free RSV, encapsulated RSV NPs and conjugated RSV NPs. Through the IP cohort, the effectiveness of conjugated RSV NPs in providing higher therapeutic concentration of RSV at the tumour site compared to free RSV and encapsulated RSV NPs by decreasing the metabolism and degradation rates of RSV *in vivo* was evident. Tumour

growth was suppressed throughout the 14-day study even after treatments were stopped at day 8. Other treatment groups showed exponential tumour growth after treatments ceased due to the lack of bioavailable RSV caused by extensive metabolism and degradation of RSV *in vivo* prior to arrival at the tumour site.

It was concluded that conjugated RSV NPs containing mPEG750-PLA1000-succ-RSV and unconjugated RSV provided an enhanced anticancer effect in B16-F10 tumours subcutaneously implanted in C57BL/6J mice possibly by decreasing the hepatic metabolism and plasma degradation rates of RSV *in vivo*.

CHAPTER 1. INTRODUCTION

1.1 Resveratrol

1.1.1 Background and physicochemical properties

Resveratrol (3,5,4'-trihydroxystilbene, **Error! Reference source not found.**) is a naturally occurring polyphenolic phytoalexin found in food products such as grapes, wine, peanuts and berries (Augustin *et al.* 2013, Kulkarni *et al.* 2015, Summerlin *et al.* 2015, Das *et al.* 2016). It was first isolated in 1939 from the roots of the white hellebore *Veratrum grandiflorum* (Bhullar *et al.* 2015, Weiskirchen *et al.* 2016). RSV is found abundantly in the Japanese knotweed root *Polygonum cuspidatum* (Summerlin *et al.* 2015) and is mainly sourced from the skin of grape vines and Mojave yucca plant (*Yucca schidigera*) (Chinembiri *et al.* 2014).

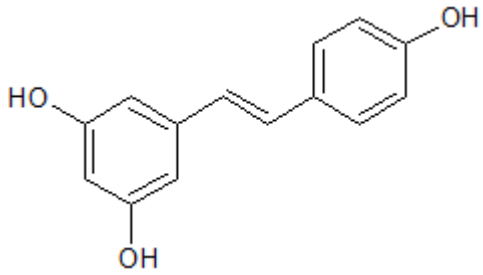

Figure 1.1 Molecular structure of resveratrol (RSV)

The synthesis of RSV in plants occurs through the phenylpropanoid pathway (Figure 1.2) (Planas *et al.* 2012) triggered by exogenous stress factors such as injury, ultraviolet radiation (UVR) and fungal infection (Ndiaye *et al.* 2011, Aluyen *et al.* 2012, Chinembiri *et al.* 2014). Presence of these stress factors rapidly activates the stilbene synthase enzyme which facilitates the biosynthesis of *trans*-RSV using the precursor, L-phenylalanine (Cimino *et al.* 2012, Summerlin *et al.* 2015). Structurally, RSV is classified as a stilbene which is part of the naturally found stilbenoid family of compounds characterised by two aromatic rings linked by a methylene bridge (Xiao *et al.* 2008, Yu *et al.* 2013). RSV exists in two geometric isomers with the *trans* isomer being more abundant and biologically active than the *cis* isomer (Morris *et al.* 2015).

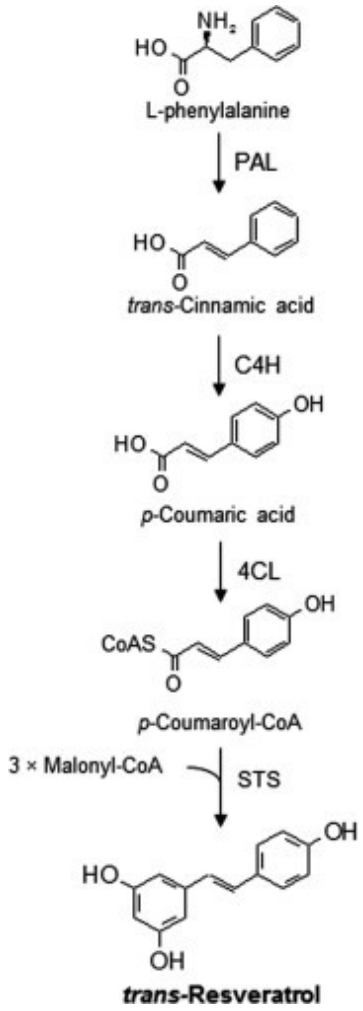

Figure 1.2 Biosynthesis of RSV *via* phenylpropanoid pathway in plants

L-phenylalanine undergoes deamination by phenylalanine ammonia-lyase (PAL) forming *trans*-cinnamic acid. Cinnamate-4-hydroxylase (C4H) catalyzed the addition of a hydroxyl group yielding *p*-coumaric acid, which is modified to *p*-coumaryl-CoA by the enzyme *p*-coumarate-CoA ligase (4CL). Finally, stilbene synthase (STS) condenses one molecule of *p*-coumaryl-CoA and three molecules of malonyl-CoA to form *trans*-RSV (Planas *et al.* 2012)

RSV (Chemical Abstracts Service Registry Number 501-36-0) is an off-white solid powder with a molecular formula $C_{14}H_{12}O_3$, MW of 228.25g/mol and a melting point between 253 and 255°C (CAS Registry 2002, O'Neil 2006). RSV is highly hydrophobic with a partition coefficient (log $P_{o/w}$) of 3.1 and its aqueous solubility is very low at 0.03g/L (Mattarei *et al.* 2013) but solubilises at 50g/L and 16g/L in ethanol (EtOH) and dimethyl sulfoxide (DMSO), respectively (Amri *et al.* 2012). Due to its lipophilicity, RSV demonstrated high membrane permeability (Summerlin *et al.* 2015). *Trans*-RSV is stable at RT for at least 42 hours when protected from light and for at least 28 days when in buffers at pH1-7 (Trela *et al.* 1996) although we have experimentally shown

instability of RSV at pH7.4 at RT (Appendix 7.10). Amri *et al.* (2012) also reported that *trans*-RSV is more biologically active than *cis* isomer probably due to its non-planar conformation.

1.1.2 Biological benefits and mechanisms of action

Weiskirchen *et al.* (2016) reported some biological benefits of RSV on various organ functions (Figure 1.3).

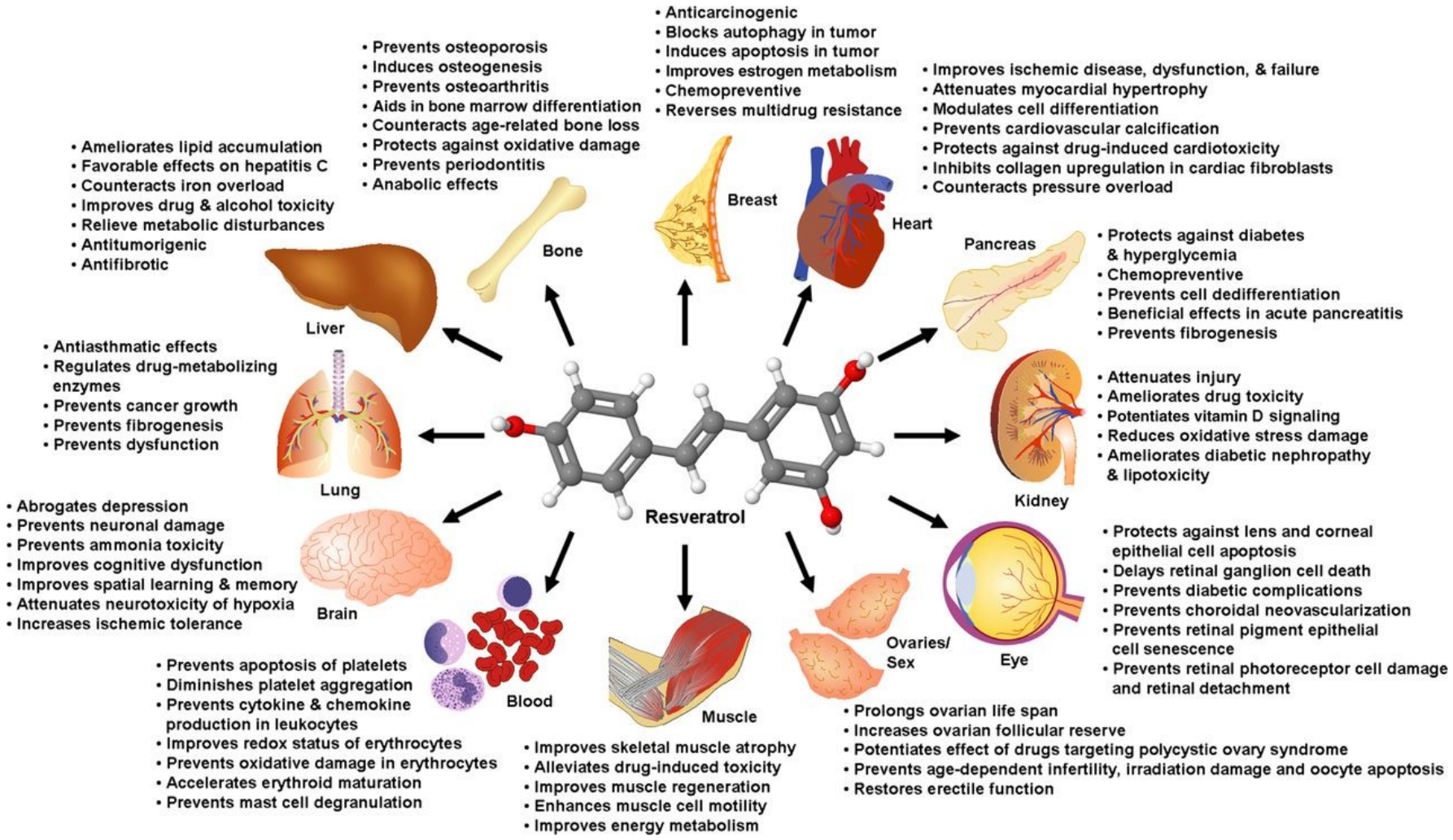

Figure 1.3 Some reported benefits of RSV on organ function (Weiskirchen *et al.* 2016)

The list of biological benefits of RSV is non-exhaustive and ever-growing, however, the exact mechanism of action for RSV remains unclear and not fully understood (Kulkarni *et al.* 2015, Summerlin *et al.* 2015, Pavan *et al.* 2016). Polyphenols are known to have non-specific actions unlike traditional therapeutical molecule where only one or very few targets are specific to the compound. The plurality of molecular targets is common in natural compounds in particular phytochemicals like RSV (Singh *et al.* 2015). Nonetheless, the biological benefits could be due to the combined effects of multiple molecular targets (Kulkarni *et al.* 2015). For example, RSV was proposed to mimic a state of cell starvation which triggered the calorie restriction pathway which contributed to its anti-aging properties in healthy and metabolically compromised mammals (Catalgol *et al.* 2012, Bhullar *et al.* 2015), cardio-protective properties (reviewed in Kulkarni *et al.* (2015)) and anticancer properties (Fouad *et al.* 2013). Das *et al.* (2016) reviewed the effect of RSV on the protein kinase C (PKC) signalling pathway which plays a key role in biological functions such as apoptosis, cell proliferation, immune responses, cell signalling and neurological functions of learning and memory. Bhullar *et al.* (2015), alternatively, hypothesised that the mammalian sirtuins SIRT1 was possibly a primary target of RSV which regulates numerous cellular processes such as deoxyribonucleic acid (DNA) repair, fat differentiation, glucose output, insulin sensitivity, fatty acid oxidation and neurogenesis. Current meta-analysis of the use of high daily oral doses (≥300 mg/day) RSV suggested that RSV played an active role to promote cardiovascular health in diabetic patients (Fogacci *et al.* 2018). In addition, Diaz-Gerevini *et al.* (2016) stated that RSV prevented bisphenol A-induced autism, type 2 diabetes mellitus and metabolic syndrome by augmenting the brain-derived neurotrophic factor (BDNF) synthesis and action. RSV also altered the gut microbiota and influenced stem cell proliferation and differentiation which could explain its multitude of benefits (Qiao *et al.* 2014, Chen *et al.* 2015b). RSV was found by Frozza *et al.* (2013) to protect against synaptic degeneration induced by fibrillar amyloid-β (Aβ) peptides simulating neurodegeneration in Alzheimer's disease. In various preclinical studies reviewed by Vang *et al.* (2011), there was sufficient evidence to suggest RSV, at the right dose, reduced the incidence of hypertension, heart failure, ischemia heart disease and had chemopreventive effects in experimental animal models. Kulkarni *et al.* (2015)

presented a systematic review on metabolic actions of RSV and its potential role on a sirtuin enzyme SIRT1 and the AMP-activated protein kinase (AMPK). The paper also reviewed other possible effectors for RSV including inhibition of cyclooxygenases (COX) and mammalian target of rapamycin (mTOR) signalling which resulted in anticancer properties.

RSV was found to be antioxidative which allowed protection against atherosclerosis at higher doses but at lower doses, was pro-oxidative by increasing intracellular superoxide production (Catalgol *et al.* 2012). This dual role was also observed in RSV derivatives where normal cells were protected from oxidative stress due to the antioxidant (AOX) nature of RSV derivatives whereas cancer or pre-malignant cells experienced necrotic death by RSV acting as a cytotoxic prooxidant (Gorlach *et al.* 2015). Madreiter-Sokolowski *et al.* (2017) reviewed the mechanisms of action of RSV in the mitochondria and described the hormetic characteristic of RSV where low doses of less than 50μM (11.4μg/mL) showed cytoprotective properties which was beneficial for aging, neurodegenerative, cardiovascular and metabolic diseases; and, a higher dose of more than 50μM induced apoptosis *via* the caspase-dependent apoptosis pathway in the mitochondria of cancer cells by increasing intracellular Ca^{2+} levels. This was evident in SW620 colon cancer cells where an increase in oxygen consumption supported by mitochondrial biogenesis and increased fatty acid oxidation followed by the hyperpolarization of mitochondrial membrane and reactive oxygen species (ROS) production led to an enhanced apoptosis effect of RSV (Blanquer-Rossello *et al.* 2017). This behaviour was further described to be dissimilar to what happens in normal cells where RSV reduces energy metabolism mimicking a calorie-restricted environment. Saunier *et al.* (2017) supported this mitochondrial metabolic effect of RSV in Caco2 colon cancer cells by proposing that RSV reverses the Warburg effect, that is the altered metabolic activity in cancer cells, by targeting the pyruvate dehydrogenase (PDH) complex through the Ca^{2+}/AMPK signaling pathway. Another colon cancer cell line was found to be affected by the hormetic nature of RSV where HCT116 cell numbers were increased when 1-10μM (0.2-2.3μg/mL) RSV was added and at 50-100μM (11.4-22.8μg/mL), RSV reduced cell numbers and increased the percentage of apoptotic and necrotic cells (San Hipolito-

Luengo *et al.* 2017).

Although there is a plethora of literature findings on the effectiveness of RSV in colon cancer cell lines, the chemopreventive effects of RSV *in vivo* was first demonstrated by Jang (1997) which described the multi-stage carcinogenesis of RSV in an *in vivo* melanoma model by affecting the carcinogenesis process in the tumour initiation, promotion and progression phases (Chinembiri *et al.* 2014). RSV was found to induce caspase-dependent apoptosis in several cancer cell types by Gogada *et al.* (2011) and was further confirmed to induce autophagy of cancer cells by Prabhu *et al.* (2013). Angiogenesis generally depicts a progressive, more severe cancer and RSV was shown to exert anti-angiogenic activity by modulation of the tumour cell release of thrombospondin-1 (TSP1) and vascular endothelial growth factor (VEGF) (Catalgol *et al.* 2012). Although RSV appeared to have a biphasic effect on cell proliferation by stimulating cell growth at low concentrations and suppressing growth at high concentrations, it was found to inhibit cell proliferation in estrogen receptor (ER)-negative cancer cell lines at all concentrations as reviewed in Mense *et al.* (2008). Table 1.1 lists recent comprehensive reviews on molecular mechanisms of RSV by various authors.

Table 1.1 Recent literature reviews on molecular mechanisms of RSV

Reference	Review topic
Berman *et al.* (2017)	Clinical trials on RSV in cancer, neurological disorders, cardiovascular diseases, diabetes, non-alcoholic fatty liver disease (NAFLD) and obesity Discussed effect of RSV on disease biomarkers
Pan *et al.* (2018)	Molecular modulations by RSV for obesity treatment and/or improvement of obesity-related metabolic diseases
Abbasi Oshaghi *et al.* (2017)	Mechanisms of action of RSV in management of insulin-resistant and related conditions
Madreiter-Sokolowski *et al.* (2017)	Mechanisms of action of RSV in the mitochondria
Ko *et al.* (2017)	Intracellular molecular targets of RSV evidenced by *in vitro* and *in vivo* studies in various cancers Clinical trials of RSV as therapeutic and chemopreventive agent
Rauf *et al.* (2016)	Mechanism of actions of RSV in cancer therapy specifically AOX modulation
Aziz *et al.* (2018)	Molecular mechanisms of RSV in chemoprevention in UVR-induced skin carcinogenesis
Zhang *et al.* (2018)	Signaling pathway targets of RSV in cancer stem cells
Li *et al.* (2018)	Relationship between RSV and aging biomarkers including oxidative stress, inflammation and high-calorie diets Mechanisms of action of RSV in age-associated disorders
Mohammed *et al.* (2018)	Modulation of mechanisms in drug-resistant cancer cells and induction of chemosensitization by RSV
Tsai *et al.* (2017)	Recent findings on the mechanisms of action and biological effects of RSV

1.1.3 Limitations

Despite numerous biological benefits, RSV has low oral bioavailability due to its short biological $t_{1/2}$, rapid metabolism and poor water solubility (Peng *et al.* 2018). It was shown that clinical translation of RSV was limited by its rapid metabolism following single or multiple oral doses of RSV between 0.5 to 5.0g dose, which led to a reduced *in vivo* bioavailability (Chinembiri *et al.* 2014, Smoliga *et al.* 2014, Singh *et al.* 2015). Kulkarni *et al.* (2015) summarised findings of PK studies on RSV where RSV levels in plasma were either non-detectable or below micromolar range after ingestion of RSV at doses achievable through a normal diet. RSV orally administered in humans reached a peak plasma concentration after 1.1 hour and a second peak after 5.4 hours (Zu *et al.* 2016). 5mg/kg RSV dissolved in a mixture of 1:1 *v/v* Cremophor EL and EtOH was injected intravenously (IV) into male Balb/c mice and found to have an area under curve (AUC) of 0.15μg/mL·h with plasma $t_{1/2}$ of 1h (Ramalingam *et al.* 2016). RSV metabolised in the intestine and liver by glucuronidation and sulfation led to less than 1% free RSV available *in vivo* post oral administration in humans (Walle 2011, Amri *et al.* 2012, Diaz-Gerevini *et al.* 2016). The RSV metabolites then accumulated in the liver; however the location of the metabolism is debatable between the small intestine and liver (Amri *et al.* 2012). Bohmdorfer *et al.* (2017) reported that the metabolism of RSV in mice after intragastric (IG) administration was due to the high level of enzymes in certain organs including the liver and colon which led to the high concentrations of RSV glucuronide and sulfate metabolites. Lou *et al.* (2014), on the other hand, briefly studied the distribution of RSV administered IV at 20mg/kg in rats over a 4-hour period where native RSV was significantly metabolised into glucuronidated and sulphated metabolites and distributed to plasma, urine, heart, kidney, liver and brain by the first sampling time point of 0.5 hours. Unfortunately, PK parameters were not determined in the paper as the focus was on the development and validation of an ultra-performance liquid chromatography-tandem mass spectrometry (UPLC-MS/MS). Although this has shed some light as to where RSV is metabolised *in vivo*, interspecies difference (Ruivo *et al.* 2015, Wang *et al.* 2018) and effects of administration route (Berman *et al.* 2017, Menet *et al.* 2017) should be considered. Effects of administration route by IG and IV was compared by

Qiu *et al.* (2017) where 50mg/kg RSV in 0.5% sodium carboxyl methyl cellulose was administered IG and 10mg/kg RSV in 10:80:10 *v/v/v N,N*-dimethylformamide-PEG400-physiological saline was administered IV in Sprague-Dawley rats. Both routes produced similar AUC values at 7.4 and 8.3μM·h and $t_{1/2}$ at 2.2 and 3.6h, respectively, however, peak plasma concentration was much higher when RSV was administered IV at 18μM than when administered IG at 1.7μM. This indicated that RSV was absorbed rapidly into the circulation system post IG administration and underwent immediate metabolism into glucuronides and sulfates (Qiu *et al.* 2017). Even though low bioavailability was assessed by evaluating RSV content in blood plasma, it may not be an accurate indicator of RSV absorption and exposure as biodistribution of RSV and RSV metabolites into other tissues apart from blood was highly possible and may have beneficial effects (Andres-Lacueva *et al.* 2012, Lou *et al.* 2014). Extensive metabolism of RSV and its PK profile *in vivo* has been studied and reviewed by a non-exhaustive list of authors including Walle (2011), Rotches-Ribalta *et al.* (2012), Bhullar *et al.* (2015), Summerlin *et al.* (2015), Diaz-Gerevini *et al.* (2016), de Vries *et al.* (2018) and Wang *et al.* (2018). The effect of low bioavailability of RSV on the therapeutic outcome of RSV was observed in Stakleff *et al.* (2012) where RSV was effective in inhibiting the *in vitro* invasion of NuTu-19 ovarian cancer cells but not in mice xenografted with the same cancer cells. Nonetheless, there is growing evidence that biotransformation of RSV by colonic microbiota into bioactive metabolites contributed to the protective effects of RSV (Augustin *et al.* 2013) but was highly dependent on the variation of fractional ratio of metabolites among individuals (Bode *et al.* 2013). Patel *et al.* (2013) reported on the bioconversion of RSV metabolites to free RSV in human colorectal cancer cells which contributed to its anticancer activity. The bioavailability of RSV was also affected by time of intake, prior food intake and fat content in food (Bhullar *et al.* 2015).

Besides the rapid metabolism of RSV contributing to its limited bioavailability, less favourable physicochemical properties of RSV including hydrophobicity and photosensitivity was also attributed to its limited bioavailability. RSV was found to undergo photodegradation when exposed to ultraviolet-visible (UV-Vis) irradiation (Silva *et al.* 2013). This confirmed findings by Trela *et al.* (1996) where 90.6% *trans*-

RSV converted to *cis*-RSV after UV irradiation for 120 minutes at 366nm. Therefore, exposure to sunlight and high intensity white light or UV light would cause isomerisation (Summerlin *et al.* 2015) and decrease the amount of the more biologically active *trans*-RSV (Amri *et al.* 2012). The high lipophilicity of RSV also decreased *in vivo* absorption especially when RSV was administered orally (Bhullar *et al.* 2015). The hydrophobicity of RSV also reduced aqueous solubility rendering it difficult to formulate into orally administered medication (Diaz-Gerevini *et al.* 2016, Pavan *et al.* 2016). The intracellular AOX properties of RSV were also limited by its lipophilicity where RSV tended to embed within the lipid bilayer of the cell membrane post penetration (Whitehouse *et al.* 2016). This property might also have attributed to the low plasma levels as intratissular and intracellular levels of RSV might be higher (Kulkarni *et al.* 2015).

Patel *et al.* (2010) reported non-adverse effects when RSV was administered in colorectal cancer patients *via* oral route at doses 0.5-1.0g/day for up to 8 days before surgical removal of cancer whereas Brown *et al.* (2010) revealed mild to moderate gastrointestinal symptoms at 2.5 and 5g doses in healthy volunteers ingesting 0.5-5.0g RSV daily for 29 days. The study also found significant increase of RSV metabolites compared to RSV and a decrease in circulating insulin-like growth factors indicative of chemopreventive activity. Although RSV is less toxic than traditional chemotherapeutics (Patel *et al.* 2011), its low bioavailability warranted much higher doses for RSV to be effective (Augustin *et al.* 2013, Smoliga *et al.* 2014) which unfortunately has led to unwanted side effects (Mukherjee *et al.* 2010) including digestive disorders and high bilirubin levels at doses more than 1g/day (Chedea *et al.* 2017). Due to its unfavourable PK profile and low bioavailability, RSV was suggested by Hubbard *et al.* (2014) as unsuitable as a clinical drug candidate unless its limitations were addressed.

1.2 Strategies to overcome limitations of resveratrol

Due to the rapid *in vivo* metabolism of RSV and physicochemical limitations, translating *in vitro* results into *in vivo* models has proven difficult due to the inability of achieving and maintaining elevated levels of RSV in the blood enough to produce

the therapeutic effect seen *in vitro* (Syed *et al.* 2011) which has attributed to the use of high doses *in vivo*. Hence, the need to overcome the limitations of RSV was warranted to decrease the dose required to produce the desired clinical effect by reducing its metabolism and degradation rate and enhancing its solubility. A sustained intake of RSV favoured the presence of native RSV in the heart and brain instead of RSV metabolites as seen in Menet *et al.* (2017) where a sustained intake of RSV in food was given over 3 months to mice at 40mg/kg daily as opposed to a single high dose intake of 150mg/kg by oral gavage. The high presence of RSV in the heart and brain was also observed in an organ distribution study by Lou *et al.* (2014) where RSV was administered IV at 20mg/kg in rats. Various researchers and pharmaceutical companies have adopted strategies to improve the bioavailability and physicochemical properties of RSV (reviewed by Singh *et al.* (2015) and Peng *et al.* (2018)) by re-deriving RSV using medicinal chemistry techniques (Osmond *et al.* 2013, Park *et al.* 2016a, Wang *et al.* 2016), reformulating RSV using formulation technology or nanotechnology (Ranganathan *et al.* 2012, Wei *et al.* 2012, Neves *et al.* 2013, Aras *et al.* 2014, Ruivo *et al.* 2015, Siddiqui *et al.* 2015, Summerlin *et al.* 2015, Subramanian *et al.* 2016, Arora *et al.* 2018), and utilising combination therapy with other known therapeutic agents such as quercetin, curcumin or paclitaxel (PTX) (Shakibaei *et al.* 2011, Cadena *et al.* 2013, Coradini *et al.* 2014, Meng *et al.* 2016).

1.2.1 Chemical modification strategies

Chemical modification of drug molecules has been utilised as a tool to enhance the bioactivity of drugs or improve on unfavourable physicochemical properties, for example solubility. Modifications to the structure of RSV at hydroxyl group locations were used to reduce their metabolic and degradation rate *in vivo* which then could improve on their therapeutic action. Ryu *et al.* (2015) showed a tri-substituted RSV with acetate groups (RTA) was more resistant to oxidation and less cytotoxic than RSV which was then confirmed in clinical trials where the RSV analogue was used for skin-whitening purposes. Park *et al.* (2016a) further improved this analogue by using glycolate groups which enhanced its solubility and increased its anti-melanogenic effects when compared to RTA and RSV. RSV was modified to include the tubulin polymerisation inhibitor E7010 (2-anilinopyridine sulphonamaide) which enhanced

the anticancer properties of RSV more than 10-fold and of E7010 by 2-fold against human cervical HepG2 cancer cell lines through cell cycle arrest at the G2/M-phase (Kamal *et al.* 2016). Scherzberg *et al.* (2015) showed that methylation of RSV led to substantial changes in the mode of action of RSV despite having an increased anti-proliferative effect in cancer cells by tubulin polymerisation inhibition and cell cycle arrest at G2/M phase. (*Z*)3,4,5,4′-*trans*-tetramethoxystilbene, an RSV analogue, showed significant inhibitory effect on gefitinib-resistant non-small-cell lung cancer (NSCLC) cells but not in normal lung epithelial cells by intervening the Ca^{2+} signalling pathway and inducing apoptosis and autophagy in NSCLC cells (Fan *et al.* 2015). An impressive paper by Goh *et al.* (2017) on the synthesis of RSV modified to a bicyclo[1.1.1]-pentane (BCP) showed superior PK properties indicated by a three-fold increase of clearance and a 10-fold increase of plasma $AUC_{0\text{-}4h}$ compared to free RSV. The *in vitro* metabolic stability of RSV was also significantly improved by the replacement of one of the phenyl rings of RSV with BCP. Substitutions to the hydroxyl groups of RSV with selected moieties so far showed increased anticancer effect compared to native RSV. In addition, substitutions to these groups also showed better PK profiles than RSV *in vivo*. A review by Biasutto *et al.* (2017) on RSV derivatives as RSV prodrugs showed that the prodrugs were able to modulate physical properties, influence *in vivo* biodistribution, enhance absorption from the gastrointestinal tract and hinder phase II metabolism which contributed to a higher bioavailability of RSV. A PK study carried out on RSV and the RSV prodrug 3,5,4′-tri-O-acetylresveratrol in rats by Liang *et al.* (2013) showed a slower elimination of the prodrug compared to RSV albeit non-significantly. Mattarei *et al.* (2015a) modulated the hydrolysis of RSV at pH 1, pH 6.8 and in whole blood by conjugating the molecule with natural amino acids *via* a *N*-monosubstituted carbamate ester linker. Oral administration to rats showed significant absorption and protection from first-pass metabolism indicating an appropriate stability profile of RSV. The same research group (Mattarei *et al.* 2015b) conjugated RSV with the same linker to methoxy-oligo(ethylene glycol) (mOEG) at varying low MW ranges as promoieties. The RSV prodrugs then underwent the same stability and *in vivo* evaluations and was found to have achieved optimal stability for use as prodrugs where the chain length of the mOEG played a role in modulating the stability profiles.

Conjugation of RSV with polymers was explored by Siddalingappa *et al.* (2015) and found to protect RSV from *in vitro* metabolism in liver microsomes and rat plasma. *In vivo* IV administration in rats found an improved PK profile of RSV when conjugated with mPEG-PLA (2,000Da) using a succ link and with poly(ethylene glycol (PEG) (2,000 and 5,000Da) using an ether link. The profiles showed a significant increase in plasma AUC, decrease in clearance and small volume of distribution when compared to RSV. RSV conjugated with mPEG (2,000Da) *via* a glycine linker showed an accelerated release rate of RSV compared to RSV conjugated mPEG without a linker with both showing a sustained release profile (Wang *et al.* 2016). Both conjugates however did not show significant improvement of cytotoxicity in MCF-7 breast cancer and HeLa cervical cancer cells compared to free RSV. This could be due to the conjugation of the hydroxyl groups of RSV which were known to be responsible for their anticancer properties (Szekeres *et al.* 2010); however, the hydroxyl groups on RSV are the only functional groups easily modified chemically. It would be prudent then to consider the linker or type of covalent bond to ensure release of native RSV for therapeutic effect. Zhang *et al.* (2014a) demonstrated that conjugation of PEG (2,000Da) to RSV and various amino acids *via* succinyl or carboxymethyl spacers improved the solubility of RSV from 0.03mg/mL to more than 900mg/mL and provided sustained release profiles dependent on the type of spacer and number of amino acids present in the conjugate, however, these data were not compared with free RSV. These characteristics of polymer-drug conjugates were also supported by Yang *et al.* (2017) showing prolonged drug circulation and enhanced therapeutic efficacy. The covalent bond between drug and polymer can be easily cleaved enzymatically or through acid/base catalysed hydrolysis *in vivo* (Ke *et al.* 2014) which then released the therapeutic effect of RSV at the target site. Ng *et al.* (2015) explored the *in vitro* plasma stability of RSV when conjugated to various PCL MWs of mPEG-PCL using a glu linker. The paper found a slight improvement in the stability of RSV in rat plasma when RSV was conjugated to higher PCL MW mPEG-PCL. RSV conjugated to gold NPs showed enhanced cellular uptake, anticancer activity and bioavailability (de Vries *et al.* 2018). Park *et al.* (2016b) demonstrated RSV capped with gold NPs using green nanotechnology inhibited several molecular biomarkers related to breast cancer cell progression. Conjugation of RSV was shown to increase the MW of RSV which

resulted in longer blood circulation time, enhanced tumour accumulation and reduced renal clearance of RSV (Yang *et al.* 2012b). Therefore, chemical modification strategies in substituting hydroxyl groups to RSV could improve the PK profile and reduce the metabolic rate of RSV which may enhance the anticancer effect of RSV.

1.2.2 Formulation strategies

Most strategies to overcome the limitations of RSV involve nanotechnology due to its rapid and simple preparation techniques and increasing popularity in disease management and therapy, particularly in cancer therapy (Galvin *et al.* 2012, Gao *et al.* 2012, Parhi *et al.* 2012, Ranganathan *et al.* 2012, Wei *et al.* 2012, Zhang *et al.* 2012, Tang *et al.* 2014, Wang *et al.* 2014, Summerlin *et al.* 2015, Chen *et al.* 2016, Masood 2016, Shi *et al.* 2016, Naves *et al.* 2017, Ye *et al.* 2018, Yue *et al.* 2018). Nanotechnology was able to prolong circulation of RSV *in vivo* (Kobayashi *et al.* 2014), enhance solubility (Li *et al.* 2017a) and stability (Torres *et al.* 2018) of RSV, prevent non-specific cellular uptake (Ye *et al.* 2014), increase drug concentration at localised sites and provide a controlled release of RSV (Zhang *et al.* 2017). Surface modification on particles was also possible which provided active targeting strategies (Edelman *et al.* 2017, Hao *et al.* 2017) and triggered release of RSV based on environmental pH (Caddeo *et al.* 2017). There was a vast array of literature available in the positive *in vitro* and *in vivo* effects of nano-sized RSV formulations in overcoming the limitations of RSV but we have selected some recent (from the year 2015) literature on different types of nano-sized delivery systems of RSV which improved the bioavailability or decreased the metabolism of RSV.

1.2.2.1 Polymeric nanoparticles (NPs)

Polymeric NPs were used to overcome the low bioavailability of RSV by controlling and prolonging the drug release to help reduce toxicity in non-specific cells and tissues (da Rocha Lindner *et al.* 2013) thus extending the residence time of RSV rather than decreasing the metabolism of RSV *in vivo*. In addition, polymeric NPs have the flexibility of conjugating ligands on their surface for targeted drug delivery (Shen *et al.* 2013, Ke *et al.* 2014, Bonferoni *et al.* 2017) which then increases the drug concentration at a localised site. Patel *et al.* (2017) reviewed various preparation

techniques of polymeric NPs modified with targeting ligands and their future prospects.

RSV encapsulated in carboxymethyl chitosan NPs were found by Zu *et al.* (2016) to enhance aqueous solubility which improved the AOX properties of RSV *in vitro* when compared to RSV alone. A sustained release of RSV from the NPs was also observed with increased *in vivo* oral bioavailability by absorption up to 3.5 times more than RSV alone. The size of the carboxymethyl chitosan NPs (155nm) was suitable for uptake by the intestinal cells which could have decreased the clearance rate of RSV and enhanced its gastrointestinal residence time compared to RSV. Geng *et al.* (2017) encapsulated RSV into albumin NPs with the tumour targeting ligand, arginine–glycine–aspartate (RGD), and found that the NPs had a longer *in vivo* blood circulation and active targeting of human pancreatic PANC-1 tumour tissue in comparison to free RSV following IV administration. Using an innovative nanotechnology technique called Solution Enhanced Dispersion by Supercritical Fluids (SEDS), Dal Magro *et al.* (2017) co-precipitated RSV into poly(3-hydroxybutyrate-co-3-hydro-xyvalerate) (PHBV) which showed high encapsulation efficiency, improved AOX activity and photostability of RSV. The release profile of an initial burst followed by a steady release phase allowed the particles to be used for long-term delivery. The authors speculated that this biphasic release pattern would be able to partially avoid rapid metabolism and elimination of RSV by rapidly producing an effective concentration in plasma then maintaining the concentration for a long period of time, thus extending its *in vivo* $t_{1/2}$, however, it was not confirmed experimentally. It should be noted that the amount of RSV metabolised was not decreased when encapsulated in NPs but rather, the rate at which RSV was metabolised was decreased. This was different than the chemical modification strategy because modifying the structure of RSV could cause a disruption to the enzyme-substrate relationship and possibly change the metabolism of modified RSV entirely. RSV was encapsulated in an unknown MW of polylactic-co-glycolic acid (PLGA) resulting in NPs with enhanced cytotoxicity against LNCaP prostate cancer cells mediated by apoptosis and cell cycle arrest at the G1/S transition phase in comparison to free RSV (Nassir *et al.* 2018). The enhanced cytotoxic activity of the RSV encapsulated in PLGA NPs was attributed to

the selective internalisation of PLGA NPs through inhibition of efflux out of cells by p-glycoproteins. The NPs were also non-toxic against murine macrophages up to 200μM (44μg/mL) RSV demonstrating the safety of RSV and PLGA in normal cells (Nassir *et al.* 2018). However, the weakness of this model is that the rapid metabolism and degradation of RSV and the possible degradation of PLGA *in vivo* was not considered. It would be prudent for the authors to conduct further evaluations regarding the stability of their NPs and also the effect of the *in vivo* environment on the NPs and the therapeutic efficacy of the RSV within the NPs.

PEG is often used to stabilise NPs *via* steric repulsion forces to avoid mononuclear phagocyte system (MPS) uptake thereby increasing circulation time *in vivo* (Khalil *et al.* 2013). In general, mPEG (2,000Da) or mPEG2000 was used in preparing liposomes for hydrophobic drug delivery however the significance of the MW of mPEG was not studied or clarified (Saw *et al.* 2015). In amphiphilic copolymers, the length and type of the hydrophilic and hydrophobic blocks can affect the NP properties such as polydispersity and particle size (Pang *et al.* 2016). RSV encapsulated in PEG5000-PLA5000 NPs improved the chemical stability of RSV and provided a sustained release of RSV with a reduction in ROS compared to free RSV (Jung *et al.* 2015). *In vivo* murine model of CT26 colon cancer showed tumour suppression and enhanced survival by the NPs administered by IV at a dose of 100mg/kg of RSV compared to an unloaded PEG5000-PLA5000 NP. The authors demonstrated that by stabilising and increasing residence time of RSV *in vivo* through encapsulation in polymeric NPs, *in vivo* anti-tumour effects of RSV were enhanced, however, a very large dose of 100mg/kg was administered to possibly compensate for the rapid metabolism of RSV which decreased its effective dose in the tumours. However, we find that 100mg/kg dose of RSV to be implausible as the NPs prepared would have had an EE of 52% which meant at each IV injection of 0.2mL twice a week for 3 weeks contained 300mg/mL PEG5000-PLA5000 which is extremely high and possibly toxic. Wang *et al.* (2015b) co-encapsulated RSV with d-α-tocopherol polyethylene glycol succ (TPGS succ) in mPEG2000-PCL4000 which enhanced the cellular uptake of RSV and translated to improved cytotoxicity by apoptosis in drug-resistant breast cancer MCF-7 cells when compared to free RSV. Despite being an aggressive tumour, Carletto *et al.* (2016)

demonstrated that encapsulation of RSV in PCL nanocapsules improved cellular uptake and tissue distribution of RSV in a melanoma mouse model with the ability to decrease tumour volume. The encapsulation also prevented metastasis and pulmonary haemorrhaging in the mice. Interestingly, Guo *et al.* (2018b) showed that RSV encapsulated in low MW mPEG2000-PLA2600 NPs could not improve cytotoxicity of RSV in MCF-7 cells but there was a synergistic effect when co-encapsulated with docetaxel evident by a prolonged release profile and better *in vivo* bioavailability after IV administration compared to individual drugs. Although it showed lack of sufficient cytotoxicity in MCF-7 cells when used alone, with the addition of docetaxel in the NPs, enzymatic reaction rate on RSV could have been affected and thus decreased the metabolic rate of RSV *in vivo* due to enzyme-substrate competition. Wang *et al.* (2017) explored two forms of stabilisers based on PEG to encapsulate RSV and studied the effects on long-term stability and *in vitro* and *in vivo* anticancer efficacy. Both RSV nanosuspensions each stabilised with TPGS succinate and folate modified distearoylphosphatidyl ethanolamine-polyethylene glycol (DSPE-PEG) showed long term stability of RSV for up to 20 days at room temperature (RT) and significant *in vitro* and *in vivo* anticancer activity against human alveolar carcinoma A549 cells compared with RSV solution (*in vitro* studies) and saline groups (*in vivo* studies). The RSV nanosuspensions were able to target cancer cells at a much lower IV dosage of 10mg/kg using folate as a targeting ligand although a PK study on the nanosuspensions would have been beneficial to assess the metabolic stability of RSV in nanosuspensions with targeting ligands.

From the selected literature presented here, encapsulation of RSV could overcome the low chemical stability of RSV with the possibility of sustained release of RSV *in vivo* (Singh *et al.* 2018) and also possibly enhance cellular uptake hence increasing the local concentration of RSV. However, the rapid metabolism of RSV could not be addressed by encapsulation by polymeric NPs alone. Targeting ligands like RGD and folate on the surface of NPs were used to direct NPs to specific sites quicker *in vivo* which would have minimised the chance of exposure of RSV to metabolic enzymes. Also, additional drugs co-encapsulated with RSV could have diverted enzymes from RSV either by saturation or by mediating the release of RSV from NPs to be slower in

order for the RSV in NPs to achieve its therapeutic effect nearer to targeted sites. Therefore, chemical modifications of RSV mentioned in the previous section would still be essential to address the problem of rapid metabolism of RSV *in vivo*.

1.2.2.2 Liposomes

Vijayakumar *et al.* (2016) studied the effects of RSV encapsulated in TPGS-coated liposomes and non-coated liposomes for glioma treatment in rats *via* IV administration. The authors found a sustained drug release and cellular internalisation in C6 glioma cells with prolonged *in vivo* systemic circulation and passive brain targeting. Plasma $t_{1/2}$ of the coated liposomes were found to be 7-fold higher than uncoated liposomes and 30-fold higher than RSV alone. This demonstrated that liposomes, whether uncoated or coated with TPGS could improve on the bioavailability of RSV for anticancer treatment. Liposomes with the hydrophilic PEG prevented opsonisation of liposomes by phagocytosis which prolonged its circulation time in the blood. This was demonstrated by Caddeo *et al.* (2018) where PEGylated liposomes containing RSV showed long-term stability and circulation with longer $t_{1/2}$ in blood and maintained antioxidative properties of RSV *in vitro*. Using an *in vitro* AOX assay using 2,2-diphenyl-1-picrylhydrazyl (DPPH), empty liposomes were found to have 24% AOX activity whereas PEGylated liposomes containing RSV (93.1%) did not alter AOX activity of RSV in methanolic solution (92.9%) significantly. This could mean that the nett AOX property of RSV in liposomes was a combination of decrease in encapsulated RSV AOX properties and inherent AOX properties of empty liposomes. Therefore, in this report, the strategy using liposome improved the physical stability of RSV but not the inherent AOX activity of RSV. Jhaveri *et al.* (2018) further modified the surface of PEGylated liposomes by adding transferrin moieties to enable active targeting of U-87 glioblastoma cells. The liposomes were found to be more cytotoxic than free RSV and unmodified PEGylated liposomes containing RSV through an enhanced caspase-activated apoptosis activity and cell cycle arrest. A subcutaneous xenograft mouse model of glioblastoma showed the superior effectiveness of transferrin-modified PEGylated liposomes containing RSV in inhibiting tumour growth and improving survival rates of mice (Jhaveri *et al.* 2018). Again, liposomes could not fully address the issue of rapid metabolism of RSV as

stated for polymeric NPs.

1.2.2.3 Other formulation strategies

Due to the growing research in combined therapy with enzyme inhibitory excipients to reduce the metabolism of RSV, Yang *et al.* (2018a) co-encapsulated RSV and RSV 3-O-glucuronide in a self-emulsifying (SME) drug delivery system (DDS) and increased bioavailability of RSV in rats orally administered with 10mg/kg RSV from 6.5% for free RSV to 12.9% for RSV-only SMEs to 76.1% for RSV and RSV 3-O-glucuronide SMEs by reducing the glucuronidation by UDP-glucuronosyltransferase. Nanoemulsions are another strategy to overcome some limitations of RSV. Li *et al.* (2017c) optimised a self-assembling micelle consisting of RSV, lecithin and Pluronic® P123 to provide high EE and DL of RSV with particle sizes less than 200nm. Compared with RSV solubilised in hydroxypropyl-β-cyclodextran (HPCD), stability of RSV at pH7 was enhanced at various temperatures using these micelles and the micelles revealed a controlled *in vitro* release of RSV. Using IV and oral routes, the micelles were found to enhance absolute bioavailabilities of RSV by 40% and 2.17-fold, respectively, when compared to RSV in HPCD. Mamadou *et al.* (2017) studied the effects of a semi-solid and liquid SME DDS containing RSV on intestinal permeation and presystemic metabolism of RSV. Both formulations significantly increased intestinal permeation across rat jejunum due to inhibition of intestinal metabolism which could potentially benefit oral delivery of RSV.

There have not been many literatures which studied the combination of both synthetic chemistry and nanotechnology to overcome the limitations of RSV. Recently, Siddalingappa *et al.* (2015) used synthetic methods to conjugate RSV to polymers whereby the conjugates were then formulated into NPs and found to have better *in vivo* PK profiles in comparison to RSV. The conjugation of RSV increased the MW of RSV which resulted in longer blood circulation time, enhanced tumour accumulation and reduced renal clearance of RSV (Yang *et al.* 2012b). Along with the benefits of using NPs which allowed longer circulation time in the blood stream (Kobayashi *et al.* 2014), reduced plasma protein adsorption and low rate of non-specific cellular uptake (Ye *et al.* 2014), the combined strategy of conjugating RSV to polymers and formulating them into NPs could have enhance stability of RSV when

administered *in vivo*. In addition, the release rates of these type of NPs could be controlled by several factors including polymer-RSV conjugate degradation rate and polymer-drug link cleavage rate (Yang *et al.* 2012b, Zhang *et al.* 2017, Yang *et al.* 2018b).

1.3 Cancer and nanotechnology

The current trend worldwide is to utilise nanotechnology for several biomedical applications including diagnosis, treatment and theranostics (Chen *et al.* 2013a, Brys *et al.* 2016, Mahato 2017, Naves *et al.* 2017). Nanotechnology is the design, synthesis, development, fabrication, characterisation and application of materials and devices on the nanoscale (Naves *et al.* 2017). Nanotechnology has enabled lower cost, faster production, minimized toxic side effects and increased drug delivery efficiency compared to conventional chemotherapeutics (Rigon *et al.* 2015). Torchilin (2014) reviewed recent developments of advanced nanoparticulate DDS and their therapeutic potential for diseases. The author also mentioned the benefits of nano-sized DDS which include prolonged circulation times with targetability due to the increased vascular permeability and poor lymphatic drainage in tumours leading to enhanced permeability and retention (EPR) effect, increased solubility and bioavailability, capability of attaching targeting ligands for active targeting and controllable behaviour and/or properties of DDS when exposed to particular stimuli in the body (Torchilin 2014). Rigon *et al.* (2015) tabulated the advantages and disadvantages of nano-sized DDS and infers DDS as an alternative strategy for antineoplastic agent carriers. Chen *et al.* (2013a) provided some examples of common DDS used in melanoma treatment including liposomes, carbon-based NPs and human albumin NPs. A recent review by Chou *et al.* (2017) highlighted the progress on the development of polymeric NPs for melanoma treatment by passive and active targeting. Qi *et al.* (2017) reviewed on the current state of co-delivery of anticancer drugs with nanotechnology for chemotherapy and examined the challenges and strategies in the area of combination chemotherapy.

Interestingly, cancer is found less prevalent in certain geographic locations in the world possibly due to the local dietary habits and/or use of natural agents as

medicines and remedies (Singh *et al.* 2015). This has led to further research into the use of natural products as chemotherapeutic and chemopreventative agents. Naturally occurring compounds are advantageous against traditional chemotherapeutic agents due to being less cytotoxic to non-cancerous cells (Hussain *et al.* 2014, Sim *et al.* 2016, Caddeo *et al.* 2017), having better accessibility and cost-effectiveness (Purushotham *et al.* 2016, Caddeo *et al.* 2017) and capable to overcome multi-drug resistance in tumour cells (Xie *et al.* 2016); however, they are highly lipophilic (Rajagopal *et al.* 2017) and metabolises rapidly *in vivo* which limited their bioavailability. For example, contradictory *in vitro* and *in vivo* findings on the anticancer effects of RSV in breast cancer and pancreatic cancer models were seen by Bartolacci *et al.* (2018) and Vendrely *et al.* (2017), respectively, and was attributed to the limited *in vivo* bioavailability of RSV. As natural products are less potent, they require higher doses (Pavan *et al.* 2016) and also have multiple mechanisms of action which may or may not lead to a particular desired therapeutic effect (Whitehouse *et al.* 2016, Xie *et al.* 2016). Due to the limitations of natural products, nanotechnology-based DDS have been used to enhance their bioavailability by prolonging their circulation time and by overcoming some of their limitations (Wang *et al.* 2014, Li *et al.* 2015a, Liu *et al.* 2015, Pavan *et al.* 2016, Sangsen *et al.* 2016, Xie *et al.* 2016). Current research in drug delivery is gearing towards using nanotechnology for diagnostic and therapeutic purposes (Hull *et al.* 2014, Coccia *et al.* 2015) as nano-sized DDS have ideal sizes to:

(1) efficiently transport into tissues or cells (Gu *et al.* 2013, Kumar *et al.* 2016),
(2) prevent rapid leakage into the urine (Yu *et al.* 2015),
(3) evade macrophage capture in the reticuloendothelial system and eventual elimination by the liver and spleen (Meng *et al.* 2016), and
(4) preferentially accumulate in tumour sites through the EPR effect resulted from a hyperpermeable tumour vasculature and insufficient lymphatic drainage (Gulcur *et al.* 2013, Ho *et al.* 2013, Shalgunov *et al.* 2017).

There are numerous review articles written on the delivery of natural products including RSV for cancer therapeutics by nanotechnology for further reading (Bonferoni *et al.* 2017, Davatgaran-Taghipour *et al.* 2017).

1.3.1 Resveratrol as anticancer or chemopreventive agent for melanoma

de Oliveira Júnior *et al.* (2017) provided a systematic review of 20 years' worth of literature on natural products, in particular flavonoids, used for the treatment of melanoma using *in vitro* or *in vivo* models. At least 97 flavonoids were investigated including RSV which showed efficacy in limiting tumour growth and inhibiting invasiveness of highly aggressive melanoma cells due to their anti-angiogenic activity. Chinembiri *et al.* (2014) reviewed the potential of natural products including RSV as skin cancer treatment by inducing apoptosis (Niles *et al.* 2003, Gatouillat *et al.* 2010) and possessing anti-metastatic properties by inhibiting the nuclear factor kappa-light-chain-enhancer (NF-κB) signalling pathway (Chen *et al.* 2012, Mohammed *et al.* 2018, Ratz-Łyko *et al.* 2018). RSV was first discovered to have anticancer effects against melanoma in tumour-bearing mice by Jang (1997). RSV was shown to have anti-proliferative effects on melanoma cells by Osmond *et al.* (2012), Habibie *et al.* (2014), Tang *et al.* (2014), Gorlach *et al.* (2015), Lee *et al.* (2015), Sim *et al.* (2016) and Wu *et al.* (2017). Shanmugam *et al.* (2017) presented a review article on selected natural compounds including RSV with anti-angiogenic potential to disrupt tumour growth and metastasis. Fang *et al.* (2013) demonstrated that RSV enhanced the radiation sensitivity of metastatic melanoma cells by inhibiting proliferation and promoting apoptosis. Rigon *et al.* (2015) explained that melanoma proliferation can be controlled or prevented by increasing apoptosis through the NF-κB pathway and decreasing ROS which are known modes of action of RSV. Pangeni *et al.* (2014) also reviewed on the therapeutic potential of RSV in various applications and some challenges associated with its delivery. Zubair *et al.* (2017), on the other hand, presented a review article on how RSV analogs and nanoformulations were able to overcome the limited bioavailability issues of RSV for cancer chemoprevention. Due to the advancement of nanotechnology DDS and increasing research in the use of natural products in chemotherapy and chemoprevention, the popularity of RSV as an anticancer and chemopreventive agent against melanoma has amplified for the past decade. Nanotechnology DDS have improved the bioavailability of RSV for melanoma and this was evident in Teskac *et al.* (2010) where RSV in solid lipid NPs (SLNs) showed better cellular uptake and cytostatic effect in skin keratinocyte cells. RSV

encapsulated in PCL nanocapsules were found to be effective against B16-F10 melanoma cells by decreasing tumour size and increasing necrotic area and inflammatory infiltrate of melanoma tumour *in vivo* (Carletto *et al.* 2016). Cosco *et al.* (2015) demonstrated co-encapsulation of 5-fluorouracil and RSV in ultradeformable liposomes enhanced skin permeation which allowed AOX and antiproliferative effects of RSV to be exerted in melanoma cells. Dermal delivery of RSV has improved due to nanotechnology which aided in the delivery of necessary therapeutic effects of RSV for skin cancer treatment (Scognamiglio *et al.* 2013, Friedrich *et al.* 2015, Juskaite *et al.* 2015). Last but not least, RSV was proposed for chemoprevention in melanoma by enhancing the chemosensitivity of melanoma cells to current therapies at possibly lower dosages (Guan *et al.* 2012, Cheng *et al.* 2015) or by inhibiting migratory and invasive properties in both drug-resistant and non-drug-resistant melanoma cells (Bhattacharya *et al.* 2011, Chen *et al.* 2013b, Menicacci *et al.* 2017). RSV encapsulated in SLNs were also found effective in inhibiting tyrosinase which is valuable in skin cancer prevention (Rigon *et al.* 2016). Despite these promising anticancer effects against melanoma *in vitro*, RSV was found ineffective towards *in vivo* A375, DM738 and DM443 melanoma models (Niles *et al.* 2006, Osmond *et al.* 2012, Osmond *et al.* 2013) which could be attributed to the rapid metabolism and lack of bioavailability of RSV *in vivo* contributing to a reduced therapeutic dose post-administration (Singh *et al.* 2015, Tou 2015).

1.4 Objective and significance of research

The main objective of this project was to produce a DDS for RSV with enhanced metabolic and plasma stability profiles of RSV by using conjugation of RSV with polymers which would then translate into enhanced anticancer activity for melanoma *in vitro* assays and an *in vivo* model. Firstly, low MW polymers were synthesised to prevent *in vivo* accumulation and systemic toxicity. RSV was conjugated to these polymers through synthetic chemistry techniques to reduce the *in vivo* metabolism and degradation of RSV. In order to improve the stability of RSV conjugated to mPEG750-PLA1000 with a succ linker, we have explored using a longer linker by one carbon called glu, a more hydrophobic polymer PCL to replace PLA and a longer mPEG chain of 2,000Da. A dual strategy of conjugation and encapsulation of free RSV was then employed when formulating the synthesised RSV conjugates into NPs to be used as a DDS of RSV (conjugated RSV NPs). In order to demonstrate the superior properties of these conjugated RSV NPs, physically entrapped RSV in the corresponding polymers (encapsulated RSV NPs) were used as comparisons. DL of novel conjugated RSV NPs were higher than encapsulated RSV NPs whilst maintaining nano-sized particles and sustained release of RSV. NPs were prepared using formulation techniques which were fast, economical and simple.

A novel HPLC gradient method was developed and validated for concurrent analysis of free RSV and conjugated RSV using a dual detection of FL and UV. A rapid isocratic HPLC method using UV detection was also optimised and validated for the analysis of assays with RSV alone. Both methods were validated for biological assay analysis. Both conjugated and encapsulated RSV NPs were tested in aggressive B16-F10 melanoma cell cultures for anti-proliferation and apoptosis followed by an *in vivo* mouse model. We established the lack of correlation between *in vitro* and *in vivo* data which proved that in most cases, *in vitro* experiments were insufficient to give a complete view of the properties of conjugated RSV NPs unlike *in vivo* models where the systemic effects on the formulation can be observed (Peng *et al.* 2018). In our *in vivo* study, we have confirmed the IP administration of NPs showed the full effect of our NPs by protecting RSV through decreasing metabolism and degradation of RSV for passive targeting and suppression of the melanoma tumour.

1.5 Thesis overview

The whole thesis is divided into four main research chapters followed by a general discussion and conclusion:

1) Chapter 2 describes the synthesis and characterisation of mPEG750-PCL1000, mPEG2000-PLA1000 and mPEG2000-PCL with varying PCL lengths. The synthesis and characterisation of RSV conjugated with these amphiphilic copolymers *via* succ and glu linkers will be discussed.
2) Chapter 3 elucidates the development and validation of a novel HPLC gradient method used to concurrently analyse free RSV and conjugated RSV in conjugated RSV NPs at various stages of the project. It also describes the development and validation of a simpler HPLC isocratic method for the analysis of free RSV alone in encapsulated RSV NPs.
3) Chapter 4 details the development and characterisation of novel NPs of RSV conjugates synthesised in Chapter 2 together with unconjugated RSV (conjugated RSV NPs) and also, as a comparison, RSV encapsulated with corresponding amphiphilic copolymers used in the conjugations (encapsulated RSV NPs).
4) Lastly, chapter 5 reports the stability of the RSV NPs in rat plasma and HLM followed by an *in vitro* evaluation of cell viability and apoptosis carried out in the B16-F10 melanoma cell line. One conjugated RSV NPs and one encapsulated RSV NPs were then tested for cytotoxicity in non-cancerous murine NIH/3T3 fibroblast cells. The chapter finishes with the *in vivo* evaluation of anticancer properties of selected RSV NPs in subcutaneously implanted B16-F10 cells in mice *via* the IT and IP route.

CHAPTER 2. SYNTHESIS OF POLYMERIC RESVERATROL CONJUGATES

2.1 Introduction

The low bioavailability of RSV is widely known to be due to its rapid metabolism and degradation *in vivo* especially after oral consumption (Walle 2011, Chinembiri *et al.* 2014, Singh *et al.* 2014c). Several approaches using chemical synthesis were able to enhance the bioavailability of RSV by slowing down its metabolism rate. This was achieved by conjugating the RSV with suitable removable small molecules known as promoieties to create prodrugs or by conjugating RSV with small or large molecules to create analogues which protected the hydroxyl group on RSV and prevented RSV from being metabolised or degraded *in vivo* by altering the enzyme-substrate relationship. Prodrugs of RSV were molecules which underwent biotransformation or chemical transformation *in vivo* resulting in the release of the biologically active RSV which then produced the desired therapeutic outcome (Sofia 2013). Mattarei *et al.* (2014) has shown conjugation of RSV with a sugar moiety enhanced solubility and allowed absorption after oral administration without any hydrolysis. Analogues of RSV that can enhance physicochemical properties and biological activity of RSV as demonstrated by Jeong *et al.* (2014) and Kim *et al.* (2014) where an RSV analogue, HS-1793, was found to be more metabolically stable, less photosensitive and more potent than RSV.

Conjugation of drugs to amphiphilic copolymers was known to enhance bioavailability of hydrophobic drugs by increasing its water solubility (Mattarei *et al.* 2014). However, the properties of drug-polymer conjugates including DL are dependent on the type and nature of the polymer and suitability of linkers used between the drug and polymer. Longer hydrophilic PEG chains led to an increase in water solubility and prolonged plasma $t_{1/2}$ but also resulted in a decrease of drug activity (Greenwald *et al.* 2003). Shorter oligo-PEG chains (130Da to 260Da) conjugated to RSV *via* amide and acetal linkers, however, allowed for higher DL when compared to longer PEG chains (Mattarei *et al.* 2013, Mattarei *et al.* 2015b). These RSV prodrugs were also assessed for phase II metabolism and *in vivo* PK studies in

rats by oral and IG administration and found to bypass the phase II metabolism stage after absorption which enhanced the bioavailability of RSV *in vivo*. Susceptibility of polymer conjugates to degradation or hydrolysis can be influenced by various hydrophobic chains covalently linked to PEG, for example, PLGA, PLA, PCL and poly(glycolic acid) (PGA) (Chen *et al.* 2015a). PCL is known to be more crystalline than PLA which made PLA more susceptible to water permeation and hydrolysis (Chu *et al.* 2016). The hydrolytic degradation rate of ciprofloxacin conjugated to PEG-PCL *via* ester linkers was slower compared to ciprofloxacin conjugated to PEG-PLA due to the higher degree of crystallinity of PCL resulting in a slower *in vitro* release of ciprofloxacin from the conjugates. The presence of hydrophilic PEG in the conjugates caused higher water permeation which increased chemical scission of ester linkers by a water molecule (Sobczak 2010). The chemical bonds used between RSV and polymers can be temporary like ester bonds or permanent like ether bonds (Mattarei *et al.* 2013, Siddalingappa *et al.* 2015). Ester bonds were liable to acid or basic hydrolysis and enzymatic cleavage (Greenwald *et al.* 1996, Biasutto *et al.* 2009a). This degradable aliphatic ester linkage was also utilised when synthesising RSV on a PCL scaffold for *in vitro* mineralization and *in vivo* bone regeneration, whereby the free RSV was released in the host tissue by hydrolytic cleavage *in vivo* (Li *et al.* 2011). Carbamate ester bonds were found to be more stable than carboxyl ester bonds and depending on their promoiety, the hydrolysis rate could be controlled (Mattarei *et al.* 2015b). In addition, the length of the carbon chain adjacent to an ester bond influenced the hydrolysis rate, thermal stability and enzymatic stability of the bond as demonstrated by Hinds (2004), Worzakowska (2014) and Ikhuoria *et al.* (2005).

Despite many reports on the conjugation of RSV and its effects on the bioavailability and activity of RSV, there have been no specific studies found which explored the combination of low MW polymer conjugation and nanotechnology formulation to enhance the bioavailability of RSV by decreasing its metabolism and degradation *in vivo*. As such, this chapter reports on the synthesis of polymers and polymer-RSV conjugates using amphiphilic copolymers for further development into NPs. To date, the author is unaware of any studies investigated on conjugated RSV NPs prepared from low MW amphiphilic copolymers for bioavailability and anticancer activity *in*

vitro and *in vivo*.

2.2 Aim

In this study, the aim was to synthesise RSV conjugated to low MW amphiphilic copolymers, which were made of hydrophilic mPEG and hydrophobic PLA or PCL. Two MW of mPEG that is, 750Da and 2,000Da, and PLA (1,000Da) or PCL with varying MWs (120Da to 12,000Da) were synthesized. Esterification between RSV and copolymers was achieved with an activated amphiphilic copolymer having either a two-carbon succ or three-carbon glu end group to explore the different hydrolysis and/or degradation rates of resulting RSV conjugates. Once polymeric RSV conjugate compounds were synthesized, they were formulated into NPs (Chapter 4) for *in vitro* characterisation and *in vivo* biological evaluations (Chapter 5).

2.3 Materials

mPEG MW 2,000Da (repeating units, *m*=45, Figure 2.1) (catalogue number, cat# 202509-250G) and MW 750Da (*m*=17, cat# 202435-250G), *ε*-caprolactone (*ε*-CL) (cat# 704067-100G), tin (II) ethylhexanoate (cat# S3252-100G), succinic anhydride (≥99%, cat# 239690-50G), glutaric anhydride (95%, cat# G3806-100G), triethylamine (≥99%, cat# T0886-100ML) and pyridine (≥99%, cat# 360570-100ML) were obtained from Sigma Aldrich (NSW, Australia). Methoxy-poly(ethylene glycol)-block-poly(L-lactic acid) (mPEG-PLLA, total MW 2,000Da with *m*=17 and *n*=14, Figure 2.1; cat# AK25) was procured from Akina Inc. (Indiana, USA). D,L-Lactide (LA) monomer (Purasorb^{D}, 99.9%; cat# unknown) was purchased from PURAC International (Holland) and purified by recrystallisation in ethyl acetate. PEG standards purchased from Jordi Labs LLC (MA, USA; cat# STD20300) in the M_p (MW at peak maxima) range of 960-26,100g/mol was used as MW calibration for GPC analysis and were stored in the dark at 4°C. *Trans*-RSV was purchased from DND Pharma-Tech Co., Inc. (Shanghai, China) (99%; cat# 20110905). (3-dimethylaminopropyl)-N'-ethylcarbodiimide hydrochloride (EDC.HCl; ≥98.5%, cat# 00805) was purchased from GL Biochem (Shanghai, China). Deuterated chloroform ($CDCl_3$, cat# DLM-7-100S) or deuterated dimethyl sulfoxide (d_6-DMSO; cat# DLM-10-10) for NMR analyses were obtained from

Novachem (VIC, Australia). Other solvents such as dichloromethane (DCM), diethyl ether (ether) and tetrahydrofuran (THF) were obtained from local sources. All materials, unless specified, were of analytical grade and used without further purification or modification.

2.4 Methodology

2.4.1 Synthesis of amphiphilic polymers

2.4.1.1 Synthesis of methoxy-poly(ethylene glycol)-polylactic acid (mPEG-PLA)

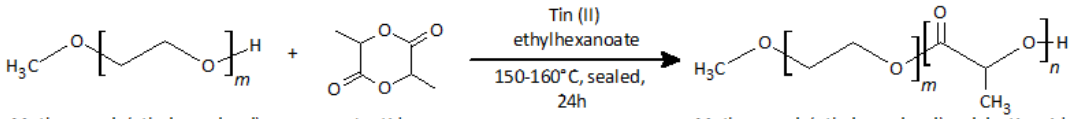

Figure 2.1 General scheme for the synthesis of amphiphilic copolymer mPEG-PLA from mPEG and monomer LA

(*m* and *n* denoted number of repeating units in polymer)

mPEG-PLA with a number-average MW (M_n) of 2,960Da as determined by NMR was synthesized under vacuum *via* ring-opening polymerization (Figure 2.1) using a modified method by Zhang *et al.* (2005). 5g (2.5mmol) mPEG (2,000Da; macro-initiator) and 0.16g (1.7mmol) LA at 1.45:1 molar amounts were heated in a round bottom flask until melted. Then, 0.5g tin (II) ethylhexanoate (10% *w/w* mPEG) was added as a catalyst and the reaction mixture (RM) was sealed under vacuum and stirred at 150-160°C for 24 hours. The RM was then allowed to cool and dissolved in 5mL of DCM. The flask was resealed and allowed to sit at RT for 4 hours. 100mL ice-cold ether was then added to precipitate the co-polymer and the flask was resealed under vacuum and left in the fridge at 4°C overnight to allow further precipitation. The precipitate was filtered under vacuum and dried using a Daihan WiseVen® vacuum oven (Thermoline Scientific: NSW, Australia) to produce the final white solid compound mPEG-PLA at the yield of 99.1%. The compound was freeze-dried using a Dynavac freeze dryer (Dynapumps: WA, Australia) over 24 hours for storage under vacuum at -20°C. Freeze-dried compounds were analysed using NMR and GPC. The copolymer was labelled as mPEG2000-PLA1000 henceforth based on the calculated

MW of PLA by NMR in Section 2.4.4.2. Synthesis of mPEG750-PLA1000 using mPEG (750Da) as a macro-initiator was also conducted using the method above.

2.4.1.2 Synthesis of methoxy-poly(ethylene glycol)-poly-(ε-caprolactone) (mPEG-PCL)

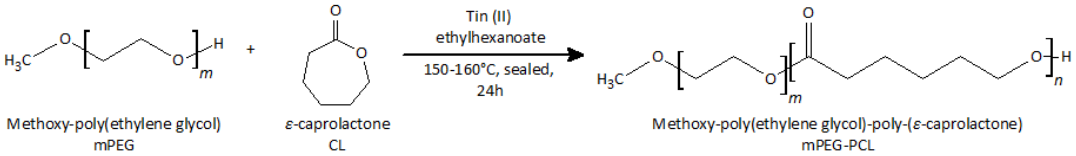

Figure 2.2 General scheme for the synthesis of amphiphilic copolymer mPEG-PCL from mPEG and monomer CL

(*m* and *n* denoted number of repeating units in polymer)

Varying MW combinations of mPEG-PCL were synthesized under vacuum *via* ring-opening polymerization (Figure 2.2) using a modified method by Yuan *et al.* (2000). In general, mPEG with MWs 2,000Da or 750Da was used as a macro-initiator and ε-CL was added as a monomer at different molar feed ratios to produce mPEG-PCL with varying MWs (Table 2.1).

Table 2.1 Molar feed ratio of mPEG and ε-CL and targeted PCL length of resulting mPEG-PCL

Macro-initiator	**Molar feed ratio mPEG to ε-CL**	**Targeted MW of PCL (Da)**
mPEG (750Da; *m*=17)	0.8:1	1,000
mPEG (2,000Da; *m*=45)	1.8:1	1,000
mPEG (2,000Da; *m*=45)	13:1 to 0.2:1	100 to 12,000

For the synthesis of mPEG-PCL with a M_n of 1,530Da based on calculations by NMR (labelled as mPEG750-PCL1000), 5g (6.7mmol) mPEG (750Da) and 0.98g (8.5mmol) ε-CL at 0.78:1 molar amounts were heated in a round bottom flask until melted. Then, 0.5g tin (II) ethylhexanoate (10% *w/w* mPEG) was added as a catalyst and the RM was sealed under vacuum and stirred at 150-160°C for 24 hours. The RM was then allowed to cool and dissolved in 5mL of DCM. The flask was resealed and allowed to sit at RT

for 4 hours. 100mL ice-cold ether was then added to precipitate the co-polymer and the flask was resealed under vacuum and left in the fridge at 4°C overnight to allow further precipitation. The precipitate was filtered under vacuum and discarded. Organic solvent in the filtrate was removed by rotary evaporation using a Büchi R-200 rotary evaporator (In Vitro Technologies: VIC, Australia) to produce a white soft wax of mPEG-PCL at the yield of 99.9%. The compound was freeze-dried over 24 hours and stored under vacuum at -20°C. Freeze-dried compounds were analysed using NMR and GPC.

For the synthesis of mPEG-PCL with a M_n of 3,090Da based on calculations by NMR (labelled as mPEG2000-PCL1000 henceforth), 5g (2.5mmol) mPEG (2,000Da) and 0.16g (1.4mmol) *ε*-CL at 1.75:1 molar amounts were heated in a round bottom flask until melted. Then, 0.5g tin (II) ethylhexanoate (10% *w/w* mPEG) was added as a catalyst and the RM was sealed under vacuum and stirred at 150-160°C for 24 hours. The RM was then allowed to cool and dissolved in 5mL of DCM. The flask was resealed and allowed to sit at RT for 4 hours. 100mL ice-cold ether was then added to precipitate the co-polymer and the flask was resealed under vacuum and left in the fridge at 4°C overnight to allow further precipitation. The precipitate was filtered under vacuum to produce a cream solid of mPEG-PCL at the yield of 99.1%. The compound was freeze-dried over 24 hours and stored under vacuum at -20°C. Freeze-dried compounds were analysed using NMR and GPC. The synthesis of remaining mPEG-PCL using mPEG (2,000Da) as macro-initiator was prepared as such with different mPEG:*ε*-CL molar feed ratios (Table 2.1).

2.4.2 Synthesis of activated amphiphilic copolymers

Amphiphilic copolymers were activated using succinic anhydride or glutaric anhydride which converted the hydroxyl end group in the amphiphilic copolymers to an active carboxylic acid end group for eventual conjugation to RSV.

2.4.2.1 Synthesis of succinated amphiphilic copolymers

Figure 2.3 revealed the general synthetic scheme for activating amphiphilic copolymers mPEG-PLA (Figure 2.3A) and mPEG-PCL (Figure 2.3B) using succinic anhydride based on a modified method by Lu *et al.* (2010). Briefly, 2g of mPEG-PLA

or mPEG-PCL (varying molar amounts depending on MW of polymer, Table 2.2) was dissolved in 10mL anhydrous toluene in a round bottom flask with 0.6g (6.0mmol, 30% *w/w* polymer) succinic anhydride and 1.7μL (11.9μmol, 0.06% *w/w* polymer) triethylamine. The flask was evacuated and the RM was heated to 90-100°C for 24 hours with stirring. After 24 hours, the RM was cooled, fully dissolved in 5mL DCM and allowed to stand at RT for 1 hour. Approximately 50mL ice-cold ether was then added to precipitate the activated copolymer and the flask was resealed under vacuum and left in the fridge at 4°C overnight to allow further precipitation. The precipitate was filtered under vacuum to produce the final compounds of succinated mPEG-PLA or mPEG-PCL in yields ranging from 42.3-82.5%. The resulting precipitate was analysed using NMR and stored under vacuum at -20°C after being freeze-dried over 24 hours. Similarly, mPEG (2,000Da) was succinated to produce a white powder with 97.5% yield.

Table 2.2 Molar feed amounts of 2g mPEG-PLA, mPEG-PCL and mPEG for synthesis of succinated polymers

Polymer	**M_n and repeating units**			**Molar feed amount of 2g copolymer (mmol)**
	mPEG	**PCL**	**PLA**	
mPEG750-PLA1000[a]	750Da *m*=17	n/a	1,000Da *n*=14	1.1
mPEG2000-PLA1000[b]	2,040Da *m*=46	n/a	920Da *n*=13	0.6
mPEG750-PCL1000[b]	680Da *m*=15	850Da *n*=7	n/a	1.2
mPEG2000-PCL1000[b]	1,940Da *m*=43	1,150Da *n*=10	n/a	0.5
mPEG2000[a]	2,000Da *m*=45	n/a	n/a	1.0

n/a = not applicable

[a]labelled according to MW provided by supplier

[b]determined by NMR using end-group analysis (Table 2.5 and Table 2.6)

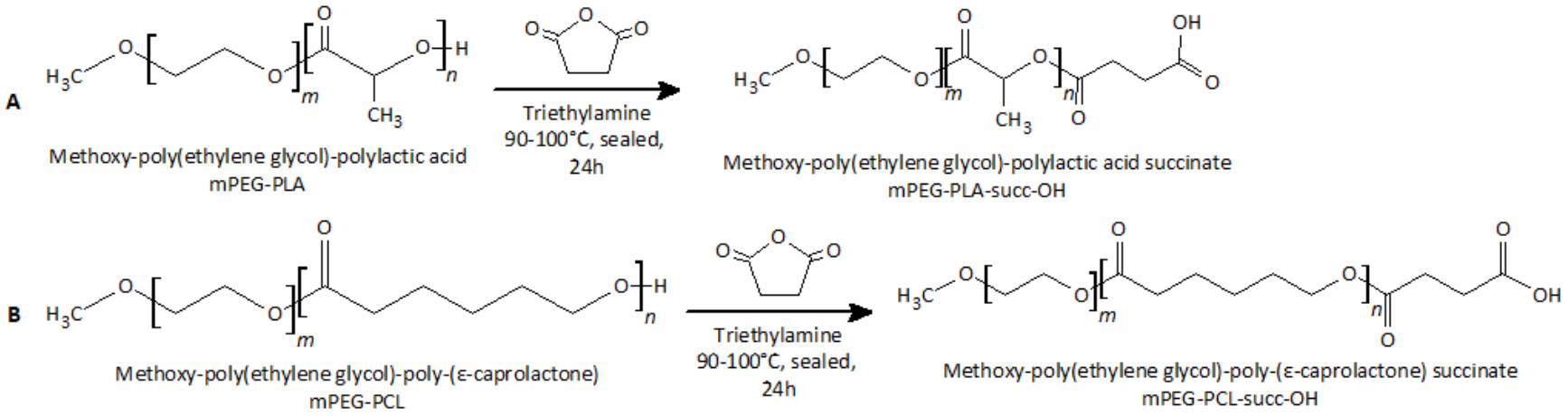

Figure 2.3 General schemes for the activation of mPEG-PLA (A) and mPEG-PCL (B) copolymers by succinic anhydride

2.4.2.2 Synthesis of glutarated amphiphilic copolymers

Figure 2.4 showed the general synthetic scheme for activating amphiphilic copolymers mPEG-PLA (Figure 2.4A) and mPEG-PCL (Figure 2.4B) using glutaric anhydride. Synthesis of glutarated amphiphilic copolymers was similar to the synthesis of succinated amphiphilic copolymers in Section 2.4.2.1. Briefly, 2g of mPEG-PLA or mPEG-PCL (varying molar amounts depending on MW of polymer, Table 2.3) was dissolved in 10mL anhydrous toluene into a round bottom flask with 0.6g (5.3mmol, 30% *w/w* polymer) glutaric anhydride and 1.7μL (11.9μmol, 0.06% *w/w* polymer) triethylamine. The flask was evacuated and the RM was heated to 90-100°C for 24 hours with stirring. After 24 hours, the RM was cooled, fully dissolved in 5mL DCM and allowed to stand at RT for 1 hour. Approximately 50mL ice-cold ether was then added to precipitate the activated copolymer and the flask was resealed under vacuum and left in the fridge at 4°C overnight to allow further precipitation. The precipitate was filtered under vacuum to produce the final compounds of glutarated mPEG-PLA or mPEG-PCL in yields ranging from 40.9-100.0%. Similarly, mPEG (2,000Da) was glutarated to a white powder with 98.1% yield. The resulting precipitates were analysed using NMR and stored under vacuum at -20°C after being freeze-dried over 24 hours.

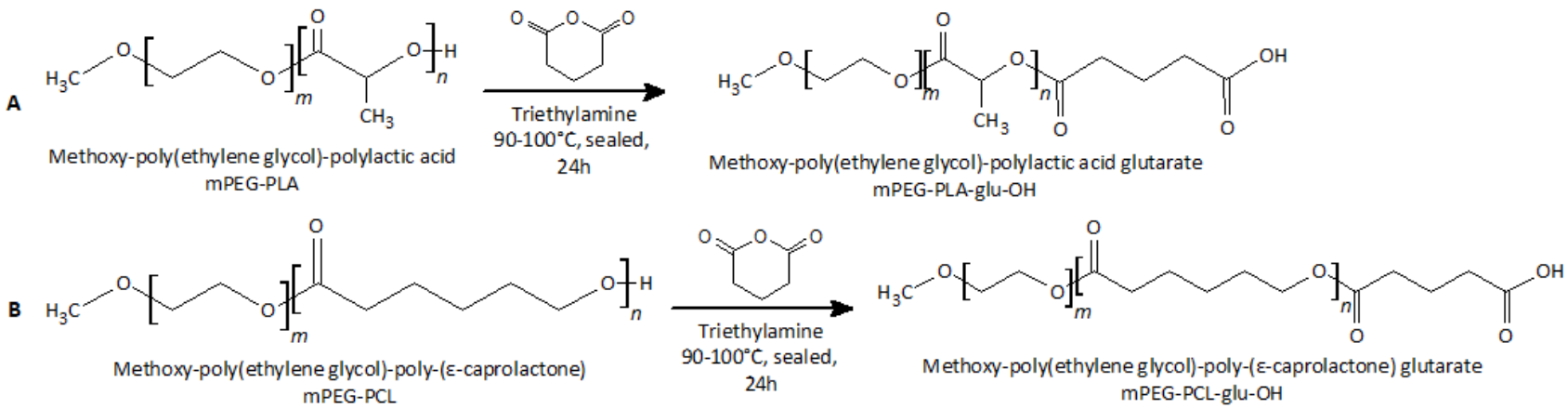

Figure 2.4 General schemes for the activation of mPEG-PLA (A) and mPEG-PCL (B) copolymers by glutaric anhydride

Table 2.3 Molar feed amounts of 2g mPEG-PLA, mPEG-PCL and mPEG for synthesis of glutarated polymers

Amphiphilic copolymer	M_n and repeating units			Molar feed amount of 2g copolymer (mmol)
	mPEG	PCL	PLA	
mPEG750-PLA1000[a]	750Da *m*=17	n/a	1,000Da *n*=14	1.1
mPEG2000-PLA1000[b]	2,040Da *m*=46	n/a	920Da *n*=13	0.6
mPEG750-PCL1000[b]	680Da *m*=15	850Da *n*=7	n/a	1.2
mPEG2000-PCL1700[b]	1,940Da *m*=43	1,150Da *n*=10	n/a	0.5
mPEG2000-PCL_n[b]	1,880 to 2,120Da *m*=42 to 47	130 to 11,660Da *n*=1 to 102	n/a	0.9 to 0.1
mPEG2000[a]	2,000Da *m*=45	n/a	n/a	1.0

[a]labelled according to MW provided by supplier
[b]determined by NMR using end-group analysis (Table 2.5 and Table 2.6)

2.4.3 Conjugation of activated amphiphilic polymers to resveratrol

The conjugation of RSV to synthesised activated amphiphilic copolymers (Section 2.4.2) with an ester bond was achieved by a carbodiimide coupling reaction (Figure 2.5) as reported in Basavaraj (2011) with a slight modification to the purification procedure.

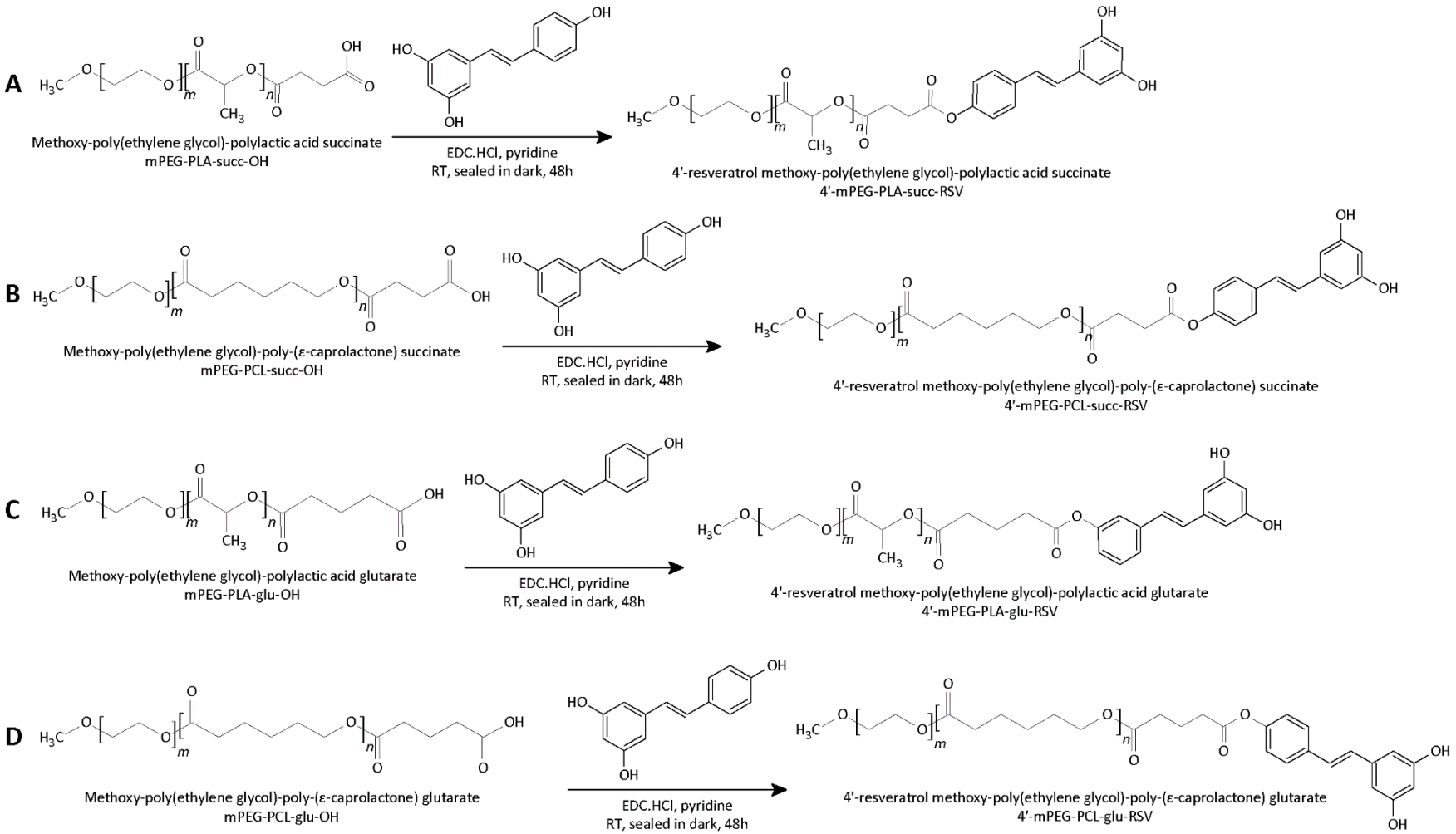

Figure 2.5 General schemes for conjugation of RSV to activated amphiphilic copolymers mPEG-PLA-succ-OH (A), mPEG-PCL-succ-OH (B), mPEG-PLA-glu-OH (C) and mPEG-PCL-glu-OH (D) by carbodiimide coupling reaction

Excess amount of RSV (approximately 4× molar amount of copolymer), 1.5g of an activated amphiphilic copolymer (Section 2.4.2) and EDC.HCl, in 4× molar amount of copolymer, was dissolved in pyridine (20 mL) in a round bottom flask (See Table 2.4 for molar and weight amounts of each component). The RM was stirred at RT in the dark under vacuum for 48 hours. The RM was then dissolved in 10mL DCM and washed once with 10mL 0.1M hydrochloric acid to remove the dicyclohexylurea from the reaction and twice with 5mL of 10% *w/v* copper (II) sulphate aqueous solution diluted 1:4 in 0.1M hydrochloric acid to remove pyridine. The organic layer was collected and dried with sodium sulphate and filtered. Excess ice-cold ether (approximately 50mL) was then added to the filtrate to precipitate the conjugated RSV copolymer and the flask was resealed under vacuum and left in the fridge overnight to allow further precipitation. The precipitate was filtered under vacuum to produce RSV conjugated to amphiphilic copolymers in yields ranging from 16.8-54.9%. Synthesized products were analyzed using NMR and HPLC. HPLC analyses will be described further in Chapter 3.

Table 2.4 Weight and molar feed amounts of selected succinated or glutarated (activated) polymers, RSV and EDC.HCl for conjugation of RSV with activated polymers by carbodiimide coupling reaction

Activated polymer	**Weight and molar amounts used**		
	Activated polymer	**RSV**	**EDC.HCl**
mPEG750-PLA1000	1.5g (0.8mmol)	0.7g (3.2mmol)	0.6g (3.2mmol)
mPEG2000-PLA1000	1.5g (0.5mmol)	0.5g (2.0mmol)	0.4g (2.0mmol)
mPEG750-PCL1000	1.5g (0.8mmol)	0.7g (3.2mmol)	0.6g (3.2mmol)
mPEG2000-PCL1700	1.5g (0.4mmol)	0.4g (1.6mmol)	0.3g (1.6mmol)

Similarly, glutarated mPEG2000-PCL_n (PCL MW 130Da-11,660Da), succinated and glutarated mPEG2000 was conjugated to RSV and characteristics of these conjugates are presented in Appendix 7.4 along with *in vitro* stability data in buffers at pH4.5 and

pH7.4 at different temperatures and in rat plasma. Stability data was published in Ng *et al.* (2015).

2.4.4 Characterisation of synthesised products

2.4.4.1 Yield

Percentage yield of synthesised products were calculated using the following equation based on the assumptions that the chemical reaction was a stoichiometric reaction and that all limiting reagents were consumed. As the conjugation reactions can result in multiple substitutions of RSV, the percentage yield was calculated assuming the reactions resulted in mono-substituted RSV conjugates with no unconjugated RSV unless the reactions resulted in 100% di-substituted RSV conjugates where the percentage yield would be calculated based on the mass of di-substituted RSV conjugates instead of mono-substituted RSV conjugates.

$$\text{Percentage yield (\%)} = \frac{\text{Actual mass yield (g)}}{\text{Theoretical mass yield (g)}} \times 100\%$$

2.4.4.2 Nuclear magnetic resonance (NMR) spectroscopy

^{1}H NMR spectroscopy was used to analyse and elucidate the structural properties of all synthesised products by observing the local magnetic fields around proton nuclei in a sample (Roberts 1961). Wiegand *et al.* (2008) stated that NMR end-group analysis was more suitable for polymers with less than 30,000Da as end groups in higher MW polymers would be impractical for quantitation. One-dimensional proton and two-dimensional COSY (homonuclear correlation spectroscopy) NMR spectra were obtained by dissolving approximately 10mg of synthesized products in 0.5mL to 1mL $CDCl_3$ or d_6-DMSO and analysed with a Bruker Avance III 400MHz spectrometer (Bruker Pty Ltd: NSW, Australia). Chemical shifts (δ) of peaks with corresponding proton labels in structure and peak areas or integrals were analysed using a TopSpin™ v3.5 software (Bruker Pty Ltd: NSW, Australia) and a Spectrus Processor vS60S41 software (Advanced Chemistry Development Inc.: Toronto, Canada) and depicted at the top and bottom of each NMR spectra, respectively. In this manuscript, δ were expressed in ppm with multiplicities indicated by s (singlet), d (doublet), t (triplet), q (quartet), m (multiplet) and br (broad). Both one-dimensional and two-dimensional

NMR spectra were used to determine and confirm the chemical structure of synthesised products according to methods detailed in Furniss *et al.* (1996). The peak areas or integration is proportional to the molar concentration of the protons analysed.

M_n of low MW amphiphilic copolymers was determined by end-group analysis using distinguishable proton signals originating from the end-group of mPEG and repeating units of PCL or PLA (Wiegand *et al.* 2008, Paulsen *et al.* 2016). Izunobi *et al.* (2011) gave an example of M_n calculation of polymers using end-group analysis and in our instance, Appendix 7.1 specified the calculations for M_n of mPEG2000-PLA1000 as a representation of our polymers.

Molar ratios of free RSV and substituted RSV in final conjugated RSV products was determined by comparing proton integrals in NMR spectra as described in Section 2.5.3 for the calculation of percentage weight-per-weight (% *w/w*) of components and total RSV equivalent concentrations of each synthesised product. % *w/w* of each component, that is mono-substituted RSV, di-substituted RSV and free unconjugated RSV, was calculated against the total weight of all components in the final synthesised RSV-conjugated product. The determination of total RSV content or total RSV equivalent concentration in a batch of synthesized products was based on its % *w/w* whereby the total RSV equivalent concentration was the summation of the concentration of unconjugated RSV and concentrations of RSV equivalent of any conjugated RSV in the synthesised products. As an example, the calculation of % *w/w* and total RSV equivalent concentration of 1mg/mL mPEG750-PCL1000-succ-RSV is presented in Appendix 7.2.

2.4.4.3 Gel permeation chromatography (GPC)

GPC was used as confirmation of M_n calculations using end-group analysis by NMR and to calculate the M_n, weight-average MW (M_w) and PDI of synthesised amphiphilic copolymers (Section 2.4.1) using an Agilent GPC system (Agilent Technologies Australia; VIC, Australia) with a Jordi Gel DVB organic column (5μm, 1000Å, 25cm × 4.6mm) (Jordi Labs LLC: MA, USA). PEG calibration standards in the M_p range of 960-26,100g/mol (Jordi Labs LLC: MA, USA) and co-polymers were prepared fresh in THF

for each analysis. Briefly, a copolymer or PEG standard solution (approximately 1mg/mL) was dissolved in THF and 100μL was injected and eluted with THF at 1.2mL/min for 5 minutes. Detection was by an Agilent model G1362A refractive index detector (RID) (Agilent Technologies Australia: VIC, Australia) with a cell temperature of 40°C. The PEG calibration curve was prepared by plotting log(M_p) against retention time (t_R) and used for the determination of the M_w, M_n, and PDI (M_w/M_n) of synthesised amphiphilic copolymers according to Holding *et al.* (1995) (See Appendix 7.3 for calculations). M_p was quoted for copolymers where calculations of average MWs were not possible.

2.5 Results and discussion

2.5.1 Synthesis of amphiphilic polymers

2.5.1.1 mPEG-PLA

Table 2.5 shows the characteristics of mPEG-PLA synthesized using mPEG (2,000Da; *m*=45) as a macro-initiator and LA was added as a monomer at 1.45:1 molar ratio. The degree of polymerization of the monomer LA on mPEG-PLA was calculated using end-group analysis by comparing integral intensity of characteristic resonance of the PLA at 5.2ppm (-C(=O)-C**H**CH_3O-) (Alibolandi *et al.* 2015) with the PEG resonance at 3.4ppm (-OC$\mathbf{H_2}$C$\mathbf{H_2}$-) in the ^{1}H NMR spectrum (Figure 2.6). Appendix 7.1 details the calculation using end-group analysis.

Table 2.5 Characteristics of mPEG-PLA using NMR and GPC

Macro-initiator	Molar feed ratio mPEG:LA	Product description	Yield (%)	GPC analyses[a]			NMR analyses[b]			Product label
				M_w	M_n	PDI	M_n (Da) and repeating units (*m*) of mPEG	M_n (Da) and repeating units (*n*) of PLA	Total M_n (Da)	
mPEG (2,000Da; *m*=45)	1.45:1	White powder	99.1	3,080	2,360	1.31	2,040 (*m*=46)[c]	920 (*n*=13)[d]	2,960	mPEG2000-PLA1000
mPEG (750Da; *m*=17)	Unsuccessful									

[a]see Appendix 7.3 for detailed calculation

[b]see Appendix 7.2 for detailed calculation

[c]MW of a single monomer in mPEG is 44Da. Therefore, with an Mn of *ca.* 2,040Da, the number of repeating units in the mPEG was $\frac{2040}{44} \approx 46$

[d]MW of a single monomer in PLA is 72Da. Therefore, with an Mn of *ca.* 920Da, the number of repeating units in the PLA was $\frac{920}{72} \approx 13$

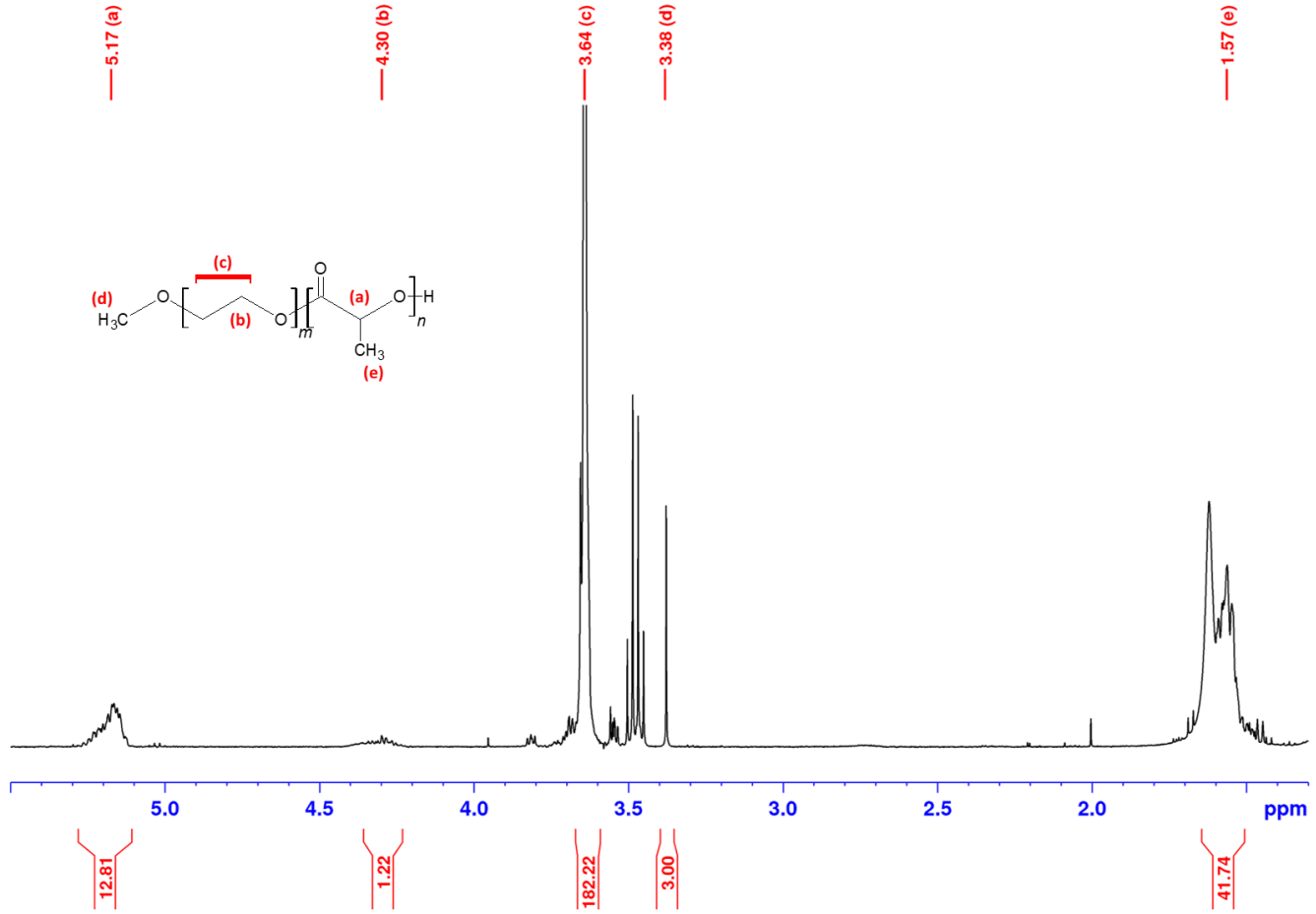

Figure 2.6 ^{1}H NMR spectra of mPEG2000-PLA1000 in $CDCl_3$

δ ppm 1.45 - 1.61 (m, -C(=O)-CHC**H$_3$**O-, H_e) 3.38 (s, -OC**H$_3$**, H_d) 3.60 - 3.69 (m, -OC**H$_2$**C**H$_2$**OC(=O)-, H_c) 4.22 - 4.40 (m, end groups of -OCH$_2$C**H$_2$**OC(=O)- and -C(=O)-C**H**CH$_3$O-, H_b and H_a) 5.13 - 5.30 (m, -C(=O)-C**H**CH$_3$O-, H_a)

The MW of mPEG was verified as close to 2,000Da using the end-group analysis by comparing integral intensity of characteristic resonance of the methyl group on mPEG at 3.4ppm (-OC**H**$_3$) with the PEG chain resonance at 3.6ppm (-OC**H**$_2$C**H**$_2$-), therefore, it was safe to assume that there was no hydrolysis or breakdown of mPEG during the synthesis of the amphiphilic copolymer mPEG2000-PLA1000. In addition, there was no sign of other degradation products present in the synthesized compound from NMR spectra and GPC chromatograms. The polymerization of LA onto mPEG was confirmed by the lack of the methine signals (labelled H_a in Figure 2.7) present in the monomer LA which had a chemical shift at *ca.* 5.0ppm with a quadruplet multiplicity (Inkinen *et al.* 2011).

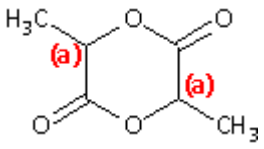

Figure 2.7 Structure of D,L-lactide (LA) monomer with labelled methine signal

^{1}H NMR spectra in Appendix 7.5, Figure 7.3

PLA was calculated to have an M_n of 920Da by NMR, however, analyses by GPC revealed a total M_n of 2,360Da for mPEG-PLA which indicated that PLA had an M_n of 360Da with mPEG at 2,000Da (Table 2.5). As GPC elution is based on the hydrodynamic volume of polymer (Wong *et al.* 2012), the linear type polymer of the PEG standards might not be comparable with our synthesized copolymers as synthesized products might have different hydrodynamic volume than PEG when eluted (Izunobi *et al.* 2011) hence affecting the average MW calculations. Nonetheless, GPC analyses allowed for the determination of MW distribution of polymers.

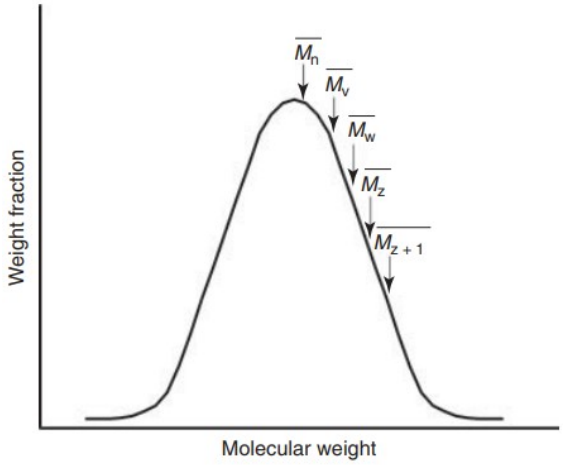

Figure 2.8 Schematic view of average MW distributions in eluted peaks on a typical GPC chromatogram

Picture taken from Neira-Velázquez *et al.* (2013); M_n = number-average MW, M_v = viscosity-average MW, M_w = weight-average MW, M_z = *Z*-average MW, M_{z+1} = *Z*+1-average MW

Figure 2.8 shows a schematic overview of different average MWs obtained from a GPC chromatogram and where our average MW distribution of interest, M_w and M_n, lies within an eluted peak (Neira - Velázquez *et al.* 2013). M_w is dependent on the size of the polymer chains whereas the M_n is dependent on the number of polymer chains in a polymer, therefore, M_w affects bulk properties of a polymer such as viscosity and toughness whereas M_n affects colligative properties of a polymer such as boiling and freezing points (Carraher 2007). As our mPEG-PLA is amphiphilic, the properties of mPEG-PLA would differ significantly from the PEG standards. Similar values of average MWs indicate a monodispersed polymer system (Carraher 2007). PDI is obtained by $\frac{M_w}{M_n}$ and a PDI value of 1.30 implied a fairly narrow distribution for mPEG2000-PLA1000 (Khanna *et al.* 1996, Agilent Technologies Inc. 2015) whereas a PDI of 1.00 indicates a monodispersed polymer system (Umoren *et al.* 2016).

Although controlling the feed ratio between initiator and monomer for a fixed reaction time was a known synthesis approach (Kim *et al.* 2004), this was not possible with the synthesis of mPEG750-PLA1000 with targeted MWs of 750Da for mPEG and 1,000Da for PLA using the macro-initiator mPEG (750Da; *m*=17). Several trials were conducted to study the influence of feed ratio on the resulting copolymer MW using mPEG (750Da) as macro-initiator. Although NMR analyses of the raw RMs prior to precipitation revealed presence of the desired product mPEG750-PLA1000,

precipitation by ice-cold ether did not produce the desired product or any mPEG-PLA signals when analysed by NMR. It was assumed that the purification step was not ideal for this copolymer. Subsequently, several trials were conducted to explore other anti-solvents such as MeOH or hexane to precipitate the desired copolymer, and to explore trituration as an alternative to precipitation but were unsuccessful. Due to time limitations, the decision was made to purchase mPEG750-PLA1000 from a commercial source for further synthesis and use (Certificate of Analysis attached in Appendix 7.6).

2.5.1.2 mPEG-PCL

The degree of polymerization of the monomer *ε*-CL on mPEG-PCL was calculated using end-group analysis similar to mPEG-PLA but by comparing integral intensity of characteristic resonance of the PCL at 2.3 ppm (-C(=O-C**H₂**) (Kim *et al.* 2005) with the PEG resonance at 3.4ppm (-OC**H₂**C**H₂**-) in the ^{1}H NMR spectrum represented by mPEG750-PCL1000 in Figure 2.10. The M_n of mPEG was verified as *ca.* 2,000Da or 750Da using the NMR end-group analysis (Table 2.6), therefore, there was no hydrolysis or breakdown of mPEG during the synthesis of the amphiphilic copolymer mPEG-PCL. The polymerization of *ε*-CL onto mPEG was confirmed by the lack of the methylene signals (labelled H_d in Figure 2.9) in CL which had a chemical shift at *ca.* 2.6ppm with a triplet multiplicity (Abraham *et al.* 2008).

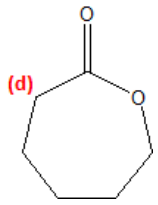

Figure 2.9 Structure of *ε*-CL monomer with labelled methylene signal

^{1}H NMR spectra in Appendix 7.5 (Figure 7.4)

The M_n of PCL in mPEG-PCL was calculated by end-group analysis using NMR and summarized in Table 2.6. The average MWs and PDI of copolymers were also calculated after analysis by GPC and reported in Table 2.6.

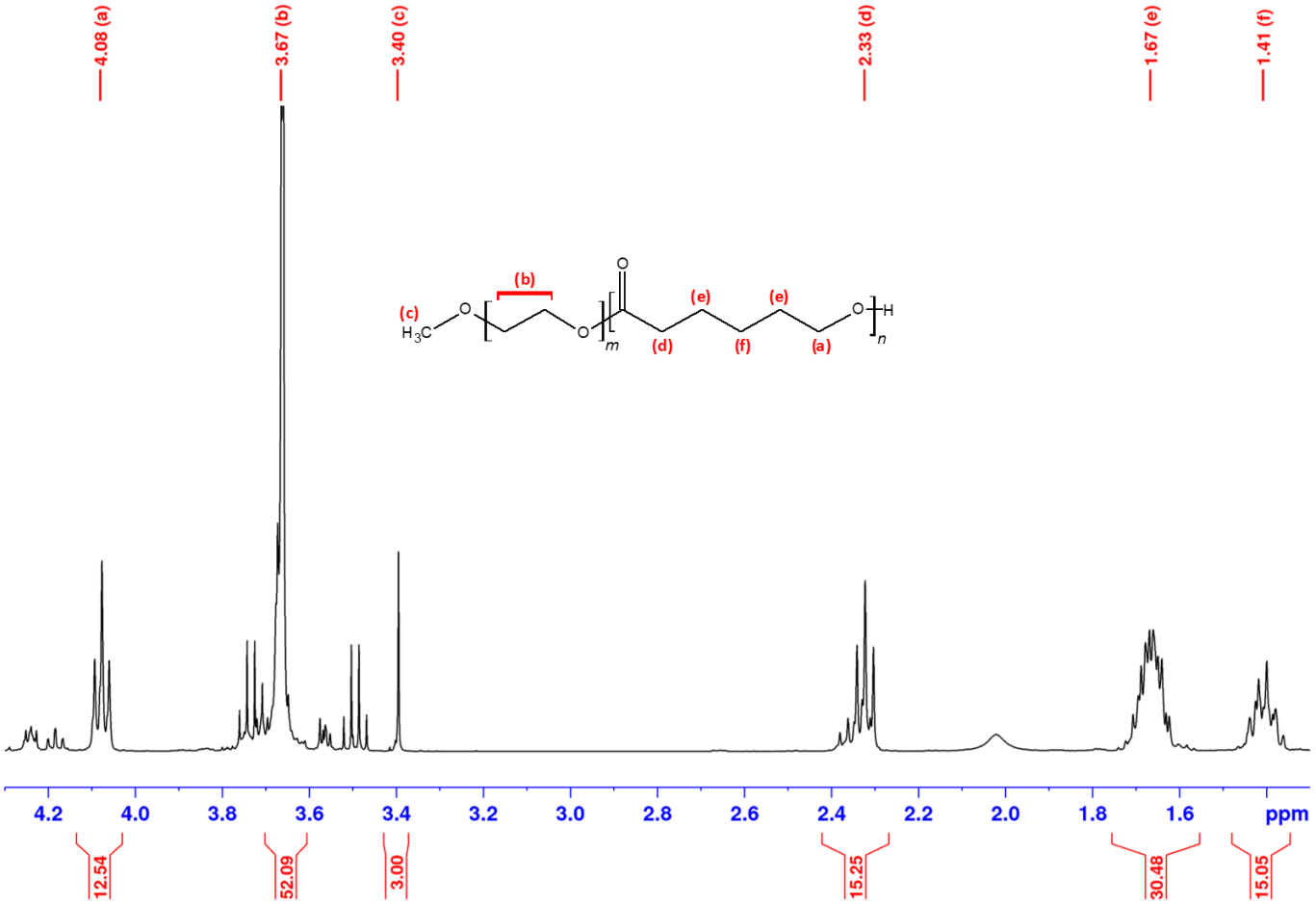

Figure 2.10 ^{1}H NMR spectra of mPEG750-PCL1000 in $CDCl_3$

δ ppm 1.30 - 1.55 (m, -C(=O)-$C_2H_5C\underline{\mathbf{H_2}}C_2H_5O$-, H_f) 1.57 - 1.74 (m, -C(=O)-$CH_2C\underline{\mathbf{H_2}}CH_2C\underline{\mathbf{H_2}}CH_2O$-, H_e) 2.33 (t, -C(=O)-$C\underline{\mathbf{H_2}}CH_2CH_2CH_2CH_2O$-, H_d) 3.40 (s, -$OC\underline{\mathbf{H_3}}$, H_c) 3.61 - 3.76 (m, -$OC\underline{\mathbf{H_2}}C\underline{\mathbf{H_2}}OC(=O)$-, H_b) 4.08 (t, -C(=O)-$CH_2CH_2CH_2CH_2C\underline{\mathbf{H_2}}O$-, H_a)

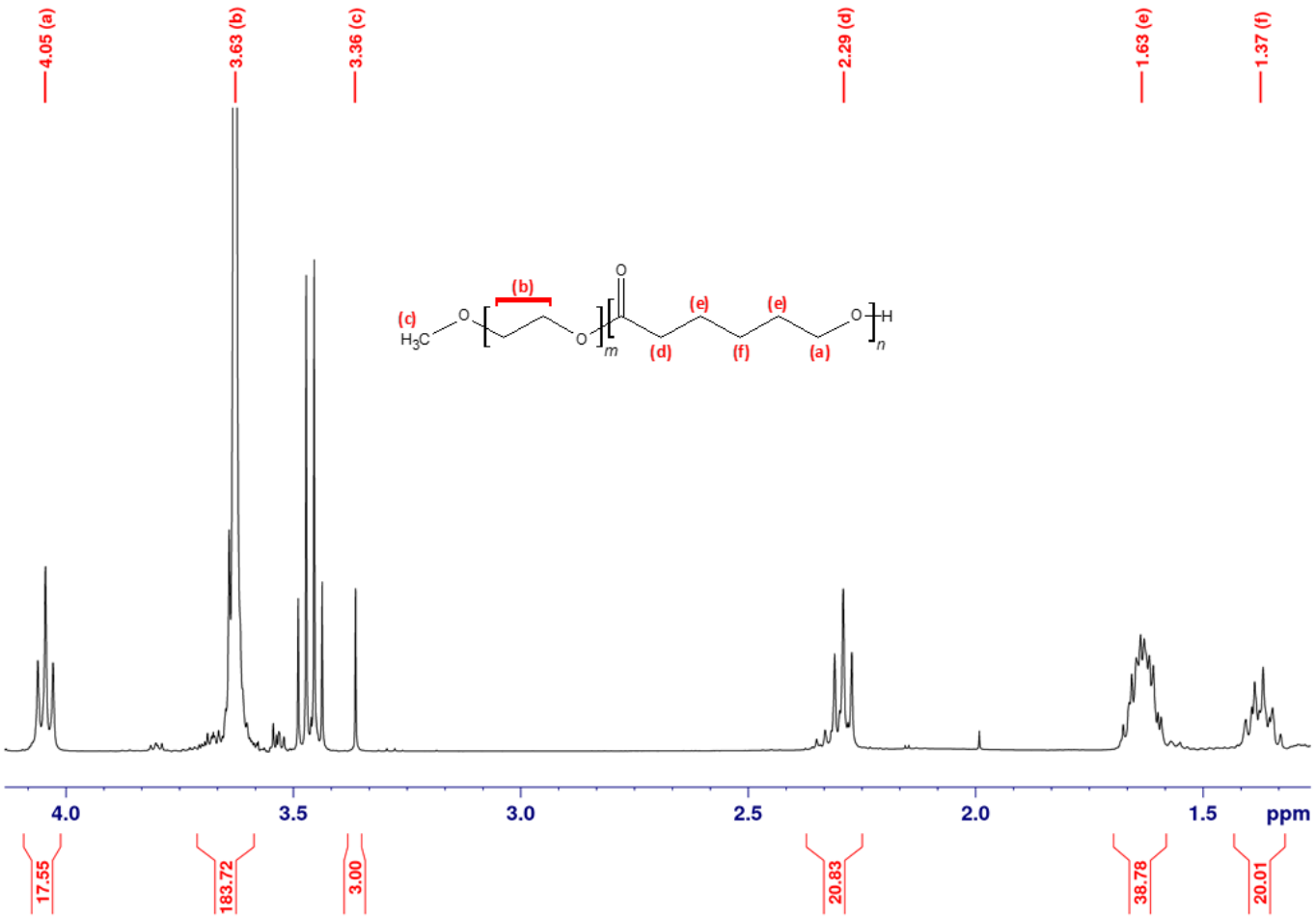

Figure 2.11 ^{1}H NMR spectra of mPEG2000-PCL1000 in $CDCl_3$

δ ppm 1.32 - 1.43 (m, -C(=O)-$C_2H_5C\underline{\mathbf{H_2}}C_2H_5O$-, H_f) 1.58 - 1.70 (m, -C(=O)-$CH_2C\underline{\mathbf{H_2}}CH_2C\underline{\mathbf{H_2}}CH_2O$-, H_e) 2.29 (t, -C(=O)-$C\underline{\mathbf{H_2}}CH_2CH_2CH_2CH_2O$-, H_d) 3.36 (s, -OC$\underline{\mathbf{H_3}}$, H_c) 3.59 - 3.71 (m, -OC$\underline{\mathbf{H_2}}C\underline{\mathbf{H_2}}$OC(=O)-, H_b) 4.05 (t, -C(=O)-$CH_2CH_2CH_2CH_2C\underline{\mathbf{H_2}}O$-, H_a)

Table 2.6 Characteristics of mPEG-PCL using NMR and GPC

Macro-initiator	Molar feed ratio mPEG:CL	Product description	Yield (%)	GPC analyses[a]			NMR analyses[b]			Product label
				M_w (Da)	M_n (Da)	PDI	M_n (Da) and repeating units (*m*) of mPEG	M_n (Da) and repeating units (*n*) of PCL[c]	Total M_n (Da)	
mPEG (750Da; *m*=17)	0.78:1	White soft wax	99.9	1,740	1,070	1.63	680 (*m*=15)	850 (*n*=7)	1,530	mPEG750-PCL1000
mPEG (2,000Da; *m*=45)	1.75:1	Cream powder	98.0	3,190	2,230	1.44	1,940 (*m*=43)	1,150 (*n*=10)	3,050	mPEG2000-PCL1000
	13.43:1	White powder	99.5	2,390	1,700	1.41	2,060 (*m*=46)	130 (*n*=1)	2,190	mPEG2000-PCL_n[d]
	7.00:1	Off-white flakes	96.9	2,670	1,780	1.50	2,050 (*m*=46)	230 (*n*=2)	2,280	
	3.55:1	Cream powder	95.6	3,170	1,990	1.59	2,090 (*m*=47)	500 (*n*=4)	2,590	
	0.59:1	Cream powder	72.8	7,970	6,300	1.27	2,120 (*m*=47)	3,240 (*n*=28)	5,360	
	0.29:1	Cream powder	71.9	15,320	13,870	1.10	1,880 (*m*=42)	5,190 (*n*=45)	7,070	
	0.20:1	Cream waxy powder	79.4	M_p = 12,940 Da			1,980 (*m*=44)	11,660 (*n*=102)	13,640	

[a]see Appendix 7.3 for calculation example using mPEG2000-PLA1000

[b]see Appendix 7.2 for calculation example using mPEG2000-PLA1000

[c]MW of a single monomer in PCL is 114Da. Therefore, with an Mn of *ca.* 1,150Da, the number of repeating units in the PCL was $\frac{1150}{114} \approx 10$

[d]*n* denotes PCL repeating units

From the NMR and GPC data, it was evident that controlling molar feed ratios were able to control the degree of polymerization of *ε*-CL onto mPEG (2,000Da). Interestingly, mPEG-PCL copolymer synthesised using mPEG (750Da) as a macro-initiator were not precipitated solids but was found in the filtrate of the precipitation process with ice-cold ether. Desired products were obtained by evaporating the organic solvent from the filtrate at 50°C under vacuum using a rotary evaporator. Although M_n calculated by NMR was not an exact correlation with M_n calculation by GPC for all copolymers, it should be noted that the PEG standards used for the calibration of GPC would not have the same structural properties as mPEG-PCL and hence have different hydrodynamic volumes which would affect the calculation of average MWs using eluted peaks of GPC chromatograms of copolymers. Nonetheless, the GPC data showed a range of average MWs which correlated with M_n of NMR. As GPC was known to be less accurate than NMR when dealing with low MW polymers due to different refractive indices of low MW polymers compared to their higher MW counterparts (Chance *et al.* 1995, Wong *et al.* 2012, Oberlerchner *et al.* 2015), we have used NMR as our main reference to label our copolymers as seen in the last column of Table 2.6.

The M_n calculated from the NMR spectra of the longer copolymers with the macro-initiator mPEG (2,000Da) synthesised at molar feed ratios of 0.29:1 and 0.20:1 was lower than the average MW range calculated from GPC analyses possibly due to the reduced sensitivity of the NMR end-group analysis owing to the diminishing quantifiable end-groups compared to the polymer protons in higher MW polymers (Umoren *et al.* 2016). It was also possible that as the length of PCL increased, the conformation of the polymer in solution differed from that in copolymers with shorter PCL lengths which affected the elution time of the copolymer hence the average MW calculation (Carraher 2007).

2.5.2 Synthesis of activated amphiphilic copolymers

In order to conjugate RSV to the copolymers or mPEG, the hydroxyl group of copolymers needed to be activated by converting the hydroxyl group to a carboxylic acid group to allow for an esterification process between the carboxylic acid of the

activated polymer and the hydroxyl group of RSV. Two different carbon chain lengths of anhydride were used to activate the hydroxyl group of polymers, that is, succinic anhydride (two-carbon) and glutaric anhydride (three-carbon). The succ linker was chosen based on the enhanced PK profile of mPEG750-PLA1000-succ-RSV compared to RSV found in Basavaraj (2011) whereas the glu linker was elected owing to a report by Safavy *et al.* (2004) which showed an improved stability, antitumour activity and sustained drug release of PEGylated PTX glu conjugates compared to the PEGylated PTX succ conjugates.

Table 2.7 Characteristics of activated amphiphilic copolymers

Activated amphiphilic copolymer	Product description	Yield (%)
mPEG750-PLA1000-succ-OH	White powder	56.8
mPEG750-PLA1000-glu-OH	White powder	51.6
mPEG750-PCL1000-succ-OH	Cream-coloured gel	49.3
mPEG750-PCL1000-glu-OH	White powder	76.4
mPEG2000-PLA1000-succ-OH	White flakes	82.5
mPEG2000-PLA1000-glu-OH	White flakes	40.9
mPEG2000-PCL1000-succ-OH	Cream powder	42.3
mPEG2000-PCL1000-glu-OH	Cream powder	88.6
mPEG2000-PCL$_n$-glu-OH	Cream powder	76.3-100.0
mPEG2000-succ-OH	White powder	97.5
mPEG2000-glu-OH	White powder	98.1

n denotes PCL repeating units for MW from 130 to 11,660Da (see Table 2.6 for individual copolymer MW)

Synthesis of activated amphiphilic copolymers was straight-forward by refluxing the amphiphilic copolymer with either succinic or glutaric anhydride in anhydrous toluene and resulted in average to high yields (Table 2.7). Chemical shifts of protons in the succinate group distinctly moved upfield from 3.0ppm to 2.6ppm whereas in the glutarate group, the chemical shifts of the protons adjacent to the carboxyl groups moved upfield from 2.8ppm to 2.4ppm (Yamaguchi *et al.* 2013, Worzakowska 2014). As peak integrations denote molar concentrations of protons in NMR samples,

we would expect the succinate and glutarate protons aforementioned would have an integration of 4.00 with the methyl group of mPEG showing an integration of 3.00 which was the case for most of our synthesized products as seen in Figure 2.12, Figure 2.14 and Figure 2.15 as representative NMR spectra of mPEG-PLA-succ-OH, mPEG-PCL-succ-OH and mPEG-PCL-glu-OH. This was not the case for mPEG750-PLA1000-glu-OH (Figure 2.13) where the integration for the glu protons at 2.47ppm was in an excess of 17.16. A comparison with the NMR spectra of the copolymer mPEG750-PLA1000 (Appendix 7.6) revealed an overlapping signal at *ca.* 2.5ppm which could have augmented the integration of the methylene group superficially. The methylene group (H_f) of the glu group at 2.00ppm on the NMR spectra of mPEG750-PLA1000-glu-OH (Figure 2.13) was also found to have an integration in excess of 9.14 when it should be 2. This was probably due to the overlapping signals of water. This observation was also seen for the synthesis of mPEG2000-PLA-glu-OH (NMR spectra in Appendix 7.5, Figure 7.5).

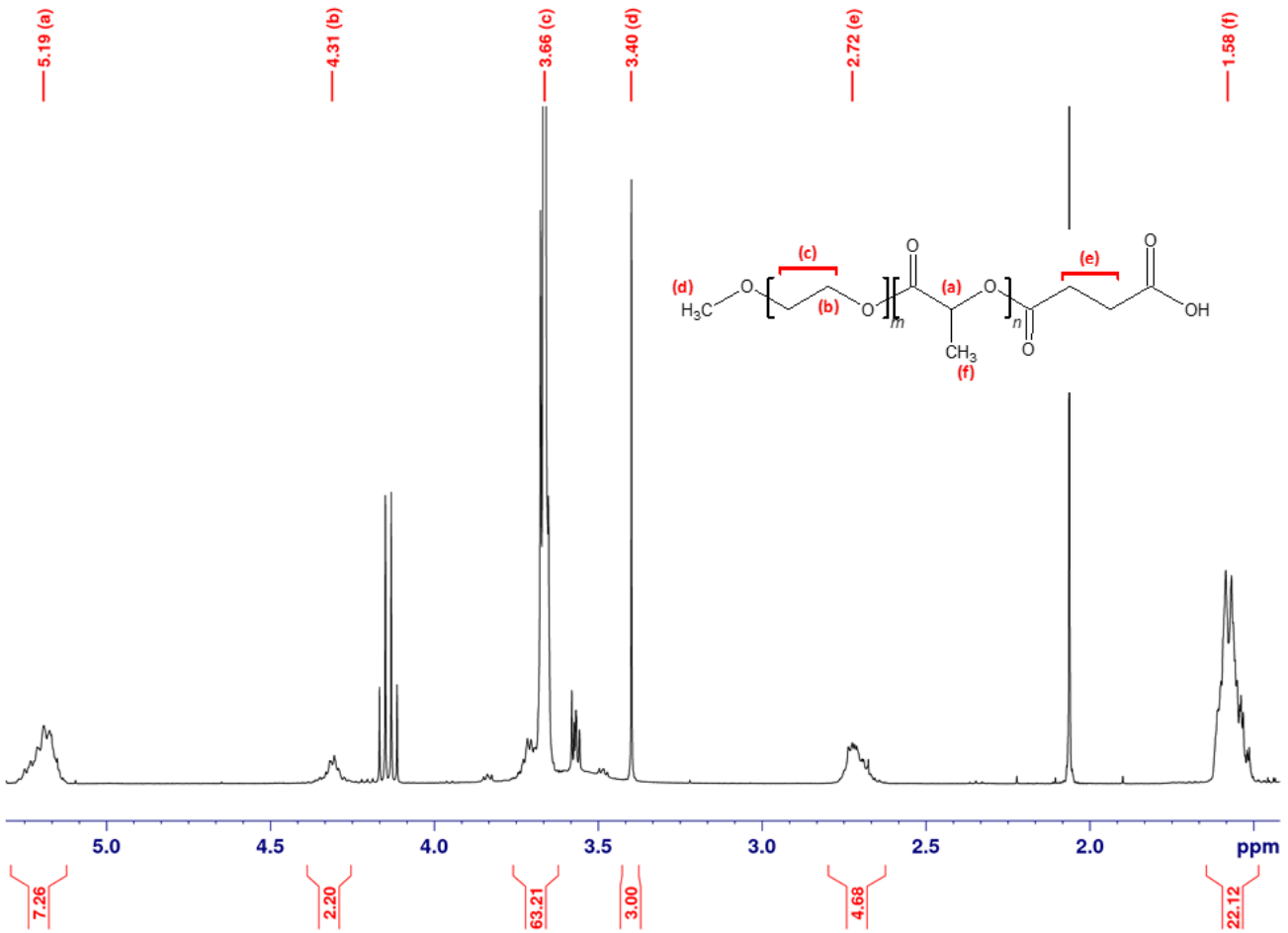

Figure 2.12 ^{1}H NMR spectra of mPEG750-PLA1000-succ-OH (representing mPEG-PLA-succ-OH) in $CDCl_3$

δ ppm 1.49 - 1.65 (m, -C(=O)-CHC**H**$_3$O-, H_f) 2.62 - 2.80 (m, -OC(=O)-C**H**$_2$C**H**$_2$-C(=O)O-, H_e) 3.40 (s, -OC**H**$_3$, H_d) 3.62 - 3.76 (m, -OC**H**$_2$C**H**$_2$OC(=O)- , H_c) 4.26 - 4.39 (m, end groups of -OCH$_2$C**H**$_2$OC(=O)- and -C(=O)-C**H**CH$_3$O-, H_b and H_a) 5.12 - 5.29 (m, -C(=O)-C**H**CH$_3$O-, H_a)

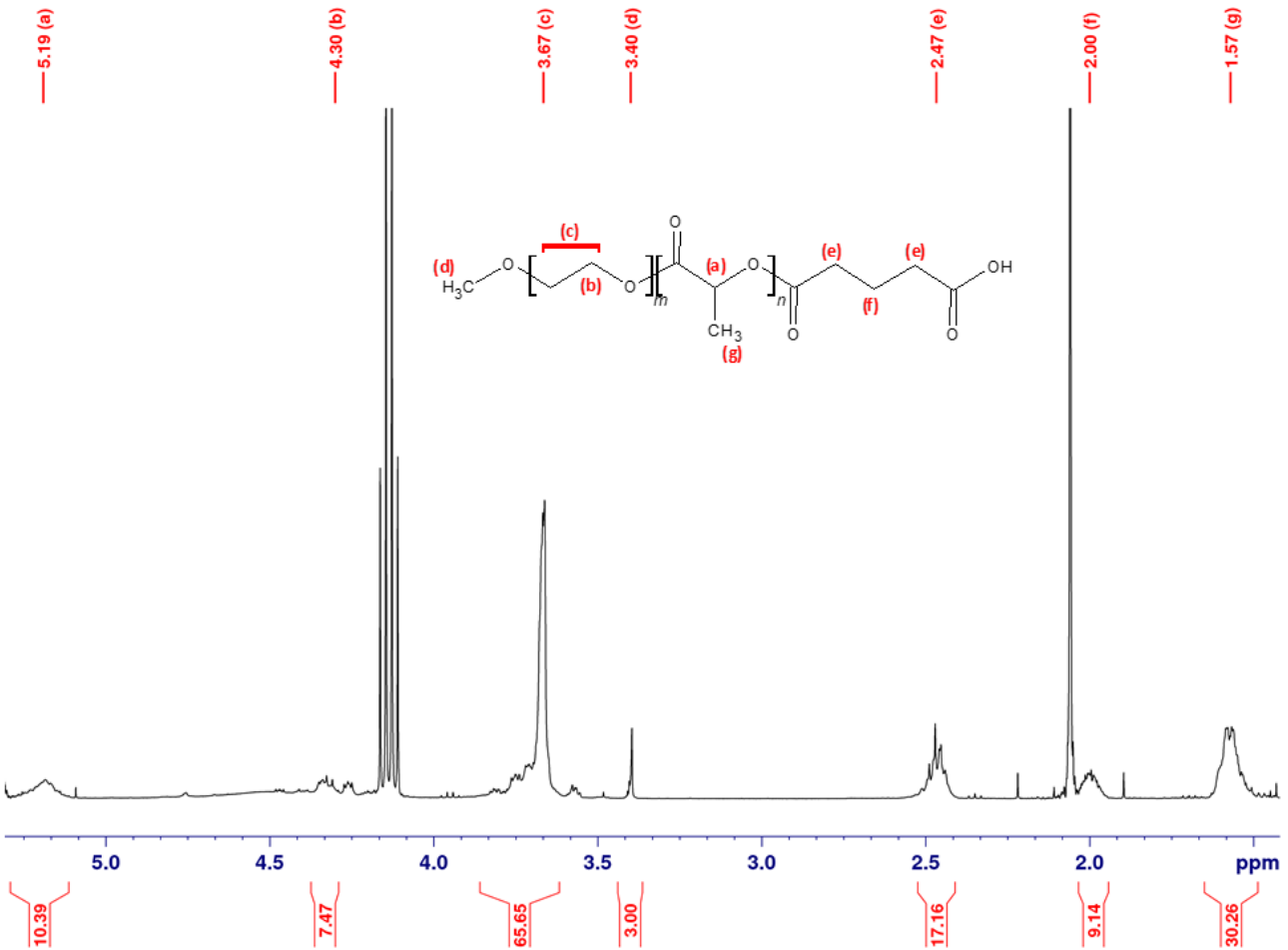

Figure 2.13 ^{1}H NMR spectra of mPEG750-PLA1000-glu-OH (representing mPEG-PLA-glu-OH) in $CDCl_3$

δ ppm 1.49 - 1.65 (m, -C(=O)-CHC**H$_3$**O-, H_g) 1.94 - 2.03 (m, -OC(=O)-CH$_2$C**H$_2$**CH$_2$-C(=O)O-, H_f) 2.41 - 2.53 (m, -OC(=O)-C**H$_2$**CH$_2$C**H$_2$**-C(=O)O-, H_e) 3.40 (s, -OC**H$_3$**, H_d) 3.62 - 3.86 (m, -OC**H$_2$**C**H$_2$**OC(=O)-, H_c) 4.29 - 4.37 (m, end groups of -OCH$_2$C**H$_2$**OC(=O)- and -C(=O)-C**H**CH$_3$O-, H_b and H_a) 5.11 - 5.29 (m, -C(=O)-C**H**CH$_3$O-, H_a)

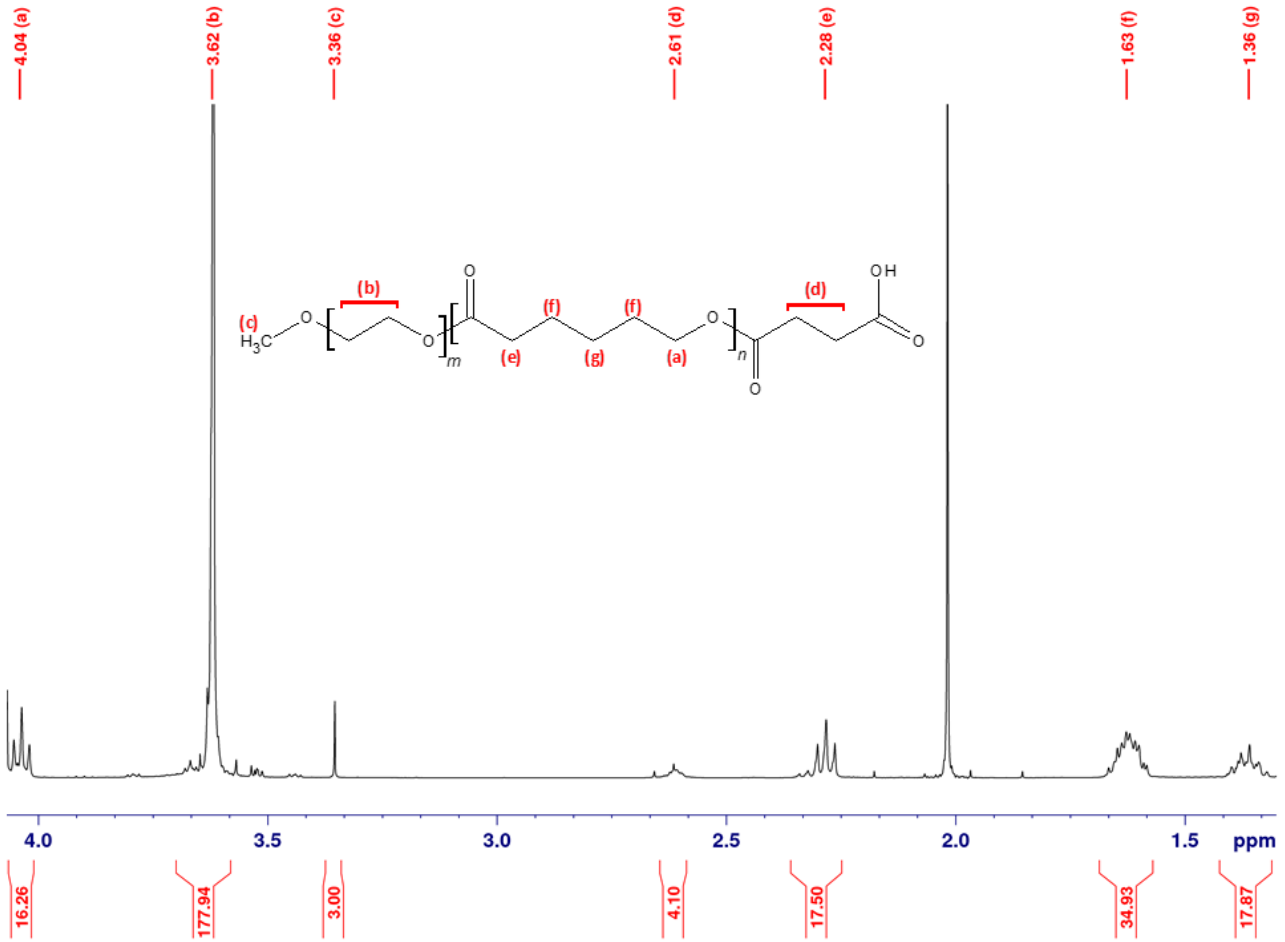

Figure 2.14 ^{1}H NMR spectra of mPEG2000-PCL1000-succ-OH (representing mPEG-PCL-succ-OH) in $CDCl_3$

δ ppm 1.31 - 1.43 (m, -C(=O)-$C_2H_5C\underline{\mathbf{H_2}}C_2H_5O$-, H_g) 1.57 - 1.69 (m, -C(=O)-$CH_2C\underline{\mathbf{H_2}}CH_2C\underline{\mathbf{H_2}}CH_2O$-, H_f) 2.28 (t, -C(=O)-$C\underline{\mathbf{H_2}}CH_2CH_2CH_2CH_2O$-, H_e) 2.59 - 2.65 (m, -OC(=O)-$C\underline{\mathbf{H_2}}C\underline{\mathbf{H_2}}$-C(=O)O-, H_d) 3.36 (s, -OC$\underline{\mathbf{H_3}}$, H_c) 3.58 - 3.70 (m, -OC$\underline{\mathbf{H_2}}C\underline{\mathbf{H_2}}$OC(=O)-, H_b) 4.04 (t, -C(=O)-$CH_2CH_2CH_2CH_2C\underline{\mathbf{H_2}}$O-, H_a)

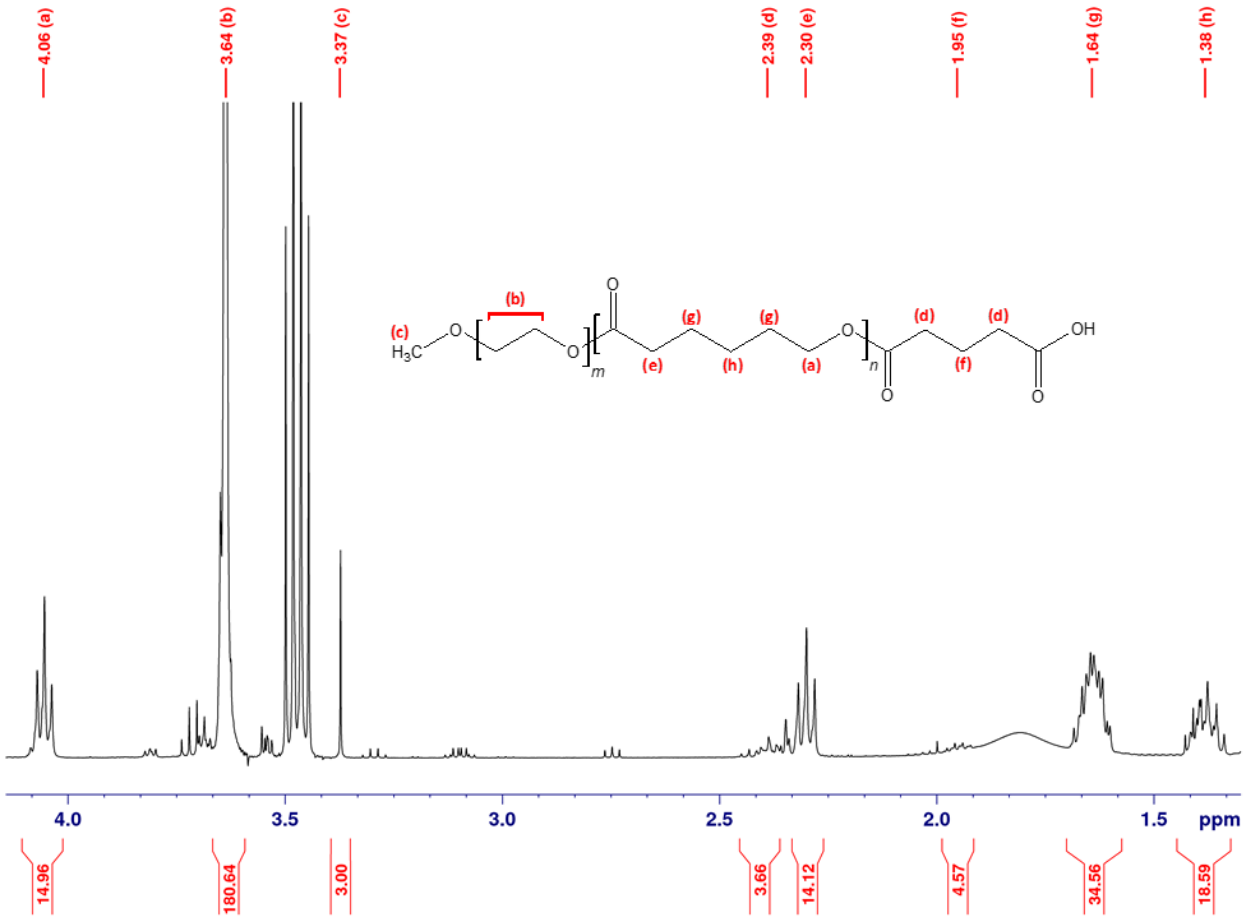

Figure 2.15 ^{1}H NMR spectra of mPEG2000-PCL1000-glu-OH (representing mPEG-PCL-glu-OH) in $CDCl_3$

δ ppm 1.32 - 1.45 (m, -C(=O)-$C_2H_5C\underline{\mathbf{H_2}}C_2H_5O$-, H_h) 1.57 - 1.70 (m, -C(=O)-$CH_2C\underline{\mathbf{H_2}}CH_2C\underline{\mathbf{H_2}}CH_2O$-, H_g) 1.91 - 1.99 (m, -OC(=O)-$CH_2C\underline{\mathbf{H_2}}CH_2$-C(=O)O-, H_f) 2.30 (t, -C(=O)-$C\underline{\mathbf{H_2}}CH_2CH_2CH_2CH_2O$-, H_e) 2.36 - 2.45 (m, -OC(=O)-$C\underline{\mathbf{H_2}}CH_2C\underline{\mathbf{H_2}}$-C(=O)O-, H_d) 3.37 (s, -OC$\underline{\mathbf{H_3}}$, H_c) 3.59 - 3.67 (m, -OC$\underline{\mathbf{H_2}}C\underline{\mathbf{H_2}}$OC(=O)-, H_b) 4.06 (t, -C(=O)-$CH_2CH_2CH_2CH_2C\underline{\mathbf{H_2}}$O-, H_a)

2.5.3 Synthesis of resveratrol-conjugated amphiphilic polymers

RSV was conjugated to the activated amphiphilic copolymers by a simple carbodiimide coupling reaction as seen in Figure 2.5 (Section 2.4.3). The coupling occurred between the carboxylic acid group of the succ or glu group on the activated amphiphilic copolymers and the hydroxyl group in the RSV forming a carboxyl ester bond. Herein, we have included synthesis data for RSV conjugated to selected activated amphiphilic copolymers. Synthesis, DL and stability data of RSV conjugated to glutarated mPEG2000-PCL$_n$ (PCL MW 130Da-11,660Da), succinated and glutarated mPEG2000 are presented in Appendix 7.4 which can also be found in Ng *et al.* (2015).

As RSV had three possible coupling sites, the probability of mono- and di-substituted RSV conjugated with amphiphilic copolymers was high whereas a tri-substituted RSV was unlikely due to steric hindrance (Siddalingappa *et al.* 2015). Figure 2.16 showed the possible substitutions on RSV by mPEG750-PCL1000-glu-OH which also illustrated the steric hindrance aforementioned for a tri-substituted RSV. Hence to minimise multiple substitution, excess RSV was used. However, this undertaking produced final synthesised products which contained unconjugated RSV along with conjugated RSV which could not be separated by simple recrystallisation or dialysis. Separation of unconjugated RSV from conjugated RSV could be possible through preparative chromatography which required specific instrumentation and resources which were not readily available. Purification of polymeric conjugates also required large amounts of synthesised products which entailed large scale synthesis of copolymers and activated copolymers. Due to the number and nature of conjugates synthesised thus far, our resources and time was limited. Nonetheless, we determined the quantity of unconjugated and unconjugated RSV in the final product using HPLC assay method which will be discussed in Chapter 3 before we proceeded onto formulation development of the synthesised products. Chapter 4 will reveal the benefits of having unconjugated RSV along with RSV conjugates during NP formulation where high DL was achieved while maintaining nano-sized particles for delivery of RSV.

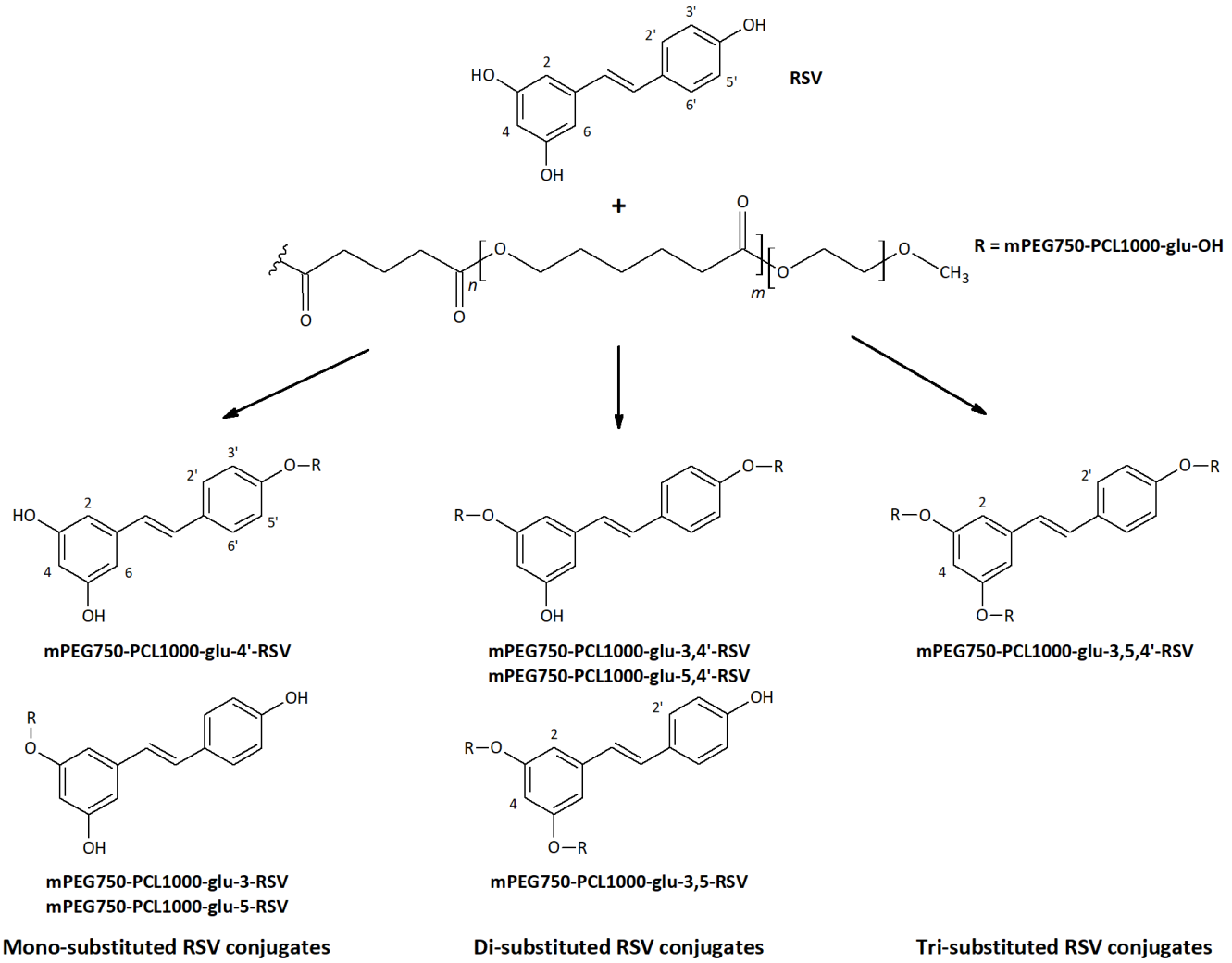

Figure 2.16 Possible substitutions on RSV molecule after esterification with mPEG750-PCL1000-glu-OH

As NMR analyses on mPEG750-PCL1000-glu-RSV showed a good mixture of two mono-substituted conjugates and free RSV (Figure 2.17, Table 2.8), we have used this RSV conjugate to describe NMR analyses of the conjugate as a representative of other synthesised RSV conjugates. NMR spectra of mPEG750-PCL1000-glu-RSV showed corresponding data of mono-substituted RSV using NMR data of RSV conjugated to PEG with a glycine linkage by Wang *et al.* (2016). NMR data in Figure 2.17 also concurred with relevant chemical shifts in synthesized PEG-succinyl-amino acid-RSV conjugates by Zhang *et al.* (2014a). This phenomenon of multiple substitutions of RSV was also observed in Basavaraj's work (Basavaraj 2011, Basavaraj *et al.* 2013, Siddalingappa *et al.* 2015) whereby the conjugates were further confirmed by NMR analysis following acid hydrolysis.

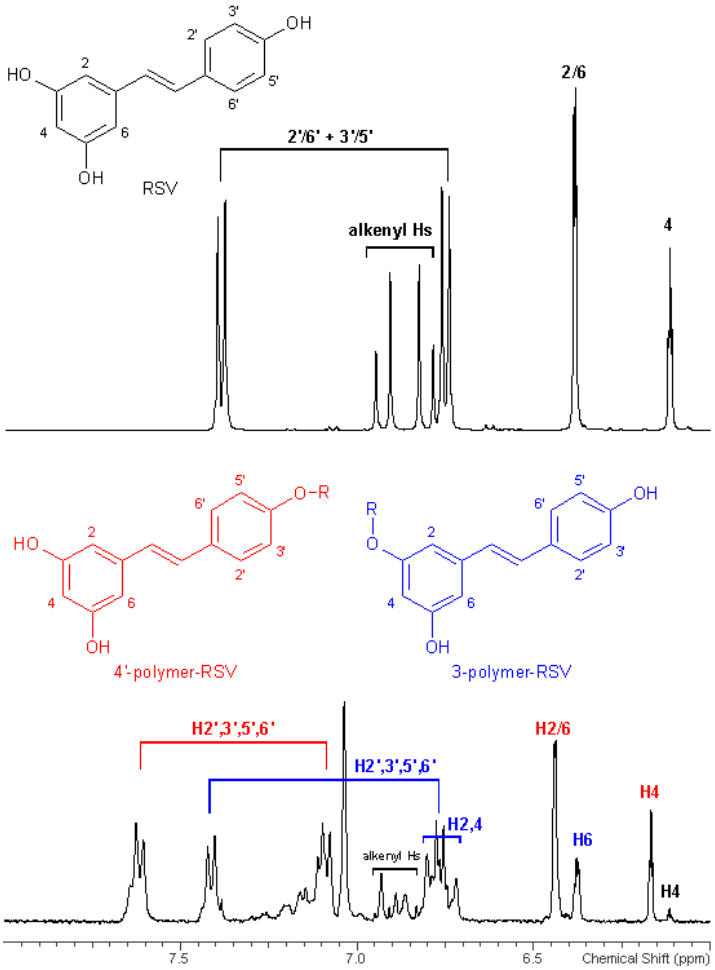

Figure 2.17 ^{1}H NMR spectra of mPEG750-PCL1000-glu-RSV in d_6-DMSO showing mono-substituted (red and blue) and free unconjugated RSV (black)

Following this, synthesized products were analysed and found to be mainly mono-

substituted RSV conjugates with minimal or non-detectable di- and tri-substituted RSV conjugates and portions of free unconjugated RSV (Table 2.8). Molar ratios were estimated based on H4 integral values on mono-substituted 4'- (*ca.* 6.2ppm), H6 integral values on mono-substituted 3- or 5- conjugates (*ca.* 6.4ppm) and H4 integral values of free RSV (*ca.* 6.1ppm) as seen in Figure 2.17. Percentage weights of mono-substituted conjugates and free RSV against total weight of final synthesised products and total RSV equivalent concentrations in 1mg/mL product were also calculated as per Section 2.4.4.2 and tabulated in Table 2.8. For some conjugates, 3- and 5-substituted RSV was not favourable compared to 4'-substituted RSV possibly due to steric hindrance of the phenolic hydroxyl groups (Li *et al.* 2011). As speculated by Zhang *et al.* (2014a) that the type of copolymer used influenced the synthesis outcome of RSV conjugates, we observed a higher weight percentage of mono-substituted RSV conjugates than unconjugated free RSV when mPEG-PCL was used to synthesise polymeric RSV conjugates compared with mPEG-PLA. The more compact structure of PLA compared to the straight chain of PCL could have caused steric or mechanistic hindrance during the synthesis causing less RSV to conjugate to mPEG-PLA as compared to mPEG-PCL, however, this was not investigated as it was not within the scope of this project. Yields were calculated based on the assumption that conjugations were mono-substituted unless specifically found to be 100% di-substituted as seen in the synthesis of mPEG2000-PCL_n-glu-RSV (Appendix 7.4). It was found that yields of synthesized products were inconsistent and varied widely. This could be due to the different physicochemical properties of the copolymers attached to the RSV which could have influenced the washing stages during purification. The oily products were resulted from waxy copolymers (low MW <2,000Da) and freeze-drying did not improve the physical appearance of the products.

As mentioned earlier, all synthesised products contained unconjugated RSV and purification was not possible due to limited resources, however, the presence of unconjugated RSV had an advantage of possibly increasing the DL of RSV of selected RSV conjugates (highlighted yellow in Table 2.8) during NP formulation which will be discussed in Chapter 4. Full NMR spectra of representative RSV conjugates can be found in Appendix 7.5 (Figure 7.6 to Figure 7.11).

Table 2.8 Characteristics of synthesized products from conjugation of RSV to activated amphiphilic copolymers

Synthesized product	Product description	Yield (%)	% *w/w* of components in final product[a]		Total RSV equivalent concentration (mg/mL)[a]
			Mono-substituted RSV	Free RSV	
mPEG750-PLA1000-succ-RSV	White powder	54.9	63.9	36.1	0.431
mPEG750-PLA1000-glu-RSV	Brown oil	ND	54.8	45.2	0.511
mPEG750-PCL1000-succ-RSV	Brown oil	22.3	99.3	0.7	0.128
mPEG750-PCL1000-glu-RSV	Clear oil	45.1	96.1	3.9	0.155
mPEG2000-PLA1000-succ-RSV	White waxy solid	32.5	76.1	23.9	0.291
mPEG2000-PLA1000-glu-RSV	White solid	49.8	97.9	2.1	0.089
mPEG2000-PCL1000-succ-RSV	White solid	45.1	98.1	1.9	0.085
mPEG2000-PCL1000-glu-RSV	White powder	16.8	98.8	1.2	0.078
mPEG2000-PCL$_n$-glu-RSV					
mPEG2000-succ-RSV			See Appendix 7.4		
mPEG2000-glu-RSV					

ND = not determined

Highlighted synthesised products used for NP formation in Chapter 4

[a]% *w/w* of components and total RSV equivalent concentration in 1mg/mL synthesised final products were calculated as per Section 2.4.4.2 (Calculation example in Appendix 7.2)

2.6 Conclusion

Mono-substituted RSV conjugated with different low MW amphiphilic PEGylated copolymers *via* either succinate or glutarate linkers were successfully synthesized. Despite the straight-forward methodology used, there were challenges in synthesising low MW amphiphilic PEGylated copolymer mPEG750-PLA1000. Nonetheless, RSV was conjugated to low MW polymers using excess RSV to ensure mono-substitution, however, this resulted in a mixture of unconjugated and conjugated RSV in the final product, with mPEG-PCL producing more mono-substituted RSV compared to mPEG-PLA. All mixtures were quantified for both unconjugated and conjugated RSV in the final product by HPLC and selected products were used for incorporation into NPs (Chapter 4) which showed high DL while maintaining nano-sized particles. Because of this, it is imperative to factor in the levels of unconjugated and conjugated RSV in final products when data is discussed henceforth. It should also be noted that individual mono-substituted conjugates were not differentiated by their bonding sites (3- or 5- or 4'-) as it did not provide additional information in determining the concentration of RSV within the compound, however, the different substitution sites could affect its NP formation and characteristics.

CHAPTER 3. DEVELOPMENT OF HIGH-PERFORMANCE LIQUID CHROMATOGRAPHY METHOD FOR ANALYSIS OF RESVERATROL AND POLYMERIC RESVERATROL CONJUGATES

3.1 Introduction

To evaluate the effectiveness of the polymeric RSV conjugates, a simple and sensitive analytical method was needed to selectively detect and quantify both free RSV and polymeric RSV conjugate in a single assay. RSV consists of two benzene rings which can be detected within the UV-Vis range, hence HPLC systems with either UV or FL detectors (UVD or FLD) would be ideal for detection and quantitation. Detectors of such will also be able to differentiate between RSV conjugated with copolymers and unconjugated copolymers as the unconjugated copolymers used in this project do not have light absorption ability. Developing a HPLC method which separated free RSV and a polymeric RSV conjugate with good resolution would enable us to quantify both analytes concurrently with good accuracy and precision.

For more than a decade, HPLC methods have been used to detect and quantify free RSV in various matrices. PEGylated RSV conjugates synthesised by Zhang *et al.* (2014) were not detectable but free RSV was quantifiable using an isocratic HPLC method with UV detection to assess the release rate of RSV after lipase catalytic hydrolysis of the conjugates. An isocratic method with a UV detector was developed by Kumar *et al.* (2016) to simultaneously detect and estimate both free RSV and quercetin, another polyphenol, with a mobile phase of MeOH, ACN and phosphoric acid in water. This method used a wavelength at the isosbestic point of RSV and quercetin which referred to a common wavelength that allows sufficient absorptivities of both compounds which had different absorption maxima. In their paper, the method was validated according to the International Conference on Harmonization (ICH) guidelines and assessed for its applicability in a nanoformulation and human plasma (Kumar *et al.* 2016). *Trans*-RSV and *cis*-RSV were detected and quantified using an isocratic HPLC system with MeOH and water adjusted to pH 2.6 with acetic acid at 306nm and 280nm UV detection wavelength, respectively (Sessa *et al.* 2011). RSV

encapsulated into polymeric NPs were orally administered into rats and the PK profiles of RSV in the NPs were assessed by Singh *et al.* (2013) using an isocratic HPLC-UV method with a mobile phase containing MeOH, a phosphate buffer and acetic acid.

Due to the polarity differences between free RSV and RSV conjugated with amphiphilic copolymers, a gradient elution system would be more suitable to separate and detect both free RSV and conjugated RSV. A gradient HPLC system with ACN, water and acetic acid using a UV detector was used to assess the extraction of RSV from a medicinal plant and was further confirmed by HPLC-MS/MS and ^{1}H NMR (Wang *et al.* 2013a). Extraction of RSV and other molecules from fruits were also detected and quantified by HPLC-MS using a 60-minute gradient system consisting of 0.1% formic acid in ACN and 0.1% formic acid in water (Huang *et al.* 2011). Similarly, RSV, RSV dimer isomers and RSV analogues extracted from wine grape stems were measured using HPLC-MS with a gradient system consisting of MeOH and water (Kong *et al.* 2011). Gradient HPLC systems were also used to evaluate RSV nanoformulations. Matos *et al.* (2014) evaluated RSV encapsulated in water-in-oil and water-in-oil-in-water emulsions using a gradient mobile system of ACN and water followed by an extensive column wash sequence. RSV in liposomes were also evaluated using a gradient method consisting of MeOH and water (Catania *et al.* 2013).

An Italian research group which has done extensive work on RSV and the synthesis of its prodrugs developed and validated a HPLC-UV gradient method consisting of ACN, water and formic acid or trifluoroacetic acid to selectively detect and quantify RSV and/or its prodrugs from PK studies on rodents (Biasutto *et al.* 2009b, Biasutto *et al.* 2010, Mattarei *et al.* 2015b). A PEGylated RSV conjugate was synthesised by this same group (Biasutto *et al.* 2009a) and a HPLC-UV method was used to detect and quantify both free RSV and RSV conjugates. The mobile phase system used was a gradient of ACN and water supplemented with 0.1% trifluoroacetic acid and RSV was detected at approximately 19 minutes after subjecting the PEGylated RSV conjugate to enzymatic hydrolysis in an *ex vivo* intestinal environment (Biasutto *et al.* 2009a). Detection of polymeric RSV conjugates using HPLC has been previously developed in-

house and reported using FL detection (Basavaraj *et al.* 2013, Siddalingappa *et al.* 2015) with good selectivity of free RSV and polymeric RSV conjugate eluting at approximately 18 minutes and 21 minutes, respectively. FL intensity was found to be more sensitive than UV detection for both RSV and polymeric RSV conjugate, most likely due to the different extinction coefficients between free RSV and conjugated RSV. In the paper by Siddalingappa *et al.* (2015), a simple protein precipitation was employed using cold ACN to remove proteins from rat plasma samples containing RSV or polymeric RSV conjugates collected from a PK study. This allowed for rapid sample clean-up resulting in shorter sample preparation time (Singh *et al.* 2013).

From the literature aforementioned, *trans*-RSV dissolved in acidic solvent systems using water and MeOH or ACN was quantifiable commonly using UV or FL detectors. Therefore, it was imperative to select a solvent system suitable for the detection wavelengths employed in this project for analysis of synthesised RSV conjugates containing both polymeric RSV conjugates and free RSV described in Chapter 2. We have developed two HPLC methods for the analysis of 1) conjugated RSV NPs which contained both RSV conjugates and free RSV, and 2) encapsulated RSV NPs which contained only free RSV. The latter is a rapid assay. Figure 3.1 summarised the application of the HPLC methods developed in this chapter.

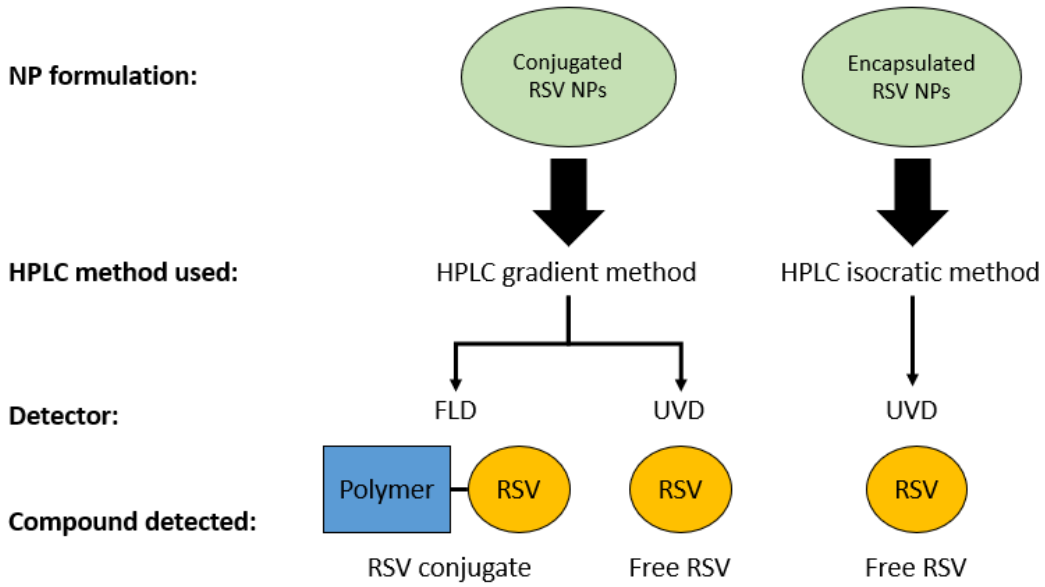

Figure 3.1 Application of developed HPLC methods for characterisation of free RSV and RSV conjugates

3.2 Aim

The aim of this part of the project is to develop two HPLC methods for 1) concurrent detection and analysis of free RSV and RSV conjugates in conjugated RSV NPs, and 2) rapid determination of free RSV in DL and drug release from encapsulated RSV NPs. Both methods were utilised for the analysis of *in vitro* release studies in Chapter 4 and biological assays in Chapter 5 and the choice of method was dependent on the type of NP formulation assessed in the assay. As part of the method development, the effect of solvent systems on the UVD and FLD wavelengths used in the HPLC gradient method was studied and the best solvent system and detection wavelengths were established. Following that, HPLC methods were optimised and validated in clean and biological samples using rat plasma and HLM matrices.

3.3 Materials

Trans-RSV was purchased from DND Pharma-Technology Co., Inc. (Shanghai, China) with 99% purity. Polymeric RSV conjugates were synthesised and characterised in-house (Section 2.5.3). ACN Optima® (HPLC grade), MeOH Optima® (HPLC grade), formic acid (90%, analytical grade) and aqueous orthophosphoric acid (85%, analytical grade) were purchased from Thermo Fisher Scientific (VIC, Australia). Milli-Q ultrapure water (MQ) was obtained using a Millipore Milli-Q Ultrapure Water purification system (Merck Millipore: VIC, Australia) at 18.2MΩcm purity. DMSO (molecular biology grade; cat# D8418-100ML) and PBS was purchased from Sigma Aldrich (NSW, Australia; cat# P3813-10PAK). PBS solution was made as per manufacturer's instructions in MQ with no further modification. Solvents were de-gassed and filtered with 0.2 μm polyvinylidene fluoride (PVDF) filters prior to use. The supernatant of blank mPEG750-PLA1000 NPs (prepared according to Section 4.4.3.1) was collected after centrifugation of blank NPs at 10,000*g* for 5 minutes at 4°C using a 5415R Eppendorf® microcentrifuge (Perth Scientific Pty Ltd: WA, Australia). Outbred rat plasma was obtained from the Animal Resource Centre (ARC) (WA, Australia), stored at -20°C in 1mL aliquots to avoid freeze-thaw cycles and thawed at RT when needed before use as is. The HLM matrix were prepared as per Section 5.4.2

without the co-factor uridine 5'-diphosphoglucuronic acid trisodium salt (UDPGA).

3.4 Methodology

3.4.1 Preparation of samples

3.4.1.1 Stock and standard solutions for HPLC assays

Stock solutions of free RSV and RSV conjugates were prepared weekly, kept in the dark at 4°C and used for both HPLC method validations and analytical assays. Standard solutions, however, were freshly prepared daily from stock solutions and used for each HPLC analytical assay. 10mg/mL stock solution of free RSV was prepared in DMSO and diluted to 100μg/mL with 50:50 *v/v* ACN:MQ as a working stock solution which was then further diluted to 1μg/mL free RSV in 50:50 *v/v* ACN:MQ as a standard solution for each HPLC assay. 1mg/mL RSV conjugate (synthesised in Chapter 2) stock solutions were prepared in DMSO and diluted to 80μg/mL with 50:50 *v/v* ACN:MQ to be used as standard solutions for HPLC assays. The purity of RSV conjugate was considered in the calculation of RSV conjugate concentration based on NMR analyses in Chapter 2 (Appendix 7.2). The approximate stock and standard solution concentrations of the RSV conjugate component in each final synthesised product is found in Table 3.1.

Table 3.1 Approximate stock and standard solution concentrations of RSV conjugates for each HPLC analytical assay

Polymeric RSV conjugate	**Solution concentration (μg/mL)***	
	Stock	**Standard**
mPEG750-PLA1000-succ-RSV	18	1.4
mPEG750-PLA1000-glu-RSV	13	1.0
mPEG2000-PLA1000-succ-RSV	12	1.0
mPEG750-PCL1000-succ-RSV	116	9.3
PEG5000-O-RSV	43	3.4

*Concentration of RSV conjugate component in final synthesised product calculated using ^{1}H NMR data as per Appendix 7.2

3.4.1.2 Analytical samples for HPLC method validation

Samples were prepared by dilution of the stock solutions prepared as per Section 3.4.1.1 in 50:50 *v/v* ACN:MQ and analysed without further modification. For assessing the recovery of free RSV from a polymeric NP matrix, the free RSV working stock solution was diluted with supernatant of blank mPEG750-PLA1000 NPs and analysed using the HPLC isocratic method. For validation of gradient assay method for analysis of biological samples, HPLC samples were prepared by spiking either rat plasma or HLM mix with stock solutions of RSV and RSV conjugates and analytes were extracted by adding ice-cold ACN to precipitate the proteins and centrifuged at 10,000*g* for 5 minutes at 4°C using a 5415R Eppendorf® microcentrifuge. The supernatant was further diluted with MQ to required final concentrations and analysed. Specific sample concentrations for each validation will be described below.

3.4.2 Development of HPLC gradient method for concurrent analysis of RSV conjugates and free RSV

3.4.2.1 Selection of solvent system and detection wavelengths

In order to obtain the most sensitive detection for free RSV and RSV conjugate, the effect of free RSV and three RSV conjugates dissolved in two separate solvent systems, 50:50 *v/v* MeOH:MQ and 50:50 *v/v* ACN:MQ and analysed with two different UV wavelengths and two different FL wavelengths, were assessed according to Table 3.2.

Table 3.2 Assessment of solvent system on detector sensitivity at different wavelengths

Sample	UV detection wavelengths		FL detection wavelengths[a]	
	307nm	320nm	307nm(ex) 400nm(em)	320nm(ex) 400nm(em)
Free RSV	‡ ¥	‡ ¥	‡ ¥	‡ ¥
PEG5000-O-RSV[b]	‡ ¥	‡ ¥	‡ ¥	‡ ¥
mPEG2000-glu-RSV[c]	‡ ¥	‡ ¥	‡ ¥	‡ ¥
mPEG2000-PCL150-glu-RSV[c]	¥	¥	¥	¥

‡ = 50:50 *v/v* MeOH:MQ
¥ = 50:50 *v/v* ACN:MQ
[a]ex = excitation; em = emission
[b]Synthesised by Basavaraj (2011) (see Appendix 7.7 for further information)
[c]Synthesised in Chapter 2

Optimal detection wavelengths were chosen based on sensitivity parameters of limits of detection (LOD) and limits of quantitation (LOQ) obtained. This was carried out by preparing a linear curve using 5μg/mL free RSV and 0.001 to 0.2μg/mL RSV conjugate prepared either in 50:50 *v/v* ACN:MQ or 50:50 *v/v* MeOH:MQ and injected at six different volumes between 1μL to 100μL resulting in a linear range of 5 to 500ng free RSV or 1 to 20ng RSV conjugate. The absorbance was measured at both 307nm and 320nm using a UV detector and at both 307nm and 320nm(ex) with 400nm(em) using a FLD. Using the peak areas and peak heights, LOD and LOQ was calculated as per Section 3.4.4.3 and compared.

3.4.2.2 HPLC conditions

Concurrent HPLC analysis of RSV conjugate and free RSV was developed from a gradient method by Biasutto *et al.* (2009a) and Biasutto *et al.* (2010). The gradient was modified to allow earlier detection of RSV and RSV conjugates. Reverse-phased HPLC was achieved using an Agilent 1200 HPLC system with dual detection (G1312A FLD and G1365B multiwavelength detector MWD), a quartenary pump (G1312A), an autosampler (G1329A), a degasser (G1379B) and a column oven (G1316A) (Agilent Technologies Australia: VIC, Australia). Separation was carried out on an Alltech

Apollo C18 (150 × 4.6 mm, 5μm) (Grace: MD, USA) using a mobile phase gradient of solution A (0.1% *v/v* formic acid in ACN) and solution B (0.1% *v/v* formic acid in MQ) at 1mL/min flow rate and 50μL injection (20μL for PEG5000-O-RSV and free RSV) with a run time of 33 minutes. The autosampler was maintained at 4°C and protected from light while the column temperature was set at 25°C. The gradient was as follows:

Table 3.3 Gradient for concurrent HPLC analysis of RSV conjugates and free RSV

Time (min)	**% solution A (0.1% formic acid in ACN)**
0	35
1	35
30	80
31	100
32	35

Absorbance was monitored at 307nm using a UVD for free RSV and FL was measured at 307nm(ex) and 400nm(em) using a FLD for RSV conjugates. All calculations for RSV conjugates and free RSV were carried out using peak areas.

3.4.3 Development of HPLC isocratic method for analysis of free RSV

Reverse-phased HPLC was achieved using an Agilent 1200 HPLC system with variable wavelength detection (VWD) (G1314B), a binary pump (G1312A), an autosampler (G1329A) and a degasser (G1379B). Isocratic HPLC analysis of free RSV was developed from a method by Frozza *et al.* (2013) with slight modifications. The final HPLC isocratic separation was carried out on an Alltech Apollo C18 (150 × 4.6 mm, 5μm) using a mobile phase 50:50:0.05 *v/v/v* ACN:MQ:85% orthophosphoric acid at 1mL/min flow rate and 20μL injection with a run time of 5 minutes. The autosampler and column temperature were not controlled. Absorbance was monitored at 307nm and all calculations were carried out using peak areas.

3.4.4 Validation of HPLC methods

3.4.4.1 Selectivity

5μg/mL free RSV or 0.6 to 5.8μg/mL RSV conjugates were prepared from their respective stock solutions by dilution with 50:50 *v/v* ACN:MQ and analysed using an Agilent diode-array detector (DAD) (G1315B) in replacement of the VWD and MWD mentioned in Section 3.4.3 and Section 3.4.2.2, respectively, to assess the selectivity of the HPLC methods. A minimum of three spectral scans from 300 to 308nm of the peak of free RSV or RSV conjugate was performed along with a purity factor calculation. Overlapping UV spectral scans and purity factors within the calculated threshold limit indicated that the peak did not have impurities present. Matrix interference from blank mPEG750-PLA1000 NP supernatant, rat plasma and HLM was also investigated in similar fashion.

3.4.4.2 Linearity

RSV conjugates and free RSV were prepared from stock solutions with 50:50 *v/v* ACN:MQ to achieve concentrations ranging from 0.006μg/mL to 24μg/mL and 0.003μg/mL to 10μg/mL, respectively. The calibration curves were obtained by plotting mean peak areas against concentration. Linearity was evaluated by linear regression analysis, which was calculated using the least squares method. Linearity of RSV conjugates and free RSV were also assessed in rat plasma by having compounds spiked in rat plasma to a concentration of 0.01 to 42μg/mL RSV conjugate and 50μg/mL free RSV. Biological samples were processed by adding ice-cold ACN (1:4 dilution) to precipitate the proteins and centrifuged at 10,000*g* for 5 minutes at 4°C using a 5415R Eppendorf® microcentrifuge. The supernatant was further diluted with MQ (1:1 dilution) to a final concentration of 0.001 to 4.2μg/mL RSV conjugate and 5μg/mL free RSV. Samples were injected once and calibration curves were obtained by plotting peak areas against concentration. Linearity was evaluated by linear regression analysis, which was calculated using the least squares method.

3.4.4.3 Limits of detection and quantitation

Limitations of the method to detect and quantify free RSV and RSV conjugate were determined by obtaining noise levels (σ*6) of blank samples of RSV and RSV

conjugates and calculated according to LOD = 3.3σ/S and LOQ = 10σ/S (Arayne *et al.* 2013), where σ is the standard deviation of minimum five noise response levels and S is the slope of the calibration curve obtained in Section 3.4.4.2 using peak heights against concentration. The concentrations calculated were used as the lowest amount of analyte detectable (LOD) and lowest amount of analyte in a sample which can be quantitatively determined (LOQ) with suitable precision and accuracy.

3.4.4.4 Accuracy

Accuracy expresses the closeness of agreement between the true value and the value found, which examines the interference of matrices present in the sample. The recovery of free RSV and RSV conjugate was carried out to determine the interference of NP, rat plasma and HLM matrices and to assess the extraction procedure for biological samples. Ideally, the recovery for non-biological samples should not exceed ±2% of the nominal concentration (Swartz *et al.* 2012a) whereas for biological samples should not exceed ±20% of nominal concentrations except at lower limit of quantification concentrations (US FDA 2013).

As our synthesised RSV conjugates contained both RSV conjugate and free RSV (Table 2.8), an indirect method was employed to calculate the accuracy of RSV conjugates by spiking RSV conjugate solutions with a known amount of free RSV and accuracy was based on the spiked free RSV concentration. Six samples of RSV conjugates in 50:50 *v/v* ACN:MQ were spiked with a known amount of free RSV to a final concentration of 0.6 to 2.2μg/mL RSV conjugate and 5μg/mL free RSV. Similarly, six samples in each rat plasma and HLM mix matrix were spiked to a concentration of 6 to 22μg/mL RSV conjugate and 50μg/mL free RSV. Biological samples were processed by adding ice-cold ACN (1:4 dilution) to precipitate the proteins and centrifuged at 10,000*g* for 5 minutes at 4°C using a 5415R Eppendorf® microcentrifuge. The supernatant was further diluted with MQ (1:1 dilution) to a final concentration of 0.6 to 2.2μg/mL RSV conjugate and 5μg/mL free RSV and analysed once. Percentage recovery and relative standard deviation (RSD) was calculated.

To validate the accuracy of the HPLC isocratic method using free RSV, six samples were prepared with free RSV spiked in the supernatant of blank mPEG750-PLA1000

NPs to a final concentration of 5μg/mL free RSV. Each sample was injected once and derived concentrations from linear curve was compared with actual prepared concentrations. Similarly, rat plasma and HLM mix was spiked to a concentration of 50μg/mL free RSV. Biological assays were added with ice-cold ACN (1:4 dilution) to precipitate proteins and centrifuged 10,000*g* for 5 minutes at 4°C. Supernatant was further diluted with MQ (1:1 dilution) to a final concentration of 5μg/mL free RSV and analysed once. Percentage recovery and RSD was calculated with samples in 50:50 *v/v* ACN:MQ as initial concentrations.

3.4.4.5 Precision

The precision of the method was evaluated by injecting in triplicate three different concentrations of free RSV and RSV conjugate ranging 20-100% of the maximum concentration in the calibration curve concentration range in Section 3.4.4.2. The percentage RSD of free RSV and RSV conjugate at each concentration was calculated and an average was obtained to assess the degree of scatter from the multiple injections of the samples. A method was precise when RSD was below 2% except at lower limit of quantification concentrations (Swartz *et al.* 2012a).

3.4.4.6 Storage stability during HPLC analysis

This section evaluated the storage stability of free RSV and RSV conjugates in different conditions during HPLC analysis (Table 3.4).

Table 3.4 Storage conditions of free RSV and RSV conjugates for evaluation of stability of analytes during HPLC isocratic and gradient analyses, respectively

Storage stability conditions[a]	
Matrix[b]	**Temperature**
HPLC isocratic method	
50:50 *v/v* ACN:MQ	4°C and RT
Supernatant of blank mPEG750-PLA1000 NPs	4°C
PBS	4°C and RT
HPLC gradient method	
50:50 *v/v* ACN:MQ	4°C
PBS	4°C

[a]All samples were kept in dark
[b]50:50 *v/v* ACN:MQ represents a general analyte assay; Supernatant of blank NPs represents general assays containing encapsulated RSV NPs; PBS represents the pH of biological assays post-processing

The stability of compounds was determined by injecting a known concentration of 5μg/mL free RSV and 0.6 to 2.2μg/mL RSV conjugate + 5μg/mL free RSV at time of preparation, 4 hours, 8 hours and 24 hours post-preparation while being stored in conditions outlined in Table 3.4. Stability of compounds during HPLC isocratic analysis was assessed up to 8 hours due to the much shorter run time compared to the HPLC gradient method. Percentage of free RSV and RSV conjugate at each time point was calculated relative to the concentration at time of preparation. The results should be within ±15% of initial concentrations (US FDA 2013) to indicate acceptable stability of solutions during HPLC analysis.

3.5 Results and discussion

3.5.1 Development and validation of HPLC gradient method for concurrent analysis of RSV conjugates and free RSV

In order to quantify both RSV conjugates and free RSV in novel RSV conjugates, its consequent NPs formulations and biological evaluation, a gradient HPLC assay

method was developed and validated.

3.5.1.1 Selection of solvent system and detection wavelengths

Free RSV can be dissolved in MeOH and ACN and can be detected at 307nm or 320nm by UV detection as reviewed in Section 3.1. In order to select a standardised solvent system and detection wavelength for free RSV and RSV conjugates, we have chosen free RSV, PEG5000-O-RSV (an ether conjugate), mPEG2000-glu-RSV (a PEGylated RSV conjugate) and mPEG2000-PCL130-glu-RSV (an amphiphilic copolymer conjugated to RSV) in two types of solvents systems detected by different wavelengths in UV and FL using HPLC gradient method. The most optimum solvent system and detection conditions were assessed by comparing LOD and LOQ values as these values revealed the sensitivity of the system. The lower the value, the more sensitive the system is for that particular solvent system detected at a particular wavelength. We also compared detection by UV and FL to determine which detector would be more sensitive for the detection of free RSV and RSV conjugates. Table 3.5 and Table 3.6 summarised results obtained in the preliminary evaluation of the effect of the sample solvent on LOD and LOQ at different UV detection wavelengths and FL excitation wavelengths, respectively. Free RSV and RSV conjugates were assessed within the linearity range of 5 to 500ng and linearity correlation coefficient (R^2), LOD and LOQ were quoted. The lower LOD and LOQ values between both UV detection wavelengths of 307nm and 320nm for each compound were highlighted in yellow (Table 3.5) and lower LOD and LOQ values between two sample solvents were in bold font. All compounds except PEG5000-O-RSV were best detected at 307nm where RSV in 50:50 *v/v* MeOH:MQ had better sensitivity than RSV conjugates. This showed the different absorption properties of each compound. Similarly, Table 3.6 showed that the best detection wavelengths in FL for all RSV conjugates except mPEG2000-PCL150-glu-RSV was 307nm(ex) and 400nm(em) in 50:50 *v/v* ACN:MQ whereas free RSV was best detected at 307nm(ex) and 400nm(em) in 50:50 *v/v* MeOH:MQ.

Table 3.5 LOD and LOQ calculations of compounds in 50:50 *v/v* MeOH:MQ and 50:50 *v/v* ACN:MQ at 307nm and 320nm UV detection wavelengths using HPLC gradient method

Compound	Dissolution solvent	UV detection wavelength 307nm			UV detection wavelength 320nm		
		R^2	LOD (ng/mL)	LOQ (ng/mL)	R^2	LOD (ng/mL)	LOQ (ng/mL)
RSV	50:50 *v/v* MeOH:MQ	0.97	**1.35**	**4.49**	0.97	1.41	4.69
PEG5000-O-RSV		1.00	6.89	22.97	1.00	6.12	20.39
mPEG2000-glu-RSV		0.97	16.64	55.45	0.96	18.98	63.26
RSV	50:50 *v/v* ACN:MQ	0.97	5.12	17.07	0.97	6.82	22.72
PEG5000-O-RSV		1.00	0.44	1.48	1.00	**0.39**	**1.29**
mPEG2000-glu-RSV		1.00	**1.33**	**4.42**	1.00	1.46	4.87
mPEG2000-PCL150-glu-RSV		1.00	9.34	31.15	1.00	11.56	38.53

Table 3.6 LOD and LOQ calculations of compounds in 50:50 *v/v* MeOH:MQ and 50:50 *v/v* ACN:MQ at 307nm or 320nm(ex) and 400nm(em) FL detection wavelengths using HPLC gradient method

Compound	Dissolution solvent	Fluorescence detection wavelengths 307nm(ex), 400nm(em)			Fluorescence detection wavelengths 320nm(ex), 400nm(em)		
		R^2	LOD (ng/mL)	LOQ (ng/mL)	R^2	LOD (ng/mL)	LOQ (ng/mL)
RSV	50:50 *v/v* MeOH:MQ	0.97	**1.77**	**5.89**	0.97	2.68	8.93
PEG5000-O-RSV		1.00	4.82	16.07	1.00	6.12	20.40
mPEG2000-glu-RSV		1.00	0.77	2.56	1.00	3.31	11.05
RSV	50:50 *v/v* ACN:MQ	0.98	14.52	48.40	0.98	15.14	50.46
PEG5000-O-RSV		1.00	**0.30**	**1.00**	1.00	0.55	1.82
mPEG2000-glu-RSV		1.00	**0.14**	**0.47**	1.00	0.33	1.11
mPEG2000-PCL150-glu-RSV		1.00	7.71	25.71	1.00	6.76	22.53

Therefore, the best solvent systems and detection wavelengths in UV and FL for each compound were as follows (Table 3.7).

Table 3.7 Optimum solvent system and detection wavelengths for free RSV and RSV conjugates based on LOD and LOQ values

Sample	UV detection wavelengths		FL detection wavelengths	
	307nm	320nm	307nm(ex) 400nm(em)	320nm(ex) 400nm(em)
Free RSV	‡		‡	
PEG5000-O-RSV		¥	¥	
mPEG2000-glu-RSV	¥		¥	
mPEG2000-PCL150-glu-RSV	¥			¥

‡ = 50:50 *v/v* MeOH:MQ
¥ = 50:50 *v/v* ACN:MQ

Comparing Table 3.5 and Table 3.6, FL detection produced lower LOD and LOQ values for RSV conjugates but not free RSV. The UV detection was found to be more sensitive for free RSV. In order to standardise sample preparation methods for HPLC analysis in this project, the solvent system of 50:50 *v/v* ACN:MQ was chosen. Therefore, concurrent analysis of free RSV and RSV conjugates with the HPLC gradient method used a dual detector system of UV at 307nm for free RSV and FL at 307nm(ex) and 400nm(em) for RSV conjugates. This allowed us to concurrently detect both free RSV and RSV conjugates with high sensitivity at sub-microgram per millilitre range. Following this, we have validated the HPLC gradient method with free RSV and selected RSV conjugates intended for further studies and the HPLC isocratic method with free RSV. Validation results are presented and discussed in the following sections.

3.5.1.2 Selectivity

Peak purity analysis of RSV and RSV conjugates in 50:50 *v/v* ACN:MQ was performed using an Agilent ChemStation® software (Agilent Technologies Australia: VIC, Australia) with a DAD. The peak purity results of free RSV (Figure 3.2) demonstrated specificity of HPLC method employed.

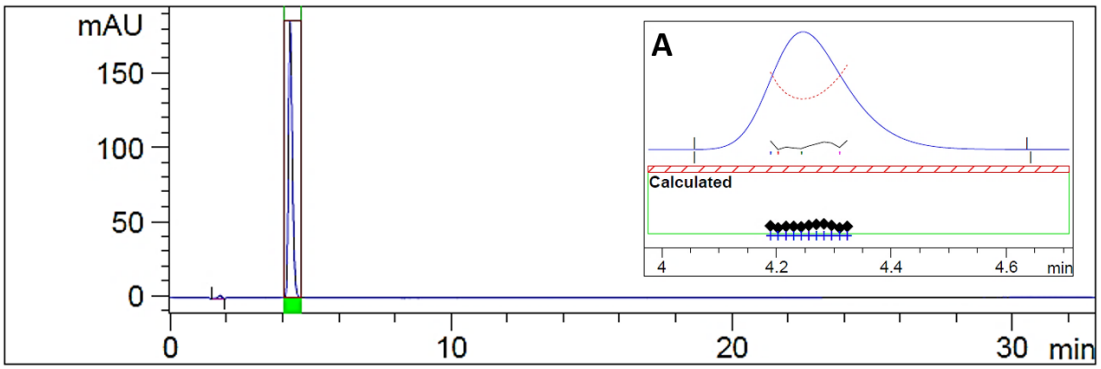

Figure 3.2 Typical HPLC chromatogram of free RSV analysed by DAD using the HPLC gradient method. (A) Purity calculation of free RSV peak

Figure 3.2 showed a sharp and resolved peak of free RSV at t_R of 4.25 minutes. Figure 3.2A showed that the purity factor of free RSV analysed by HPLC gradient method was within the calculated threshold limit. Figure 3.3 showed a partially resolved peak of mPEG2000-PLA1000-succ-RSV at t_R of 13.8 minutes and free RSV at approximately 4.5 minutes.

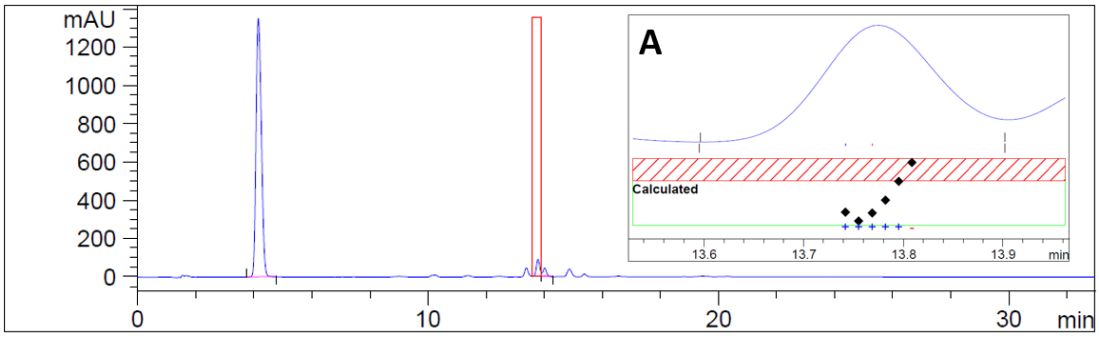

Figure 3.3 Typical HPLC chromatogram of mPEG2000-PLA1000-succ-RSV (76.1% *w/w* RSV conjugate of final product) analysed by DAD using the HPLC gradient method. (A) Purity calculation of mPEG2000-PLA1000-succ-RSV peak

It should be noted that DAD is different from FLD so the extinction coefficient of free RSV and RSV conjugate would differ significantly due to the different structural properties of both compounds. As such, the peak height in the mPEG2000-PLA1000-succ-RSV peak height and area cannot be a direct reflection of the purity and concentration of the conjugate. Therefore, the concentration of RSV conjugates was calculated based on purity levels from NMR spectra described in Chapter 2. Nonetheless, Figure 3.3A showed that the purity factor of mPEG2000-PLA1000-succ-RSV analysed by HPLC gradient method was within the calculated threshold limit. RSV

conjugates PEG5000-O-RSV and mPEG750-PLA1000-succ-RSV did not produce enough data for a peak purity analysis.

3.5.1.3 Linearity and limitations of HPLC method

Calibration curves for free RSV, PEG5000-O-RSV and synthesized RSV conjugates in 50:50 *v/v* ACN:MQ were obtained by plotting mean peak areas (mAU*s or LU*s) against concentration (ng/mL or μg/mL). Concentrations of RSV conjugates were calculated based on its purity obtained by NMR analyses in Chapter 2. Linearity parameters of compounds were summarised in Table 3.8. Free RSV and RSV conjugates have a good linear response over corresponding linear ranges with excellent R^2 (>0.9590). LOD and LOQ values of RSV conjugates in 50:50 *v/v* ACN:MQ obtained were found to be of nanogram per millilitre range and lower to what was ascertained by the HPLC gradient method in Basavaraj *et al.* (2013) where LOD and LOQ values of a PEGylated RSV was 0.1μg/mL and 0.3μg/mL, respectively.

Table 3.8 Linearity parameters of RSV conjugates and free RSV in 50:50 *v/v* ACN:MQ using HPLC gradient method

Compound	Linearity parameters				Limitations	
	Retention time, t_R (minutes)[a]	Linearity range	Linear regression equation	Correlation coefficient, R^2	LOD (ng/mL)	LOQ (ng/mL)
Free RSV[b]	4.4±0.2	2.5ng/mL to 8.2μg/mL	y = 477.1x – 0.1777	1.0000	0.4	1.1
mPEG750-PLA1000-succ-RSV[c]	13.6±0.3	0.08μg/mL to 3.3μg/mL	y = 6.3528x + 0.6425	0.9935	4.5	13.7
mPEG750-PLA1000-glu-RSV[c]	15.6±0.2	6.0ng/mL to 2.5μg/mL	y = 154.0537x + 0.1909	0.9999	0.5	1.6
mPEG2000-PLA1000-succ-RSV[c]	13.9±0.2	6.0ng/mL to 1.2μg/mL	y = 111.0306x + 0.8178	0.9999	1.1	3.3
mPEG750-PCL1000-succ-RSV[c]	15.3±0.1	0.06μg/mL to 24.1μg/mL	y = 18.8777x + 6.5683	0.9598	8.3	25.1
PEG5000-O-RSV[c]	10.2±0.5	0.05μg/mL to 4.7μg/mL	y = 33.6050x – 0.5539	0.9984	9.1	27.6

[a]Data presented as mean (*n*=3) ± standard deviation (SD)
[b]detection by UV at 307nm
[c]detection by FL at 307nm(ex) and 400nm(em)

Basavaraj (2011) validated a HPLC-FLD gradient method of MeOH and pH7 aqueous buffer made with triethyl amine and formic acid using mPEG750-PLA1000-succ-RSV and PEG2000-O-RSV and obtained much higher LOD and LOQ values than our values in low microgram per millilitre range (Table 3.9).

Table 3.9 Published LOD and LOQ values of RSV conjugates (Basavaraj 2011)

Compound	LOD (μg/mL)	LOQ (μg/mL)
mPEG750-PLA1000-succ-RSV	2.2	3.2
PEG2000-O-RSV	0.7	5.0

mPEG750-PLA1000-succ-RSV used by Basavaraj (2011) was the same compound re-synthesised in Section 2.5.3, however, consisted of 100% RSV conjugate with no unconjugated RSV unlike our mPEG750-PLA1000-succ-RSV which contained 63.9% *w/w* RSV conjugate in the final product. PEG2000-O-RSV differed from the PEG5000-O-RSV used for this validation by its MW but can be used as a representative of the type of compound validated for comparison. Therefore by using our developed HPLC gradient method, the method was found to be more sensitive for PEGylated RSV than the gradient method developed by Basavaraj (2011) and simpler in preparation. Free RSV was validated for linearity and LOD and LOQ values in 50:50 *v/v* ACN:MQ was 0.4ng/mL and 1.1ng/mL, respectively. These values were at least three times lower than best published values from gradient methods developed by Basavaraj *et al.* (2013) and Nour *et al.* (2012). Hence, the HPLC gradient method developed in this chapter also showed better sensitivity than published methods for free RSV.

3.5.1.4 Accuracy

The recovery of free RSV and an RSV conjugate from a mixture of both compounds in 50:50 *v/v* ACN:MQ was assessed using the HPLC gradient method (Table 3.10).

Table 3.10 Recovery of RSV conjugates and 5μg/mL free RSV from a physical mixture of both compounds in 50:50 *v/v* ACN:MQ using HPLC gradient method

Mixture	RSV conjugate concentration (μg/mL)	Recovery (%)	
		Free RSV	RSV conjugate
mPEG750-PLA1000-succ-RSV	0.9	89.4±18.0	89.9±14.8
mPEG2000-PLA1000-succ-RSV	0.6	113.2±32.8	107.8±30.0
PEG5000-O-RSV	2.2	105.3±10.1	91.7±4.5

Data presented as mean (*n*=6) ± SD

Recovery of free RSV and RSV conjugate from a physical mixture of both compounds in 50:50 *v/v* ACN:MQ was found to be outside of acceptable limits of 100±2% for the analysis of pure compounds (Swartz *et al.* 2012a). The recovery range of three RSV conjugates analysed in Table 3.10 was within 100±10% which could be explained by the instability of the ester linkers due to hydrolysis in ester RSV conjugates when exposed to water affecting the amount of free RSV and RSV conjugate components in the mixture. The ether RSV conjugate PEG5000-O-RSV being more stable produced a smaller recovery range when compared to the ester conjugates.

3.5.1.5 Precision

Table 3.11 revealed the precision study results of RSV conjugates and free RSV using HPLC gradient method. All compounds were prepared in three concentrations spanning 20% to 100% of the calibration curve concentration range in Table 3.8 except for mPEG750-PLA1000-succ-RSV where the lower concentration was the minimum concentration in its calibration curve. Each concentration was analysed in triplicate. Average RSD values of all compounds were below 2.30% which was close to the acceptable limit of ≤2% for the method to be precise (Swartz *et al.* 2012a). mPEG750-PLA1000-succ-RSV and PEG5000-O-RSV produced a higher average RSD of more than 2% due to the lower concentrations analysed which were much closer to their respective LOD values compared to the other compounds analysed.

Table 3.11 Precision study on RSV conjugates and free RSV using HPLC gradient method

Compound	Concentrations analysed (μg/mL)	Average RSD (%)
Free RSV	2.1, 4.1 and 8.2	0.02
mPEG750-PLA1000-succ-RSV	0.08, 0.8 and 3.3	2.26
mPEG750-PLA1000-glu-RSV	0.6, 1.3 and 2.5	1.03
mPEG2000-PLA1000-succ-RSV	0.2, 0.6 and 1.2	0.72
mPEG750-PCL1000-succ-RSV	6.0, 12.1 and 24.1	0.46
PEG5000-O-RSV	0.9, 2.3 and 4.6	2.09

3.5.1.6 Storage stability during HPLC analysis

Free RSV and selected RSV conjugates were assessed in various matrices to ensure that short-term stability during HPLC analysis was within acceptable limits. Analytes were prepared in matrices outlined in Table 3.4 and analysed with initial potency (100%) at 0 hours or time of preparation. Aliquots of the prepared analytes were then kept in the dark at 4°C which represented the environment of the HPLC autosampler and analysed at 4 hours, 8 hours and 24 hours post-preparation. 50:50 *v/v* ACN:MQ was chosen because stock solutions and processed samples were dissolved in 50:50 *v/v* ACN:MQ for HPLC analyses. On the other hand, PBS represented pH storage conditions in biological *in vitro* assays post-processing which was approximately pH7.4. Table 3.12 summarised the stability of all compounds using HPLC gradient method.

Table 3.12 Stability of free RSV and RSV conjugates at 4°C during HPLC gradient analysis

Compound	Concentration (μg/mL)	Potency post-preparation (%)*		
		4h	8h	24h
Compounds in 50:50 *v/v* ACN:MQ				
Free RSV	5.0	80.2±3.3	86.5±1.3	85.0±2.7
mPEG750-PLA1000-succ-RSV	0.9	100.2±1.6	100.8±3.5	101.3±2.5
mPEG2000-PLA1000-succ-RSV	0.6	96.8±1.3	94.6±0.8	95.9±9.4
PEG5000-O-RSV	2.2	89.8±1.1	92.4±2.4	94.8±2.6
Compounds in PBS				
Free RSV	5.0	99.6±0.1	99.7±0.1	95.1±0.1
mPEG750-PLA1000-succ-RSV	0.9	103.7±5.3	95.3±11.3	83.6±4.8
mPEG2000-PLA1000-succ-RSV	0.6	96.5±1.6	102.4±1.4	84.5±0.0
PEG5000-O-RSV	2.2	105.1±3.8	101.8±2.9	105.9±5.7

Data presented as mean (*n*=2) ± SD
*Initial potency = 100%

All RSV conjugate solutions in 50:50 *v/v* ACN:MQ was stable at 4°C and within acceptable limits of 100±15% for up to 24 hours. This indicated that the 33-minute HPLC gradient method did not affect the potency of free RSV and RSV conjugates if analysis was carried out within 8 hours of preparation. This also implied that the stock solutions in 50:50 *v/v* ACN:MQ did not degrade and were acceptable to be re-analysed for up to 24 hours. Free RSV solutions in 50:50 *v/v* ACN:MQ at 4°C were within acceptable limits of 100±15% except free RSV analysed after 4 hours post-preparation. Nonetheless, data at 8 hours and 24 hours showed acceptable limits. Free RSV and RSV conjugates in PBS were found to be within acceptable limits of 100±15% except for mPEG2000-PLA1000-succ-RSV and mPEG750-PLA100-succ-RSV after 24 hours. As the ester link succinate was sensitive to degradation at pH7.4 (Li *et al.* 2011), this was expected. It was possible that the RSV conjugates degraded to free RSV as the free RSV peak area was observed to increase slightly after 24 hours. Therefore, analyses of these two RSV conjugates needed to be carried out within 8 hours of processing biological assays. Consequently, in order to establish a standard

method, all samples for HPLC gradient analyses were analysed within 8 hours of preparation or processing to avoid decrease in potency of free RSV and RSV conjugates which would affect data henceforth.

3.5.1.7 Bioanalytical validation

This section discussed the validation of free RSV, PEG5000-O-RSV and mPEG2000-PLA1000-succ-RSV in biological matrices. Remaining RSV ester conjugates were not used to validate due to their instability in rat plasma and HLM mix as demonstrated by results in Table 3.15 and Table 3.16 using mPEG2000-PLA1000-succ-RSV where only 76% and 21% of the RSV conjugate was recovered, respectively. Figure 3.4 portrayed a typical HPLC gradient chromatograms of rat plasma spiked with RSV conjugates mPEG2000-PLA1000-succ-RSV and PEG5000-O-RSV. mPEG2000-PLA1000-succ-RSV and PEG5000-O-RSV showed a t_R of 14.1 and 9.5 minutes, respectively, corresponding to what was found in Section 3.5.1.3. There was insufficient data to produce a peak purity report on both RSV conjugates in rat plasma.

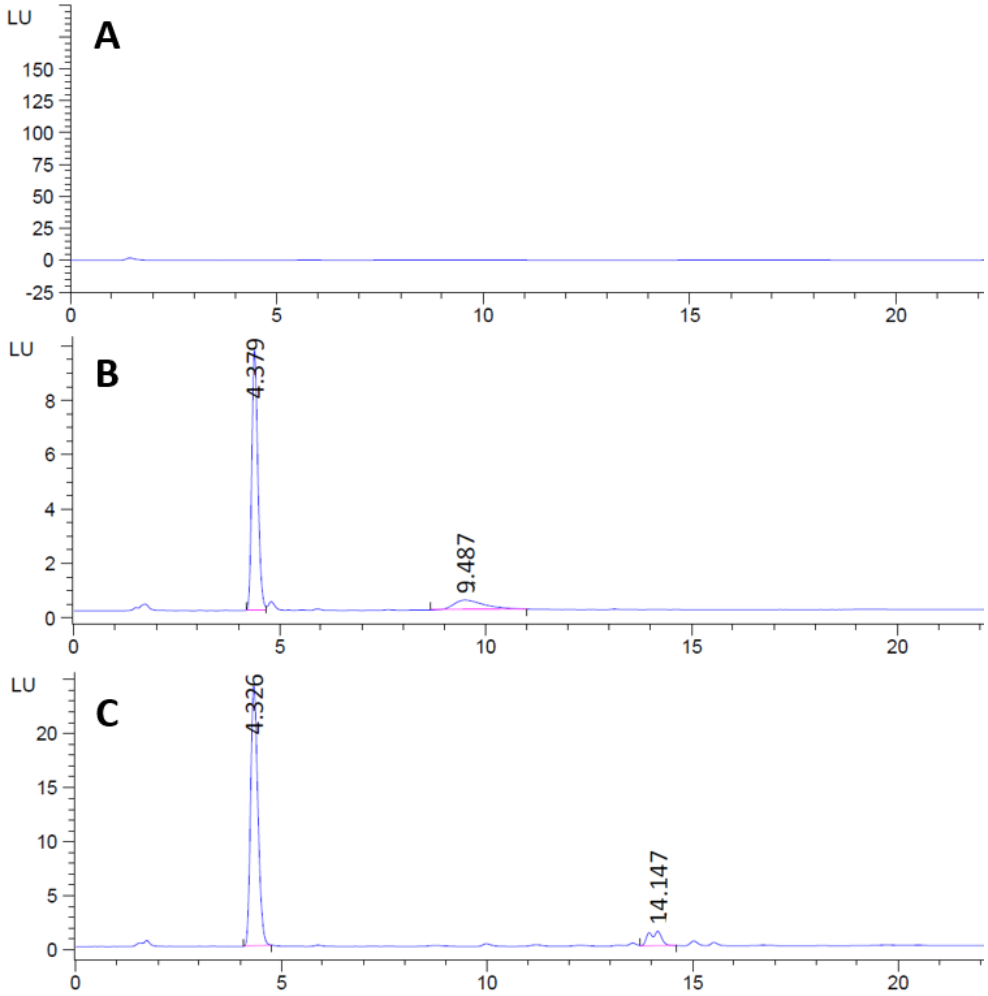

Figure 3.4 Typical gradient HPLC chromatogram of (A) non-spiked rat plasma (B) spiked rat plasma with 2.2μg/mL PEG5000-O-RSV (t_R 9.5min) (C) spiked rat plasma with 0.6μg/mL mPEG2000-PLA1000-succ-RSV (t_R 14.1min). Free RSV detected at t_R 4.3min

Figure 3.5, on the other hand, portrayed a typical HPLC gradient chromatogram of non-spiked and spiked HLM mix with PEG5000-O-RSV and mPEG2000-PLA1000-succ-RSV. All chromatograms showed excellent selectivity with no matrix interference for free RSV and RSV conjugates in HLM. A peak purity analysis on the RSV conjugates peaks was not performed due to insufficient data.

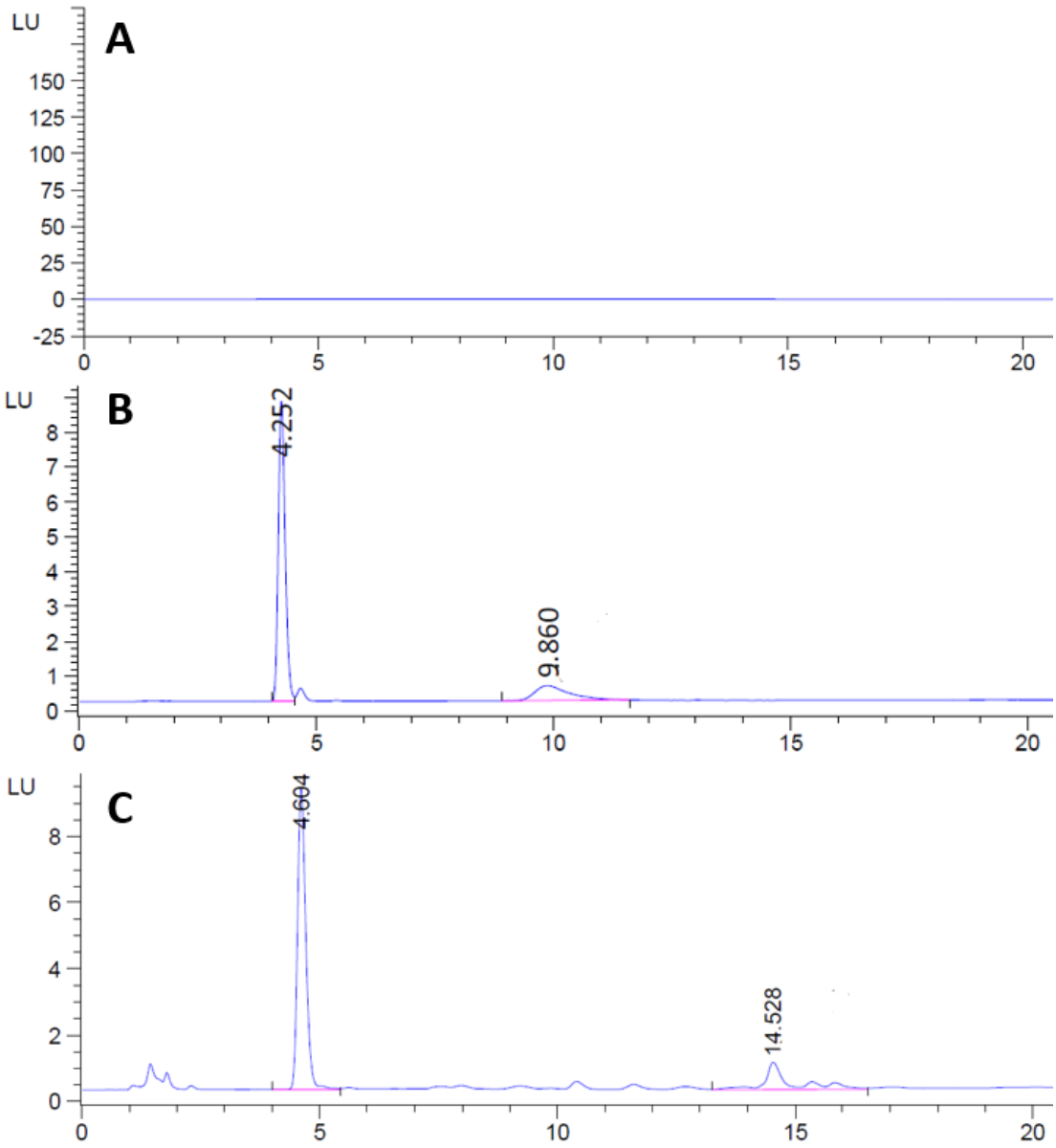

Figure 3.5 Typical gradient HPLC chromatogram of (A) non-spiked HLM mix (B) spiked HLM mix with 2.2μg/mL PEG5000-O-RSV (t_R 9.9min) (C) spiked HLM mix with 0.6μg/mL mPEG2000-PLA1000-succ-RSV (t_R 14.5min). Free RSV detected at t_R 4.3-4.6min

Similarly, rat plasma and HLM mix was spiked with free RSV and analysed using the HPLC gradient method and the t_R corresponded to what was found in Section 3.5.1.3,

that is, 4.3 minutes (Figure 3.6). The peak purity report (Appendix 7.8.1) showed no interference of free RSV by the HLM mix allowing for selective analysis of free RSV in HLM using the HPLC gradient method. Purity of free RSV peak in rat plasma was not assessable due to insufficient data.

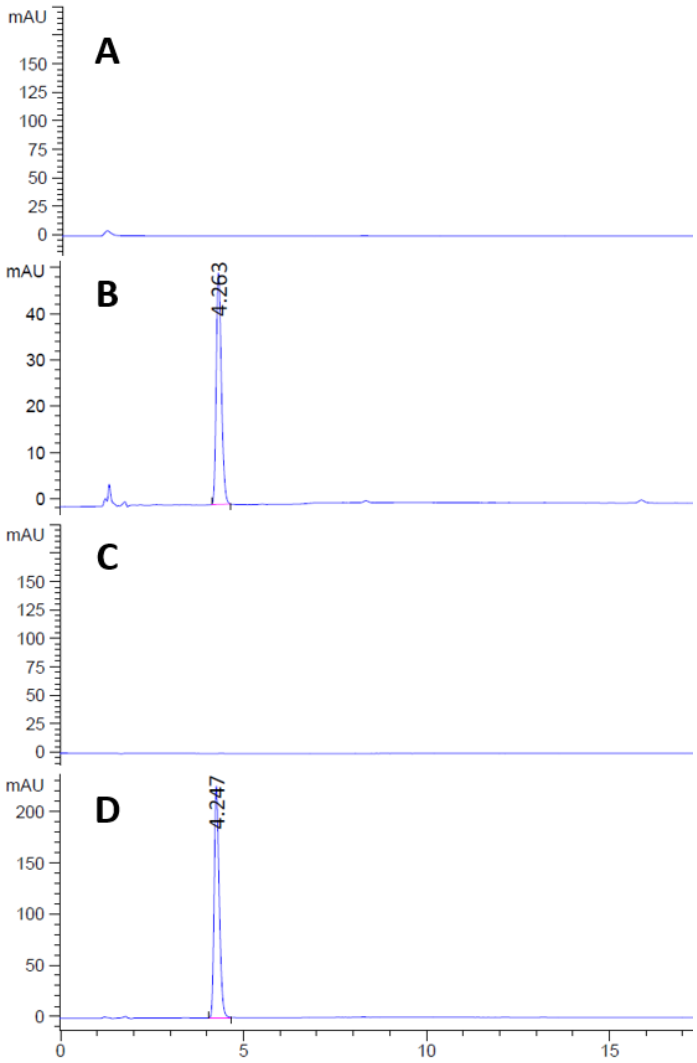

Figure 3.6 Typical gradient HPLC chromatogram of (A) non-spiked rat plasma (B) spiked rat plasma with 5μg/mL RSV (t_R 4.3min) (C) non-spiked HLM mix (D) spiked HLM mix with 5μg/mL RSV (t_R 4.2min)

Linearity and precision of the gradient method for biological assays was summarised in Table 3.13 and Table 3.14, respectively. In general, free RSV and RSV conjugates in rat plasma showed excellent R^2 (>0.9800) over linear ranges quoted. LOD and LOQ values in rat plasma more than tripled the LOD and LOQ values found in 50:50 *v/v* ACN:MQ except for PEG5000-O-RSV where LOD and LOQ values were slightly improved than those dissolved in 50:50 *v/v* ACN:MQ (Table 3.8).

Table 3.13 HPLC linearity parameters of biological assays of free RSV, mPEG2000-PLA1000-succ-RSV and PEG5000-O-RSV conjugates in rat plasma using HPLC gradient method

Linearity parameters	Free RSV	mPEG2000-PLA1000-succ-RSV	PEG5000-O-RSV
Linearity range	10.0ng/mL to 1.0μg/mL	1.2ng/mL to 1.2μg/mL	0.04μg/mL to 4.25μg/mL
Linear regression equation	y = 3.1327x + 0.1520	y = 115.6534x – 1.1830	y = 20.2369x – 0.5443
Correlation coefficient, R^2	0.9989	0.9828	0.9987
LOD (ng/mL)	6.8	3.6	7.2
LOQ (ng/mL)	20.6	10.8	11.8

Most notable increase in LOD and LOQ values was free RSV which increased more than ten-fold compared to its counterpart in 50:50 *v/v* ACN:MQ possibly due to the noisy baseline and interference of species in the rat plasma (Sagirli *et al.* 2004). A better extraction method could improve the recovery; however, this was not further pursued due to time and resource limitation. The change of gradient in the HPLC solvent system could also contribute to the higher noise levels, and hence, higher LOD and LOQ values (Schellinger *et al.* 2006). Therefore, the higher LOD and LOQ values for mPEG2000-PLA1000-succ-RSV was expected. Although this should be the case for PEG5000-O-RSV, the LOD and LOQ values of this ether conjugate was much lower than its counterpart in 50:50 *v/v* ACN:MQ. It was possible that due to its earlier elution compared to the ester conjugates, the effect of gradient change in the method was not as notable. Nonetheless, all LOD and LOQ values at nanogram per millilitre range for samples extracted from rat plasma was sufficiently sensitive for this project. Using the same concentrations for precision validation in Section 3.5.1.5, precision of free RSV and selected RSV conjugates in rat plasma using HPLC gradient method was assessed and reported in Table 3.14.

Table 3.14 Precision study on selected RSV conjugates and free RSV in rat plasma using HPLC gradient method

Compound	**Concentrations analysed (μg/mL)**	**Average RSD (%)**
Free RSV	2.1, 4.1 and 8.2	4.96
mPEG2000-PLA1000-succ-RSV	0.2, 0.6 and 1.2	2.00
PEG5000-O-RSV	0.9, 2.3 and 4.6	0.51

RSD values compared to samples in 50:50 *v/v* ACN:MQ were slightly higher except for PEG5000-O-RSV. This could be due to the noisy baseline from the plasma despite protein extraction; however, RSD values were still below the acceptable limit of 15% (US FDA 2013) and hence, the HPLC gradient method employed were also precise for biological assays. The recovery of free RSV and selected RSV conjugates extracted from rat plasma and their RSD values was summarised in Table 3.15. As expected, the recovery of free RSV from rat plasma using the gradient method was not satisfactory due to its fast degradation by plasma esterases prior to extraction, being more than

100±20% of the acceptable limit for biological samples (US FDA 2013). The RSV ester conjugate mPEG2000-PLA1000-succ-RSV did not recover well from rat plasma and this was possibly due to its tendency to degrade very fast in rat plasma. The stability of ester conjugates NPs in rat plasma was assessed and discussed in Chapter 5. The RSV ether conjugate PEG5000-O-RSV, however, recovered excellently from rat plasma with 102% on average. This showed that the HPLC gradient method was accurate to analyse PEG5000-O-RSV in rat plasma.

Table 3.15 Recovery of free RSV and RSV conjugate from rat plasma using HPLC gradient method

Compound	Concentration (*μg*/mL)	Recovery (%)	RSD (%)
Free RSV	5	71.8±1.4	2.00
mPEG2000-PLA1000-succ-RSV	0.6	75.7±6.2	0.08
PEG5000-O-RSV	2.2	102.2±0.8	0.01

Data presented as mean (*n*=6) ± SD

Table 3.16 exhibits the recovery of free RSV and PEG5000-O-RSV from HLM mix and was found to be excellent and within acceptable limits of 100±20% using the HPLC gradient method (US FDA 2013). However, the recovery of mPEG2000-PLA1000-succ-RSV from HLM mix was not satisfactory due to the lack of stability of the ester bond within the RSV conjugate especially when exposed to the HLM matrix although the selectivity for the ester conjugate was good as per Figure 3.5. The stability of this RSV conjugate as NPs in HLM was investigated and discussed in Chapter 5.

Table 3.16 Recovery of free RSV and RSV conjugate from HLM mix using HPLC gradient method

Compound	Concentration (*μg*/mL)	Recovery (%)	RSD (%)
Free RSV	5	99.6±4.4	4.39
mPEG2000-PLA1000-succ-RSV	0.6	21.4±11.0	0.51
PEG5000-O-RSV	2.2	110.0±0.6	0.01

Data presented as mean (*n*=6 except mPEG2000-PLA1000-succ-RSV where *n*=3) ± SD

In conclusion, a novel HPLC gradient method has been developed for the concurrent analysis of free RSV and RSV conjugates with dual detection in assays containing conjugated RSV NPs. The method was validated in non-biological and biological assays and found to be suitable for the purpose of this project.

3.5.2 Development and validation of HPLC isocratic method for analysis of free RSV

We have developed a rapid and sensitive isocratic method for the analysis of assays containing encapsulated RSV NPs (preparation described in Chapter 4) where RSV was not conjugated to any moiety and remained as a free compound. Although the gradient method described earlier could be used for this purpose, a more rapid method was useful and more economical especially for assays containing encapsulated RSV NPs. The isocratic method was based on Frozza *et al.* (2013) with slight modifications. The ratio between ACN and water was adjusted to 50:50 *v/v* as opposed to 40:60 *v/v* and a slower flow rate of 1.0ml/min was employed. Detection was made using a UV detector at 307nm as optimised in Section 3.5.1.1 and free RSV was eluted at approximately 2.4 minutes (Figure 3.7).

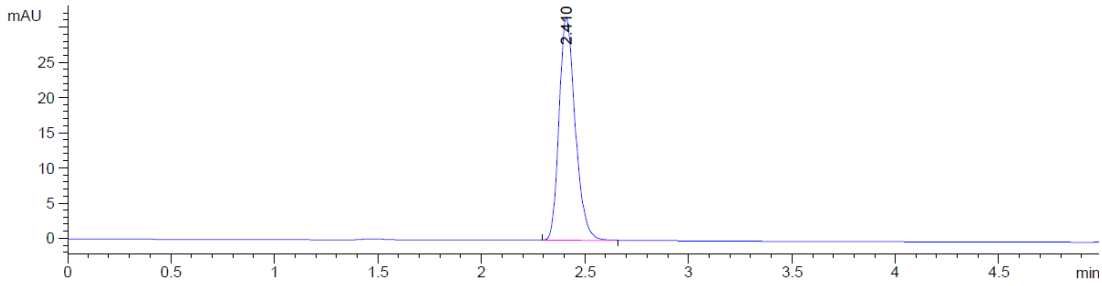

Figure 3.7 Typical HPLC chromatogram of free RSV in 50:50 *v/v* ACN:MQ (t_R 2.4min) analysed using HPLC isocratic method

3.5.2.1 Selectivity

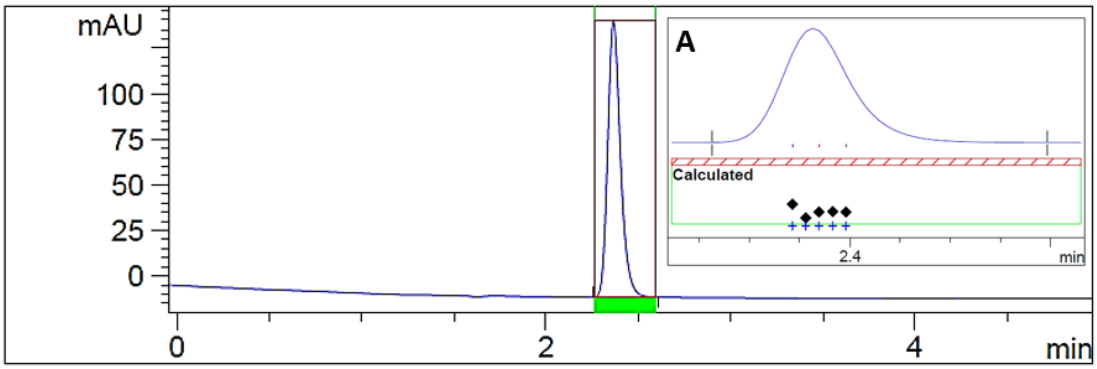

Figure 3.8 Typical HPLC chromatogram of free RSV analysed using the HPLC isocratic method. (A) Purity calculation of free RSV peak

Figure 3.8 showed a sharp and resolved peak of free RSV at the t_R of 2.36 minutes. Figure 3.8A showed that the purity factor of free RSV analysed by HPLC isocratic method was within the calculated threshold limit.

3.5.2.2 Linearity and limitations of HPLC method

The calibration curve for free RSV in 50:50 *v/v* ACN:MQ were obtained by plotting mean peak areas (mAU*s) against concentration (ng/mL or μg/mL). Linearity parameters of free RSV were summarised in Table 3.17 and showed a good linear response over the linear range with excellent R^2 (0.9998).

Table 3.17 Linearity and limitations of HPLC isocratic method using free RSV in 50:50 *v/v* ACN:MQ

Linearity parameters	
Retention time, t_R (minutes)	2.1±0.3
Linearity range	3.2ng/mL to 10.8μg/mL
Linear regression equation	y = 193.6x + 2.3
Correlation coefficient, R^2	0.9998
LOD (ng/mL)	0.7
LOQ (ng/mL)	2.1

Data presented as mean (*n*=3) ± SD

The LOD and LOQ values in 50:50 *v/v* ACN:MQ was 0.7ng/mL and 2.1ng/mL, respectively. These values were at least three times lower than best published values by Singh *et al.* (2014b). An isocratic method using ACN, MeOH and aqueous phosphoric acid as a mobile phase provided almost similar LOD and LOQ values of 0.62ng/mL and 1.87ng/mL, respectively (Kumar *et al.* 2016), however, the HPLC isocratic method employed in this research project used a simpler ACN and aqueous phosphoric acid system with a faster flow rate and shorter run time. Nonetheless, it should be noted that a direct comparison cannot be made as the column and application was not identical.

3.5.2.3 Accuracy

As this method was used exclusively for assays containing encapsulated RSV NPS, it was essential to determine the recovery of free RSV in a representative polymeric matrix to eliminate the possibility of shielding of RSV by the polymers which would affect its detection and quantification. An accuracy test was carried out with six individually prepared samples of 5μg/mL free RSV in 50:50 *v/v* ACN:MQ in the supernatant of blank mPEG750-PLA1000 NPs. The recovery of free RSV spiked in the supernatant of blank NPs was compared with those prepared in 50:50 *v/v* ACN:MQ and RSD was determined (Table 3.18). Recovery of free RSV from the supernatant of blank NPs was outside of acceptable limits of 100±2% (Swartz *et al.* 2012b).

Table 3.18 Recovery of free RSV from supernatant of blank mPEG750-PLA1000 NPs using HPLC isocratic method

Compound	Recovery (%)	RSD (%)
Free RSV	117.3±12.7	10.9

Data presented as mean (*n*=6) ± SD

Figure 3.9 showed a typical HPLC chromatogram of non-spiked and spiked samples of supernatant of blank mPEG750-PLA1000 NPs with free RSV analysed using the HPLC isocratic method. The peak at approximately 2 minutes corresponding to the blank mPEG750-PLA1000 did not interfere with the RSV peak at 2.4 minutes. Peak purity report on the free RSV peak also showed no impurity was present and the purity factor was within calculated threshold limits (Appendix 7.8.2).

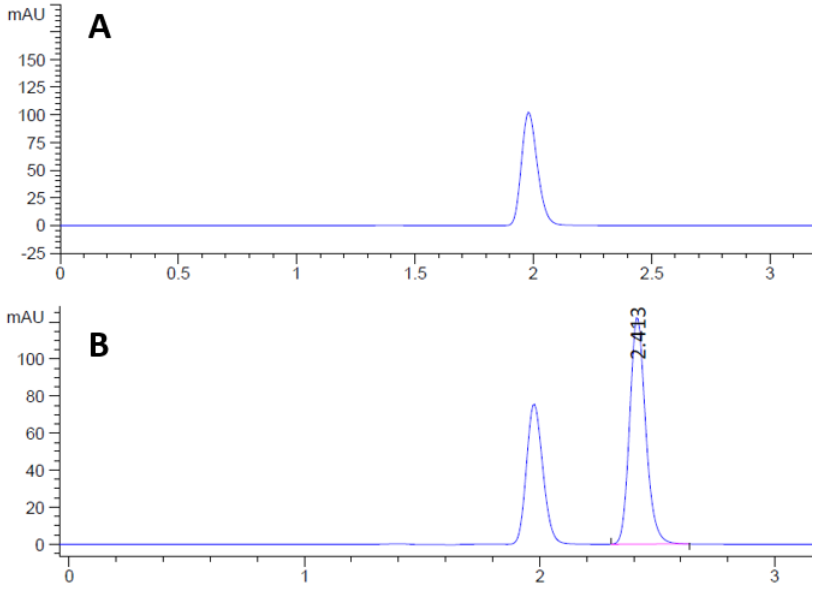

Figure 3.9 HPLC chromatogram using the HPLC isocratic method of (A) supernatant of blank mPEG750-PLA1000 NPs, and (B) supernatant of blank mPEG750-PLA1000 NPs spiked with 5μg/mL free RSV (t_R 2.4min)

3.5.2.4 Precision

Table 3.19 revealed the precision study results of free RSV prepared in 50:50 *v/v* ACN:MQ at three concentrations spanning 20% to 100% of the calibration curve concentration range in Table 3.17 and analysed in triplicate. Average RSD value of all concentrations was well below 0.1% which was well within the acceptable limit for the method to be precise (Swartz *et al.* 2012a).

Table 3.19 Precision study on free RSV using HPLC isocratic method

Compound	Concentrations analysed (μg/mL)	Average RSD (%)
Free RSV	2.2, 5.4 and 10.8	0.07

3.5.2.5 Storage stability during HPLC analysis

Similar to Section 3.5.1.6, the stability of free RSV in three matrices was studied to ensure that free RSV maintained its potency during the analysis using the HPLC isocratic method. As the HPLC isocratic method developed was short, validation was done up to 8 hours as opposed to 24 hours. The three matrices were 50:50 *v/v* ACN:MQ, PBS and the supernatant of blank mPEG750-PLA1000 NPs. The two former matrices were chosen similarly to what was discussed in Section 3.5.1.6 and analysed

at 4°C and RT to represent storage temperature of encapsulated RSV NPs and HPLC autosampler temperature, respectively. The supernatant of blank NPs was chosen to ensure that the matrix did not affect the potency of free RSV over time during storage at 4°C which represented the storage temperature of encapsulated RSV NPs. As samples in the autosampler would be processed NPs in 50:50 *v/v* ACN:MQ, the stability study of free RSV in supernatant of blank NPs at RT was not necessary.

Table 3.20 Stability of free RSV at 4°C and RT during HPLC isocratic analysis

Matrix	**Potency post-preparation (%)***	
	4h	**8h**
4°C		
50:50 *v/v* ACN:MQ	108.0±4.7	99.4±5.3
PBS	99.6±0.1	99.5±0.1
Supernatant of blank NPs	97.6±2.6	116.3±20.0
RT		
50:50 *v/v* ACN:MQ	93.9±4.1	97.7±2.6
PBS	100.6±0.1	85.3±1.7

Data presented as mean (*n*=2) ± SD
*Initial potency = 100%

Free RSV in supernatant of blank NPs showed acceptable limits for stability at 4°C which allowed us to analyse the samples for up to 4 hours with excellent stability. Samples of free RSV in both 50:50 *v/v* ACN:MQ and PBS analysed by the HPLC isocratic method at 4°C and RT for up to 8h were found to be within acceptable limits of 100±15%. Therefore, analyses of free RSV can be carried out up to 8 hours post-processing without variation of potency regardless of matrix and temperature, however, as a standard practice, the samples were analysed within 4 hours of post-processing.

3.5.2.6 Bioanalytical validation

Rat plasma and HLM mix spiked with free RSV was analysed using the HPLC isocratic method and the t_R corresponded to what was found in Section 3.5.2.2, that is, 2.3 minutes (Figure 3.10).

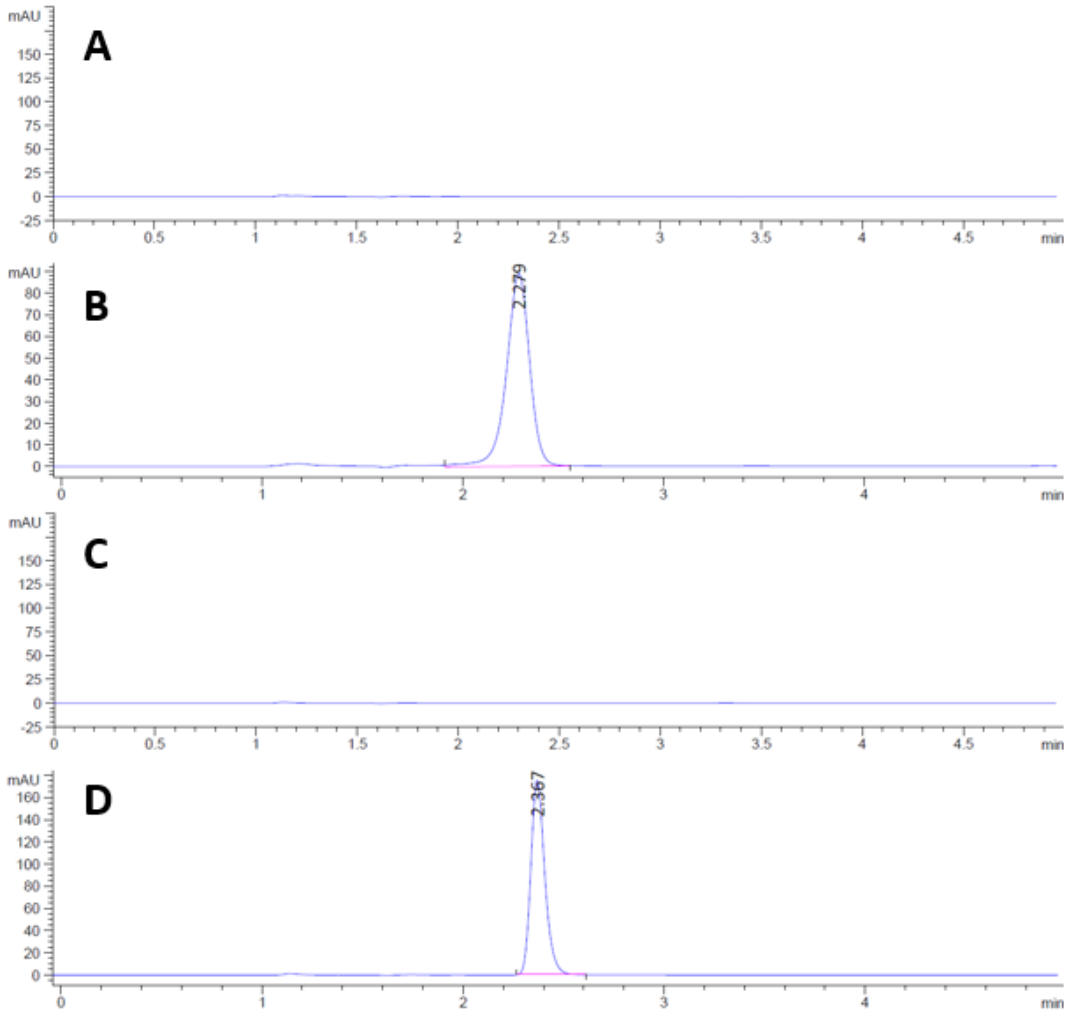

Figure 3.10 Typical isocratic HPLC chromatogram of (A) non-spiked rat plasma (B) spiked rat plasma with 5μg/mL RSV (t_R 2.3min) (C) non-spiked HLM mix (D) spiked HLM mix with 5μg/mL RSV (t_R 2.4min)

Peak purity reports (Appendices 7.8.3 and 7.8.4) of both biological matrices showed no interference was present with the free RSV peak which allowed selective analysis of free RSV in biological assays using the HPLC isocratic method. Following this, linearity, recovery from rat plasma and precision of the isocratic method using biological assays was carried out. In general, free RSV in rat plasma showed excellent R^2 (=0.9953) over the linear range quoted. LOD and LOQ values in rat plasma approximately doubled the LOD and LOQ values found in 50:50 *v/v* ACN:MQ (Table 3.17). The increase in limitation values were possibly due to the interference of species present in the rat plasma (Sagirli *et al.* 2004). Published LOD and LOQ values of 5ng/mL and 7ng/mL by Singh *et al.* (2013) using a HPLC isocratic method were

found higher than our LOD and LOQ values of 1.9ng/mL and 5.6ng/mL, respectively. Therefore, our HPLC isocratic method was highly sensitive when analysing free RSV in non-biological and biological matrices.

Table 3.21 Linearity parameters of free RSV in rat plasma using HPLC isocratic method

Linearity parameters	
Linearity range	16.0ng/mL to 10.8μg/mL
Linear regression equation	y = 250.9x + 53.9
Correlation coefficient, R^2	0.9953
LOD (ng/mL)	1.9
LOQ (ng/mL)	5.6

Data presented as mean (*n*=3) ± SD

Using the same concentrations for precision validation in Section 3.5.2.4 at 2.2, 5.4 and 10.8μg/mL, precision of free RSV in rat plasma using HPLC isocratic method was calculated to be an average RSD of 2.28%. Compared to samples in 50:50 *v/v* ACN:MQ where the average RSD was 0.07%, this value was higher due to the interference from the plasma matrix despite protein extraction; however, RSD values were still below the acceptable limit of 15% (US FDA 2013) and hence, the HPLC isocratic method employed was also precise for biological assays.

Recovery of free RSV from rat plasma and HLM mix using the isocratic method was found to be excellent and within acceptable limits of 100±20% (US FDA 2013) (Table 3.22), however free RSV could be undergoing degradation in rat plasma as seen with the gradient method validation (Section 3.5.1.7) hence the recovery was found to be close to 80%.

Table 3.22 Recovery of 5μg/mL free RSV from rat plasma and HLM mix using HPLC isocratic method

Biological matrix	**Recovery (%)**	**RSD (%)**
Rat plasma	82.6±3.7	4.51
HLM mix	104.6±3.8	3.66

Data presented as mean (*n*=6) ± SD

In conclusion, HPLC using an isocratic mode was successfully optimised and validated in non-biological and biological assays which allowed us to quantify free RSV in assays evaluating encapsulated RSV NPs described in Chapter 4 and 5. This method also allowed us to conduct a rapid and economic analysis of free RSV where RSV conjugates were not present in an assay.

3.6 Conclusion

Apart from the aforementioned in-house research done by Basavaraj (2011), there is no known HPLC method which detects both free RSV and polymeric RSV conjugates simultaneously with good separation and selectivity of both compounds using a combination of both FL and UV detectors. Herein, we have developed a gradient method which simultaneously detected free RSV by UV and polymeric RSV conjugates by FL. Separation between free RSV and polymeric RSV conjugates were at least 5 to 10 minutes elution time apart, which allowed better resolution between analytes. This method was useful when analysing assays containing conjugated RSV NPs formulated in Chapter 4. We have also developed a rapid and economic isocratic method which detected free unconjugated RSV with high selectivity and sensitivity allowing us to assess assays containing encapsulated RSV NPs also formulated in Chapter 4. All methods were validated in non-biological and biological matrices for linearity, limitations, accuracy, precision and storage stability during HPLC analyses.

CHAPTER 4. DEVELOPMENT AND CHARACTERISATION OF NANOPARTICLES OF FREE RSV AND RSV CONJUGATES

4.1 Introduction

RSV is known to have low bioavailability due to several reasons, including a short biological $t_{1/2}$ of less than 15 minutes (Chauhan 2015), low aqueous solubility (Frozza *et al.* 2013), fast metabolism and elimination in the liver *via* phase II metabolic processes (Baur *et al.* 2006) and its instability in plasma (Davidov-Pardo *et al.* 2014). The extensive metabolism of RSV *in vivo* decreases the cell availability of RSV resulting in reduction of bioactivity of RSV (Arora *et al.* 2018). A good review prepared by Amri *et al.* (2012) discussed the shortcomings of RSV which led to its low bioavailability *in vivo* and described nano-sized formulation approaches for RSV and its controlled release. Nanocarriers were known to have sustained release of drugs as demonstrated for PLGA NPs by Rafiei *et al.* (2017) and for polymeric methoxy-poly(ethylene glycol)-poly(lactic acid)-(glycolic acid) (mPEG-PLGA) NPs by Yuan *et al.* (2018). Suktham *et al.* (2018) also showed sustained release of RSV encapsulated in protein NPs. DDSs have also shown to slow down enzyme degradation and the metabolism rate of RSV *in vivo* (Augustin *et al.* 2013, Frozza *et al.* 2013). DDS comprising of nano-sized formulations were developed because they have been touted to be advantageous in cancer therapy due to their preferential accumulation or passive targeting in cancer tissues *via* the EPR effect (Summerlin *et al.* 2015, Carletto *et al.* 2016) resulted from the poor lymphatic system and hyperpermeable vasculature structure in some tumours with pore size ranges of up to 800nm (Fang *et al.* 2011). The ability of nano-sized DDS to enhance cell uptake of its drug cargo into cancer cells in addition to providing protection of the drug and sustained drug release is advantageous and should be considered for the delivery of RSV into cancer cells to ensure its therapeutic effect.

mPEG-PLA and mPEG-PCL are amphiphilic biocompatible copolymers commonly used in DDS of anticancer drugs by encapsulation or conjugation (Letchford *et al.* 2008, Biswas *et al.* 2016). As seen in Figure 4.1, mPEG-PLA and mPEG-PCL NPs structurally

contain the hydrophilic component mPEG to prevent aggregation and provide good dispersion in water and stability in blood circulation against clearance by the MPS (Khalil *et al.* 2013, Natesan *et al.* 2017); and a hydrophobic component PLA or PCL to encourage hydrophobic interaction between RSV and polymer for RSV incorporation.

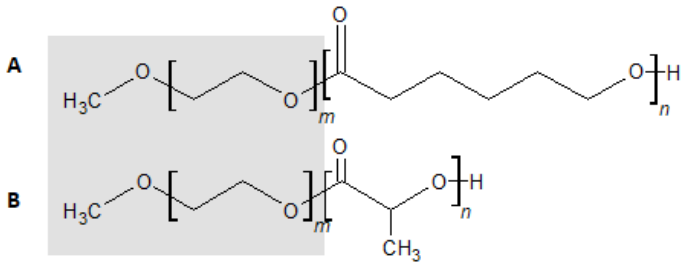

Figure 4.1 Structure of (A) mPEG-PCL and (B) mPEG-PLA with mPEG component highlighted

PEGylated NPs also demonstrated higher tumour accumulation versus control and relatively lower accumulation in the liver compared to non-PEGylated NPs (Jokerst *et al.* 2011), however the length and density of PEG affected the brush layer protecting the hydrophobic core from interactions with blood proteins (Ho *et al.* 2013). This has initiated an interest in the use of low MW polymers because of its potential in producing relatively lower toxicity (Palacio *et al.* 2011) and modulating the p-glycoprotein to overcome multi-drug resistant cancer cells (Wan *et al.* 2013). In a recently published report, Guo *et al.* (2018a) used low MW oligohyaluronic acid of 3,000-10,000Da to co-encapsulate RSV and curcumin which showed better stability of NP particle size than NPs made with high MW hyaluronic acid polymers. Palacio *et al.* (2011) attributed the benefits of low MW PLA NPs in biomedical applications, compared to high MW PLA NPs, to their faster degradation in the human body and hence lower toxicity. Letchford *et al.* (2009) and Wan *et al.* (2013) showed PTX loaded in low MW mPEG-PCL NPs overcame the issue of drug resistance in cancer cells. This was further expanded by Elamanchili *et al.* (2009) where low MW mPEG750-PCL580, better than mPEG750-PCL1200, modulated the p-glycoprotein transporter function in multi-drug resistant cancer cells. To date, as far as authors are aware, mPEG2000-PLA1100 was the lowest MW mPEG-PLA found in literature which was used to encapsulate another hydrophobic compound, coumarin-6, to study the effects of particle rigidity on cellular uptake and penetration (Stern *et al.* 2017). Carstens *et al.* (2008) and Khonkarn *et al.* (2011) used mPEG750-PCL with PCL MWs of 550 to 800

Da to solubilise and encapsulate various anticancer drugs. We have selected amphiphilic biocompatible polymers, mPEG-PLA and mPEG-PCL, to protect RSV against premature degradation and to possibly increase therapeutic concentration and stability in biological fluids (Jiang *et al.* 2015) thereby improving the bioavailability of RSV *in vitro* and *in vivo* for anticancer therapy. Although there is limited literature evidence in the usage of low MW mPEG-PLA and mPEG-PCL for NP formulation of RSV, there has been no published research on the use of low MW (<3,000Da in total) mPEG-PLA and mPEG-PCL for specific conjugation with and encapsulation of RSV.

Several research groups used the approach of conjugating drugs to polymers in order to further increase drug loading capacity (LC) and stability, improve drug retention within the NP core and prolong its blood circulation time (Matsumura *et al.* 2004, Yang *et al.* 2012c, Song *et al.* 2015, Xu *et al.* 2015). Compared to physical entrapment, conjugated drugs prevented premature release and loss of cargos in the blood stream due to the stronger covalent interaction between drugs and polymers in NPs (Yang *et al.* 2012a, Ke *et al.* 2014). Conjugation to RSV increased its MW which reduced kidney clearance of RSV *in vivo* (Kolate *et al.* 2014), and more importantly the conjugation will prevent RSV from enzymatic degradation or rapid metabolism due to the change of enzyme substrate. With a cleavable linker between the drug and polymer, the therapeutic effect of the drug was targeted at sites where these linkers were hydrolysed, for example acidic hydrolysis at tumour sites (Yang *et al.* 2012b, Zhang *et al.* 2017). Due to the synthetic outcomes of RSV conjugates in Chapter 2, a unique DDS approach to producing NPs containing both conjugated RSV and free RSV was needed.

Although there is numerous literature which covered either encapsulation or conjugation of RSV into nano-sized formulations, there were none which combined both encapsulation and conjugation approaches to form RSV NPs. The following literature encompassed other drugs in this unique form of NPs or a combination with other drugs. Ekladious *et al.* (2018) developed NPs containing physically entrapped free PTX and polymer-PTX conjugate which showed very high DL with tunable release kinetics. Yang *et al.* (2012c) reported a significant increase in DL when curcumin was

conjugated to mPEG-PLA and formulated together with unconjugated curcumin (8.5% at 81nm) whereas free curcumin encapsulated in mPEG-PLA had a DL of 2.3% at 60nm. This was attributed to the ability of conjugates enhancing the hydrophobic interaction with unconjugated curcumin within the micelles. Huang *et al.* (2018) investigated the physicochemical and cellular uptake of PEGylated PTX prodrug micelles formed with free PTX which showed superior DL of 60.3% whilst maintaining nano-sized particles of 210nm for *in vitro* delivery by the EPR effect. When comparing with free PTX, these NPs showed similar *in vitro* anticancer activity in cervical and breast carcinoma cells as free PTX below 1μg/mL but exhibited superior anti-proliferative effect when higher than 1μg/mL as free PTX could not be internalised by the cells due to its poor solubility. This showed the notable characteristic of NPs formed by conjugates together with unconjugated drugs where DL can be enhanced whilst maintaining a small particle size suitable for passive targeting. Free RSV and free curcumin were co-encapsulated into low MW oligo-hyaluronic acid polymers conjugated with curcumin and showed sustained release of both drugs in simulated gastrointestinal environment, better stability in PBS and higher ability in reducing free radicals compared to single-drug NPs (Guo *et al.* 2018a). Danafar *et al.* (2017) showed interesting release profiles of free doxorubicin (DOX) and free curcumin encapsulated in mPEG-PCL conjugated to DOX in different physiological environments and pH buffers. NPs made by polymer-pterostilbene conjugates with encapsulated clofazimine showed low toxicity, highly stable NP dispersions, increased stability due to encapsulation and cellular internalisation (Romio *et al.* 2018). Most literature researched on the encapsulation of RSV in NPs formed with a different drug-polymer conjugate due to one of the numerous biological effects of RSV which aided the delivery of the conjugated drug (Washington *et al.* 2018). Therefore, NPs with drug conjugates and free drug are able to increase DL while maintaining nano-sized particles, provide sustained release of drug and decrease or prevent *in vivo* degradation and metabolism of some drugs. To our knowledge, there is no known literature that has reported on the study of RSV both encapsulated in and conjugated to amphiphilic copolymeric NPs with low MW polymers.

4.2 Aim

The aims of the work described in this chapter were 1) to develop novel nano-sized formulations using polymeric RSV conjugates synthesized in Chapter 2.5.3 containing both RSV conjugates and free RSV (conjugated RSV NPs); 2) to develop novel nano-sized formulations of free RSV encapsulated in low MW amphiphilic copolymers synthesised in Chapter 2.5.1 (encapsulated RSV NPs); and, 3) to assess the properties of both conjugated RSV NPs and encapsulated RSV NPs. Assessments include particle size, zeta potential, DL and release characteristics in a simulated physiological pH environment.

4.3 Materials

Trans-RSV was purchased from Shanghai DND Pharma-Technology Co., Inc. (Shanghai, China) with 99% purity. Polymeric RSV conjugates and amphiphilic copolymers were synthesised and characterised in-house (Chapter 2). mPEG750-PLLA1000 was procured from Akina Inc. (IN, USA). PEG5000-O-RSV ether conjugate was synthesised by Basavaraj (2011). ACN Optima® (HPLC grade), MeOH Optima® (HPLC grade), acetone (analytical grade), DCM (analytical) and EtOH (analytical grade) were purchased from Thermo Fisher Scientific (VIC, Australia). MQ was obtained using a Millipore Milli-Q Ultrapure Water purification system by Merck Millipore (VIC, Australia) at 18.2MΩcm purity. Solvents were de-gassed and filtered with 0.2 μm PVDF filters prior to use. PVA (MW 9,000-10,000Da, 80% hydrolyzed; cat# 360627-500G), dialysis tubing (MW cut-off MWCO 12,400Da; cat# D0530-100FT) used for release studies, molecular grade DMSO and PBS were purchased from Sigma-Aldrich (NSW, Australia). PBS solution was made as per manufacturer's instructions in MQ with no further modification.

4.4 Methodology

4.4.1 Development of conjugated RSV NPs

Conjugated RSV NPs were prepared using a selection of synthesised products

discussed in Chapter 2. Final synthesised products of ester RSV conjugates mPEG750-PLA1000-succ-RSV, mPEG750-PCL1000-succ-RSV, mPEG750-PLA1000-glu-RSV and mPEG2000-PLA1000-succ-RSV were prepared using solvent diffusion, however, NPs prepared using mPEG750-PLA1000-succ-RSV was not of satisfactory characteristics thus solvent evaporation was employed. Table 4.1 summarises methods trialled for preparing ester conjugated RSV NPs and final methods are described below. PEG5000-O-RSV, an ether conjugate, synthesised by Basavaraj (2011) (Appendix 7.7) was prepared using a self-assembly method also described below.

Table 4.1 Summary of methods used for preparing conjugated RSV NPs

Conjugate used for formulation	**Methods used for NP formulation**	
	Solvent diffusion	**Solvent evaporation**
mPEG750-PLA1000-succ-RSV	×	✓
mPEG750-PLA1000-glu-RSV	✓	Not trialled
mPEG2000-PLA1000-succ-RSV	✓	Not trialled
mPEG750-PCL1000-succ-RSV	✓	Not trialled

× = unsuccessful trials
✓ = successful trials

4.4.1.1 Solvent evaporation method

mPEG750-PLA1000-succ-RSV conjugate was formulated into NPs by dissolving 5.5mg of the conjugate in 1mL 60:40 *v/v* DCM:MeOH and adding the solution dropwise into 1mL 3% *w/v* aqueous PVA while stirring at 300rpm. This mixture was then ultrasonicated with a UP200S ultrasonicator probe (200W, 24kHz) (Hielscher Ultrasonics GmbH: Germany) for 2 minutes at 70% amplitude (0.6 cycle) in an ice bath to prevent overheating. The solution was diluted with 4mL MQ and stirred in the dark at 300rpm for 10 minutes. The organic phase was removed by a rotary evaporator under vacuum at 60°C for 5 minutes at 200rpm resulting in a clear and translucent suspension.

4.4.1.2 Solvent diffusion method

mPEG750-PLA1000-glu-RSV NPs were prepared by solvent diffusion method by dissolving 6.1mg of the conjugate in 50μL MeOH and 1mL MQ. The solution was

bubbled with an inert nitrogen gas flow for 15 minutes to remove MeOH resulting in 1mL milky white suspension.

Similarly, mPEG750-PCL1000-succ-RSV NPs were prepared by dissolving 6.6mg mPEG750-PCL1000-succ-RSV conjugate in 50μL MeOH and 1mL MQ. The solution was then bubbled with an inert nitrogen gas flow for 15 minutes to remove MeOH resulting in 1mL milky white suspension.

mPEG2000-PLA1000-succ-RSV NPs were prepared by sonicating 2.8mg of the conjugate in 50μL ACN in a Bransonic® ultrasonic water bath (Branson Ultrasonics Corporation: CT, USA). 50μL MQ was then added and the solution was bubbled with an inert nitrogen gas flow for 15 minutes to remove ACN and MQ was added to make up a total of 100μL clear translucent suspension.

4.4.1.3 Self-assembly

1mg PEG5000-O-RSV powder was added to 1mL MQ and dispersed using an ultrasonic water bath for 10 minutes.

4.4.2 Characterisation of conjugated RSV NPs

4.4.2.1 Size and zeta potential analysis

All conjugated RSV NPs excluding mPEG750-PLA1000-succ-RSV NPs and PEG5000-O-RSV NPs were diluted 1:9 with MQ and evaluated for their mean particle size, PDI and zeta potential using a Zetasizer Nano ZSP (Malvern Instruments Ltd: Worcestershire, UK) with a He-Ne laser at 633nm. mPEG750-PLA1000-succ-RSV NPs and PEG5000-O-RSV NPs were evaluated undiluted. Each sample was measured by dynamic light scattering at a scattering angle of 90° and a temperature of 25°C. For zeta potential, samples were placed in a folded capillary cell and subjected to an electric field at 25°C. All measurements were carried out in triplicate and an average number was reported.

4.4.2.2 Drug loading (DL)

The DL of conjugated RSV NPs was total RSV equivalent weight against the total weight of NPs in 1mL of NP suspension. As EE of conjugated RSV NPs were not assessed, we have excluded soluble RSV from the free RSV component of the NPs

using solubility of RSV at 0.03mg/mL (Mattarei *et al.* 2013). Therefore, DL of conjugated RSV NPs were as follows:

$$\text{Drug loading in 1mL NPs (\%)} = \frac{\text{Total RSV equivalent (mg) - 0.03mg}}{\text{Total final synthesised product (mg)}} \times 100\%$$

4.4.2.3 Release study of RSV from conjugated RSV NPs

Release studies were carried out to profile the release characteristics of conjugated RSV NPs in a simulated physiological environment at pH7.4 in PBS solution at 37°C using the dialysis bag method. 1mL conjugated RSV NPs containing known amounts of RSV equivalent in NPs was added in a dialysis tubing (MWCO 12,400Da), sealed and placed in an amber jar containing 49mL of PBS as release medium which gave released RSV a dilution factor of 50. The jar was placed on an orbital shaker mixing at 100rpm in a dark hot room maintained at 37°C. At time intervals of 0, 15, 30, 45 minutes, and 1, 2, 4, 7, 24 and 48 hours, 200μL aliquot release medium was removed from the container and replaced with an equivalent volume of fresh pre-warmed PBS to maintain sink conditions. The aliquot was then measured for RSV and RSV conjugate using the HPLC gradient method detailed in Section 3.4.2.2. Data was presented as percentage cumulative amounts of total RSV equivalent in conjugated RSV NPs released against time. Cumulative percentage released was determined by comparing the amount of total RSV equivalent in conjugated RSV NPs released per time point against the initial amount of total RSV equivalent in conjugated RSV NPs added into the dialysis bag. As a control, 100μg/mL of free RSV prepared using an RSV stock in DMSO diluted with PBS solution was used.

4.4.2.4 Stability of conjugated RSV NPs in buffers

Stability of conjugated RSV NPs was assessed in PBS at pH7.4. Known concentrations of RSV in conjugated RSV NPs were diluted 1:9 with PBS to a total volume of 1mL. 200μL aliquots were maintained in sealed 1.5mL centrifuge tubes in the dark at 37°C. At 5 minutes, 24 and 48 hours, one aliquot was removed and solubilised with an equal volume of 50:50 *v/v* ACN:MQ and analysed for RSV and RSV conjugate with the HPLC gradient method detailed in Section 3.4.2.2. Data was presented as % *w/w* of RSV and RSV conjugate components in conjugated RSV NPs against time with initial potency

being the initial % *w/w* of each RSV and RSV conjugate component in conjugated RSV NPs added into the PBS.

4.4.3 Development of encapsulated RSV NPs

Purchased mPEG750-PLA1000 and two different amphiphilic copolymers synthesised in Section 2.5.1 (mPEG750-PCL1000 and mPEG2000-PLA1000) were selected to encapsulate RSV into NPs for further *in vitro* and *in vivo* evaluation as a comparison with conjugated RSV NPs. Encapsulation of RSV into these three different amphiphilic copolymers were achieved after several trials and developments. Due to the difference in polymeric hydrophilicity and hydrophobicity properties, we have used additional methods with varying drug:polymer ratios and anti-solvent systems for the encapsulation of RSV compared to how conjugated RSV NPs were prepared. Trials were summarised in Table 4.2 and methods used which produced the satisfactory NPs are described here.

Table 4.2 Summary of methods used for preparing encapsulated RSV NPs

Polymer used for encapsulation of RSV	Methods used for NP formulation		
	Solvent diffusion	Solvent evaporation	Thin film hydration
mPEG750-PLA1000	✓	×	Not trialled
mPEG750-PCL1000	×	✓	✓
mPEG2000-PLA1000	×	✓	Not trialled

× = unsuccessful trials
✓ = successful trials

4.4.3.1 Solvent diffusion method

10.2mg mPEG750-PLA1000 and 1.1mg RSV was dissolved in 2mL acetone. This solution was added dropwise into 10mL MQ while stirring at 300rpm. Acetone was evaporated in a fumehood for approximately 17 hours in the dark under an inert nitrogen gas flow resulting in a slightly turbid suspension. A blank NP formulation was prepared similarly with 11.6mg copolymer and no RSV producing a clear translucent suspension.

4.4.3.2 Solvent evaporation method

RSV encapsulated in mPEG750-PCL1000 NPs was best formulated using the solvent evaporation method. 108.2mg mPEG750-PCL1000 and 10.2mg RSV was dissolved in 4mL 60:40 *v/v* DCM:acetone. The solution was then added dropwise into 4mL 3% *w/v* aqueous PVA while stirring at 300rpm. The mixture was ultrasonicated at 70% amplitude (0.4 cycle) for 2 minutes. The solution was diluted with an addition of 16mL MQ (1:4 dilution) and then stirred at 300rpm for 10 minutes in the dark. This resulted in a final PVA concentration of 0.6%. The organic phase was removed under vacuum at 50°C for 20 minutes at 150rpm resulting in a milky white suspension. Similarly, a blank formulation was prepared with 102.8mg mPEG750-PCL1000 without RSV producing a less turbid milky white suspension than the encapsulated formulation. Both suspensions were then diluted 1:9 with MQ for further assessments and use.

RSV encapsulated in mPEG2000-PLA1000 NPs was prepared similarly to the mPEG750-PCL1000 NPs with slight modifications. 51.7mg of copolymer and 10.3mg of RSV were dissolved in 5mL 60:40 *v/v* DCM:ACN and then added dropwise into 2mL 3% *w/v* aqueous PVA while stirring at 300rpm. The vial containing the mixture was placed in an ice bath to prevent overheating and ultrasonicated at 70% amplitude (0.8 cycle). The solution was diluted 1:4 with MQ and then stirred at 300rpm for 10 minutes in the dark. The organic solvent was removed by a rotary evaporator at 150rpm at 55°C for 15 minutes resulting in a milky-white turbid suspension. A blank formulation was prepared similarly with 53.2mg mPEG2000-PLA1000 and no RSV resulting in a slightly turbid suspension.

4.4.3.3 Thin film hydration method

10.9mg of mPEG750-PCL1000 and 1.1mg of RSV was dissolved in 2mL acetone. The organic solvent was evaporated to a thin film using a rotary evaporator at 55°C for 15 minutes at 200rpm. The film was cooled and 20mL of MQ was then added to solubilise the thin film using a rotary evaporator (45°C, 200rpm, 15 minutes, in the dark) without vacuum resulting in a slightly turbid suspension. A blank formulation was prepared similarly with 10.7mg polymer and no RSV resulting in a turbid suspension.

4.4.4 Characterisation of encapsulated RSV NPs

4.4.4.1 Size and zeta potential analysis

All NPs were evaluated as is for their mean particle size, polydispersity and zeta potential as per Section 4.4.2.1.

4.4.4.2 Encapsulation efficiency (EE) and drug loading (DL)

An indirect measurement of the efficiency of the encapsulation of RSV in loaded NPs was used. A suspension was centrifuged at 10,000*g* for 5 minutes at RT using a 5415R Eppendorf® microcentrifuge. The supernatant was removed and diluted appropriately for HPLC analysis in the isocratic mode as described in Section 3.4.3. The EE denoted how much free RSV was successfully entrapped in the NPs and was calculated as follows:

$$\text{EE (\%)} = \frac{\text{Initial drug added - drug in supernatant (mg)}}{\text{Initial drug added (mg)}} \times 100\%$$

The DL represented the drug content in 1mL NP suspension. This was done by calculating the amount of drug entrapped in 1mL of NP suspension using the EE and compared against the weight of 1mL of NP suspension dried in a Daihan WiseVen® vacuum oven (Thermoline Scientific: NSW, Australia) at 60°C until the weight was consistent, usually for about 24 hours.

$$\text{DL (\%)} = \frac{\text{Amount of drug entrapped in 1mL suspension (mg)}}{\text{Weight of 1mL NPs after drying (mg)}} \times 100\%$$

4.4.4.3 Yield

The yield of the NPs was determined by drying 1mL of the NP suspension in a vacuum oven at 60°C until the weight was consistent, usually for about 24 hours. The yield was calculated as follows:

$$\text{Yield (\%)} = \frac{\text{Amount of dried NPs from 1mL suspension (mg)}}{\text{Weight of combined components to make 1mL suspension (mg)}} \times 100\%$$

The components to make NPs included the copolymer, RSV and PVA (if used). 1mL of MQ was treated similarly to ensure dried NPs did not contain any impurities from MQ.

4.4.4.4 Release study of RSV from encapsulated RSV NPs

Release studies were carried out as per Section 4.4.2.3, however, analysis of RSV was by HPLC isocratic method detailed in Section 3.4.3. Data was presented as percentage cumulative amounts of RSV released against time. Cumulative percentage released was determined by comparing total amount of RSV released per time point against the initial amount of RSV added into the dialysis bag. As a control, 100μg/mL of free RSV prepared using 1mg/mL RSV stock in DMSO diluted with PBS solution was added to the dialysis bag and used.

4.4.4.5 Stability of encapsulated RSV NPs in PBS

Stability of encapsulated RSV NPs was assessed in PBS at pH7.4 as per Section 4.4.2.4 and samples were analysed for RSV with the HPLC isocratic method detailed in Section 3.4.3. Data was presented as percentage of RSV remaining against time with initial potency being the amount of RSV in NP suspension added into the PBS.

4.5 Results and discussion

4.5.1 Development of conjugated RSV NPs

In this section, we described the development of NPs using RSV conjugated to three amphiphilic copolymers mPEG750-PLA1000, mPEG750-PCL1000 and mPEG2000-PLA1000 synthesised in Section 2.5.3. The purpose of conjugating RSV to the polymers was to decrease the metabolism and possibly improve the stability of RSV *in vivo* thereby enhancing its therapeutic effect. In addition, conjugation can also improve DL and enhance interactions between hydrophobic blocks which can produce more stable NPs (Yang *et al.* 2012c). RSV conjugates synthesised in Chapter 2 contained free unconjugated RSV which was not further separated from the conjugates because the free RSV could be used to increase the DL of conjugated RSV NPs by physical entrapment of free RSV in the NP core similar to what was reviewed by Xu *et al.* (2015) and Zhang *et al.* (2017).

4.5.1.1 Formulation development process

Basavaraj (2011) successfully formulated conjugated RSV NPs with mPEG750-

PLA1000-succ-RSV using a solvent diffusion method. However, despite being the same conjugate, our mPEG750-PLA1000-succ-RSV could not be formulated into NPs using the solvent diffusion method due to the presence of free RSV in the final synthesised product which resulted in more hydrophobic content rendering it more suitable for a solvent evaporation method. Table 4.3 summarises the physical attributes of conjugated RSV NPs and selected relevant data from Basavaraj (2011) was also included.

Table 4.3 Summary of physical characteristics of conjugated RSV NPs

Conjugate used for formulation	Preparation method	Particle size (nm)[a]	Polydispersity index (PDI)[a]	Zeta potential (mV)[a]	Total RSV equivalent concentration (mg/mL)[b]	DL (%)	% *w/w* component in final synthesised product[b]	
							RSV conjugate	Free RSV
mPEG750-PLA1000-succ-RSV NPs	Solvent evaporation	269.0±50.2	0.317±0.037	-2.8±1.0	0.431	40.1	63.9	36.1
mPEG750-PLA1000-glu-RSV NPs	Solvent diffusion	356.4±13.3	0.668±0.113	-26.6±0.6	0.511	48.1	54.8	45.2
mPEG750-PCL1000-succ-RSV NPs	Solvent diffusion	205.0±1.9	0.196±0.018	-34.7±3.4	0.128	9.8	99.3	0.7
mPEG2000-PLA1000-succ-RSV NPs	Solvent diffusion	27.5±6.5	0.337±0.170	-9.3±3.1	0.291	26.1	76.1	23.9
PEG5000-O-RSV NPs	Self-assembly	579.0±85.8	0.533±0.069	-0.2±2.3	0.043	4.3	100.0	0
Data from Basavaraj (2011)								
mPEG750-PLA1000-succ-RSV NPs	Solvent diffusion	249.0±10.4	0.59±0.03	ND	ND; reported no free RSV present but multiple substitution of RSV present			
PEG5000-O-RSV NPs	Self-assembly	ND	ND	ND				

[a]Data presented as mean (*n*=3 except PEG5000-O-RSV particle size and zeta potential analyses where *n*=2) ± SD where calculated
[b]determined by NMR analyses (Appendix 7.2 for calculation example, Table 2.8 for data)

4.5.1.2 Particle size and distribution

Conjugated RSV NPs size and distribution varied drastically despite using the same MW of amphiphilic copolymer. Several factors could have influenced this including the type of copolymers used to synthesise the RSV conjugates, the weight levels of each RSV conjugate and unconjugated free RSV components in the final synthesised product and the method used to prepare the NPs. mPEG750-PLA1000 was conjugated with RSV using two types of linkers, that is, succinate and glutarate (Section 2.5.3). mPEG750-PLA1000-glu-RSV was approximately 100nm larger than mPEG750-PLA1000-succ-RSV and this could be due to the extra carbon in the glutarate linker and a slightly higher % *w/w* of free RSV compared to RSV conjugates which affected the hydrophobicity of the overall product and thus the NP formation (Yang *et al.* 2012c). Observing the particle size report of both mPEG750-PLA1000 conjugates (Appendices 7.9.1 and 7.9.2), each NPs consisted of at least two size distributions. This could be due to the almost equivalent weight levels of free RSV to RSV conjugates and possibly unconjugated polymers which produced both blank and encapsulated forms of NPs while mPEG750-PLA1000-succ-RSV NPs and mPEG750-PLA1000-glu-RSV NPs were prepared.

mPEG750-PCL1000-succ-RSV NPs produced a single particle size distribution of 205.0nm average with a low PDI value compared to the other conjugated RSV NPs (Appendix 7.9.3). The low PDI value could be due to the minimal amount of unconjugated RSV in the final synthesised product which allowed for a more homogenous formation of NPs. mPEG2000-PLA1000-succ-RSV NPs, on the other hand, had a Z-average of less than 30nm which was the smallest particle size formulated thus far (Appendix 7.9.4). This could be due to the effect of conjugating RSV to mPEG2000-PLA1000 which changed the hydrophobicity of the polymer in favour of a more compact NP. From Appendix 7.9.4, we observed two particle size populations, that is 18.7nm (83%) and 140.7nm (17 %) which caused a higher PDI value. It was possible that the size population of 18.7nm in mPEG2000-PLA1000-succ-RSV NPs could have aggregated to the minor 140.7nm size population. Further investigation using blank and RSV-loaded mPEG2000-PLA1000 NPs was necessary to draw a definite conclusion.

PEG5000-O-RSV NPs presented large particle sizes with a moderate PDI. This could be due to aggregation of micelles as the suspension was clear upon addition to MQ with no evidence of precipitation. Despite this result, PEG5000-O-RSV was further assessed due to its long-term stability in buffers and plasma, and its favourable PK profile as demonstrated by Siddalingappa *et al.* (2015).

4.5.1.3 Zeta potential

All conjugated RSV NPs excluding mPEG750-PLA1000-succ-RSV and PEG5000-O-RSV NPs had mid to high range of negative zeta potential despite the presence of the neutral PEG (Appendices 7.9.1 to 7.9.4). This could be due to the stronger covalent interaction between RSV and the polymers *via* an ester bond which aided in the folding of RSV in the hydrophobic core of the NP resulting in a more stable compact NP. High zeta potential values in the conjugated RSV NPs could be indicative of physically stable NPs (Neves *et al.* 2013) or the presence of RSV on the NP surface brought on by the development of anionic phenoxyl radicals as suggested by Soo *et al.* (2016). The presence of a steric stabiliser PVA in the preparation of mPEG750-PLA1000-succ-RSV NPs could have affected its nett zeta potential as PVA could shield the particle surface charge, lowering it closer to zero (Cooper *et al.* 2014, Zhang *et al.* 2014b). On the other hand, PEG5000-O-RSV NPs showed near zero zeta potential as expected with PEGylated NPs (Ho *et al.* 2013). This result explained the possible aggregation which was shown with its particle size report as there was a lack of electrostatic repulsion between particles to prevent aggregation.

4.5.1.4 Drug loading (DL)

Due to the unique nature of the conjugated RSV NPs, the DL of RSV in conjugated RSV NPs was calculated based on the combination of the RSV equivalent in RSV conjugates and unconjugated RSV encapsulated in the conjugated RSV NPs. Using NMR analyses described in Section 2.4.4.2, the weight percentage of each component was calculated and a total concentration of RSV equivalent was calculated for each RSV conjugate synthesised (Table 2.8). Using this information, the DL of conjugated RSV NPs was calculated and tabulated in Table 4.4.

Table 4.4 Weight percentage of components in and DL of conjugated RSV NPs

Conjugated RSV NPs	% *w/w* component in NPs*		DL (%)
	RSV conjugate	Free RSV	
mPEG750-PLA1000-succ-RSV NPs	63.9	36.1	40.1
mPEG750-PLA1000-glu-RSV NPs	54.8	45.2	48.1
mPEG750-PCL1000-succ-RSV NPs	99.3	0.7	9.8
mPEG2000-PLA1000-succ-RSV NPs	76.1	23.9	26.1

*determined by NMR analyses (Appendix 7.2 for calculation example, Table 2.8 for data)

As seen from Table 4.4, higher DL of conjugated RSV NPs were a result from the presence of unconjugated free RSV encapsulated in conjugated RSV NPs. This was speculated by observing the DL of mPEG750-PCL1000-succ-RSV NPs where 99.3% of the NPs were RSV conjugate whereas the remaining conjugated RSV NPs had substantially higher amounts of free RSV. Higher DLs of this type of NPs were also observed in Huang *et al.* (2018) and Xu *et al.* (2011) where DLs of NPs of drug conjugates formulated together with free drug were 56-62% at 200nm and 16nm, respectively. Therefore, our conjugated RSv NPs will be able to deliver higher amounts of RSV due to its DL by passive targeting *via* the EPR effect due to its particle size.

4.5.2 Development of encapsulated RSV NPs

In order to compare the effects of unconjugated free RSV encapsulated in conjugated RSV NPs, we have developed NPs with free RSV encapsulated in the same amphiphilic copolymers used for the preparation of conjugated RSV NPs. Unlike the development of conjugated RSV NPs, extensive trials were employed to encapsulate RSV into three different amphiphilic PEGylated polymers, that is, synthesised mPEG750-PCL1000, mPEG2000-PLA1000 (Section 2.5.1) and commercially available mPEG750-PLA1000. The development of the NPs involved different preparation methods, different polymer to RSV ratios and varying final suspension volume. NPs prepared with solvent evaporation method were experimented with different energy input from the ultrasonicator probe. During the development of the NPs, aggregation was observed

in unsuccessful trials and this could possibly be caused by insufficient polymer to completely saturate the particle surface (Davidov-Pardo *et al.* 2015) in order to stabilise the particle, thus the addition of stabilisers at differing concentrations were experimented. This time-consuming exercise was possibly due to the difficulty of formulating low MW polymers into NPs and the lack of literature in formulating such NPs was a possible indication of this problem. The development process of each NP will first be described followed by a discussion of individual physical properties of encapsulated RSV NPs compared with the physical properties of conjugated RSV NPs.

4.5.2.1 Formulation development process

mPEG750-PLA1000 was dispersible in water and found to form polymeric micelle-like particles as evident when 10mg of the polymer was stirred in 10mL MQ producing 22.8nm particles with a PDI of 0.347. The particle size report of these mPEG750-PLA1000 NPs (Appendix 7.9.5) revealed larger particles (683.1nm and 4.5μm) present in low percentage (total 18.6%) which could be a result of aggregation of the micelle-like particles. This is not surprising as mPEG750-PLA1000 is amphiphilic. Similarly, amphiphilic PEGylated polycarbonates were found to have two size populations at 40nm and about 130nm resulting in a polydispersed distribution (Yang *et al.* 2012a). The authors hypothesized that the polymer molecules tended to fold upon themselves due to intra-molecular hydrogen-bonding in the same polymer chain leading to aggregation of the primary micelles at 130nm whereas the smaller size distribution was probably due to inter-molecular hydrogen-bonding interactions between two polymer chains. Nonetheless, this dispersion of mPEG750-PLA1000 NPs in water was not optimal and therefore required an addition of a stabiliser like PVA to encourage a more homogenous dispersion. Blank and RSV-loaded mPEG750-PLA1000 NPs were then prepared using the solvent evaporation method in the presence of PVA but this method produced heterogenous dispersions with large microparticles present which had to be abandoned. The solvent diffusion method was therefore used for preparation of blank and RSV-loaded mPEG750-PLA1000 NPs in MQ and its physical attributes will be discussed in the next section.

mPEG750-PCL1000 NPs were successfully made using two methods, that is the thin film hydration and solvent evaporation methods. In order to highlight the effect of

preparation method on the physical characteristics of NPs, particle size and zeta potential values of mPEG750-PCL1000 NPs prepared by both methods are summarised in Table 4.5.

Table 4.5 Physical characteristics of blank and RSV encapsulated in mPEG750-PCL1000 NPs prepared by thin film hydration and solvent evaporation

Physical characteristic	Thin film hydration		Solvent evaporation*	
	Blank NPs	Encapsulated NPs	Blank NPs	Encapsulated NPs
Size (nm)	464.1±16.6	331.1±5.6	243.5±3.4	116.7±2.0
PDI	0.602±0.104	0.422±0.302	0.388±0.176	0.418±0.013
Zeta potential (mV)	-29.4±5.0	-32.2±1.6	-3.8±2.4	-4.8±1.6

*mPEG750-PCL1000 NPs were analysed prior to 1:9 dilution as per Section 4.4.3.2 to ensure comparable concentrations of polymer and RSV between both methods
Data presented as mean (*n*=3) ± SD

Despite size and zeta potential measurements reported as good quality, the particle sizes and PDI values for mPEG750-PCL1000 NPs prepared by thin film hydration were not favourable where multiple size distributions were observed in both blank and encapsulated NPs. mPEG750-PCL1000 NPs prepared using a solvent evaporation method at comparable polymer and RSV concentrations produced smaller particles with slightly better PDI values although zeta potential values were lower. The lower zeta potential values could be explained by the presence of PVA as a stabiliser. A further 1:9 dilution of the NPs with MQ for size and zeta potential measurements produced smaller particle sizes with much lower PDI values and higher zeta potential magnitudes which will be discussed in the next section as the final encapsulated RSV NPs using mPEG750-PCL1000.

Due to the higher hydrophilicity in mPEG2000-PLA1000 compared to mPEG750-PLA1000 because of the longer mPEG chain length, it was assumed that a solvent diffusion method could produce NPs, however, despite extensive trials using polymer:RSV amount ratios of 5:1 and 10:1, acetone or ACN as anti-solvents and 0.6% *w/v* PVA as stabilisers, NPs were large with polydispersed distributions. Thus, solvent evaporation was employed similar to the method used for preparing RSV in

mPEG750-PCL1000 NPs. A polymer:drug ratio of 10:1 was not successful, producing large particles and high PDI values. The ratio of 5:1 was then trialled yielding a suspension with smaller particle sizes but still very polydispersed due to microparticles present. Different anti-solvent systems were then trialled and 60:40 *v/v* DCM:ACN was found to be more superior than 60:40 *v/v* DCM:acetone, 60:40 *v/v* DCM:EtOH, 60:40 *v/v* DCM:MeOH or 100% DCM. Physical properties of blank and RSV-loaded mPEG2000-PLA1000 NPs will be discussed in the following section.

As the development of encapsulated RSV NPs was necessary to compare and critically evaluate some physical attributes of conjugated RSV NPs, it should be pointed out that the conjugation to RSV altered the hydrophobicity level of the amphiphilic polymers and thus produced more thermodynamically stable NPs. This difference could be observed in the choice of preparation method for both encapsulated and conjugated RSV NPs. Also, in general, the development of conjugated RSV NPs was less tedious and time-consuming than encapsulated RSV NPs. Regardless of preparation method, it was clear that conjugation of RSV to the amphiphilic copolymers produced more stable NPs using less energy input compared to encapsulation. Yang *et al.* (2017) concluded that a delicate balance between hydrophilic and lipophilic components of a polymer-drug conjugate was needed in order to form nano-sized structures which we believe was the case for our conjugated RSV NPs. As a summary, Table 4.6 presents the final preparation methods and physical characteristics of NPs of blank and RSV encapsulated in three types of amphiphilic polymers. The following sections discusses the physical attributes of blank and encapsulated RSV NPs and compares with those of conjugated RSV NPs prepared with comparable amphiphilic copolymers.

Table 4.6 Summary of final preparation methods and physical characteristics of blank and encapsulated RSV NPs

Polymer used for encapsulation	Preparation method	Type of formulation	Particle size (nm)	Polydispersity index (PDI)	Zeta potential (mV)	EE (%)	DL (%)	Yield (%)
mPEG750-PLA1000	Solvent diffusion	Blank	239.6±12.8*	0.641±0.064*	-5.3±1.6	NR	NR	ND
		Encapsulated	162.2±2.9	0.062±0.024	-11.0±0.4	95.1±0.1*	8.7±0.1*	98.4±0.9
mPEG750-PCL1000	Solvent evaporation	Blank	107.6±3.0	0.234±0.008	-21.3±1.9	NR	NR	ND
		Encapsulated	201.0±4.2	0.042±0.038	-20.1±0.4	72.4±4.5	2.7±0.2	121.6±11.9
mPEG2000-PLA1000	Solvent evaporation	Blank	124.0±1.4	0.699±0.023	2.2±0.5	NR	NR	66.5±2.0
		Encapsulated	345.5±5.5	0.087±0.074	-0.5±0.1	96.9±0.1*	8.8±0.1*	87.3±1.0

NR = not relevant

Data presented as mean (*n*=3 unless indicated by * where *n*=2) ± SD

4.5.2.2 Particle size and distribution

Overall, Z-average of the encapsulated RSV NPs were between 160nm and 350nm with exceptional PDI values of below 0.1. Particle size reports of all encapsulated RSV NPs were of good quality showing single size distributions (Appendices 7.9.7, 7.9.9 and 7.9.11). The addition of another hydrophobic component, that is RSV, could have strengthened the non-covalent interactions between the hydroxyl groups in RSV and carboxylic acid or carboxyl groups in the PCL and PLA, respectively, thus compacting the NP further resulting in a more densely packed particle (Yang *et al.* 2012a, Ke *et al.* 2014). RSV encapsulated in mPEG2000-PLA1000 NPs was found to be largest in particle size amongst all encapsulated NPs. One of the reasons to the larger particle sizes could be the high feed amounts of mPEG2000-PLA1000 and RSV in a 10ml suspension, that is 50mg and 10mg respectively (Table 4.7).

Table 4.7 Polymer and RSV feed amounts and final suspension volume for preparation of encapsulated RSV NPs

Polymer for RSV encapsulation	Amount of polymer (mg)	Amount of RSV (mg)	Total final suspension volume
mPEG750-PLA1000	10	1	10mL each NP formulation
mPEG750-PCL1000	10	1	
mPEG2000-PLA1000	50	10	

This particle size increase was observed in Cheng *et al.* (2007) where an increase of polymer concentration increased the particle size. The increase of polymer concentration also led to higher DL due to enhanced non-covalent interaction between RSV and PLA of mPEG2000-PLA1000 which contributed to an increase in particle size (Sharma *et al.* 2016). This further demonstrated the impact of the drug:polymer feed ratio and the concentration of each component on the particle size of NPs during a NP formation. In addition, particle size of NPs were dependent on the MW of copolymer dissolved in the organic phase prior to nanoprecipitation as demonstrated by Riley *et al.* (2001) where the particle size of mPEG-PLA block copolymers (PEG MW 5,000Da and PLA varying MWs 2,000-110,000Da) NPs increased with increasing lengths of the hydrophobic chain PLA, however, this trend

was not followed after the PLA length reached 30,100Da. Homs *et al.* (2018) also showed that an increase in PLGA polymer concentration increased the NP size. In addition, the preparation method using mPEG2000-PLA1000 was solvent evaporation method which involved the formation of oil-in-water emulsion in the presence of PVA as a stabiliser and this could have increased its overall particle size.

Blank NPs were between 107nm and 240nm with higher PDI values than the encapsulated RSV NPs. Although particle size reports of blank mPEG750-PLA1000 and mPEG2000-PLA1000 NPs were of good quality, the reports each showed two size distributions leading to PDI values of more than 0.6 (Appendices 7.9.6 and 7.9.10, respectively). The PDI values of these blank NPs asserted that the polymers by themselves could not form a homogenous dispersion possibly due to insufficient PEG for colloidal stability (Wieczorek *et al.* 2015). Despite the mPEG750-PLA1000 being commercially prepared, blank mPEG750-PLA1000 NPs showed two particle size distributions possibly due to the capability of mPEG750-PLA1000 to form micelle-like particles in MQ as discussed in Section 4.5.2.1. In contrast, blank mPEG750-PCL1000 NPs were of single size distributions (Appendix 7.9.8). Following size and zeta potential data from two preparation methods in Table 4.5, the mPEG750-PCL1000 NPs prepared with solvent evaporation method was diluted 1:9 with MQ which not only decreased its particle sizes but also improved the PDI values (data shown in Table 4.6) despite having less PVA at 0.06% *w/v* compared to encapsulated RSV NPs prepared with mPEG2000-PLA1000. This showed that the low PVA concentration was sufficient to provide a stabilising effect on the NP (Agarwal *et al.* 2016). The discussion thus far showed that the fabrication conditions and hydrophobic content of NPs influenced the particle size and distribution of blank and encapsulated RSV NPs.

Conjugated RSV NPs made with mPEG750-PLA1000 were larger than comparable encapsulated RSV NPs with mPEG750-PLA1000-succ-RSV NPs producing almost twice as large and mPEG750-PLA1000-glu-RSV NPs producing more than twice as large as their encapsulated counterpart. This could be due to a larger hydrophobic moiety comprising of RSV, succ or glu linker and PLA in the polymer which created a bigger core in the NP (Yang *et al.* 2012c). Another reason for the larger size of mPEG750-PLA1000-succ-RSV NPs compared to the encapsulated RSV NPs was the preparation

method, that is, solvent evaporation and solvent diffusion, respectively. mPEG750-PLA1000-succ-RSV NPs involved the formation of oil-in-water emulsions using 0.6% *w/v* PVA as a stabiliser which could have enlarged the particles. mPEG750-PLA1000-glu-RSV NPs, however, was prepared by solvent diffusion, similar to the preparation of encapsulated RSV NPs in mPEG750-PLA1000. Almost 45% *w/w* of the conjugated RSV NPs was made up of unconjugated RSV and this could explain the particle size distribution at 190nm (Appendix 7.9.2) which was similar in size to the encapsulated RSV NPs made with mPEG750-PLA1000. Nonetheless, the presence of unconjugated RSV resulted in both conjugated RSV NPs having PDI values much higher than the encapsulated RSV NPs most likely due to the mixture of unconjugated RSV, unconjugated amphiphilic copolymer and RSV conjugated with mPEG750-PLA1000 at various substitution points creating heterogenous suspensions with multiple size distributions as seen in the particle size reports of both conjugated RSV NPs (Appendices 7.9.1 and 7.9.2).

The low percentage of unconjugated RSV in mPEG750-PCL1000-succ-RSV NPs allowed for a single size distribution (Appendix 7.9.3) almost similar in size with the encapsulated RSV NPs made with mPEG750-PCL1000 (Appendix 7.9.9). Nonetheless, the substitution variations of conjugated RSV and small percentage of unconjugated RSV in mPEG750-PCL1000-succ-RSV NPs produced a slightly wider distribution compared to the encapsulated RSV NPs made with mPEG750-PCL1000. The preparation method, however, did not influence the particle size as heavily as conjugated and encapsulated NPs made with mPEG750-PLA1000, possibly due to the very low amount of PVA used for the encapsulated RSV NPs in mPEG750-PCL1000. This observation in addition to those seen in conjugated and encapsulated RSV NPs using mPEG750-PLA1000 demonstrated the effect of the presence of unconjugated RSV when preparing conjugated RSV NPs.

mPEG2000-PLA1000-succ-RSV NPs had a Z-average of less than 50nm with two size distributions (Appendix 7.9.4) which was the smallest particle size formulated in the project as opposed to its encapsulated NPs counterpart being the largest particle size with one size distribution (Appendix 7.9.11) in the project. mPEG2000-PLA1000-succ-RSV NPs were significantly smaller than RSV encapsulated in mPEG2000-PLA1000 as

conjugation to RSV vastly improved the hydrophobic and hydrophilic equilibrium of the polymer for better NP formation. As such, the preparation method for the conjugated RSV NPs required lesser energy input (solvent diffusion) compared with the encapsulated RSV NPs in mPEG2000-PLA1000 prepared by solvent evaporation. Due to the use of solvent evaporation method for the encapsulated RSV NPs, the larger size compared to the conjugated RSV NPs could be explained by the necessary oil-in-water emulsion to incorporate RSV into its oil phase or polymer core. Blank mPEG2000-PLA1000 NPs showed a small distribution of particles at 25nm (Appendix 7.9.10) whereas the mPEG2000-PLA1000-succ-RSV NPs showed a large distribution of particles at 20nm. Both NPs showed another size distribution at 190nm and 140nm, respectively. Although these two NPs were prepared by different methods, it could be an indication that mPEG2000-PLA1000-succ-RSV NPs was capable of micellar formation to form NPs similarly to what was observed in blank mPEG2000-PLA1000 NPs.

Although conjugation of RSV to amphiphilic copolymers has aided in producing NPs with lesser energy input compared with encapsulated RSV NPs, the mixture of unconjugated RSV, unconjugated copolymers and RSV conjugates with various substitutions produced more heterogenous suspensions compared to encapsulated RSV NPs. A direct comparison between conjugated and encapsulated RSV NPs of the same amphiphilic copolymer cannot be made due to the different preparation methods used for respective NPs but some observations could be done with regards to the effect of the presence of unconjugated RSV whilst preparing conjugated RSV NPs and its particle size and distributions.

4.5.2.3 Zeta potential

Blank and encapsulated NPs using mPEG750-PCL1000 had zeta potentials of -20mV whereas blank and encapsulated NPs using mPEG750-PLA1000 with -5mV and -11mV, respectively. Nearly zero zeta potential magnitudes seen in the blank and encapsulated mPEG2000-PLA1000 NPs did not necessarily indicate a physically unstable formulation (Rachmawati *et al.* 2016) as these NPs were stabilised by mPEG and PVA *via* steric stabilisation. The low zeta potential range of RSV encapsulated in mPEG-PLA NPs was also reported in several literatures (Guo *et al.* 2013, Jung *et al.*

2015). A distinct shift to a more negative zeta potential in RSV-loaded mPEG750-PLA1000 and mPEG2000-PLA1000 NPs compared to its corresponding blank NPs might be due to the aromatic ring possessed by RSV which shifted its negative charge to an oxygen atom of the hydroxyl groups, enabling the development of anionic phenoxyl radicals (Soo *et al.* 2016); however, this warrants further investigation. Also, depending on how PVA, the polymer and RSV formed structurally as a NP, the PVA could have led to a more negative zeta potential charge due to the hydroxyl groups present in the PVA or presence of acidic impurities (Xu *et al.* 2009) in the case of mPEG2000-PLA1000 NPs. Blank and encapsulated mPEG750-PCL1000 NPs showed high magnitudes of zeta potential (more than -20mV) despite PEGylated NPs showing a neutral surface charge (Ho *et al.* 2013). The significantly lower concentration of PVA was sufficient to stabilise the mPEG750-PCL1000 NPs as indicated by its zeta potential (Agarwal *et al.* 2016) but was likely not enough to have affected the zeta potential magnitude.

The conjugation to RSV clearly altered the hydrophobicity of the amphiphilic polymers to produce more thermodynamically stable NPs which was discussed in previous sections. As mentioned, this difference was observed in the choice of preparation method for both encapsulated and conjugated RSV NPs. Further scrutiny into their zeta potential values showed a better zeta potential range (-9mV to -35mV) for all conjugated RSV NPs compared to their encapsulated counterparts (0mV to -20mV) except for mPEG750-PLA1000-succ-RSV NPs (-3mV) and this could be attributed to the presence of PVA as a stabiliser. For example, the physical entrapment of RSV in mPEG750-PLA1000 required less external energy input in order to produce a formulation with acceptable physical characteristics whereas the conjugated compounds needed a high energy input *via* solvent evaporation method to emulsify the phases to produce nano-sized particles. Contrary to this polymer, both mPEG750-PCL1000 and mPEG2000-PLA1000 required energy input to entrap RSV into the polymers but when conjugated to RSV, the polymers could form NPs with less energy input *via* solvent diffusion method. Regardless of preparation method, it was clear that conjugation of RSV to the amphiphilic copolymers produced more stable NPs with lesser energy input compared to encapsulation.

4.5.2.4 Drug loading (DL)

Encapsulated RSV NPs allowed for high EE (70%-100%) of RSV and high DL (8.7 and 8.8%) for two out of three NPs assessed. It was interesting to note that the high DL were in mPEG-PLA NPs whereas the low DL of RSV was encapsulated in mPEG750-PCL1000 (2.7%) despite having the same polymer:RSV feed ratio and final suspension volume with RSV encapsulated in mPEG750-PLA1000 (Table 4.7). This difference could be explained by the higher crystalline properties of PCL compared to PLA in our copolymers which decreased the DL capacities as seen in Shuai *et al.* (2004a) where mPEG-PCL copolymers were used to encapsulate DOX. However, when mPEG-PCL was used to encapsulate PTX, a more hydrophobic drug than DOX, an increase in DL was found to be proportional to the increase in the PCL length, indicative of increased crystallinity in the polymer (Shuai *et al.* 2004b). Despite having a similar log P value with PTX (Kim *et al.* 2016), RSV transitioned into an amorphous state when encapsulated in nanosuspensions (Hao *et al.* 2015, Natesan *et al.* 2017) and although shorter PCL lengths have lower crystallinity (Shuai *et al.* 2004a), the non-covalent interactions between amorphous RSV and the low MW PCL component while forming NPs was probably insufficiently strong enough to produce NPs with high DL.

The length of mPEG could have played a crucial role in encapsulating RSV in mPEG750-PCL1000 as found by Wieczorek *et al.* (2015) where a PEG-peptide polymer could not load a hydrophobic compound, m-THPC, due to insufficient PEG to envelope the NP and provide a core for the compound to reside in. As PCL is more hydrophobic than PLA, the mPEG length could have had a greater influence as to how RSV was loaded in the NPs. Therefore, factors like hydrophobicity relative to copolymers and crystallinity transitions of RSV during NP precipitation affected the amount of drug encapsulated in mPEG-PCL. These factors were most likely specific to the drug as drug-polymer affinity and drug partition coefficient in internal and external phases with and without polymer would rely heavily on drug properties (Mittal *et al.* 2007, Grossen *et al.* 2017).

As the preparation method used for mPEG750-PLA1000 and mPEG750-PCL1000 NPs were different, that is, solvent diffusion and solvent evaporation, respectively, the presence of PVA as stabiliser in the solvent evaporation method could have affected

the DL of the NP (Cooper *et al.* 2014). In addition, excess drug during NP preparation could have led to an increase of unentrapped drug which caused a decrease in EE as observed by Pandita *et al.* (2014). Interestingly, the presence of PVA did not affect the production of mPEG2000-PLA1000 NPs. The high concentration of PVA (3% *w/v*) initially used to emulsify the organic and water phases provided a better coating around the particles generating a repulsive force between particles against aggregation (Rachmawati *et al.* 2016) thus preventing drug loss during dilution and precipitation. The high mPEG2000-PLA1000 polymer concentration compared to other polymers also led to higher DL as there was more polymer present to coat the NP core (Sharma *et al.* 2016).

Although we cannot directly compare DL of encapsulated RSV NPs and conjugated RSV NPs because EE was not determined for the latter, we see that the high presence of free RSV in combination with RSV conjugated to amphiphilic copolymers allowed for a higher DL compared to the encapsulated RSV NPs whilst maintaining nano-sized particles. The loading of curcumin was found to be much higher than conventional encapsulated curcumin NPs when curcumin was conjugated to mPEG-PLA with a tris(hydroxymethyl)aminomethane linker *via* ester bonds (Yang *et al.* 2012c).

Although most of our encapsulated RSV NPs had high drug EE, the DL in final NP suspensions were lesser than what was found in conjugated RSV NPs implying that conjugated RSV NPs were able to deliver a higher dose of RSV compared to encapsulated RSV NPs in 1mg NPs. This would be particularly useful since unconjugated RSV could be metabolised rapidly *in vivo* essentially decreasing the dose available for therapeutic effect. In addition, conjugated RSV NPs contained conjugated RSV which were able to decrease the metabolism rate of RSV due to change of the enzyme substrate. It would now be imperative to study the release profiles of conjugated RSV NPs and compare with data obtained from encapsulated RSV NPs to further evaluate their physical attributes.

4.5.3 Release profiles of RSV NPs

Polymeric NPs were not only used to protect its cargo from enzymatic degradation *in vivo* (Masood 2016) but also for cancer therapy due to their preferential

accumulation in cancer tissues *via* the EPR effect (Summerlin *et al.* 2015, Carletto *et al.* 2016) which was useful for passive targeting of cancer tissues by anticancer drugs. Once the NPs were taken up by cancer cells, the cargo, namely anticancer drugs, were released at a sustained rate for maximum therapeutic efficiency (Masood 2016). As demonstrated in this chapter so far, polymeric NPs containing RSV could be formed by a combination of polymeric conjugated with RSV and physical entrapment of free RSV into NPs (conjugated RSV NPs) or by physical entrapment of RSV into polymeric NPs (encapsulated RSV NPs). The release of RSV from conjugated RSV NPs was dependent on the polymer architecture, the interaction between RSV and the polymer-drug conjugate, the DL of RSV in NPs and the particle size (Yang *et al.* 2014). Using PBS as release medium to imitate the physiological fluid in the body (Soo *et al.* 2016), the release profiles of conjugated RSV NPs were ascertained. Release profiles of free RSV and encapsulated RSV NPs were also obtained as a comparison.

4.5.3.1 Release profiles of conjugated RSV NPs

Slower release rates of RSV were generally obtained from NPs with larger particle sizes and higher MW (Wang *et al.* 2016) and considering our conjugated RSV NPs encompassed those characteristics, it was expected that the conjugated RSV NPs would provide a more sustained release profile of total RSV equivalent compared to encapsulated RSV NPs. In addition to the sustained release provided by polymer-drug conjugates (Yang *et al.* 2017), conjugated RSV NPs containing RSV conjugates were able to decrease metabolism rate of RSV by altering the enzyme substrate which could further prolong circulation of RSV *in vivo* and enhance therapeutic efficacy. The covalent bond between drug and polymer can then be easily cleaved enzymatically or through acid/base catalysed hydrolysis *in vivo* (Ke *et al.* 2014). Figure 4.2 depicts the release profiles of conjugated RSV NPs in PBS using total RSV equivalent concentrations, that is, total concentrations of unconjugated RSV and RSV equivalent in RSV conjugates, against free RSV up to 50 hours at 37°C. Note that small error bars will not be visible if smaller than symbols used.

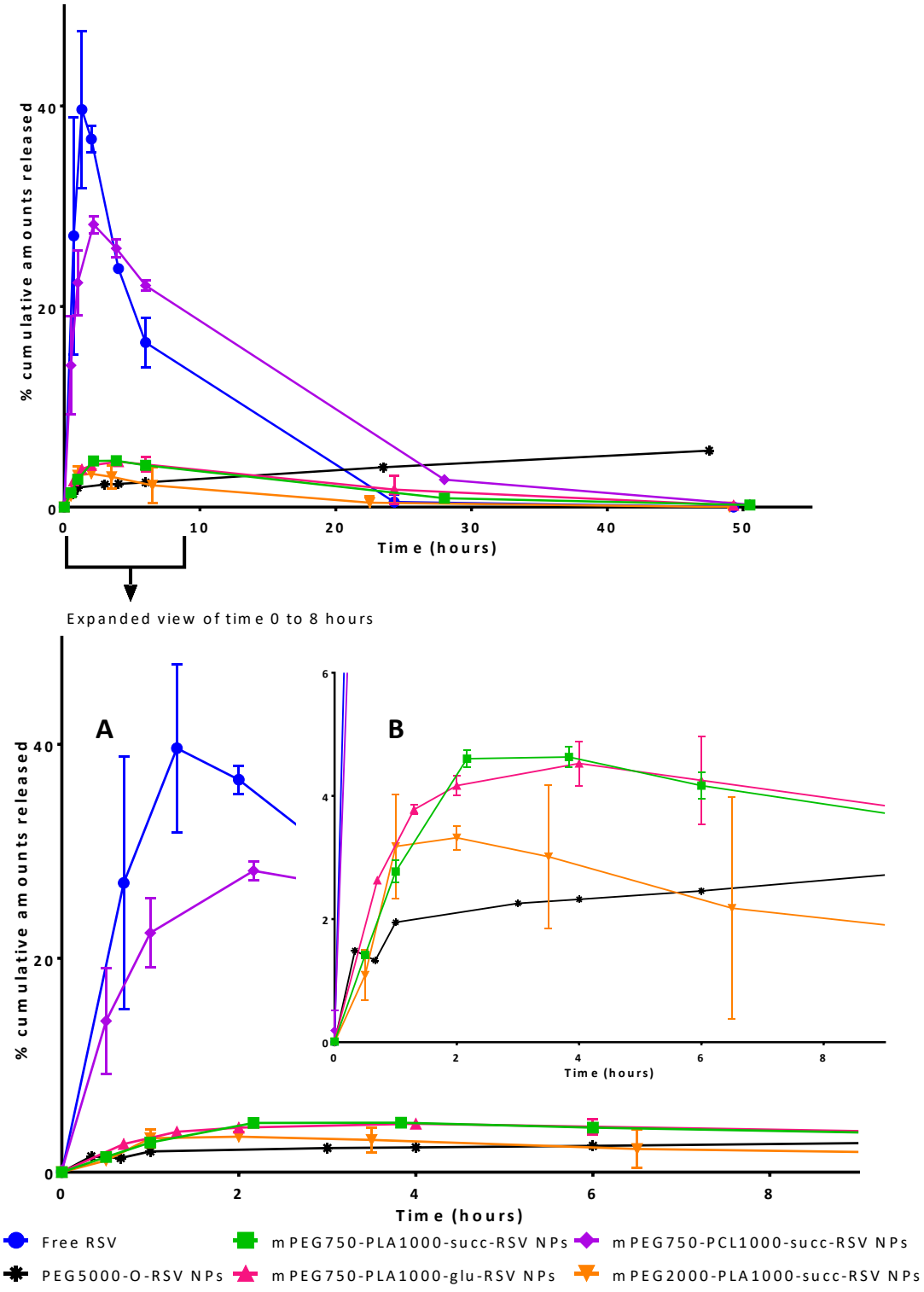

Figure 4.2 Release profiles of total RSV equivalent from conjugated RSV NPs in PBS at 37°C against free RSV for up to 50 hours with (A) an expanded view from 0 to 8 hours (inset B: Smaller scale of % cumulative amounts released of graph A)

Data presented as mean (*n*=2 except mPEG750-PCL1000-succ-RSV NPs where *n*=3 and PEG5000-O-RSV NPs where *n*=1) ± SD where calculated

From Figure 4.2, conjugated RSV NPs provided a sustained release profile of total RSV equivalent when compared to free RSV where approximately 40% of free RSV was released by 1.3 hours followed by a degradation leaving almost no detectable free RSV released by 24 hours. Release profiles of free RSV in PBS at pH7.4 observed by Sanna *et al.* (2013) and Wang *et al.* (2015b) showed an initial burst release the first two hours with almost 100% being released by 3 hours, however, data beyond 6 hours was not reported in both papers. It was unknown whether a degradation of free RSV in the release media PBS was observed beyond 6 hours, however, degradation of RSV in release media in our study was observed by change of colour from colourless or turbid white of NPs and free RSV to dark brown at the end of the release studies in both the release medium and remaining dialysis bag contents. Degradation of curcumin, a natural product similar to RSV, was observed in release studies of encapsulated curcumin NPs by Wang *et al.* (2015a) and Yang *et al.* (2012c).

The degradation of RSV was also possibly translated into the decrease of % cumulative amounts of total RSV equivalent in the release profiles of conjugated RSV NPs. mPEG750-PCL1000-succ-RSV NPs showed higher release rates than other conjugated RSV NPs which peaked at 2.2 hours followed by a decrease in % total RSV equivalent amounts in the NPs. Due to the much lower % total RSV equivalent amounts released by the other conjugated RSV NPs, an expansion was depicted in Figure 4.2B which showed % total RSV equivalent amounts released at its maximum at 3.8 hours, 4 hours and 2 hours for mPEG750-PLA1000-succ-RSV NPs, mPEG750-PLA1000-glu-RSV NPs and mPEG2000-PLA1000-succ-RSV NPs, respectively. After this maximum point, the % cumulative amounts of total RSV equivalent in conjugated RSV NPs decreased steadily possibly due to the degradation of RSV conjugates and/or unconjugated RSV encapsulated in the NPs. The effect of the unconjugated RSV encapsulated in the conjugated RSV NPs will be discussed in Section 4.5.3.2.

The release rates of our ester conjugates depended on several factors including those influencing encapsulated RSV NPs, polymer-RSV conjugate degradation rate, polymer-drug link cleavage, and physical interaction of excess free RSV and polymer-RSV conjugate (Yang *et al.* 2012b, Khalil *et al.* 2013, Alibolandi *et al.* 2015, Yang *et al.* 2018b). The release of RSV from the conjugated RSV NPs could have followed the

sequence depicted in Figure 4.3. Nonetheless, the mechanism of release of RSV from each conjugated RSV NPs is unique and each sequence step could overlap producing a complex order of release mechanisms of RSV from the NPs (Mandal *et al.* 2017).

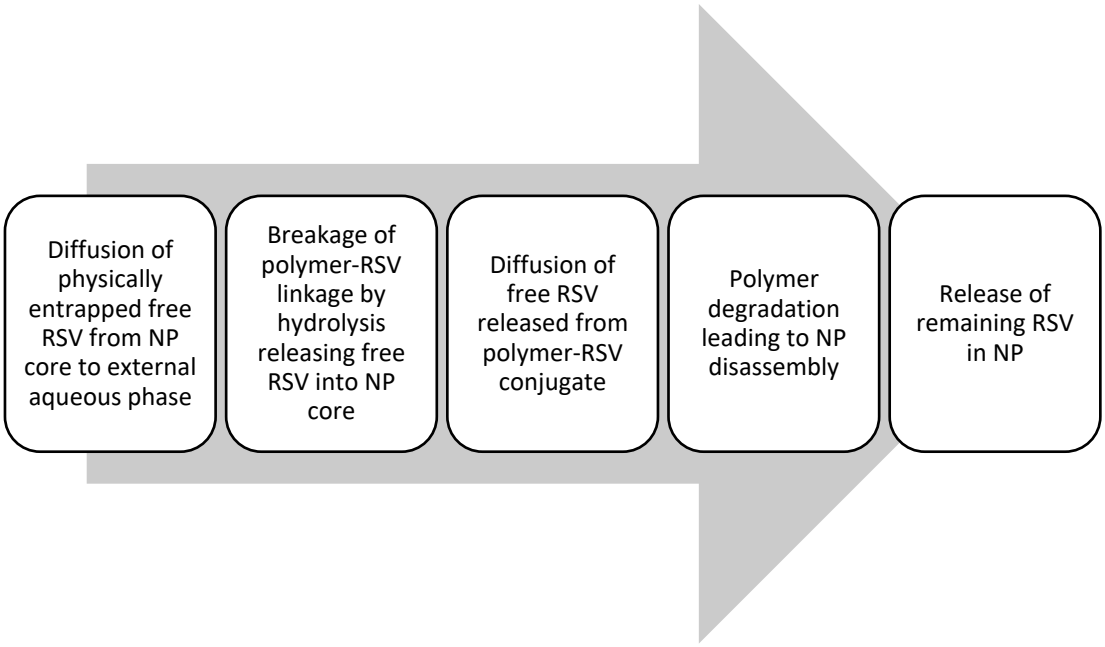

Figure 4.3 Possible sequence of release of RSV from conjugated RSV NPs

mPEG750-PLA1000-succ-RSV NPs and mPEG750-PLA1000-glu-RSV NPs showed favourable release profiles and this could be attributed to its large particle size and presence of PVA. The large particle size decreased the surface area to volume ratio which increased the diffusion barrier required for encapsulated RSV or RSV cleaved from RSV conjugates to be released into external aqueous phase (Alibolandi *et al.* 2015). Sharma *et al.* (2016) suggested that the rapid solvent evaporation method used to prepare mPEG750-PLA1000-succ-RSV NPs produced a smooth NP surface which resulted in a slower release compared to the solvent diffusion methods used for the remaining ester conjugates which utilised a longer solvent evaporation time comparatively, however, this warrants further investigation into the morphology of the NPs which was not carried out due to time limitations.

Despite having the advantage of higher MW for mPEG2000-PLA1000-succ-RSV NPs, and higher crystallinity in mPEG750-PCL1000-succ-RSV NPs, their small particle size (<210nm) could have outweighed those advantages by increasing the surface area to

volume ratio significantly enough to release RSV faster than the other conjugates (Sharma *et al.* 2016). mPEG2000-PLA1000-succ-RSV NPs would have been heavily influenced by its particle size being the smallest particle size (28nm) produced in this project thus far. Small particle sizes encouraged water permeation which led to faster degradation of the polymer-RSV conjugate by hydrolysis of the ester bond between RSV and polymer (Alibolandi *et al.* 2015). This was substantiated by the faster degradation rate of % total RSV equivalent amounts in mPEG2000-PLA1000-succ-RSV NPs and mPEG750-PCL1000-succ-RSV NPs after maximum cumulative amounts were achieved compared to the other ester conjugates. In order to further assess the release profiles of ester conjugated RSV NPs, the release profiles of ester conjugated RSV NPs were depicted according to their two components, which is the % cumulative amounts of RSV conjugate and free RSV component released up to 25 hours (Figure 4.4). The % cumulative amounts of free RSV component (black circle) released was calculated against the initial amounts of total RSV equivalent (RSV and RSV conjugate, black square) in ester conjugated RSV NPs depicted in Figure 4.2. This was carried out similarly for the calculation of % cumulative amounts of RSV conjugate component (grey circle). This allowed us to visualise the release profiles of each component in the conjugated RSV NPs.

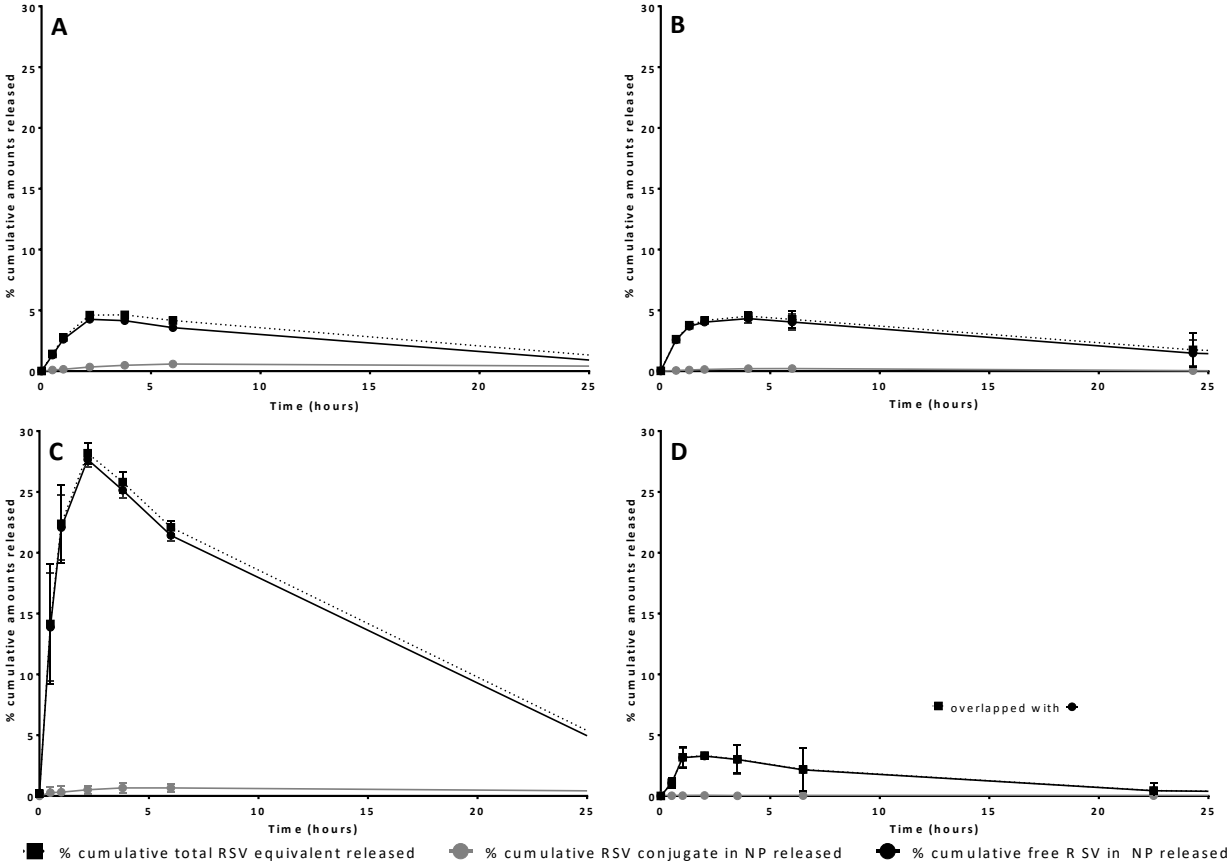

Figure 4.4 Further analysis of % cumulative amounts of free RSV and RSV conjugate components released against initial amount of total RSV equivalent in ester conjugated RSV NPs up to 25 hours in PBS at 37°C

A: mPEG750-PLA1000-succ-RSV NPs, B: mPEG750-PLA1000-glu-RSV NPs, C: mPEG750-PCL1000-succ-RSV NPs, D: mPEG2000-PLA1000-succ-RSV NPs
Data presented as mean (*n*=2 except mPEG750-PCL1000-succ-RSV NPs where *n*=3) ± SD where calculated

Using HPLC gradient method (Section 3.4.2.2), individual free RSV and RSV conjugate peak areas detected over the release study experiment were converted into amounts of RSV and RSV conjugate, respectively, and % of each component released was calculated against the total RSV equivalent amounts initially added to form conjugated RSV NPs and depicted in Figure 4.4. The % cumulative release of ester conjugated NPs using the total RSV equivalent amounts released against the initial total RSV equivalent amounts added into the dialysis bags was presented in Figure 4.2 and with this, Table 4.8 summarises their maximum % of cumulative amounts of RSV equivalent released. In addition, the time points when maximum % cumulative amounts of each component (RSV conjugate and RSV) in the conjugated RSV NPs were also summarised in this table (t_{max}). Beyond these time points, a decrease in % cumulative amounts at varying degrees was observed in both components, less so in RSV conjugate components. Even though the total RSV equivalent in mPEG750-PLA1000-succ-RSV NPs were released to a maximum of 4.6% at 3.8 hours, the RSV conjugate component in the NPs was only released to a maximum of 0.6% at 6 hours whereas the free RSV component in the NPs was released to a maximum of 4.3% at 2.2 hours. This showed the different release rates of RSV when encapsulated in and conjugated to polymeric NPs. Table 4.8 summarises the time points at which maximum % cumulative amounts of each component and total RSV equivalent in conjugated RSV NPs were released.

Table 4.8 Time points when maximum % cumulative amounts of each component against total RSV equivalent was released (t_{max}) from ester conjugated RSV NPs in PBS at 37°C

Conjugated RSV NPs	% *w/w* RSV conjugate in NPs	Total RSV equivalent		Free RSV component		RSV conjugate component[a]	
		t_{max} (h)	Maximum cumulative amounts released (%)	t_{max} (h)	Maximum cumulative amounts released (%)	t_{max} (h)	Maximum cumulative amounts released (%)
Free RSV[b]	NR	1.3	39.6±7.9	1.3	39.6±7.9	NR	
mPEG750-PLA1000-succ-RSV NPs	63.9	3.8	4.6±0.2	2.2	4.3±0.1	6.0	0.6±0.10
mPEG750-PLA1000-glu-RSV NPs	54.8	4.0	4.5±0.4	4.0	4.3±0.4	6.0	0.2±0.02
mPEG750-PCL1000-succ-RSV NPs	99.3	2.2	28.2±0.9	2.2	27.7±0.6	6.0	0.7±0.30
mPEG2000-PLA1000-succ-RSV NPs	76.1	2.0	3.3±0.2	2.0	3.3±0.3	2.0	0.04±0.06

Data presented as mean (*n*=2 except mPEG750-PCL1000-succ-RSV NPs where *n*=3) ± SD where calculated

[a]RSV conjugate component was calculated using RSV equivalent amounts in RSV conjugate

[b]RSV stock in DMSO diluted with PBS and loaded into dialysis bag (Section 4.4.2.3)

All ester conjugated RSV NPs showed that their free RSV components were initially released almost similarly to non-formulated free RSV followed by a slower degradation than free RSV possibly due to the protective layer of the polymeric NPs. Interestingly, mPEG750-PLA1000-glu-RSV NPs released its free RSV component maximally at 4.0 hours, 2 hours longer than the other NPs, most likely due to its large particle size. The highest release of free RSV components amongst all other ester conjugated RSV NPs was by mPEG750-PCL1000-succ-RSV NPs with 27.7% released by 2.2 hours. It was possible that the higher crystallinity environment within the NPs due to the presence of the PCL chain and high % *w/w* of RSV conjugate compared to free RSV in NPs caused a rapid release of free RSV, which was amorphous in nature, into the release media. The RSV conjugate components of all ester conjugated RSV NPs showed a slower release of RSV equivalent amounts where maximum % cumulative amounts were released at 6 hours except for mPEG2000-PLA1000-succ-RSV. This rapid release of mPEG2000-PLA1000-succ-RSV component compared to the other RSV conjugate components of conjugated RSV NPs could possibly be due to the small particle size of mPEG2000-PLA1000-succ-RSV NPs. Therefore, the release profiles of total RSV equivalent and individual components were related to the NP particle size where the larger particles allowed for slower release of components, however, due to the weaker hydrophobic interactions between free RSV encapsulated in conjugated RSV NPs compared to the strong covalent bonds in RSV conjugates, most of the total RSV equivalent amounts released up to 50h were attributed to the free RSV component of the conjugated RSV NPs. Another factor to consider is the stability of each component in the ester conjugated RSV NPs as the stability of the RSV conjugate affects the stability of the NP structure which in turn affects the stability and release of RSV (free RSV and RSV cleaved from RSV conjugate). Figure 4.5 depicts the change of % *w/w* of RSV and RSV conjugate components in ester conjugated RSV NPs up to 48 hours in PBS at 37°C compared with the initial % *w/w* of each component in ester conjugated RSV NPs. This gave us a representation of how NPs behaved in PBS without considering the release kinetics of NPs in dialysis bags.

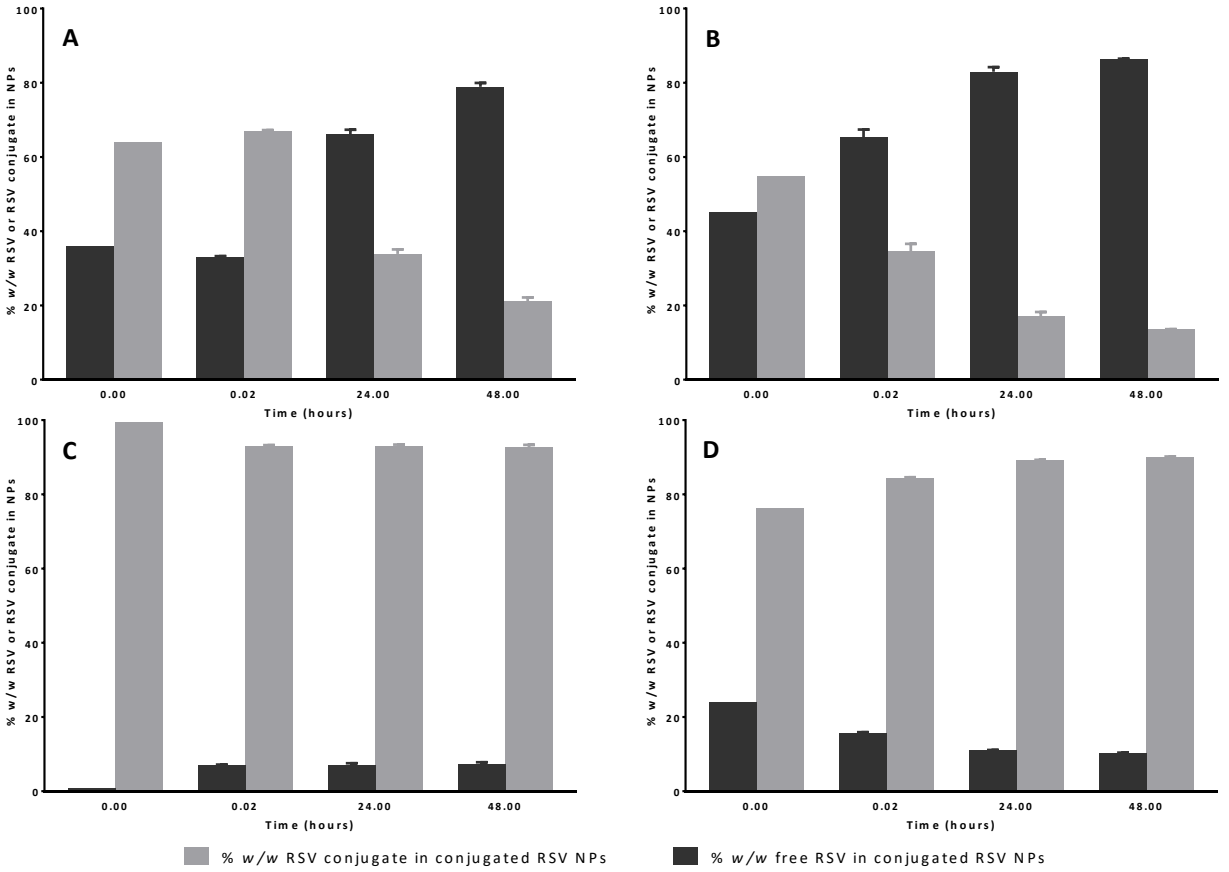

Figure 4.5 Stability of ester conjugated RSV NPs by individual component weights of free RSV (black) and RSV conjugate (grey) in PBS pH7.4 at 37°C for up to 48 hours

A: mPEG750-PLA1000-succ-RSV NPs, B: mPEG750-PLA1000-glu-RSV NPs, C: mPEG750-PCL1000-succ-RSV NPs, D: mPEG2000-PLA1000-succ-RSV NPs
Data presented as mean (*n*=3 except mPEG750-PLA1000-glu-RSV NPs and mPEG2000-PLA1000-succ-RSV NPs where *n*=2) ± SD where calculated

Components in mPEG750-PCL1000-succ-RSV NPs were stable from point of addition into release media without dialysis bag to up to 48 hours. The addition of NPs into PBS slightly decreased the amount of RSV conjugate and increased the amount of RSV within the NPs due to the hydrolysis of polymer-RSV bond releasing RSV into the NP core or the breakdown of some RSV conjugates on NP surface. This could explain the high amount of free RSV released from the NPs into the release media in Figure 4.6. The hydrolysable ester bond in mPEG750-PCL1000-succ-RSV could have been protected within the NP core to a certain extent which also contributed to the NP structure stability (Zhang *et al.* 2017) hence the very low amount of RSV conjugate component and slower release of the conjugate from the dialysis bag. In other words, the release of total RSV equivalent amounts from mPEG750-PCL1000-succ-RSV NPs was more dependent on the RSV encapsulated or cleaved from the RSV conjugate than the conjugate itself.

Conversely, the components in mPEG750-PLA1000-succ-RSV NPs were not affected as much by the release media at the point of addition which showed that the NP formation included all RSV conjugates and free RSV found in the final synthesised product. However, the amount of RSV conjugate decreased over time with an increase of the RSV component. This showed a breakdown of the NP structure which released RSV into the NP core however the encapsulated RSV was not fully released into the media which would be depicted with a decrease in the amounts of RSV as well. This was portrayed similarly by the components in mPEG750-PLA1000-glu-RSV NPs with the RSV conjugate component being slightly less stable than its succinated counterpart. These observations explain the lower cumulative amounts of RSV conjugate in mPEG750-PLA1000-glu-RSV NPs released into the release media PBS compared to the conjugate in mPEG750-PLA1000-succ-RSV NPs. Nonetheless, the slower release rates of both components in mPEG750-PLA1000-glu-RSV NPs compared to mPEG750-PLA1000-succ-RSV NPs was most likely due to the particle size rather than the stability of the components within the NPs as the larger mPEG750-PLA1000-glu-RSV NPs would require a longer diffusion time for the release of its components into the release media.

mPEG2000-PLA1000-succ-RSV NPs components revealed an interesting pattern

where the % *w/w* RSV conjugate component increased and the free RSV component decreased. This could be explained by a rapid release of the free RSV component from within the NP core due to the small particle size. There was also a possibility of the presence of free RSV on the particle surface rather than entrapped RSV within the core (Coradini *et al.* 2014) which was released more easily and incidentally could explain the small particle size of mPEG2000-PLA1000-succ-RSV NPs. The RSV conjugate component in the NPs was most likely stable as the % *w/w* of the conjugate component continued to increase instead of decrease which was expected with the rapid release and degradation of RSV from the NP core. This correlated with the maximum % cumulative amount of RSV conjugate component released at 2.0 hours (3.3%) where the stable RSV conjugate was only minimally released. Nonetheless, the small particle size of mPEG2000-PLA1000-succ-RSV NPs would have heavily influenced the degradation of the RSV conjugate itself as water permeation into the NP core would have encouraged hydrolysis of the conjugate.

Overall, the stability of the RSV conjugate components in the ester conjugated RSV NPs correlated with the type and MW of their respective polymers with mPEG750-PLA1000 degrading the fastest followed by either mPEG750-PCL1000 or mPEG2000-PLA1000. It was difficult to differentiate between mPEG750-PCL1000-succ-RSV and mPEG2000-PLA1000-succ-RSV components as mPEG2000-PLA1000-succ-RSV NPs was highly affected by its very small particle size compared to the other ester conjugated RSV NPs. The stability order of ester conjugate components was related to the length of mPEG where a longer mPEG length (Bolourchian *et al.* 2013) and a more hydrophobic PCL (Goyal *et al.* 2016) improved the stability of polymers. The longer glu linkage in mPEG750-PLA1000-glu-RSV did not improve the stability of mPEG750-PLA1000-succ-RSV where the degradation of the conjugate was 73% as opposed to 80%, respectively, because of easier access for hydrolysis of the ester bonds. It would be noteworthy to synthesise this conjugate with much longer linkers to effectively observe the effect. Nonetheless, it should be noted that the succ and glu linkages on the ester conjugates have electron withdrawing groups which destabilised drug-polymer link which could have led to hydrolysis (Wang *et al.* 2016). In addition, the ester bond between mPEG and the hydrophobic PCL or PLA could

cause the depolymerization of the NP which led to release of RSV (Ye *et al.* 2014).

The higher PDI values in all ester conjugated RSV NPs except mPEG750-PCL1000-succ-RSV NPs (Appendices 7.9.1, 7.9.2 and 7.9.4) showed heterogenous suspensions which could explain the complicated release profiles where different types of NPs (encapsulated, conjugated or encapsulated-conjugated particles) were releasing RSV concurrently each with different release kinetics. The complex release kinetics of ester conjugated RSV NPs was influenced by the amount of free RSV present, degradation rate of encapsulated RSV and conjugated RSV components and the release kinetics of individual components in the NPs (Mandal *et al.* 2017). The complex release kinetics of total RSV equivalent from the ether conjugate PEG5000-O-RSV NPs could also be explained by the cumulative release profiles and the stability profiles of each component in the ether conjugated RSV NPs.

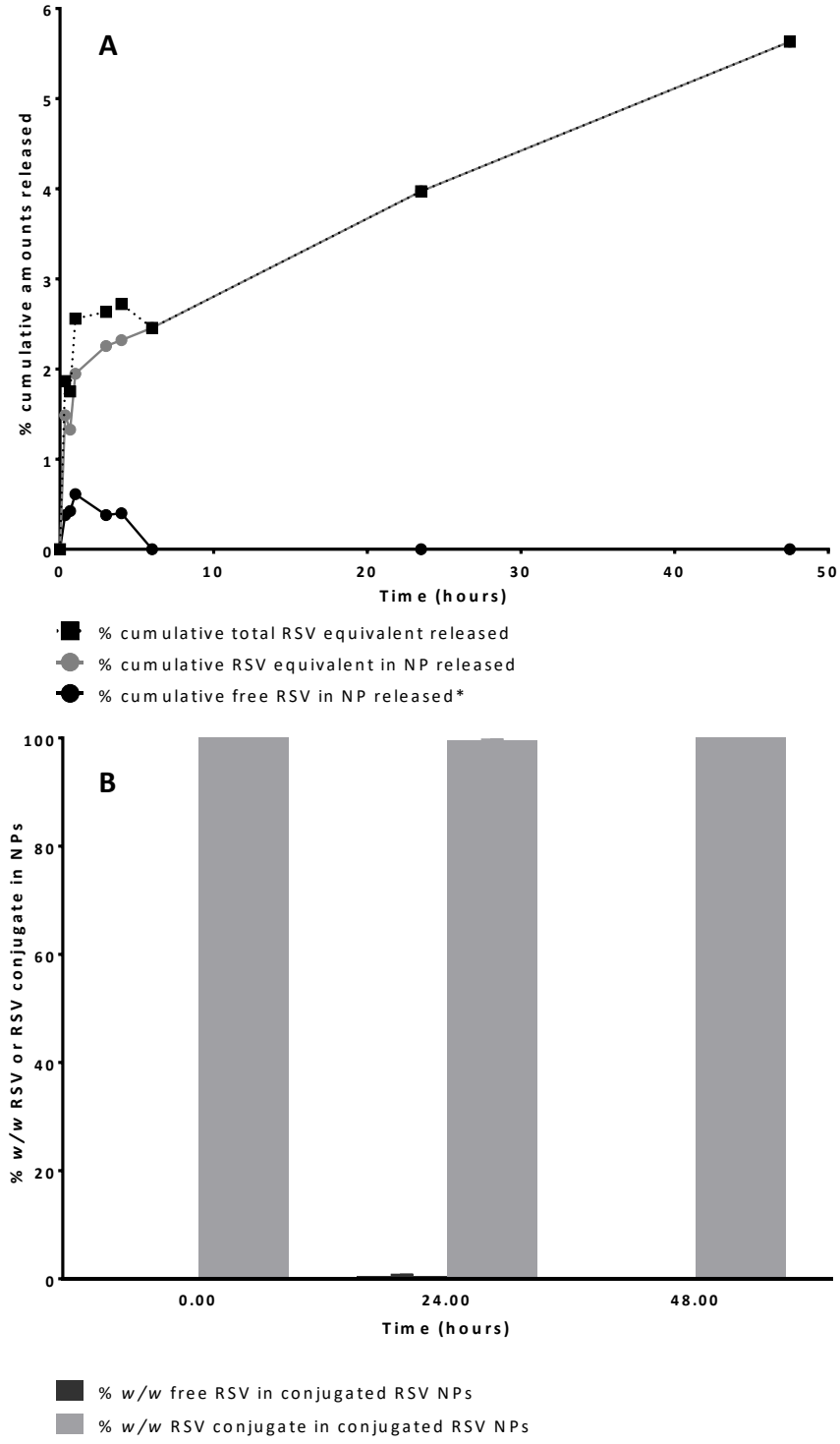

Figure 4.6 (A) Further analysis of % cumulative amounts of free RSV and RSV conjugate components released against initial amount of total RSV equivalent in PEG5000-O-RSV NPs up to 25 hours in PBS at 37°C (*n*=1) and (B) Stability of free RSV and RSV conjugate components in PEG5000-O-RSV NPs in PBS pH7.4 at 37°C for up to 48 hours

Stability data presented as mean (*n*=2) ± SD with no free RSV present at time 0 hours
*% cumulative amounts of free RSV component in NPs released was calculated against total amount of free RSV released throughout release study as opposed to amount initially added as no free RSV was initially present in NPs

As expected due to its strong ether bond, the PEG5000-O-RSV NPs showed a slow sustained release throughout the study up to 50 hours where at 50 hours, only 5.6% total RSV equivalent of the RSV conjugate in the NPs were released. From Figure 4.6A, the cumulative release of free RSV was rapid for the first hour similar to what was seen for free RSV followed by degradation of RSV. As the conjugate did not have free RSV present (Table 4.3), the free RSV component in its cumulative release profile was minor and the overall release profile of PEG5000-O-RSV was mainly dependent on the RSV conjugate component. Due to the very stable ether conjugate compared to the ester conjugates, the release profiles of the ether conjugate component in PEG5000-O-RSV NPs did not show degradation as seen in the release profiles of individual components in ester conjugated RSV NPs in Figure 4.4. The stability of PEG5000-O-RSV conjugate was due to its stronger covalent bond to the polymer *via* the ether bond compared to the ester conjugates making it an ideal sustained release candidate in cancer therapy (Basavaraj 2011), however, this bond could be detrimental as RSV could not be released in a timely and convenient manner *in vivo*.

As previously discussed, the complex release profile of conjugated RSV NPs was due to the combination of having free RSV encapsulated in and conjugated RSV forming the conjugated RSV NPs. Therefore, a study on the release profiles of encapsulated RSV NPs was warranted. Although the encapsulated RSV NPs could not be a direct comparison to the conjugated RSV NPs due to the diverse physical attributes caused by different preparation methods and levels of free RSV and RSV conjugates, a correlation could be drawn between the release profiles of encapsulated RSV NPs and the release profiles of the free RSV components in conjugated RSV NPs. The following section discusses the release profiles of encapsulated RSV NPs and possible correlations with release profiles of conjugated RSV NPs, in particular the release profiles of the free RSV component in conjugated RSV NPs.

4.5.3.2 Release profiles of encapsulated RSV NPs

Figure 4.7 depicts the release profiles of encapsulated RSV NPs against free RSV for up to 30 hours.

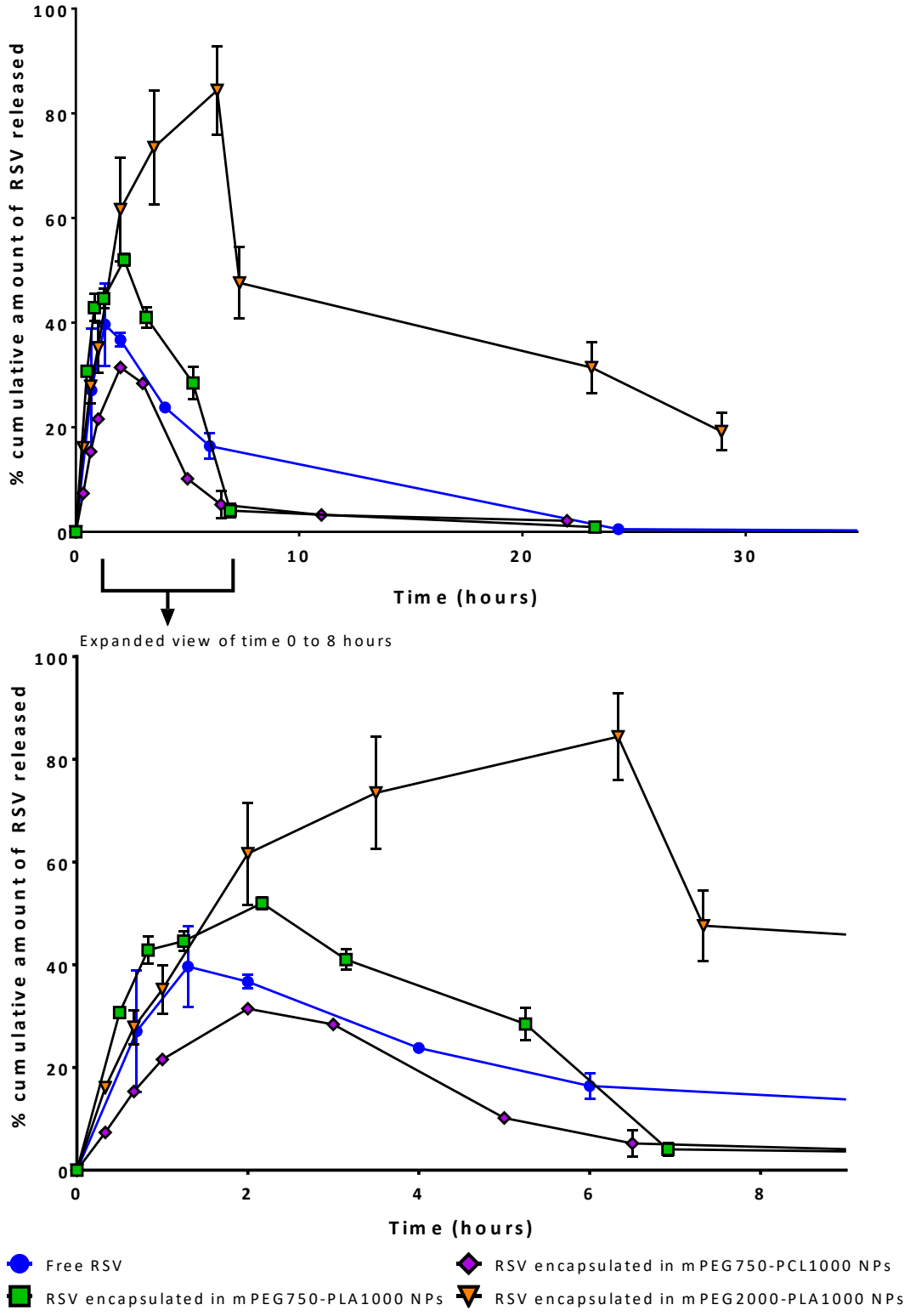

Figure 4.7 Release profiles of encapsulated RSV NPs against free RSV for up to 30 hours with an expanded view from 0 to 8 hours in PBS at 37°C

Data presented as mean (*n*=2 except RSV encapsulated in mPEG750-PLA1000 NPs where *n*=3) ± SD

The degradation of RSV in nano-structures was reported recently by Zupancic *et al.* (2015) where RSV loaded into PCL nanofibers showed a sustained release of RSV in PBS at pH7.4 and 37°C for up to three hours followed by a degradation. It was speculated that for the first three hours, release kinetics was more dominant than the degradation kinetics of RSV which showed the sustained release profile. Following this, the sustained release was slower compared to the degradation rate of RSV translating into the decreasing amount of RSV in the release medium. This could be the case for our encapsulated RSV NPs and also our conjugated RSV NPs where the conjugated RSV NPs were not only influenced by the degradation rate of RSV but also of RSV conjugate. Due to differing degradation kinetics of each conjugate and RSV, the release profiles of conjugated RSV NPs and encapsulated RSV NPs depicted in Figure 4.2 and Figure 4.7, respectively, were more complex than previously discussed.

Encapsulated RSV NPs provided a slower release of RSV than free RSV until degradation of RSV was seen from 2 hours for RSV encapsulated in mPEG750-PLA1000 and mPEG750-PCL1000 NPs and from 6.5 hours for RSV encapsulated in mPEG2000-PLA1000 NPs. Sanna *et al.* (2013) showed a sustained release of RSV encapsulated in PEG-PLGA-PCL NPs with 55% of RSV released in PBS at pH7.4 at 37°C within 7 hours whereas Wang *et al.* (2015b) showed 51% of RSV encapsulated in mPEG-PCL NPs with TPGS was released within 6 hours in PBS at pH7.4 at 37°C. Figure 4.7 showed both mPEG750-PLA1000 and mPEG750-PCL1000 NPs (maximum cumulative amounts released at 52.0% and 31.4% respectively) had similar release profile patterns with higher amounts of RSV released by mPEG750-PLA1000 NPs due to higher crystallinity of PCL component in mPEG750-PCL1000 polymers compared to PLA component in mPEG750-PLA1000 polymers (Yin *et al.* 2014, Gupta *et al.* 2015, Goyal *et al.* 2016) which attributed to a more stable polymer. This factor also contributed to the slower initial release rate of mPEG750-PCL1000 NPs compared to mPEG750-PLA1000 NPs. RSV encapsulated in mPEG2000-PLA1000 NPs produced a sustained release profile with a maximum of 84.4% of RSV was released at 6.3 hours. Following that, a much slower degradation rate of RSV was observed compared to mPEG750-PLA1000 and mPEG750-PCL1000 NPs where at 8 hours, 50% of RSV still

remained compared to less than 10% in free RSV and mPEG750-PLA1000 NPs and mPEG750-PCL1000 NPs. RSV encapsulated in mPEG2000-PLA1000 NPs was largest in particle size in the project thus far (Table 4.6) being almost twice larger than encapsulated NPs made with mPEG750-PLA1000 and mPEG750-PCL1000. This decreased its surface area to volume ratio significantly and increased the barrier distance between the NP core and external aqueous phase (Alibolandi *et al.* 2015, Sharma *et al.* 2016). Due to these characteristics, diffusion of RSV from the NP core to the external phase was slower compared to mPEG750-PLA1000 and mPEG750-PCL1000 NPs (Vassiliou *et al.* 2010). Table 4.9 summarises the t_{max} and maximum % cumulative amounts of RSV released from encapsulated RSV NPs.

Table 4.9 Time points when maximum % cumulative amounts of RSV was released from encapsulated RSV NPs in PBS at 37°C

Encapsulated RSV NPs	**Initial concentration in release study (mg/mL)[a]**	**t_{max} (h)**	**Maximum cumulative amounts released (%)**
Free RSV[b]	≈0.1	1.3	39.6±7.9
RSV in mPEG750-PLA1000 NPs	0.11	2.2	52.0±1.2
RSV in mPEG750-PCL1000 NPs	0.04	2.0	31.4±0.4
RSV in mPEG2000-PLA1000 NPs	1.02	6.3	84.4±8.5

[a]Concentration of encapsulated RSV NPs according to EE except free RSV
[b]RSV stock in DMSO diluted with PBS and loaded into dialysis bag (Section 4.4.4.4)
Data presented as mean (*n*=2 except RSV encapsulated in mPEG750-PLA1000 NPs where *n*=3) ± SD

As the release rate of RSV from various nano-sized DDS in water at 37°C (Hao *et al.* 2016, Siu *et al.* 2018) and the degradation rate of RSV in PBS pH7.4 at 37°C was according to first-order kinetics (Robinson *et al.* 2015, Zupancic *et al.* 2015), the concentration of RSV in the encapsulated RSV NPs should be a direct proportion to the release and degradation rates of the NPs. It should be noted that the release kinetics of RSV in nanosuspensions *in situ* gels was found to fit a few release models including zero-order, first-order and Higuchi model as demonstrated by Hao *et al.* (2016) which indicated that NPs containing RSV could follow several release models.

From Table 4.9, the release rate of RSV from encapsulated RSV NPs, that is amount released over time, was correlated with the concentration of RSV in the NPs however we could not substantiate this when amount of RSV released started to decrease due to the overlapping effects of release and degradation rates of RSV from encapsulated RSV NPs. Nonetheless, the release profiles of encapsulated RSV NPs should not ignore the factors of particle size and polymer architecture which could also influence the stability of the NPs. When RSV diffuses into release media PBS from the dialysis bags, PBS diffuses into the dialysis bag due to the concentration gradient between the contents of the dialysis bag (encapsulated RSV NPs) and release media. Thus, the presence of PBS and its pH in the dialysis bag containing the encapsulated RSV NPs could affect the stability of the NPs. Figure 4.8 portrays the stability of encapsulated RSV NPs in PBS at 37°C against free RSV up to 48 hours at 37°C without the use of a dialysis bag.

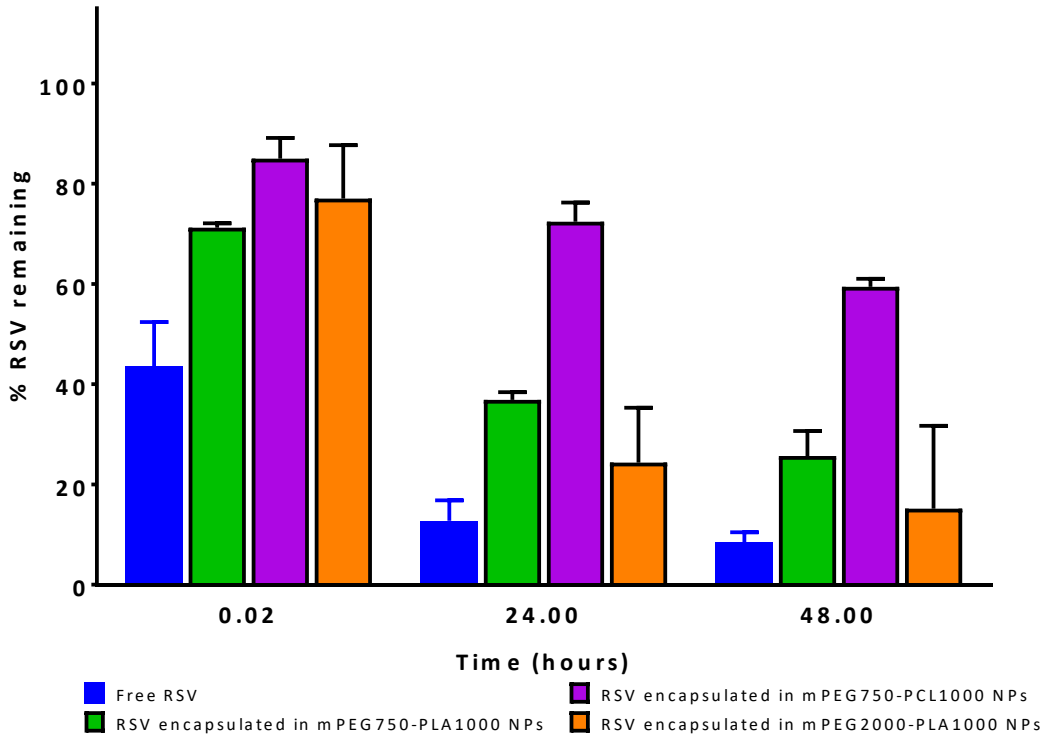

Figure 4.8 Stability of encapsulated RSV NPs in PBS pH7.4 at 37°C against free RSV for 48 hours without dialysis bag

Data presented as mean (*n*=2 except free RSV where *n*=3) ± SD

It was clear that encapsulation of RSV protected RSV from degradation as seen in

Sessa *et al.* (2014) with RSV encapsulated in mPEG750-PCL1000 giving the best protection due to higher crystallinity compared to mPEG-PLA NPs (Gupta *et al.* 2015, Goyal *et al.* 2016). Interestingly, mPEG2000-PLA1000 was less stable than mPEG750-PLA1000 NPs despite having a higher MW and longer hydrophilic mPEG chain length which warrants further investigation. Although physical entrapment of RSV by polymeric NPs have increased the chemical stability of RSV compared to free RSV, degradation of the surrounding polymeric NP and subsequent release and degradation of RSV when exposed to physiological pH of 7.4 in the dialysis bag would have possibly degraded the RSV before it could be released from the dialysis bag into the release media for analysis. As the specific release and degradation rates were not studied in this project, it was difficult to discern which rate was faster at precise stages of the release study. Therefore, the release profiles of encapsulated RSV NPs in Figure 4.7 were a result of a combination of factors including the individual release rates of RSV from NPs followed by the degradation rate of RSV in the release media, the individual stability profiles of NPs which led to premature release of RSV in the dialysis bag, the degradation of RSV in the dialysis bag thereafter and the release and degradation rates of remaining RSV released into the release media.

Using the data from the release study of encapsulated RSV NPs (Table 4.9), we could draw some conclusions for the release profiles of conjugated RSV NPs, in particular the release profiles of the free RSV component of the NPs in Table 4.8. Encapsulated RSV NPs using mPEG750-PLA1000 achieved a % maximum cumulative amount of RSV released at 2.2 hours which was similar to what was achieved by the free RSV component in mPEG750-PLA1000-succ-RSV NPs, however this was not the case for mPEG750-PLA1000-glu-RSV NPs where the % maximum cumulative amount of free RSV released was at 4.0 hours. This could be explained by its larger particle size compared to mPEG750-PLA1000-succ-RSV NPs which caused a slower diffusion of RSV from the NP core into the release media. The rapid release of free RSV component in mPEG750-PCL1000-succ-RSV NPs was similar to its encapsulated RSV NPs counterpart at approximately 2 hours, however, the high amounts of RSV released from the conjugated RSV NPs compared to the encapsulated RSV NPs was probably due to the minimal % *w/w* of free RSV possibly on the surface of the

conjugated RSV NPs which caused a fast release of all of the RSV in the NPs. Interestingly, the release of RSV from encapsulated RSV NPs made with mPEG2000-PLA1000 (% maximum cumulative amounts of RSV achieved at 6.3 hours) was contradictory to the release of free RSV component in mPEG2000-PLA1000-succ-RSV NPs (2.0 hours) which could be due to the particle size difference of both NPs where the encapsulated RSV NPs was the largest (350nm) in the project and conjugated RSV NPs was the smallest (25nm) in the project. The smaller conjugated RSV NPs was more prone to water permeation and because of the shorter diffusion distance between the NP core to the external phase, the free RSV component was released much earlier than its encapsulated RSV NPs counterpart.

4.5.3.3 Comparison of release profiles of RSV NPs

As a general comparison, the release profiles of free RSV, RSV encapsulated in mPEG750-PLA1000 NPs and two conjugated RSV NPs (PEG5000-O-RSV ether conjugate NPs and mPEG750-PLA1000-succ-RSV ester conjugate NPs) were displayed in Figure 4.9.

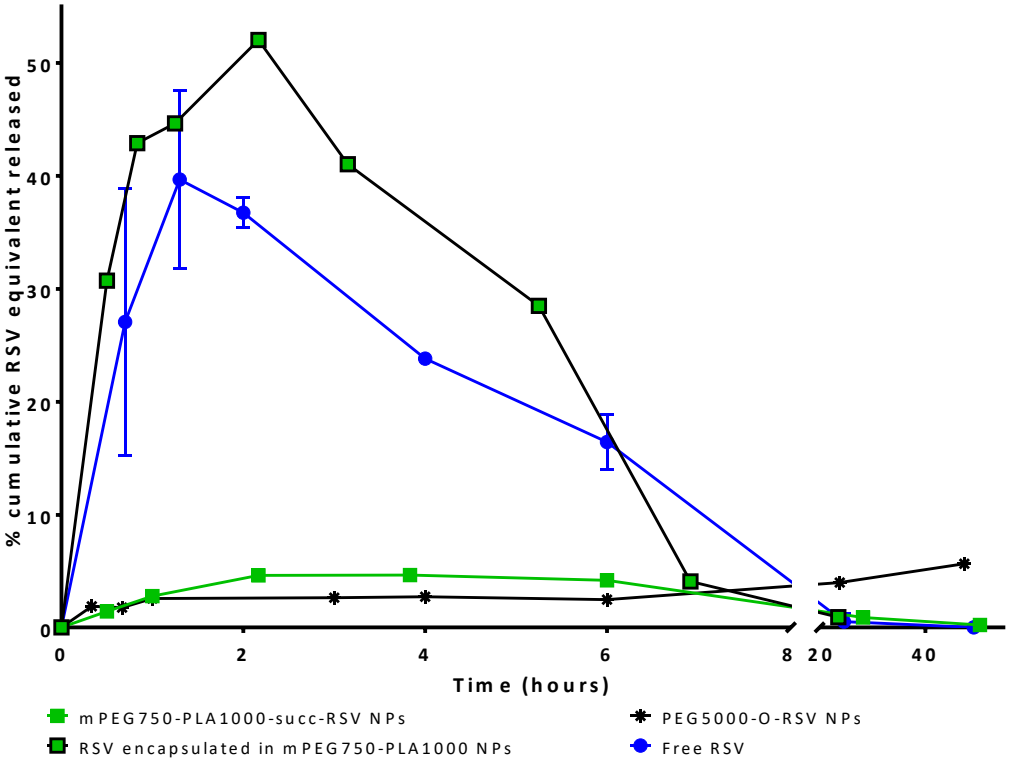

Figure 4.9 Comparison of release profiles of % cumulative amounts of RSV released from free RSV, ester conjugated mPEG750-PLA1000-succ-RSV NPs, RSV encapsulated in mPEG750-PLA1000 NPs and ether conjugated PEG5000-O-RSV NPs in PBS at 37°C for up to 40 hours

Data presented as mean (*n*=3 except free RSV where *n*=2 and PEG5000-O-RSV NPs where *n*=1) ± SD where calculated

Firstly, NP formulation provides a slower or sustained release of total RSV equivalent regardless of type, that is, encapsulation or conjugation. The release rate of RSV from encapsulated RSV NPs was faster and higher in % released than both conjugated RSV NPs due to its weaker non-covalent interaction between RSV and mPEG750-PLA1000 whereas mPEG750-PLA1000-succ-RSV NPs and PEG5000-O-RSV NPs had stronger covalent bonds between RSV and their respective polymers in the RSV conjugates (Wang *et al.* 2016) and better non-covalent interaction between RSV and RSV-polymer conjugate. The release rate was dependent on the type of polymer-RSV bond where the ether bond in PEG5000-O-RSV conjugate provided a much stronger bond than the ester bond in mPEG750-PLA1000-succ-RSV conjugate, rendering the PEG5000-O-RSV NPs having a longer and slower sustained release comparatively. The lower % cumulative amounts of total RSV equivalent released from mPEG750-PLA1000-succ-RSV NPs and PEG5000-O-RSV NPs (<6% maximum) compared to RSV

encapsulated in mPEG750-PLA1000 NPs (52.0% maximum) could have significant tumour suppression efficacy (Luo *et al.* 2016b) by allowing enough time for tumour tissues to uptake the NPs for maximum therapeutic effect of RSV (Sessa *et al.* 2014). The longer sustained release of RSV from PEG5000-O-RSV NPs could be applied *in vivo* however the therapeutic effects of the NPs are yet to be confirmed due to the strong ether bond between PEG5000 and RSV and high stability of the RSV conjugate in PBS (Figure 4.6).

4.5.4 Selection of suitable formulations for further *in vitro* and *in vivo* studies

In order to establish the suitability of NP formulations developed in this chapter for further *in vitro* and *in vivo* studies, the characteristics of NPs are summarised in Table 4.10 for blank and encapsulated RSV NPs and Table 4.11 for conjugated RSV NPs.

Table 4.10 Summary data of novel blank and encapsulated RSV NPs using low MW polymers

Formulation	Particle size (nm)	PDI	Zeta potential (mV)	EE (%)	DL (%)	Release study		Stability of NPs in PBS at 37°C after 24 hours (%)[b]
						t_{max} (h)	$\%_{max}$[a]	
Free RSV	NR	NR	NR	NR	NR	1.3	39.6±7.9[2]	12.8±4.1[3]
Blank NPs								
mPEG750-PLA1000	239.6±12.8[2]	0.641±0.064[2]	-5.3±1.6[3]	NR	NR	NR		ND
mPEG750-PCL1000	107.6±3.0[3]	0.234±0.008[3]	-21.3±1.9[3]	NR	NR	NR		ND
mPEG2000-PLA1000	124.0±1.4[3]	0.699±0.023[3]	2.2±0.5[3]	NR	NR	NR		ND
Encapsulated RSV NPs								
RSV in mPEG750-PLA1000	162.2±2.9[3]	0.062±0.024[3]	-11.0±0.4[3]	95.1±0.1[2]	8.7±0.1[2]	2.2	52.0±1.2[3]	36.9±1.6[2]
RSV in mPEG750-PCL1000	201.0±4.2[3]	0.042±0.038[3]	-20.1±0.4[3]	72.4±4.5[3]	2.7±0.2[3]	2.0	31.4±0.4[2]	72.4±3.8[2]
RSV in mPEG2000-PLA1000	345.5±5.5[3]	0.087±0.074[3]	-0.5±0.1[3]	96.9±0.1[2]	8.8±0.1[2]	6.3	84.4±8.5[2]	24.4±10.9[2]

Data presented as mean (*n*=superscript numbers) ± SD where calculated

[a]Maximum % cumulative amounts of RSV released

[b]Data presented as % RSV remaining after NPs were in PBS pH7.4 at 37°C for 24 hours

Table 4.11 Summary data of novel conjugated RSV NPs made with low MW polymers conjugated to RSV and unconjugated RSV

Formulation	Particle size (nm)	PDI	Zeta potential (mV)	DL (%)	% *w/w* RSV conjugate in NPs	Release study		Stability of NPs in PBS at 37°C after 24 hours (%)[b]
						t_{max} (h)	$\%_{max}$[a]	
Free RSV	NR	NR	NR	NR	NR	1.3	39.6±7.9[2]	12.8±4.1[3]
Conjugated RSV NPs								
mPEG750-PLA1000-succ-RSV	269.0±50.2[3]	0.317±0.037[3]	-2.8±1.0[3]	40.1	63.9	3.8	4.6±0.2[2]	33.9±1.2[3]
mPEG750-PLA1000-glu-RSV	356.4±13.3[3]	0.668±0.113[3]	-26.6±0.6[3]	48.1	54.8	4.0	4.5±0.4[2]	17.0±1.2[2]
mPEG750-PCL1000-succ-RSV	205.0±1.9[3]	0.196±0.018[3]	-34.7±3.4[3]	9.8	99.3	2.2	28.2±0.9[3]	92.9±0.5[3]
mPEG2000-PLA1000-succ-RSV	27.5±6.5[3]	0.337±0.170[3]	-9.3±3.1[3]	26.1	76.1	2.0	3.3±0.2[2]	89.1±0.2[2]
PEG5000-O-RSV	579.0±85.8[2]	0.533±0.069[2]	-0.2±2.3[2]	4.3	100.0	>47.5	5.6[1]	99.5±0.1[2]

Data presented as mean (*n*=superscript numbers) ± SD where calculated

[a]Maximum % cumulative amounts of total RSV equivalent released

[b]Data presented as % *w/w* RSV conjugate remaining after NPs were in PBS pH7.4 at 37°C for 24 hours except free RSV where % RSV remaining was quoted

Several selection criteria were utilised to choose best performing NPs for further *in vitro* and *in vivo* studies. Firstly, particle size should be below 250nm with low to moderate PDI values (<0.6) so the NPs could still preferentially accumulate in the tumours *via* the EPR effect (Mei *et al.* 2016). Secondly, it would be preferred that the NPs have high negative-charged zeta potential values (>-20mV) as NPs with negative charge were shown to have longer circulation time in the blood stream (Kobayashi *et al.* 2014), reduced plasma protein adsorption, aggregation of NPs in the body (Yang *et al.* 2011, Li *et al.* 2015b) and low rate of non-specific cellular uptake (Ye *et al.* 2014). Thirdly, a high DL of more than 10% in NPs would be beneficial in allowing a large dose of RSV to be administered and lastly, a sustained release of RSV with maximum amounts released would aid in providing a continuous supply of RSV for longer periods of time instead of a burst effect.

In general, all of our NPs except RSV encapsulated in mPEG2000-PLA1000 NPs and mPEG750-PLA1000-glu-RSV NPs were 240nm or smaller. The presence of PEG on NP surfaces could prevent opsonisation, producing the 'stealth' effect thus increasing circulation time *in vivo* (Shalgunov *et al.* 2017) and also provide an additional stabilising effect to the electrostatic repulsion (Rachmawati *et al.* 2016) which high negative-charged zeta potential values can provide. Hence, the need for negatively-charged NPs was not essential although desirable in our case. Apart from that, PEG-PLA and PEG-PCL were known polymers in nano-sized DDS for cancer therapy (Biswas *et al.* 2016, Grossen *et al.* 2017). Low MW mPEG-PCL has also been used to release an anti-inflammatory drug dexamethasone efficiently, possibly maximising the drug bioavailability for skin disease treatment (Du *et al.* 2016). The use of low MW polymers reduced the likelihood of toxicity making it more biocompatible (Wang *et al.* 2016). The following table (Table 4.12) gives an overview of which NPs fulfilled the selection criteria for further *in vitro* and *in vivo* studies.

Table 4.12 Characteristics of novel RSV NPs against selection criteria

RSV NPs	Particle size	Zeta potential	DL	Sustained release
RSV in mPEG750-PLA1000 NPs	++	+	-	+
RSV in mPEG750-PCL1000 NPs	++	++	-	-
RSV in mPEG2000-PLA1000 NPs	-	-	-	++
mPEG750-PLA1000-succ-RSV NPs	+	+	++	+
mPEG750-PLA1000-glu-RSV NPs	-	++	++	+
mPEG750-PCL1000-succ-RSV NPs	++	++	-	-
mPEG2000-PLA1000-succ-RSV NPs	++	+	+	-
PEG5000-O-RSV NPs	-	-	-	++

++ fulfils criteria
+ partially fulfils criteria
- does not fulfil criteria

Thus far, physical characteristics of mPEG750-PLA1000-succ-RSV NPs fulfilled all criteria and this was advantageous due to its promising PK profile established by Siddalingappa *et al.* (2015). Even though our mPEG750-PLA1000-succ-RSV NPs consisted of 63.9% *w/w* RSV conjugate rather than 100%, further *in vitro* studies would help in determining the effect of this percentage. Lee *et al.* (2010) demonstrated *in vivo* efficacy against subcutaneous B16-F10 melanoma tumour growth using PTX-loaded in low MW mPEG750-PCL2400 which displayed good mechanical strength and rapid sol-to-gel phase transitions. The same group showed *in vivo* efficacy when the same block copolymers were used to encapsulate DOX (Kang *et al.* 2011). In our observations, encapsulated mPEG750-PCL1000 NPs displayed similar sol-to-gel characteristics and this warranted further investigation into its pre-clinical application. Although the encapsulated and conjugated mPEG750-PCL1000 NPs exceeded the criteria for particle size and zeta potential, they did not provide high DL or sustained release (Table 4.12). It was unfortunate as the conjugated mPEG750-PCL1000-succ-RSV NPs composed of the highest % *w/w* RSV conjugate (99.3%) in the NPs compared to the other ester conjugated RSV NPs and would have been a good comparison with other ester conjugated RSV NPs where there were high %

of free RSV in the NPs. The other two ester conjugated RSV NPs, mPEG750-PLA1000-glu-RSV NPs and mPEG2000-PLA1000-succ-RSV NPs fulfilled three out of four criteria but mPEG2000-PLA1000-succ-RSV NPs did not provide a sustained release of RSV equivalent which was more important than the unfulfilled particle size criteria by mPEG750-PLA1000-glu-RSV NPs. Despite being very stable and having a long-sustained release of RSV, PEG5000-O-RSV NPs did not have the right physical attributes for further *in vitro* and *in vivo* studies. Despite unfavourable physical attributes of encapsulated RSV NPs, the encapsulated RSV NPs would be used as a comparison with the conjugated RSV NPs to assess the benefits of conjugation over encapsulation.

4.6 Conclusion

This chapter was to develop novel nano-sized NPs by physical entrapment of RSV into low MW polymeric NPs (encapsulated RSV NPs) and by using low MW polymeric RSV conjugates with encapsulated free RSV (conjugated RSV NPs). Encapsulated RSV NPs were of good particle size and distribution albeit with low zeta potential values, however, this was not expected to have impact on the physical stability of NPs due to the presence of PVA and mPEG on the NP surface. The release profiles were not significantly improved from free RSV with physical encapsulation but RSV was protected from degradation to a certain extent in PBS at 37°C. Conjugation of RSV vastly improved the ease of developing NPs with good particle size and distribution along with excellent zeta potential values which boded well for *in vivo* stability and circulation. We established that conjugation of RSV produced NPs with higher DL than encapsulated RSV NPs while maintaining nano-sized particles. Conjugated RSV NPs also either produced a sustained release profile and prevented an initial burst release of RSV seen in encapsulated RSV NPs. The covalent bond between RSV and polymers provided better stability profiles for RSV in PBS at 37°C and a sustained release of RSV. As the physico-chemical characteristics of NPs affect their *in vitro* and *in vivo* properties (Li *et al.* 2017b), all encapsulated and conjugated RSV NPs will undergo *in vitro* stability evaluations in rat plasma and HLM which would allow us to select candidates for anticancer activity assessments and other biological assessments.

CHAPTER 5. BIOLOGICAL EVALUATION OF ENCAPSULATED AND CONJUGATED RESVERATROL NANOPARTICLES

5.1 Introduction

During the drug product development process, various *in vitro* and *in vivo* methods have been used to determine the therapeutic properties of the drug formulation before clinical trials in humans (Tillement *et al.* 2007). Depending on its administration route and pharmacological purpose, drugs were selected based on their pharmacodynamic (PD) and PK properties (Chung *et al.* 2015). *In vitro* stability of a drug in rat plasma indicated a drug formulation was less affected by enzymes like esterases in plasma which could imply better *in vivo* bioavailability for therapeutic effect (Chung *et al.* 2015). RSV was known to be rapidly metabolised *via* hepatic enzymes *in vivo* which decreased its bioavailability and therapeutic efficacy (Iwuchukwu *et al.* 2008). Despite these bioavailability limitations, RSV is a natural polyphenol which suppresses the proliferation of cancer cells through several mechanisms including inhibition of angiogenesis, induction of apoptosis and cell cycle arrest (Csiszar *et al.* 2015, Dun *et al.* 2015, Lee *et al.* 2015, Meng *et al.* 2016). RSV has been proven by various research groups to induce and/or enhance apoptosis which led to cell death (Kundu *et al.* 2008) in melanoma cell lines such as murine melanoma B16-F10 (Guan *et al.* 2012, Lee-Chang *et al.* 2013), human melanoma SK-Mel-5 (Fang *et al.* 2013), human melanoma SK-Mel-28 and A375 (Niles *et al.* 2003) and DOX-resistant murine B16 melanoma cells (Gatouillat *et al.* 2010). The effectiveness of RSV as an anticancer therapeutic drug was further seen in several rodent cancer models (Jang 1997, Bhattacharya *et al.* 2011, Lee *et al.* 2012b, Lee-Chang *et al.* 2013, Park *et al.* 2015). Unfortunately, this effectiveness was only significant when very high doses of RSV were used which were not clinically feasible and caused renal toxicity as suggested by Popat *et al.* (2013) in a Phase II clinical study in human patients with multiple myeloma given 5g of RSV daily for almost a year.

The need for high doses was due to the low bioavailability and rapid metabolism of RSV *in vivo* (Lee-Chang *et al.* 2013, Poulsen *et al.* 2013, Chinembiri *et al.* 2014).

Evidence of its low bioavailability was shown in humans with nearly no native RSV detectable in blood plasma after oral consumption (Walle 2011, Singh *et al.* 2014a). Elimination $t_{1/2}$ values of RSV administered IV in rats and humans were found to be 11.4 hours and 17.2 hours, respectively (Walle *et al.* 2004, Li *et al.* 2017c). Nanotechnology has been employed as a strategy to enhance the bioavailability of RSV and/or decrease its metabolism rate in the body (Wang *et al.* 2014, Summerlin *et al.* 2015, Weiskirchen *et al.* 2016). Nanotechnological DDS of RSV were also developed to increase cytotoxicity of RSV in cancer cell lines. Many of these research claimed that the DDS have allowed an increase of cellular uptake of RSV (Guo *et al.* 2013, Sanna *et al.* 2013), protection of RSV before it reaches target site (Lu *et al.* 2013, Sessa *et al.* 2014) and overcome the issue of poor solubility of RSV (Ansari *et al.* 2011, Lee *et al.* 2012a, Bolko *et al.* 2014) which led to increased therapeutic activity of RSV *in vivo*. Pandita *et al.* (2014) showed RSV encapsulated in SLNs increased the oral bioavailability of RSV in Wistar rats. Bu *et al.* (2013) showed RSV in chitosan NPs extended the residence time of RSV in blood in a PK study in rats. Conjugation of RSV to polymers were also shown to decrease metabolism of RSV *in vitro* and found to enhance the bioavailability of RSV *in vivo.* Siddalingappa *et al.* (2015) showed an enhanced *in vivo* bioavailability of RSV conjugated with mPEG750-PLA1000 *via* succinate linker and RSV conjugated to PEG5000 *via* ether bond NPs administered IV in rats at 2mg/kg where *in vivo* $t_{1/2}$ was 1.7h and 5.3h, respectively (RSV $t_{1/2}$ 1.4h, 10mg/kg). Both compounds demonstrated stability against rat microsomal enzymes after incubation for 1h at 37°C whereas RSV was fully metabolised within 10min. The ester conjugate NPs also showed enhanced stability in rat plasma where $t_{1/2}$ was 3h compared to RSV ($t_{1/2}$ 0.1h). Thus, the combination of conjugation of RSV and nanotechnology could decrease metabolism rate and enhance bioavailability of RSV which will then increase the therapeutic effect of RSV *in vivo*.

RSV encapsulated in mPEG-PLA NPs showed enhanced cytotoxicity and apoptosis in glioma cell lines which was then translated to increased survival and better tumour growth inhibition in mice models at 15mg/kg RSV injected IV every 48 hours for 14 days (Guo *et al.* 2013). Similarly, Jung *et al.* (2015) showed encapsulation of RSV in mPEG-PLA NPs showed better cytotoxicity and apoptosis properties than RSV and

these properties were further demonstrated in colon cancer mice models where 100mg/kg RSV was administrated IV twice daily for 21 days. RSV encapsulated in high MW PCL nanocapsules showed improved cytotoxicity in B16-F10 cell lines when compared to free RSV (Carletto *et al.* 2016). These nanocapsules were injected at 5mg/kg IP daily for 10 days and decreased tumour volumes in B16-F10 tumour models with enhanced apoptosis and necrosis histological properties indicating a good prognosis for cancer patients. Despite these promising anticancer effects *in vitro* and *in vivo*, most research of RSV in melanoma model were found to be contradictory where RSV was sometimes found to be cytotoxic *in vitro* but not *in vivo* (Niles *et al.* 2006, Osmond *et al.* 2012, Lee-Chang *et al.* 2013, Osmond *et al.* 2013). This again could be attributed to the rapid metabolism and lack of bioavailability of RSV *in vivo* which effectively reduced the drug level at the target cells (Singh *et al.* 2015, Tou 2015). In the case of a drug which is prone to plasma degradation and/or liver metabolism, the *in vitro* cell culture data will not be able to reflect the trend/data obtained from *in vivo* studies using animals. For example, Liu et al. (2015) depicted that conjugated pterostilbene with PEG was less cytotoxic than native pterostilbene in *in vitro* Lewis lung carcinoma (LLC) cell assays but showed significant tumour growth suppression in a subcutaneous implanted LLC C57BL/6 mouse model. Asensi *et al.* (2002) and Stakleff *et al.* (2012) highlighted the lack of correlation between and reliability of *in vitro* and *in vivo* data which potentially could undermine the potential therapeutic effects of RSV due to the fact that all *in vitro* studies focused on a particular cell-related drug mechanism and not the holistic biological processes to which a drug would be exposed to in the body. In addition, the hormetic nature of RSV could affect its biological effects when administered in much larger doses *in vivo* compared to the small doses *in vitro* (Scott *et al.* 2012). This further emphasises the importance of carrying out both *in vitro* and *in vivo* biological evaluations on drug formulations, in particular RSV formulations, to study the full extent of the effectiveness of the formulations.

In Chapter 4, we have developed novel nano-sized formulations using nanotechnology to formulate both free RSV NPs (encapsulated RSV NPs) and conjugated RSV synthesised in chapter 2 together with free RSV (conjugated RSV NPs)

using low MW amphiphilic PEGylated copolymers. We have seen in the previous chapter the superior characteristics of conjugated RSV NPs in sustained release and formulation physical attributes over encapsulated RSV NPs. In order to further differentiate and understand the effectiveness of these two different formulation strategies, the *in vitro* and *in vivo* stability and therapeutic effect needs to be addressed. *In vitro* assays employed in this chapter could describe the stability and therapeutic effectiveness of formulations in an isolated environment, however, an *in vivo* model will enable us to evaluate the effectiveness of the formulations in a holistic environment where various biological factors affect the efficacy of a formulation. This would be particularly useful in differentiating the two formulation strategies, that is encapsulation and conjugation, for possibly improving the bioavailability of RSV *in vivo* by stabilising RSV against plasma enzymes and liver metabolism.

5.2 Aim

The aim of this chapter was to evaluate the biological activities of RSV formulations (encapsulated and conjugated RSV NPs developed in Chapter 4) *in vitro* for plasma stability and liver metabolism followed by *in vitro* cell culture assessment using B16-F10 melanoma cells. One set each of encapsulated and conjugated RSV NPs was then selected and assessed *in vivo* using a mouse melanoma model. The following flow chart summarises the studies carried out on RSV NPs.

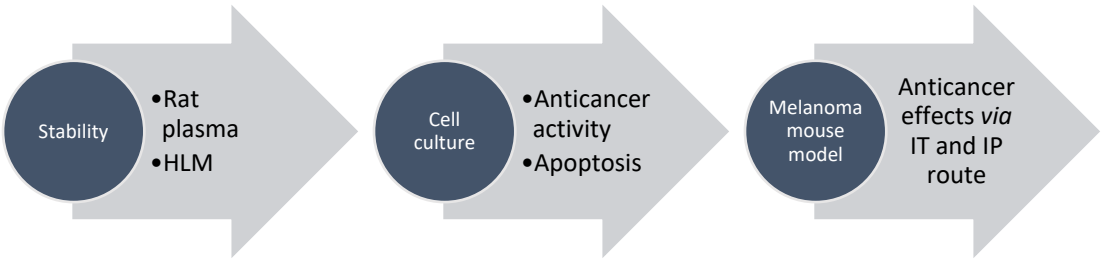

Figure 5.1 Flow chart of biological evaluations carried out on encapsulated and conjugated RSV NPs developed in Chapter 4

Firstly, stability of all RSV NPs in rat plasma and HLM were assessed and compared. NPs which were found capable of improving the stability of RSV *in vitro* were then

used to assess their anti-proliferative effect on B16-F10 melanoma cells. One encapsulated RSV NPs and one conjugated RSV NPs were elected to be tested for their apoptosis effect in B16-F10 melanoma cells and for their cytotoxicity in non-cancerous NIH/3T3 fibroblast cells. The NPs were then evaluated for *in vivo* efficacy *via* two administration routes, IT and IP, in a melanoma mouse model established by C57BL/6J male mice with subcutaneously implanted B16-F10 cells.

5.3 Materials

Materials used throughout this chapter included 0.01M PBS solution and molecular biology grade DMSO purchased from Sigma-Aldrich (NSW, Australia).

Stability of RSV NPs against plasma esterases was assessed using outbred rat plasma. Rat plasma was stored at -20°C in 1mL aliquots to avoid freeze-thaw cycle effects. HLM was a Gibco® 50-donor pool mix purchased from Life Technologies Pty Ltd (VIC, Australia; cat# HMMCPL) and used as is. UDPGA (98-100%; cat# U6751-25MG), alamethicin from *Trichoderma viride* (≥98%; cat# A4665-5MG), magnesium chloride $MgCl_2$ (>98%; cat# M8266-100G) and Trizma® base (≥99.9%; cat# T4661-100G) for Tris buffer was purchased from Sigma-Aldrich (NSW, Australia). Tris buffer (100mM) was prepared as per manufacturer's instructions and used to dissolve UDPGA, alamethicin and $MgCl_2$ to concentrations of 50mM, 0.25mg/mL and 10mM, respectively. CGM was a combination of 500mL high glucose Dulbecco's Modified Eagle's Medium (DMEM) (Sigma-Aldrich: NSW, Australia; cat# D5671-500ML) supplemented with 50mL Serana® foetal bovine serum (FBS) (Fisher Biotec: WA, Australia; cat# S-FBS-AU-015), 5mL of 200mM L-glutamine solution (Sigma-Aldrich: NSW, Australia, cat# G7513-20ML) and 5mL of penicillin-streptomycin solution with 10,000 units/mL of penicillin and 10mg/mL streptomycin (Sigma-Aldrich: NSW, Australia; cat# P4333-20ML).

General cell culture used a Gibco® TrypLE™ Express (Life Technologies Australia Pty Ltd: VIC, Australia; cat# 12604-021), various Greiner Bio-One conical tube volumes (Interpath Services Pty Ltd: VIC, Australia), MTT (≥97.5%, cat# M5655-1G), 0.4% *w/v* trypan blue (Sigma-Aldrich: NSW, Australia; cat# T6146-25G) in PBS and 2mL Greiner Bio-One Cryo.s™ cryopreservation vial (Interpath Services Pty Ltd: VIC, Australia). To

prepare for our apoptosis assays, a 50μg/mL propidium iodide (PI, ≥94.0%; cat# P4170-25MG) (Sigma-Aldrich: NSW, Australia) solution in PBS was prepared. The Annexin binding buffer (1×) was prepared using 10mM 4-(2-Hydroxyethyl)piperazine-1-ethanesulfonic acid (HEPES, ≥99.5%, cat# H3375-100G) buffer, 140mM sodium chloride (≥99%; cat# S9888-500G) and 2.5mM calcium chloride (≥97%; cat# C4901-100G) in water, adjusted to pH7.4, sterilised by autoclave and stored at 4°C when not in use. All components for the binding buffer were purchased from Sigma-Aldrich (NSW, Australia). A BD Pharmingen™ Annexin V-fluorescein isothiocyanate (V-FITC) (BD Biosciences: NSW, Australia; cat# 556419) was used as is and kept in the dark at 4°C when not in use. 5μL of Annexin V-FITC optimally stains approximately 100,000 cells as per manufacturer's documentation but was optimised according to B16-F10 cells and flow cytometer used prior to experiments. Tumour growth evaluation specifically used Hanks' balanced salt solution (HBSS, 10×; cat# H6648) and HPCD from Sigma-Aldrich (NSW, Australia). HPCD was prepared in PBS as described. PathClear® Cultrex® Basement Membrane Extract (BME) from In Vitro Technologies Pty Ltd (WA, Australia; cat# RDS343200501P) was used as is.

5.4 Methodology

5.4.1 Stability of RSV formulations in rat plasma

The stability of RSV formulations in rat plasma was assessed using the methodology by Siddalingappa *et al.* (2015). Briefly, 50mg/mL of final conjugated RSV product synthesised in Chapter 2 was prepared as conjugated RSV NPs as per Section 4.4.1 and diluted 1:4 with defrosted rat plasma to a final concentration of 10mg/mL. 50mg/mL of conjugated RSV NPs were also diluted 1:4 with MQ to 10mg/mL as controls. As a comparison, 2mg/mL final concentration of free RSV was prepared in rat plasma from freshly prepared 10mg/mL RSV in DMSO. After dilution, 50μL aliquots were placed into 1.5mL centrifuge tubes, sealed and incubated in the dark in a hot water bath at 37°C. At varying time intervals, one aliquot was removed at each time point and 450μL of cold ACN (1:9 dilution) was added to precipitate the plasma proteins. The sample was then centrifuged at 10,000*g* for 5 minutes at 4°C in a 5415R Eppendorf® microcentrifuge and the supernatant was diluted with 50:50 *v/v* ACN:MQ

to an appropriate concentration for HPLC gradient analysis (Section 3.4.2.2). Experiments were carried out in minimum of duplicates and the data was presented as percentage total RSV equivalent remaining over time. For encapsulated RSV NPs, NPs prepared as per Section 4.4.3 were diluted 1:4 with defrosted rat plasma to final concentrations between 10μg/mL to 20μg/mL depends on EE of NPs. Free RSV controls diluted in rat plasma from 1mg/mL RSV in DMSO to concentrations of 40μg/mL were used as comparisons. Samples were aliquoted and processed similarly to what was done with conjugated RSV NPs and data was presented as percentage RSV remaining over time after analysis with HPLC isocratic method as per Section 3.4.3. Plasma stability data was analysed by GraphPad Prism version 7.0.3 for Windows software (GraphPad Software: CA, USA) using a non-linear regression analysis of a one-phase decay model for plasma $t_{1/2}$.

5.4.2 Stability of RSV formulations in human liver microsomes (HLM)

Stability of RSV formulations in HLM was assessed for phase II metabolism with the enzyme co-factor UDPGA using Life Technologies Pty Ltd protocols (Life Technologies Pty Ltd 2015) with slight modifications. 5μL human microsomes (1mg/mL final protein concentration), 2μL alamethicin (5μg/mg protein final concentration), 10μL $MgCl_2$ (1mM final concentration) and 63μL 100mM Tris buffer was pre-incubated in ice for 1 hour to allow for microsomal pore opening by alamethicin. 10μL of 5mg/mL conjugated RSV NPs prepared as per Section 4.4.1 were then added to obtain final concentrations of 500μg/mL NPs whereas 10μL encapsulated RSV NPs were added to obtain final concentrations of 0.2 to 2.5μg/mL RSV depending on EE of NPs. Assays were incubated at 37°C in the dark for a further 5 minutes. The metabolic reaction was initiated by adding 10μL of UDPGA (final concentration of 5mM). Aliquots of 20μL were separated into 0.5mL centrifuge tubes, sealed and kept in the dark at 37°C. At time intervals of up to 1 hour, one aliquot per time point was removed and proteins were precipitated by adding 80μL cold ACN (1:4 dilution). The sample was then centrifuged at 10,000*g* for 5 minutes at 4°C in a microcentrifuge and the supernatant was diluted with 50:50 *v/v* ACN:MQ to an appropriate concentration for HPLC analysis as per Section 3.4.2.2 (for conjugated RSV NPs) and Section 3.4.3 (for encapsulated RSV NPs). As a comparison, a final concentration of 300μg/mL RSV in

HLM was used. Experimental controls at comparable concentrations with each RSV NPs were employed in each experiment replicate as follows:

1) Test assay without UDPGA (negative control)
2) Test assay without test article (blank control)
3) Test assay without HLM and UDPGA (control)

A final reaction volume of 100μL was maintained by substituting omitted components with 100mM Tris buffer. The experiment was carried out in minimum of duplicates and the data was plotted as percentage total RSV equivalent or RSV remaining against time. Data was analysed using the first-order equation for microsomal $t_{1/2}$.

5.4.3 Stability of RSV formulations in complete growth media (CGM)

Stability of RSV formulations was assessed in CGM used for *in vitro* cell culture studies. 5mg/mL conjugated RSV NPs prepared as per Section 4.4.1 were diluted 1:9 with CGM to 500μg/mL. 20μL aliquots were maintained in sealed 0.5mL centrifuge tubes in the dark at 37°C for up to 48 hours. At 0.02, 24 and 48 hours, one aliquot was removed and 180μL cold ACN (1:9 dilution) was added to precipitate any proteins. The sample was then centrifuged at 10,000*g* for 5 minutes at 4°C in a microcentrifuge and the supernatant was diluted with 50:50 *v/v* ACN:MQ to an appropriate concentration for analysis using HPLC gradient method as per Section 3.4.2.2 and presented as percentage of total RSV equivalent remaining. Encapsulated RSV NPs prepared as per Section 4.4.3 were diluted with CGM to final RSV concentrations of 20μg/mL and treated similarly to that of conjugated RSV NPs. Analyses were done using HPLC isocratic method as per Section 3.4.3 and presented as percentage of RSV remaining. As a control, 20μg/mL free RSV was diluted in CGM from 1mg/mL RSV in DMSO.

5.4.4 Cell cultures

Two mouse cell lines were used in this project, that is B16-F10 melanoma cells and NIH/3T3 fibroblast cells. Culturing details of both cell lines were detailed in Table 5.1. Cell morphology and growth were monitored using an Eclipse TS100 light microscope (Nikon Instruments Inc.: Tokyo, Japan) and imaged using a DS-Fi2 digital camera with

a DS-L3 controller (Nikon Instruments Inc.: Tokyo, Japan). Cell culture procedures were carried out in GELAIRE® Ultrasafe Class II biological safety cabinets (Gelaire Pty Ltd: NSW, Australia) with aseptic working techniques and centrifugation was performed using an Allegra® X-12 centrifuge (Beckman Coulter Pty Ltd: NSW, Australia) and incubation was in a NuAire CO_2 incubator (In Vitro Technologies: VIC, Australia) at 37°C with 5% CO_2 and 95% humidified air unless specified otherwise. See Appendix 7.11 for details on basic cell culture techniques used. All procedures were carried out in a Physical Containment II (PC2) facility at the Curtin Health and Innovation Research Institute (CHIRI) at Curtin University (Perth, Australia).

Table 5.1 Culturing details for B16-F10 and NIH/3T3 cell lines for biological *in vitro* evaluation

		B16-F10	**NIH/3T3**
Cell type		Mouse melanoma	Mouse fibroblast
Origin		American Type Culture Collection® (ATCC®) (Virginia, USA)	
Product code		ATCC® CRL-6475™	ATCC® CRL-1658™
Passage number used		5-20	10-20
Culturing flasks (medium volume)*		T25: 25cm^2 Nunc™ EasYFlask™ (5-7mL) T75: 75cm^2 Nunc™ EasYFlask™ (20-25mL)	
Experimental culturing plates (medium volume)*	Cytotoxicity	Nunc™ MicroWell™ 96-Well microplate (100μL per well)	
	Apoptosis	Nunc™ 6-well plate (1mL per well)	
CGM	Medium	500mL high glucose DMEM	
	Serum	50mL Serana® FBS	
	Supplements	5mL of 200mM L-glutamine solution 5mL of penicillin-streptomycin solution (10,000 units/mL of penicillin and 10mg/mL streptomycin)	

*All culturing flasks and plates were purchased from Life Technologies Australia Pty Ltd (VIC, Australia)

5.4.5 Dose and incubation time response of free RSV in B16-F10 cells

A quantitative and colorimetric MTT assay was used to assess the IC_{50} (half-maximal

inhibitory concentration) of free RSV and the most effective incubation time in B16-F10 cells. B16-F10 cells were seeded at 2000 cells per well in quadruplet for each variable and allowed to adhere in a humidified atmosphere with 5% CO_2 at 37°C. After 24 hours, media was removed by aspiration and cells in each well were treated with 100μL of 0, 5, 10, 20, 50, 80 and 100μg/mL free RSV freshly prepared in CGM. The plates were incubated for 24 and 48 hours. At the end of the treatments, media was removed by aspiration and 100μL of filter-sterilised 1mg/mL MTT prepared in PBS was added to each well. The plates were incubated at 37°C covered in foil for a further 2 hours to allow cleavage of the yellow MTT salt to the insoluble purple formazan crystals by the mitochondrial dehydrogenase of viable cells (Riss *et al.* 2013), after which the well contents were aspirated and replaced with 100μL molecular grade DMSO and incubated at 37°C covered in foil for 15 minutes to allow solubilization of the formazan crystals. Absorbance of the formazan crystals was read at 570nm using an EnSpire® multimode plate reader (Perkin Elmer: Waltham, USA) with pre-set shaking of 20 seconds prior to readings.

To prepare test articles, a 50mg/mL RSV was prepared in DMSO to be used as stock solution and kept at -20°C for a maximum of one week. To decrease the amount of DMSO present in the assay due to its toxicity (Timm *et al.* 2013), thawed 50mg/mL RSV was diluted with CGM to 1mg/mL RSV which was then diluted further to 5 to 100μg/mL RSV with CGM. Blank control (0μg/mL RSV) was DMSO diluted with CGM equivalent to the highest DMSO concentration cells were exposed to, which was 0.2% (*v/v*). All test articles were freshly prepared to avoid possible chemical degradation effects and contamination in cell culture.

Assays were carried out in duplicates of assay plates, and results were expressed as a percentage of viable cells, with 100% representing control cells. IC_{50} of RSV after 24-hour and 48-hour treatment was determined at the concentration where viable cells decreased by approximately 50%. A practical and suitable concentration and incubation time for further assays was chosen based on the results obtained which will be explained in Section 5.5.4.

5.4.6 Anticancer effect of RSV formulations in B16-F10 cells

Following the dose response evaluation of free RSV, IC_{50} of RSV was between 10 and 20μg/mL after a 48-hour treatment whereas a 24-hour treatment produced an IC_{50} between 20 and 50μg/mL. We have chosen 10 and 20μg/mL as our treatment concentrations and 48 hours as our treatment period due to the lower concentration necessary to inhibit 50% of B16-F10 cells after a 48-hour treatment.

Similarly, anticancer effect of RSV formulations in B16-F10 cells was assessed using the MTT assay used in the previous section (Section 5.4.5). Briefly, B16-F10 cells were seeded at 2000 cells per well in quadruplet for each variable and allowed to adhere in a humidified atmosphere with 5% CO_2 at 37°C. After 24 hours, media was removed by aspiration and cells in each well were treated for 48 hours with 100μL of 0, 10 and 20μg/mL RSV equivalent concentrations of RSV formulations freshly prepared in CGM and 100μL of 0, 10 and 20μg/mL free RSV prepared as per Section 5.4.5 as controls. Table 5.2 lists the RSV formulations tested and details the preparation of blank control (0μg/mL RSV) test articles, which were same as per medium used in NP dispersion.

Table 5.2 Preparation of blank controls for the study of anticancer effect of RSV formulations in B16-F10 cells

RSV formulation[a]	Blank control[b]
RSV encapsulated in mPEG750-PLA1000 NPs	Water diluted with CGM
RSV encapsulated in mPEG750-PCL1000 NPs	0.6% PVA diluted with CGM
RSV encapsulated in mPEG2000-PLA1000 NPs	0.6% PVA diluted with CGM
mPEG750-PLA1000-succ-RSV NPs	0.6% PVA diluted with CGM
mPEG750-PLA1000-glu-RSV NPs	Water diluted with CGM
mPEG750-PCL1000-succ-RSV NPs	Water diluted with CGM
mPEG2000-PLA1000-succ-RSV NPs	Water diluted with CGM
PEG5000-O-RSV NPs	Water diluted with CGM

[a]prepared as per Sections 4.4.1 and 4.4.3
[b]Dilution used was same dilution factor used when preparing 20μg/mL test articles in CGM

In addition, blank encapsulated NPs were used as controls alongside their

corresponding encapsulated RSV NPs listed in Table 5.2. The NPs were prepared as per Section 4.4.3 and listed below:

1) Blank mPEG750-PLA1000 NPs
2) Blank mPEG750-PCL1000 NPs
3) Blank mPEG2000-PLA1000 NPs

Blank encapsulated NPs were prepared similarly to corresponding encapsulated NPs as per Table 5.2 without RSV. In general, one type of encapsulated RSV NPs and its corresponding blank NPs and free RSV controls were plated in one 96-well plate whereas two or three conjugated RSV NPs and a free RSV control were able to fit in one 96-well plate. At the end of the treatment (48 hours), media was removed by aspiration and 100μL of filter-sterilised 1mg/mL MTT prepared in PBS was added to each well. The plates were incubated for a further 2 hours after which the well contents were aspirated and replaced with 100μL molecular grade DMSO and incubated at 37°C covered in foil for 15 minutes. Absorbance of the formazan crystals was read at 570nm using an EnSpire® multimode plate reader with pre-set shaking of 20 seconds prior to readings. Assays were carried out in triplicate assay plates and results were expressed as a percentage of viable cells, with 100% representing control cells.

5.4.7 Cytotoxicity of selected RSV formulations in NIH/3T3 cells

Murine fibroblast NIH/3T3 cells were used as a representative of non-cancerous cells to assess the cytotoxicity of free RSV and selected RSV formulations to ensure formulations were not producing toxicity effect *in vivo*. The choice of one conjugated and one encapsulated RSV NPs was made based on their anticancer effects. The cytotoxicity was evaluated using the MTT cell viability assay detailed in Sections 5.4.5.

Briefly, NIH/3T3 cells were seeded at 2000 cells per well in quadruplet for each variable and allowed to adhere in a humidified atmosphere with 5% CO_2 at 37°C. After 24 hours, media was removed by aspiration and cells in each well were treated for 48 hours with 100μL of 0, 10 and 20μg/mL RSV equivalent concentrations of conjugated mPEG750-PLA1000-succ-RSV NPs and RSV encapsulated in mPEG750-PLA1000 NPs freshly prepared in CGM as per Section 5.4.6 and 100μL of 0, 10 and

20μg/mL free RSV prepared in CGM as per Section 5.4.5. At the end of the treatment, media was removed by aspiration and 100μL of filter-sterilised 1mg/mL MTT prepared in PBS was added to each well. The plates were incubated for a further 2 hours after which the well contents were aspirated and replaced with 100μL molecular grade DMSO and incubated for further 15 minutes. Absorbance of the formazan crystals was read at 570 nm using an EnSpire® multimode plate reader with pre-set shaking of 20 seconds prior to readings. Assays were carried out in duplicate assay plates and results were expressed as a percentage of viable cells, with 100% representing control cells.

5.4.8 Apoptosis evaluation of selected RSV formulations in B16-F10 cells by flow cytometry

Flow cytometric analysis for apoptosis in B16-F10 cells was assessed using a double Annexin V-FITC and PI staining in cells. Gating strategies of apoptosis assays can be found in Appendix 7.15. Apoptotic cells were characterised by translocated phosphatidylserine molecules to the outer cell membrane which allowed for the binding of Annexin V and due to the lack of integrity in the cell membrane of necrotic cells, PI would permeate into the nucleus and bind to nucleic acid within (Alkan *et al.* 2014). Free RSV, conjugated mPEG750-PLA1000-succ-RSV NPs and RSV encapsulated in mPEG750-PLA1000 NPs were assessed for apoptosis in B16-F10 cells at RSV equivalent concentrations of 20μg/mL and 50μg/mL for 24 hours and 48 hours. A higher concentration of 50μg/mL which produced a higher anti-proliferative effect in B16-F10 cells (discussed in Section 5.5.4) was used to compare with the apoptotic and necrotic effects observed in 20μg/mL RSV formulations. Two treatment periods were also selected for the purpose of comparison.

In order to obtain sufficient events for quantification, large number of cells were needed and hence, 6-well plates were used to seed 250,000 cells per well and allowed to adhere. After 24 hours, media was removed and cells in each well were treated for 24 hours or 48 hours with 1mL of 20μg/mL and 50μg/mL RSV equivalent concentrations of free RSV freshly prepared as per Section 5.4.5 and two RSV formulations freshly prepared in CGM, namely conjugated mPEG750-PLA1000-succ-

RSV NPs and RSV encapsulated in mPEG750-PLA1000 NPs as per Section 5.4.6. At the end of specified treatment periods, individual well contents were aspirated and kept in separate centrifuge tubes for each well. Cells were trypsinised, collected and added to corresponding centrifuge tubes. Wells were then washed twice with ice-cold PBS and aspirated into corresponding centrifuge tubes. Cells and washings were pelleted by centrifugation at 930*g* for 5 minutes at RT. The dark-coloured cell pellet was resuspended in 1mL Annexin binding buffer and maintained on ice. 10μL Annexin V-FITC was added to the cell suspension followed by 5μL 50μg/mL PI solution and incubated on ice for 15 minutes in the dark. Suspensions were further added with 400μL of binding buffer and analysed within 4 hours while kept on ice in the dark throughout. Ten thousand events were collected with a FACSCanto^{TM} II flow cytometer (BD Biosciences: NSW, Australia) using standard optics to detect FITC and PI. Data was analysed using FlowJo 10.4 software (FlowJo, LLC: OR, USA).

5.4.9 Evaluation of RSV formulations in *in vivo* cancer model

5.4.9.1 Preparation of RSV formulations test and control articles

Conjugated mPEG750-PLA1000-succ-RSV NPs and RSV encapsulated in mPEG750-PLA1000 NPs were selected for anticancer evaluation in a C57BL/6J mouse model with a subcutaneous B16-F10 tumour. Various controls were appointed and listed as follows:

1) 20% *w/v* HPCD in PBS
2) Free RSV in 20% *w/v* HPCD in PBS
3) 100mg/mL mPEG750-PLA1000 polymer dissolved in PBS
4) Blank mPEG750-PLA1000 NPs

This section will describe the preparation methods for each formulation and control for *in vivo* studies. mPEG750-PLA1000-succ-RSV NPs were prepared as per Section 4.4.1 in concentration ranges of approximately 5.8 to 6.65mg/mL final product synthesised in Chapter 2 which resulted in concentrations of 5.0 to 5.7mg/mL total RSV equivalent.

Both RSV encapsulated in mPEG750-PLA1000 NPs and blank mPEG750-PLA1000 NPs were prepared as per Section 4.4.3.1. Due to the low DL and high dose required for

in vivo experiments, encapsulated RSV NPs were prepared in multiples of 2 or 3, combined and concentrated to allow for higher dose injections. To concentrate the NPs, the NPs were pelleted using an Avanti-JE centrifuge fitted with a JA-20 rotor (Beckman Coulter: CA, USA) at 15,000*g* for 20 minutes at 5°C. The supernatant was used to determine the total amount of RSV in the NP pellet as per Section 4.4.4.2 and then, with the supernatant discarded, the pellet was redispersed in MQ followed by 15 minutes in an ultrasonic water bath to concentrations of 5.0 to 5.7mg/mL RSV. The blank NPs were pelleted and redispersed with the same volume of MQ used to redisperse the encapsulated NPs which produced about 60mg/mL mPEG750-PLA1000. RSV formulations were prepared fresh on each treatment day to maintain sterility.

20% *w/v* HPCD in PBS and 100mg/mL mPEG750-PLA1000 polymer was prepared, filter-sterilised and kept in a sterile environment at 4°C for a maximum of 10 days. 5 to 5.7mg/mL free RSV in 20% HPCD was freshly prepared each treatment, filter-sterilised and kept in a sterile vial covered with aluminium foil to prevent RSV degradation by light.

5.4.9.2 Preparation of B16-F10 cells for subcutaneous tumour inoculation in animals

B16-F10 cells were prepared according to Overwijk *et al.* (2001) for subcutaneous tumour inoculation in C57BL/6J mice. B16-F10 cells were cultured into a 175cm^2 Nunc™ EasYFlask™ (T175) with a CGM volume of 30-35mL. When exponentially growing cells were at approximately 45-50% confluency, cells were detached from flasks with 5mL cold Gibco® TrypLE™ Express and vigorously pipetted to obtain a suspension of single cells. 20mL of CGM was added to halt the trypsinisation and cells were then transferred into a 50mL Greiner Bio-One conical tube and centrifuged at 930*g* for 5 minutes at RT to pellet the cells. The supernatant was decanted and the dark-coloured pellet was resuspended in 1mL ice-cold HBSS and kept on ice while 20μL of the suspension was used for cell counting using a haemocytometer as per Appendix 7.11.1. The number of cells were then adjusted using ice-cold HBSS to a final concentration of 2.5×10^5 cells in 25μL HBSS per mouse. An equivalent volume of PathClear® Cultrex® BME was added for better support for tumour growth *in vivo*

(Fliedner *et al.* 2016) to produce a final cell concentration of 1.25×10^5 cells in 50μL 50:50 *v/v* HBSS:Cultrex® per mouse. 50μL of this cell suspension was loaded into a 1mL 27-gauge insulin syringe (Nipro Australia Pty Ltd: NSW, Australia) and inoculated into mice within 2 hours to avoid decrease in cell viability. Remaining cell suspension was maintained in a conical tube on ice on standby and discarded when inoculations were completed.

5.4.9.3 Animal model and tumour inoculation

Animal experiments were approved by the Animal Ethics Committee (AEC) of Curtin University (Perth, Australia) with the application approval number AEC_2016_28 (Appendix 7.16) and conducted in accordance with the Australian Code of Practice for the care and use of animals for scientific purposes. C57BL/6J mice have been used as melanoma *in vivo* models (Belleri *et al.* 2008, Cheng *et al.* 2015, Carletto *et al.* 2016) for evaluating the biological benefits of RSV. 4-week old C57BL/6J male mice were purchased and individually ear-tagged from the ARC. Animals were housed in maximum of five per cage according to husbandry protocols at the Life Sciences Research Facility at Curtin University (Perth, Australia) and allowed to acclimatise for 5 days before the start of experiments. Throughout the experiment, animals were in a controlled temperature climate with 12-hour dark-light cycles and provided with food and water *ad libitum*. All studies were carried out in a Physical Containment III (PC3) facility with appropriate standard operating procedures and aseptic working techniques.

B16-F10 cells were inoculated using a protocol by Overwijk *et al.* (2001) with slight modifications. Once the animals were acclimatised, mice in groups of five maximum were weighed and anaesthesised using 4% isoflurane-oxygen mixture at 2-3L/min in an anaesthetic chamber. Once mice were found without reflex, that is sufficiently anaesthesised, the isoflurane flow was ceased to the closed chamber. One mouse was removed from the chamber and maintained under anaesthesia using 1.5% isoflurane-oxygen mixture at 0.5-1.0L/min by a nose cone and shaved in the dorsal mid-back region for inoculation. Approximately 1.25×10^5 B16-F10 cells in 50μL of 50:50 *v*/*v* HBSS:Cultrex® prepared in Section 5.4.9.2 were carefully injected subcutaneously in the shaved region to avoid leakage of cell suspension. A successful

injection was indicated by a 'bleb' visible on the skin which produced a spherical-shaped tumour when cells grow. Mice were returned into cages ventrally to avoid cell leakage and allowed to recover.

5.4.9.4 Treatment and data collection

Tumour-bearing mice were sorted by weight and split into two groups where heavier mice were administered *via* the IP route and the lighter mice were administered *via* the IT route. Figure 5.2 summarises the treatment plan for both IP and IT administration.

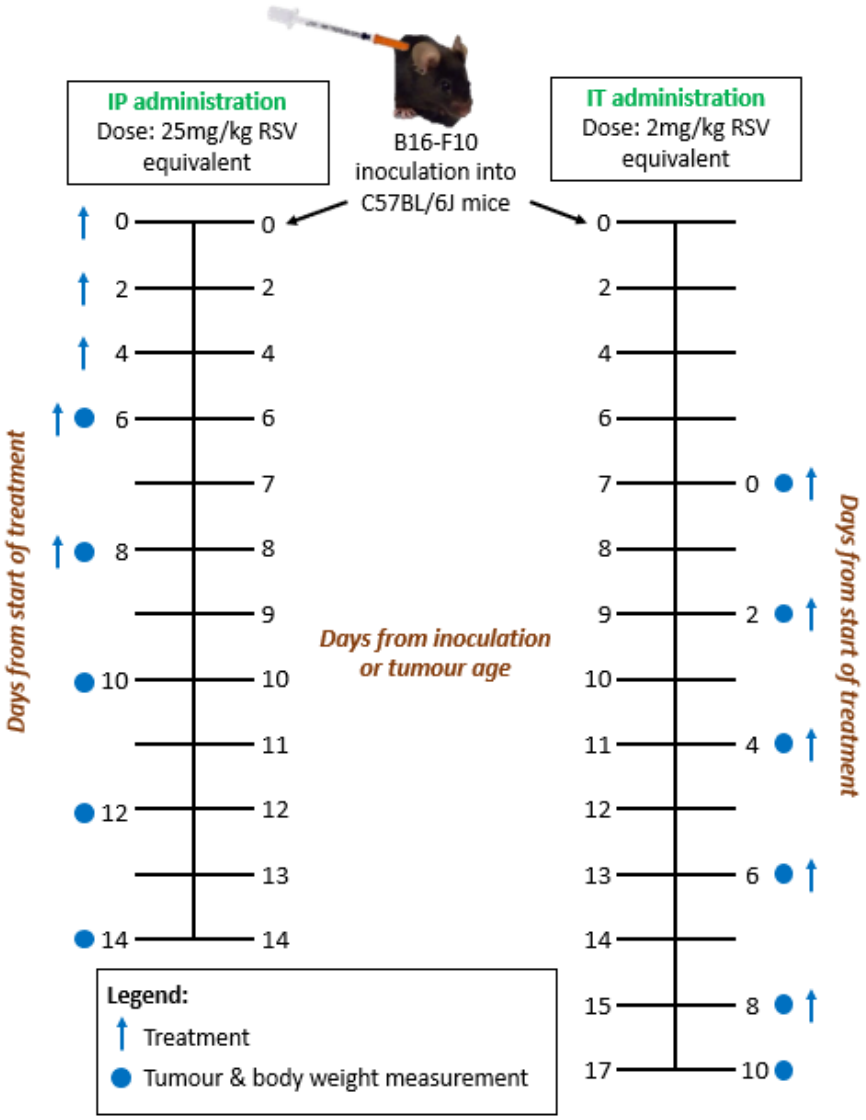

Figure 5.2 Graphical representation of treatment plan for both IP and IT administration

Mice in the IT cohort were allowed to recover after tumour inoculation and observed

daily until tumour was palpable (approximately day 7, see Appendix 7.19). Mice were then sorted into treatment groups summarised in Table 5.3 and 10μL treatments were injected directly into the tumour under anaesthesia at approximately 2mg/kg RSV equivalent per mouse for 5 times, that is days 7, 9, 11, 13 and 15 post-inoculation.

Table 5.3 Treatment groups for tumour-bearing C57BL/6J mice administered *via* IT route

Treatment group	Dose or concentration	Sample size
Conjugated mPEG750-PLA1000-succ-RSV NPs	2mg/kg	7
Encapsulated RSV in mPEG750-PLA1000 NPs	2mg/kg	7
RSV in 20% HPCD	2mg/kg	6
20% HPCD in PBS	200mg/mL	8
Blank mPEG750-PLA1000 NPs	60mg/mL	6

Mice in the IP cohort, on the other hand, were randomly sorted into treatment groups (Table 5.4) and injected with 25mg/kg RSV equivalent in volumes between 80-110μL in the left or right abdominal region right after inoculation of tumours. 20% HPCD and mPEG750-PLA1000 polymer controls were injected at a standardised 100μL volume per mouse. Treatment was repeated every 48 hours for a total of 5 injections per mouse, that is days 0, 2, 4, 6 and 8 after tumour inoculation which was assumed as day 0.

Table 5.4 Treatment groups for tumour-bearing C57BL/6J mice administered *via* IP route

Treatment group	Dose or concentration	Sample size
Conjugated mPEG750-PLA1000-succ-RSV NPs	25mg/kg	7
Encapsulated RSV in mPEG750-PLA1000 NPs	25mg/kg	8
RSV in 20% HPCD	25mg/kg	7
20% HPCD in PBS	200mg/mL	8
mPEG750-PLA1000 polymer in PBS	100mg/mL*	7

*concentration was chosen based on maximum possible amount of mPEG750-PLA1000 polymer present without RSV if encapsulated RSV NP structures were to disintegrate releasing mPEG750-PLA1000 polymers *in vivo*

Tumours were measured every 48 hours once palpable (day 6 for IP cohort; day 7 for IT cohort) using a 150mm digital vernier caliper with ±0.01mm accuracy (Kincrome Australia Pty Ltd: VIC, Australia) under anaesthesia and tumour volumes were calculated from the formula length × width × height × 0.52, where length and width were tumour diameters in mutually perpendicular directions (Fahmy *et al.* 2003). Toxicity was also observed by measuring the body weight of mice before each tumour measurement and was indicated by a decrease in body weight of more than 10% from previous weigh-in. At 14 and 17 days post-inoculation for IP and IT cohorts, respectively, mice were euthanised as per our animal experiment protocol approved by the AEC. Data was presented based on days from start of treatment.

5.4.10 Statistical analyses

All data were presented in mean ± SD for all *in vitro* stability and cell culture studies or standard error of the mean (SEM) for all *in vivo* mouse studies. Error bars may not appear if smaller than the symbol. Statistical analyses were done using student's *t*-test or two-way analysis of variance (ANOVA) followed by a Dunnett's multiple comparisons test using GraphPad Prism version 7.0.3. A p-value of less than 0.05 was considered to be statistically significant.

5.5 Results and discussion

5.5.1 In vitro stability of RSV formulations in rat plasma and human liver microsomes (HLM)

Low bioavailability of RSV was mainly due to its instability in circulation and fast elimination by metabolism *in vivo*. We have used two preliminary *in vitro* screening methods to characterise stability profiles of our conjugated RSV NPs in rat plasma and HLM, which could determine the effect of formulation on the likelihood bioavailability and biological efficacy of RSV (Ng *et al.* 2014, Chung *et al.* 2015). Rat plasma was used to ascertain a preliminary stability profile of the NPs when exposed to plasma esterases. Metabolic enzyme levels in plasma are generally lower than levels in microsomes unless there is an injury to the liver which causes the enzymes to leak out into the plasma. An assessment on the stability of the conjugated RSV NPs

in HLM would assist us in understanding whether conjugation and nano-formulation techniques maintained or altered the metabolic profile of RSV. Although rodent liver microsomes was more relevant due to the use of plasma from the rat species, rodent liver enzymes were known to be more active than human liver enzymes (Sakai *et al.* 2015) and therefore, the use of HLM was employed whereby a slower metabolism rate could be practically observed. Essentially, a stable formulation in both rat plasma and HLM would elucidate that a formulation would stay in circulation and remain intact *in vivo* thus being more bioavailable for better pharmacological effect at target sites (Chung *et al.* 2015, Ma *et al.* 2016). Several factors affect the stability of conjugated RSV NPs including the stability of RSV itself, the stability of the copolymers mPEG-PLA and mPEG-PCL and the stability of the ester links between RSV and the copolymers. These factors will be discussed as results are presented as follows. Due to the unique nature of conjugated RSV NPs containing unconjugated RSV, encapsulated RSV NPs were also assessed for stability in rat plasma and HLM to further elucidate stability profiles of conjugated RSV NPs.

5.5.1.1 In vitro *stability of RSV formulations in rat plasma*

The stability of RSV could be improved by covalent conjugation of RSV to polymers and forming the conjugates into NPs (Siddalingappa *et al.* 2015). Our conjugated RSV NPs were made with an RSV conjugate and encapsulated free RSV as discussed in Section 4.5.1. Figure 5.3 shows the *in vitro* stability of 10mg/mL conjugated RSV NPs in rat plasma against 2mg/mL free RSV control at 37°C for up to 5 hours. Appendix 7.4 summarises plasma stability data of mPEG2000-PCL$_n$-glu-RSV synthesised in Chapter 2 along with buffer stability data published in Ng *et al.* (2015).

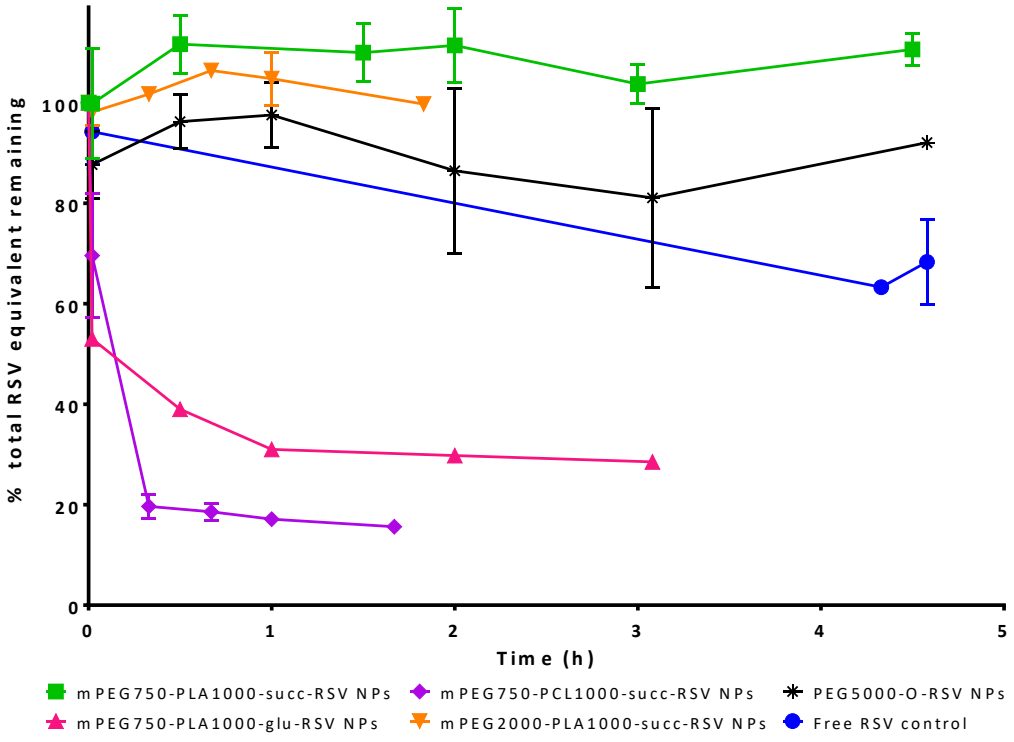

Figure 5.3 Stability of 10mg/mL conjugated RSV NPs in rat plasma at 37°C against 2mg/mL free RSV for up to 5 hours

Data presented as mean (*n*=2 except mPEG750-PLA1000-succ-RSV NPs where *n*=3 and mPEG750-PLA1000-glu-RSV NPs where *n*=1) ± SD where calculated

Using a non-linear regression analysis of the one-phase decay model in GraphPad Prism 7.0.3, plasma $t_{1/2}$ of conjugated RSV NPs and free RSV control was calculated and presented in Table 5.5.

Table 5.5 Calculation of plasma half-life ($t_{1/2}$) of 10mg/mL conjugated RSV NPs and 2mg/mL free RSV control using non-linear regression analysis of one-phase decay model

Formulation	$t_{1/2}$ in rat plasma (h)	% *w/w* RSV conjugate in conjugated RSV NPs
Free RSV	7.7	NR
mPEG750-PLA1000-succ-RSV NPs	Stable	63.9
mPEG750-PLA1000-glu-RSV NPs	0.02	54.8
mPEG750-PCL1000-succ-RSV NPs	0.04	99.3
mPEG2000-PLA1000-succ-RSV NPs	Stable	76.1
PEG5000-O-RSV NPs	Stable	100.0

Data presented as best-fit values from non-linear regression analysis of one-phase decay model; model does not fit data when NPs are stable

2mg/mL free RSV control was seen to have a $t_{1/2}$ of 7.7h, slightly faster than 11.4h found by Li *et al.* (2017c) where RSV in HPCD was administered IV in rats. Robinson *et al.* (2015) discovered that free RSV degraded in an apparent first-order process when 500μg/mL RSV was incubated with rat plasma at 37°C resulting in a $t_{1/2}$ of 25h. This was vastly different from the data we have obtained even when we calculated $t_{1/2}$ of free RSV control as 8.0h using the first-order equation where $t_{1/2}$ is $\frac{0.693}{k}$ to compare. The longer plasma $t_{1/2}$ obtained by Robinson *et al.* (2015) could be due to the concentration used. In enzyme kinetics, the rate of degradation is directly proportional to the substrate concentration, hence the higher concentration of free RSV in our plasma stability assay increased the degradation rate of RSV resulting in a shorter plasma $t_{1/2}$.

From Figure 5.3, it was obvious that mPEG750-PCL1000-succ-RSV NPs and mPEG750-PLA1000-glu-RSV NPs were least stable conjugated RSV NPs in rat plasma at 37°C. The plasma $t_{1/2}$ calculated by one-phase decay model was 0.04h and 0.02h, respectively whereas for mPEG750-PLA1000-succ-RSV NPs, mPEG2000-PLA1000-succ-RSV NPs and PEG5000-O-RSV NPs, plasma $t_{1/2}$ could not be calculated because the one-phase decay model could not fit the data presented in Figure 5.3 where conjugated RSV NPs appeared stable in rat plasma at 37°C. The stable plasma profile of PEG5000-O-RSV NPs was reported by Siddalingappa *et al.* (2015) along with a plasma $t_{1/2}$ of 3h for

mPEG750-PLA1000-succ-RSV NPs. Our mPEG750-PLA1000-succ-RSV NPs was more stable possibly due to the presence of unconjugated RSV encapsulated in the NPs (36.1% *w/w* NPs). The release of unconjugated RSV from the NPs could have saturated the plasma enzymes before mPEG750-PLA1000-succ-RSV conjugate could be complexed rendering a more stable plasma profile than what was found by Siddalingappa *et al.* (2015). These conjugated RSV NPs were less susceptible to plasma esterases than free RSV and could benefit in increasing the bioavailability of RSV *in vivo* (Siddalingappa *et al.* 2015).

Figure 5.3 and Table 5.5 also showed that a longer linker using glutarate (mPEG750-PLA1000-glu-RSV NPs $t_{1/2}$ 0.02 hours) or a more hydrophobic component PCL instead of PLA (mPEG750-PCL1000-succ-RSV NPs $t_{1/2}$ 0.04 hours) did not improve the stability of a conjugated RSV NPs when compared with mPEG750-PLA1000-succ-RSV NPs. Despite synthetic method approaches to improve the stability properties of mPEG750-PLA1000-succ-RSV NPs in Section 2.5.3, the results here showed that the approaches did not produce a significant positive effect to the conjugate mPEG750-PLA1000-succ-RSV NPs as the plasma proteins could have affected the surface charge, aggregation point and particle size of NPs (Curran *et al.* 2011, Wang *et al.* 2013b). Although conjugated RSV NPs were negatively charged (Table 4.11) which usually prevented non-specific protein adsorption (Li *et al.* 2015b), the particle size of the NPs could have played a bigger role in affecting its interaction with plasma proteins (Sanfins *et al.* 2014, Lata *et al.* 2015). HPLC chromatograms of plasma stability experiments could not elucidate other species of RSV other than the conjugate and free RSV but this should not be disregarded as it was possible that the other species degraded at a rapid rate rendering them undetectable by HPLC or the HPLC method employed was not sensitive enough for these species. Nonetheless, data for mPEG2000-PLA1000-succ-RSV NPs in rat plasma was stable up to 2 hours. It would be prudent to repeat the assay with a longer period as the lack of degradation for the first 2 hours showed that the longer hydrophilic component of the conjugate avoided rapid degradation seen in mPEG750-PLA1000-glu-RSV NPs and mPEG750-PCL1000-succ-RSV NPs. A longer assay period would also enable us to determine whether the longer hydrophilic component improved the plasma stability of mPEG750-PLA1000-

succ-RSV NPs. To further elucidate the plasma stability profiles of conjugated RSV NPs, we observed the % change of individual components in conjugated RSV NPs, that is the RSV conjugate and the unconjugated RSV (Figure 5.4).

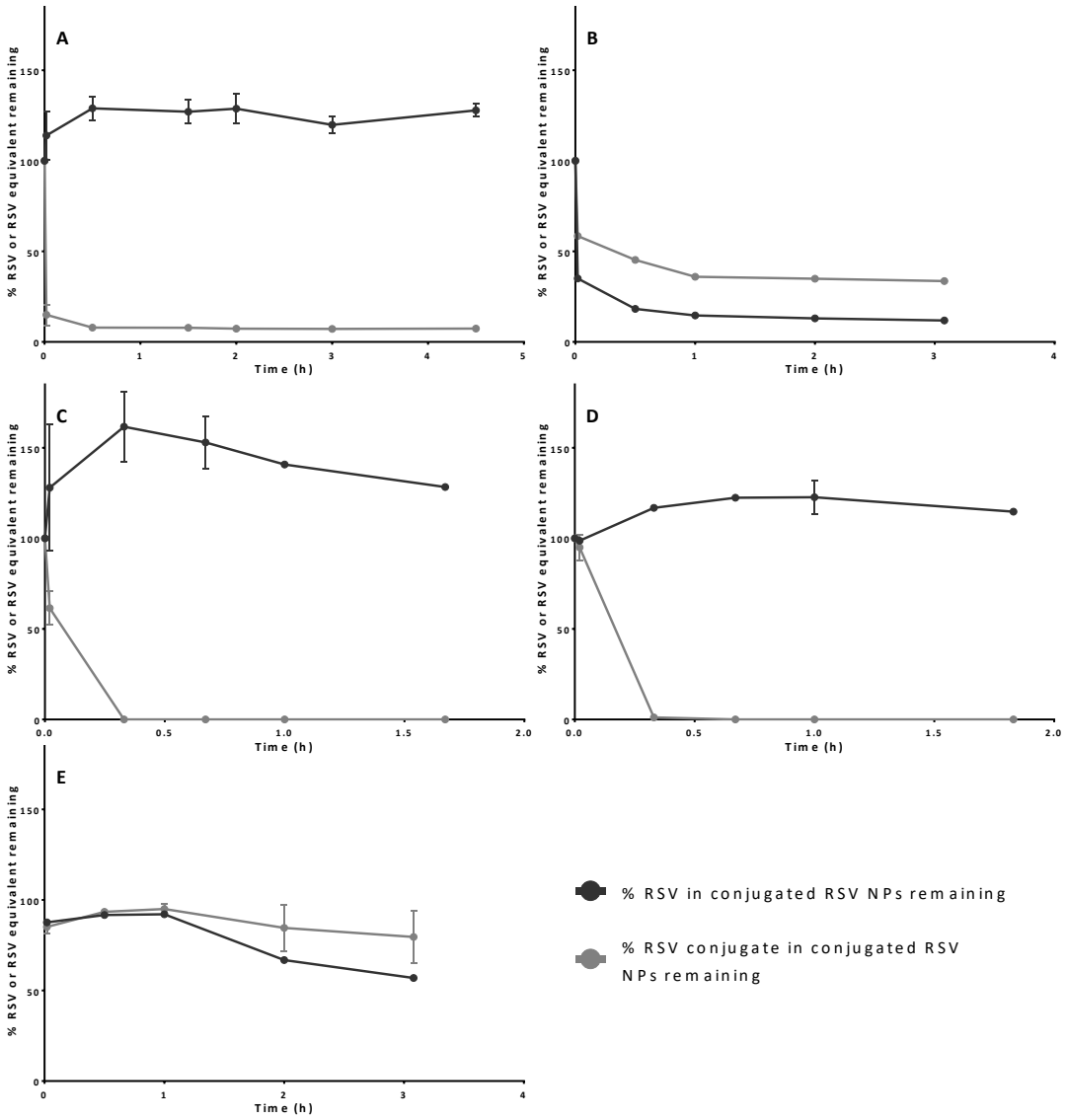

Figure 5.4 Stability profile of conjugated RSV NPs by individual components of unconjugated RSV (black) and RSV conjugate (grey) in rat plasma at 37°C for up to 4.5 hours

A: mPEG750-PLA1000-succ-RSV NPs, B: mPEG750-PLA1000-glu-RSV NPs, C: mPEG750-PCL1000-succ-RSV NPs, D: mPEG2000-PLA1000-succ-RSV NPs, E: PEG5000-O-RSV NPs
Data presented as mean (*n*=2 except mPEG750-PLA1000-succ-RSV NPs where *n*=3 and mPEG750-PLA1000-glu-RSV NPs where *n*=1) ± SD where calculated

In each graph, the % of unconjugated RSV (black) and RSV conjugate (grey) remaining over time in each conjugated RSV NPs after exposure to rat plasma was presented.

Due to the unique combination of components in our conjugated RSV NPs, several factors could affect the overall plasma stability profile of a conjugated RSV NPs including the stability of individual components in plasma over time which can affect the physical stability of NPs in plasma. Other components to consider are possible presence of unconjugated polymers which could encapsulate unconjugated RSV to form encapsulated RSV NPs.

In general, Figure 5.4 further confirms that the stable profiles of mPEG750-PLA1000-succ-RSV NPs (A) and PEG5000-O-RSV NPs (E) in rat plasma was due to presence of a stable RSV conjugate throughout the experiment although hydrolysis of RSV conjugates was seen for up to 0.5h of the experiment for mPEG750-PLA1000-succ-RSV NPs. Despite the hydrolysis, the remaining RSV conjugates in the NPs were able to sustain the physical stability of mPEG750-PLA1000-succ-RSV NPs against plasmatic enzymes. The structural formation of the NPs could have also limited access to active sites of enzymes. This proves that these conjugated RSV NPs provided a better stability profile than free RSV in rat plasma. Conversely, the stability profiles of the RSV conjugate component in mPEG2000-PLA1000-succ- RSV NPs (D) showed a rapid degradation of the conjugate where no conjugate was detectable by 0.5h, however the unconjugated RSV showed a fairly stable profile up to 2h. It was possible that the NPs contained unconjugated RSV encapsulated in unconjugated mPEG2000-PLA1000 which maintained a good stability against plasma enzymes translating into an overall stable plasma profile for mPEG2000-PLA1000-succ-RSV NPs seen in Figure 5.3. Due to the high % of mPEG750-PCL1000-succ-RSV conjugate component in mPEG750-PCL1000-succ-RSV NPs (99.3% *w/w*), the overall plasma stability profile of the NPs was heavily dependent on the stability of the RSV conjugate. Therefore, the rapid degradation of mPEG750-PCL1000-succ-RSV NPs (C) was due to the rapid degradation of RSV conjugate which showed a rapid increase in unconjugated RSV cleaved from the RSV conjugates followed by a steady degradation. This steady degradation would have attributed to the apparent plateau in the overall plasma stability profile of mPEG750-PCL1000-succ-RSV NPs in Figure 5.3 due to enzyme saturation of RSV, however, as the experiment was not carried out longer than 2h, we cannot conclude whether this plateau was sustained.

Interestingly, mPEG750-PLA1000-glu-RSV NPs (B) showed a profile with rapid degradation followed by a plateau in both RSV conjugate and unconjugated RSV components. It was possible that the structural integrity of the conjugated RSV NPs was compromised due to the hydrolysis of the mPEG750-PLA1000-glu-RSV conjugate as the longer glu linker provided an easier access to the ester bond by plasma enzymes, however, the non-existent increase in unconjugated RSV levels showed that the hydrolysis of RSV conjugate releasing unconjugated RSV was not probable. As such, a different mechanism was possibly at play in the stability of mPEG750-PLA1000-glu-RSV NPs in rat plasma. From Section 4.5.1.2, we have described the presence of two particle size distribution in mPEG750-PLA1000-glu-RSV NPs, one of which was possibly encapsulated RSV NPs formed with unconjugated RSV and mPEG750-PLA1000. The simultaneous degradation of both unconjugated RSV and RSV conjugate could mean that two different types of NPs, that is pure conjugated RSV NPs and encapsulated RSV NPs, existed in this NP dispersion and was exposed to rat plasma enzymes and degraded simultaneously. Furthermore, the plateau in both overall and individual component stability profiles depicted enzyme saturation where no further degradation could be observed. Due to the influence of encapsulated unconjugated RSV in some conjugated RSV NPs, we have conducted the plasma stability study of encapsulated RSV NPs with corresponding amphiphilic copolymers mPEG750-PLA1000, mPEG750-PCL1000 and mPEG2000-PLA1000 as a comparison (Figure 5.5).

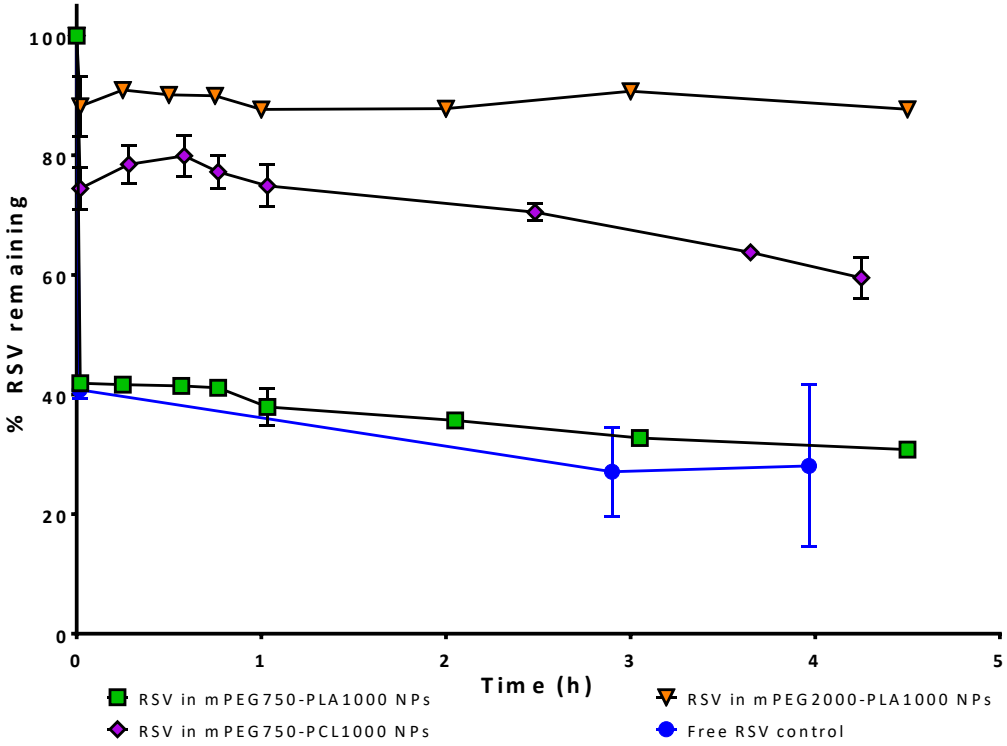

Figure 5.5 Stability of 10-20μg/mL encapsulated RSV NPs against 40μg/mL free RSV control in rat plasma at 37°C for up to 4.5 hours

Data presented as mean (n=3 except RSV in mPEG2000-PLA1000 NPs and free RSV control where n=2) ± SD

All encapsulated RSV NPs with 10-20μg/mL of RSV showed a more stable profile than 40μg/mL free RSV control ($t_{1/2}$ 0.01h) in rat plasma with mPEG2000-PLA1000 NPs being most stable. Encapsulation of RSV into NPs rendered a more stable RSV than free RSV in PK studies and prevented further metabolism of RSV *in vitro* as reviewed by Davidov-Pardo *et al.* (2014). Calculation of plasma $t_{1/2}$ of encapsulated RSV NPs using the one-phase decay model similar to what was applied to conjugated RSV NPs was not possible due to their apparent stable profile which did not fit the model. A longer experiment on encapsulated RSV NPs would have been useful; however, this was not performed. Nonetheless, the plasma stability profiles of encapsulated RSV NPs were used to assist in interpreting the plasma stability profiles of conjugated RSV NPs previously discussed. Before comparing with corresponding conjugated RSV NPs, plasma stability profiles of encapsulated RSV NPs will be evaluated.

Both RSV in mPEG750-PLA1000 NPs and RSV in mPEG750-PCL1000 NPs were less stable than RSV in mPEG2000-PLA1000 NPs possibly due to their low MW and hence

higher hydrolysis rate of the polymers by plasma esterases when compared with the larger mPEG2000-PLA1000 (Davidov-Pardo *et al.* 2014). This effect of higher MW was also observed in release studies conducted in Section 4.5.3.2 where RSV encapsulated in mPEG750-PLA1000 and mPEG750-PCL1000 NPs achieved 100% cumulative release of RSV at 2 hours compared to RSV in mPEG2000-PLA1000 NPs at 6.3 hours due to a faster polymer hydrolysis rate of the mPEG750 copolymers in the release medium PBS. Between RSV in mPEG750-PLA1000 and mPEG750-PCL1000 NPs, the mPEG-PCL NPs was more stable than mPEG-PLA NPs due to the lower crystallinity in mPEG750-PLA1000 polymer compared to mPEG750-PCL1000 polymer which attributed to its higher polymer hydrolysis rate by plasma esterase and hence a lower stability of the NPs in rat plasma (Carletto *et al.* 2016).

The stable plasma profile of mPEG750-PLA1000-succ-RSV NPs was most likely due to the combination of a stable RSV conjugate and stable NPs formed with unconjugated RSV and unconjugated mPEG750-PLA1000. Although the stability profile of RSV encapsulated in mPEG750-PLA1000 NPs was not substantially better than free RSV control (Figure 5.5), the combination of a stable RSV conjugate maintaining the NPs structure could have allowed a better stability of unconjugated RSV encapsulated within the NP core. The higher stability of RSV in mPEG2000-PLA1000 NPs could also explain the higher plasma stability of conjugated mPEG2000-PLA1000-succ-RSV NPs where unconjugated polymers was responsible for protecting remaining encapsulated RSV from plasma degradation. As the conjugate mPEG2000-PLA1000-succ-RSV was seen to degrade rapidly in Figure 5.4 where by 1h, no conjugate was present, the overall plasma stability profile of mPEG2000-PLA1000-succ-RSV NPs was largely due to NPs formed with unconjugated RSV encapsulated in unconjugated mPEG2000-PLA1000. Similarly, the moderate stability of RSV encapsulated in mPEG750-PCL1000 NPs corroborated with the steady degradation of unconjugated RSV component of mPEG750-PCL1000-succ-RSV NPs in rat plasma (Figure 5.4). Apart from stability of individual components in conjugated RSV NPs, in particular RSV conjugates which affect the structural integrity and physical stability of the NPs, we should be aware that the morphology of the NPs, compared to its aqueous dispersion, could be altered when exposed to the plasma environment which had a slightly

different pH, presence of proteins and different viscosity (Cavallaro *et al.* 2004, Chung *et al.* 2015). There was also a factor of the formulations binding to the plasma proteins or to the cellular membrane which could affect the extraction of RSV and underestimating the true value of remaining RSV (Ruivo *et al.* 2015).

5.5.1.2 In vitro *stability of RSV formulations in human liver microsomes (HLM)*

In order to assess the ability of conjugated RSV NPs to decrease the metabolism rate of RSV, conjugated RSV NPs developed in Chapter 4 was incubated in HLM at 37°C for up to 1.5 hours to be assessed against phase II metabolism and compared with free RSV (Figure 5.6).

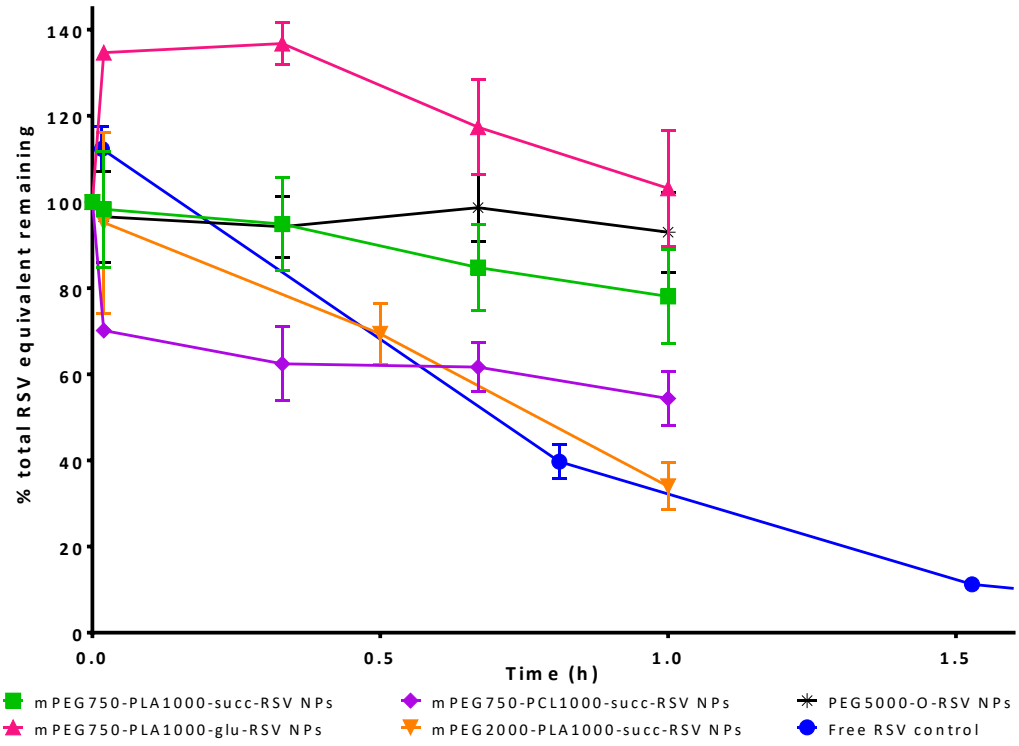

Figure 5.6 Stability of 500μg/mL conjugated RSV NPs in HLM at 37°C up to 1.5 hours against 300μg/mL free RSV control

Data presented as mean (n=2 except mPEG750-PLA1000-succ-RSV NPs and mPEG750-PCL1000-succ-RSV NPs where n=3) ± SD

Using the first-order equation and data from Figure 5.6, free RSV control had a microsomal $t_{1/2}$ of 0.5h, longer than what was quoted by Siddalingappa *et al.* (2015), that is 0.2h using rat liver microsomes. Goh *et al.* (2017) showed that the $t_{1/2}$ of RSV was 0.4h and less than 0.1h when incubated in human and rat hepatocytes,

respectively. Asensi *et al.* (2002) found 80% of 4.6mg/mL RSV incubated in rat hepatocytes was metabolised within 20 minutes with nothing detectable by 60 minutes. This further highlighted the different metabolic activity and rates between species and individuals (Ruivo *et al.* 2015, Singh *et al.* 2015) which prompted the assessment of phase II metabolism using pooled HLM instead of rat liver microsomes where a more practical stability profile could be observed. Table 5.6 summarises the microsomal $t_{1/2}$ of conjugated RSV NPs and free RSV control calculated using the first-order equation and further confirmed by a non-linear regression analysis using a one-phase decay model by GraphPad Prism 7.0.3.

Table 5.6 Microsomal half-life ($t_{1/2}$) of conjugated RSV NPs and free RSV control using first-order equation and non-linear regression analysis with one-phase decay model

Formulation	**First-order equation[a]**		**One-phase decay model[b]**	
	R^2	**$t_{1/2}$ (h)**	**R^2**	**$t_{1/2}$ (h)**
Free RSV	0.998	0.5	0.976	0.6
mPEG750-PLA1000-succ-RSV NPs	0.980	2.8	0.977	2.9
mPEG750-PLA1000-glu-RSV NPs	0.877[c]	2.4	UD[d]	
mPEG750-PCL1000-succ-RSV NPs	0.640[e]	1.6	0.135[e]	0.9
mPEG2000-PLA1000-succ-RSV NPs	0.967	0.7	0.970	0.7
PEG5000-O-RSV NPs	0.308[e]	17.7	0.03[e]	10.6

[a]ln(concentration) = -rate constant × time + concentration at 0 hours; calculations were done using mean values of % total RSV equivalent (concentration) remaining over time
[b]Calculated using non-linear regression analysis with one-phase decay model by GraphPad Prism 7.0.3
[c]First-order equation excluded data at 0 hours; ln(concentration) = -rate constant × time + concentration at 0.02 hours
[d]UD = undetermined; model does not fit data
[e]R^2 value low due to lack of data beyond 1h or lack of degradation profile

All conjugated RSV NPs were found to have better stability against phase II metabolism compared to free RSV albeit at varying degrees, however their stability was not as high as that seen in rat plasma, which could be due to the concentrated amount of enzymes in microsomes compared to plasma. This proved our hypothesis that conjugation of RSV improved the stability of RSV against phase II metabolism in

HLM due to change of substrate for the enzymes. Although chemical modifications to mPEG750-PLA1000-succ-RSV was expected to improve the stability of the RSV conjugate, all ester conjugated RSV NPs (mPEG750-PLA1000-glu-RSV NPs, mPEG750-PCL1000-succ-RSV NPs and mPEG2000-PLA1000-succ-RSV NPs) did not portray a better stability profile than mPEG750-PLA1000-succ-RSV NPs in HLM. It can be speculated that the low MW of polymers in the conjugates was not significantly different enough to cause metabolic rate changes amongst the ester conjugated RSV NPs. The ether conjugated RSV NPs PEG5000-O-RSV was very stable due to its stronger ether bond compared to the ester bonds and could not fit the first-order equation using data obtained. The high concentrations of mPEG750-PLA1000-glu-RSV NPs was unexplainable despite being replicated twice. It was possible that evaporation occurred during the experiment or the extractions at time 0 hours was not conducted properly. Therefore, for the calculation of $t_{1/2}$ for mPEG750-PLA1000-glu-RSV NPs using first-order equation, data at 0 hours was excluded and first time point was at 0.02h. To further elucidate the microsomal stability profiles of conjugated RSV NPs, stability profiles of individual components, that is unconjugated RSV and RSV conjugate, is depicted in Figure 5.7.

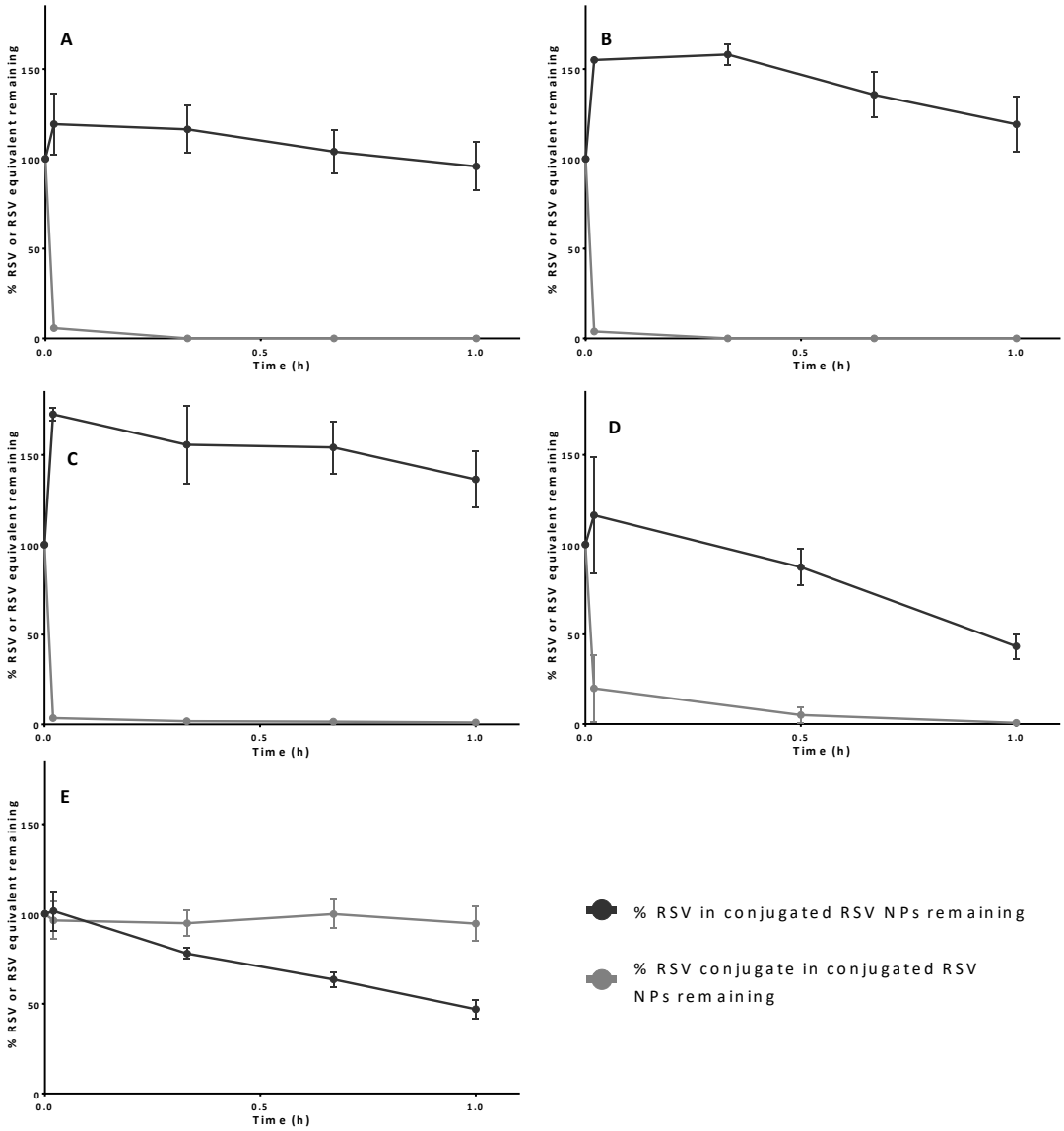

Figure 5.7 Stability profile of conjugated RSV NPs by individual components of unconjugated RSV (black) and RSV conjugate (grey) in HLM at 37°C for up to 1 hour

A: mPEG750-PLA1000-succ-RSV NPs, B: mPEG750-PLA1000-glu-RSV NPs, C: mPEG750-PCL1000-succ-RSV NPs, D: mPEG2000-PLA1000-succ-RSV NPs, E: PEG5000-O-RSV NPs
Data presented as mean (*n*=2 except mPEG750-PLA1000-succ-RSV NPs and mPEG750-PCL1000-succ-RSV NPs where *n*=3) ± SD

From Figure 5.7, the stability profile of components in PEG5000-O-RSV NPs (E) showed that the RSV conjugate was highly stable for up to 1h whereas the unconjugated RSV component degraded rapidly. As the unconjugated RSV component was less than 4% of total RSV equivalent of PEG5000-O-RSV NPs, its degradation was not significant to the overall microsomal stability of the NPs in Figure

5.6. Conversely, all ester conjugate components degraded rapidly in HLM which released significant amounts of cleaved RSV within 0.5h. The RSV component in the ester conjugated RSV NPs was then a combination of unconjugated RSV encapsulated in the conjugated RSV NPs and cleaved RSV from ester RSV conjugates hence values of more than 100% were seen. This component then proceeded to degrade at varying degrees as seen in Figure 5.7 with RSV from mPEG2000-PLA1000-succ-RSV NPs (D) having degraded the fastest followed by RSV from mPEG750-PLA1000-glu-RSV NPs (B) and RSV from mPEG750-PLA1000-succ-RSV NPs (A) and the slowest degradation of RSV was from mPEG750-PCL1000-succ-RSV NPs (C). Using first-order equation on the degradation profile of the RSV component of conjugated RSV NPs in HLM, microsomal $t_{1/2}$ was calculated and presented in Table 5.7.

Table 5.7 Microsomal half-life ($t_{1/2}$) of RSV component in conjugated RSV NPs and free RSV control using first-order equation

RSV component in conjugated RSV NPs	**First-order equation***	
	R^2	**$t_{1/2}$ (h)**
Free RSV	0.998	0.5
mPEG750-PLA1000-succ-RSV NPs	0.959	2.9
mPEG750-PLA1000-glu-RSV NPs	0.868	2.4
mPEG750-PCL1000-succ-RSV NPs	0.915	3.2
mPEG2000-PLA1000-succ-RSV NPs	0.949	0.7
PEG5000-O-RSV NPs	0.994	0.9

Calculations were done using mean values of % RSV (concentration) remaining over time
*ln(concentration) = -rate constant × time + concentration at 0.02 hours except for free RSV and PEG5000-O-RSV NPs where ln(concentration) = -rate constant × time + concentration at 0 hours

Comparing with microsomal $t_{1/2}$ calculated for overall microsomal stability profiles of conjugated RSV NPs, the microsomal $t_{1/2}$ of RSV component in all conjugated RSV NPs were similar to that of the microsomal $t_{1/2}$ of conjugated RSV NPs as expected, however this was not the case for mPEG750-PCL1000-succ-RSV NPs where the microsomal $t_{1/2}$ was 1.6h and its RSV component was 3.2h. This could be due to the high % of mPEG750-PCL1000-succ-RSV conjugate (99.3% *w/w*) in the NPs which when

metabolised, released a high amount of RSV cleaved from mPEG750-PCL1000-succ-RSV causing saturation of microsomal enzymes resulting in a longer microsomal $t_{1/2}$ of RSV component in mPEG750-PCL1000-succ-RSV NPs. Nonetheless, the degradation profile of unconjugated RSV components could possibly be further expounded by stability profiles of encapsulated RSV NPs in mPEG750-PLA1000, mPEG750-PCL1000 and mPEG2000-PLA1000 (Figure 5.8).

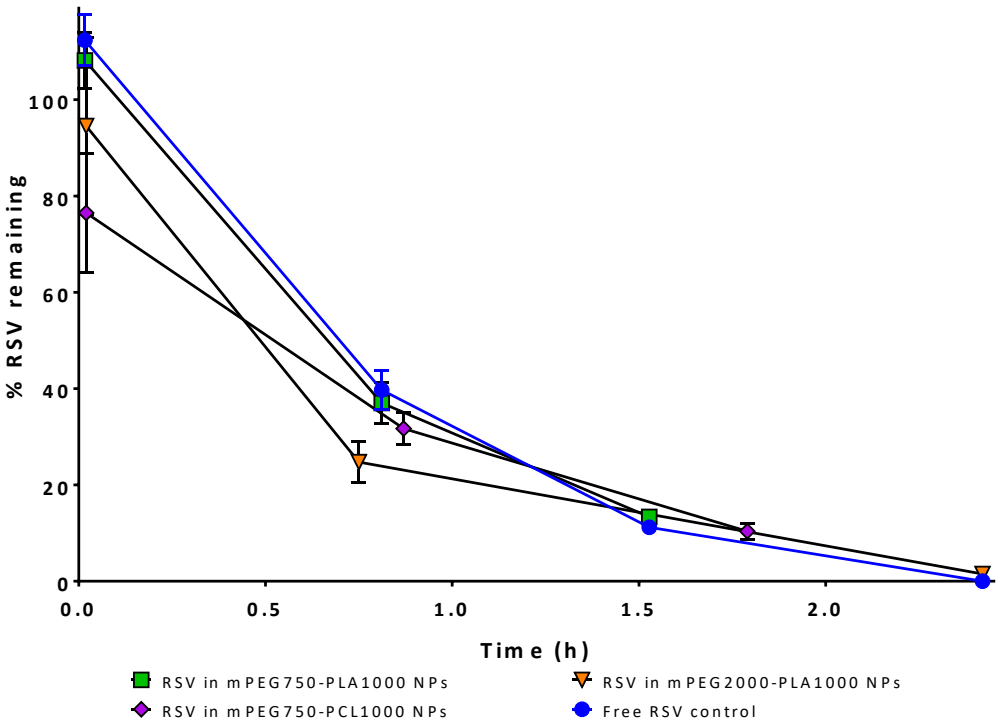

Figure 5.8 Stability profile of up to 0.2-2.5μg/mL encapsulated RSV NPs in HLM at 37°C for up to 2.5h against 300μg/mL free RSV control

Data presented as mean (*n*=3 except free RSV control where *n*=2) ± SD

Although the stability profiles of encapsulated RSV NPs in rat plasma were favourable, stability profiles of all encapsulated RSV NPs in HLM were similar to the free RSV control revealing that nano-encapsulation did not protect free RSV from *in vitro* metabolism. Microsomal $t_{1/2}$ of encapsulated RSV NPs was obtained by using the first-order equation similarly to what was conducted on conjugated RSV NPs and tabulated in Table 5.8.

Table 5.8 Microsomal half-life ($t_{1/2}$) of encapsulated RSV NPs and free RSV control using first-order equation

Formulation	First-order equation*	
	R^2	$t_{1/2}$ (h)
Free RSV	0.998	0.5
RSV in mPEG750-PLA1000 NPs	0.998	0.5
RSV in mPEG750-PCL1000 NPs	0.990	0.6
RSV in mPEG2000-PLA1000 NPs	0.999	0.4

Calculations were done using mean values of % RSV (concentration) remaining over time
*ln(concentration) = -rate constant × time + concentration at 0 hours

Data from microsomal stability studies on encapsulated RSV NPs further confirmed that the overall microsomal stability of conjugated RSV NPs (Figure 5.6) was due to the RSV conjugate components and its role in altering the enzyme-substrate mechanism and thus modified the kinetics of HLM enzymes when conjugated RSV NPs were used as opposed to encapsulated RSV NPs. The RSV conjugate components also contributed to a more stable NP structure which decreased the unconjugated RSV available for enzymatic activity. The presence of unsubstituted hydroxyl groups in RSV contributed to the higher metabolism rate as they were prone to conjugation by liver enzymes (Teng *et al.* 2012, Chung *et al.* 2015) and thus, chemically attaching RSV to amphiphilic copolymers in conjugated RSV NPs as opposed to physically entrapping RSV into the copolymers in encapsulated RSV NPs attributed to the difference in the overall microsomal stability profiles of the RSV formulations seen in Figure 5.6 and Figure 5.8, respectively (Ho *et al.* 2013, Luo *et al.* 2016b).

It should be noted, however, that all ester conjugated RSV NPs underwent significant chemical degradation at initial exposure to HLM matrix without the co-factor UDPGA which showed other unknown metabolic mechanisms (Figure 5.9). Following this, mPEG750-PLA1000-glu-RSV and mPEG2000-PLA1000-succ-RSV conjugates underwent further degradation significantly decreasing the amount of RSV conjugates in the NPs after 1h incubation in HLM matrix without co-factor.

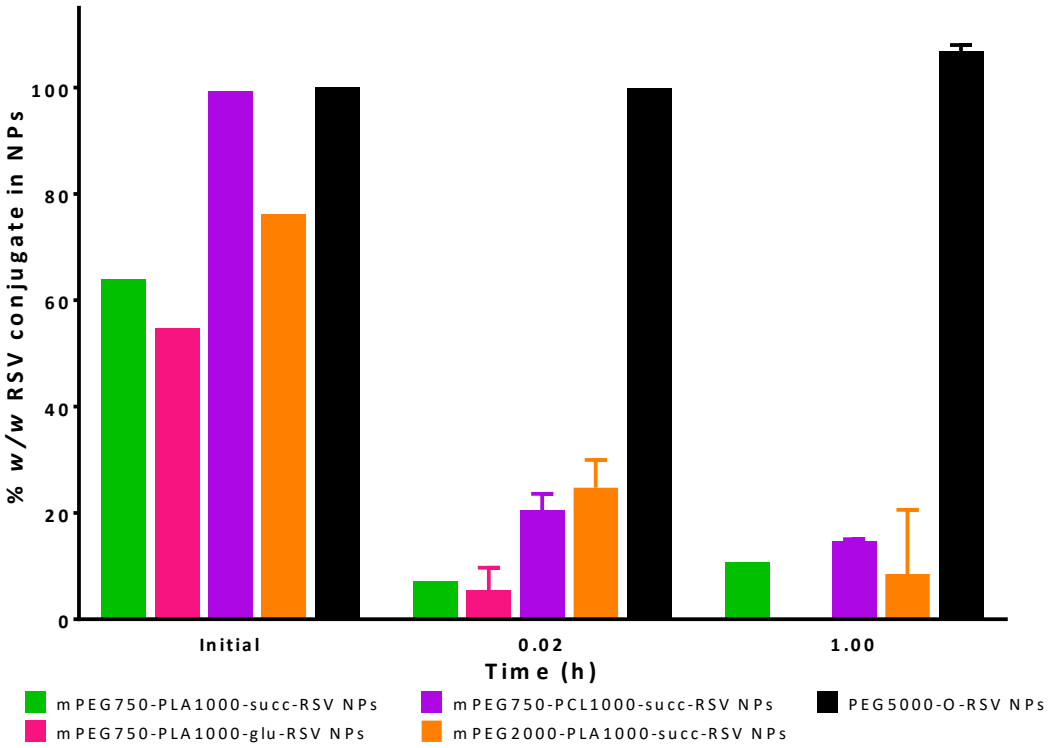

Figure 5.9 Percentage *w/w* of RSV conjugate in conjugated RSV NPs at initial (before incubation) and at 0.02 hour and 1 hour of incubation in HLM without co-factor UDPGA at 37°C for 1 hour

Data presented as mean (*n*=2 except mPEG750-PLA1000-succ-RSV NPs and mPEG750-PCL1000-succ-RSV NPs where *n*=1 and 3, respectively) ± SD where calculated

The chemical instability of mPEG2000-PLA1000-succ-RSV conjugate was also seen when performing validations on the HPLC gradient method for analysing mPEG2000-PLA1000-succ-RSV conjugate in biological samples (Table 3.16). As such, the stability profile of RSV conjugate components in conjugated RSV NPs (Figure 5.7) could be explained by the rapid degradation at the initial point of exposure to the HLM matrix which resulted in low amounts of RSV conjugates detected throughout the experiment and initial burst of free RSV at the beginning of the experiment. This chemical degradation was sufficient enough to disrupt the structural integrity of the NP which resulted in the rapid release of RSV and further enzyme degradation of the RSV conjugate and free RSV.

5.5.2 Selection of formulations for biological evaluation

Preliminary *in vitro* studies have enabled us to select formulations for further *in vitro*

cell culture and *in vivo* studies. Table 5.9 summarised selected preliminary data thus far for each formulation. As one of the aims of the project was to decrease the metabolism or slow down the degradation rate of RSV, the main criteria for further assessment should be based on stability in rat plasma and HLM. Two conjugated RSV NPs (PEG5000-O-RSV NPs and mPEG750-PLA1000-succ-RSV NPs) that showed better stability in both rat plasma and HLM were allocated into Group 1 in Table 5.9. Both conjugated RSV NPs also showed a sustained release of RSV which could assist in the therapeutic effect of RSV *in vivo.* Group 2 formulations were NPs that showed high stability in rat plasma but did not improve the metabolic stability of RSV whereas Group 3 formulations showed good metabolic stability in HLM but was rapidly degraded in rat plasma. Between Group 2 and Group 3, stability in HLM was considered more important because even though stability in rat plasma may be low, hydrolysis by plasma enzymes could be beneficial by maximising exposure of RSV close to the site of administration depending on the route. Also, lack of plasma stability indicates that if an IT administration was employed, the impact of plasma instability of NPs would be minimum. Nonetheless, the plasma stability data allowed us to elucidate possible hurdles which could occur during *in vivo* experiments including storage of samples. Following this, all formulations including free RSV should be further assessed for anticancer activity in B16-F10 melanoma cells to narrow down to a maximum of two for final *in vitro* biological assays and *in vivo* assessment in a B16-F10 mouse model.

Table 5.9 Summary of selected preliminary data for RSV formulations and group allocation

Formulation	**% *w/w* RSV conjugate**	**Formulation selection criteria***	**t_{max} (h)**	**$t_{1/2}$ in rat plasma (h)**	**$t_{1/2}$ in HLM (h)**
Reference tables	Table 2.8	Table 4.12	Table 4.10 and Table 4.11	Table 5.5	Table 5.6 and Table 5.8
Free RSV	NR	NR	1.3	7.7 (2mg/mL) and 0.01 (40μg/mL)	0.5
			Group 1		
PEG5000-O-RSV	100.0	-	>47.5	Stable	17.7
mPEG750-PLA1000-succ-RSV	63.9	++	3.8	Stable	2.8
			Group 2		
RSV in mPEG2000-PLA1000	NR	-	6.3	Stable	0.4
mPEG2000-PLA1000-succ-RSV	76.1	+	2.0	Stable	0.7
RSV in mPEG750-PLA1000	NR	+	2.2	Stable	0.5
RSV in mPEG750-PCL1000	NR	-	2.0	Stable	0.6
			Group 3		
mPEG750-PLA1000-glu-RSV	54.8	+	4.0	0.02	2.4
mPEG750-PCL1000-succ-RSV	99.3	-	2.2	0.04	1.6

*++ fulfils all criteria; + fulfils more than half of all criteria; – fulfils half or less than half of all criteria

5.5.3 Stability of RSV formulations in cell culture growth media

As the efficacy of RSV formulations is dependent on their stability in CGM used to grow B16-F10 and NIH/3T3 cells, we have assessed their stability over 48 hours by incubating the formulations in CGM. Figure 5.10 displays the % of total RSV equivalent or RSV remaining over time.

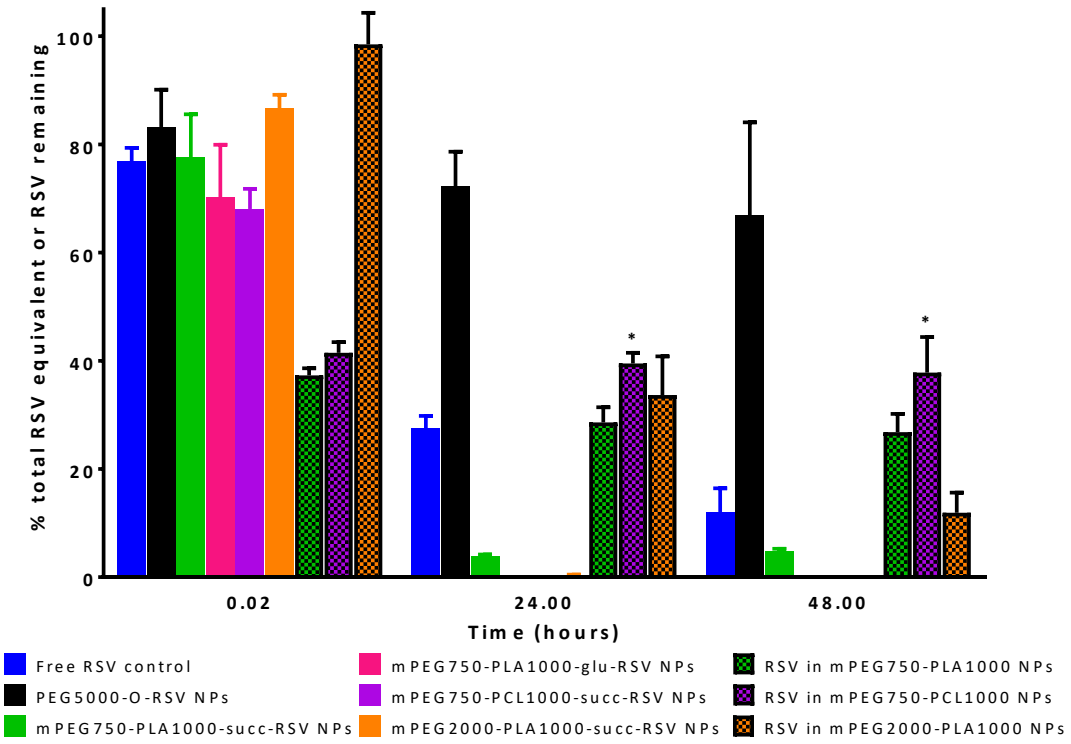

Figure 5.10 Stability of RSV formulations in complete growth media (CGM) at 37°C for up to 48 hours

Data presented as mean (*n*=3 except mPEG750-PLA1000-glu-RSV NPs, PEG5000-O-RSV NPs and RSV encapsulated in mPEG2000-PLA1000 NPs where *n*=2) ± SD
*not significant compared to t=0.02h, remaining t=24h and 48h results were significant ($p<0.05$) compared to t=0.02h

From the figure above, it was clear that RSV itself was not stable in CGM with about 30% remained after 24 hours of incubation at 37°C. This degradation was also seen by Long *et al.* (2010), Yang *et al.* (2010) and Chang *et al.* (2018) in cell-free systems. There was speculation by Yang *et al.* (2010) that RSV degraded by oxidation yielding hydrogen peroxide (H_2O_2) which affected cell growth leading to artificial results, however, Long *et al.* (2010) showed no significant H_2O_2 production although there

was significant degradation over 24 hours when 11μg/mL to 0.2mg/mL of RSV was incubated in DMEM. The presence of bicarbonate ions in Base Modified Eagle Medium which is similar to our CGM was revealed to have cause the significant degradation of RSV (Yang *et al.* 2010). Recently, Chang *et al.* (2018) reported that a combination of 10% FBS and 1mM pyruvate in DMEM completely avoided degradation of RSV and oxy-RSV but not acetyl-RSV. We speculate that the presence of ester bonds in acetyl-RSV could have been affected by the pH of the media which culminated in its significant degradation which explained the instability of our ester conjugated RSV NPs and encapsulated RSV NPs over 48 hours in Figure 5.10. Although our CGM did not contain pyruvate, the presence of 9% FBS should have been sufficient to avoid the degradation of RSV by superoxide dismutase (SOD) activity according to results shown by Chang *et al.* (2018). The ether conjugated RSV NPs (PEG5000-O-RSV) showed lesser degradation compared to other formulations and could be due to its strong ether covalent bond. Although both conjugated and encapsulated RSV NPs were found unstable in CGM, we have continued to assess them by cell culture as cellular uptake of the NPs could avoid the degradation of NPs in CGM and improve the cytotoxicity of the RSV formulations. Nonetheless, cell culture results should be considered with the knowledge that RSV formulations are unstable in CGM after 24 hours of incubation at 37°C and formulations needed to be freshly prepared in CGM to avoid further artificial results.

5.5.4 Dose and incubation time response of RSV

In order to select an appropriate dose for further anticancer evaluation, a dose and incubation time response assay was conducted on free RSV as per Section 5.4.5.

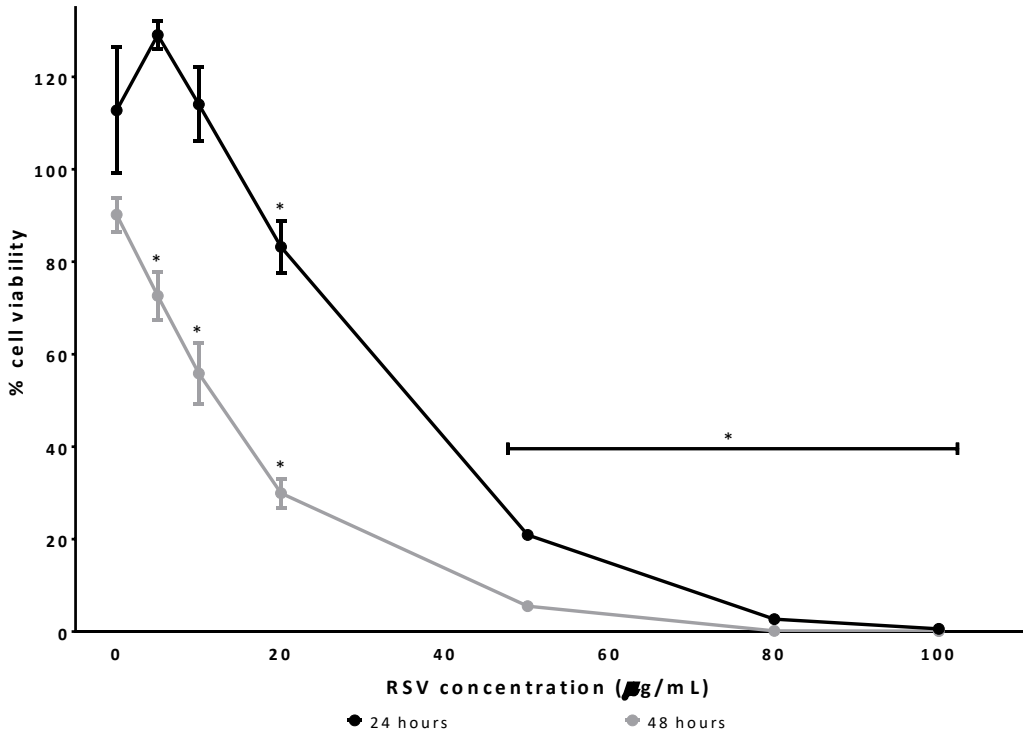

Figure 5.11 Dose and incubation time response of free RSV on B16-F10 cells
Data presented as mean (*n*=2) ± SD *p<0.05 compared to 0μg/mL

Figure 5.11 showed that when treated for 24 hours, a low concentration of RSV (<10μg/mL) encouraged cell growth and higher than 10μg/mL RSV produced a dose-dependent anti-proliferative effect. The hormesis characteristic was observed when RSV was tested in various cell lines by Calabrese *et al.* (2010), Dun *et al.* (2015) and Su *et al.* (2013), which incidentally led to difficulty in choosing the right dose for clinical studies (Zordoky *et al.* 2015). Ruivo *et al.* (2015) described that the dual mechanism of action of RSV in cell protection and cell apoptosis depended on the cellular conditions, concentration used, cytosolic redox status and duration of contact. The IC_{50} of RSV after a 24-hour treatment was found to be 33.6±1.2μg/mL, however, Caltagirone *et al.* (2000) quoted an IC_{50} of 1.1μg/mL for RSV in another B16 variant, B16-BL6 cells. The anti-proliferative effect of RSV was shown in other cell lines with varying IC_{50} values (Junco *et al.* 2013, Karthikeyan *et al.* 2013, Lee-Chang *et al.* 2013, Schaafsma *et al.* 2016) demonstrating the cell-specific anti-proliferative properties of RSV. A distinct decrease in B16-F10 cell viability was observed when cells were treated with 50μg/mL compared to 20μg/mL of RSV along with visible

cellular shrinkage and detachment indicating apoptosis (Dun *et al.* 2015) (see Appendix 7.13 for microscopic images of cells). When treated for 48 hours, cell viability was dose-dependent and the IC_{50} of RSV was found to be 10.8±1.1μg/mL. Therefore, with a longer 48-hour treatment, a lower dose of RSV achieved the same effect compared to the 24-hour treatment. It should be noted that cells were not over-confluent which could result in cell death. We chose a 48-hour treatment with 10 and 20μg/mL RSV equivalent as the dose for our *in vitro* evaluations as the IC_{50} was in between the two concentrations. Interestingly, degradation of RSV in CGM seen in Figure 5.10 did not affect the anti-proliferative effect of RSV on B16-F10 cells and this could be attributed to the possible cell uptake of RSV which prevented the exposure of RSV to the CGM components which were critical to degradation. It would be pertinent to conduct a cellular uptake study on RSV and possibly other RSV formulations to further understand the biological effect of RSV on B16-F10 cells.

5.5.5 Anti-proliferative effect of RSV formulations in B16-F10 cells

B16-F10 cells were treated with 10 and 20μg/mL RSV equivalent concentrations of all formulations excluding mPEG750-PLA1000-glu-RSV NPs due to lack of raw material to prepare the NPs.

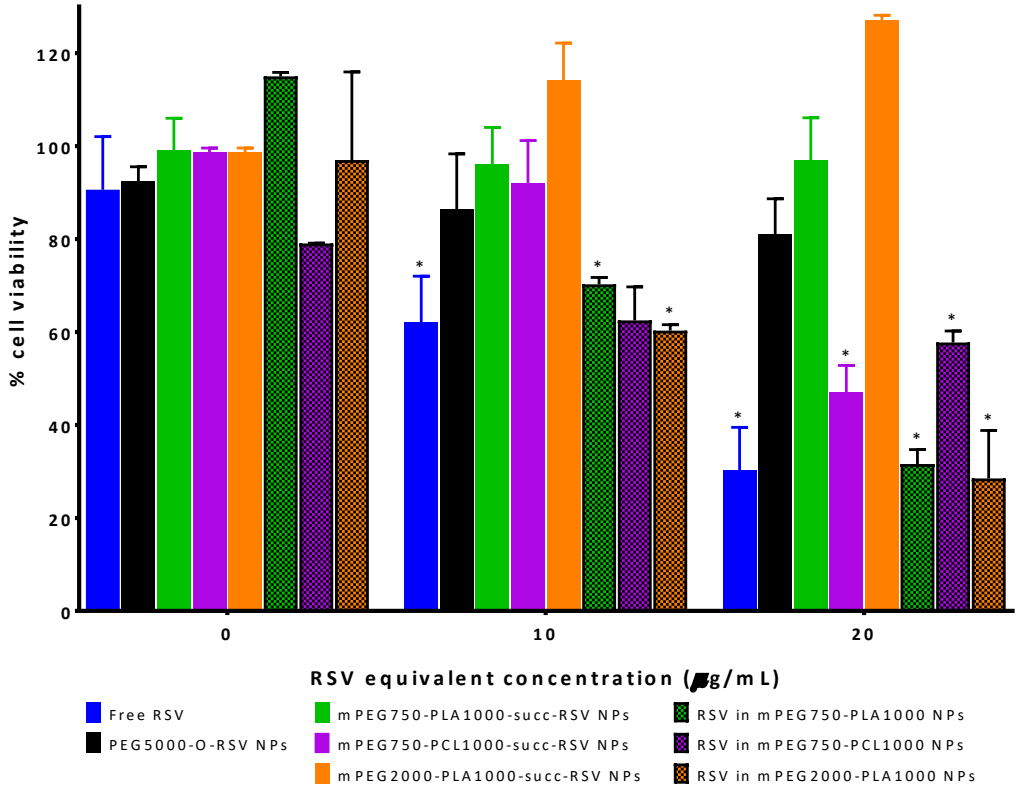

Figure 5.12 B16-F10 cell viability after treatment with 0, 10 and 20μg/mL RSV formulations for 48 hours

Data presented as mean (n=3) ± SD *p<0.05 compared to 0μg/mL

All conjugated RSV NPs did not improve the anti-proliferative effect of RSV on B16-F10 cells as seen by Duan *et al.* (2016) using RSV analogues although 20μg/mL of mPEG750-PCL1000-succ-RSV NPs showed a significant decrease in cell viability when compared to its 0μg/mL dose. Conjugated RSV NPs reduced the cytotoxicity of RSV due to its lower drug availability during the course of the assay due to sustained RSV release from the formulation. Both PEG5000-O-RSV NPs and mPEG2000-PLA1000-succ-RSV NPs revealed slowest release of RSV (Figure 4.4) and this could have rendered low amount of RSV available for reducing B16-F10 cell viability. This was reported by Cavallaro *et al.* (2004) where PTX was conjugated to polymers *via* a succ bond and the cytotoxicity of conjugated PTX was 40-fold less cytotoxic than free PTX in murine myeloid leukaemia NFS-60 cells due to the slow release of PTX. Liu *et al.* (2015) also showed that pterostilbene conjugated with PEG did not increase the potency of pterostilbene in murine Lewis lung carcinoma cells and claimed that unlike *in vivo* studies, *in vitro* experiments using cancer cell cultures did not fully portray the

advantages of prodrugs or polymeric conjugates which underestimated the efficacy of the conjugates. Another reason for the lack of potency in conjugated RSV NPs was due to the nature of the conjugation which reduced the number of hydroxyl groups on RSV available as the active site for anticancer activity in RSV (Lee *et al.* 2004, Szekeres *et al.* 2010), however the mechanism of action of conjugated RSV NPs should be studied in detail before a conclusion can be drawn. The high % of cumulative amounts of total RSV equivalent released from mPEG750-PCL1000-succ-RSV NPs (Figure 4.2) due to the high % of free RSV component released from the NPs (Figure 4.4) could have contributed to the only statistically significant cytotoxic effect on B16-F10 cells amongst conjugated RSV NPs. This showed that the cytotoxic effect on B16-F10 cells required conjugated RSV NPs to convert to free RSV as the conjugated RSV was biologically less active *in vitro* as evident from the remaining conjugated RSV NPs. In addition, the stability of NPs in CGM could have influenced its anti-proliferative properties because conversion to free RSV is preferred but not further degradation in the media before cellular uptake as it would decrease the efficacy of the formulation (Lu *et al.* 2013). The non-existent anti-proliferative effect of mPEG2000-PLA1000-succ-RSV NPs could be due to lack of cellular uptake of the NPs for any biological effect or its failed conversion to release the active form of RSV. The same reasons could also be applicable to mPEG750-PLA1000-succ-RSV NPs and PEG5000-O-RSV NPs. Unfortunately, due to time and resource constraint, cellular uptake studies were not carried out.

When compared with free RSV at 20μg/mL, encapsulated RSV NPs did not have significant improvement on the anti-proliferative effect of RSV on B16-F10 cells, however, encapsulated RSV NPs outperformed conjugated RSV NPs in anti-proliferative effect in B16-F10 cells. The lack of enhanced cytotoxicity, compared to free RSV control, from encapsulated RSV NPs was contrary to what was found by Guo *et al.* (2013) where encapsulated RSV in mPEG-PLA NPs was found to decrease glioma cells viability at 10μg/mL after 72 hours when compared to free RSV, however, a direct comparison could not be made as the MW of mPEG-PLA used was not disclosed which could have affected the integrity of the NP polymeric shell which in turn affected the biological efficacy of its cargo. In addition, in our study, cell viability was

assessed 48 hours, not 72 hours after treatment. Despite a more rapid release of RSV from encapsulated RSV NPs compared to conjugated RSV NPs (Section 4.5.3.2), the cytotoxic effect of encapsulated RSV NPs was equal to or worse than the cytotoxic effect of free RSV. Therefore, the lack of anticancer activity of mPEG750-PLA1000-succ-RSV NPs and mPEG2000-PLA1000-succ-RSV NPs, which contained unconjugated RSV in the NP core, was probably because the cells did not take up the NPs which would have shown some anticancer effect. This did not bode well for these conjugated RSV NPs which was purposed for anticancer treatment, however, due to the superior properties of mPEG750-PLA1000-succ-RSV NPs thus far in decreasing metabolism and maintaining plasma stability *in vitro*, data from *in vitro* cancer cell culture cannot provide a holistic view of the anticancer effect of mPEG750-PLA1000-succ-RSV NPs. Using data we have obtained thus far, we have summarised pertinent information on the RSV formulations evaluated in order to select suitable formulations for further *in vitro* and *in vivo* assessment (Table 5.10).

Table 5.10 Summary of physical characteristics and *in vitro* data for RSV formulations

RSV formulation	% *w/w* RSV conjugate	t_{max} (h)	$t_{1/2}$ in rat plasma (h)[a]	$t_{1/2}$ in HLM (h)[a]	% B16-F10 cell viability[b]	% RSV equivalent remaining in CGM[b]
Free RSV	NR	1.3	7.7 (2mg/mL) 0.01 (40μg/mL)	0.5	30.3±9.2^{6}	12.0±4.4^{3}
PEG5000-O-RSV NPs	100.0	>47.5	Stable	17.7	80.9±7.8^{3}	66.9±17.2^{2}
mPEG750-PLA1000-succ-RSV NPs	63.9	3.8	Stable	2.8	96.9±9.2^{3}	4.7±0.5^{3}
mPEG750-PCL1000-succ-RSV NPs	99.3	2.2	0.04	1.6	47.0±5.8^{2}	0^{3}
mPEG2000-PLA1000-succ-RSV NPs	76.1	2.0	Stable	0.7	127.0±1.1^{2}	0^{3}
RSV in mPEG750-PLA1000 NPs	NR	2.2	Stable	0.5	31.6±3.1^{2}	26.8±3.4^{3}
RSV in mPEG750-PCL1000 NPs	NR	2.0	Stable	0.6	71.2±8.6^{3}	37.8±6.6^{3}
RSV in mPEG2000-PLA1000 NPs	NR	6.3	Stable	0.4	57.8±2.5^{2}	11.9±3.7^{2}

Data presented as mean (*n*=superscript numbers) ± SD where calculated

[a] conducted at 37°C, see Section 5.5.1

[b] treated with 20μg/mL RSV equivalent dose for 48 hours at 37°C

From Table 5.10, RSV in mPEG750-PLA1000 NPs was highlighted yellow due to its better anti-proliferative effect on B16-F10 cells compared to free RSV and other RSV formulations (conjugated and encapsulated RSV NPs), however, its release and microsomal stability profiles, being almost identical to free RSV, were not favourable. As such, mPEG750-PLA1000-succ-RSV NPs (highlighted blue) was considered as a comparison between encapsulated and conjugated RSV NPs and despite having very poor *in vitro* anti-proliferative effect on B16-F10 cells and low stability in CGM, its release, plasma stability and microsomal stability profiles were more favourable than free RSV and all other RSV formulations excluding PEG5000-O-RSV NPs indicating that this formulation might be able to overcome *in vivo* hurdles for improving the bioavailability of RSV for anticancer treatment. Another conjugate with *in vivo* therapeutic potential was PEG5000-O-RSV NPs (highlighted green) despite having poor *in vitro* anti-proliferative effect on B16-F10 cells. As discussed, its great potential was due to its strong ether bond between RSV and PEG. Nonetheless, this formulation was not chosen for further *in vitro* and *in vivo* evaluations as its strong ether bond might in turn become a limitation where RSV cannot be released easily for therapeutic effect (Mattarei *et al.* 2013) and eventually lead to *in vivo* drug resistance (Gupta *et al.* 2015). Therefore, we have chosen both encapsulated and conjugated mPEG750-PLA1000 NPs for further assessment and comparison.

5.5.6 Cytotoxicity of mPEG750-PLA1000 formulations

Conjugated and encapsulated mPEG750-PLA1000 NPs and free RSV were used to treat mouse fibroblast NIH/3T3 cells to assess the cytotoxicity effect of the formulations on non-cancerous cells. Similar to the anti-proliferative evaluations on B16-F10 cells, 10 and 20μg/mL RSV equivalent doses were used.

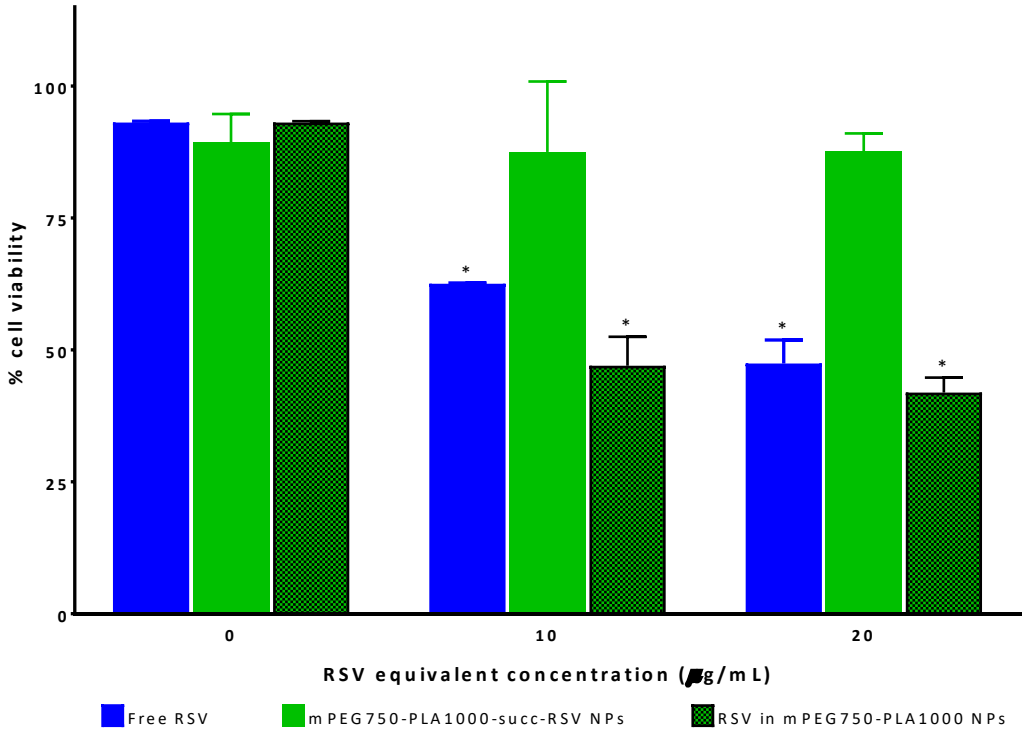

Figure 5.13 Cytotoxicity of RSV encapsulated in mPEG750-PLA1000 NPs and conjugated mPEG750-PLA1000-succ-RSV NPs on NIH/3T3 cells treated at 0, 10 and 20μg/mL for 48 hours at 37°C

Data presented as mean (n=2) ± SD *p<0.05 compared to 0μg/mL

It was evident from Figure 5.13 that RSV itself was toxic at 10-20 µg/mL to non-cancerous fibroblast cells although not as toxic in B16-F10 cancerous cells. This effect was transferred to the encapsulated RSV NPs and less so in conjugated RSV NPs, possibly due to the same reasons as the B16-F10 assays such as sustained release, conjugated hydroxyl groups of RSV and instability in CGM. Imamura *et al.* (2017) assessed the anti-obesity properties of RSV in murine 3T3-L1 preadipocytes and found a significant (p<0.01) decrease in cell viability to approximately 65% when treated with 22μg/mL RSV for 72 hours which was comparable to our data in Figure 5.13. It would be pertinent to study the cytotoxicity of RSV and the formulations in other non-cancerous cell lines such as HaCaT cells (Nogueira *et al.* 2011, Pinazo *et al.* 2016) but a more holistic approach was taken by studying the effect of RSV and the formulation *in vivo*.

5.5.7 Apoptosis assay of mPEG750-PLA1000 formulations

A standard Annexin V-FITC and PI assay was employed to evaluate the effect of mPEG750-PLA1000 formulations on the apoptosis of B16-F10 cells after being treated with 20 and 50μg/mL RSV equivalent for 24 and 48 hours. 50μg/mL was additionally tested because of the higher anti-proliferative and apoptosis effect of 50μg/mL free RSV on B16-F10 compared to 20μg/mL free RSV (Figure 5.11). Two treatment times were selected in order to observe the time-lapse apoptosis and necrosis process on B16-F10 post-treatment.

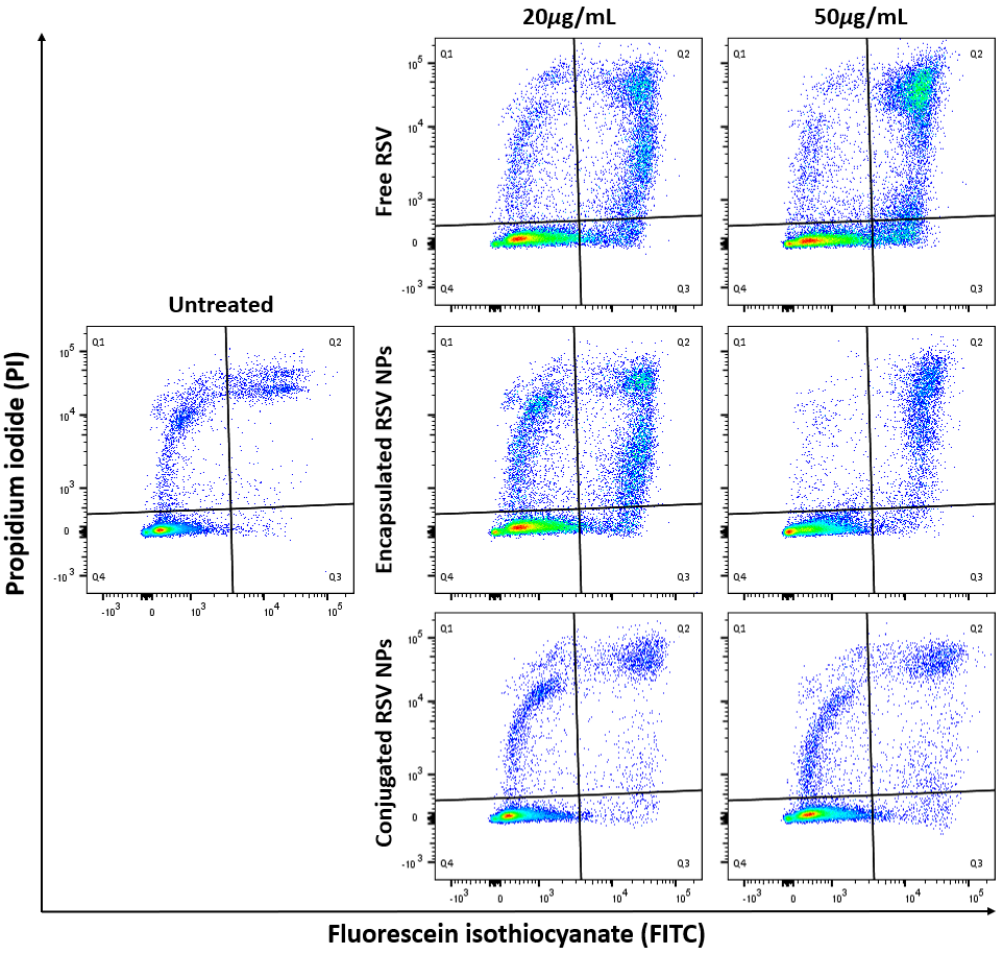

Figure 5.14 Representative coloured dot plots of 24-hour treated B16-F10 cells with 20 and 50μg/mL RSV equivalent RSV formulations

Q1 = necrotic cells, Q2 = late apoptotic cells, Q3 = early apoptotic cells, Q4 = viable cells

In general, Figure 5.14 showed that all RSV formulations followed an apoptotic pathway of cell death after 24-hour treatments. Quantified data of each cell population according to each treatment was presented in Table 5.11.

Table 5.11 Cell population percentages of B16-F10 cells treated with free RSV, encapsulated RSV in mPEG750-PLA1000 NPs and conjugated mPEG750-PLA1000-succ-RSV NPs for 24 hours

Formulation & concentration	Viable (Q4)	Early apoptotic (Q3)	Late apoptotic (Q2)	Necrotic (Q1)
No treatment	89.4±0.0	0.4±0.0	4.2±0.0	5.9±0.0
20μg/mL free RSV	68.1±3.2*	5.4±0.4*	19.5±1.2*	7.1±1.6
50μg/mL free RSV	62.5±1.4*	6.9±0.5*	23.6±4.2*	7.1±3.3
20μg/mL encapsulated RSV NPs	62.5±5.1*	4.3±0.7*	23.3±6.8*	9.8±2.4
50μg/mL encapsulated RSV NPs	83.8±2.0	1.7±0.2	11.4±3.4	3.1±1.6
20μg/mL conjugated RSV NPs	86.3±2.1	1.2±0.1	5.2±0.1	7.3±1.8
50μg/mL conjugated RSV NPs	82.8±4.0	2.1±0.3	8.8±3.7	6.3±0.1

Data presented as mean (n=2) ± SD *p<0.05 compared to untreated cells

Correlating with MTT data on free RSV (Section 5.5.4), both concentrations had an anti-proliferative effect on B16-F10 cells by significantly increasing apoptotic populations and less so necrotic populations. As expected, the lower concentration of encapsulated RSV NPs (20μg/mL) was more effective than 20μg/mL free RSV, behaving very similarly to 50μg/mL free RSV with a higher percentage of necrotic cells. The increased effect of apoptosis due to encapsulation was seen in CT26 colon cancer cells treated with RSV encapsulated in a mPEG5000-PLA5000 at 4.6μg/mL RSV equivalent for 72 hours (Jung *et al.* 2015) and also in glioma cells where encapsulated RSV NPs were also found to have higher intracellular levels than free RSV which contributed to its enhanced apoptotic effect (Guo *et al.* 2013). The enhanced cellular uptake of RSV in NPs was seen in Wang *et al.* (2015b) where RSV-loaded mPEG-PCL micelles showed higher apoptotic cells in MCF-7 breast cancer cells than cells treated with free RSV. This further confirmed the benefits of nano-formulation of RSV in enhancing cellular uptake. Interestingly, 50μg/mL encapsulated RSV NPs did not perform as expected where there should be a higher percentage population of apoptotic and necrotic cells than 20μg/mL encapsulated RSV NPs. It was possible that a higher RSV content within the NPs increased the degradation rate of RSV as RSV is rapidly released reducing its biological efficacy. The slower release rate of RSV from conjugated RSV NPs due to the stronger covalent bonds (Section 4.5.3.1) and possibly due to the low stability in CGM (Section 5.5.3) also impeded the apoptosis effect of RSV at both concentrations. 50μg/mL conjugated RSV NPs did not perform better than 20μg/mL conjugated RSV NPs with only a very slight increase in apoptotic cells and this was most likely due to the increased degradation of the NPs in CGM due to higher concentration of the NPs. Therefore, a longer treatment period of 48 hours was adopted to ascertain whether the release rate of RSV from conjugated RSV NPs could be a factor in its biological efficacy.

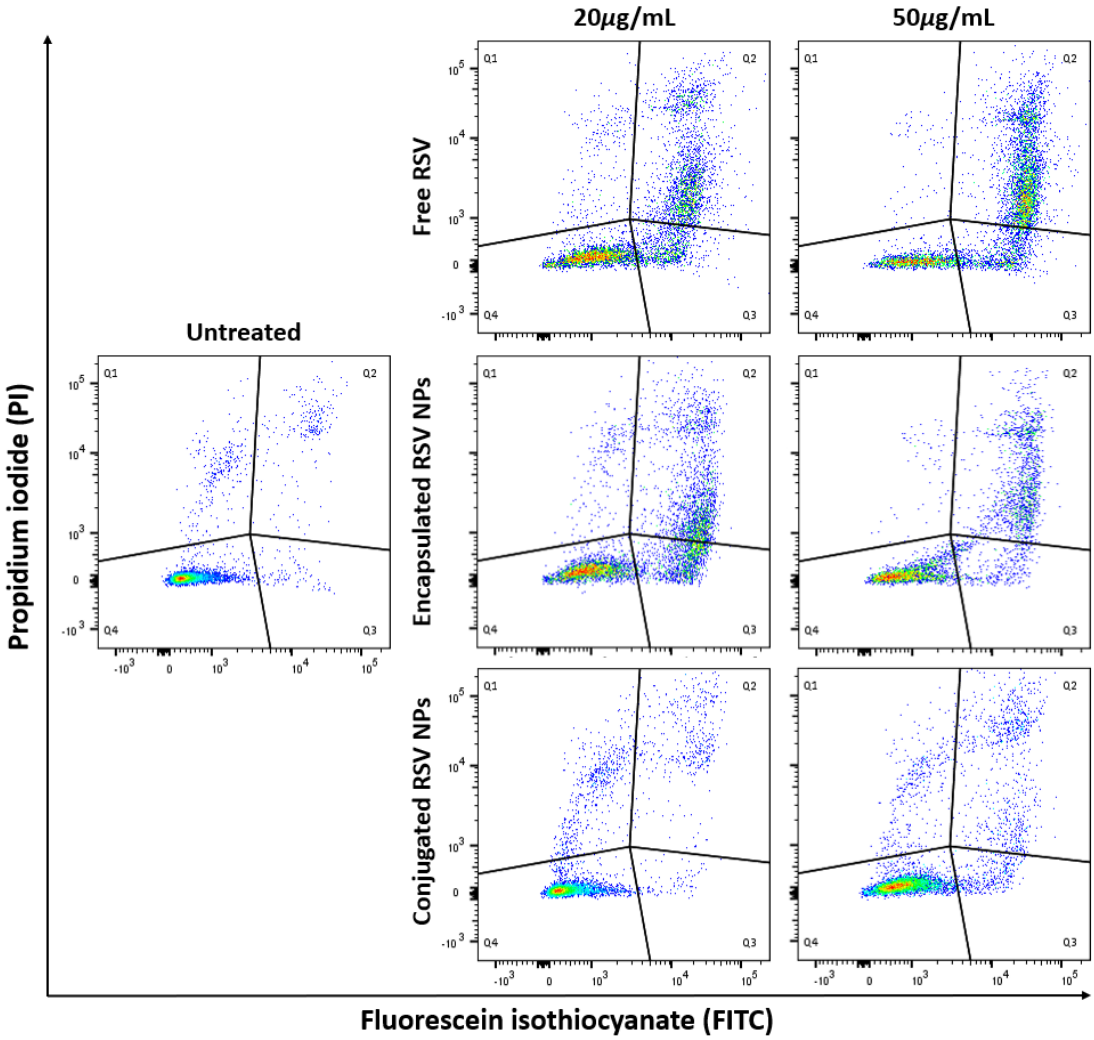

Figure 5.15 Representative coloured dot plots of 48-hour treated B16-F10 cells with 20 and 50μg/mL RSV equivalent RSV formulations

Q1 = necrotic cells, Q2 = late apoptotic cells, Q3 = early apoptotic cells, Q4 = viable cells

Figure 5.15 showed that all RSV formulations followed an apoptotic pathway of cell death after 48-hour treatments. Quantified data of each cell population according to each treatment was presented in Table 5.12.

Table 5.12 Cell population percentages of B16-F10 cells treated with free RSV, encapsulated RSV in mPEG750-PLA1000 NPs and conjugated mPEG750-PLA1000-succ-RSV NPs for 48 hours

Formulation & concentration	Viable (Q4)	Early apoptotic (Q3)	Late apoptotic (Q2)	Necrotic (Q1)
No treatment	93.1±0.0	1.2±0.0	2.7±0.0	3.0±0.0
20μg/mL free RSV	42.3±1.8*	15.3±0.3*	36.7±0.9*	5.9±2.9
50μg/mL free RSV	26.1±0.5*	15.6±1.6*	56.3±0.6*	2.1±1.6
20μg/mL encapsulated RSV NPs	40.6±5.4*	21.8±1.7*	34.0±3.2*	3.7±0.5
50μg/mL encapsulated RSV NPs	53.2±1.8*	9.8±0.9*	35.9±1.2*	1.2±0.3
20μg/mL conjugated RSV NPs	86.9±0.2	1.2±0.1	5.7±0.8	6.3±0.7
50μg/mL conjugated RSV NPs	76.6±2.8*	5.7±0.9	12.1±0.7*	5.6±1.3

Data presented as mean (n=2) ± SD *p<0.05 compared to untreated cells

As speculated, a longer treatment period of 48 hours allowed free RSV to assert its apoptosis effect on B16-F10 cells. Both concentrations of free RSV showed a dose dependent anti-proliferative effect on B16-F10 cells *via* the apoptotic pathway. As expected, the biological efficacy of conjugated RSV NPs could be observed after 48 hours of treatment where some RSV has been released from conjugated RSV NPs. The higher concentration of conjugated RSV NPs resulted in a faster hydrolysis of polymer-RSV ester bonds resulting in more biologically active RSV. Duan *et al.* (2016) reported an RSV analogue, where the hydroxyl groups of RSV were conjugated to acetyl groups, did not show significant increase in apoptosis cells when compared to comparable free RSV concentrations. No explanation was given by the authors for this observation but this further asserted our speculation that hydroxyl groups on RSV was responsible for apoptosis in B16-F10 cells (Lee *et al.* 2004, Szekeres *et al.* 2010). Also, conjugated RSV NPs could have influenced its cellular uptake and mechanism of biological activity due to the different structure of RSV (Nikhil *et al.* 2014).

Results from the apoptosis assay conducted on free RSV, encapsulated RSV NPs and conjugated RSV NPs confirmed that the apoptotic mechanism of RSV in B16-F10 cells was structure-specific, concentration-dependent and time-dependent as seen by others (Khan *et al.* 2013, Su *et al.* 2013, Chong *et al.* 2014, Summerlin *et al.* 2015). Further studies including cell cycle assays could be carried out in the near future to further elucidate the apoptotic mechanisms of the RSV formulations. Nonetheless, *in vitro* apoptosis assays cannot be directly translated or used to predict outcomes in *in vivo* models as tumour cells *in vivo* were capable of suppressing apoptosis for tumorigenesis (Proskuryakov *et al.* 2010). Therefore, there is a need to further assess these RSV formulations in an *in vivo* model to further understand and elucidate the biological efficacy and compare the effectiveness of encapsulation and conjugation in NPs.

5.5.8 Tumour growth evaluation in a melanoma mouse model

From the results of the apoptosis and MTT assays in B16-F10 cancer cells, RSV, encapsulated or conjugated, did not produce the same cytotoxicity as free RSV at a

cytotoxic dose. Although encapsulation has slightly enhanced the cytotoxicity of free RSV in B16-F10 cells possibly by enhanced cellular uptake of NPs, conjugation significantly decreased the cytotoxicity despite being more stable *in vitro*. From previous experiments, we knew that conjugation of RSV to polymers increased the stability profile of RSV in rat plasma and HLM. In addition, conjugation provided a sustained release profile of RSV when compared to encapsulated RSV NPs and free RSV. With these properties, the therapeutic effect of RSV *in vivo* would logically be better than *in vitro* due to the increased bioavailability of RSV, however, through our *in vitro* cell culture studies (Sections 5.5.5 to 5.5.7) we have discovered that the therapeutic effect was even lesser than free RSV. The *in vitro* models did not take into consideration of bioavailability of RSV *in vivo* and were much more simplified systems with no simulation of metabolism or plasma degradation. The benefit of ester bond cleavage by plasma enzymes to release the therapeutic effect of RSV from conjugated RSV NPs cannot be fully observed in *in vitro* models. It would be imprudent not fully explore the possible benefits of conjugation *in vivo* and hence, our hypotheses on the potential of our formulations can only be further evaluated and confirmed by *in vivo* experiments.

5.5.8.1 Study rationale

We have evaluated free RSV, RSV encapsulated in mPEG750-PLA1000 NPs and conjugated mPEG750-PLA1000-succ-RSV NPs in C57BL/6J mice with subcutaneously implanted B16-F10 tumours. RSV treatment in melanoma models produced mixed outcomes as reviewed by Park *et al.* (2015) where doses of RSV in various C57BL/6 mice cancer models were as low as 0.1mg/kg body weight to as high as 200mg/kg. Asensi *et al.* (2002) administered 20mg/kg *trans*-RSV orally twice a day in C57BL/6 mice and did not find any tumour growth suppression of B16M cells grown into the footpad of the hind limb of mice compared to the control group. 50mg/kg RSV, however, was found to inhibit *in vivo* melanoma B16-BL6 tumour in C57BL/6N mice after daily IP administration for 19 days but also showed a decrease in body weight indicating *in vivo* toxicity (Caltagirone *et al.* 2000). The same group found that at 25mg/kg, the tumour size decreased by 4% whereas a 50mg/kg dose did not have significant decrease when compared to the control group.

In our study, the formulations were injected *via* two routes, that is, IT which was an injection directly into the tumour once palpable (Appendix 7.19) and IP which was an injection into the lower abdominal cavity of the mouse. The IT route allowed us to assess the therapeutic efficacy of a precise dose of a particular formulation at a lower dose (Lee *et al.* 2010, Fakhari *et al.* 2015). Lee *et al.* (2010) used a C57BL/6 mouse model with subcutaneous B16-F10 tumours for IT injections of PTX-loaded mPEG-PCL gels hence this study using IT administration allowed us to evaluate the suitability of the *in vivo* melanoma tumour model and to better understand the limitation of this model in the case of RSV NPs. Although not perfect, IT administration has been used frequently in the research to assess formulations. A polymeric DDS of DOX administered IT in prostate cancer rat models was found to enhance both tumour drug concentrations and tumour-to-organ ratios, resulting in improved efficacy of single dose chemotherapy when compared with IV administrations (Lammers *et al.* 2006, Shen *et al.* 2017). As RSV formulations were injected directly into the tumour, a much lower dose than of RSV formulations can be used. The IT dose in this study was 2mg/kg every 48 hours, with a total of 5 injections. However, the IT route administration did not allow us to assess developed formulations in overcoming issues related to drug metabolism in the blood circulation and liver. Thus, the adoption of the IP route was necessary to assess the effectiveness of our formulations, comparing between conjugated RSV NPs and encapsulated RSV NPs, in decreasing the metabolism rate and providing a sustained release of RSV for anticancer therapy in a melanoma model. In addition, the IP route was more practical in a clinical setting where treatments for tumours at multiple sites can be administered at one site and also used at early stages of cancer where tumours have limited accessibility to *via* direct injections (Cheng *et al.* 2007). We started our *in vivo* tumour growth evaluation using the IT administration to assess the suitability and limitations of this B16-F10 model. This cohort also allowed us to view the effectiveness of our RSV formulations in tumour-bearing mice models which assisted in our study design using the IP administration.

5.5.8.2 Intratumoral (IT) administration

The IT cohort was administered with two controls and three RSV formulations as per

Table 5.3 with a minimum of 6 mice per treatment. To reiterate the treatment plan for the IT cohort, a summary was prepared in Table 5.13 below.

Table 5.13 Summary of treatment dosing, data collection days and sample size per treatment group during IT treatment period

Procedure	Days from start of treatment					
	0	**2**	**4**	**6**	**8**	**10**
Dosing (refer to Table 5.3)	‡	‡	‡	‡	‡	
Body weight measurement	‡	‡	‡	‡	‡	‡
Tumour volume measurement	‡	‡	‡	‡	‡	‡
Remaining sample size of treatment groups by treatment days						
20% HPCD	8	8	8	6	3	0
Blank mPEG750-PLA1000 NPs	6	6	6	4	2	0
RSV in 20% HPCD	6	6	6	6	2	2
RSV in mPEG750-PLA1000 NPs (encapsulated)	7	7	7	1	0	0
mPEG750-PLA1000-succ-RSV NPs (conjugated)	7	7	7	5	2	1

Most reasons for early termination of animals was due to onset of necrosis and/or a sudden growth of tumour which was beyond the approved 100mm^2 (length × width) hence the need to have larger sample sizes for treatment groups, in particle control groups. Appendix 7.18 showed various tumour characteristics observed during the *in vivo* study which included the onset of necrosis. However, it should be noted that a cancer treatment was deemed successful when the tumour develops necrosis (Carletto *et al.* 2016) and/or shrinks in volume (Ogston *et al.* 2003). The Kaplan-Meier survival curve for the IT cohort (Figure 5.16) showed that the median survival for all treatment groups was 6 days except encapsulated RSV NPs which was 4 days.

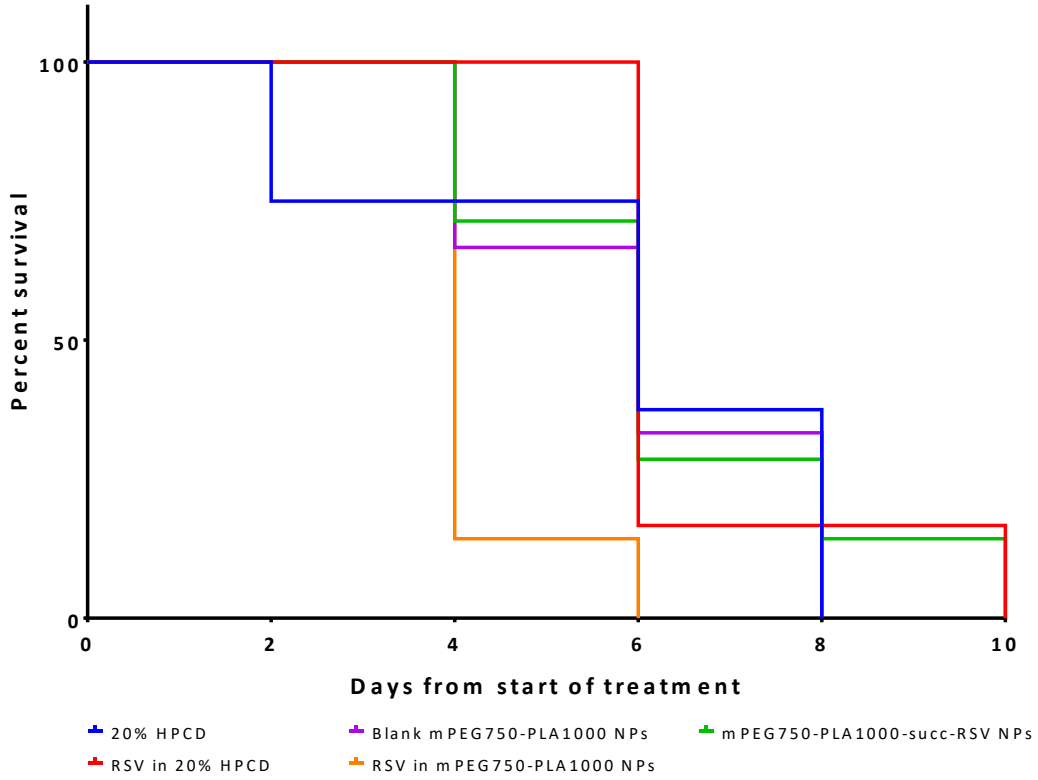

Figure 5.16 Kaplan-Meier survival curve of animals treated in IT cohort for each treatment group

From cytotoxicity data of RSV formulations in non-cancerous fibroblast cells (Section 5.5.6), our main concern was whether the formulations would cause any ill-effects on the mice treated especially due to multiple treatment injections which led to an increased dose in a short time frame. One observation would be the body weight trend which should be a steady increase for the duration of our study as per Appendix 7.17. Mice in the IT cohort were 40 days old at the start of treatment with a weight range of 18.7-21.2g which was within the range supplied by the supplier. At the end of the treatment, remaining mice were 50 days old and within a healthy weight range of 19.1-22.3g. Figure 5.17 shows the body weight change in percentage for each treatment group throughout the treatment period.

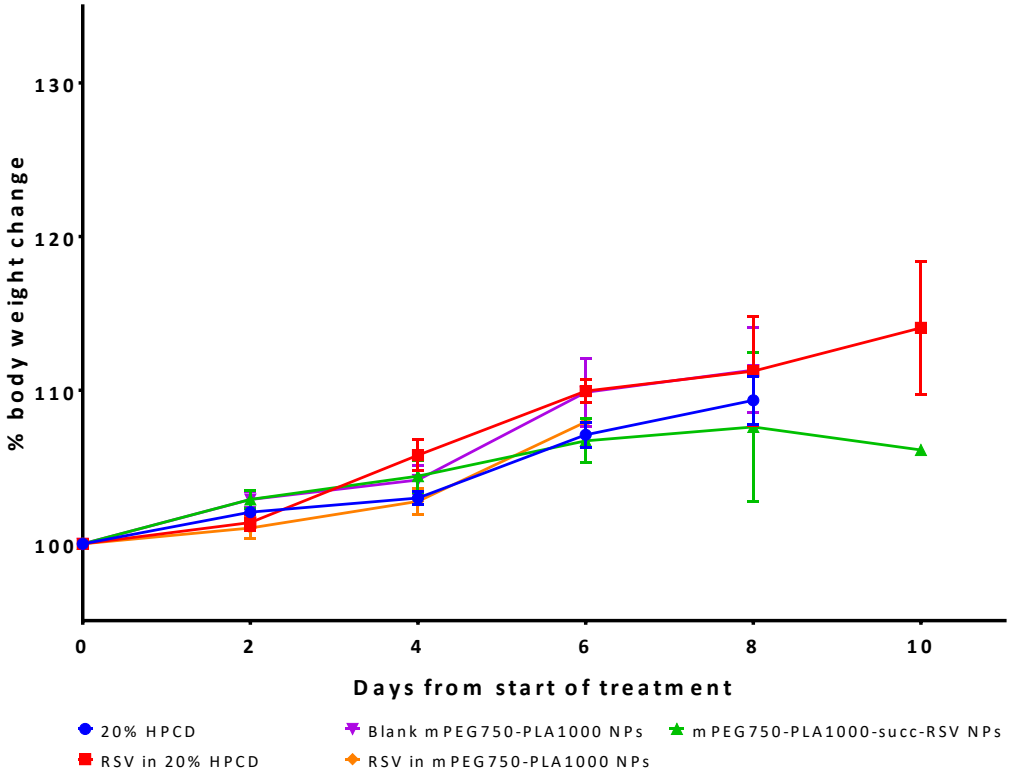

Figure 5.17 Body weight percentage changes of animals in IT cohort throughout treatment period

Data presented as mean (*n* as per Table 5.13) ± SEM

The body weight of animals progressed as expected although there was a slight dip in body weight at day 10 in the conjugated RSV NPs treatment group (green line), however, this should be noted that the sample size was one in that case and the weight of the same mouse increased as expected compared to the previous time point. Although the study required necessary early termination of mice, the body weights of the animals suggest that the formulations were not toxic *in vivo* (Gao *et al.* 2015). The physical appearances of the mice were also healthy according to the health monitoring score card used for each observation day. Mean tumour volumes of each treatment group throughout the treatment period was presented in Figure 5.18.

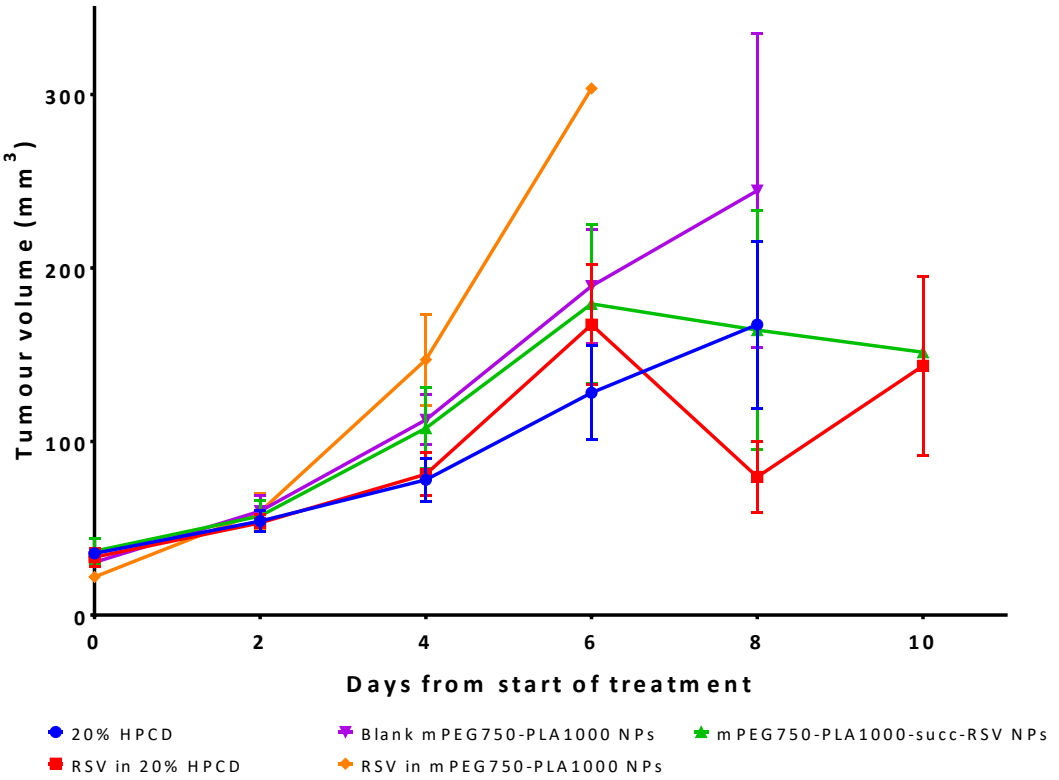

Figure 5.18 Tumour volumes for all treatment groups in IT cohort from the start of treatment

Data presented as mean (*n* as per Table 5.13) ± SEM (no significant results for all treatment groups compared to 20% HPCD control group)

From details in Table 5.13 and the survival curve (Figure 5.16), sample sizes from day 8 decreased to one or two mice per treatment group with no mice in the encapsulated RSV NPs group due to early terminations. Therefore, data from day 8 were biased due to a much smaller sample size. Nonetheless, statistical analyses of treatments compared to control group and between treatments showed no significant results ($p>0.5$). Interestingly, the control group (20% HPCD) maintained smaller tumour volumes throughout the treatment compared to the other groups inferring that the treatments containing RSV may have worked adversely to what was seen through the project thus far. However, the large tumours could be due to the apoptotic and necrotic effect of the treatments where fluid seepage and inflammation was not visible externally and thus, gave an exaggerated measurement of the tumour. Appendix 7.20 displayed visual characteristics of excised tumours from each treatment group which showed fluid seepage and inflammation. In addition to our *in vitro* apoptotic data, Lee *et al.* (2006) also found 17% of tumour

cells in excised tumours in lung cancer bearing C57BL/6 mice treated daily with 20mg/kg RSV orally for 14 days were apoptotic by histological quantitative TUNEL staining compared to 9% in vehicle treated mice. Also, the physical act of direct injection into the tumour could have encouraged necrosis due to the stress of injury from multiple injections which also caused fluid seepage from cytoplasm of the cells (Rock *et al.* 2008). Such effects could potentially mask therapeutic effects from RSV formulations and also cause difficulties in obtaining consistent tumour measurements. Distinct changes in mean tumour volumes in the IT cohort from start of treatments were from day 6 onwards and thus, a comparison of individual tumour volumes between the start of treatment and from days 6 onwards is shown in Figure 5.19.

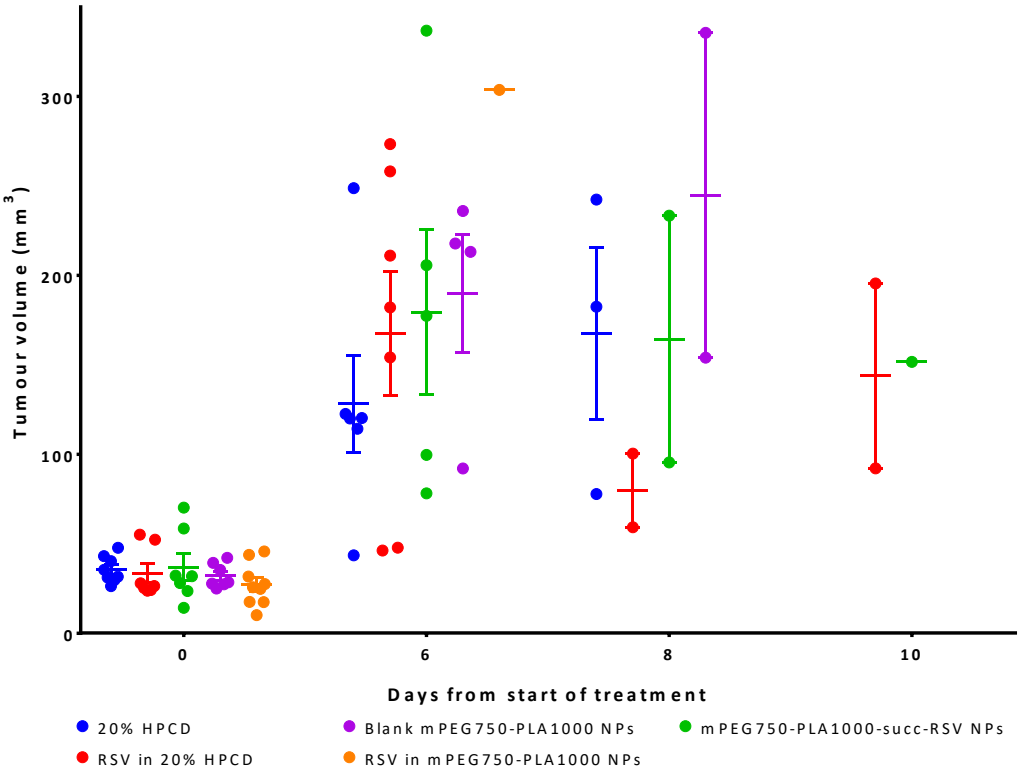

Figure 5.19 Individual tumour volumes (dots) of each treatment group in IT cohort at beginning of treatment and days 6, 8 and 10 of treatment

Data presented as individual dots and mean ± SEM (line and error)

From Figure 5.19, tumour growth of all groups was scattered in a wide range at days 6 and 8 despite being closely clustered at the beginning of treatments. There were several possible reasons to this which could not be controlled, mainly due to the

nature of the tumour. This was supported by Zang *et al.* (2015) and Fairchild *et al.* (2011) where B16-F10 tumours were known to be highly aggressive, invasive and metastasize at early stages of tumour growth. The tumours in the control group consisted of mice with various tumour sizes by day 6 despite being untreated. The lower outliers seen at day 6 and 8 could be due to the tumours not growing healthily in some individuals. The high outliers could be due to the trauma of injection or the treatments containing RSV which led to apoptosis or necrosis of cells in some tumours. Due to early termination due to the size and state of the implanted tumours, sample sizes from day 8 significantly decreased and appeared even more scattered. This further highlighted the interindividual variation in tumour growth patterns within an *in vivo* study due to the interindividual metabolic variation (Bode *et al.* 2013).

Although the sample size decreased, we can postulate that free RSV and conjugated RSV NPs was able to control the tumour growth more than the other treatment groups evident from their survival at day 10. This could be attributed to the sustained release of RSV from conjugated RSV NPs and the possible acid hydrolysis of conjugates which could occur within the acidic tumour environment (Dubey *et al.* 2017). Nonetheless, the multiple dosing could have increased the potency of the conjugated RSV NPs over time. Free RSV was complexed with HPCD to aid its solubilisation in our *in vivo* study hence, the physicochemical properties of free RSV in a HPCD complex was not considered which could have led to a better sustained release and stability profile than free RSV in DMSO in the *in vitro* studies. HPCD was found to increase the aqueous solubility of RSV and improve its cytotoxicity in HeLa, Hep3B and MCF-7 cell lines as reviewed by Summerlin *et al.* (2015).

As mentioned before, the tumour volumes of both control groups steadily increased throughout the treatment period but was culled before the end of the treatment period due to large tumour volumes and onset of necrosis which could be an indication of an aggressive tumour consistent with the nature of B16-F10 tumour models (Proskuryakov *et al.* 2010). This highlighted another factor to consider for B16-F10 tumour-bearing C57BL/6 mice that is the age of the tumour. In our case, at day 10 of the treatment period, the tumour was 17 days old and evidently from Figure

5.19, the control groups were eliminated due to their large volume and necrosis unlike free RSV and conjugated RSV NPs treatment groups.

Due to the rapid release of RSV from encapsulated RSV NPs compared to conjugated RSV NPs and multiple dosing during the study, the amount of RSV available for therapeutic effect would be much more than what was made available by the conjugated RSV NPs. As encapsulated RSV NPs caused apoptosis which could have eventually led to necrosis as described in Section 5.5.7, the measurement of tumours could be superficially larger due to the inflammation and fluid seepage entailing apoptotic and necrotic processes. Furthermore, RSV was found to trigger cell death by both apoptosis and necrosis individually and concurrently which further affirmed its multi-faceted biological mechanism (Scarlatti *et al.* 2008). Although the results from the IT cohort could not explain the effects of RSV formulations clearly, there were several points which could be utilised for our IP cohort:

1) Early termination due to possible necrosis from multiple IT dosing could be avoided by using another administration route, for example IP.
2) As B16-F10 tumours are aggressive tumours (Mathieu *et al.* 2012, Danciu *et al.* 2015), it would be imperative to design a study with tumours less than 17 days to avoid early termination due to tumour size and onset of necrosis.
3) The therapeutic difference between three RSV formulations (free RSV, encapsulated RSV NPs and conjugated RSV NPs) may be better differentiated using a different route administration, particularly one considering the metabolism pathway of RSV in plasma and liver.

5.5.8.3 Intraperitoneal (IP) administration

With the knowledge from the IT cohort, the IP cohort was treated slightly differently from the IT cohort. Firstly, treatment was carried out on the same day as tumour inoculation to accommodate the aggressive tumour growth. A larger sample size of treatment groups was also used at the beginning to account for possible loss of mice due to early termination from overly large tumours or onset of necrosis. Secondly, the tumour volume and body weight measurements were completed at 14 days after the start of treatment. As such, a summary of the treatment plan is depicted below.

Table 5.14 Summary of treatment dosing, data collection days and sample size per treatment group during IP treatment period

Procedure	Days from start of treatment							
	0	**2**	**4**	**6**	**8**	**10**	**12**	**14**
Dosing (refer to Table 5.4)	‡	‡	‡	‡	‡			
Body weight measurement	‡	‡	‡	‡	‡	‡	‡	‡
Tumour volume measurement				‡	‡	‡	‡	‡
Remaining sample size of treatment groups by treatment days								
20% HPCD	8	8	8	8	8	8	8	6
mPEG750-PLA1000 polymer in MQ	7	7	7	7	7	7	7	6
RSV in 20% HPCD	7	7	7	7	7	7	7	6
RSV in mPEG750-PLA1000 NPs (encapsulated)	8	8	8	8	8	8	8	7
mPEG750-PLA1000-succ-RSV NPs (conjugated)	7	7	7	7	7	7	7	6

As treatments were started on the same day of tumour inoculation, tumours were not palpable for measurement, as a result, measurement of tumour only started from day 6 when tumours were palpable. All treatment groups majority survived to the end of the treatment period of 14 days with a median survival of 14 days (Figure 5.20A). There was also no sign of toxicity due to the steady increase of body weight in all treatment groups (Figure 5.20B).

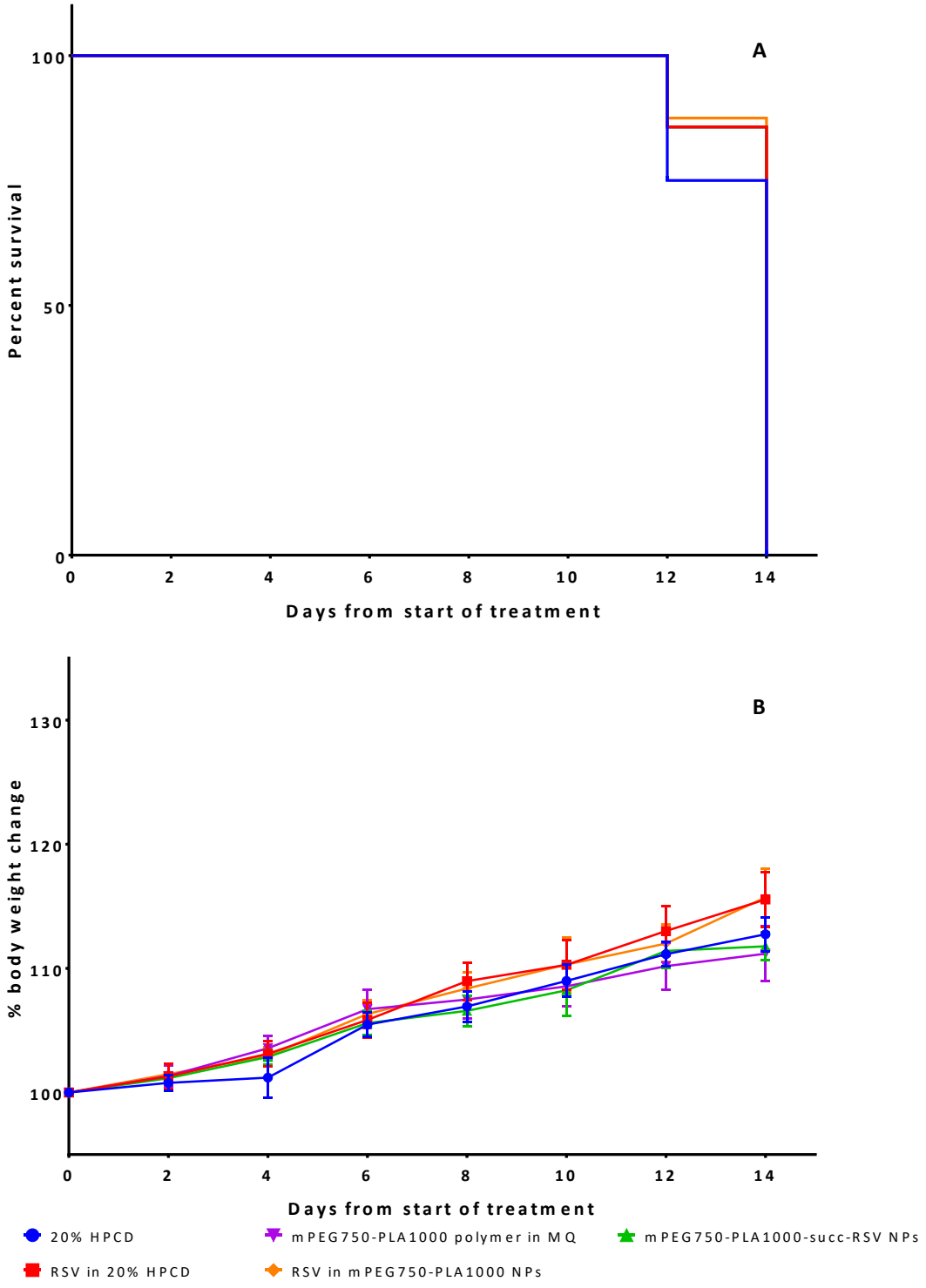

Figure 5.20 Kaplan-Meier survival curve (A) and body weight percentage changes (B) of animals treated in IP cohort for each treatment group

Data (B) presented as mean (*n* as per Table 5.14) ± SEM

Overall, the difference in mean tumour volumes between each treatment throughout the study showed no statistical significance but there were patterns observed especially after treatment period (Figure 5.21).

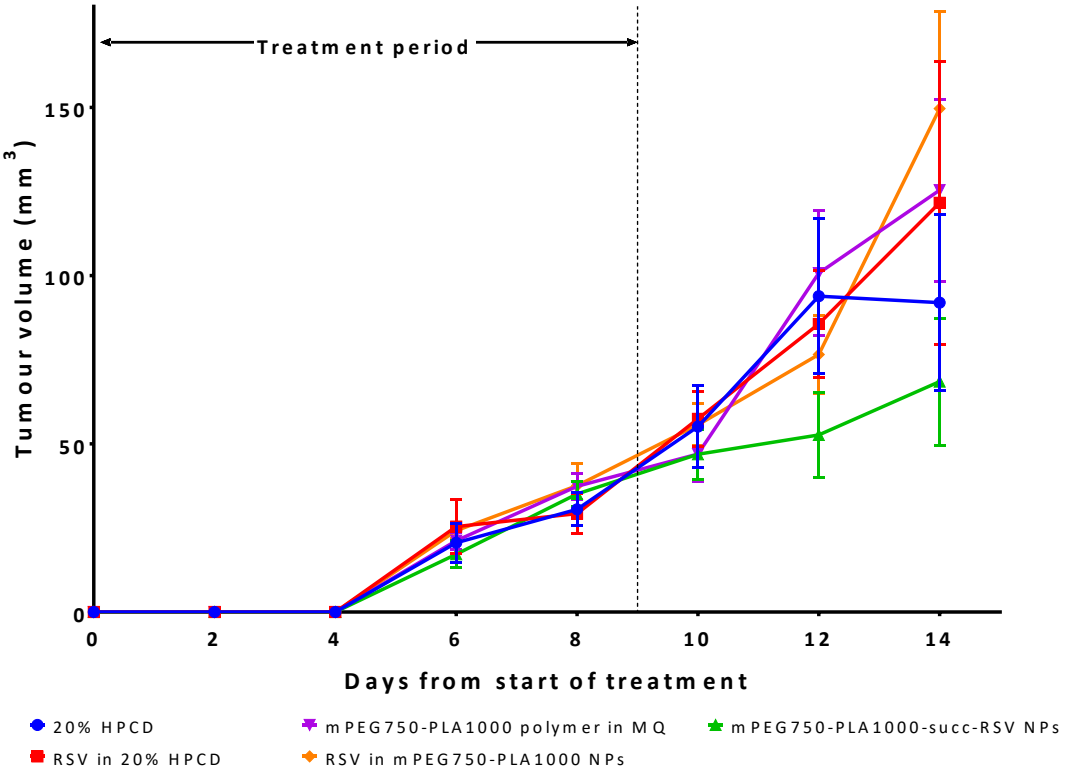

Figure 5.21 Tumour volumes for all treatment groups in IP cohort from the start of treatment Data presented as mean (*n* as per Table 5.14) ± SEM (no significant results for all treatment groups compared to 20% HPCD control group)

During the treatment period, tumour volumes were not distinguishable between treatment groups, however, once treatments were stopped, the treatment group with conjugated RSV NPs had a distinct decrease in tumour growth for up to 14 days when compared with the other treatment and control groups. At day 12, the tumour volumes were as expected where the control groups had higher tumour volumes followed by free RSV and encapsulated RSV NPs with the conjugated RSV NPs being the smallest tumour volumes. Figure 5.22 details the individual tumour volumes of each treatment group at days 8 which is the last day of treatment and days 12 and 14 since the start of treatment.

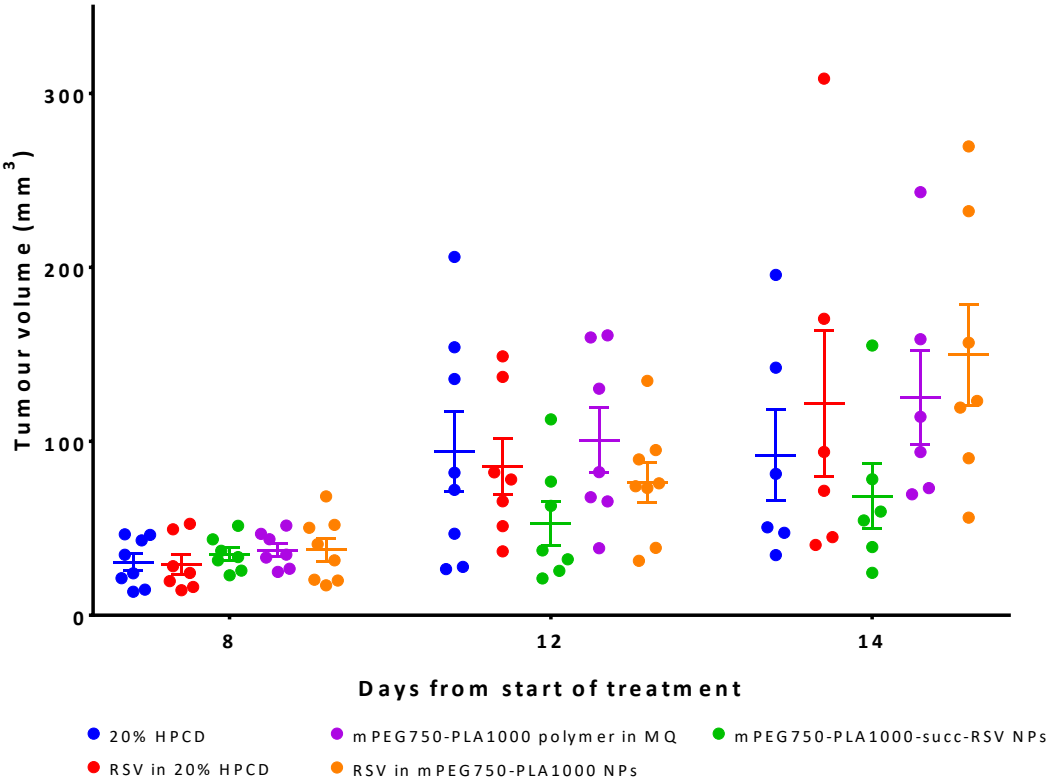

Figure 5.22 Individual tumour volumes of each treatment group in IP cohort at beginning of treatment (day 8), days 12 and 14 of study

Data presented as individual dots and mean ± SEM (line and error)

By day 14 since start of treatment, the sample size of the control group treated with 20% HPCD was decreased by 2 mice due to tumours being too large. This reduction of mice samples size has caused the mean tumour volume appear artificially smaller as the tumour size of culled mice would be much greater than those analysed. The mean tumour volumes of treatment groups with free RSV and encapsulated RSV NPs were high due to the fluid seepage and inflammation which led to an overestimation of tumour volumes as seen in the IT cohort. Appendix 7.21 showed excised tumours of each treatment group after culling which depicted the fluid seepage and inflammation in both free RSV and encapsulated RSV NPs. The conjugated RSV NPs treatment group showed decrease in tumour growth with no fluid seepage or inflammation compared to the other RSV treatment groups. Despite being ineffective in *in vitro* assays, the *in vivo* study demonstrated that the sustained release (Figure 4.2) and better stability profiles of conjugated RSV NPs in rat plasma and HLM (Section 5.5.1) increased the availability of RSV for the decrease of B16-F10 tumour

growth over time. In addition, the presence of mPEG on the conjugated RSV NPs allowed for prolonged residence time in the body leading to passive tumour targeting (Yang *et al.* 2014). We also speculate that the acidic tumour environment was able to hydrolyse the covalent ester bonds between the polymer and RSV (Dubey *et al.* 2017, Zhang *et al.* 2017) which then released RSV at the tumour site for therapeutic effect, however, this would need further investigation to confirm this. Both free RSV and encapsulated RSV NPs were not able to produce any tumour suppression effect compared to the control group due to its fast metabolism and plasma degradation (Section 5.5.1) and fast release of RSV (Section 4.5.3) as demonstrated by our *in vitro* studies. The similar benefits of conjugated RSV NPs against encapsulated RSV NPs in anticancer studies were observed in Luo *et al.* (2016b) where, campothericin, another natural product, was conjugated to PEG and used for treatment of breast cancer cells *via* IV administration.

Despite reports on RSV being ineffective in melanoma (Niles *et al.* 2006, Osmond *et al.* 2013), our IP cohort proved that by formulating NPs using RSV conjugates and free RSV, conjugated RSV NPs could suppress melanoma in mice. The IP route enabled administration of the RSV formulations before the tumour was palpable which could be useful when early tumour detection was made or when a tumour was located in locations within the body where IT injections would be impractical. Early tumour treatment or tumours with a small burden were known to be more sensitive to anticancer agents, therefore an early treatment as demonstrated in the IP cohort would be clinically favourable (Temple *et al.* 2005). As B16-F10 is a highly aggressive tumour, repeated doses was needed to reduce the total number of cells for the immune system to kill any remaining cells (Barton-Burke *et al.* 2006). Our study also showed undetectable *in vivo* systemic toxicity of the conjugated RSV NPs (Section 5.5.6) as determined by body weight, which could be due to rapid clearance of low MW polymers (Kolate *et al.* 2014, Wang *et al.* 2016) and RSV in general (Park *et al.* 2015). Park *et al.* (2015) reviewed various pre-clinical studies using free RSV, carried out on various cancer cells with doses equal to or more than 50mg/kg body weight injected daily for at least 2 weeks *via* the IP route. For example, IP treatment of 50mg/kg/day of RSV for 6 weeks in DU145 prostate xenografts reduced tumour

growth and progression. Our IP cohort showed that at a lower dose of 25mg/kg, our novel conjugated RSV NPs containing both polymeric RSV conjugates and free RSV produced therapeutic effect with a shorter duration of treatment and less dosing frequency. Nonetheless, it should be noted that the % *w/w* of mPEG750-PLA1000-succ-RSV in the conjugated RSV NPs was 63.9% and a better purification of the conjugate during the chemical synthesis stage discussed in Chapter 2 would expect to produce even more therapeutic beneficial in B16-F10 tumour growth suppression *in vivo*. However, the high DL due to encapsulated of free RSV in conjugated RSV NPs could have contributed to higher RSV concentration at tumour sites. The nano-sized particles would have also encouraged passive targeting of B16-F10 tumour.

5.6 Conclusion

The low bioavailability of RSV is known to be mainly due to its rapid *in vivo* metabolism and degradation. We have developed novel RSV NPs using low MW amphiphilic copolymers and polymeric RSV conjugates in Chapter 4. We have found that nano-formulations of RSV by either encapsulation or conjugation protected RSV from degradation in rat plasma. Furthermore, we confirmed that conjugated RSV NPs reduced the phase II metabolism of RSV in HLM when compared to free RSV and encapsulated RSV NPs. The NPs were then assessed for anticancer activity in B16-F10 melanoma cells *in vitro* where the conjugated RSV NPs were found to be ineffective in increasing the anti-proliferative and apoptotic properties of RSV. The encapsulated RSV NPs performed either on-par or only slightly better than free RSV for those properties. As the effect of conjugation in decreasing the metabolism and degradation of RSV could not be fully evaluated in *in vitro* assays, *in vivo* evaluation of these NPs and their effect was undertaken to study the therapeutic effectiveness of conjugated RSV NPs in tumour suppression compared to encapsulated RSV NPs and free RSV using a B16-F10 mouse model with IT and IP route administrations. Conjugated RSV NPs were found to have decreased the growth of tumours better than encapsulated RSV NPs and free RSV alone despite its contradictory *in vitro* anticancer data, most likely due to its enhanced plasma and HLM stability and sustained release. In conclusion, this chapter has established that novel RSV

formulations made with RSV conjugated with low MW polymers and unconjugated RSV increased therapeutic activity of RSV in tumour bearing mice *via* the reduction of the metabolism rate of RSV in the melanoma mouse model. The outcomes of our study also strongly suggest that *in vitro* cytotoxicity work cannot be used to predict the therapeutic effectiveness of a drug delivery system. For a drug which undergoes extensive metabolisms, the use of chemical conjugation and NP formulation is an effective strategy to enhance its drug efficacy.

CHAPTER 6. GENERAL DISCUSSION, CONCLUSION AND FUTURE WORK

6.1 General discussion and conclusion

RSV is a simple and yet elegant molecule which has plenty of potential for an array of biological effects including anticancer with low toxicity (Gorlach *et al.* 2015). Although there are still discoveries need to be made to clarify its mechanisms of action and *in vivo* behaviour, it has been well documented that the therapeutic potential of RSV was limited by its low bioavailability due to its rapid degradation and hepatic metabolism *in vivo*. Our approach was to utilise both synthetic chemistry and nanotechnology techniques to improve on the stability profile of RSV by conjugating RSV to low MW PEGylated amphiphilic copolymers and formulating the conjugates into NPs. This research project aimed to produce nano-sized RSV formulations with better stability profiles than native RSV in order to enhance its anticancer properties in murine B16-F10 melanoma cells.

Low MW polymers with less than 3,000Da in total were used to optimise the DL of RSV formulations and to reduce likelihood of *in vivo* toxicity of polymers. However, the synthesis and purification of low MW mPEG750-PLA1000 was challenging despite various trials and purification techniques. Further studies into the mechanistic factors were needed to successfully synthesise the low MW polymer with high efficiency, however, this was not possible in this project. In this project, activated amphiphilic copolymers were synthesised using two-carbon and three-carbon linear chains, that is succ and glu, respectively, as a linker for the conjugation to RSV. With these, RSV was conjugated to the amphiphilic copolymers *via* an ester bond which can be easily cleaved *in vivo* for the release of RSV and hence, to produce its therapeutic effect. During the synthesis of the RSV conjugates, excess RSV was used in order to maintain mono-substitution of RSV by the amphiphilic copolymer and remaining unconjugated RSV was not removed after the chemical reaction so that we could utilise the unsubstituted free RSV to increase the DL of the nano-sized formulation. In order to study the effects of hydrophobic chain length, type of hydrophobic chain, hydrophilic chain length and type of linker used, we synthesised RSV conjugates with several

variables (Table 6.1) to mPEG750-PLA1000-succ-RSV with known enhanced PK and *in vitro* stability profile compared to free RSV (Basavaraj 2011).

Table 6.1 Synthesis variables of mPEG750-PLA1000-succ-RSV conjugate studied and expected outcome

RSV conjugate	Effect studied	Hypothesis
mPEG750-PLA1000-glu-RSV	Longer chain linker	More stable linker compared to succ leading to slower hydrolysis
mPEG750-PCL1000-succ-RSV	More hydrophobic chain	Slower polymer hydrolysis compared to mPEG750-PLA1000
mPEG2000-PLA1000-succ-RSV	Longer hydrophilic chain	Better formulation stability compared to mPEG750-PLA1000-succ-RSV
mPEG2000-PCL1000-succ-RSV	More hydrophobic chain	Slower polymer hydrolysis compared to mPEG2000-PLA1000

Using RSV conjugates synthesised in Chapter 2, we then successfully formulated the RSV conjugates into NPs by simple and affordable nanotechnology formulation techniques, that is solvent evaporation, solvent diffusion or thin film hydration (conjugated RSV NPs). With the presence of free RSV in the final synthesised RSV conjugate compound, DL of conjugated RSV NPs was higher (10%-48%) when compared to free RSV encapsulated in low MW amphiphilic PEGylated copolymers (encapsulated RSV NPs) with DL of below 10%. The particle sizes and zeta potential values were highly dependent on the polymer hydrophilicity and hydrophobicity, RSV-polymer covalent and non-covalent interaction and hydrophilicity-hydrophobicity properties of RSV conjugates. Overall, all NPs were smaller than 240nm except RSV encapsulated in mPEG2000-PLA1000 NPs with good PDI values which was suitable for passive tumour targeting. Zeta potential values were generally negative or zero which were explained extensively in Chapter 4 with conjugated RSV NPs being more negative than the encapsulated RSV NPs. This showed that conjugated RSV NPs were of high DL whilst maintaining nano-sized particles.

Conjugation also allowed for a sustained release of RSV equivalent as opposed to a

rapid release of RSV from encapsulated RSV NPs within 2 hours. Using a novel HPLC gradient method developed to analyse free RSV and RSV conjugates concurrently, we were able to elucidate the release profile of conjugated RSV NPs by the release profiles of each component in the NPs, that is free unconjugated RSV and RSV conjugate. Conjugated RSV NPs provided a sustained release of RSV by protecting the encapsulated free RSV and maintaining a NP shell using the RSV conjugate which slowly released the covalently bonded RSV by hydrolysis cleavage. The release of RSV from conjugated RSV NPs was found to be complex and varied depending on the type of polymer, particle size, release kinetics of encapsulated RSV, release kinetics of RSV cleaved from RSV conjugate and the degradation kinetics of the RSV conjugate and RSV. Encapsulated RSV NPs were able to reduce the degradation rate of RSV in PBS but was not able to provide a sustained release of RSV except for RSV encapsulated in mPEG2000-PLA1000 NPs due to its higher MW and large particle size.

A distinct difference between conjugation and encapsulation was also seen in the stability of RSV formulations when exposed to rat plasma esterases and human microsomal enzymes. Almost all encapsulated RSV NPs were stable against plasma esterases due to the protective polymeric shell but not against microsomal enzymes due to the availability of hydroxyl groups on RSV and the rapid degradation of polymeric shell upon exposure to microsomal enzyme in the study. The stability of conjugated RSV NPs against plasma esterases and microsomal enzymes were again studied using concurrent analysis of free unconjugated RSV and RSV conjugate by HPLC and were found to be dependent on the stability of the RSV conjugate itself which maintained the integrity of the NP structure and provided the release of RSV which was then degraded or metabolised. As the amount of free RSV within each conjugated RSV NPs varied, this perceived advantage was now contributing to the complexity of the stability and physical properties of conjugated RSV NPs. Nonetheless, all conjugated RSV NPs outperformed encapsulated RSV NPs in terms of release profile and stability profile against plasmatic and microsomal enzymes. Most RSV formulations were then evaluated for anti-proliferative effects on B16-F10 melanoma cell line which showed conjugated RSV NPs less effective than encapsulated RSV NPs and free RSV. This suggests that the conjugated RSV NPs may

have to be converted to free RSV to be therapeutically effective. This is not surprising as the conjugation of RSV prevented the use of the hydroxyl groups on RSV which was reported essential for anti-proliferative effect (Lee *et al.* 2004, Szekeres *et al.* 2010). The *in vitro* cell culture studies were not able to expound the *in vivo* effect of conjugated RSV NPs when reduction of metabolism and degradation rates were directly related to the therapeutic activity of RSV at the tumour site.

With data thus far, mPEG750-PLA1000-succ-RSV NPs was selected as the top candidate for further *in vitro* and *in vivo* studies. The polymeric conjugate properties were most balanced for NP preparation and for sustaining the NP integrity which provided stable profiles against plasma and liver enzymes. Its sustained release of total RSV equivalent was also favourable compared to the other RSV formulations regardless of encapsulated or conjugated NPs except RSV encapsulated in mPEG2000-PLA1000 NPs. As a comparison, RSV encapsulated in mPEG750-PLA1000 NPs was used for similar studies as well. In order to understand the mechanisms of anti-proliferative activity seen in B16-F10 cells, apoptosis assays were carried out. Correlating with the anti-proliferative assays, mPEG750-PLA1000-succ-RSV NPs was not effective when compared with encapsulated mPEG750-PLA1000 NPs or free RSV. The apoptotic effect of the encapsulated RSV NPs was enhanced when compared to free RSV but not after being treated for 48 hours which could be due to the rapid release of RSV from the encapsulated RSV NPs and subsequent degradation in CGM rendering it ineffective after a certain period of time post-release.

With a clear understanding that the full extent of the effectiveness of conjugated RSV NPs could not be assessed in *in vitro* experiments, we carried out *in vivo* studies on tumour-bearing mice where using the IT route enabled us to determine the suitability of the formulations and model at precise doses whereas with the IP route, the full effect and benefit of conjugation was evident. The tumour model we have chosen was highly aggressive and any positive effect rendered from our RSV formulations would have therapeutic potential. Through the IT cohort, we observed apoptotic and necrotic effects on the tumour of the treatment at low doses. However, tumour growth was too fast and aggressive to enable us to differentiate the treatments. A decrease of tumour growth trend was observed in the conjugated RSV NPs treatment

group when administered *via* the IP route although statistically not significant when compared with the control group. It should be noted that the control group had mice culled earlier due to their excessive tumour size and onset of necrosis. Furthermore, our conjugated NPs did not contain 100% RSV conjugate but 63.9% *w/w* of mPEG750-PLA1000-succ-RSV conjugate in conjugated RSV NPs (remaining was free unconjugated RSV), hence, the effect of the RSV conjugate as a treatment for the B16-F10 mouse model could have improved if purification was carried out on the final products synthesised to obtain 100% pure RSV conjugate for formulation of NPs which could lessen the DL. Nonetheless, this project has proven a few key points which should be considered in future research of RSV conjugates in NPs.

1) Low MW PEGylated amphiphilic copolymers is effective in conjugating RSV to reduce its metabolism rate and also suppress a highly aggressive tumour growth
2) Despite synthetic chemistry approaches to improve on the stability of the RSV conjugate mPEG750-PLA1000-succ-RSV, NP architecture and properties could have affected the stability profiles, release of RSV and anti-proliferative effect
3) DL of RSV in NPs was increased substantially when free RSV was encapsulated into NPs together with RSV conjugates and this has not been reported in literature thus far, in particular for RSV
4) The use of concurrent analysis of free RSV and RSV conjugates allowed us to examine the release profile and stability profiles of conjugated RSV NPs which has not been presented in literature before
5) In order to observe or evaluate the full effect of conjugation, *in vitro* cell culture assays were insufficient and animal models were necessary to allow the revelation of the full effectiveness of NP formulation

In conclusion, we successfully prepared RSV NPs within the size range possible for passive tumour targeting and enhanced the DL of NPs by encapsulating free RSV into NPs formulated with RSV conjugates. Conjugated RSV NPs showed better release and stability profiles against plasmatic and microsomal enzymes than free RSV and was ineffective against melanoma cell lines in anti-proliferative and apoptosis *in vitro* assays, however these NPs suppressed tumour growth in an *in vivo* model. Therefore,

the strategy to conjugate RSV to low MW PEGylated amphiphilic copolymers and formulate into NPs together with unconjugated RSV enhanced the anticancer activity of RSV. It was proven to be more effective than the approach of encapsulating free RSV into low MW PEGylated amphiphilic copolymers by effectively reducing the plasma degradation and liver metabolism rates of RSV, producing the more active form of RSV for anticancer effects.

6.2 Future work

This research project also revealed that there were many additional works which could be done in order to produce a better holistic understanding of the effects of RSV conjugation and its nano-sized formulation on improving the bioavailability of RSV for anticancer treatment. Due to time and resource constraints, they could not be conducted. It was imperative that the scope of the research project remained succinct to produce high quality research and deductions. Nonetheless, future work for this project are listed here.

1) Purification of final products synthesised in Chapter 2 to obtain conjugated RSV NPs with 100% RSV conjugates and evaluating the NPs for comparison with data in this project
2) Mechanistic cellular uptake studies of RSV formulations in B16-F10
3) Mechanistic apoptosis assays of RSV formulations in B16-F10
4) Anti-proliferative assay of RSV formulations in other cancerous cell lines
5) Modification of the current *in vivo* study to include a longer treatment period and longer evaluation period in the IP cohort; and also, to test other conjugated RSV NPs in the animal model
6) Biodistribution study and PK study of conjugated RSV NPs
7) Tumour histology of excised tumour tissue to assess apoptotic and necrotic effect of RSV formulations
8) *In vitro* and *in vivo* effects of RSV formulations on metastatic properties of B16-F10 cells due to the anti-metastatic properties of RSV

REFERENCES

Abbasi Oshaghi, E., Goodarzi, M.T., Higgins, V. and Adeli, K. (2017). "Role of resveratrol in the management of insulin resistance and related conditions: Mechanism of action." Critical Reviews in Clinical Laboratory Sciences **54**(4): 267-293.

Abraham, R.J. and Mobli, M. (2008, Retrieved February 2018). "Modelling 1H NMR Spectra of Organic Compounds: Theory, Applications and NMR Prediction Software." from http://atb.uq.edu.au/molecule.py?molid=16765#panel-nmr.

Agarwal, V., Rathore, D. and Bajpai, M. (2016). "Investigation of Effect of Non-Ionic Stabilizers on the Physical Stability of Drug Nanosuspension Prepared By Bottom Up Approach." International Journal of Pharmaceutical Sciences and Drug Research **8**(4): 189-198.

Agilent Technologies Inc. (2015) "Polymer Molecular Weight Distribution and Definitions of MW Averages." USA; Agilent Technologies, Inc.

Alibolandi, M., Sadeghi, F., Sazmand, S.H., Shahrokhi, S.M., Seifi, M. and Hadizadeh, F. (2015). "Synthesis and self-assembly of biodegradable polyethylene glycol-poly (lactic acid) diblock copolymers as polymersomes for preparation of sustained release system of doxorubicin." International Journal of Pharmaceutical Investigation **5**(3): 134-141.

Alkan, F.U., Anlas, C., Cinar, S., Yildirim, F., Ustuner, O., Bakirel, T. and Gurel, A. (2014). "Effects of curcumin in combination with cyclophosphamide on canine mammary tumour cell lines." Veterinarni Medicina **59**(11): 553-572.

Aluyen, J.K., Ton, Q.N., Tran, T., Yang, A.E., Gottlieb, H.B. and Bellanger, R.A. (2012). "Resveratrol: potential as anticancer agent." Journal of Dietary Supplements **9**(1): 45-56.

Amri, A., Chaumeil, J.C., Sfar, S. and Charrueau, C. (2012). "Administration of resveratrol: What formulation solutions to bioavailability limitations?" Journal of Controlled Release **158**(2): 182-193.

Andres-Lacueva, C., Macarulla, M.T., Rotches-Ribalta, M., Boto-Ordonez, M., Urpi-Sarda, M., Rodriguez, V.M. and Portillo, M.P. (2012). "Distribution of resveratrol metabolites in liver, adipose tissue, and skeletal muscle in rats fed different doses of this polyphenol." Journal of Agricultural and Food Chemistry **60**(19): 4833-4840.

Animal Resources Centre. (2018). "Rat and Mice Weights." Retrieved 24 April 2018, from http://www.arc.wa.gov.au/?page_id=125.

Ansari, K.A., Vavia, P.R., Trotta, F. and Cavalli, R. (2011). "Cyclodextrin-based nanosponges for delivery of resveratrol: in vitro characterisation, stability, cytotoxicity and permeation study." AAPS PharmSciTech **12**(1): 279-286.

Aras, A., Khokhar, A.R., Qureshi, M.Z., Silva, M.F., Sobczak-Kupiec, A., Pineda, E.A.G., Hechenleitner, A.A.W. and Farooqi, A.A. (2014). "Targeting Cancer with Nano-Bullets: Curcumin, EGCG, Resveratrol and Quercetin on Flying Carpets." Asian Pacific Journal of Cancer Prevention **15**(9): 3865-3871.

Arayne, M.S., Sultana, N. and Tabassum, A. (2013). "RP-LC simultaneous quantitation of co-administered drugs for (non-insulin dependent) diabetic mellitus induced dyslipidemia in active pharmaceutical ingredient, pharmaceutical formulations and human serum with UV-detector." Clinica Chimica Acta **425**(2013): 54-61.

Arora, D. and Jaglan, S. (2018). "Therapeutic applications of resveratrol nanoformulations." Environmental Chemistry Letters **16**(1): 35-41.

Asensi, M., Medina, I., Ortega, A., Carretero, J., Carmen Baño, M., Obrador, E. and Estrela, J.M. (2002). "Inhibition of cancer growth by resveratrol is related to its low bioavailability." Free Radical Biology & Medicine **33**(3): 387-398.

Augustin, M.A., Sanguansri, L. and Lockett, T. (2013). "Nano- and micro-encapsulated systems for enhancing the delivery of resveratrol." Annals of the New York Academy of Sciences **1290**(2013): 107-112.

Aziz, S.W. and Aziz, M.H. (2018). "Protective molecular mechanisms of resveratrol in UVR-induced Skin carcinogenesis." Photodermatology, Photoimmunology & Photomedicine **34**(1): 35-41.

Bartolacci, C., Andreani, C., Amici, A. and Marchini, C. (2018). "Walking a Tightrope: A Perspective of Resveratrol Effects on Breast Cancer." Current Protein and Peptide Science **19**(3): 311-322.

Barton-Burke, M. and Wilkes, G. (2006). Cancer chemotherapy and cell cycle kinetics. Cancer Therapies. Barton-Burke, M. and Wilkes, G.M. (Eds). Massachusetts; Jones & Bartlett Publishers.

Basavaraj (2011). Development of Novel Formulation Strategies to Improve Pharmacokinetic Profile of Resveratrol. PhD thesis, Curtin University.

Basavaraj, S., Benson, H.A.E., Brown, D.H. and Chen, Y. (2013). "Application of Solvent Influenced Fluorescence-quenching and Enhancement to Develop a Highly Sensitive HPLC Methodology for Analysis of Resveratrol-PEG Conjugates." Current Pharmaceutical Analysis **9**(2): 199-207.

Baur, J.A. and Sinclair, D.A. (2006). "Therapeutic potential of resveratrol: the in vivo evidence." Nature Reviews Drug Discovery **5**(6): 493-506.

Belleri, M., Ribatti, D., Savio, M., Stivala, L.A., Forti, L., Tanghetti, E., Alessi, P., Coltrini, D., Bugatti, A., Mitola, S., Nicoli, S., Vannini, V. and Presta, M. (2008). "alphavbeta3 Integrin-dependent antiangiogenic activity of resveratrol stereoisomers." Molecular Cancer Therapeutics **7**(12): 3761-3770.

Berman, A.Y., Motechin, R.A., Wiesenfeld, M.Y. and Holz, M.K. (2017). "The therapeutic potential of resveratrol: a review of clinical trials." NPJ Precision Oncology **1**(35): 1-9.

Bhattacharya, S., Darjatmoko, S.R. and Polans, A.S. (2011). "Resveratrol modulates the malignant properties of cutaneous melanoma through changes in the activation and attenuation of the antiapoptotic protooncogenic protein Akt/PKB." Melanoma Research **21**(3): 180-187.

Bhullar, K.S. and Hubbard, B.P. (2015). "Lifespan and healthspan extension by resveratrol." Biochimica et Biophysica Acta **1852**(6): 1209-1218.

Biasutto, L., Caliceti, P., Marotta, E., Garbisa, S., Mattarei, A., Salmaso, S., Zoratti, M., Beltramello, S., Bernkop-Schnürch, A. and Paradisi, C. (2009a). "Absorption and Metabolism of Resveratrol Carboxyesters and Methanesulfonate by Explanted Rat Intestinal Segment." Cellular Physiology and Biochemistry **24**(5-6): 557-566.

Biasutto, L., Marotta, E., Bradaschia, A., Fallica, M., Mattarei, A., Garbisa, S., Zoratti, M. and Paradisi, C. (2009b). "Soluble polyphenols: synthesis and bioavailability of 3,4',5-tri(alpha-D-glucose-3-O-succinyl) resveratrol." Bioorganic & Medicinal Chemistry Letters **19**(23): 6721-6724.

Biasutto, L., Marotta, E., Garbisa, S., Zoratti, M. and Paradisi, C. (2010). "Determination of quercetin and resveratrol in whole blood--implications for bioavailability studies." Molecules **15**(9): 6570-6579.

Biasutto, L., Mattarei, A., Azzolini, M., La Spina, M., Sassi, N., Romio, M., Paradisi, C. and Zoratti, M. (2017). "Resveratrol derivatives as a pharmacological tool." Annals of the New York Academy of Sciences **1403**(1): 27-37.

Biswas, S., Kumari, P., Lakhani, P.M. and Ghosh, B. (2016). "Recent advances in polymeric micelles for anti-cancer drug delivery." European Journal of Pharmaceutical Sciences **83**(2016): 184-202.

Blanquer-Rossello, M.D., Hernandez-Lopez, R., Roca, P., Oliver, J. and Valle, A. (2017). "Resveratrol induces mitochondrial respiration and apoptosis in SW620 colon cancer cells." Biochimica et Biophysica Acta **1861**(2): 431-440.

Bode, L.M., Bunzel, D., Huch, M., Cho, G.S., Ruhland, D., Bunzel, M., Bub, A., Franz, C.M. and Kulling, S.E. (2013). "In vivo and in vitro metabolism of trans-resveratrol by human gut microbiota." The American Journal of Clinical Nutrition **97**(2): 295-309.

Bohmdorfer, M., Szakmary, A., Schiestl, R.H., Vaquero, J., Riha, J., Brenner, S., Thalhammer, T., Szekeres, T. and Jager, W. (2017). "Involvement of UDP-Glucuronosyltransferases and Sulfotransferases in the Excretion and Tissue Distribution of Resveratrol in Mice." Nutrients **9**(12): 1347.

Bolko, K., Zvonar, A. and Gasperlin, M. (2014). "Mixed lipid phase SMEDDS as an innovative approach to enhance resveratrol solubility." Drug Development and Industrial Pharmacy **40**(1): 102-109.

Bolourchian, N., Mahboobian, M.M. and Dadashzadeh, S. (2013). "The Effect of PEG Molecular Weights on Dissolution Behavior of Simvastatin in Solid Dispersions." Iranian Journal of Pharmaceutical Research **12**(Supplement): 11-20.

Bonferoni, M.C., Rossi, S., Sandri, G. and Ferrari, F. (2017). "Nanoparticle formulations to enhance tumor targeting of poorly soluble polyphenols with potential anticancer properties." Seminars in Cancer Biology **46**(2017): 205-214.

Brown, V.A., Patel, K.R., Viskaduraki, M., Crowell, J.A., Perloff, M., Booth, T.D., Vasilinin, G., Sen, A., Schinas, A.M., Piccirilli, G., Brown, K., Steward, W.P., Gescher, A.J. and Brenner, D.E. (2010). "Repeat Dose Study of the Cancer Chemopreventive Agent Resveratrol in Healthy Volunteers: Safety, Pharmacokinetics, and Effect on the Insulin-like Growth Factor Axis." Cancer Research **70**(22): 9003-9011.

Brys, A.K., Gowda, R., Loriaux, D.B., Robertson, G.P. and Mosca, P.J. (2016). "Nanotechnology-based strategies for combating toxicity and resistance in melanoma therapy." Biotechnology Advances **34**(5): 565-577.

Bu, L., Gan, L.C., Guo, X.Q., Chen, F.Z., Song, Q., Qi, Z., Gou, X.J., Hou, S.X. and Yao, Q. (2013). "Trans-resveratrol loaded chitosan nanoparticles modified with biotin and avidin to target hepatic carcinoma." International Journal of Pharmaceutics **452**(1-2): 355-362.

Burghoff, S., Gong, X., Viethen, C., Jacoby, C., Flögel, U., Bongardt, S., Schorr, A., Hippe, A., Homey, B. and Schrader, J. (2014). "Growth and metastasis of B16-F10 melanoma cells is not critically dependent on host CD73 expression in mice." BMC Cancer **14**(14): 898.

Caddeo, C., Pons, R., Carbone, C., Fernandez-Busquets, X., Cardia, M.C., Maccioni, A.M., Fadda, A.M. and Manconi, M. (2017). "Physico-chemical characterization of succinyl chitosan-stabilized liposomes for the oral co-delivery of quercetin and resveratrol." Carbohydrate Polymers **157**(2017): 1853-1861.

Caddeo, C., Pucci, L., Gabriele, M., Carbone, C., Fernandez-Busquets, X., Valenti, D., Pons, R., Vassallo, A., Fadda, A.M. and Manconi, M. (2018). "Stability, biocompatibility and antioxidant activity of PEG-modified liposomes containing resveratrol." International Journal of Pharmaceutics **538**(1-2): 40-47.

Cadena, P.G., Pereira, M.A., Cordeiro, R.B., Cavalcanti, I.M., Barros Neto, B., Pimentel Mdo, C., Lima Filho, J.L., Silva, V.L. and Santos-Magalhaes, N.S. (2013). "Nanoencapsulation of quercetin and resveratrol into elastic liposomes." Biochimica et Biophysica Acta **1828**(2): 309-316.

Calabrese, E.J., Mattson, M.P. and Calabrese, V. (2010). "Resveratrol commonly displays hormesis: occurrence and biomedical significance." Human & Experimental Toxicology **29**(12): 980-1015.

Caltagirone, S., Rossi, C., Poggi, A., Ranelletti, F.O., Natali, P.G., Brunetti, M., Aiello, F.B. and Piantelli, M. (2000). "Flavonoids apigenin and quercetin inhibit melanoma growth and metastatic potential." International Journal of Cancer **87**(4): 595-600.

Carletto, B., Berton, J., Ferreira, T.N., Dalmolin, L.F., Paludo, K.S., Mainardes, R.M., Farago, P.V. and Favero, G.M. (2016). "Resveratrol-loaded nanocapsules inhibit murine melanoma tumor growth." Colloids and Surfaces B: Biointerfaces **144**(2016): 65-72.

Carraher, C.E. (2007). Introduction to Polymer Chemistry. USA; Taylor & Francis Group, LLC.

Carstens, M.G., de Jong, P.H., van Nostrum, C.F., Kemmink, J., Verrijk, R., de Leede, L.G., Crommelin, D.J. and Hennink, W.E. (2008). "The effect of core composition in biodegradable oligomeric micelles as taxane formulations." European Journal of Pharmaceutics and Biopharmaceutics **68**(3): 596-606.

CAS Registry. (2002, Retrieved 12 December 2017). "Resveratrol." 3 June 2002. from http://www.cas.org/motw/resveratrol.html.

Catalgol, B., Batirel, S., Taga, Y. and Ozer, N.K. (2012). "Resveratrol: French paradox revisited." Frontiers in Pharmacology **3**(141): 1-18.

Catania, A., NicolosI, S., Barrajón-Catalán, E., Cicirata, F. and Micol, V. (2013). "Immunoliposome encapsulation increases cytotoxic activity and selectivity of curcumin and resveratrol against HER2 overexpressing human breast cancer cells." Breast Cancer Research and Treatment **141**(1): 55–65.

Cavallaro, G., Licciardi, M., Caliceti, P., Salmaso, S. and Giammona, G. (2004). "Synthesis, physico-chemical and biological characterization of a paclitaxel macromolecular prodrug." European Journal of Pharmaceutics and Biopharmaceutics **58**(1): 151-159.

CellularChronicler (2016). "Said no more dollars, we'll be counting cells…." Cell Culture Chronicles https://cellculturechronicles.wordpress.com/2016/06/30/said-no-more-dollars-well-be-counting-cells/. Accessed March 2018.

Chance, R.R., Baniukiewicz, S.P., Mintz, D., Strate, G.V. and Hadjichristidis, N. (1995). "Characterization of Low-Molecular-Weight Polymers: Failure of Universal Calibration in Size Exclusion Chromatography." International Journal of Polymer Analysis and Characterization **1**(1): 3-34.

Chang, Y.J., Chang, Y.C., Liu, R.H., Chen, C.W., Lee, I. and Yang, N.C. (2018). "Resveratrol Can Be Stable in a Medium Containing Fetal Bovine Serum with Pyruvate but Shortens the Lifespan of Human Fibroblastic Hs68 Cells." Oxidative Medicine and Cellular Longevity **2018**(2371734): 1-15.

Chauhan, A.S. (2015). "Dendrimer nanotechnology for enhanced formulation and controlled delivery of resveratrol." Annals of the New York Academy of Sciences **1348**(1): 134-140.

Chedea, V.S., Vicas, S.I., Sticozzi, C., Pessina, F., Frosini, M., Maioli, E. and Valacchi, G. (2017). "Resveratrol: from diet to topical usage." Food & Function **8**(11): 3879-3892.

Chen, J., Shao, R., Zhang, X.D. and Chen, C. (2013a). "Applications of nanotechnology for melanoma treatment, diagnosis, and theranostics." International Journal of Nanomedicine **2013**(8): 2677-2688.

Chen, M.C., Chang, W.W., Kuan, Y.D., Lin, S.T., Hsu, H.C. and Lee, C.H. (2012). "Resveratrol inhibits LPS-induced epithelial-mesenchymal transition in mouse melanoma model." Innate Immunity **18**(5): 685-693.

Chen, Q. and Thouas, G. (2015a). Bioresorbable Polymers. Biomaterials: A Basic Introduction. Boca Raton; CRC Press. **10:** 339-384.

Chen, S., Yang, K., Tuguntaev, R.G., Mozhi, A., Zhang, J., Wang, P.C. and Liang, X.J. (2016). "Targeting tumor microenvironment with PEG-based amphiphilic nanoparticles to overcome chemoresistance." Nanomedicine **12**(2): 269-286.

Chen, Y.-B., Lan, Y.-W., Hung, T.-H., Chen, L.-G., Choo, K.-B., Cheng, W.T.K., Lee, H.-S. and Chong, K.-Y. (2015b). "Mesenchymal stem cell-based HSP70 promoter-driven VEGFA induction by resveratrol promotes angiogenesis in a mouse model." Cell Stress & Chaperones **20**(4): 643-652.

Chen, Y.J., Chen, Y.Y., Lin, Y.F., Hu, H.Y. and Liao, H.F. (2013b). "Resveratrol inhibits alpha-melanocyte-stimulating hormone signaling, viability, and invasiveness in melanoma cells." Evidence-Based Complementary and Alternative Medicine **2013**(632121): 1-8.

Cheng, J., Teply, B.A., Sherifi, I., Sung, J., Luther, G., Gu, F.X., Levy-Nissenbaum, E., Radovic-Moreno, A.F., Langer, R. and Farokhzad, O.C. (2007). "Formulation of functionalized PLGA-PEG nanoparticles for in vivo targeted drug delivery." Biomaterials **28**(5): 869-876.

Cheng, Y.J., Chang, M.Y., Chang, W.W., Wang, W.K., Liu, C.F., Lin, S.T. and Lee, C.H. (2015). "Resveratrol Enhances Chemosensitivity in Mouse Melanoma Model Through Connexin 43 Upregulation." Environmental Toxicology **30**(8): 877-886.

Chinembiri, T.N., du Plessis, L.H., Gerber, M., Hamman, J.H. and du Plessis, J. (2014). "Review of natural compounds for potential skin cancer treatment." Molecules **19**(8): 11679-11721.

Chong, S.J., Low, I.C. and Pervaiz, S. (2014). "Mitochondrial ROS and involvement of Bcl-2 as a mitochondrial ROS regulator." Mitochondrion **19**(2014): 39-48.

Chou, Y.-P., Lin, Y.-K., Chen, C.-H. and Fang, J.-Y. (2017). "Recent Advances in Polymeric Nanosystems for Treating Cutaneous Melanoma and Its Metastasis." Current Pharmaceutical Design **23**(35): 5301-5314.

Chu, B., Zhang, L., Qu, Y., Chen, X., Peng, J., Huang, Y. and Qian, Z. (2016). "Synthesis, characterization and drug loading property of Monomethoxy-Poly(ethylene glycol)-Poly(epsilon-caprolactone)-Poly(D,L-lactide) (MPEG-PCLA) copolymers." Scientific Reports **6**(34069): 1-15.

Chung, T.D.Y., Terry, D.B. and Smith, L.H. (2015). In Vitro and In Vivo Assessment of ADME and PK Properties During Lead Selection and Lead Optimization – Guidelines, Benchmarks and Rules of Thumb. Assay Guidance Manual. Sittampalam, G.S. and Coussens, N.P. (Eds). Bethesda; Eli Lilly & Company and the National Center for Advancing Translational Sciences**:** 15.

Cimino, S., Sortino, G., Favilla, V., Castelli, T., Madonia, M., Sansalone, S., Russo, G.I. and Morgia, G. (2012). "Polyphenols: key issues involved in chemoprevention of prostate cancer." Oxidative Medicine and Cellular Longevity **2012**(632959): 1-8.

Coccia, M. and Wang, L. (2015). "Path-breaking directions of nanotechnology-based chemotherapy and molecular cancer therapy." Technological Forecasting and Social Change **94**(2015): 155-169.

Cooper, D.L. and Harirforoosh, S. (2014). "Design and Optimization of PLGA-Based Diclofenac Loaded Nanoparticles." PLoS One **9**(1): e87326.

Coradini, K., Lima, F.O., Oliveira, C.M., Chaves, P.S., Athayde, M.L., Carvalho, L.M. and Beck, R.C. (2014). "Co-encapsulation of resveratrol and curcumin in lipid-core nanocapsules improves their in vitro antioxidant effects." European Journal of Pharmaceutics and Biopharmaceutics **88**(1): 178-185.

Correa, M., Machado, J., Jr., Carneiro, C.R., Pesquero, J.B., Bader, M., Travassos, L.R., Chammas, R. and Jasiulionis, M.G. (2005). "Transient inflammatory response induced by apoptotic cells is an important mediator of melanoma cell engraftment and growth." International Journal of Cancer **114**(3): 356-363.

Cosco, D., Paolino, D., Maiuolo, J., Marzio, L.D., Carafa, M., Ventura, C.A. and Fresta, M. (2015). "Ultradeformable liposomes as multidrug carrier of resveratrol and 5-fluorouracil for their topical delivery." International Journal of Pharmaceutics **489**(1-2): 1-10.

Csiszar, A., Csiszar, A., Pinto, J.T., Gautam, T., Kleusch, C., Hoffmann, B., Tucsek, Z., Toth, P., Sonntag, W.E. and Ungvari, Z. (2015). "Resveratrol encapsulated in novel fusogenic liposomes activates Nrf2 and attenuates oxidative stress in cerebromicrovascular endothelial cells from aged rats." The Journals of Gerontology. Series A, Biological Sciences and Medical Sciences **70**(3): 303-313.

Curran, R.E., Claxton, C.R., Hutchison, L., Harradine, P.J., Martin, I.J. and Littlewood, P. (2011). "Control and measurement of plasma pH in equilibrium dialysis: influence on drug plasma protein binding." Drug Metabolism and Disposition **39**(3): 551-557.

da Rocha Lindner, G., Khalil, N.M. and Mainardes, R.M. (2013). "Resveratrol-loaded polymeric nanoparticles: validation of an HPLC-PDA method to determine the drug entrapment and evaluation of its antioxidant activity." Scientific World Journal **2013**(506083): 1-9.

Dal Magro, C., Aguiar, G.P.S., Veneral, J.G., dos Santos, A.E., de Chaves, L.M.P.C., Oliveira, J.V. and Lanza, M. (2017). "Co-precipitation of trans -resveratrol in PHBV using Solution Enhanced Dispersion by Supercritical Fluids technique." The Journal of Supercritical Fluids **127**(2017): 182-190.

Danafar, H., Rostamizadeh, K., Davaran, S. and Hamidi, M. (2017). "Co-delivery of hydrophilic and hydrophobic drugs by micelles: a new approach using drug conjugated PEG-PCLNanoparticles." Drug Development and Industrial Pharmacy **43**(11): 1908-1918.

Danciu, C., Oprean, C., Coricovac, D.E., Andreea, C., Cimpean, A., Radeke, H., Soica, C. and Dehelean, C. (2015). "Behaviour of four different B16 murine melanoma cell sublines: C57BL/6J skin." International Journal of Experimental Pathology **96**(2): 73-80.

Das, J., Ramani, R. and Suraju, M.O. (2016). "Polyphenol compounds and PKC signaling." Biochimica et Biophysica Acta **1860**(10): 2107-2121.

Davatgaran-Taghipour, Y., Masoomzadeh, S., Farzaei, M.H., Bahramsoltani, R., Karimi-Soureh, Z., Rahimi, R. and Abdollahi, M. (2017). "Polyphenol nanoformulations for cancer therapy: experimental evidence and clinical perspective." International Journal of Nanomedicine **12**: 2689-2702.

Davidov-Pardo, G., Joye, I.J. and McClements, D.J. (2015). "Encapsulation of resveratrol in biopolymer particles produced using liquid antisolvent precipitation. Part 1: Preparation and characterization." Food Hydrocolloids **45**(2015): 309-316.

Davidov-Pardo, G. and McClements, D.J. (2014). "Resveratrol encapsulation: Designing delivery systems to overcome solubility, stability and bioavailability issues." Trends in Food Science & Technology **38**(2): 88-103.

de Oliveira Júnior, R.G., Ferraz, C.A.A., e Silva, M.G., de Lavor, E.M., Rolim, L.A., de Lima, J.T., Fleury, A., Picot, L., de Souza Siqueira Quintans, J., Quintans Júnior, L.J. and da Silva Almeida, J.R.G., Eds. (2017). Flavonoids: Promising Natural Products for Treatment of Skin Cancer (Melanoma). Natural Products and Cancer Drug Discovery; IntechOpen. from https://www.intechopen.com/books/natural-products-and-cancer-drug-discovery/flavonoids-promising-natural-products-for-treatment-of-skin-cancer-melanoma-.

de Vries, K., Strydom, M. and Steenkamp, V. (2018). "Bioavailability of resveratrol: Possibilities for enhancement." Journal of Herbal Medicine **11**(2018): 71-77.

Diaz-Gerevini, G.T., Repossi, G., Dain, A., Tarres, M.C., Das, U.N. and Eynard, A.R. (2016). "Beneficial action of resveratrol: How and why?" Nutrition **32**(2): 174-178.

Du, F., Honzke, S., Neumann, F., Keilitz, J., Chen, W., Ma, N., Hedtrich, S. and Haag, R. (2016). "Development of biodegradable hyperbranched core-multishell nanocarriers for efficient topical drug delivery." Journal of Controlled Release **242**(2016): 42-49.

Duan, J., Yue, W., E, J., Malhotra, J., Lu, S.E., Gu, J., Xu, F. and Tan, X.L. (2016). "In vitro comparative studies of resveratrol and triacetylresveratrol on cell proliferation, apoptosis, and STAT3 and NFkappaB signaling in pancreatic cancer cells." Scientific Reports **6**(31672): 1-10.

Dubey, R.D., Klippstein, R., Wang, J.T.-W., Hodgins, N., Mei, K.-C., Sosabowski, J., Hider, R.C., Abbate, V., Gupta, P.N. and Al-Jamal, K.T. (2017). "Novel Hyaluronic Acid Conjugates for Dual Nuclear Imaging and Therapy in CD44-Expressing Tumors in Mice In Vivo." Nanotheranostics **1**(1): 59-79.

Dun, J., Chen, X., Gao, H., Zhang, Y., Zhang, H. and Zhang, Y. (2015). "Resveratrol synergistically augments anti-tumor effect of 5-FU in vitro and in vivo by increasing S-phase arrest and tumor apoptosis." Experimental Biology and Medicine (Maywood) **240**(12): 1672-1681.

Edelman, R., Assaraf, Y.G., Levitzky, I., Shahar, T. and Livney, Y.D. (2017). "Hyaluronic acid-serum albumin conjugate-based nanoparticles for targeted cancer therapy." Oncotarget **8**(15): 24337-24353.

Ekladious, I., Liu, R., Varongchayakul, N., Mejia Cruz, L.A., Todd, D.A., Zhang, H., Oberlies, N.H., Padera, R.F., Colson, Y.L. and Grinstaff, M.W. (2018). "Reinforcement of polymeric nanoassemblies for ultra-high drug loadings, modulation of stiffness and release kinetics, and sustained therapeutic efficacy." Nanoscale **2018**(18): 8360-8366.

Elamanchili, P., McEachern, C. and Burt, H. (2009). "Reversal of multidrug resistance by methoxypolyethylene glycol-block-polycaprolactone diblock copolymers through the inhibition of P-glycoprotein function." Journal of Pharmaceutical Sciences **98**(3): 945-958.

Fahmy, R.G., Dass, C.R., Sun, L.Q., Chesterman, C.N. and Khachigian, L.M. (2003). "Transcription factor Egr-1 supports FGF-dependent angiogenesis during neovascularization and tumor growth." Nature Medicine **9**(8): 1026-1032.

Fairchild, E.T. and Carson, W.E. (2011). Animal Models of Melanoma. Tumor Models in Cancer Research. Teicher, B.A. (Eds). New York; Humana Press. **11**.

Fakhari, A. and Anand Subramony, J. (2015). "Engineered in-situ depot-forming hydrogels for intratumoral drug delivery." Journal of Controlled Release **220**(2015): 465-475.

Fan, X.X., Yao, X.J., Xu, S.W., Wong, V.K., He, J.X., Ding, J., Xue, W.W., Mujtaba, T., Michelangeli, F., Huang, M., Huang, J., Xiao, D.K., Jiang, Z.B., Zhou, Y.L., Kam, R.K., Liu, L. and Leung, E.L. (2015). "(Z)3,4,5,4'-trans-tetramethoxystilbene, a new analogue of resveratrol, inhibits gefitinb-resistant non-small cell lung cancer via selectively elevating intracellular calcium level." Scientific Reports **5**(16348): 1-18.

Fang, J., Nakamura, H. and Maeda, H. (2011). "The EPR effect: Unique features of tumor blood vessels for drug delivery, factors involved, and limitations and augmentation of the effect." Advanced Drug Delivery Reviews **63**(3): 136-151.

Fang, Y., Bradley, M.J., Cook, K.M., Herrick, E.J. and Nicholl, M.B. (2013). "A potential role for resveratrol as a radiation sensitizer for melanoma treatment." Journal of Surgical Research **183**(2): 645-653.

Fliedner, F.P., Hansen, A.E., Jorgensen, J.T. and Kjaer, A. (2016). "The use of matrigel has no influence on tumor development or PET imaging in FaDu human head and neck cancer xenografts." BMC Medical Imaging **16**(5): 1-8.

Fogacci, F., Tocci, G., Presta, V., Fratter, A., Borghi, C. and Cicero, A.F.G. (2018). "Effect of resveratrol on blood pressure: A systematic review and meta-analysis of randomized, controlled, clinical trials." Critical Reviews in Food Science and Nutrition **2018**: 1-14.

Fouad, M.A., Agha, A.M., Merzabani, M.M. and Shouman, S.A. (2013). "Resveratrol inhibits proliferation, angiogenesis and induces apoptosis in colon cancer cells: calorie restriction is the force to the cytotoxicity." Human Experimental Toxicology **32**(10): 1067-1080.

Friedrich, R.B., Kann, B., Coradini, K., Offerhaus, H.L., Beck, R.C. and Windbergs, M. (2015). "Skin penetration behavior of lipid-core nanocapsules for simultaneous delivery of resveratrol and curcumin." European Journal of Pharmaceutical Sciences **78**: 204-213.

Frozza, R.L., Bernardi, A., Hoppe, J.B., Meneghetti, A.B., Matte, A., Battastini, A.M., Pohlmann, A.R., Guterres, S.S. and Salbego, C. (2013). "Neuroprotective effects of resveratrol against Abeta administration in rats are improved by lipid-core nanocapsules." Molecular Neurobiology **47**(3): 1066-1080.

Furniss, B.S., Hannaford, A.J., Smith, P.W.G. and Tatchell, A.R. (1996). Vogel's Textbook of Practical Organic Chemistry. UK; Pearson Education Limited.

Galvin, P., Thompson, D., Ryan, K.B., McCarthy, A., Moore, A.C., Burke, C.S., Dyson, M., Maccraith, B.D., Gun'ko, Y.K., Byrne, M.T., Volkov, Y., Keely, C., Keehan, E., Howe, M., Duffy, C. and MacLoughlin, R. (2012). "Nanoparticle-based drug delivery: case studies for cancer and cardiovascular applications." Cellular and Molecular Life Sciences **69**(3): 389-404.

Gao, H., Zhang, Q., Yang, Y., Jiang, X. and He, Q. (2015). "Tumor homing cell penetrating peptide decorated nanoparticles used for enhancing tumor targeting delivery and therapy." International Journal of Pharmaceutics **478**(1): 240-250.

Gao, Z., Zhang, L. and Sun, Y. (2012). "Nanotechnology applied to overcome tumor drug resistance." Journal of Controlled Release **162**(1): 45-55.

Gatouillat, G., Balasse, E., Joseph-Pietras, D., Morjani, H. and Madoulet, C. (2010). "Resveratrol induces cell-cycle disruption and apoptosis in chemoresistant B16 melanoma." Journal of Cellular Biochemistry **110**(4): 893-902.

Geng, T., Zhao, X., Ma, M., Zhu, G. and Yin, L. (2017). "Resveratrol-Loaded Albumin Nanoparticles with Prolonged Blood Circulation and Improved Biocompatibility for Highly Effective Targeted Pancreatic Tumor Therapy." Nanoscale Research Letters **12**(1): 437.

Gogada, R., Prabhu, V., Amadori, M., Scott, R., Hashmi, S. and Chandra, D. (2011). "Resveratrol induces p53-independent, X-linked inhibitor of apoptosis protein (XIAP)-mediated Bax protein oligomerization on mitochondria to initiate cytochrome c release and caspase activation." Journal of Biological Chemistry **286**(33): 28749-28760.

Goh, Y.L., Cui, Y.T., Pendharkar, V. and Adsool, V.A. (2017). "Toward Resolving the Resveratrol Conundrum: Synthesis and in Vivo Pharmacokinetic Evaluation of BCP-Resveratrol." ACS Medicinal Chemistry Letters **8**(5): 516-520.

Gorlach, S., Fichna, J. and Lewandowska, U. (2015). "Polyphenols as mitochondria-targeted anticancer drugs." Cancer Letters **366**(2): 141-149.

Goyal, R., Macri, L.K., Kaplan, H.M. and Kohn, J. (2016). "Nanoparticles and nanofibers for topical drug delivery." Journal of Controlled Release **240**(2016): 77-92.

Greenwald, R.B., Pendri, A., Conover, C., Gilbert, C., Yang, R. and Xia, J. (1996). "Drug Delivery Systems. 2. Camptothecin 20-O-Poly(ethylene glycol) Ester Transport Forms." Journal of Medicinal Chemistry **39**(10): 1938-1940.

Greenwald, R.B., Yang, K., Zhao, H., Conover, C.D., Lee, S. and Filpula, D. (2003). "Controlled Release of Proteins from Their Poly(Ethylene Glycol) Conjugates: Drug Delivery Systems Employing 1,6-Elimination." Bioconjugate Chemistry **14**(2): 395-403.

Grossen, P., Witzigmann, D., Sieber, S. and Huwyler, J. (2017). "PEG-PCL-based nanomedicines: A biodegradable drug delivery system and its application." Journal of Controlled Release **260**(2017): 46-60.

Gu, G., Gao, X., Hu, Q., Kang, T., Liu, Z., Jiang, M., Miao, D., Song, Q., Yao, L., Tu, Y., Pang, Z., Chen, H., Jiang, X. and Chen, J. (2013). "The influence of the penetrating peptide iRGD on the effect of paclitaxel-loaded MT1-AF7p-conjugated nanoparticles on glioma cells." Biomaterials **34**(21): 5138-5148.

Guan, H., Singh, N.P., Singh, U.P., Nagarkatti, P.S. and Nagarkatti, M. (2012). "Resveratrol prevents endothelial cells injury in high-dose interleukin-2 therapy against melanoma." PLoS One **7**(4): e35650.

Gulcur, E., Thaqi, M., Khaja, F., Kuzmis, A. and Onyuksel, H. (2013). "Curcumin in VIP-targeted sterically stabilized phospholipid nanomicelles: a novel therapeutic approach for breast cancer and breast cancer stem cells." Drug Delivery and Translational Research **3**(6): 62–574.

Guo, C., Yin, J. and Chen, D. (2018a). "Co-encapsulation of curcumin and resveratrol into novel nutraceutical hyalurosomes nano-food delivery system based on oligo-hyaluronic acid-curcumin polymer." Carbohydrate Polymers **181**(2018): 1033-1037.

Guo, W., Li, A., Jia, Z., Yuan, Y., Dai, H. and Li, H. (2013). "Transferrin modified PEG-PLA-resveratrol conjugates: in vitro and in vivo studies for glioma." European Journal of Pharmacology **718**(1-3): 41-47.

Guo, X., Zhao, Z., Chen, D., Qiao, M., Wan, F., Cun, D., Sun, Y. and Yang, M. (2018b). "Co-delivery of resveratrol and docetaxel via polymeric micelles to improve the treatment of drug-resistant tumors." Asian Journal of Pharmaceutical Sciences **Accepted** (In Press).

Gupta, R., Shea, J., Scafe, C., Shurlygina, A. and Rapoport, N. (2015). "Polymeric micelles and nanoemulsions as drug carriers: Therapeutic efficacy, toxicity, and drug resistance." Journal of Controlled Release **212**: 70-77.

Habibie, Yokoyama, S., Abdelhamed, S., Awale, S., Sakurai, H., Hayakawa, Y. and Saiki, I. (2014). "Survivin suppression through STAT3/beta-catenin is essential for resveratrol-induced melanoma apoptosis." International Journal of Oncology **45**(2): 895-901.

Hao, J., Gao, Y., Zhao, J., Zhang, J., Li, Q., Zhao, Z. and Liu, J. (2015). "Preparation and optimization of resveratrol nanosuspensions by antisolvent precipitation using Box-Behnken design." AAPS PharmSciTech **16**(1): 118-128.

Hao, J., Tong, T., Jin, K., Zhuang, Q., Han, T., Bi, Y., Wang, J. and Wang, X. (2017). "Folic acid-functionalized drug delivery platform of resveratrol based on Pluronic 127/D-alpha-tocopheryl polyethylene glycol 1000 succinate mixed micelles." International Journal of Nanomedicine **12**: 2279-2292.

Hao, J., Zhao, J., Zhang, S., Tong, T., Zhuang, Q., Jin, K., Chen, W. and Tang, H. (2016). "Fabrication of an ionic-sensitive in situ gel loaded with resveratrol nanosuspensions intended for direct nose-to-brain delivery." Colloids and Surfaces B: Biointerfaces **147**(2016): 376-386.

Hinds, K.D. (2004). Protein Conjugation, Cross-Linking, and PEGylation. Biomaterials for Delivery and Targeting of Proteins and Nucleic Acids. Mahato, R.I. (Eds). Boca Raton; CRC Press. **5**.

Ho, K.S. and Shoichet, M.S. (2013). "Design considerations of polymeric nanoparticle micelles for chemotherapeutic delivery." Current Opinion in Chemical Engineering **2**(1): 53-59.

Holding, S.R. and Meehan, E. (1995) "Molecular Weight Characterisation of Synthetic Polymers." Rapra Review Reports **7**, 16. UK; Rapra Technology Ltd.

Homs, M., Calderó, G., Monge, M., Morales, D. and Solans, C. (2018). "Influence of polymer concentration on the properties of nano-emulsions and nanoparticles obtained by a low-energy method." Colloids and Surfaces A: Physicochemical and Engineering Aspects **536**(2018): 204-212.

Huang, D., Zhuang, Y., Shen, H., Yang, F., Wang, X. and Wu, D. (2018). "Acetal-linked PEGylated paclitaxel prodrugs forming free-paclitaxel-loaded pH-responsive micelles with high drug loading capacity and improved drug delivery." Materials Science & Engineering C - Materials for Biological Applications **82**(2018): 60-68.

Huang, X. and Mazza, G. (2011). "Simultaneous analysis of serotonin, melatonin, piceid and resveratrol in fruits using liquid chromatography tandem mass spectrometry." Journal of Chromatography A **1218**(25): 3890-3899.

Hubbard, B.P. and Sinclair, D.A. (2014). "Small molecule SIRT1 activators for the treatment of aging and age-related diseases." Trends in Pharmacological Sciences **35**(3): 146-154.

Hull, L.C., Farrell, D. and Grodzinski, P. (2014). "Highlights of recent developments and trends in cancer nanotechnology research-view from NCI Alliance for Nanotechnology in Cancer." Biotechnology Advances **32**(4): 666-678.

Hussain, A., Gheewala, T.M., Vas, A.J., Shah, K., Goala, P., Khan, S., Hinduja, S. and Sharma, C. (2014). "Growth inhibitory and adjuvant therapeutic potential of aqueous extract of *Triticum aestivum* on MCF-7 and HeLa cells." Experimental Oncology **36**(1): 9-16.

Ikhuoria, E.U., Okieimen, F.E. and Aigbodion, A.I. (2005). "Evaluation of the Effect of Temperature on the Stability of Metal Soaps of Dicarboxylic Acids." Journal of Applied Sciences Environmental Management **9**(1): 127 - 130.

Imamura, H., Nagayama, D., Ishihara, N., Tanaka, S., Watanabe, R., Watanabe, Y., Sato, Y., Yamaguchi, T., Ban, N., Kawana, H., Ohira, M., Endo, K., Saiki, A., Shirai, K. and Tatsuno, I. (2017). "Resveratrol attenuates triglyceride accumulation associated with upregulation of Sirt1 and lipoprotein lipase in 3T3-L1 adipocytes." Molecular Genetics and Metabolism Reports **12**(2017): 44-50.

Inkinen, S., Hakkarainen, M., Albertsson, A.C. and Sodergard, A. (2011). "From lactic acid to poly(lactic acid) (PLA): characterization and analysis of PLA and its precursors." Biomacromolecules **12**(3): 523-532.

Iwuchukwu, O.F. and Nagar, S. (2008). "Resveratrol (trans-resveratrol, 3,5,4'-trihydroxy-trans-stilbene) glucuronidation exhibits atypical enzyme kinetics in various protein sources." Drug Metabolism and Disposition **36**(2): 322-330.

Izunobi, J.U. and Higginbotham, C.L. (2011). "Polymer Molecular Weight Analysis by 1H NMR Spectroscopy." Journal of Chemical Education **88**(8): 1098-1104.

Jang, M. (1997). "Cancer Chemopreventive Activity of Resveratrol, a Natural Product Derived from Grapes." Science **275**(5297): 218-220.

Jeong, M.H., Yang, K., Lee, C.G., Jeong, D.H., Park, Y.S., Choi, Y.J., Kim, J.S., Oh, S.J., Jeong, S.K. and Jo, W.S. (2014). "In Vitro Genotoxicity Assessment of a Novel Resveratrol Analogue, HS-1793." Toxicology Research **30**(3): 211-220.

Jhaveri, A., Deshpande, P., Pattni, B. and Torchilin, V. (2018). "Transferrin-targeted, resveratrol-loaded liposomes for the treatment of glioblastoma." Journal of Controlled Release **277**(2018): 89-101.

Jiang, Z.M., Dai, S.P., Xu, Y.Q., Li, T., Xie, J., Li, C. and Zhang, Z.H. (2015). "Crizotinib-loaded polymeric nanoparticles in lung cancer chemotherapy." Medical Oncology **32**(7): 193.

Jokerst, J.V., Tatsiana, L., Zare, R.N. and Gambhir, S.S. (2011). "Nanoparticle PEGylation for imaging and therapy." Nanomedicine **6**(4): 715-728.

Junco, J.J., Mancha, A., Malik, G., Wei, S.J., Kim, D.J., Liang, H. and Slaga, T.J. (2013). "Resveratrol and P-glycoprotein inhibitors enhance the anti-skin cancer effects of ursolic acid." Molecular Cancer Research **11**(12): 1521-1529.

Jung, K.H., Lee, J.H., Park, J.W., Quach, C.H., Moon, S.H., Cho, Y.S. and Lee, K.H. (2015). "Resveratrol-loaded polymeric nanoparticles suppress glucose metabolism and tumor growth in vitro and in vivo." International Journal of Pharmaceutics **478**(1): 251-257.

Juskaite, V., Ramanauskiene, K. and Briedis, V. (2015). "Design and Formulation of Optimized Microemulsions for Dermal Delivery of Resveratrol." Evidence-Based Complementary and Alternative Medicine **2015**(540916): 1-10.

Kamal, A., Ashraf, M., Basha, S.T., Ali Hussaini, S.M., Singh, S., Vishnuvardhan, M.V., Kiran, B. and Sridhar, B. (2016). "Design, synthesis and antiproliferative activity of the new conjugates of E7010 and resveratrol as tubulin polymerization inhibitors." Organic Biomolecular Chemistry **14**(4): 1382-1394.

Kang, Y.M., Kim, G.H., Kim, J.I., Kim, D.Y., Lee, B.N., Yoon, S.M., Kim, J.H. and Kim, M.S. (2011). "In vivo efficacy of an intratumorally injected in situ-forming doxorubicin/poly(ethylene glycol)-b-polycaprolactone diblock copolymer." Biomaterials **32**(20): 4556-4564.

Karthikeyan, S., Rajendra Prasad, N., Ganamani, A. and Balamurugan, E. (2013). "Anticancer activity of resveratrol-loaded gelatin nanoparticles on NCI-H460 non-small cell lung cancer cells." Biomedicine & Preventive Nutrition **3**(1): 64-73.

Ke, X., Ng, V.W., Ono, R.J., Chan, J.M., Krishnamurthy, S., Wang, Y., Hedrick, J.L. and Yang, Y.Y. (2014). "Role of non-covalent and covalent interactions in cargo loading capacity and stability of polymeric micelles." Journal of Controlled Release **193**(2014): 9-26.

Khalil, N.M., do Nascimento, T.C., Casa, D.M., Dalmolin, L.F., de Mattos, A.C., Hoss, I., Romano, M.A. and Mainardes, R.M. (2013). "Pharmacokinetics of curcumin-loaded PLGA and PLGA-PEG blend nanoparticles after oral administration in rats." Colloids and Surfaces B: Biointerfaces **101**(2013): 353-360.

Khan, M.D., Chan, H.-C., Wan, X.-X., Tania, M., Xu, A.-H., Chen, F.-Z. and Zhang, D.-Z. (2013). "Regulatory Effects of Resveratrol on Antioxidant Enzymes: a Mechanism of Growth Inhibition and Apoptosis Induction in Cancer Cells." Molecules and Cells **35**: 215-229.

Khanna, Y.P., McDonnell, M.E. and Han, P.K. (1996). Rheology and Molecular Weight of Polymers. A Guide to Materials Characterization and Chemical Analysis. Sibilia, J.P. (Eds). USA; VCH Publishers, Inc. **12:** 287-310.

Khonkarn, R., Mankhetkorn, S., Hennink, W.E. and Okonogi, S. (2011). "PEG-OCL micelles for quercetin solubilization and inhibition of cancer cell growth." European Journal of Pharmaceutics and Biopharmaceutics **79**(2): 268-275.

Kim, J.A., Kim, D.H., Hossain, M.A., Kim, M.Y., Sung, B., Yoon, J.H., Suh, H., Jeong, T.C., Chung, H.Y. and Kim, N.D. (2014). "HS-1793, a resveratrol analogue, induces cell cycle arrest and apoptotic cell death in human breast cancer cells." International Journal of Oncology **44**(2): 473-480.

Kim, M.S., Hyun, H., Cho, Y.H., Seo, K.S., Jang, W.Y., Kim, S.K., Khang, G. and Lee, H.B. (2005). "Preparation of methoxy poly(ethyleneglycol)-block-poly(caprolactone) via activated monomer mechanism and examination of micellar characterization." Polymer Bulletin **55**(3): 149-156.

Kim, M.S., Seo, K.S., Khang, G., Cho, S.H. and Lee, H.B. (2004). "Preparation of poly(ethylene glycol)-block-poly(caprolactone) copolymers and their applications as thermo-sensitive materials." Journal of Biomedical Materials Research A **70**(1): 154-158.

Kim, S., Thiessen, P.A., Bolton, E.E., Chen, J., Fu, G., Gindulyte, A., Han, L., He, J., He, S., Shoemaker, B.A., Wang, J., Yu, B., Zhang, J. and Byrant, S.H. (2016). "PubChem Substance and Compound databases." Nucleic Acids Research **44**: D1202–D1213.

Ko, J.H., Sethi, G., Um, J.Y., Shanmugam, M.K., Arfuso, F., Kumar, A.P., Bishayee, A. and Ahn, K.S. (2017). "The Role of Resveratrol in Cancer Therapy." International Journal of Molecular Sciences **18**(12): 2589.

Kobayashi, K., Wei, J., Iida, R., Ijiro, K. and Niikura, K. (2014). "Surface engineering of nanoparticles for therapeutic applications." Polymer Journal **46**(8): 460-468.

Kolate, A., Baradia, D., Patil, S., Vhora, I., Kore, G. and Misra, A. (2014). "PEG - a versatile conjugating ligand for drugs and drug delivery systems." Journal of Controlled Release **192**(2014): 67-81.

Kong, Q.J., Ren, X.Y., Hu, N., Sun, C.R. and Pan, Y.J. (2011). "Identification of isomers of resveratrol dimer and their analogues from wine grapes by HPLC/MS(n) and HPLC/DAD-UV." Food Chemistry **127**(2): 727-734.

Kulkarni, S.S. and Canto, C. (2015). "The molecular targets of resveratrol." Biochimica et Biophysica Acta **1852**(6): 1114-1123.

Kumar, S., Lather, V. and Pandita, D. (2016). "Stability indicating simplified HPLC method for simultaneous analysis of resveratrol and quercetin in nanoparticles and human plasma." Food Chemistry **197**(Pt A): 959-964.

Kundu, J.K. and Surh, Y.J. (2008). "Cancer chemopreventive and therapeutic potential of resveratrol: mechanistic perspectives." Cancer Letters **269**(2): 243-261.

Lammers, T., Peschke, P., Kuhnlein, R., Subr, V., Ulbrich, K., Huber, P., Hennink, W. and Storm, G. (2006). "Effect of intratumoral injection on the biodistribution and the therapeutic potential of HPMA copolymer-based drug delivery systems." Neoplasia **8**(10): 788-795.

Lata, J.P., Gao, L., Mukai, C., Cohen, R., Nelson, J.L., Anguish, L., Coonrod, S. and Travis, A.J. (2015). "Effects of Nanoparticle Size on Multilayer Formation and Kinetics of Tethered Enzymes." Bioconjugate Chemistry **26**(9): 1931-1938.

Lee-Chang, C., Bodogai, M., Martin-Montalvo, A., Wejksza, K., Sanghvi, M., Moaddel, R., de Cabo, R. and Biragyn, A. (2013). "Inhibition of breast cancer metastasis by resveratrol-mediated inactivation of tumor-evoked regulatory B cells." Journal of Immunology **191**(8): 4141-4151.

Lee, C.W., Yen, F.L., Huang, H.W., Wu, T.H., Ko, H.H., Tzeng, W.S. and Lin, C.C. (2012a). "Resveratrol nanoparticle system improves dissolution properties and enhances the hepatoprotective effect of resveratrol through antioxidant and anti-inflammatory pathways." Journal of Agricultural Food Chemistry **60**(18): 4662-4671.

Lee, E.O., Lee, H.J., Hwang, H.S., Ahn, K.S., Chae, C., Kang, K.S., Lu, J. and Kim, S.H. (2006). "Potent inhibition of Lewis lung cancer growth by heyneanol A from the roots of Vitis amurensis through apoptotic and anti-angiogenic activities." Carcinogenesis **27**(10): 2059-2069.

Lee, H., Zhang, P., Herrmann, A., Yang, C., Xin, H., Wang, Z., Hoon, D.S., Forman, S.J., Jove, R., Riggs, A.D. and Yu, H. (2012b). "Acetylated STAT3 is crucial for methylation of tumor-suppressor gene promoters and inhibition by resveratrol results in demethylation." Proceedings of the National Academy of Sciences of the United States of America **109**(20): 7765-7769.

Lee, H.J., Seo, J.W., Lee, B.H., Chung, K.-H. and Chi, D.Y. (2004). "Syntheses and radical scavenging activities of resveratrol derivatives." Bioorganic & Medicinal Chemistry Letters **14**(2): 463-466.

Lee, J.Y., Kim, K.S., Kang, Y.M., Kim, E.S., Hwang, S.J., Lee, H.B., Min, B.H., Kim, J.H. and Kim, M.S. (2010). "In vivo efficacy of paclitaxel-loaded injectable in situ-forming gel against subcutaneous tumor growth." International Journal of Pharmaceutics **392**(1-2): 51-56.

Lee, S.H., Koo, B.S., Park, S.Y. and Kim, Y.M. (2015). "Anti-angiogenic effects of resveratrol in combination with 5-fluorouracil on B16 murine melanoma cells." Molecular Medicine Reports **12**(2): 2777-2783.

Letchford, K., Liggins, R. and Burt, H. (2008). "Solubilization of hydrophobic drugs by methoxy poly(ethylene glycol)-block-polycaprolactone diblock copolymer micelles: theoretical and experimental data and correlations." Journal of Pharmaceutical Sciences **97**(3): 1179-1190.

Letchford, K., Liggins, R., Wasan, K.M. and Burt, H. (2009). "In vitro human plasma distribution of nanoparticulate paclitaxel is dependent on the physicochemical properties of poly(ethylene glycol)-block-poly(caprolactone) nanoparticles." European Journal of Pharmaceutics and Biopharmaceutics **71**(2): 196-206.

Li, H.Y., Chen, Z., Ho, L.W., Chan, P.S., Li, Q., Leung, S.C., Zhang, B., Lai, K.L., Kwon, G.S., Choi, C.H.J. and Lee, W.Y.T. (2017a). "Oligonucleotide-conjugated nanoparticles for targeted drug delivery via scavenger receptors class A: An in vitro assessment for proof-of-concept." International Journal of Pharmaceutics **532**(1): 647-655.

Li, J., Qiao, Y. and Wu, Z. (2017b). "Nanosystem trends in drug delivery using quality-by-design concept." Journal of Controlled Release **256**(2017): 9-18.

Li, J., Wang, Y., Liang, R., An, X., Wang, K., Shen, G., Tu, Y., Zhu, J. and Tao, J. (2015a). "Recent advances in targeted nanoparticles drug delivery to melanoma." Nanomedicine **11**(3): 769-794.

Li, T.P., Wong, W.P., Chen, L.C., Su, C.Y., Chen, L.G., Liu, D.Z., Ho, H.O. and Sheu, M.T. (2017c). "Physical and Pharmacokinetic Characterizations of trans-Resveratrol (t-Rev) Encapsulated with Self-Assembling Lecithin-based Mixed Polymeric Micelles (saLMPMs)." Scientific Reports **7**(1): 10674.

Li, Y., Danmark, S., Edlund, U., Finne-Wistrand, A., He, X., Norgard, M., Blomen, E., Hultenby, K., Andersson, G. and Lindgren, U. (2011). "Resveratrol-conjugated poly-epsilon-caprolactone facilitates in vitro mineralization and in vivo bone regeneration." Acta Biomaterialia **7**(2): 751-758.

Li, Y.R., Li, S. and Lin, C.C. (2018). "Effect of resveratrol and pterostilbene on aging and longevity." Biofactors **44**(1): 69-82.

Li, Z., Jiang, H., Xu, C. and Gu, L. (2015b). "A review: Using nanoparticles to enhance absorption and bioavailability of phenolic phytochemicals." Food Hydrocolloids **43**(2015): 153-164.

Liang, L., Liu, X., Wang, Q., Cheng, S., Zhang, S. and Zhang, M. (2013). "Pharmacokinetics, tissue distribution and excretion study of resveratrol and its prodrug 3,5,4'-tri-O-acetylresveratrol in rats." Phytomedicine **20**(6): 558-563.

Life Technologies Pty Ltd. (2015). "Thawing & Incubating Human & Animal Liver Microsomes." Retrieved January 2015, from https://www.thermofisher.com/au/en/home/references/protocols/drug-discovery/adme-tox-protocols/microsomes-protocol.html.

Liu, K.-f., Li, C.-x., Dai, L., Liu, J., Wang, L.-y., Lei, J.-d. and Guo, L.-q. (2015). "Design, synthesis and in vivo antitumor efficacy of novel eight-arm-polyethylene glycol–pterostilbene prodrugs." RSC Advances **5**(64): 51592-51599.

Long, L.H., Hoi, A. and Halliwell, B. (2010). "Instability of, and generation of hydrogen peroxide by, phenolic compounds in cell culture media." Archives of Biochemistry and Biophysics **501**(1): 162-169.

Lou, B.S., Wu, P.S., Hou, C.W., Cheng, F.Y. and Chen, J.K. (2014). "Simultaneous quantification of trans-resveratrol and its sulfate and glucuronide metabolites in rat tissues by stable isotope-dilution UPLC-MS/MS analysis." Journal of Pharmaceutical and Biomedical Analysis **94**(2014): 99-105.

Lu, C. and Zhong, W. (2010). "Synthesis of Propargyl-Terminated Heterobifunctional Poly(ethylene glycol)." Polymers **2**(4): 407-417.

Lu, X., Xu, H., Sun, B., Zhu, Z., Zheng, D. and Li, X. (2013). "Enhanced neuroprotective effects of resveratrol delivered by nanoparticles on hydrogen peroxide-induced oxidative stress in rat cortical cell culture." Molecular Pharmaceutics **10**(5): 2045-2053.

Luo, H., Umebayashi, M., Doi, K., Morisaki, T., Shirasawa, S. and Tsunoda, T. (2016a). "Resveratrol Overcomes Cellular Resistance to Vemurafenib Through Dephosphorylation of AKT in BRAF-mutated Melanoma Cells." Anticancer Research **36**(2016): 3585-3590.

Luo, X., Chen, M., Zhang, Y., Chen, Z. and Li, X. (2016b). "Pharmacokinetics and antitumor efficacy of micelles assembled from multiarmed amphiphilic copolymers with drug conjugates in comparison with drug-encapsulated micelles." European Journal of Pharmaceutics and Biopharmaceutics **98**(2016): 9-19.

Ma, Z., Shi, X., Zhang, G., Guo, F., Shan, L. and Cai, J. (2016). "Metabolism and Metabolic Inhibition of Xanthotoxol in Human Liver Microsomes." Evidence-Based Complementary and Alternative Medicine **2016**(5416509): 1-8.

Madreiter-Sokolowski, C.T., Sokolowski, A.A. and Graier, W.F. (2017). "Dosis Facit Sanitatem-Concentration-Dependent Effects of Resveratrol on Mitochondria." Nutrients **9**(10): 1117.

Mahato, R. (2017). "Nanoemulsion as Targeted Drug Delivery System for Cancer Therapeutics." Journal of Pharmaceutical Sciences and Pharmacology **3**(2): 83-97.

Mamadou, G., Charrueau, C., Dairou, J., Limas Nzouzi, N., Eto, B. and Ponchel, G. (2017). "Increased intestinal permeation and modulation of presystemic metabolism of resveratrol formulated into self-emulsifying drug delivery systems." International Journal of Pharmaceutics **521**(1-2): 150-155.

Mandal, A., Bisht, R., Rupenthal, I.D. and Mitra, A.K. (2017). "Polymeric micelles for ocular drug delivery: From structural frameworks to recent preclinical studies." Journal of Controlled Release **248**(2017): 96-116.

Masood, F. (2016). "Polymeric nanoparticles for targeted drug delivery system for cancer therapy." Materials Science and Engineering C - Materials for Biological Applications **60**(2016): 569-578.

Mathieu, V., de Lassalle, E.M., Toelen, J., Mohr, T., Bellahcene, A., Van Goietsenoven, G., Verschuere, T., Bouzin, C., Debyser, Z., De Vleeschouwer, S., Van Gool, S., Poirier, F., Castronovo, V., Kiss, R. and Feron, O. (2012). "Galectin-1 in melanoma biology and related neo-angiogenesis processes." Journal of Investigative Dermatology **132**(9): 2245-2254.

Matsumura, Y., Hamaguchi, T., Ura, T., Muro, K., Yamada, Y., Shimada, Y., Shirao, K., Okusaka, T., Ueno, H., Ikeda, M. and Watanabe, N. (2004). "Phase I clinical trial and pharmacokinetic evaluation of NK911, a micelle-encapsulated doxorubicin." British Journal of Cancer **91**(10): 1775-1781.

Mattarei, A., Azzolini, M., Carraro, M., Sassi, N., Zoratti, M., Paradisi, C. and Biasutto, L. (2013). "Acetal derivatives as prodrugs of resveratrol." Molecular Pharmaceutics **10**(7): 2781-2792.

Mattarei, A., Azzolini, M., La Spina, M., Zoratti, M., Paradisi, C. and Biasutto, L. (2015a). "Amino Acid Carbamates As Prodrugs Of Resveratrol." Scientific Reports **5**(15216): 1-11.

Mattarei, A., Azzolini, M., Zoratti, M., Biasutto, L. and Paradisi, C. (2015b). "N-Monosubstituted Methoxy-oligo(ethylene glycol) Carbamate Ester Prodrugs of Resveratrol." Molecules **20**(9): 16085-16102.

Mattarei, A., Carraro, M., Azzolini, M., Paradisi, C., Zoratti, M. and Biasutto, L. (2014). "New water-soluble carbamate ester derivatives of resveratrol." Molecules **19**(10): 15900-15917.

Mei, K.C., Bai, J., Lorrio, S., Wang, J.T. and Al-Jamal, K.T. (2016). "Investigating the effect of tumor vascularization on magnetic targeting in vivo using retrospective design of experiment." Biomaterials **106**(2016): 276-285.

Menet, M.C., Baron, S., Taghi, M., Diestra, R., Dargere, D., Laprevote, O., Nivet-Antoine, V., Beaudeux, J.L., Bedarida, T. and Cottart, C.H. (2017). "Distribution of trans-resveratrol and its metabolites after acute or sustained administration in mouse heart, brain, and liver." Molecular Nutrition & Food Research **61**(8): 1600686.

Meng, J., Guo, F., Xu, H., Liang, W., Wang, C. and Yang, X.D. (2016). "Combination Therapy using Co-encapsulated Resveratrol and Paclitaxel in Liposomes for Drug Resistance Reversal in Breast Cancer Cells in vivo." Scientific Reports **6**(22390): 1-11.

Menicacci, B., Laurenzana, A., Chilla, A., Margheri, F., Peppicelli, S., Tanganelli, E., Fibbi, G., Giovannelli, L., Del Rosso, M. and Mocali, A. (2017). "Chronic Resveratrol Treatment Inhibits MRC5 Fibroblast SASP-Related Protumoral Effects on Melanoma Cells." Journal of Gerontology Series A Biological Sciences and Medical Science **72**(9): 1187-1195.

Mense, S.M., Hei, T.K., Ganju, R.K. and Bhat, H.K. (2008). "Phytoestrogens and breast cancer prevention: possible mechanisms of action." Environmental Health Perspectives **116**(4): 426-433.

Mittal, G., Sahana, D.K., Bhardwaj, V. and Ravi Kumar, M.N. (2007). "Estradiol loaded PLGA nanoparticles for oral administration: effect of polymer molecular weight and copolymer composition on release behavior in vitro and in vivo." Journal of Controlled Release **119**(1): 77-85.

Mohammed, S. and Harikumar, K.B. (2018). Role of Resveratrol in Chemosensitization of Cancer. Role of Nutraceuticals in Cancer Chemosensitization. Aggarwal, B.B. and Bharti, A.C. (Eds); Academic Press. **2**. **3:** 61-76.

Morris, V.L., Toseef, T., Nazumudeen, F.B., Rivoira, C., Spatafora, C., Tringali, C. and Rotenberg, S.A. (2015). "Anti-tumor properties of cis-resveratrol methylated analogs in metastatic mouse melanoma cells." Molecular and Cellular Biochemistry **402**(1-2): 83-91.

Mukherjee, S., Dudley, J.I. and Das, D.K. (2010). "Dose-dependency of resveratrol in providing health benefits." Dose Response **8**(4): 478-500.

Nassir, A.M., Shahzad, N., Ibrahim, I.A.A., Ahmad, I., Md, S. and Ain, M.R. (2018). "Resveratrol-loaded PLGA nanoparticles mediated programmed cell death in prostate cancer cells." Saudi Pharmaceutical Journal **26**(6): 876-885.

Natesan, S., Pandian, S., Ponnusamy, C., Palanichamy, R., Muthusamy, S. and Kandasamy, R. (2017). "Co-encapsulated resveratrol and quercetin in chitosan and peg modified chitosan nanoparticles: For efficient intra ocular pressure reduction." International Journal of Biological Macromolecules **104**(Pt B): 1837-1845.

Naves, L.B., Dhand, C., Venugopal, J.R., Rajamani, L., Ramakrishna, S. and Almeida, L. (2017). "Nanotechnology for the treatment of melanoma skin cancer." Progress in Biomaterials **6**(1-2): 13-26.

Ndiaye, M., Kumar, R. and Ahmad, N. (2011). "Resveratrol in cancer management: where are we and where we go from here?" Annals of the New York Academy of Sciences **1215**(2011): 144-149.

Neira-Velázquez, M.G., Rodríguez-Hernández, M.T., Hernández-Hernández, E. and Ruiz-Martínez, A.R. (2013). Polymer Molecular Weight Measurement. Handbook of Polymer Synthesis, Characterization, and Processing. Saldívar-Guerra, E. and Vivaldo-Lima, E. (Eds). USA; John Wiley & Sons, Inc. **17:** 12.

Neves, A.R., Lucio, M., Martins, S., Lima, J.L. and Reis, S. (2013). "Novel resveratrol nanodelivery systems based on lipid nanoparticles to enhance its oral bioavailability." International Journal of Nanomedicine **8**(2013): 177-187.

Ng, S.Y., Cardullo, N., Yeo, S.C., Spatafora, C., Tringali, C., Ong, P.S. and Lin, H.S. (2014). "Quantification of the resveratrol analogs trans-2,3-dimethoxy-stilbene and trans-3,4-dimethoxystilbene in rat plasma: application to pre-clinical pharmacokinetic studies." Molecules **19**(7): 9577-9590.

Ng, Y.-J., Benson, H.A.E., Brown, D.H. and Chen, Y. (2015). "Synthesis and Characterization of Novel Copolymeric Resveratrol Conjugates." Journal of Chemistry **2015**(245625): 1-6.

Nikhil, K., Sharan, S., Chakraborty, A. and Roy, P. (2014). "Pterostilbene-isothiocyanate conjugate suppresses growth of prostate cancer cells irrespective of androgen receptor status." PLoS One **9**(4): e93335.

Niles, R.M., Cook, C.P., Meadows, G.G., Fu, Y.-M., McLaughlin, J.L. and Rankin, G.O. (2006). "Resveratrol Is Rapidly Metabolized in Athymic (Nu/Nu) Mice and Does Not Inhibit Human Melanoma Xenograft Tumor Growth." Journal of Nutrition **136**(10): 2542-2546.

Niles, R.M., McFarland, M., Weimer, M.B., Redkar, A., Fu, Y.-M. and Meadows, G.G. (2003). "Resveratrol is a potent inducer of apoptosis in human melanoma cells." Cancer Letters **190**(2): 157-163.

Nogueira, D.R., Mitjans, M., Infante, M.R. and Vinardell, M.P. (2011). "Comparative sensitivity of tumor and non-tumor cell lines as a reliable approach for in vitro cytotoxicity screening of lysine-based surfactants with potential pharmaceutical applications." International Journal of Pharmaceutics **420**(1): 51-58.

Nour, V., Trandafir, I. and Muntean, C. (2012). "Ultraviolet Irradiation of Trans-Resveratrol and HPLC Determination of Trans-Resveratrol and Cis-Resveratrol in Romanian Red Wines." Journal of Chromatographic Science **50**(10): 920-927.

O'Neil, M.J. (2006). The Merck index: an encyclopedia of chemicals, drugs, and biologicals. Whitehouse Station, N.J.; Merck.

Oberlerchner, J.T., Rosenau, T. and Potthast, A. (2015). "Overview of Methods for the Direct Molar Mass Determination of Cellulose." Molecules **20**(6): 10313-10341.

OECD (1996). Determination of the Number-Average Molecular Weight and the Molecular Weight Distribution of Polymers using Gel Permeation Chromatography (Test No. 118). OECD Guidelines for the Testing of Chemicals, Section 1. Paris; OECD Publishing.

Ogston, K.N., Miller, I.D., Payne, S., Hutcheon, A.W., Sarkar, T.K., Smith, I., Schofield, A. and Heys, S.D. (2003). "A new histological grading system to assess response of breast cancers to primary chemotherapy: prognostic significance and survival." The Breast **12**(5): 320-327.

Osmond, G.W., Augustine, C.K., Zipfel, P.A., Padussis, J. and Tyler, D.S. (2012). "Enhancing melanoma treatment with resveratrol." Journal of Surgical Research **172**(1): 109-115.

Osmond, G.W., Masko, E.M., Tyler, D.S., Freedland, S.J. and Pizzo, S. (2013). "In vitro and in vivo evaluation of resveratrol and 3,5-dihydroxy-4'-acetoxy-trans-stilbene in the treatment of human prostate carcinoma and melanoma." Journal of Surgical Research **179**(1): e141-148.

Overwijk, W.W. and Restifo, N.P. (2001). "B16 as a mouse model for human melanoma." Current Protocols in Immunology **Chapter 20**: Unit 20.21.

Palacio, J., Orozco, V.H. and López, B.L. (2011). "Effect of the Molecular Weight on the Physicochemical Properties of Poly(lactic acid) Nanoparticles and on the Amount of Ovalbumin Adsorption." Journal of the Brazilian Chemical Society **22**(12): 2304-2311.

Pan, M.H., Wu, J.C., Ho, C.T. and Lai, C.S. (2018). "Antiobesity molecular mechanisms of action: Resveratrol and pterostilbene." Biofactors **44**(1): 50-60.

Pandita, D., Kumar, S., Poonia, N. and Lather, V. (2014). "Solid lipid nanoparticles enhance oral bioavailability of resveratrol, a natural polyphenol." Food Research International **62**: 1165-1174.

Pang, X., Jiang, Y., Xiao, Q., Leung, A.W., Hua, H. and Xu, C. (2016). "pH-responsive polymer-drug conjugates: Design and progress." Journal of Controlled Release **222**: 116-129.

Pangeni, R., Sahni, J.K., Ali, J., Sharma, S. and Baboota, S. (2014). "Resveratrol: review on therapeutic potential and recent advances in drug delivery." Expert Opinion on Drug Delivery **11**(8): 1285-1298.

Parhi, P., Mohanty, C. and Sahoo, S.K. (2012). "Nanotechnology-based combinational drug delivery: an emerging approach for cancer therapy." Drug Discovery Today **17**(17-18): 1044-1052.

Park, E.J. and Pezzuto, J.M. (2015). "The pharmacology of resveratrol in animals and humans." Biochimica et Biophysica Acta **1852**(6): 1071-1113.

Park, S., Seok, J.K., Kwak, J.Y., Choi, Y.H., Hong, S.S., Suh, H.J., Park, W. and Boo, Y.C. (2016a). "Anti-melanogenic effects of resveratryl triglycolate, a novel hybrid compound derived by esterification of resveratrol with glycolic acid." Archives of Dermatological Research **308**(5): 325-334.

Park, S.Y., Chae, S.Y., Park, J.O., Lee, K.J. and Park, G. (2016b). "Gold-conjugated resveratrol nanoparticles attenuate the invasion and MMP-9 and COX-2 expression in breast cancer cells." Oncology Reports **35**(6): 3248-3256.

Patel, A., Khanna, S., Xavier, G.K., Khanna, K. and Goel, B. (2017). "Polymeric Nano-Particles for Tumor Targeting - A Review." International Journal of Drug Development and Research **9**(1): 50-59.

Patel, K.R., Andreadi, C., Britton, R.G., Horner-Glister, E., Karmokar, A., Sale, S., Brown, V.A., Brenner, D.E., Singh, R., Steward, W.P., Gescher, A.J. and Brown, K. (2013). "Sulfate Metabolites Provide an Intracellular Pool for Resveratrol Generation and Induce Autophagy with Senescence." Science Translational Medicine **5**(205): 205ra133.

Patel, K.R., Brown, V.A., Jones, D.J., Britton, R.G., Hemingway, D., Miller, A.S., West, K.P., Booth, T.D., Perloff, M., Crowell, J.A., Brenner, D.E., Steward, W.P., Gescher, A.J. and Brown, K. (2010). "Clinical pharmacology of resveratrol and its metabolites in colorectal cancer patients." Cancer Research **70**(19): 7392-7399.

Patel, K.R., Scott, E., Brown, V.A., Gescher, A.J., Steward, W.P. and Brown, K. (2011). "Clinical trials of resveratrol." Annals of the New York Academy of Sciences **1215**: 161-169.

Paulsen, K. and Frasco, D. (2016) "Determination of polymer molecular weight and composition using picoSpin NMR spectroscopy (Application Note)." USA; Thermo Fisher Scientific.

Pavan, A.R., Silva, G.D., Jornada, D.H., Chiba, D.E., Fernandes, G.F., Man Chin, C. and Dos Santos, J.L. (2016). "Unraveling the Anticancer Effect of Curcumin and Resveratrol." Nutrients **8**(11): 628.

Peng, R.M., Lin, G.R., Ting, Y. and Hu, J.Y. (2018). "Oral delivery system enhanced the bioavailability of stilbenes: Resveratrol and pterostilbene." Biofactors **44**(1): 5-15.

Pinazo, A., Petrizelli, V., Bustelo, M., Pons, R., Vinardell, M.P., Mitjans, M., Manresa, A. and Perez, L. (2016). "New cationic vesicles prepared with double chain surfactants from arginine: Role of the hydrophobic group on the antimicrobial activity and cytotoxicity." Colloids and Surfaces B: Biointerfaces **141**(2016): 19-27.

Planas, J.M., Alfaras, I., Colom, H. and Juan, M.E. (2012). "The bioavailability and distribution of trans-resveratrol are constrained by ABC transporters." Archives of Biochemistry and Biophysics **527**(2): 67-73.

Pochapsky, T.C. and Pochapsky, S.S. (2013). Nuclear Magnetic Resonance Spectroscopy. Molecular Biophysics for the Life Sciences. Allewell, N., Narhi, L.O. and Rayment, I. (Eds). New York, NY; Springer New York**:** 113-173.

Popat, R., Plesner, T., Davies, F., Cook, G., Cook, M., Elliott, P., Jacobson, E., Gumbleton, T., Oakervee, H. and Cavenagh, J. (2013). "A phase 2 study of SRT501 (resveratrol) with bortezomib for patients with relapsed and or refractory multiple myeloma." British Journal of Haematology **160**(5): 714-717.

Poulsen, M.M., Vestergaard, P.F., Clasen, B.F., Radko, Y., Christensen, L.P., Stødkilde-Jørgensen, H., Møller, N., Jessen, N., Pedersen, S.B. and Jørgensen, J.O.L. (2013). "High-Dose Resveratrol Supplementation in Obese Men." Diabetes **62**(2013): 1186-1195.

Prabhu, V., Srivastava, P., Yadav, N., Amadori, M., Schneider, A., Seshadri, A., Pitarresi, J., Scott, R., Zhang, H., Koochekpour, S., Gogada, R. and Chandra, D. (2013). "Resveratrol depletes mitochondrial DNA and inhibition of autophagy enhances resveratrol-induced caspase activation." Mitochondrion **13**(5): 493-499.

Proskuryakov, S.Y. and Gabai, V.L. (2010). "Mechanisms of Tumor Cell Necrosis." Current Pharmaceutical Design **16**(1): 56-68.

Purushotham, G., Padma, Y., Nabiha, Y. and Venkata Raju, R.R. (2016). "In vitro evaluation of anti-proliferative, anti-inflammatory and pro-apoptotic activities of the methanolic extracts of Andrographis nallamalayana Ellis on A375 and B16F10 melanoma cell lines." 3 Biotech **6**(2): 212.

Qi, S.S., Sun, J.H., Yu, H.H. and Yu, S.Q. (2017). "Co-delivery nanoparticles of anti-cancer drugs for improving chemotherapy efficacy." Drug Delivery **24**(1): 1909-1926.

Qiao, Y., Sun, J., Xia, S., Tang, X., Shi, Y. and Le, G. (2014). "Effects of resveratrol on gut microbiota and fat storage in a mouse model with high-fat-induced obesity." Food Function **5**(6): 1241-1249.

Qiu, Z., Yu, J., Dai, Y., Yang, Y., Lu, X., Xu, J., Qin, Z., Huang, F. and Li, N. (2017). "A simple LC-MS/MS method facilitated by salting-out assisted liquid-liquid extraction to simultaneously determine trans-resveratrol and its glucuronide and sulfate conjugates in rat plasma and its application to pharmacokinetic assay." Biomedical Chromatography **31**(11): e4001.

Rachmawati, H., Rahma, A., Al Shaal, L., Muller, R.H. and Keck, C.M. (2016). "Destabilization Mechanism of Ionic Surfactant on Curcumin Nanocrystal against Electrolytes." Scientia Pharmaceutica **84**(4): 685-693.

Rafiei, P. and Haddadi, A. (2017). "Pharmacokinetic Consequences of PLGA Nanoparticles in Docetaxel Drug Delivery." Pharmaceutical Nanotechnology **5**(1): 3-23.

Rajagopal, S. and Ponnusamy, M. (2017). Channelopathies: Application of Natural Products Using Nanotechnology. Calcium Signaling: From Physiology to Diseases. Singapore; Springer Singapore**:** 73-86.

Ramalingam, P. and Ko, Y.T. (2016). "Validated LC-MS/MS method for simultaneous quantification of resveratrol levels in mouse plasma and brain and its application to pharmacokinetic and brain distribution studies." Journal of Pharmaceutical and Biomedical Analysis **119**(2016): 71-75.

Ranganathan, R., Madanmohan, S., Kesavan, A., Baskar, G., Krishnamoorthy, Y.R., Santosham, R., Ponraju, D., Rayala, S.K. and Venkatraman, G. (2012). "Nanomedicine: towards development of patient-friendly drug-delivery systems for oncological applications." International Journal of Nanomedicine **7**(2012): 1043-1060.

Ratz-Łyko, A. and Arct, J. (2018). "Resveratrol as an active ingredient for cosmetic and dermatological applications: a review." Journal of Cosmetic and Laser Therapy **2018 May 8**: 1-7.

Rauf, A., Imran, M., Butt, M.S., Nadeem, M., Peters, D.G. and Mubarak, M.S. (2016). "Resveratrol as an anti-cancer agent: A review." Critical Reviews in Food Science and Nutrition **58**(9): 1428-1447.

Rigon, R.B., Fachinetti, N., Severino, P., Santana, M.H. and Chorilli, M. (2016). "Skin Delivery and in Vitro Biological Evaluation of Trans-Resveratrol-Loaded Solid Lipid Nanoparticles for Skin Disorder Therapies." Molecules **21**(1): E116.

Rigon, R.B., Oyafuso, M.H., Fujimura, A.T., Goncalez, M.L., do Prado, A.H., Gremiao, M.P. and Chorilli, M. (2015). "Nanotechnology-Based Drug Delivery Systems for Melanoma Antitumoral Therapy: A Review." BioMed Research International **2015**(841817): 1-22.

Riley, T., Stonik, S., Heald, C.R., Xiong, C.D., Garnett, M.C., Illum, L., Davis, S.S., Purkiss, S.C., Barlow, R.J. and Gellert, P.R. (2001). "Physicochemical Evaluation of Nanoparticles Assembled from Poly(lactic acid)-Poly(ethylene glycol) (PLA-PEG) Block Copolymers as Drug Delivery Vehicles." Langmuir **17**(11): 3168-3174.

Riss, T.L., Moravec, R.A., Niles, A.L., Duellman, S., Benink, H.A., Worzella, T.J. and Minor, L. (2013). Cell Viability Assays. Assay Guidance Manual [Internet]. Sittampalam, G.S., Coussens, N.P., Brimacombe, K. et al. (Eds). Bethesda, MD; Eli Lilly & Company and the National Center for Advancing Translational Sciences. from https://www.ncbi.nlm.nih.gov/books/NBK144065/.

Roberts, J.D. (1961). "Nuclear magnetic resonance spectroscopy." Journal of Chemical Education **38**(11): 581.

Robinson, K., Mock, C. and Liang, D. (2015). "Pre-formulation studies of resveratrol." Drug Development and Industrial Pharmaceutics **41**(9): 1464-1469.

Rock, K.L. and Kono, H. (2008). "The inflammatory response to cell death." Annual Review of Pathology: Mechanisms of Disease **3**: 99-126.

Romio, M., Morgese, G., Trachsel, L., Babity, S., Paradisi, C., Brambilla, D. and Benetti, E.M. (2018). "Poly(2-oxazoline)-Pterostilbene Block Copolymer Nanoparticles for Dual-Anticancer Drug Delivery." Biomacromolecules **19**(1): 103-111.

Rotches-Ribalta, M., Andres-Lacueva, C., Estruch, R., Escribano, E. and Urpi-Sarda, M. (2012). "Pharmacokinetics of resveratrol metabolic profile in healthy humans after moderate consumption of red wine and grape extract tablets." Pharmacological Research **66**(5): 375-382.

Ruivo, J., Francisco, C., Oliveira, R. and Figueiras, A. (2015). "The main potentialities of resveratrol for drug delivery systems." Brazilian Journal of Pharmaceutical Sciences **51**(3): 499-513.

Ryu, J.H., Seok, J.K., An, S.M., Baek, J.H., Koh, J.S. and Boo, Y.C. (2015). "A study of the human skin-whitening effects of resveratryl triacetate." Archives of Dermatological Research **307**(3): 239-247.

Safavy, A., Georg, G.I., Velde, D.V., Raisch, K.P., Safavy, K., Carpenter, M., Wang, W., Bonner, J.A., Khazaeli, M.B. and Buchsbaum, D.J. (2004). "Site-Specifically Traced Drug Release and Biodistribution of a Paclitaxel−Antibody Conjugate toward Improvement of the Linker Structure." Bioconjugate Chemistry **15**(6): 1264-1274.

Sagirli, O. and Ersoy, L. (2004). "An HPLC method for the determination of lisinopril in human plasma and urine with fluorescence detection." Journal of Chromatography B: Analytical Technologies in the Biomedical and Life Sciences **809**(1): 159-165.

Sakai, C., Iwano, S., Yamazaki, Y., Ando, A., Nakane, F., Kouno, M., Yamazaki, H. and Miyamoto, Y. (2015). "Species Differences in the Pharmacokinetic Parameters of Cytochrome P450 Probe Substrates between Experimental Animals, such as Mice, Rats, Dogs, Monkeys, and Microminipigs, and Humans." Journal of Drug Metabolism & Toxicology **5**(6): 173.

San Hipolito-Luengo, A., Alcaide, A., Ramos-Gonzalez, M., Cercas, E., Vallejo, S., Romero, A., Talero, E., Sanchez-Ferrer, C.F., Motilva, V. and Peiro, C. (2017). "Dual Effects of Resveratrol on Cell Death and Proliferation of Colon Cancer Cells." Nutrition and Cancer **69**(7): 1019-1027.

Sanfins, E., Augustsson, C., Dahlback, B., Linse, S. and Cedervall, T. (2014). "Size-dependent effects of nanoparticles on enzymes in the blood coagulation cascade." Nano Letters **14**(8): 4736-4744.

Sangsen, Y., Wiwattanawongsa, K., Likhitwitayawuid, K., Sritularak, B., Graidist, P. and Wiwattanapatapee, R. (2016). "Influence of surfactants in self-microemulsifying formulations on enhancing oral bioavailability of oxyresveratrol: Studies in Caco-2 cells and in vivo." International Journal of Pharmaceutics **498**(1-2): 294-303.

Sanna, V., Siddiqui, I.A., Sechi, M. and Mukhtar, H. (2013). "Resveratrol-loaded nanoparticles based on poly(epsilon-caprolactone) and poly(D,L-lactic-co-glycolic acid)-poly(ethylene glycol) blend for prostate cancer treatment." Molecular Pharmaceutics **10**(10): 3871-3881.

Saunier, E., Antonio, S., Regazzetti, A., Auzeil, N., Laprevote, O., Shay, J.W., Coumoul, X., Barouki, R., Benelli, C., Huc, L. and Bortoli, S. (2017). "Resveratrol reverses the Warburg effect by targeting the pyruvate dehydrogenase complex in colon cancer cells." Scientific Reports **7**(1): 6945.

Saw, P.E., Park, J., Lee, E., Ahn, S., Lee, J., Kim, H., Kim, J., Choi, M., Farokhzad, O.C. and Jon, S. (2015). "Effect of PEG pairing on the efficiency of cancer-targeting liposomes." Theranostics **5**(7): 746-754.

Scarlatti, F., Maffei, R., Beau, I., Codogno, P. and Ghidoni, R. (2008). "Role of non-canonical Beclin 1-independent autophagy in cell death induced by resveratrol in human breast cancer cells." Cell Death & Differentiation **15**(8): 1318-1329.

Schaafsma, E. and Hsieh, T.c. (2016). "Anticancer Activities of Resveratrol in Colorectal Cancer." Biology and Medicine **8**(5): 317.

Schellinger, A.P. and Carr, P.W. (2006). "Isocratic and gradient elution chromatography: a comparison in terms of speed, retention reproducibility and quantitation." Journal of Chromatography A **1109**(2): 253-266.

Scherzberg, M.C., Kiehl, A., Zivkovic, A., Stark, H., Stein, J., Furst, R., Steinhilber, D. and Ulrich-Ruckert, S. (2015). "Structural modification of resveratrol leads to increased anti-tumor activity, but causes profound changes in the mode of action." Toxicology and Applied Pharmacology **287**(1): 67-76.

Scognamiglio, I., De Stefano, D., Campani, V., Mayol, L., Carnuccio, R., Fabbrocini, G., Ayala, F., La Rotonda, M.I. and De Rosa, G. (2013). "Nanocarriers for topical administration of resveratrol: a comparative study." International Journal of Pharmaceutics **440**(2): 179-187.

Scott, E., Steward, W.P., Gescher, A.J. and Brown, K. (2012). "Resveratrol in human cancer chemoprevention--choosing the 'right' dose." Molecular Nutrition & Food Research **56**(1): 7-13.

Sessa, M., Balestrieri, M.L., Ferrari, G., Servillo, L., Castaldo, D., D'Onofrio, N., Donsi, F. and Tsao, R. (2014). "Bioavailability of encapsulated resveratrol into nanoemulsion-based delivery systems." Food Chemistry **147**(2014): 42-50.

Sessa, M., Tsao, R., Liu, R., Ferrari, G. and Donsi, F. (2011). "Evaluation of the stability and antioxidant activity of nanoencapsulated resveratrol during in vitro digestion." Journal of Agricultural and Food Chemistry **59**(23): 12352-12360.

Shakibaei, M., Mobasheri, A. and Buhrmann, C. (2011). "Curcumin synergizes with resveratrol to stimulate the MAPK signaling pathway in human articular chondrocytes in vitro." Genes & Nutrition **6**(2): 171-179.

Shalgunov, V., Zaytseva-Zotova, D., Zintchenko, A., Levada, T., Shilov, Y., Andreyev, D., Dzhumashev, D., Metelkin, E., Urusova, A., Demin, O., McDonnell, K., Troiano, G., Zale, S. and Safarovsmall a, C.E. (2017). "Comprehensive study of the drug delivery properties of poly(l-lactide)-poly(ethylene glycol) nanoparticles in rats and tumor-bearing mice." Journal of Controlled Release **261**(2017): 31-42.

Shanmugam, M.K., Warrier, S., Kumar, A.P., Sethi, G. and Arfuso, F. (2017). "Potential Role of Natural Compounds as Anti-Angiogenic Agents in Cancer." Current Vascular Pharmacology **15**(6): 503-519.

Sharma, N., Madan, P. and Lin, S. (2016). "Effect of process and formulation variables on the preparation of parenteral paclitaxel-loaded biodegradable polymeric nanoparticles: A co-surfactant study." Asian Journal of Pharmaceutical Sciences **11**(3): 404-416.

Shen, H., Hu, X., Szymusiak, M., Wang, Z.J. and Liu, Y. (2013). "Orally administered nanocurcumin to attenuate morphine tolerance: comparison between negatively charged PLGA and partially and fully PEGylated nanoparticles." Molecular Pharmaceutics **10**(12): 4546-4551.

Shen, L., Zhang, Z., Wang, T., Yang, X., Huang, R. and Quan, D. (2017). "Reversed lipid-based nanoparticles dispersed in oil for malignant tumor treatment via intratumoral injection." Drug Delivery **24**(1): 857-866.

Shi, J., Philip, W.K., Richard, W. and Omid, C.F. (2016). "Cancer nanomedicine: progress, challenges and opportunities." Nature Reviews Cancer **17**(1): 20-37.

Shuai, X., Ai, H., Nasongkla, N., Kim, S. and Gao, J. (2004a). "Micellar carriers based on block copolymers of poly(epsilon-caprolactone) and poly(ethylene glycol) for doxorubicin delivery." Journal of Controlled Release **98**(3): 415-426.

Shuai, X., Merdan, T., Schaper, A.K., Xi, F. and Kissel, T. (2004b). "Core-Cross-Linked Polymeric Micelles as Paclitaxel Carriers." Bioconjugate Chemistry **15**(3): 441-448.

Siddalingappa, B., Benson, H.A., Brown, D.H., Batty, K.T. and Chen, Y. (2015). "Stabilization of resveratrol in blood circulation by conjugation to mPEG and mPEG-PLA polymers: investigation of conjugate linker and polymer composition on stability, metabolism, antioxidant activity and pharmacokinetic profile." PLoS One **10**(3): e0118824.

Siddiqui, I.A., Sanna, V., Ahmad, N., Sechi, M. and Mukhtar, H. (2015). "Resveratrol nanoformulation for cancer prevention and therapy." Annals of the New York Academy of Sciences **1348**(1): 20-31.

Silva, C.G., Monteiro, J., Marques, R.R., Silva, A.M., Martinez, C., Canle, M. and Faria, J.L. (2013). "Photochemical and photocatalytic degradation of trans-resveratrol." Photochemical and Photobiological Sciences **12**(4): 638-644.

Sim, D.Y., Sohng, J.K. and Jung, H.J. (2016). "Anticancer activity of 7,8-dihydroxyflavone in melanoma cells via downregulation of alpha-MSH/cAMP/MITF pathway." Oncology Reports **36**(1): 528-534.

Singh, C.K., Ndiaye, M.A. and Ahmad, N. (2015). "Resveratrol and cancer: Challenges for clinical translation." Biochimica et Biophysica Acta **1852**(6): 1178-1185.

Singh, G. and Pai, R.S. (2014a). "In-vitro/in-vivo characterization of trans-resveratrol-loaded nanoparticulate drug delivery system for oral administration." Journal of Pharmaceutics and Pharmacology **66**(8): 1062-1076.

Singh, G. and Pai, R.S. (2014b). "A Rapid Reversed-Phase HPLC Method for Analysis ofTrans-Resveratrol in PLGA Nanoparticulate Formulation." ISRN Chromatography **2014**(248635): 1-6.

Singh, G. and Pai, R.S. (2014c). "Recent advances of resveratrol in nanostructured based delivery systems and in the management of HIV/AIDS." Journal of Controlled Release **194**(2014): 178-188.

Singh, G., Pai, R.S. and Pandit, V. (2013). "In vivo pharmacokinetic applicability of a simple and validated HPLC method for orally administered trans-resveratrol loaded polymeric nanoparticles to rats." Journal of Pharmaceutical Investigation **44**(2): 69-78.

Singh, S.K., Lillard, J.W., Jr. and Singh, R. (2018). "Reversal of drug resistance by planetary ball milled (PBM) nanoparticle loaded with resveratrol and docetaxel in prostate cancer." Cancer Letters **427**(2018): 49-62.

Siu, F.Y., Ye, S., Lin, H. and Li, S. (2018). "Galactosylated PLGA nanoparticles for the oral delivery of resveratrol: enhanced bioavailability and in vitro anti-inflammatory activity." International Journal of Nanomedicine **13**: 4133-4144.

Smoliga, J.M. and Blanchard, O. (2014). "Enhancing the delivery of resveratrol in humans: if low bioavailability is the problem, what is the solution?" Molecules **19**(11): 17154-17172.

Sobczak, M. (2010). "Synthesis and characterization of polyester conjugates of ciprofloxacin." European Journal of Medicinal Chemistry **45**(9): 3844-3849.

Sofia, M.J. (2013). "Nucleotide prodrugs for the treatment of HCV infection." Advances in Pharmacology **67**(2013): 39-73.

Song, H., Li, W., Qi, R., Yan, L., Jing, X., Zheng, M. and Xiao, H. (2015). "Delivering a photosensitive transplatin prodrug to overcome cisplatin drug resistance." Chemical Communications **51**(57): 11493-11495.

Soo, E., Thakur, S., Qu, Z., Jambhrunkar, S., Parekh, H.S. and Popat, A. (2016). "Enhancing delivery and cytotoxicity of resveratrol through a dual nanoencapsulation approach." Journal of Colloid and Interface Science **462**(2016): 368-374.

Stakleff, K.S., Sloan, T., Blanco, D., Marcanthony, S., Booth, T.D. and Bishayee, A. (2012). "Resveratrol Exerts Differential Effects in Vitro and in Vivo against Ovarian Cancer Cells." Asian Pacific Journal of Cancer Prevention **13**(4): 1333-1340.

Stern, T., Kaner, I., Laser Zer, N., Shoval, H., Dror, D., Manevitch, Z., Chai, L., Brill-Karniely, Y. and Benny, O. (2017). "Rigidity of polymer micelles affects interactions with tumor cells." Journal of Controlled Release **257**(2017): 40-50.

Su, D., Cheng, Y., Liu, M., Liu, D., Cui, H., Zhang, B., Zhou, S., Yang, T. and Mei, Q. (2013). "Comparision of piceid and resveratrol in antioxidation and antiproliferation activities in vitro." PLoS One **8**(1): e54505.

Subramanian, A.P., Jaganathan, S.K., Manikandan, A., Pandiaraj, K.N., N, G. and Supriyanto, E. (2016). "Recent trends in nano-based drug delivery systems for efficient delivery of phytochemicals in chemotherapy." RSC Advances **6**(54): 48294-48314.

Suktham, K., Koobkokkruad, T., Wutikhun, T. and Surassmo, S. (2018). "Efficiency of resveratrol-loaded sericin nanoparticles: Promising bionanocarriers for drug delivery." International Journal of Pharmaceutics **537**(1): 48-56.

Summerlin, N., Soo, E., Thakur, S., Qu, Z., Jambhrunkar, S. and Popat, A. (2015). "Resveratrol nanoformulations: challenges and opportunities." International Journal of Pharmaceutics **479**(2): 282-290.

Sun, Y., Qi, Y., Mu, Z. and Wang, K. (2015). "Quantitative determination of resveratrol in Polygonum cuspidatum and its anti-proliferative effect on melanoma A375 cells." Biomedical Research **26**(4): 750-754.

Swartz, M. and Krull, I.S. (2012a). Method Validation Basics. Handbook of Analytical Validation. Swartz, M. and Krull, I.S. (Eds). Boca Raton; CRC Press. **4:** 61-80.

Swartz, M. and Krull, I.S. (2012b). Validation by Type of Method. Handbook of Analytical Validation. Swartz, M. and Krull, I.S. (Eds). Boca Raton; CRC Press. **7:** 119-164.

Syed, D.N. and Mukhtar, H. (2011). "Botanicals for the prevention and treatment of cutaneous melanoma." Pigment Cell and Melanoma Research **24**(4): 688-702.

Szekeres, T., Fritzer-Szekeres, M., Saiko, P. and Jager, W. (2010). "Resveratrol and resveratrol analogues-structure-activity relationship." Pharmaceutical Research **27**(6): 1042-1048.

Tang, L., Yang, X., Yin, Q., Cai, K., Wang, H., Chaudhury, I., Yao, C., Zhou, Q., Kwon, M., Hartman, J.A., Dobrucki, I.T., Dobrucki, L.W., Borst, L.B., Lezmi, S., Helferich, W.G., Ferguson, A.L., Fan, T.M. and Cheng, J. (2014). "Investigating the optimal size of anticancer nanomedicine." Proceedings of the National Academy of Sciences **111**(43): 15344-15349.

Temple, S.V. and Poniatowski, B. (2005). Nursing implications of antineoplastic therapy. Core Curriculum for Oncology Nursing. Itano, J. and Taoka, K. (Eds). Philadelphia; Elsevier Saunders.

Teng, Z., Yuan, C., Zhang, F., Huan, M., Cao, W., Li, K., Yang, J., Cao, D., Zhou, S. and Mei, Q. (2012). "Intestinal absorption and first-pass metabolism of polyphenol compounds in rat and their transport dynamics in Caco-2 cells." PLoS One **7**(1): e29647.

Teskac, K. and Kristl, J. (2010). "The evidence for solid lipid nanoparticles mediated cell uptake of resveratrol." International Journal of Pharmaceutics **390**(1): 61-69.

Tillement, J.-P. and Tremblay, D. (2007). Clinical Pharmacokinetic Criteria for Drug Research. Comprehensive Medicinal Chemistry II. Testa, B. and Van de Waterbeemd, H. (Eds); Elsevier Ltd. **5:** 11-30.

Timm, M., Saaby, L., Moesby, L. and Hansen, E.W. (2013). "Considerations regarding use of solvents in in vitro cell based assays." Cytotechnology **65**(5): 887-894.

Torchilin, V.P. (2014). "Multifunctional, stimuli-sensitive nanoparticulate systems for drug delivery." Nature Reviews Drug Discovery **13**(11): 813-827.

Torres, V., Hamdi, M., Millán de la Blanca, M., Urrego, R., Echeverri, J., López-Herrera, A., Rizos, D., Gutiérrez-Adán, A. and Sánchez-Calabuig, M. (2018). "Resveratrol–cyclodextrin complex affects the expression of genes associated with lipid metabolism in bovine in vitro produced embryos." Reproduction in Domestic Animals **53**(4): 850-858.

Tou, J.C. (2015). "Resveratrol supplementation affects bone acquisition and osteoporosis: Pre-clinical evidence toward translational diet therapy." Biochimica et Biophysica Acta **1852**(6): 1186-1194.

Trela, B.C. and Waterhouse, A.L. (1996). "Resveratrol: Isomeric Molar Absorptivities and Stability." Journal of Agricultural and Food Chemistry **44**(5): 1253-1257.

Tsai, H.Y., Ho, C.T. and Chen, Y.K. (2017). "Biological actions and molecular effects of resveratrol, pterostilbene, and 3'-hydroxypterostilbene." Journal of Food and Drug Analysis **25**(1): 134-147.

Umoren, S.A. and Solomon, M.M. (2016). Polymer Characterization: Polymer Molecular Weight Determination. Polymer science: research advances, practical applications and educational aspects. Méndez-Vilas, A. and Solano, A. (Eds). Spain; Formatex Research Center.

US FDA (2013). Guidance for Industry: Bioanalytical Method Validation. Center for Drug Evaluation and Research. USA; US FDA Retrieved February 2018.

Vang, O., Ahmad, N., Baile, C.A., Baur, J.A., Brown, K., Csiszar, A., Das, D.K., Delmas, D., Gottfried, C., Lin, H.Y., Ma, Q.Y., Mukhopadhyay, P., Nalini, N., Pezzuto, J.M., Richard, T., Shukla, Y., Surh, Y.J., Szekeres, T., Szkudelski, T., Walle, T. and Wu, J.M. (2011). "What is new for an old molecule? Systematic review and recommendations on the use of resveratrol." PLoS One **6**(6): e19881.

Vassiliou, A.A., Papadimitriou, S.A., Bikiaris, D.N., Mattheolabakis, G. and Avgoustakis, K. (2010). "Facile synthesis of polyester-PEG triblock copolymers and preparation of amphiphilic nanoparticles as drug carriers." Journal of Controlled Release **148**(3): 388-395.

Vendrely, V., Peuchant, E., Buscail, E., Moranvillier, I., Rousseau, B., Bedel, A., Brillac, A., de Verneuil, H., Moreau-Gaudry, F. and Dabernat, S. (2017). "Resveratrol and capsaicin used together as food complements reduce tumor growth and rescue full efficiency of low dose gemcitabine in a pancreatic cancer model." Cancer Letters **390**: 91-102.

Vijayakumar, M.R., Vajanthri, K.Y., Balavigneswaran, C.K., Mahto, S.K., Mishra, N., Muthu, M.S. and Singh, S. (2016). "Pharmacokinetics, biodistribution, in vitro cytotoxicity and biocompatibility of Vitamin E TPGS coated trans resveratrol liposomes." Colloids and Surfaces B: Biointerfaces **145**(2016): 479-491.

Walle, T. (2011). "Bioavailability of resveratrol." Annals of the New York Academy of Sciences **1215**(2011): 9-15.

Walle, T., Hsieh, F., DeLegge, M.H., Oatis, J.E., Jr. and Walle, U.K. (2004). "High absorption but very low bioavailability of oral resveratrol in humans." Drug Metabolism and Disposition **32**(12): 1377-1382.

Wan, C.P., Letchford, K., Jackson, J.K. and Burt, H.M. (2013). "The combined use of paclitaxel-loaded nanoparticles with a low-molecular-weight copolymer inhibitor of P-glycoprotein to overcome drug resistance." International Journal of Nanomedicine **8**: 379-391.

Wang, C., Ma, C., Wu, Z., Liang, H., Yan, P., Song, J., Ma, N. and Zhao, Q. (2015a). "Enhanced Bioavailability and Anticancer Effect of Curcumin-Loaded Electrospun Nanofiber: In Vitro and In Vivo Study." Nanoscale Research Letters **10**(1): 439.

Wang, D.-G., Liu, W.-Y. and Chen, G.-T. (2013a). "A simple method for the isolation and purification of resveratrol from Polygonum cuspidatum." Journal of Pharmaceutical Analysis **3**(4): 241-247.

Wang, L., Liu, Y., Zhao, J., Li, C., Zhou, Y., Du, J. and Wang, Y. (2017). "In vitro and in vivo evaluation of targeting tumor with folate-based amphiphilic multifunctional stabilizer for resveratrol nanosuspensions." Colloids and Surfaces B: Biointerfaces **160**(2017): 462-472.

Wang, P. and Sang, S. (2018). "Metabolism and pharmacokinetics of resveratrol and pterostilbene." Biofactors **44**(1): 16-25.

Wang, S., Chen, R., Morott, J., Repka, M.A., Wang, Y. and Chen, M. (2015b). "mPEG-b-PCL/TPGS mixed micelles for delivery of resveratrol in overcoming resistant breast cancer." Expert Opinion on Drug Delivery **12**(3): 361-373.

Wang, S., Su, R., Nie, S., Sun, M., Zhang, J., Wu, D. and Moustaid-Moussa, N. (2014). "Application of nanotechnology in improving bioavailability and bioactivity of diet-derived phytochemicals." The Journal of Nutritional Biochemistry **25**(4): 363-376.

Wang, W., Zhang, L., Le, Y., Chen, J.F., Wang, J. and Yun, J. (2016). "Synergistic effect of PEGylated resveratrol on delivery of anticancer drugs." International Journal of Pharmaceutics **498**(1-2): 134-141.

Wang, Y., Zheng, Y., Zhang, L., Wang, Q. and Zhang, D. (2013b). "Stability of nanosuspensions in drug delivery." Journal of Controlled Release **172**(3): 1126-1141.

Washington, K.E., Kularatne, R.N., Biewer, M.C. and Stefan, M.C. (2018). "Combination Loading of Doxorubicin and Resveratrol in Polymeric Micelles for Increased Loading Efficiency and Efficacy." ACS Biomaterials Science & Engineering **4**(3): 997-1004.

Wei, A., Mehtala, J.G. and Patri, A.K. (2012). "Challenges and opportunities in the advancement of nanomedicines." Journal of Controlled Release **164**(2): 236-246.

Weiskirchen, S. and Weiskirchen, R. (2016). "Resveratrol: How Much Wine Do You Have to Drink to Stay Healthy?" Advances in Nutrition **7**(4): 706-718.

Whitehouse, S., Chen, P.L., Greenshields, A.L., Nightingale, M., Hoskin, D.W. and Bedard, K. (2016). "Resveratrol, piperine and apigenin differ in their NADPH-oxidase inhibitory and reactive oxygen species-scavenging properties." Phytomedicine **23**(12): 1494-1503.

Wieczorek, S., Schwaar, T., Senge, M.O. and Borner, H.G. (2015). "Specific Drug Formulation Additives: Revealing the Impact of Architecture and Block Length Ratio." Biomacromolecules **16**(10): 3308-3312.

Wiegand, S. and Köhler, W. (2008). Determination of Molecular Weights and Their Distributions. Molecular Characterization and Analysis of Polymers. Chalmers, J.M. and Meier, R.J. (Eds). UK; Elsevier B.V. **53**. **6:** 205-251.

Wong, M., Hollinger, J., Kozycz, L.M., McCormick, T.M., Lu, Y., Burns, D.C. and Seferos, D.S. (2012). "An Apparent Size-Exclusion Quantification Limit Reveals a Molecular Weight Limit in the Synthesis of Externally Initiated Polythiophenes." ACS Macro Letters **1**(11): 1266-1269.

Worzakowska, M. (2014). "Thermal properties of citronellyl diesters." Journal of Thermal Analysis and Calorimetry **118**(1): 299-309.

Wu, F. and Cui, L. (2017). "Resveratrol suppresses melanoma by inhibiting NF-kappaB/miR-221 and inducing TFG expression." Archives in Dermatological Research **309**(10): 823-831.

Xiao, K., Zhang, H.-J., Xuan, L.-J., Zhang, J., Xu, Y.-M. and Bai, D.-L. (2008). Stilbenoids: Chemistry and bioactivities. Studies in Natural Products Chemistry. Atta-ur-Rahman (Eds). UK; Elsevier. **34:** 453-646.

Xie, J., Yang, Z., Zhou, C., Zhu, J., Lee, R.J. and Teng, L. (2016). "Nanotechnology for the delivery of phytochemicals in cancer therapy." Biotechnology Advances **34**(4): 343-353.

Xu, H., Yao, Q., Cai, C., Gou, J., Zhang, Y., Zhong, H. and Tang, X. (2015). "Amphiphilic poly(amino acid) based micelles applied to drug delivery: the in vitro and in vivo challenges and the corresponding potential strategies." Journal of Controlled Release **199**(2015): 84-97.

Xu, Q., Crossley, A. and Czernuszka, J. (2009). "Preparation and characterization of negatively charged poly(lactic-co-glycolic acid) microspheres." Journal of Pharmaceutical Sciences **98**(7): 2377-2389.

Xu, R., Fisher, M. and Juliano, R.L. (2011). "Targeted albumin-based nanoparticles for delivery of amphipathic drugs." Bioconjugate Chemistry **22**(5): 870-878.

Yamaguchi, S., Tanha, M., Hult, A., Okuda, T., Ohara, H. and Kobayashi, S. (2013). "Green polymer chemistry: lipase-catalyzed synthesis of bio-based reactive polyesters employing itaconic anhydride as a renewable monomer." Polymer Journal **46**(1): 2-13.

Yang, C., Attia, A.B., Tan, J.P., Ke, X., Gao, S., Hedrick, J.L. and Yang, Y.Y. (2012a). "The role of non-covalent interactions in anticancer drug loading and kinetic stability of polymeric micelles." Biomaterials **33**(10): 2971-2979.

Yang, D., Liu, X., Jiang, X., Liu, Y., Ying, W., Wang, H., Bai, H., Taylor, W.D., Wang, Y., Clamme, J.P., Co, E., Chivukula, P., Tsang, K.Y., Jin, Y. and Yu, L. (2012b). "Effect of molecular weight of PGG-paclitaxel conjugates on in vitro and in vivo efficacy." Journal of Controlled Release **161**(1): 124-131.

Yang, F.F., Zhou, J., Hu, X., Cong, Z.Q., Liu, C.Y., Pan, R.L., Chang, Q., Liu, X.M. and Liao, Y.H. (2018a). "Improving oral bioavailability of resveratrol by a UDP-glucuronosyltransferase inhibitory excipient-based self-microemulsion." European Journal of Pharmaceutical Sciences **114**(2018): 303-309.

Yang, J., Hou, Y., Ji, G., Song, Z., Liu, Y., Dai, G., Zhang, Y. and Chen, J. (2014). "Targeted delivery of the RGD-labeled biodegradable polymersomes loaded with the hydrophilic drug oxymatrine on cultured hepatic stellate cells and liver fibrosis in rats." European Journal of Pharmacuetical Sciences **52**(2014): 180-190.

Yang, N.-C., Lee, C.-H. and Song, T.-Y. (2010). "Evaluation of Resveratrol Oxidation in Vitro and the Crucial Role of Bicarbonate Ions." Bioscience, Biotechnology and Biochemistry **74**(1): 63-68.

Yang, R., Mondal, G., Ness, R.A., Arnst, K., Mundra, V., Miller, D.D., Li, W. and Mahato, R.I. (2017). "Polymer conjugate of a microtubule destabilizer inhibits lung metastatic melanoma." Journal of Controlled Release **249**(2017): 32-41.

Yang, R., Zhang, S., Kong, D., Gao, X., Zhao, Y. and Wang, Z. (2012c). "Biodegradable Polymer-Curcumin Conjugate Micelles Enhance the Loading and Delivery of Low-Potency Curcumin." Pharmaceutical Research **29**(12): 3512–3525.

Yang, X., Shi, X., D'Arcy, R., Tirelli, N. and Zhai, G. (2018b). "Amphiphilic polysaccharides as building blocks for self-assembled nanosystems: molecular design and application in cancer and inflammatory diseases." Journal of Controlled Release **272**(2018): 114-144.

Yang, X.Z., Dou, S., Sun, T.M., Mao, C.Q., Wang, H.X. and Wang, J. (2011). "Systemic delivery of siRNA with cationic lipid assisted PEG-PLA nanoparticles for cancer therapy." Journal of Controlled Release **156**(2): 203-211.

Ye, F., Zhao, Y., El-Sayed, R., Muhammed, M. and Hassan, M. (2018). "Advances in nanotechnology for cancer biomarkers." Nano Today **18**(2018): 103-123.

Ye, W.L., Du, J.B., Zhang, B.L., Na, R., Song, Y.F., Mei, Q.B., Zhao, M.G. and Zhou, S.Y. (2014). "Cellular uptake and antitumor activity of DOX-hyd-PEG-FA nanoparticles." PLoS One **9**(5): e97358.

Yin, H., Si, J., Xu, H., Dong, J., Zheng, D., Lu, X. and Li, X. (2014). "Resveratrol-Loaded Nanoparticles Reduce Oxidative Stress Induced by Radiation or Amyloid- in Transgenic Caenorhabditis elegans." Journal of Biomedical Nanotechnology **10**(8): 1536-1544.

Yu, H., Chen, J., Liu, S., Lu, Q., He, J., Zhou, Z. and Hu, Y. (2015). "Enzyme sensitive, surface engineered nanoparticles for enhanced delivery of camptothecin." Journal of Controlled Release **216**(2015): 111-120.

Yu, L., Wang, S., Kogure, Y., Yamamoto, S., Noguchi, K. and Dai, Y. (2013). "Modulation of TRP channels by resveratrol and other stilbenoids." Molecular Pain **9**(1): 3.

Yuan, J.-D., ZhuGe, D.-L., Tong, M.-Q., Lin, M.-T., Xu, X.-F., Tang, X., Zhao, Y.-Z. and Xu, H.-L. (2018). "pH-sensitive polymeric nanoparticles of mPEG-PLGA-PGlu with hybrid core for simultaneous encapsulation of curcumin and doxorubicin to kill the heterogeneous tumour cells in breast cancer." Artificial Cells, Nanomedicine, and Biotechnology **4 Jan 2018**: 1-12.

Yuan, M., Wang, Y., Li, X., Xiong, C. and Deng, X. (2000). "Polymerization of Lactides and Lactones. 10. Synthesis, Characterization, and Application of Amino-Terminated Poly(ethylene glycol)-co-poly(ε-caprolactone) Block Copolymer." Macromolecules **33**(5): 1613-1617.

Yue, X. and Dai, Z. (2018). "Liposomal Nanotechnology for Cancer Theranostics." Current Medicinal Chemistry **25**(12): 1397-1408.

Zang, G., Gustafsson, K., Jamalpour, M., Hong, J., Genove, G. and Welsh, M. (2015). "Vascular dysfunction and increased metastasis of B16F10 melanomas in Shb deficient mice as compared with their wild type counterparts." BMC Cancer **15**: 234.

Zhang, L., Tao, L., Shi, T., Zhang, F., Sheng, X., Cao, Y., Zheng, S., Wang, A., Qian, W., Jiang, L. and Lu, Y. (2015). "Paeonol inhibits B16F10 melanoma metastasis in vitro and in vivo via disrupting proinflammatory cytokines-mediated NF-kappaB and STAT3 pathways." IUBMB Life **67**(10): 778-788.

Zhang, L., Wen, X., Li, M., Li, S. and Zhao, H. (2018). "Targeting cancer stem cells and signaling pathways by resveratrol and pterostilbene." Biofactors **44**(1): 61-68.

Zhang, X., Li, Y., Chen, X., Wang, X., Xu, X., Liang, Q., Hu, J. and Jing, X. (2005). "Synthesis and characterization of the paclitaxel/MPEG-PLA block copolymer conjugate." Biomaterials **26**(14): 2121-2128.

Zhang, X.X., Eden, H.S. and Chen, X. (2012). "Peptides in cancer nanomedicine: drug carriers, targeting ligands and protease substrates." Journal of Controlled Release **159**(1): 2-13.

Zhang, Y., Ren, T., Gou, J., Zhang, L., Tao, X., Tian, B., Tian, P., Yu, D., Song, J., Liu, X., Chao, Y., Xiao, W. and Tang, X. (2017). "Strategies for improving the payload of small molecular drugs in polymeric micelles." Journal of Controlled Release **261**(2017): 352-366.

Zhang, Y., Song, H., Shang, Z., Chen, A., Huang, D., Zhao, H. and Du, H. (2014a). "Amino Acid-PEGylated Resveratrol and Its Influence on Solubility and the Controlled Release Behavior." Biological and Pharmaceutical Bulletin **37**(5): 785-793.

Zhang, Z., Xu, L., Chen, H. and Li, X. (2014b). "Rapamycin-loaded poly(epsilon-caprolactone)-poly(ethylene glycol)-poly(epsilon-caprolactone) nanoparticles: preparation, characterization and potential application in corneal transplantation." Journal of Pharmaceutics and Pharmacology **66**(4): 557-563.

Zordoky, B.N., Robertson, I.M. and Dyck, J.R. (2015). "Preclinical and clinical evidence for the role of resveratrol in the treatment of cardiovascular diseases." Biochimica et Biophysica Acta **1852**(6): 1155-1177.

Zu, Y., Zhang, Y., Wang, W., Zhao, X., Han, X., Wang, K. and Ge, Y. (2016). "Preparation and in vitro/in vivo evaluation of resveratrol-loaded carboxymethyl chitosan nanoparticles." Drug Delivery **23**(3): 981-991.

Zubair, H., Azim, S., Ahmad, A., Khan, M.A., Patel, G.K., Singh, S. and Singh, A.P. (2017). "Cancer Chemoprevention by Phytochemicals: Nature's Healing Touch." Molecules **2017**(22): 395.

Zupancic, S., Lavric, Z. and Kristl, J. (2015). "Stability and solubility of trans-resveratrol are strongly influenced by pH and temperature." European Journal of Pharmaceutics and Biopharmaceutics **93**(2015): 196-204.

CHAPTER 7. APPENDICES

7.1 Calculation of polymer molecular weight by NMR using end-group analysis

NMR spectroscopy is an absolute method to determine the MW of polymers using end-group analysis (Umoren *et al.* 2016). For additional reading, Pochapsky *et al.* (2013) offers a comprehensive overview on the theory and standard experiments carried out on NMR spectrometers. Using mPEG-PLA synthesised based on methods detailed in Section 2.4.1.1 as an example (Figure 7.1), the methyl end-group protons of mPEG (H_d) at *ca.* 3.4ppm was used to calculate the number of repeating units of mPEG by using the methylene protons H_c at *ca.* 3.6ppm and of PLA by using the methine proton H_a at *ca.* 5.2ppm.

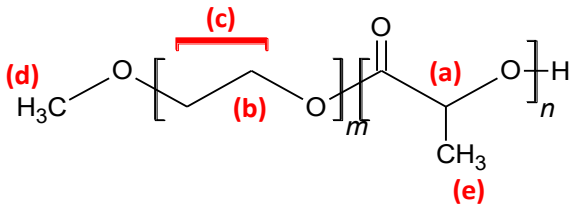

Figure 7.1 Molecular structure and proton labels of mPEG-PLA synthesised

From Table 7.1, the number of repeating units for mPEG was calculated using the following equation as described by Izunobi *et al.* (2011). OEt represented protons from the methylene protons of the mPEG chain. When calculating for the repeating units of PLA, OEt was replaced with the methine proton of PLA chain.

$$r_{mPEG} = \frac{A_{OEt} \times 3 \text{ (Number of protons in methyl end-group)}}{\text{Peak area of methyl end-group} \times B_{OEt}}$$

where,
r is the repeating units of species *i*
A is the area of the ^{1}H NMR peak of species *i*
B is the number of protons of species *i*

Table 7.1 M_n calculation for mPEG-PLA using end-group analysis by NMR

Peak	Peak integration		Number of repeating units	Formula weight of repeating unit	M_n (Da)
	Expected	Actual			
Methylene protons on mPEG -OC**H₂**C**H₂** (3.6ppm)	179	182.22	45.6	44.053	2039.9
Methine proton on PLA -C(=O)-C**H**CH_3O- (5.2ppm)	14	12.81	12.8	72.063	923.4
				Total M_n	2963.3

The number of repeating units for each polymer was then used to calculate the M_n of each polymer on the copolymer using the formula MW of each polymer as follows.

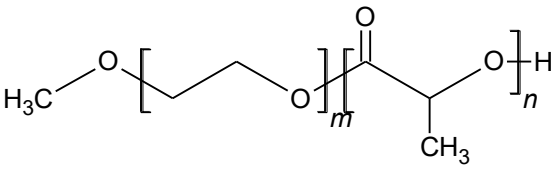

Formula MW 31.034 44.053*m* 72.063*n* 1.008 g/mol or Da

mPEG M_n
= 31.034 + 44.053 × 45.6
= 2039.8508

PLA M_n
= 72.063 × 12.8 + 1.008
= 923.4144

g/mol or Da

Total M_n = 2039.8508 + 923.4144
= 2963.2648

g/mol or Da

Therefore, by using the end-group analysis by NMR, we have determined that the M_n of the amphiphilic copolymer mPEG-PLA as 2,960Da with mPEG having a M_n of 2,040Da and PLA 920Da.

7.2 Calculation of % *w/w* of components and total RSV equivalent concentration in final RSV conjugate products by NMR

The molar ratio of components in mPEG750-PCL1000-succ-RSV were estimated based on H4 integral values on mono-substituted 4'- (*ca.* 6.2ppm), H6 integral values on mono-substituted 3- or 5- conjugates (*ca.* 6.4ppm) and H4 integral values of free RSV (*ca.* 6.1ppm) as previously discussed in Section 2.5.3. There were negligible amounts of di-substituted conjugates in the final product and was disregarded from calculations.

Table 7.2 Molar ratio of free RSV and mono-substituted RSV conjugates in mPEG750-PCL1000-succ-RSV synthesised product using NMR spectra integral values

	Free RSV	**Mono-substituted 3- or 5- RSV conjugate**	**Mono-substituted 4'- RSV conjugate**
Proton and chemical shift	H4 at 6.1ppm	H6 at 6.4ppm	H4 at 6.2ppm
Integration value	0.09	0.82	0.85
Molar ratio	$\frac{0.09}{0.09 + 0.82 + 0.85} = 0.05$	$\frac{0.82}{0.09 + 0.82 + 0.85} = 0.48$	$\frac{0.85}{0.09 + 0.82 + 0.85} = 0.47$
As mono-substituted RSV conjugates were not distinguished by substitution in this project…			
Molar ratio	**0.05**	0.48 + 0.47 = **0.95**	

Therefore, the molar ratio of free RSV to mono-substituted RSV conjugates was 0.05 to 0.95. Using the MW of each component, that is 228g/mol for RSV and 1872g/mol for mPEG750-PCL1000-succ-RSV, we determined the % *w/w* of each component in the synthesised product as follows:

$$\% \; w/w \text{ free RSV} = \frac{0.05 \times 228}{(0.05 \times 228) + (0.95 \times 1872)} \times 100\% = 0.7\%$$

$$\% \; w/w \text{ mono-substituted RSV conjugates} = \frac{0.95 \times 1872}{(0.05 \times 228) + (0.95 \times 1872)} \times 100\% = 99.3\%$$

Determination of total RSV content or total RSV equivalent concentration in RSV conjugates in a batch of synthesized products were based on the % *w/w* of its individual components. The final product contained 0.7% *w/w* free RSV (MW 228g/mol), that is 0.7g free RSV was found in 100g product. Therefore, in 1mg product, there was $\frac{0.7}{228 \times 100}$ = **0.0307μmol** free RSV.

The final product contained 99.3% *w/w* total mono-substituted conjugates (MW 1872g/mol). Therefore, in 1mg product, there was $\frac{99.3}{1872 \times 100}$ = **0.5304μmol** mono-substituted conjugates. In a mono-substituted conjugate, the molar ratio between RSV and the copolymer was 1:1. Thus, the number of moles of RSV in a mono-substituted conjugate was the same number of moles of the mono-substituted conjugates. In this case, the number of moles of RSV in the mono-substituted conjugate was then also **0.5304μmol**.

Hence, the total number of moles of RSV equivalent in 1mg final product was 0.0307μmol + 0.5304μmol = **0.5611μmol** and the total weight of RSV equivalent in 1mg of final product was 0.5611μmol × 228g/mol = 0.12793mg. Therefore, the total concentration of RSV in 1 mg/mL product was $\frac{1\text{mg/mL} \times 0.12793\text{mg}}{1\text{mg}}$ = **0.128mg/mL**.

7.3 Calculation of polymer molecular weight by GPC

Unlike the NMR technique described in Appendix 7.1, determination of MW of polymers by GPC is relative to the calibration of polymer standards with narrow PDI. We have used PEG standards (Jordi Labs LLC: MA, USA) with PDI values of less than 1.20 with the following MW distributions (Table 7.3).

Table 7.3 MW distributions and PDI of PEG standards used for GPC calibration

MW at peak maxima, M_p (Da)	**Weight-average MW, M_w (Da)**	**Number-average MW, M_n (Da)**	**Polydispersity index, PDI (M_w/M_n)**
960	985	879	1.12
3,020	3,060	2,800	1.09
6,430	6,510	5,610	1.16
26,100	25,800	22,100	1.17

A calibration curve was prepared by plotting the average t_R obtained from eluted peaks of standards measured in triplicate against $\log M_p$ (Figure 7.2).

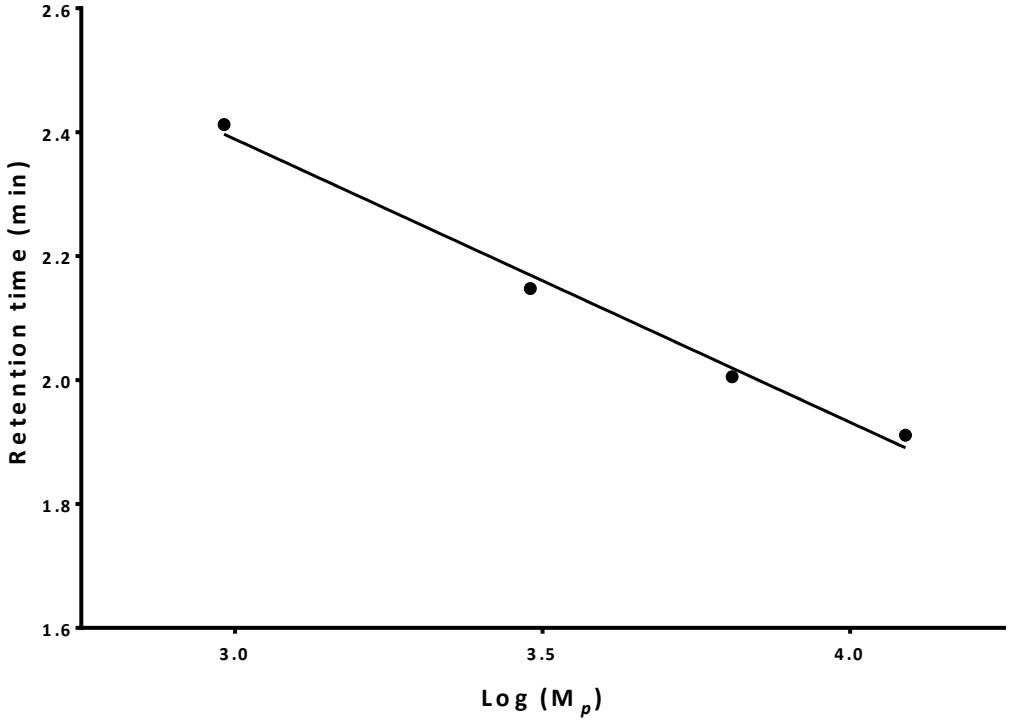

Figure 7.2 Calibration of GPC system using PEG standards (960 to 26,100Da)
Linear regression equation: y = -0.4569x + 3.759 (R^2 = 0.9906)

As an example, an mPEG-PLA synthesised as per Section 2.4.1.1 was analysed by the GPC method against these PEG standards and the raw data of the eluted peak from t_R 1.8936 minutes to 2.4552 minutes were processed as per Table 7.4. From the raw data of an eluted sample peak, the M_n and M_w was calculated by equations described as follows (Holding *et al.* 1995, Khanna *et al.* 1996, OECD 1996):

$$M_n = \frac{\sum_{i=1}^{n} H_i}{\sum_{i=1}^{n} H_i/M_i}$$

$$M_w = \frac{\sum_{i=1}^{n} H_i \times M_i}{\sum_{i=1}^{n} H_i}$$

$$PDI = \frac{M_w}{M_n}$$

where,
H_i is the response level minus noise of the RID signal for the t_R t_i,
M_i is the MW fraction of the polymer calculated from the calibration curve linear regression equation at the t_R t_i, and
n is the number of data points in the eluted peak

Table 7.4 Processed raw GPC data for M_n and M_w calculations

Retention time, t_i (minutes)	**RID response (nRIU)**	**RID response minus noise level, H_i (nRIU)***	**M_i**	**H_i/M_i**	**$H_i \times M_i$**
1.8936	4681.5098	0.0000	12098.50	0.0000	0.0000
1.9008	4766.6499	85.1401	11667.37	0.0073	993361.2975
1.9080	4868.4297	186.9199	11251.61	0.0166	2103149.9974
1.9152	4989.2598	307.7500	10850.66	0.0284	3339292.0058
1.9224	5131.8398	450.3300	10464.01	0.0430	4712255.6542
⋮	⋮	⋮	⋮	⋮	⋮
2.4336	7608.5200	2927.0102	795.89	3.6777	2329580.9934
2.4408	7451.6699	2770.1601	767.53	3.6092	2126180.2341
2.4480	7309.4800	2627.9702	740.18	3.5505	1945168.6944
2.4552	7180.7300	2499.2202	713.80	3.5013	1783951.2653
		$\sum_{1.8936}^{2.4552} H_i$ = 785354.2313		$\sum_{1.8936}^{2.4552} H_i/M_i$ = 335.5982	$\sum_{1.8936}^{2.4552} H_i \times M_i$ = 2412694771

*Noise level was determined by using the response level just before peak elution which in this case was at 1.8936 minutes.

Then, the MW distributions of this polymer mPEG-PLA were calculated and summarised in the following table (Table 7.5).

Table 7.5 Calculated MW distribution and PDI of mPEG-PLA using GPC

mPEG-PLA MW characteristic	
M_n	2340.16
M_w	3072.11
PDI	1.31

7.4 Synthesis of mPEG-PCL-RSV conjugates with different PCL chain lengths

A library of mPEG2000-PCL$_n$-glu-RSV was synthesised with PCL lengths from 130Da (*n* = 1) to 11,660Da (*n* = 102) and mPEG (2,000Da) was conjugated to RSV with either a succ or glu linker. The stability of these RSV conjugates in buffers and rat plasma were compared against free RSV and published in Ng *et al.* (2015). Rat plasma $t_{1/2}$ and physical characteristics of conjugates are tabulated in Table 7.6. The plasma stability of RSV was not significantly improved with conjugation (RSV $t_{1/2}$ <5min); however, longer PCL chain lengths were found to be slightly more stable than shorter PCL chain lengths. Similar to what was found in Section 4.5.1.4, higher DL of NPs were of those formulated with free RSV.

Table 7.6 Characteristic of synthesized products from conjugation of RSV to amphiphilic copolymers used in Ng *et al.* (2015)

Product	Product description	Yield (%)	% *w/w* of components in final product[a]		Total RSV equivalent concentration (mg/mL)[b]	DL (%)	Plasma $t_{1/2}$ (min)
			Mono-substituted RSV	Free RSV			
mPEG2000-PCL130-glu-RSV	Off-white waxy powder	22.2	67.6	32.4	0.386	35.6	5
mPEG2000-PCL230-glu-RSV	Brown wax	31.8	99.5	0.5	0.093	6.3	3
mPEG2000-PCL500-glu-RSV	Brown solid	22.3	62.0	38.0	0.429	39.9	3
mPEG2000-PCL900-glu-RSV	Brown powder	6.1	75.8	24.2	0.295	26.5	3.5
mPEG2000-PCL2590-glu-RSV	Dark brown solid	21.6	100.0	0	0.061	3.1	ND
mPEG2000-PCL5360-glu-RSV	Brown wax	4.0	100% di-substituted RSV		0.015	1.5	4
mPEG2000-PCL7070-glu-RSV	Brown solid	11.8	100.0	0	0.024	2.4	ND
mPEG2000-PCL9500-glu-RSV	Cream powder	22.3	100% di-substituted RSV		0.010	1.0	10
mPEG2000-PCL13640-glu-RSV	White powder	37.7	99.5	0.5	0.019	1.9	8
mPEG2000-succ-RSV	Cream powder	16.5	100% di-substituted RSV		0.052	5.2	ND
mPEG2000-glu-RSV	Brown powder	16.3	100% di-substituted RSV		0.051	5.1	3

[a]% *w/w* of components in synthesised final products were calculated as per Section 2.4.4.2 (Calculation example in Appendix 7.2)
[b]Total RSV equivalent concentration in 1mg/mL final product was calculated as per Section 2.4.4.2 (Calculation example in Appendix 7.2)

7.5 NMR Spectra

The following were the NMR spectra of representative synthesized products as follows:

1) D,L-lactide (Figure 7.3)
2) *ε*-caprolactone (Figure 7.4)
3) mPEG2000-PLA1000-glu-OH (Figure 7.5)
4) mPEG750-PLA1000-succ-RSV (Figure 7.6)
5) mPEG750-PLA1000-glu-RSV (Figure 7.7)
6) mPEG2000-PCL1000-succ-RSV (Figure 7.8)
7) mPEG2000-PCL1000-glu-RSV (Figure 7.9)
8) mPEG2000-succ-RSV (Figure 7.10)
9) mPEG2000-glu-RSV (Figure 7.11)

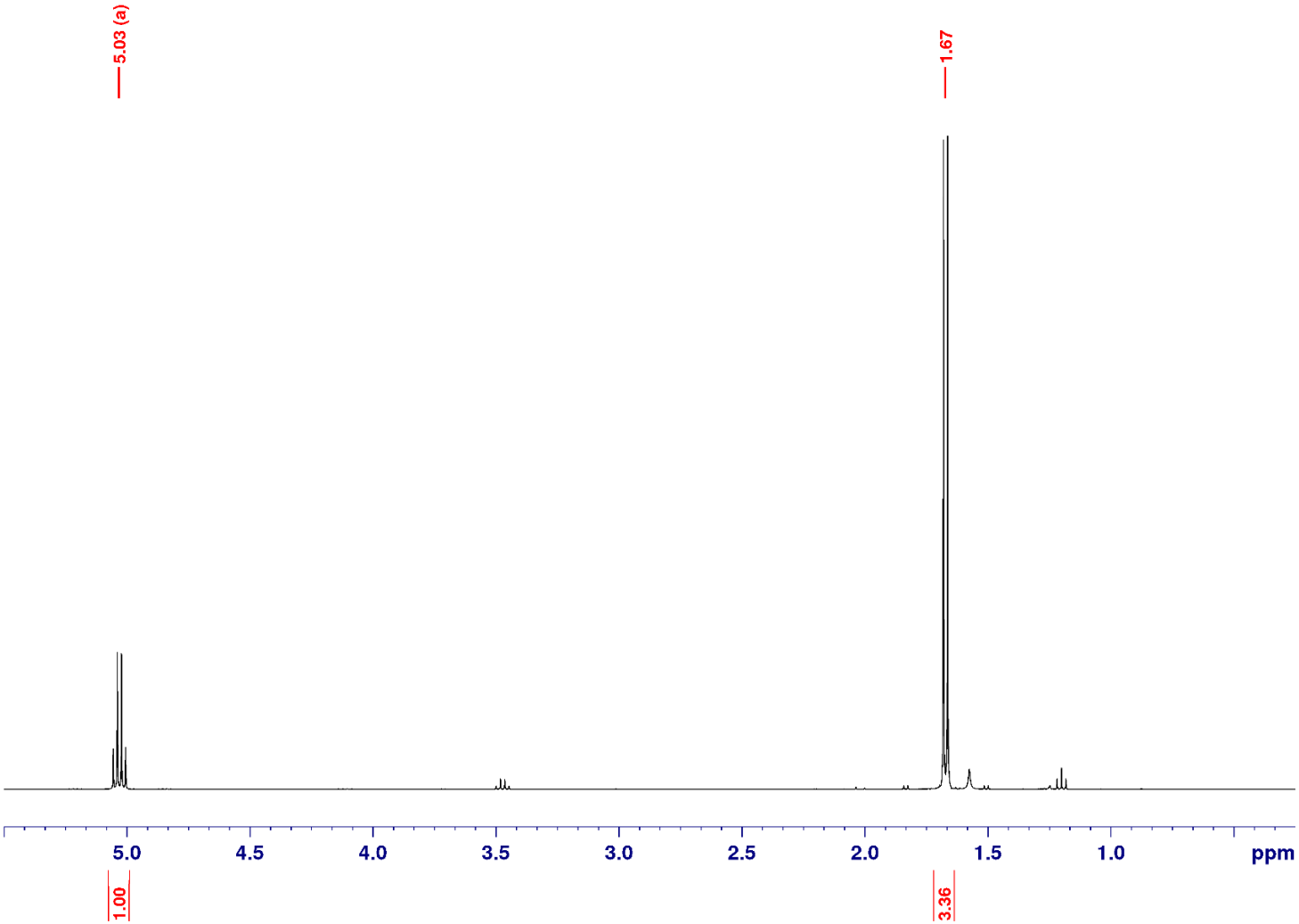

Figure 7.3 ^{1}H NMR spectra of D,L-lactide

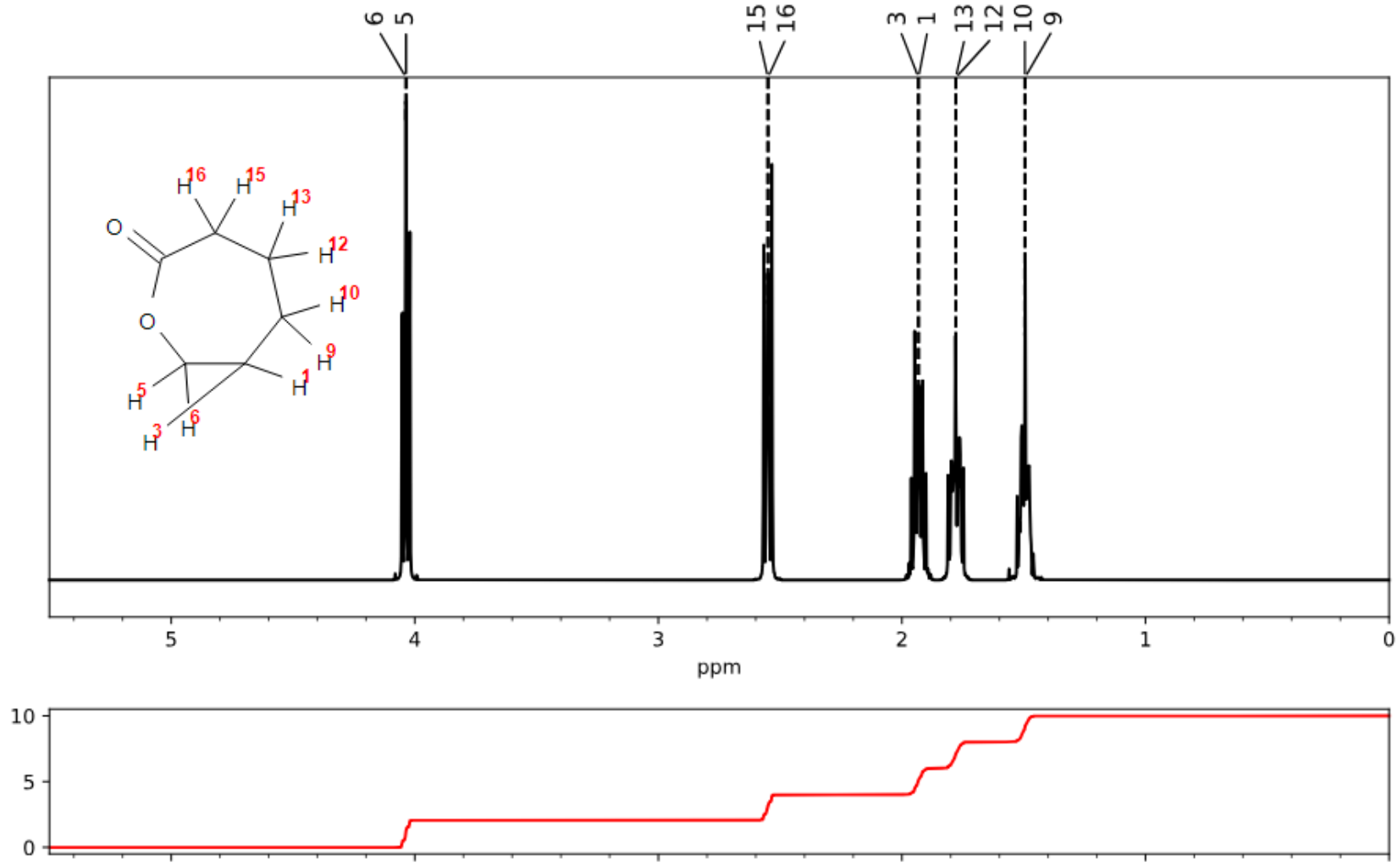

Figure 7.4 ^{1}H NMR spectra of *ε*-caprolactone (Abraham *et al.* 2008)

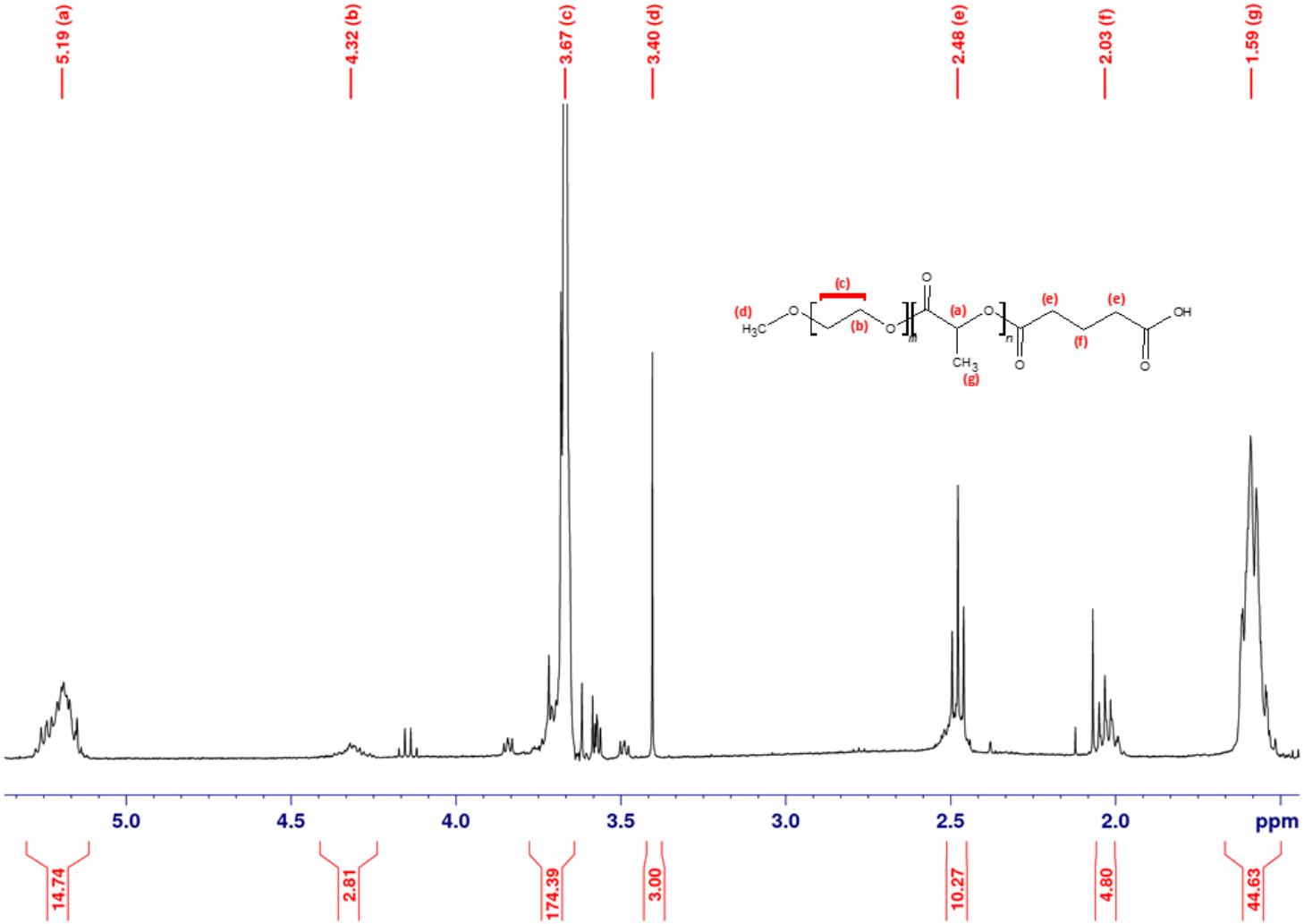

Figure 7.5 ^{1}H NMR spectra of mPEG2000-PLA1000-glu-OH

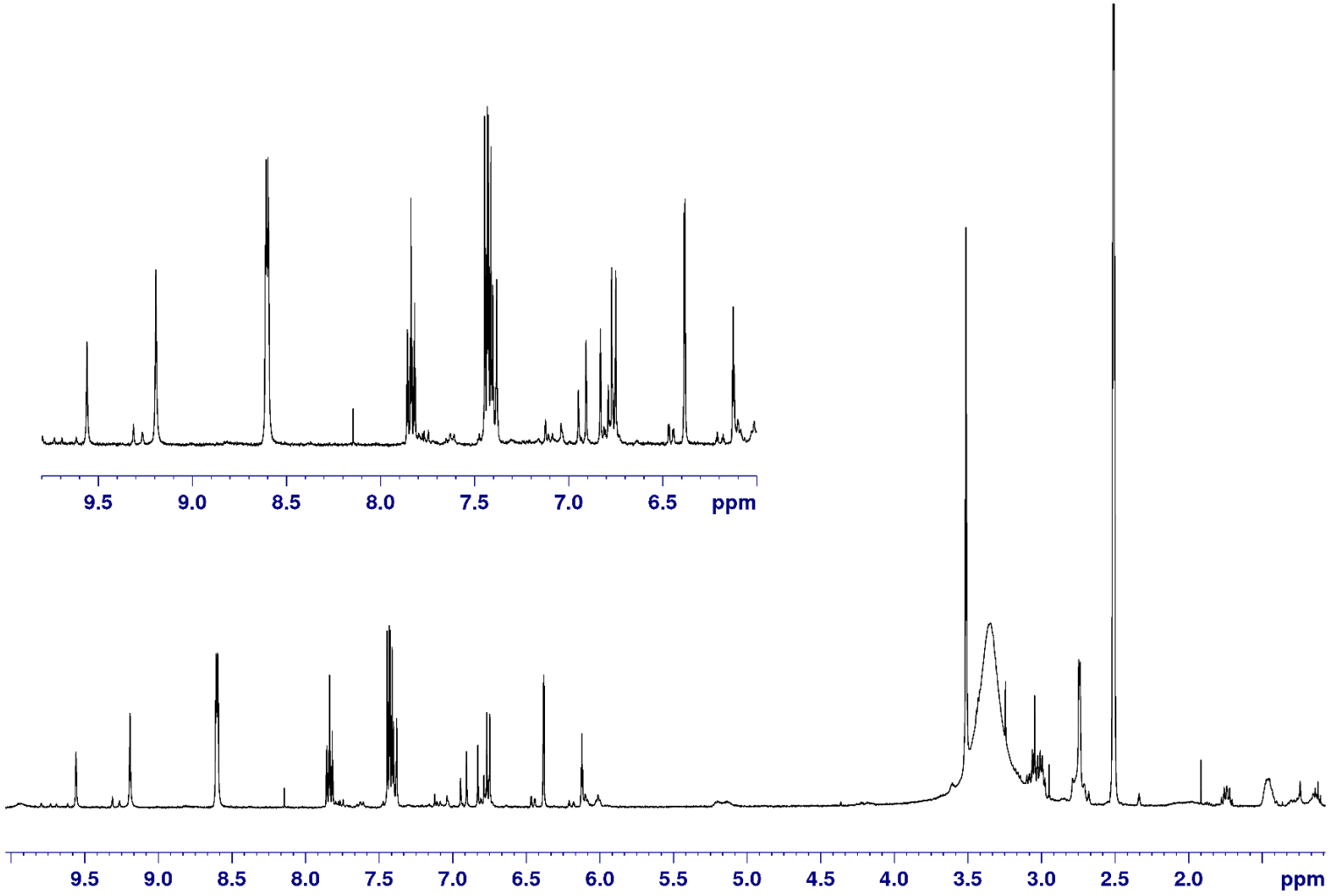

Figure 7.6 ^{1}H NMR spectra of mPEG750-PLA1000-succ-RSV (inset: RSV region)

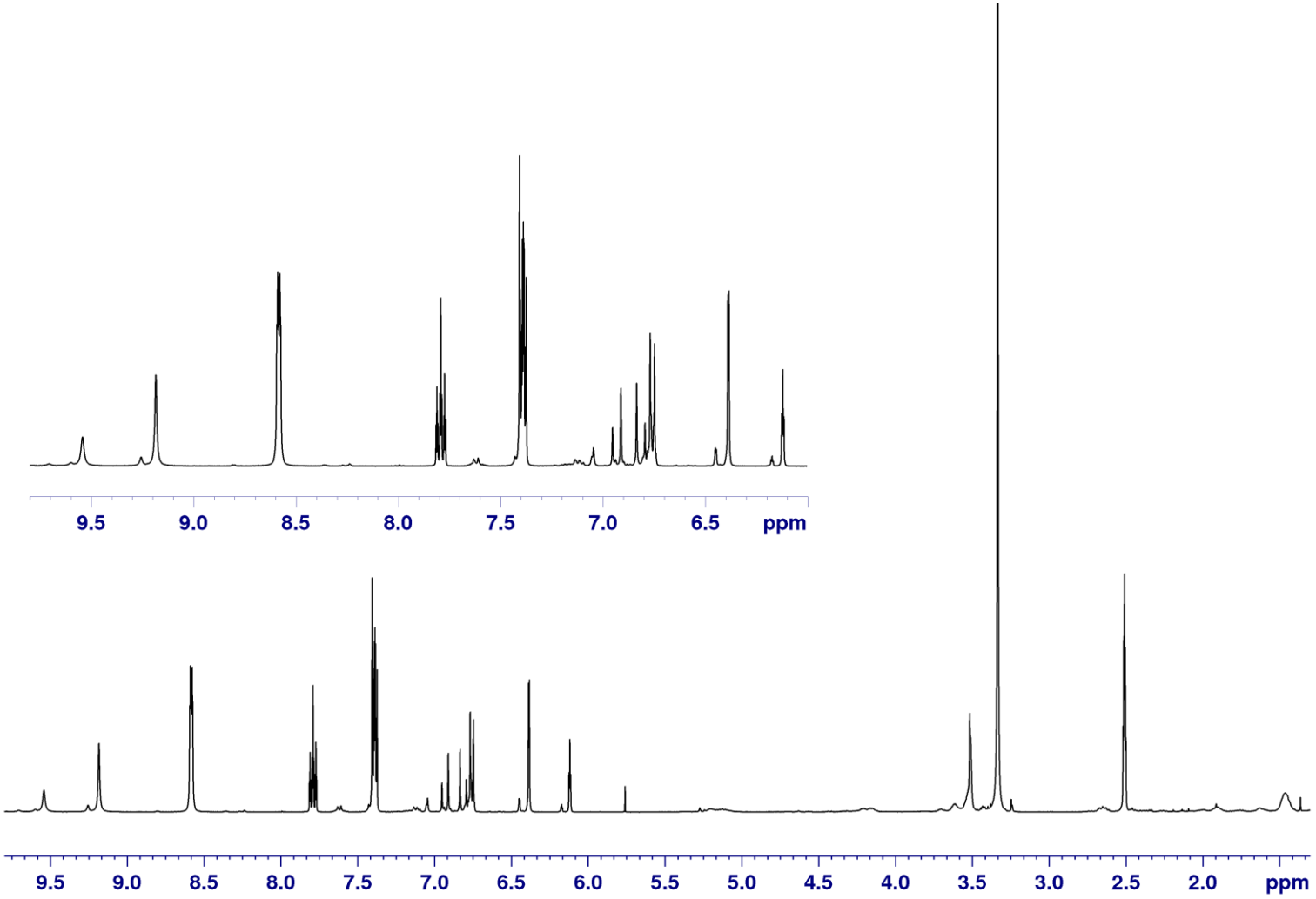

Figure 7.7 ^{1}H NMR spectra of mPEG750-PLA1000-glu-RSV (inset: RSV region)

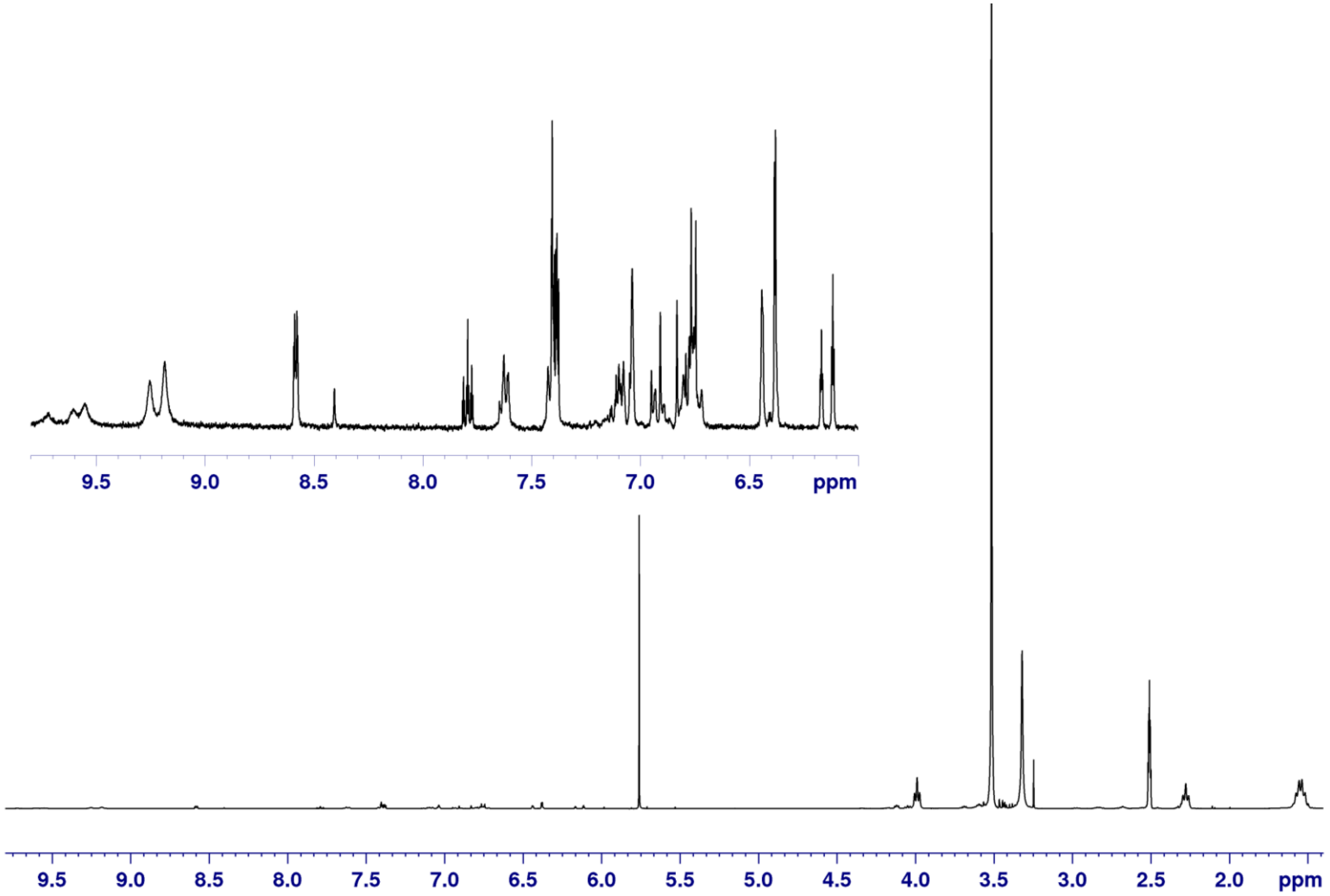

Figure 7.8 ^{1}H NMR spectra of mPEG2000-PCL1000-succ-RSV (inset: RSV region)

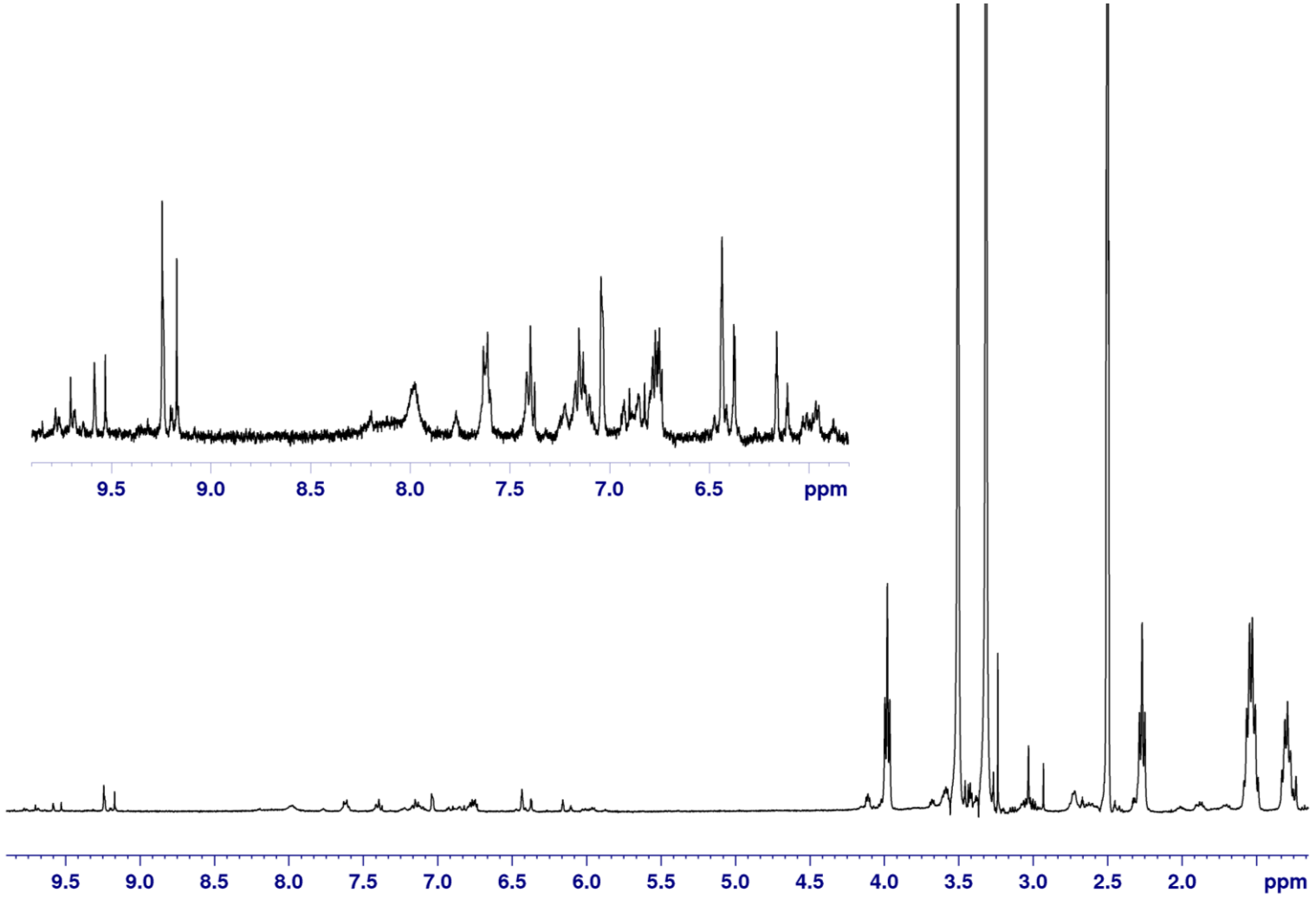

Figure 7.9 ^{1}H NMR spectra of mPEG2000-PCL1000-glu-RSV (inset: RSV region)

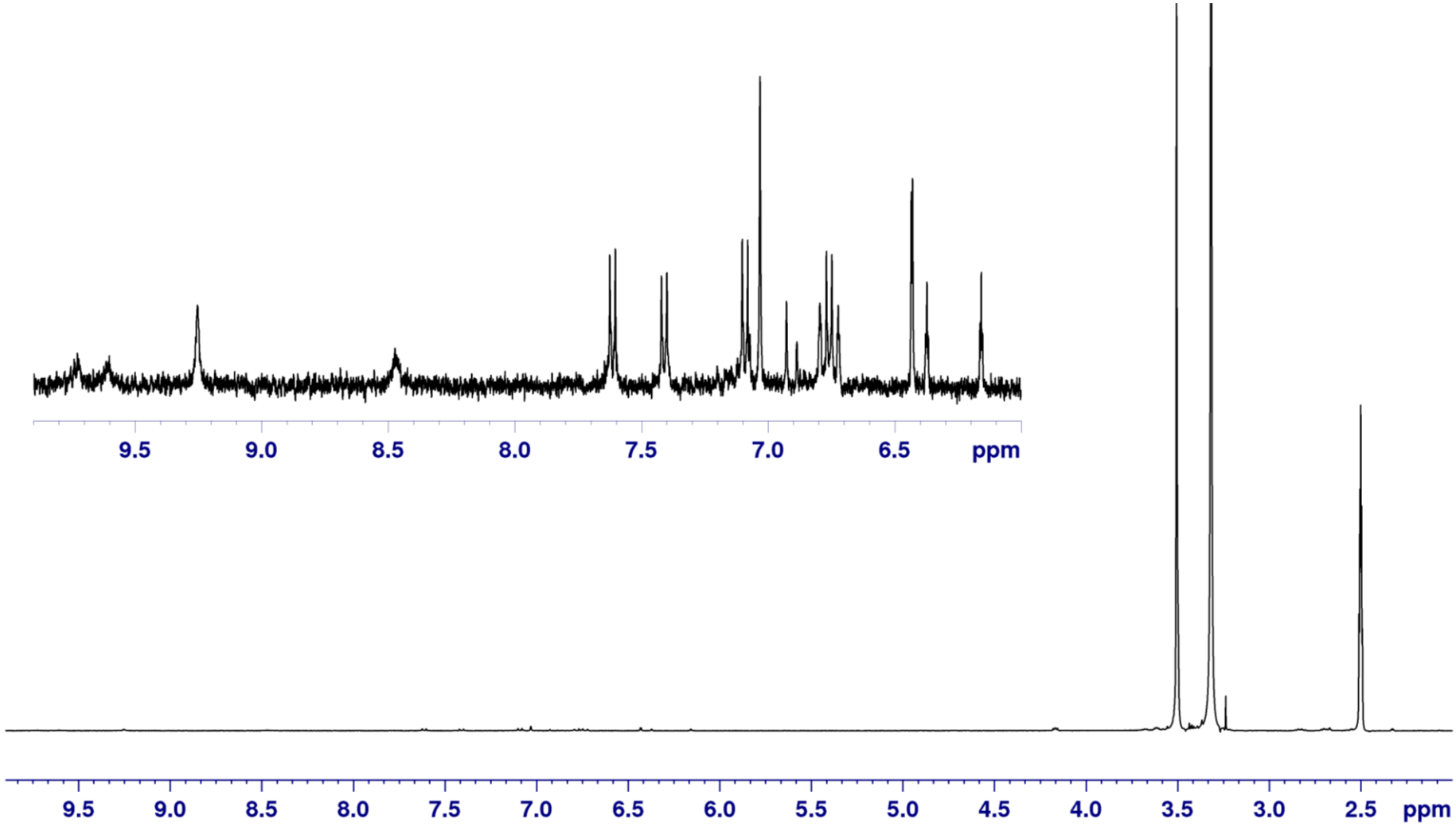

Figure 7.10 ^{1}H NMR spectra of mPEG2000-succ-RSV (inset: RSV region)

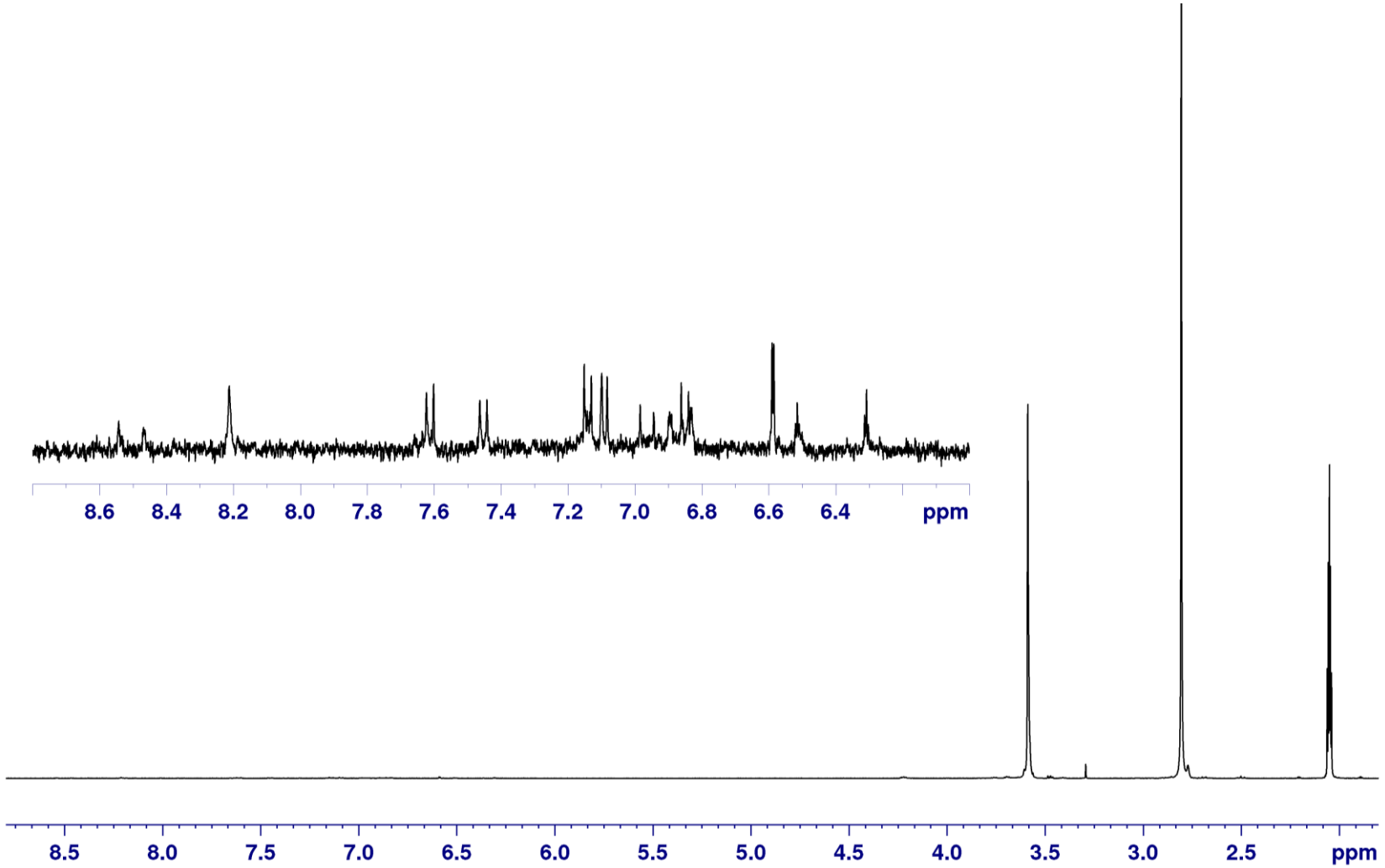

Figure 7.11 ^{1}H NMR spectra of mPEG2000-glu-RSV (inset: RSV region)

7.6 Certificate of analysis (mPEG750-PLLA1000 AK25)

No. 25 Certificate of Analysis

Product Name: Methoxy Poly(ethylene glycol)-*b*-Poly (L) Lactic Acid copolymer (nominal block weight 750-1000)

- ^{1}H-NMR Spectrum of MPEG-P(L)LA diblock copolymer in CDCl3 (Varian Inova 300 MHz instrument)

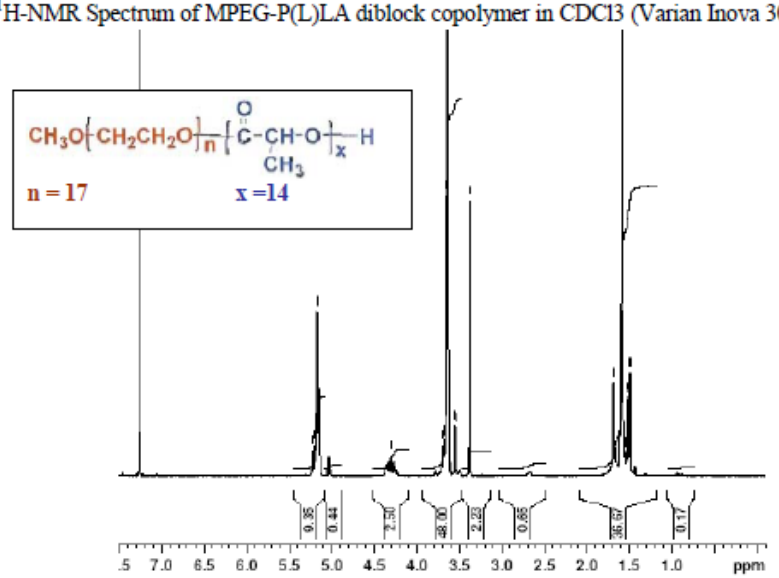

Mn(NMR) of MPEG-PLLA copolymers: 750-1000

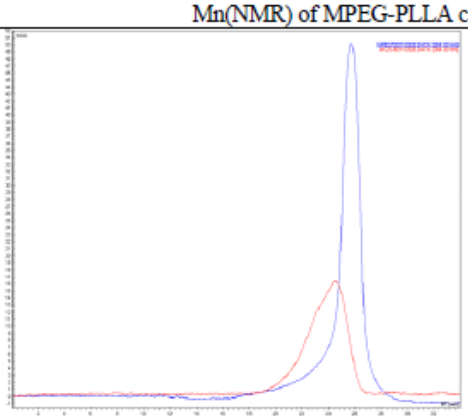

GPC analysis of mPEG initiator (blue) and mPEG-P(L)LA product (red): Analysis Method: Varian Prostar system with 1 ml/min DCM flow across two Resipore 3 um columns and one Mixed E column (Varian) and with UV-Vis (PDA) detection. Calibrated against polystyrene standards

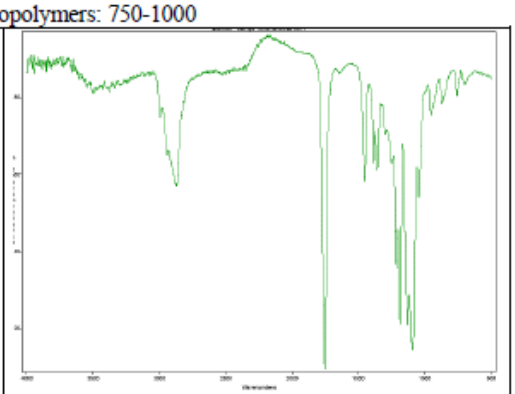

FTIR analysis: **Collected from cast-film on KBR salt-plate placed in Sattelite FTIR (Thermo-Mattson) and analyzed in transmission mode.**

Name	Mw (GPC)	Mn (GPC)	PDI
mPEG 750 initiator	1000	863	1.16
AK25	3159	1881	1.68

PolySciTech Division of Akina, Inc. | 3495 Kent Avenue, West Lafayette, IN 47906
765-464-0390 | www.polyscitech.com
For research use only.

7.7 PEG5000-O-RSV

Basavaraj (2011) synthesised an RSV conjugate where RSV was covalently bonded to a PEG (MW 5000Da) by an ether bond (Figure 7.12).

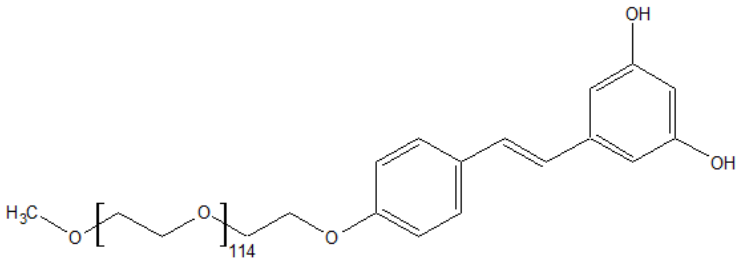

Figure 7.12 RSV conjugated to PEG5000 with an ether bond

This conjugate was found to be stable in biological buffers (Basavaraj 2011) and was warranted for future *in vitro* and *in vivo* evaluation. This conjugate contained a mixture of 26% 3- or 5- mono-substituted conjugates and 74% 4'-polymer-RSV with no free RSV. Due to its stable nature, it was chosen to fully validate our HPLC gradient method.

7.8 Peak purity reports

Peak purity reports are displayed in this section.

7.8.1 Free RSV in HLM mix using HPLC gradient method

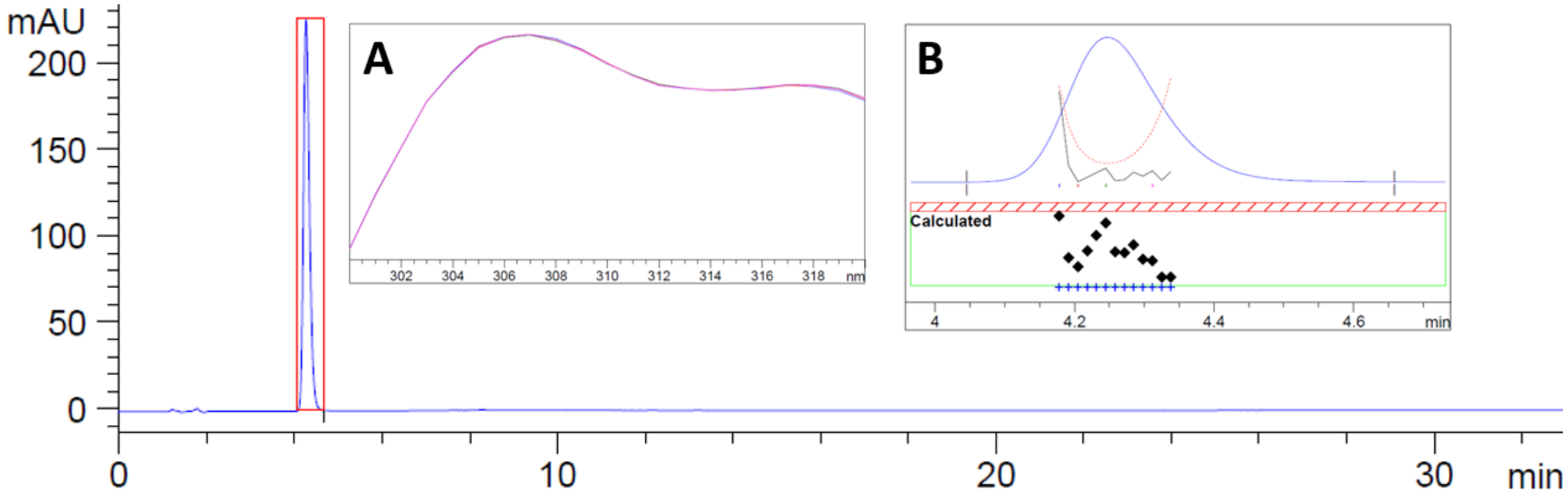

Figure 7.13 Typical HPLC chromatogram of free RSV in HLM mix analysed using the HPLC gradient method. (A) UV spectra of free RSV peak (B) Purity calculation of free RSV peak

7.8.2 Free RSV in supernatant of blank mPEG750-PLA1000 NPs using HPLC isocratic method

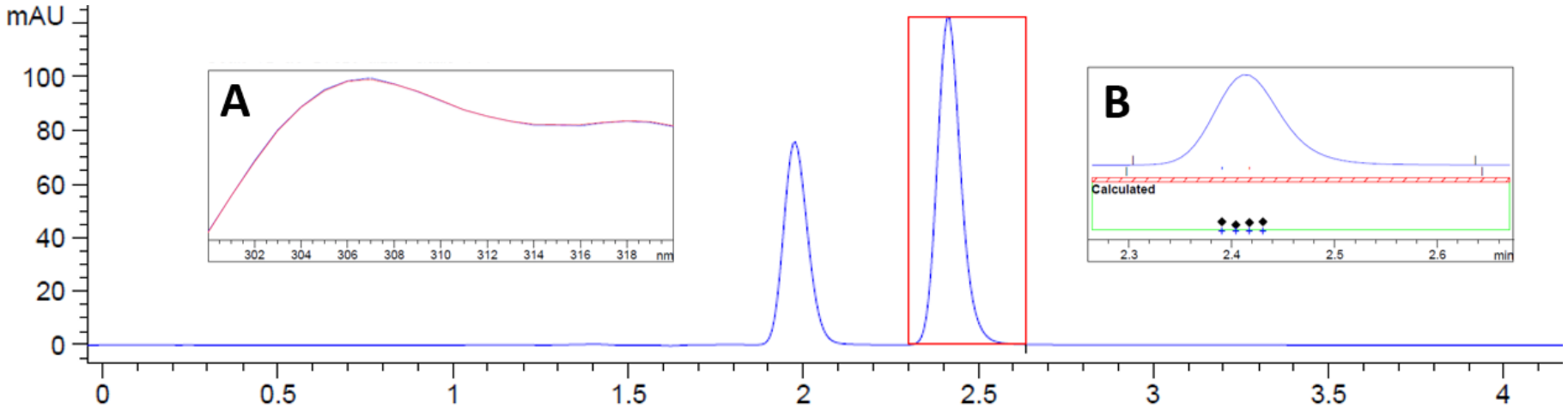

Figure 7.14 Typical HPLC chromatogram of free RSV in supernatant of blank mPEG750-PLA1000 NPs analysed using the HPLC isocratic method. (A) UV spectra of free RSV peak (B) Purity calculation of free RSV peak

7.8.3 Free RSV in rat plasma using HPLC isocratic method

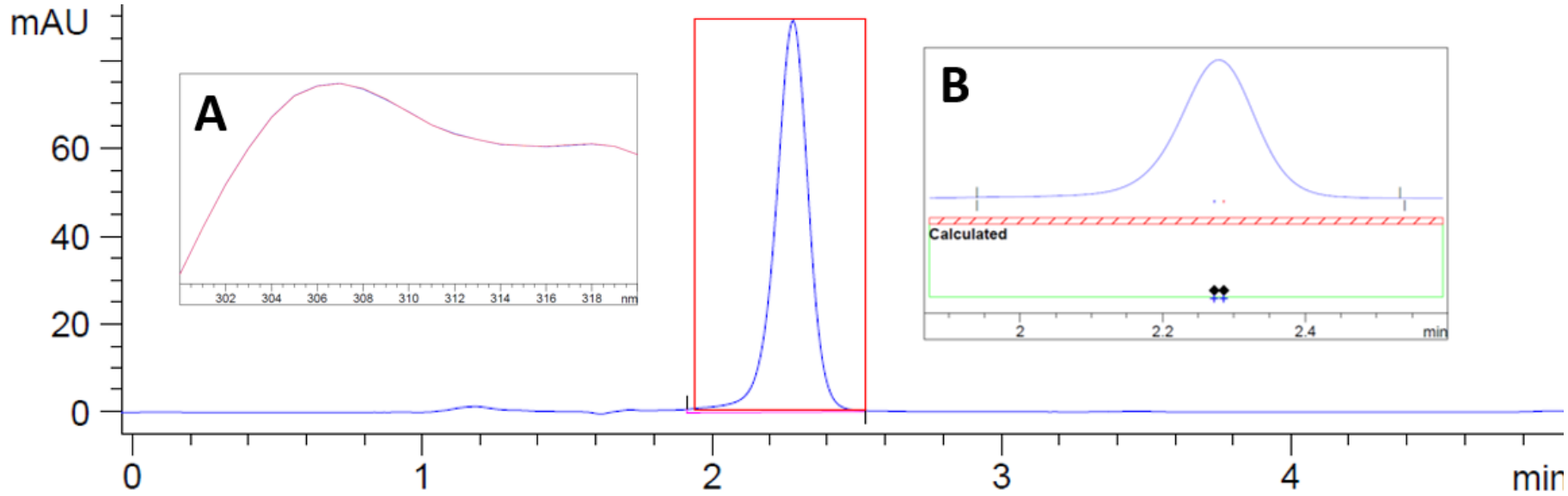

Figure 7.15 Typical HPLC chromatogram of free RSV in rat plasma analysed using the HPLC isocratic method. (A) UV spectra of free RSV peak (B) Purity calculation of free RSV peak

7.8.4 Free RSV in HLM mix using HPLC isocratic method

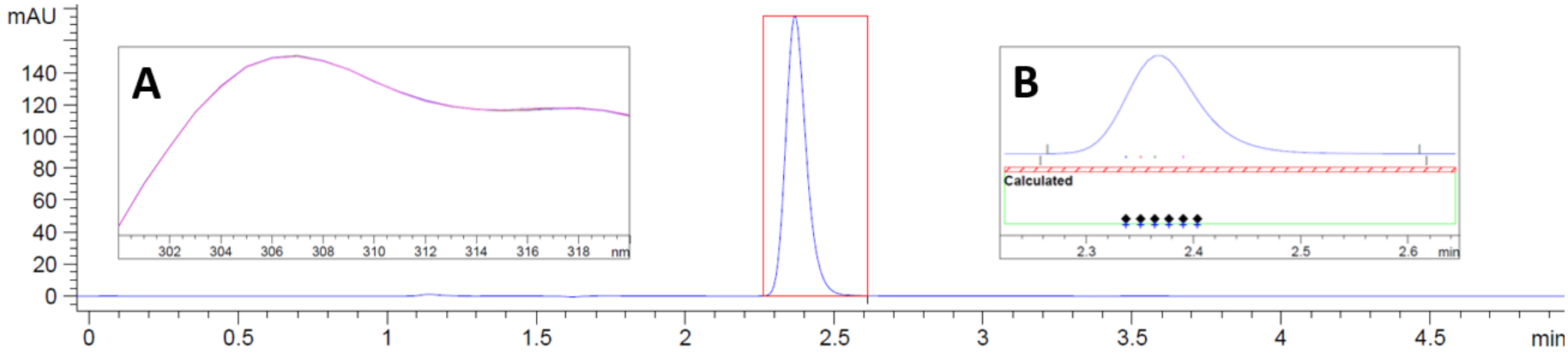

Figure 7.16 Typical HPLC chromatogram of free RSV in HLM mix analysed using the HPLC isocratic method. (A) UV spectra of free RSV peak (B) Purity calculation of free RSV peak

7.9 Size and zeta potential reports

7.9.1 mPEG750-PLA1000-succ-RSV NPs

A

		Size (d.nm):	% Intensity:	St Dev (d.nm):
Z-Average (d.nm): 277.3	Peak 1:	194.1	73.4	31.62
PdI: 0.304	Peak 2:	21.58	26.6	3.391
Intercept: 0.864	Peak 3:	0.000	0.0	0.000

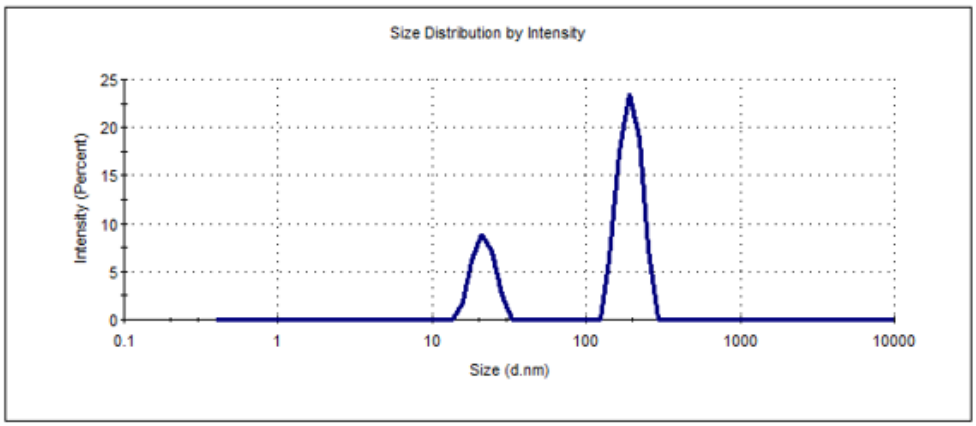

B

		Mean (mV)	Area (%)	St Dev (mV)
Zeta Potential (mV): -3.82	Peak 1:	-0.849	79.3	3.67
Zeta Deviation (mV): 7.10	Peak 2:	-16.0	20.7	3.03
Conductivity (mS/cm): 1.18	Peak 3:	0.00	0.0	0.00

Result quality : Good

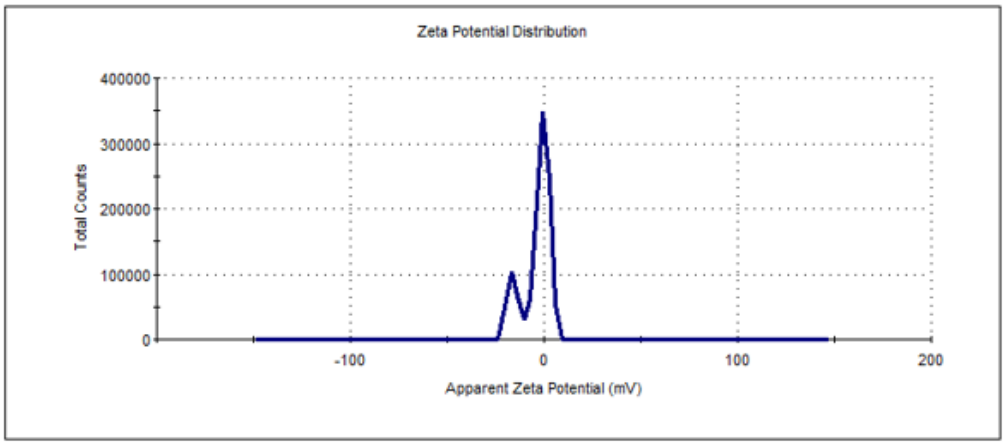

Figure 7.17 Size (A) and zeta potential (B) report of mPEG750-PLA1000-succ-RSV NPs prepared using solvent evaporation method

7.9.2 mPEG750-PLA1000-glu-RSV NPs

A

		Size (d.nm):	% Intensity:	St Dev (d.nm):
Z-Average (d.nm): 348.1	Peak 1:	839.5	55.7	377.1
PdI: 0.560	Peak 2:	192.2	39.9	68.18
Intercept: 0.699	Peak 3:	4945	4.4	634.5
Result quality : Good				

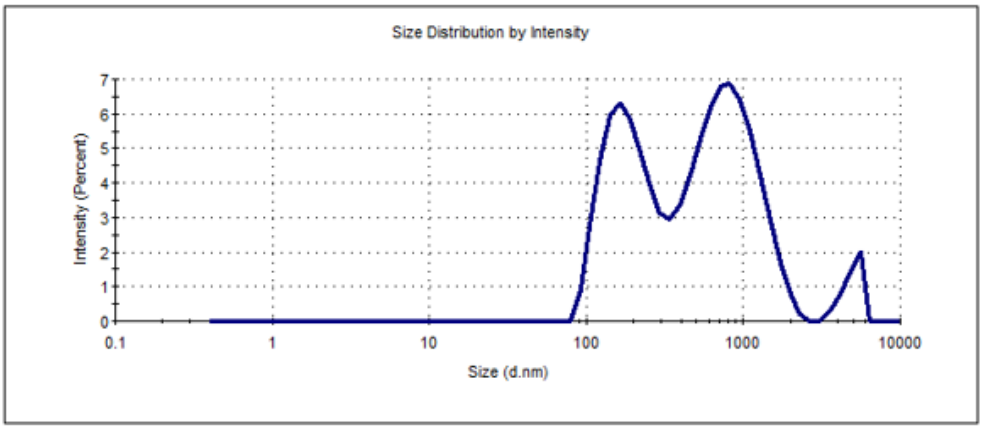

B

		Mean (mV)	Area (%)	St Dev (mV)
Zeta Potential (mV): -26.0	Peak 1:	-26.0	100.0	7.42
Zeta Deviation (mV): 7.42	Peak 2:	0.00	0.0	0.00
Conductivity (mS/cm): 0.116	Peak 3:	0.00	0.0	0.00
Result quality : Good				

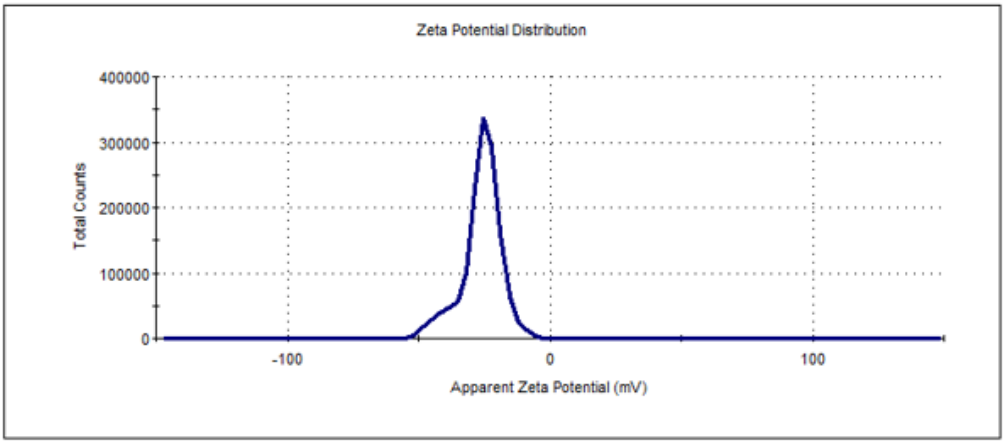

Figure 7.18 Size (A) and zeta potential (B) reports for mPEG750-PLA1000-glu-RSV NPs prepared by solvent diffusion method

7.9.3 mPEG750-PCL1000-succ-RSV NPs

A

		Size (d.nm):	% Intensity:	St Dev (d.nm):
Z-Average (d.nm):	203.7	Peak 1: 254.0	100.0	127.8
PdI:	0.176	Peak 2: 0.000	0.0	0.000
Intercept:	0.759	Peak 3: 0.000	0.0	0.000
Result quality :	Good			

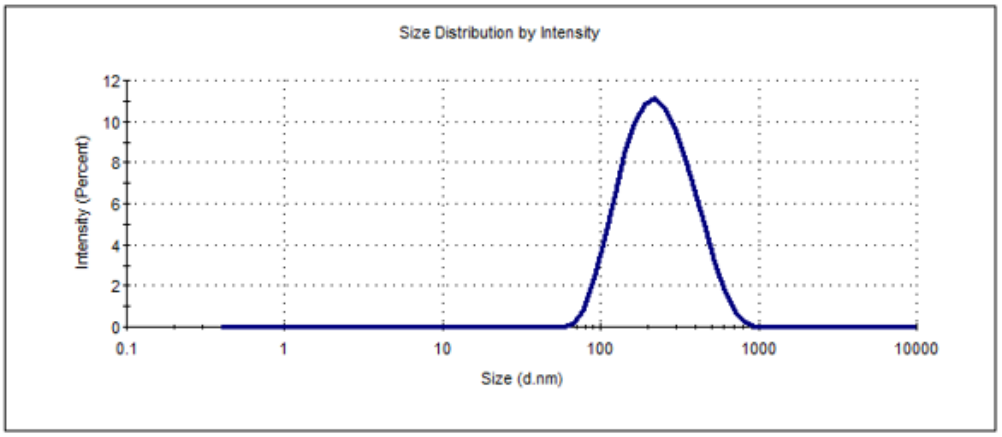

B

		Mean (mV)	Area (%)	St Dev (mV)
Zeta Potential (mV):	-37.8	Peak 1: -37.7	99.6	12.4
Zeta Deviation (mV):	12.6	Peak 2: -75.6	0.4	2.45
Conductivity (mS/cm):	0.148	Peak 3: 0.00	0.0	0.00

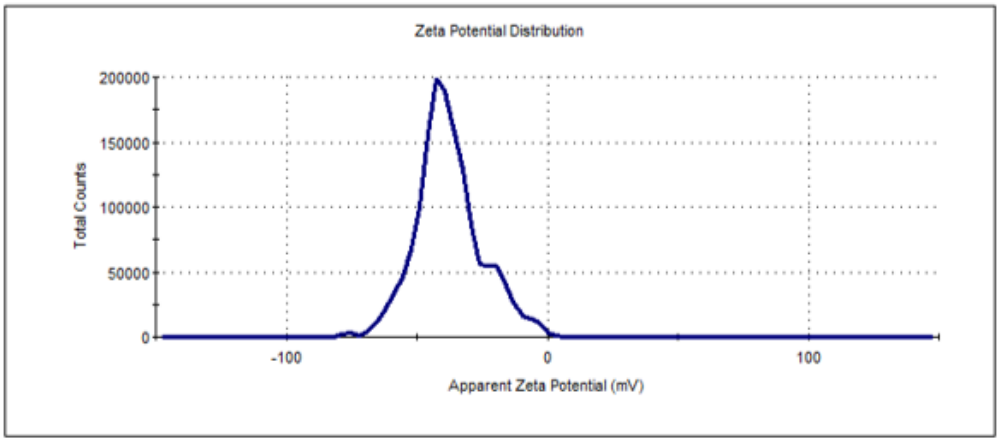

Figure 7.19 Size (A) and zeta potential (B) reports of mPEG750-PCL1000-succ-RSV NPs prepared by solvent diffusion method

7.9.4 mPEG2000-PLA1000-succ-RSV NPs

A

			Size (d.nm):	% Intensity:	St Dev (d.nm):
Z-Average (d.nm):	24.55	Peak 1:	18.71	83.2	5.278
PdI:	0.463	Peak 2:	140.7	16.8	35.43
Intercept:	0.746	Peak 3:	0.000	0.0	0.000

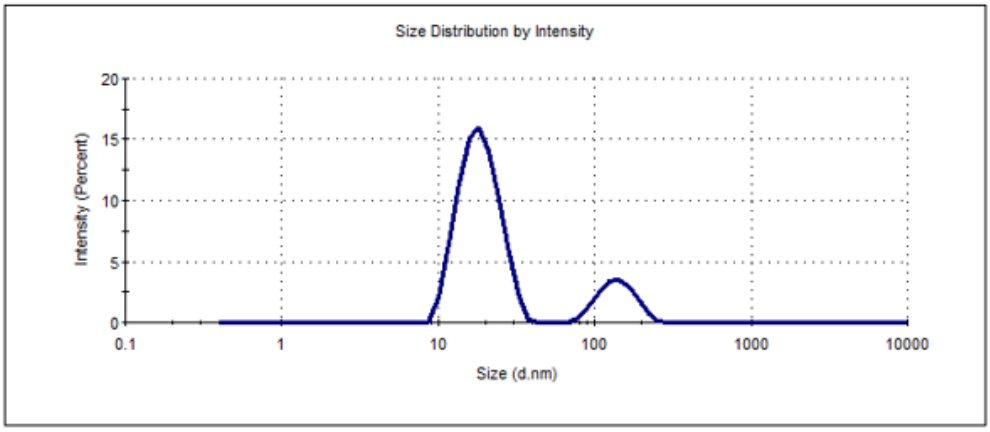

B

			Mean (mV)	Area (%)	St Dev (mV)
Zeta Potential (mV):	-7.25	Peak 1:	-6.22	100.0	7.49
Zeta Deviation (mV):	16.2	Peak 2:	0.00	0.0	0.00
Conductivity (mS/cm):	0.0176	Peak 3:	0.00	0.0	0.00

Result quality : Good

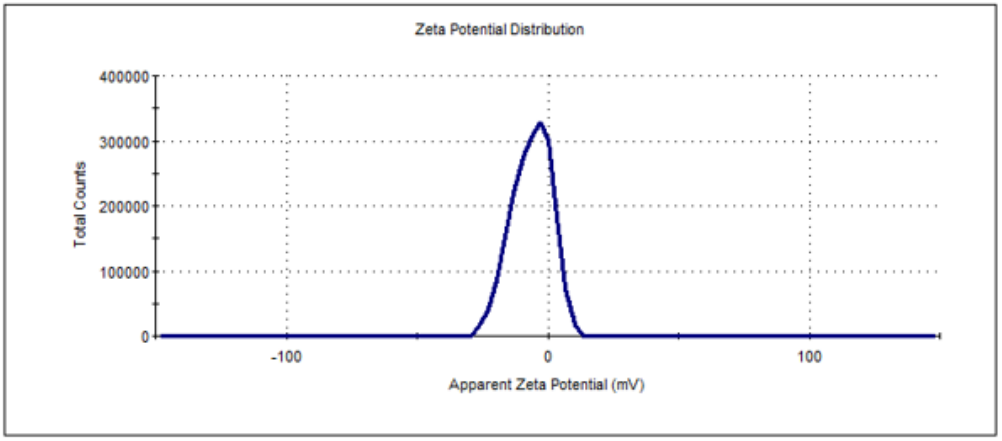

Figure 7.20 Size (A) and zeta potential (B) reports for mPEG2000-PLA1000-succ-RSV NPs prepared by solvent diffusion method

7.9.5 Blank mPEG750-PLA1000 NPs prepared by self-assembly method

			Size (d.nm):	% Intensity:	St Dev (d.nm):
Z-Average (d.nm):	22.82	Peak 1:	20.21	81.3	6.091
PdI:	0.347	Peak 2:	683.1	17.1	327.2
Intercept:	0.919	Peak 3:	4517	1.5	889.8
Result quality :	Good				

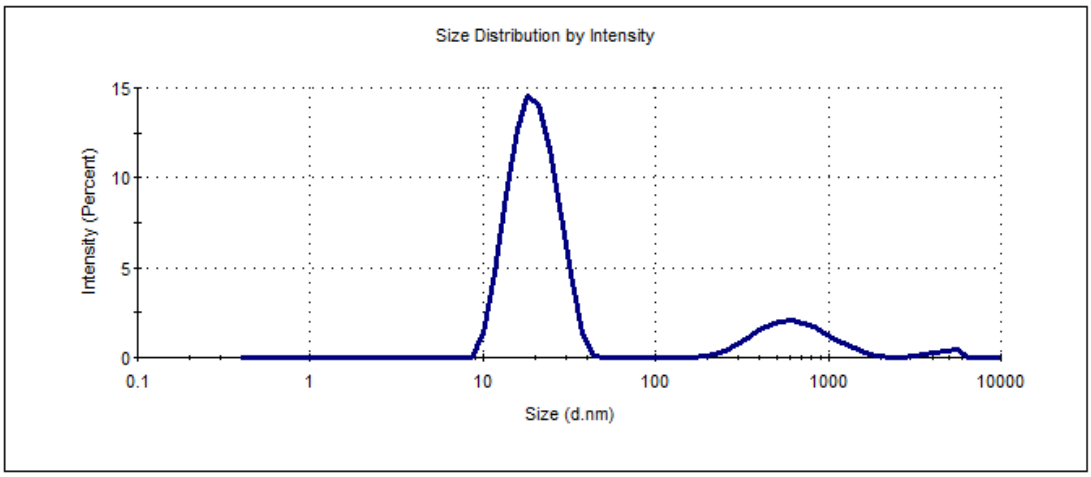

Figure 7.21 Size report of blank mPEG750-PLA1000 NPs prepared by self-assembly method

7.9.6 Blank mPEG750-PLA1000 NPs

A

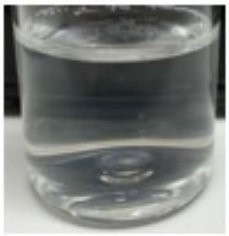

B

		Size (d.nm):	% Intensity:	St Dev (d.nm):
Z-Average (d.nm): 248.6	Peak 1:	465.1	71.5	95.75
PdI: 0.596	Peak 2:	27.34	28.5	5.073
Intercept: 0.962	Peak 3:	0.000	0.0	0.000

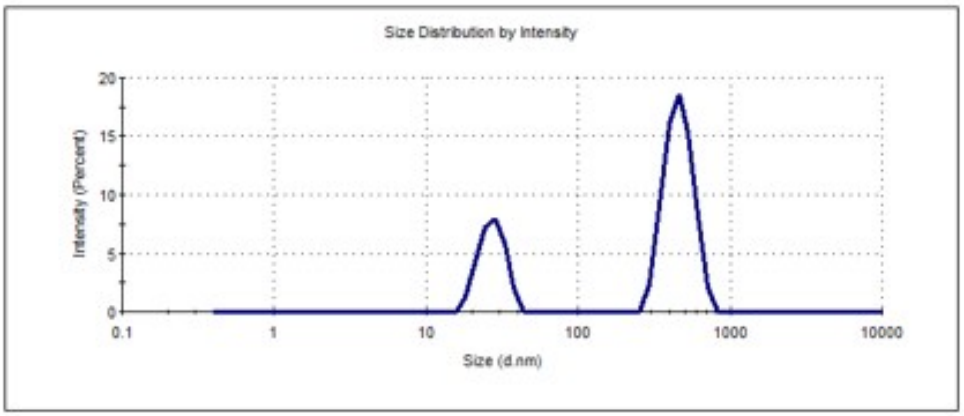

C

		Mean (mV)	Area (%)	St Dev (mV)
Zeta Potential (mV): -5.29	Peak 1:	-5.35	99.8	8.73
Zeta Deviation (mV): 8.73	Peak 2:	58.2	0.2	1.63
Conductivity (mS/cm): 0.0486	Peak 3:	58.8	0.3	6.74e-7

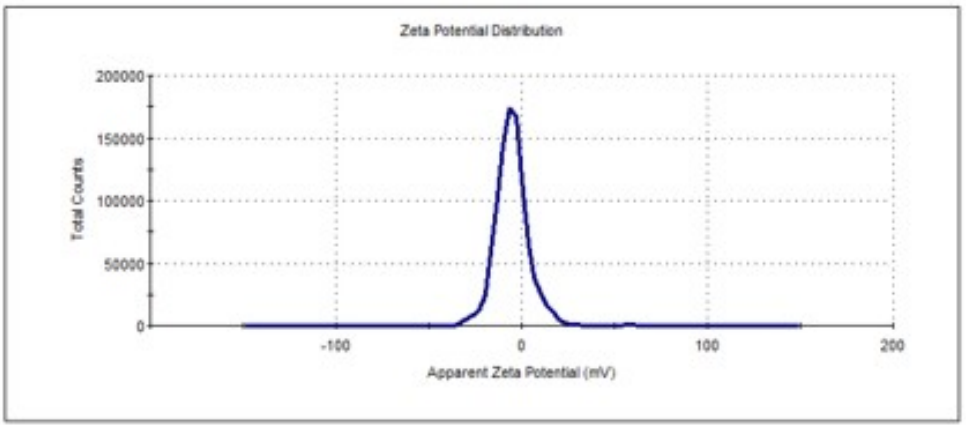

Figure 7.22 (A) Appearance of, size (B) and zeta potential (C) reports of blank mPEG750-PLA1000 NPs prepared using solvent diffusion method

7.9.7 RSV encapsulated in mPEG750-PLA1000 NPs

A

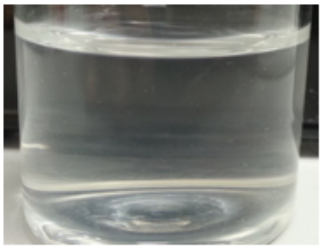

B

		Size (d.nm):	% Intensity:	St Dev (d.nm):
Z-Average (d.nm): 165.5	Peak 1:	179.6	100.0	52.73
PdI: 0.073	Peak 2:	0.000	0.0	0.000
Intercept: 0.942	Peak 3:	0.000	0.0	0.000

Result quality : Good

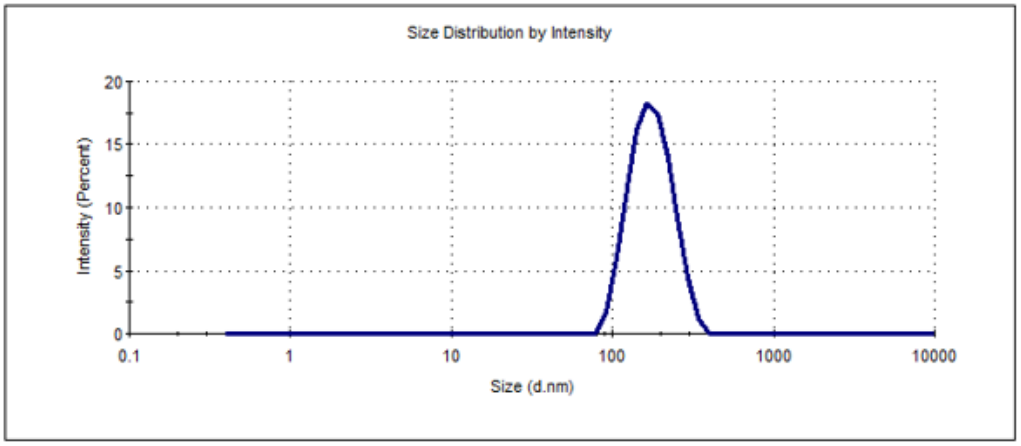

C

		Mean (mV)	Area (%)	St Dev (mV)
Zeta Potential (mV): -11.4	Peak 1:	-11.4	100.0	4.14
Zeta Deviation (mV): 4.14	Peak 2:	0.00	0.0	0.00
Conductivity (mS/cm): 0.0455	Peak 3:	0.00	0.0	0.00

Result quality : Good

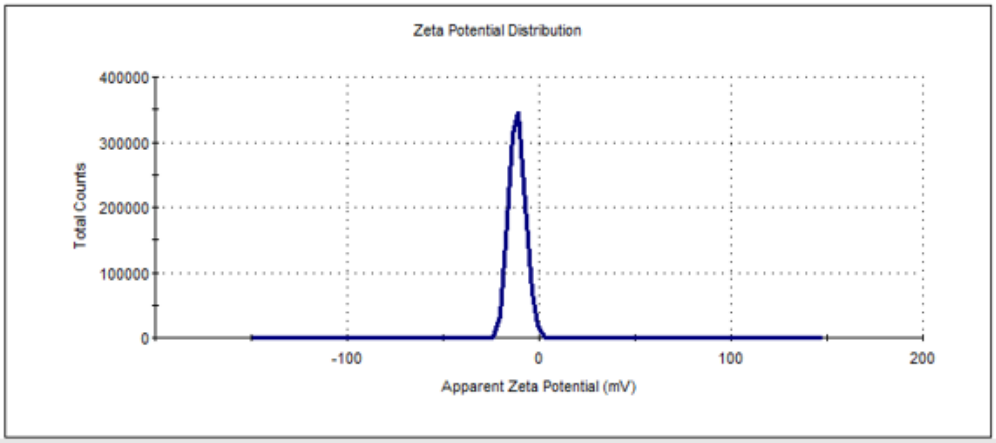

Figure 7.23 (A) Appearance of, size (B) and zeta potential (C) reports for RSV encapsulated in mPEG750-PLA1000 NPs using solvent diffusion method

7.9.8 Blank mPEG750-PCL1000 NPs

A

B

			Size (d.nm):	% Intensity:	St Dev (d.nm):
Z-Average (d.nm):	104.6	Peak 1:	143.9	100.0	84.96
PdI:	0.244	Peak 2:	0.000	0.0	0.000
Intercept:	0.878	Peak 3:	0.000	0.0	0.000
Result quality :	Good				

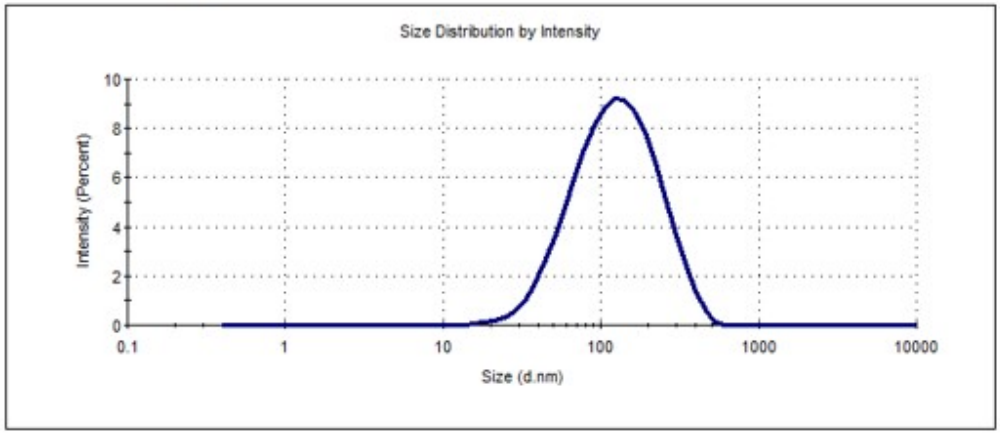

C

			Mean (mV)	Area (%)	St Dev (mV)
Zeta Potential (mV):	-19.4	Peak 1:	-11.8	50.9	5.04
Zeta Deviation (mV):	10.4	Peak 2:	-27.2	48.9	7.18
Conductivity (mS/cm):	0.0441	Peak 3:	10.1	0.2	1.55

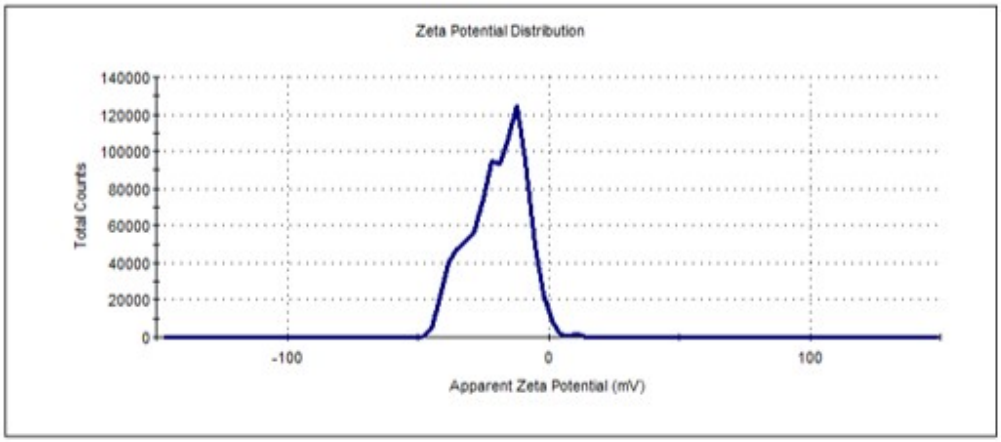

Figure 7.24 (A) Appearance of, size (B) and zeta potential (C) reports for blank mPEG750-PCL1000 NPs prepared using solvent evaporation method and diluted with MQ

7.9.9 RSV encapsulated in mPEG750-PCL1000 NPs

A

B

		Size (d.nm):	% Intensity:	St Dev (d.nm):
Z-Average (d.nm): 198.2	Peak 1:	207.0	100.0	40.03
PdI: 0.034	Peak 2:	0.000	0.0	0.000
Intercept: 0.926	Peak 3:	0.000	0.0	0.000

Result quality : Good

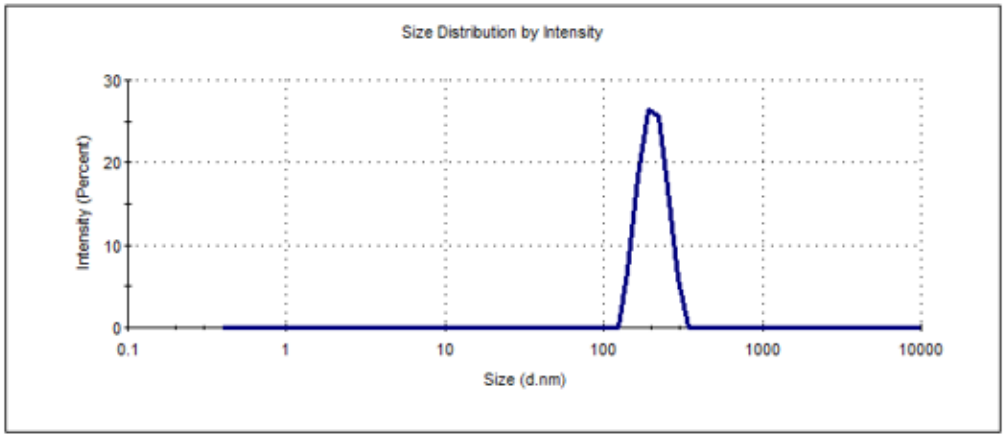

C

		Mean (mV)	Area (%)	St Dev (mV)
Zeta Potential (mV): -20.0	Peak 1:	-20.0	100.0	5.17
Zeta Deviation (mV): 5.17	Peak 2:	0.00	0.0	0.00
Conductivity (mS/cm): 0.0610	Peak 3:	0.00	0.0	0.00

Result quality : Good

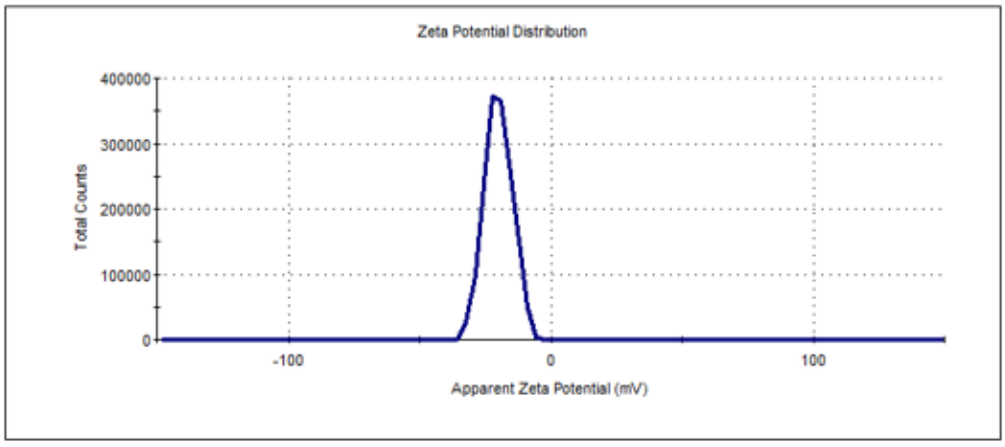

Figure 7.25 (A) Appearance of, size (B) and zeta potential (C) reports for RSV encapsulated in mPEG750-PCL1000 NPs prepared by solvent evaporation method and diluted with MQ

7.9.10 Blank mPEG2000-PLA1000 NPs

A

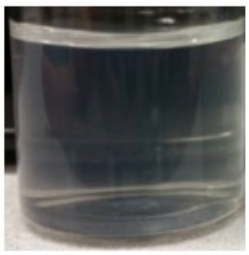

B

		Size (d.nm):	% Intensity:	St Dev (d.nm):
Z-Average (d.nm): 122.6	Peak 1:	192.4	83.9	50.83
PdI: 0.673	Peak 2:	24.33	16.1	5.002
Intercept: 0.907	Peak 3:	0.000	0.0	0.000

Result quality : Good

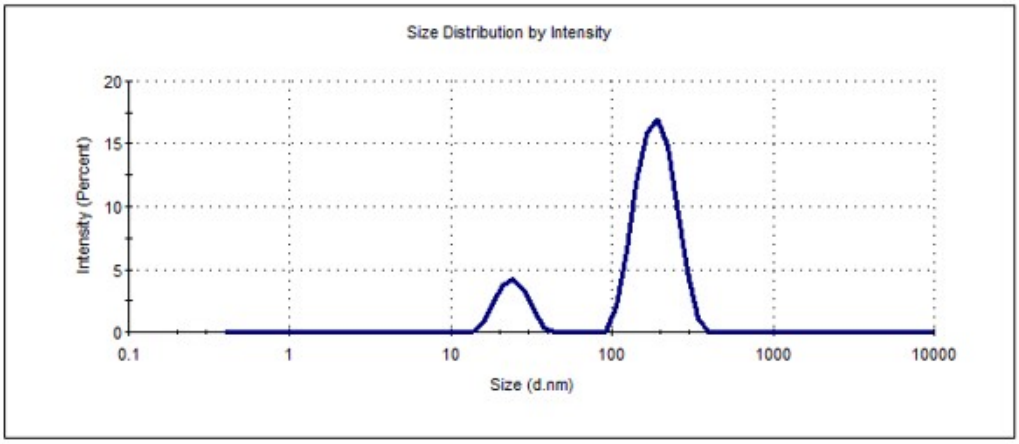

C

		Mean (mV)	Area (%)	St Dev (mV)
Zeta Potential (mV): 2.37	Peak 1:	2.37	100.0	3.61
Zeta Deviation (mV): 3.61	Peak 2:	0.00	0.0	0.00
Conductivity (mS/cm): 0.318	Peak 3:	0.00	0.0	0.00

Result quality : Good

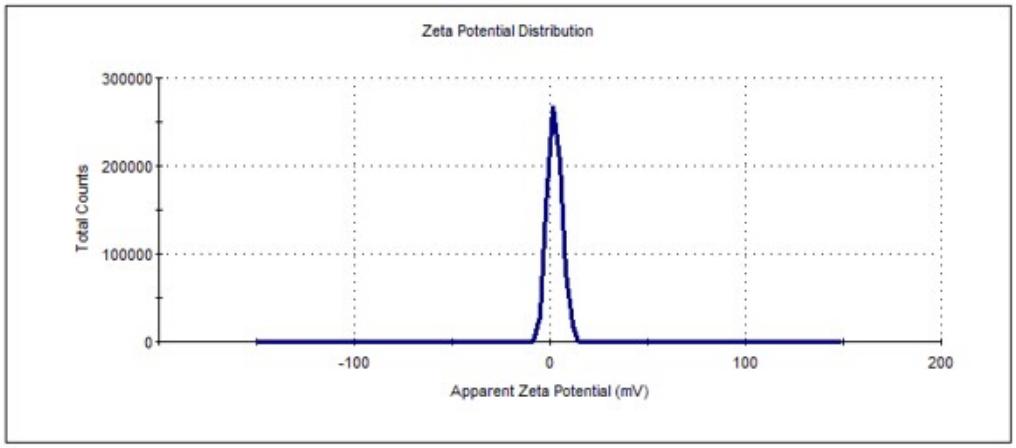

Figure 7.26 (A) Appearance of, size (B) and zeta potential (C) reports for blank mPEG2000-PLA1000 NPs using solvent evaporation method

7.9.11 RSV encapsulated in mPEG2000-PLA1000 NPs

A

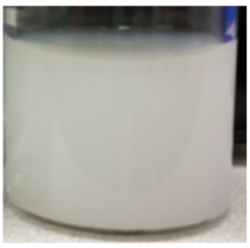

B

		Size (d.nm):	% Intensity:	St Dev (d.nm):
Z-Average (d.nm): 351.8	Peak 1:	353.0	100.0	68.10
PdI: 0.140	Peak 2:	0.000	0.0	0.000
Intercept: 0.875	Peak 3:	0.000	0.0	0.000
Result quality : Good				

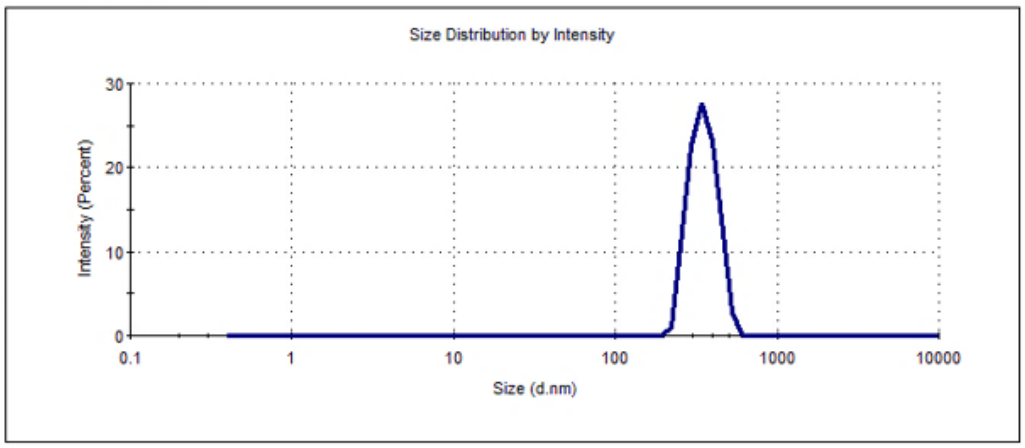

C

		Mean (mV)	Area (%)	St Dev (mV)
Zeta Potential (mV): -0.358	Peak 1:	-0.358	100.0	4.43
Zeta Deviation (mV): 4.43	Peak 2:	0.00	0.0	0.00
Conductivity (mS/cm): 0.336	Peak 3:	0.00	0.0	0.00

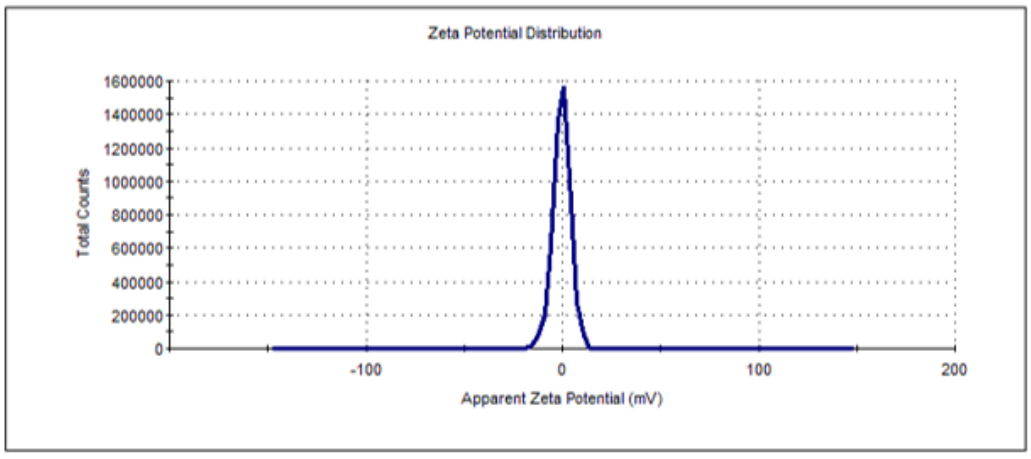

Figure 7.27 (A) Appearance of, size (B) and zeta potential (C) reports for RSV encapsulated in mPEG2000-PLA1000 NPs using solvent evaporation method

7.10 Stability of RSV in buffers at different temperatures for 24 hours

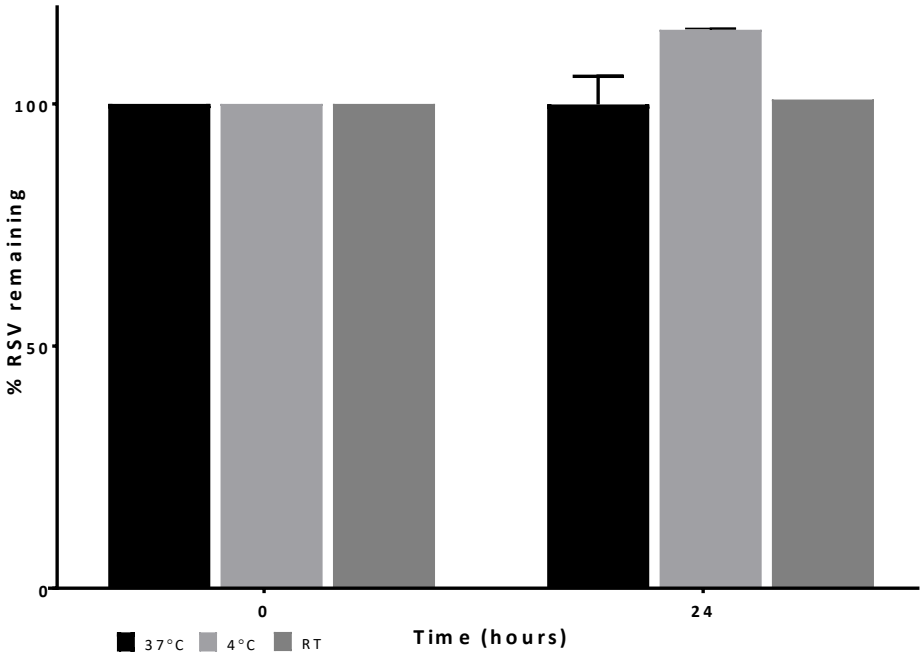

Figure 7.28 Stability of free RSV in acetate buffer (pH4.5) at 37°C, 4°C and RT for 24 hours in the dark

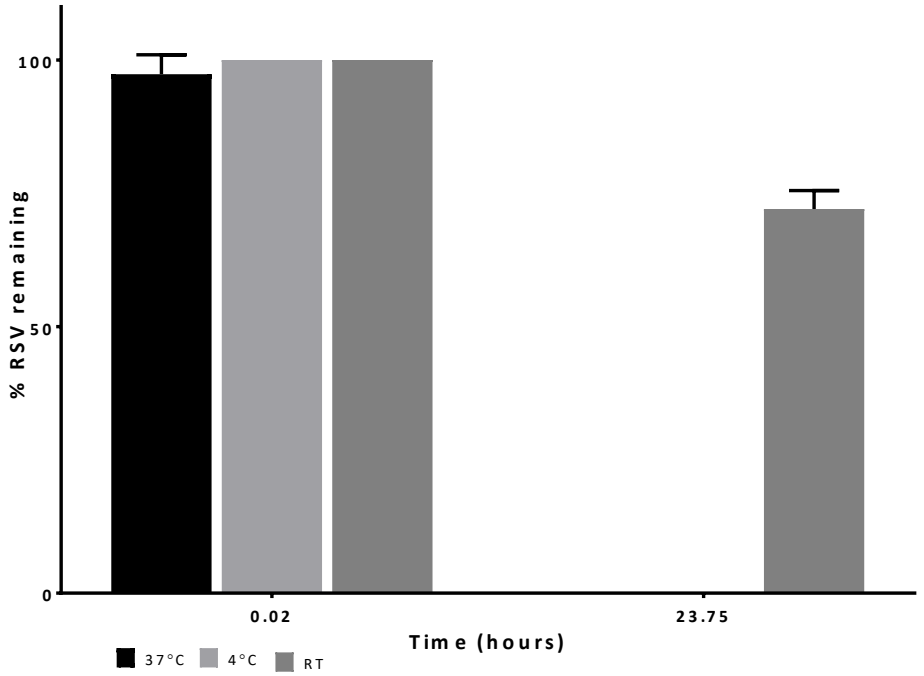

Figure 7.29 Stability of free RSV in phosphate buffer (pH7.4) at 37°C, 4°C and RT for 24 hours in the dark

7.11 Basic cell culture techniques

7.11.1 Cell passaging and plating

Cells were passaged or split into culture flasks to avoid cell death due to overpopulation and to prepare cells for seeding in multi-well plates for experiments. Both B16-F10 and NIH/3T3 cell lines were passaged and plated after achieving 70-80% confluency.

After 70-80% confluency was achieved in T25 flasks by visual microscopic inspection, CGM were aspirated carefully from the culture flask and cells were washed twice with sterile pre-warmed 0.01M PBS. 1mL of pre-warmed Gibco® TrypLE™ Express was added to the flask to dissociate cells from the flask surface and incubated at 37°C for no more than 5 minutes with periodic inspection to ensure cells were not killed by the trypsinisation process. Once cells were detached, 5mL of pre-warmed CGM was added to the flask to stop the trypsinisation followed by centrifugation at 930*g* for 5 minutes at RT in a 15mL conical tube to pellet the cells. The supernatant was discarded and 1mL of pre-warmed CGM was added to resuspend the dark-coloured pellet. Cells were split at ratios between 1:3 to 1:8 into T75 flasks or 1:5 to 1:10 into T25 flasks depending on the experimental schedule with a lower ratio used when large number of cells were needed within a short period of time. Pre-warmed CGM was added to the flask with cells after being split to the volume specified in Table 5.1 and then incubated in an incubator.

Cells were plated into multi-well plates for experiments using cells grown in T75 flasks. After trypsinisation and pelleting, the supernatant was discarded and 1mL of pre-warmed CGM was added to resuspend the pellet. A trypan blue exclusion method was used to count the number of cells using a haemocytometer. Briefly, 20μL of dispersed cells was diluted 1:1 with 20μL 0.4% *w/v* trypan blue in PBS. 10μL of the cell suspension with trypan blue was loaded onto a haemocytometer and viable cells in the four outer set of 16 squares (quadrants, labelled 1 to 4) were counted using a light microscope at 40× magnification (Figure 7.30).

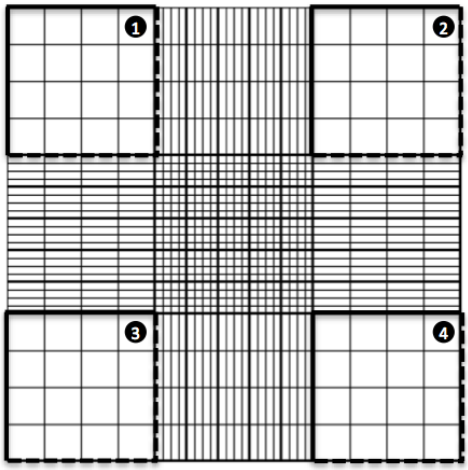

Figure 7.30 Haemocytometer grid lines and four quadrants used for counting cells
Image from CellularChronicler (2016)

Cell viability was observed and ensured to be above 95%. Only unstained viable cells were counted and the average of four quadrants were used to calculate the number of cells in 1mL resuspended cells as follows:

Number of cells in 1mL = average number of viable cells of 4 quadrants × 10^4 × 2 (dilution factor) × 1mL

Cells were then seeded at 2000 cells in 100μL pre-warmed CGM per well in 96-well plates and 250000 cells in 1mL pre-warmed CGM per well in 6-well plates. Seeding number of cells in 96-well plates were determined using a B16-F10 cell calibration curve in Appendix 7.12. Doubling time for B16-F10 cell line was about 18-24 hours and for NIH/3T3 cell line was about 24-36 hours when seeded at the exponential growth phase of the cells.

7.11.2 Cryopreservation of cells

Cryopreservation of grown B16-F10 cells was to avoid freeze-thaw cycles in the original cell line stock and to preserve lower passage numbers for long-term experiments within 6 months period. Upon receipt from the supplier, an aliquot of B16-F10 cell line stock was grown in T25 culture flasks with 7mL CGM prepared in Section 5.3 for up to three passages with remaining cell stock frozen in liquid nitrogen at the CHIRI facility. A solution of cryo-protectant was prepared with 1:4 *v/v* of molecular grade DMSO and CGM. Once cells were at exponential growing phase, cells

were detached from flasks and 500μL aliquots of minimum 1×10^6 cells were added with 500μL cryo-protectant in a 2mL Greiner Bio-One Cryo.s™ cryopreservation vial. Multiple vials of passages between 4 to 8 were cryo-frozen at -80°C. NIH/3T3 cells cryo-frozen between passages 8-10 were obtained from a colleague and treated as our cell line stock. The cell line was also cryo-frozen in multiple cryopreservation vials at passages between 10-12.

7.11.3 Resurrection of cells

Cells were removed from cryo-freeze and allowed to thaw slowly to RT. Once thawed, the cells were transferred into a 15mL Greiner Bio-One conical tube with 5mL pre-warmed CGM. The cells were pelleted at 930*g* for 5 minutes at RT to remove debris and dead cells. Once supernatant was discarded, the cells were resuspended with 7mL pre-warmed CGM and transferred into T25 culture flasks. The flask was then incubated in an incubator. Cells were observed daily for growth and passaged once more as per Section 7.11.1 before allowed to be used for experiments.

7.12 B16-F10 cell calibration for plate reader

To assess the optimal number of cells to seed in a 96-well plate for the span of the experiment, we have carried out a cell growth calibration curve by seeding 1000, 2500, 5000, 7500 and 10000 B16-F10 cells per well in quadruplet, allowed to adhere and grown for 24 hours, 48 hours and 72 hours. After incubation, an MTT assay was carried out without treatment as per Section 5.4.5 and absorbance was recorded. Results were presented as absorbance against the number of cells seeded in each well (Figure 7.31). An optimal number of cells was chosen for seeding.

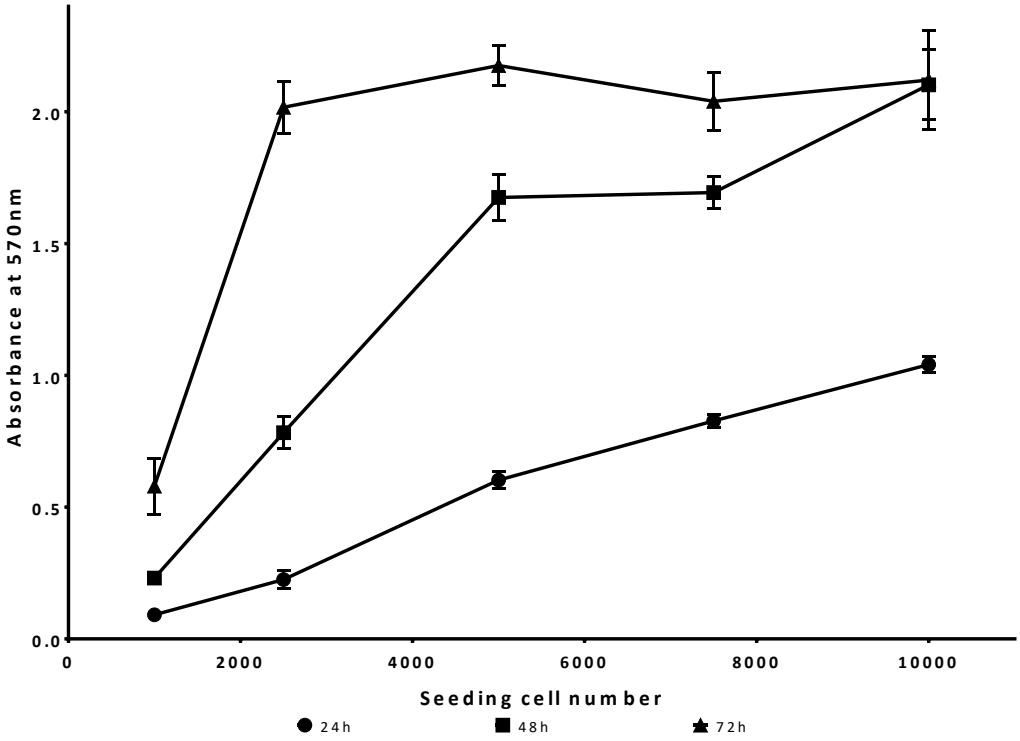

Figure 7.31 Calibration curve for seeding of cells in a 96-well cell culture plate

Figure 7.32 represented microscopic pictures of B16-F10 cells seeded at 2000 cells per well and allowed to grow for 24 hours, 48 hours and 72 hours. B16-F10 cells were spindle-shaped and epithelial-like. Cells were very dense and evidence of layering was visible after 72 hours of growth which would most likely result in cell death due to spatial and nutrition constraints.

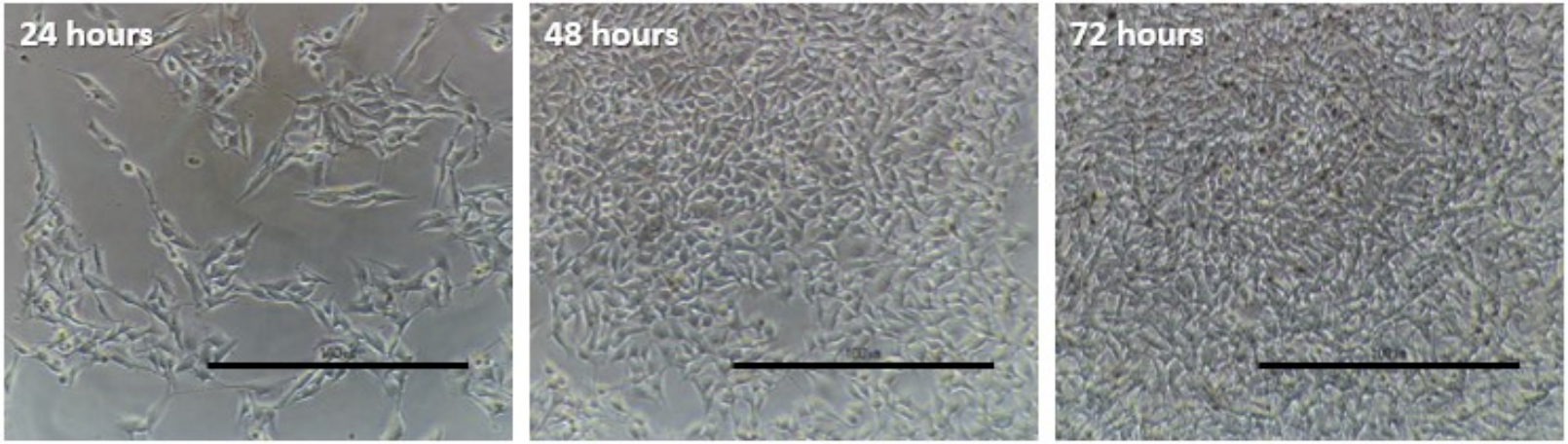

Figure 7.32 B16-F10 cells under light microscope at incubation times of 24, 48 and 72 hours

Scale bar = 100μm

7.13 Effect of RSV on B16-F10 cell morphology

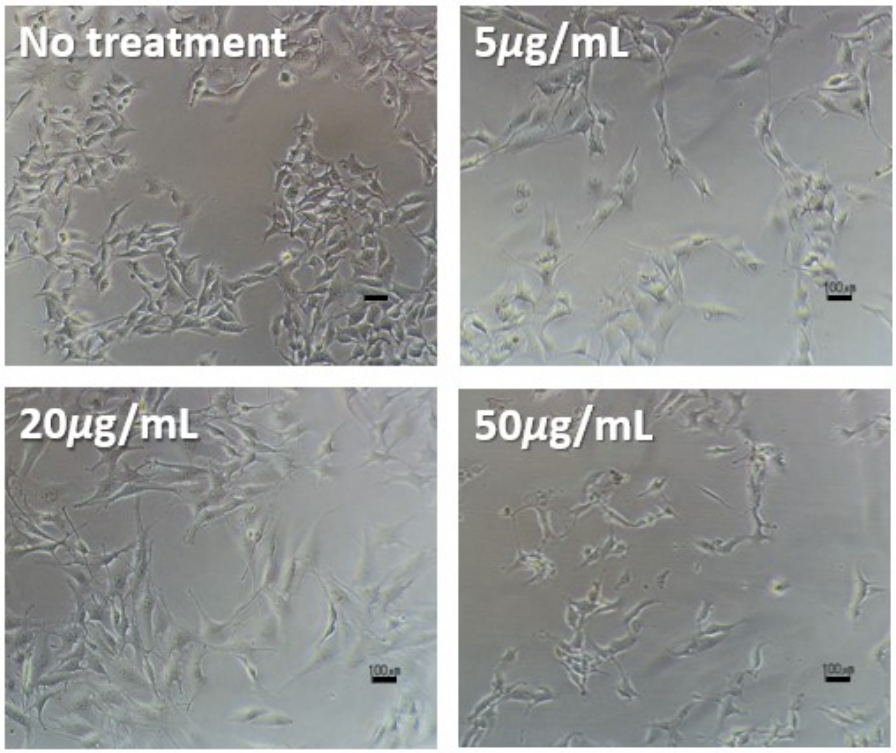

Figure 7.33 B16-F10 cells under optical microscope after treatment with free RSV at 5, 20 and 50μg/mL for 24 hours

Scale bar = 100μm

Figure 7.33 represented B16-F10 cells before treatment and after being treated with 5μg/mL, 20μg/mL and 50μg/mL free RSV for 24 hours. After treatment with 5μg/mL and 20μg/mL of RSV, the cells appeared to distend. The microscope image of cells with 50μg/mL RSV treatment showed dead cells floating as debris and cell shrinkage indicating a loss of adherence. The morphological change in the cells was observed in lung cancer cells treated with cytotoxic NPs in Jiang *et al.* (2015) and in B16-F10 cells reported by Purushotham *et al.* (2016). These characteristics were indicative of apoptosis (Dun *et al.* 2015). Figure 7.34 represented B16-F10 cells before treatment and treated with 10μg/mL and 20μg/mL free RSV for 48 hours. Similar to the 24-hour treatments, cells appeared to distend before death, however, with a longer 48-hour treatment, a lower dose of RSV achieved the same effect compared to the 24-hour treatment.

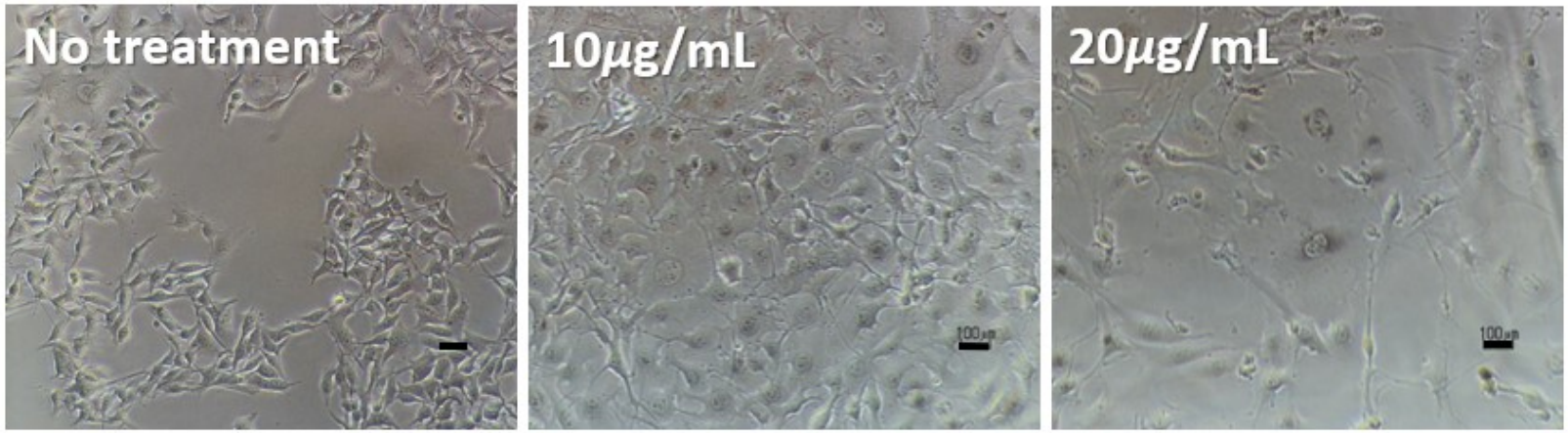

Figure 7.34 B16-F10 cells under optical microscope after treatment with free RSV at 10 and 20μg/mL for 48 hours

Scale bar = 100μm

7.14 RSV concentration in NPs in rat plasma and HLM assays

Table 7.7 shows the final RSV equivalent concentrations of conjugated RSV NPs in assays for the plasma stability study of conjugated RSV NPs.

Table 7.7 Final RSV equivalent concentrations of conjugated RSV NPs in rat plasma for *in vitro* plasma stability study of conjugated RSV NPs

Conjugated RSV NPs	**% *w/w* RSV conjugate in NPs**	**Total RSV equivalent concentration in NPs (mg/mL)**
mPEG750-PLA1000-succ-RSV NPs	63.9	0.76
mPEG750-PLA1000-glu-RSV NPs	54.8	9.27
mPEG750-PCL1000-succ-RSV NPs	99.3	1.63
mPEG2000-PLA1000-succ-RSV NPs	76.1	8.72
PEG5000-O-RSV NPs	100.0	0.44

Table 7.8 shows the final RSV equivalent concentrations of conjugated RSV NPs in assays for the HLM stability study of conjugated RSV NPs.

Table 7.8 Final RSV equivalent concentrations of conjugated RSV NPs in HLM for *in vitro* microsomal stability study of conjugated RSV NPs

Conjugated RSV NPs	**% *w/w* RSV conjugate in NPs**	**Total RSV equivalent concentration in NPs (mg/mL)**
mPEG750-PLA1000-succ-RSV NPs	63.9	0.38
mPEG750-PLA1000-glu-RSV NPs	54.8	0.54
mPEG750-PCL1000-succ-RSV NPs	99.3	0.11
mPEG2000-PLA1000-succ-RSV NPs	76.1	0.26
PEG5000-O-RSV NPs	100.0	0.022

7.15 Flow cytometry gating strategies

Selection of analysis region for apoptosis assays were carried out on untreated cells grown alongside cells with the following staining:

1) Cells with no stains
2) Cells stained with FITC
3) Cells stained with PI
4) Cells stained with both FITC and PI

Figure 7.35 displays the identification and selection of a cluster of cells as B16-F10 cells based on the size (forward scatter, FSC) and granularity (side scatter, SSC) of cells and to exclude debris in our 24-hour assay.

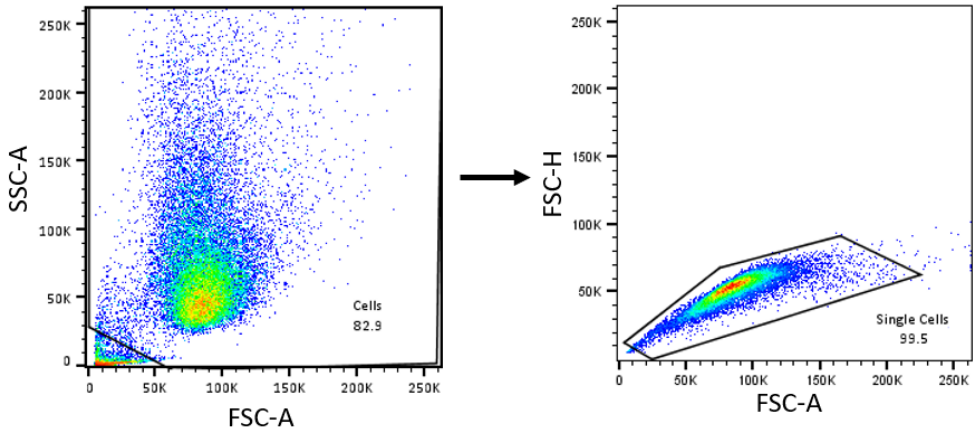

Figure 7.35 B16-F10 cell population selected for analysis in 24-hour apoptosis assays

Following this, a double-stained untreated cell sample was used for defining individual populations for apoptosis and necrosis, which automatically quantified the number of cells in each quadrant (Figure 7.36) (Jiang *et al.* 2015).

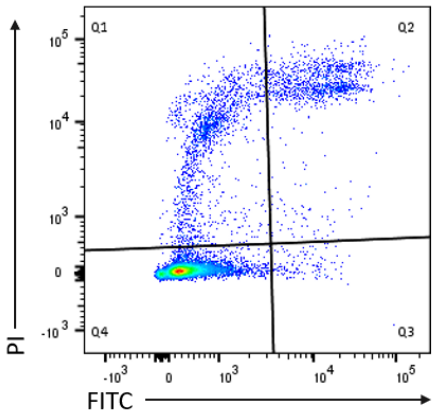

Quadrant	FITC	PI	Cell population
Q1	-	+	Necrotic
Q2	+	+	Late apoptotic
Q3	+	-	Early apoptotic
Q4	-	-	Viable

Figure 7.36 Gating for individual cell populations in 24-hour apoptosis assays

Figure 7.37 depicts the gating strategies for the 48-hour apoptosis assays determined similarly to the 24-hour assays.

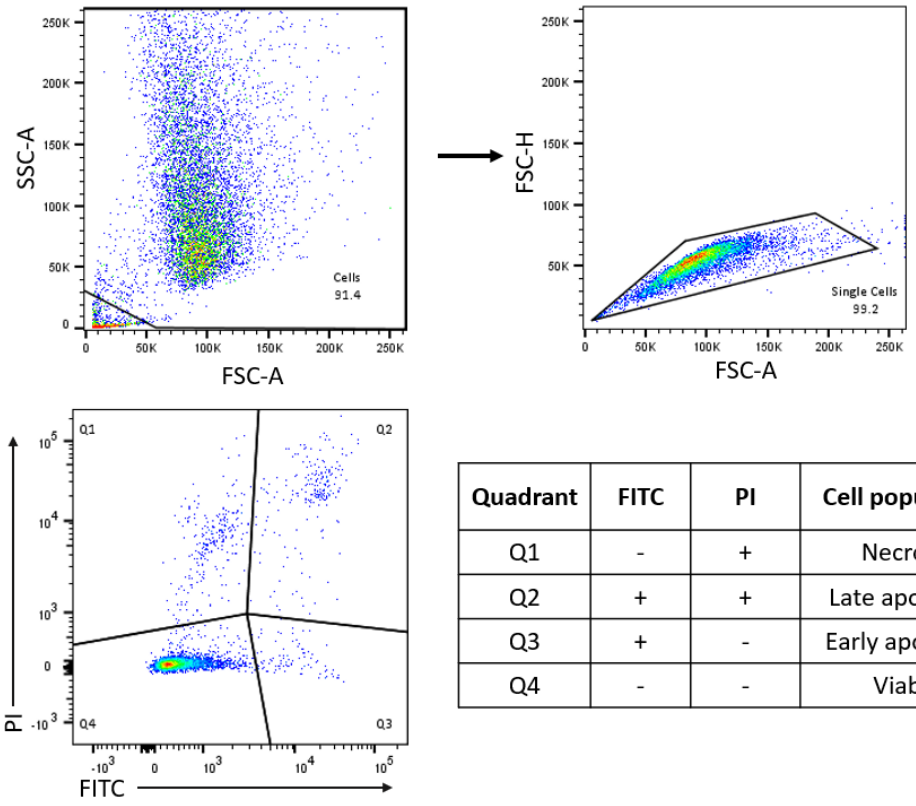

Quadrant	FITC	PI	Cell population
Q1	-	+	Necrotic
Q2	+	+	Late apoptotic
Q3	+	-	Early apoptotic
Q4	-	-	Viable

Figure 7.37 Gating strategy for 48-hour apoptosis assays

In summary, cells were discriminated into populations detailed in Table 7.9.

Table 7.9 Cell populations for Annexin V-FITC and PI apoptosis assay

Stains	Cell populations			
	Live or viable	Early apoptosis	Late apoptosis	Necrosis
FITC	-	+	+	-
PI	-	-	+	+

7.16 Animal ethics committee application approval AEC_2016_28

Curtin University

17 August 2016

Office of Research and Development

Building 100 Level 1 West
Dumas Road
Bentley Western Australia 6102

GPO Box U1987
Perth Western Australia 6845

Telephone +61 8 9266 7863
Facsimile +61 8 9266 3793
Web research.curtin.edu.au

Animal Ethics Committee

Telephone +61 8 9266 2784
Facsimile +61 8 9266 3793
Email aec@curtin.edu.au

Dr Yan Chen
Curtin University

Dear Yan

Animal Ethics

Approval Number: **AEC_2016_28**
Project Title: *An in vivo study on the anticancer properties and pharmacokinetic profiles of novel resveratrol formulations (Application Number 20-2016)*

Thank you for providing additional information for the project titled "*An in vivo study on the anticancer properties and pharmacokinetic profiles of novel resveratrol formulations*". The information you have provided has satisfactorily addressed the queries raised by the Committee.

Your application has been **approved** and the relevant approval number is **AEC_2016_28** and the period of the project approval is from 17/08/2016 to 17/08/2020.

Species Approved	No
Mouse C57BL/6J	164
Rat Wistar	38

OTHER REQUIREMENTS/NOTES

An Annual Progress Report must be submitted to the Ethics Office annually, on the anniversary of approval.

An Annual Animal Use Report that captures the relevant details regarding the number of animals used in the preceding year i.e. 1 January to 31 December must be submitted before 31 January of the following year.

Any amendments to the approved protocol must be submitted to the Ethics Office.

A Completion Report must be submitted to the Ethics Office on completion of the project.

You are reminded that it is your responsibility to maintain your own animal records and to report annually to the Committee.

Should any animal(s) experience an adverse or unexpected outcome resulting from the experimentation, the AEC is to be notified in writing immediately.

Please ensure that you quote the Animal Ethics Committee approval number whenever you order animals for this project. Note also that an AEC approval number must be displayed on the cage(s)/aquaria etc used to house/maintain animals during an approved activity.

If the results of this research will be published, citations should state: "All experiments were performed according to the Australian Code of Practice for the care and use of animals for scientific purposes".

Regards

Dr Beng Hooi Chua
Deputy Chairperson, Animal Ethics Committee

7.17 Body weight of C57BL/6J male mice from ARC

Table 7.10 Average and range of body weights of C57BL/6J male mice

Age (days)	21	42	56	84
Average (g)	8	21	23	27
Range (g)	6-10	18-23	21-25	24-29

Mice obtained from the ARC (Animal Resources Centre 2018)

7.18 *in vivo* B16-F10 tumour characteristics

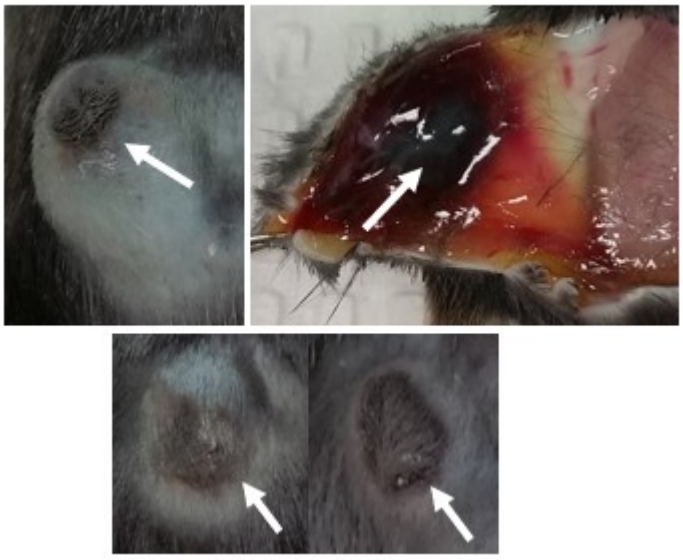

Figure 7.38 Example of tumours developing necrosis (external views and internally post-euthanasia) on B16-F10 tumour-bearing C57BL/6J mice

White arrows indicate the tumour location

Figure 7.38 depicted examples of tumours visibly developing necrosis externally and a representation of a necrotic tumour excised after euthanasia. Necrotic tumours in our studies were less intact, had high vascularisation and yellow-tinged or clear fluids surrounding the tumour. Seepage was not visible externally. Various levels of vascularisation were observed throughout the study and are represented graphically in Figure 7.39.

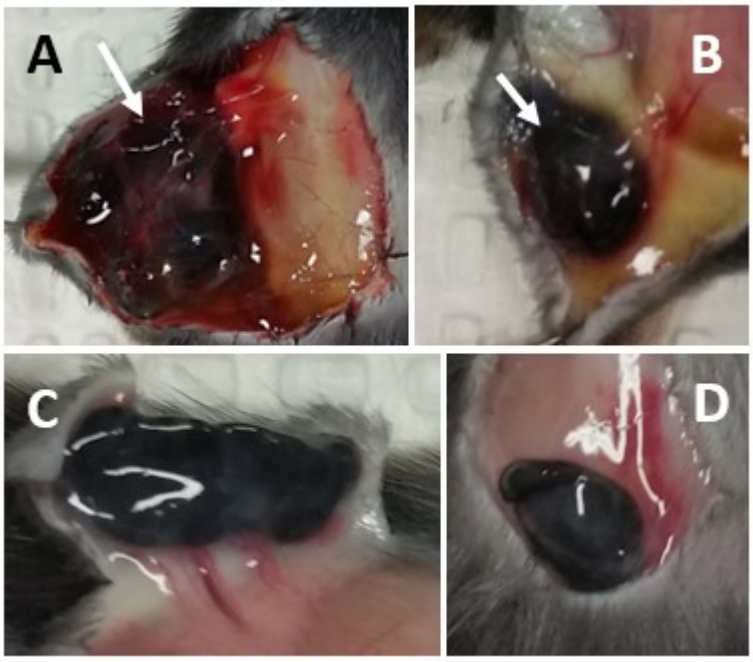

Figure 7.39 Levels of vascularisation of B16-F10 tumours in C57BL/6J mice after euthanasia (A: high; B: mid; C and D: low)

The top two images (A and B) showed high vascularisation and mid-range vascularisation, respectively. These observations were consistent with B16-F10 animal models where inflammation, haemorrhaging, necrosis and vascularisation are indicative of a healthy growing tumour (Correa *et al.* 2005, Burghoff *et al.* 2014, Danciu *et al.* 2015, Zhang *et al.* 2015). High vascularisation was characteristic of a rapidly growing tumour which was usually accompanied with inflammation and necrosis (Burghoff *et al.* 2014). The bottom two images (C and D) showed low or no vascularisation and tumours in these cases tended to be more intact in shape with very little or no fluids within the tumour environment. The tumours were easily removed from the carcass compared to their necrotic counterparts. Low or no vascularisation was indicative of a slow growing or retarded tumour (Danciu *et al.* 2015).

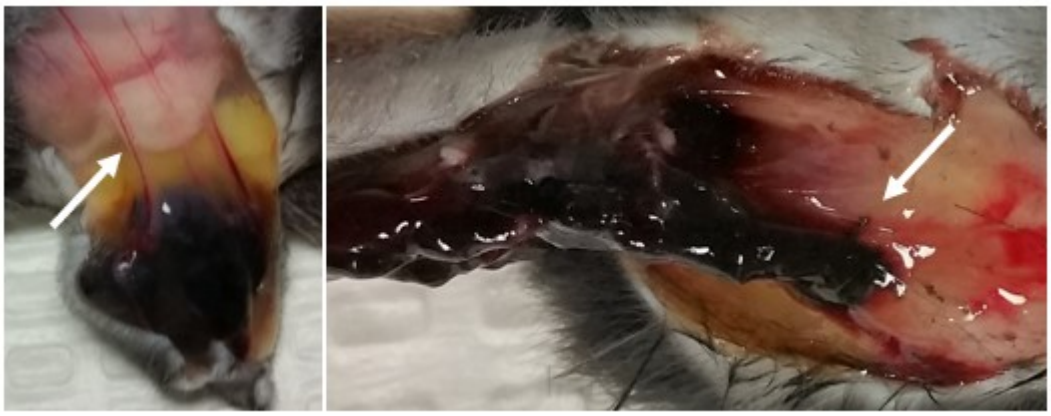

Figure 7.40 B16-F10 tumours metastasis in C57BL/6J mice
White arrow indicates tumour infiltration in dermal and fatty layers of animal

Figure 7.40 illustrated the aggressiveness of B16-F10 tumours where the tumours started to infiltrate the dermal and fatty layers of the animal. The occurrence was low (<9% in animals of the whole study) but it should be noted that these tumours had very high vascularisation and were necrotic. The incidences of these tumours were only observed in the IT cohort. This was supported by Zang *et al.* (2015) and Fairchild *et al.* (2011) where B16-F10 animal models were known to be highly invasive and metastasize at early stages of tumour growth.

7.19 Visualisation of palpable tumour

Treatment for the IT cohort started when the tumours were palpable (approximately 30-40mm^3) which took about seven days to grow from inoculation (Figure 7.41).

Figure 7.41 Example of palpable tumour (white circle) on an animal in the IT cohort

The tumour appeared as a small hump at the site of inoculation enabling us to inject the treatments directly into the tumour.

7.20 IT cohort

Figure 7.42 represented examples of tumours of each treatment group at their respective end-points in the IT cohort. Images C to E showed extra fluids surrounding the tumour (yellowish or clear) compared to tumours of the control groups (A and B). This could have contributed to its larger sizes and hence an earlier termination before the designated treatment end-point was required. Animals treated with free RSV had tumours which appeared less solid than the other treatment groups and could be due to the strong apoptotic or necrotic effect which resulted in a breakdown of cancer cells. From the apoptosis assay (Section 5.5.7) and microscope images of B16-F10 cells treated with the RSV formulations (Section 5.5.5), the cellular cytoplasm of treated cells appeared to swell which then resulted in cell death by eruption. The seepage and haemorrhaging into the tumour environment and also inflammation of the cells due to apoptosis could have increased the tumour size exaggeratedly when measured externally. Evidence of necrosis and inflammation was observed in Carletto *et al.* (2016) after histology analyses on B16-F10 tumours from tumour-bearing mice treated with free RSV and encapsulated RSV capsules.

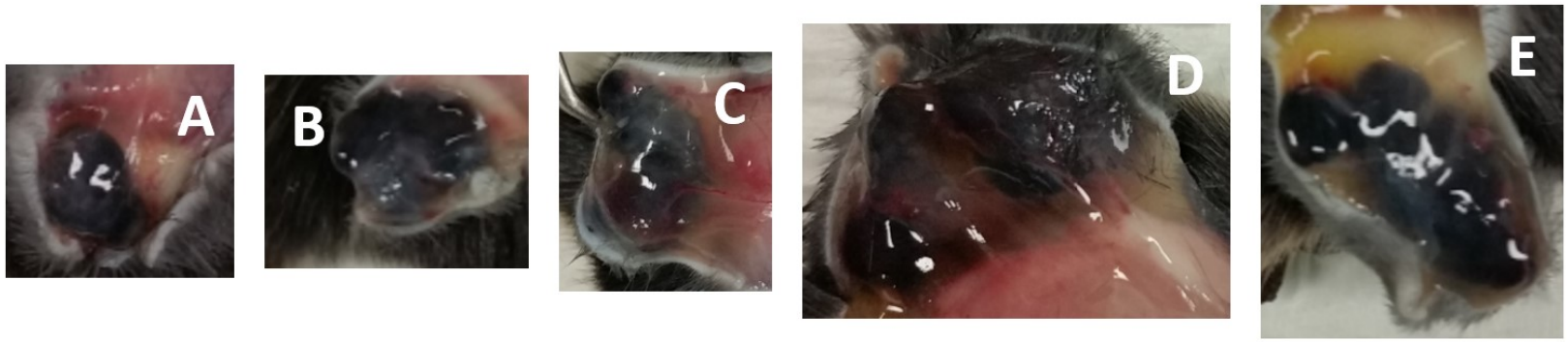

Figure 7.42 Representative tumours of each treatment group at respective end-points in IT cohort

Scale 1:1
A: 20% HPCD at day 8; B: Blank mPEG750-PLA1000 NPs at day 8; C: Encapsulated RSV NPs at day 10; D: RSV in 20% HPCD at day 6; and, E: Conjugated RSV NPs at day 10.

7.21 IP cohort

Figure 7.43 showed tumours excised from each treatment group of the IP cohort. As the tumour age of the IP cohort was younger than those in the IT cohort, less seepage and inflammation was observed in the tumour surroundings. Nonetheless, inflammation was visible in treatment groups, less so in conjugated RSV NPs.

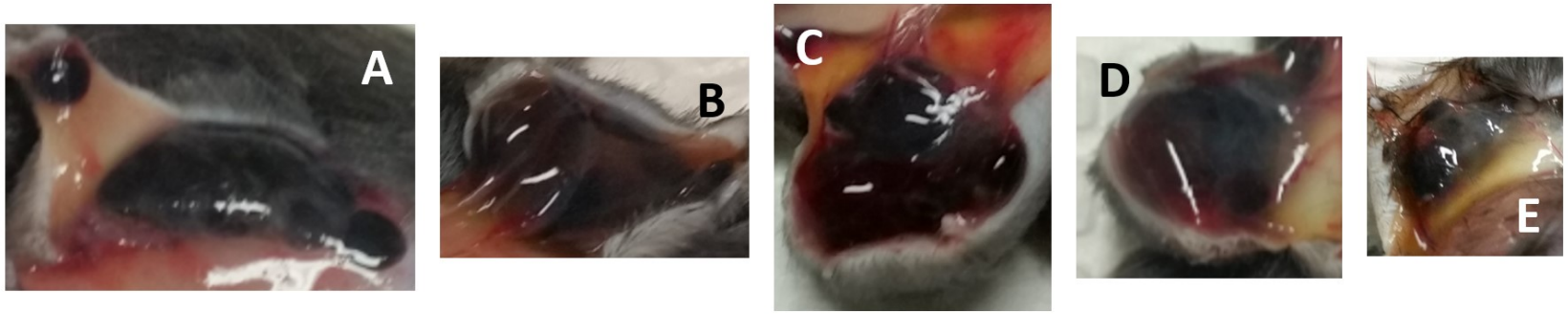

Figure 7.43 Representation of tumours from each treatment group at the end of study in IP cohort

Scale 1:1
A: 20% HPCD; B: mPEG750-PLA1000 polymer in MQ; C: Encapsulated RSV NPs; D: RSV in 20% HPCD; and, E: Conjugated RSV NPs.

LIST OF PRESENTATIONS AND PUBLICATIONS

Journal publication

- **Ng, Y.-J.**, Benson, H. A. E., Brown, D. H., & Chen, Y. (2015). Synthesis and Characterization of Novel Copolymeric Resveratrol Conjugates. *Journal of Chemistry, 2015*, 1-6

Posters

- **Yee, Y.-J.**, Benson, H., Dass, C. and Chen Y. "A Preliminary Study on the Anti-Melanoma Effect of Resveratrol Nanoparticle Formulations." In *Mark Liveris Research Student Seminar*. Perth, Australia, 2017.
- **Yee, Y.-J**., Benson, H., Dass, C. and Chen Y. "A Preliminary Study on the Anti-Melanoma Effect of Resveratrol Nanoparticle Formulations." In *Science on the Swan Conference*. Fremantle, Australia, 2017
- **Ng, Y. J.**, Benson, H.A.E., Brown, D.H. and Chen Y. "Synthesis and Characterisation of Novel Polymeric Conjugates of Resveratrol." In *Drug Delivery Australia and 6th Annual Meeting of the Australian Chapter of the Controlled Release Society*. Parkville, Australia, 2012.
- **Ng, Y. J.**, Brown, D.H., Benson, H.A. and Chen Y. "Effect of Hydrophobic Chain Length in Synthetic Methoxy-Poly(Ethylene Glycol)-Poly(*ε*-Caprolactone) for Use in Drug Delivery " In *International Conference on Nanoscience and Nanotechnology (ICONN)*. Perth, Australia, 2012.

Oral presentations

- School of Pharmacy seminars
- Curtin Health Innovation Research Institute (CHIRI) Journal Club

COPYRIGHT LICENSES AND PERMISSIONS

License for Figure 1.2

ELSEVIER LICENSE
TERMS AND CONDITIONS

Sep 10, 2018

This Agreement between Ms. Yan Jing Yee ("You") and Elsevier ("Elsevier") consists of your license details and the terms and conditions provided by Elsevier and Copyright Clearance Center.

License Number	4362470875640
License date	Jun 05, 2018
Licensed Content Publisher	Elsevier
Licensed Content Publication	Archives of Biochemistry and Biophysics
Licensed Content Title	The bioavailability and distribution of trans-resveratrol are constrained by ABC transporters
Licensed Content Author	Joana M. Planas,Irene Alfaras,Helena Colom,M. Emília Juan
Licensed Content Date	Nov 15, 2012
Licensed Content Volume	527
Licensed Content Issue	2
Licensed Content Pages	7
Start Page	67
End Page	73
Type of Use	reuse in a thesis/dissertation
Portion	figures/tables/illustrations
Number of figures/tables/illustrations	1
Format	both print and electronic
Are you the author of this Elsevier article?	No
Will you be translating?	No
Original figure numbers	Figure 1
Title of your thesis/dissertation	Evaluation of Novel Resveratrol Conjugate and Nanoparticle Formulations for Enhanced Anticancer Activity
Expected completion date	Aug 2018
Estimated size (number of pages)	300
Requestor Location	Ms. Yan Jing Yee 76 Selway Road Brentwood

	Perth, Western Australia 6153 Australia Attn: Ms. Yan Jing Yee
Publisher Tax ID	GB 494 6272 12
Total	0.00 AUD
Terms and Conditions	

INTRODUCTION

1. The publisher for this copyrighted material is Elsevier. By clicking "accept" in connection with completing this licensing transaction, you agree that the following terms and conditions apply to this transaction (along with the Billing and Payment terms and conditions established by Copyright Clearance Center, Inc. ("CCC"), at the time that you opened your Rightslink account and that are available at any time at http://myaccount.copyright.com).

GENERAL TERMS

2. Elsevier hereby grants you permission to reproduce the aforementioned material subject to the terms and conditions indicated.

3. Acknowledgement: If any part of the material to be used (for example, figures) has appeared in our publication with credit or acknowledgement to another source, permission must also be sought from that source. If such permission is not obtained then that material may not be included in your publication/copies. Suitable acknowledgement to the source must be made, either as a footnote or in a reference list at the end of your publication, as follows:

"Reprinted from Publication title, Vol /edition number, Author(s), Title of article / title of chapter, Pages No., Copyright (Year), with permission from Elsevier [OR APPLICABLE SOCIETY COPYRIGHT OWNER]." Also Lancet special credit - "Reprinted from The Lancet, Vol. number, Author(s), Title of article, Pages No., Copyright (Year), with permission from Elsevier."

4. Reproduction of this material is confined to the purpose and/or media for which permission is hereby given.

5. Altering/Modifying Material: Not Permitted. However figures and illustrations may be altered/adapted minimally to serve your work. Any other abbreviations, additions, deletions and/or any other alterations shall be made only with prior written authorization of Elsevier Ltd. (Please contact Elsevier at permissions@elsevier.com). No modifications can be made to any Lancet figures/tables and they must be reproduced in full.

6. If the permission fee for the requested use of our material is waived in this instance, please be advised that your future requests for Elsevier materials may attract a fee.

7. Reservation of Rights: Publisher reserves all rights not specifically granted in the combination of (i) the license details provided by you and accepted in the course of this licensing transaction, (ii) these terms and conditions and (iii) CCC's Billing and Payment terms and conditions.

8. License Contingent Upon Payment: While you may exercise the rights licensed immediately upon issuance of the license at the end of the licensing process for the transaction, provided that you have disclosed complete and accurate details of your proposed use, no license is finally effective unless and until full payment is received from you (either by publisher or by CCC) as provided in CCC's Billing and Payment terms and conditions. If full payment is not received on a timely basis, then any license preliminarily granted shall be deemed automatically revoked and shall be void as if never granted. Further, in the event that you breach any of these terms and conditions or any of CCC's Billing and Payment terms and conditions, the license is automatically revoked and shall be void as if never granted. Use of materials as described in a revoked license, as well as any use of the

materials beyond the scope of an unrevoked license, may constitute copyright infringement and publisher reserves the right to take any and all action to protect its copyright in the materials.
9. Warranties: Publisher makes no representations or warranties with respect to the licensed material.
10. Indemnity: You hereby indemnify and agree to hold harmless publisher and CCC, and their respective officers, directors, employees and agents, from and against any and all claims arising out of your use of the licensed material other than as specifically authorized pursuant to this license.
11. No Transfer of License: This license is personal to you and may not be sublicensed, assigned, or transferred by you to any other person without publisher's written permission.
12. No Amendment Except in Writing: This license may not be amended except in a writing signed by both parties (or, in the case of publisher, by CCC on publisher's behalf).
13. Objection to Contrary Terms: Publisher hereby objects to any terms contained in any purchase order, acknowledgment, check endorsement or other writing prepared by you, which terms are inconsistent with these terms and conditions or CCC's Billing and Payment terms and conditions. These terms and conditions, together with CCC's Billing and Payment terms and conditions (which are incorporated herein), comprise the entire agreement between you and publisher (and CCC) concerning this licensing transaction. In the event of any conflict between your obligations established by these terms and conditions and those established by CCC's Billing and Payment terms and conditions, these terms and conditions shall control.
14. Revocation: Elsevier or Copyright Clearance Center may deny the permissions described in this License at their sole discretion, for any reason or no reason, with a full refund payable to you. Notice of such denial will be made using the contact information provided by you. Failure to receive such notice will not alter or invalidate the denial. In no event will Elsevier or Copyright Clearance Center be responsible or liable for any costs, expenses or damage incurred by you as a result of a denial of your permission request, other than a refund of the amount(s) paid by you to Elsevier and/or Copyright Clearance Center for denied permissions.

LIMITED LICENSE

The following terms and conditions apply only to specific license types:
15. **Translation**: This permission is granted for non-exclusive world **English** rights only unless your license was granted for translation rights. If you licensed translation rights you may only translate this content into the languages you requested. A professional translator must perform all translations and reproduce the content word for word preserving the integrity of the article.
16. **Posting licensed content on any Website**: The following terms and conditions apply as follows: Licensing material from an Elsevier journal: All content posted to the web site must maintain the copyright information line on the bottom of each image; A hyper-text must be included to the Homepage of the journal from which you are licensing at http://www.sciencedirect.com/science/journal/xxxxx or the Elsevier homepage for books at http://www.elsevier.com; Central Storage: This license does not include permission for a scanned version of the material to be stored in a central repository such as that provided by Heron/XanEdu.
Licensing material from an Elsevier book: A hyper-text link must be included to the Elsevier homepage at http://www.elsevier.com . All content posted to the web site must maintain the copyright information line on the bottom of each image.

Posting licensed content on Electronic reserve: In addition to the above the following

clauses are applicable: The web site must be password-protected and made available only to bona fide students registered on a relevant course. This permission is granted for 1 year only. You may obtain a new license for future website posting.
17. **For journal authors:** the following clauses are applicable in addition to the above:
Preprints:
A preprint is an author's own write-up of research results and analysis, it has not been peer-reviewed, nor has it had any other value added to it by a publisher (such as formatting, copyright, technical enhancement etc.).
Authors can share their preprints anywhere at any time. Preprints should not be added to or enhanced in any way in order to appear more like, or to substitute for, the final versions of articles however authors can update their preprints on arXiv or RePEc with their Accepted Author Manuscript (see below).
If accepted for publication, we encourage authors to link from the preprint to their formal publication via its DOI. Millions of researchers have access to the formal publications on ScienceDirect, and so links will help users to find, access, cite and use the best available version. Please note that Cell Press, The Lancet and some society-owned have different preprint policies. Information on these policies is available on the journal homepage.
Accepted Author Manuscripts: An accepted author manuscript is the manuscript of an article that has been accepted for publication and which typically includes author-incorporated changes suggested during submission, peer review and editor-author communications.
Authors can share their accepted author manuscript:

- immediately
    - via their non-commercial person homepage or blog
    - by updating a preprint in arXiv or RePEc with the accepted manuscript
    - via their research institute or institutional repository for internal institutional uses or as part of an invitation-only research collaboration work-group
    - directly by providing copies to their students or to research collaborators for their personal use
    - for private scholarly sharing as part of an invitation-only work group on commercial sites with which Elsevier has an agreement
- After the embargo period
    - via non-commercial hosting platforms such as their institutional repository
    - via commercial sites with which Elsevier has an agreement

In all cases accepted manuscripts should:

- link to the formal publication via its DOI
- bear a CC-BY-NC-ND license - this is easy to do
- if aggregated with other manuscripts, for example in a repository or other site, be shared in alignment with our hosting policy not be added to or enhanced in any way to appear more like, or to substitute for, the published journal article.

Published journal article (JPA): A published journal article (PJA) is the definitive final record of published research that appears or will appear in the journal and embodies all value-adding publishing activities including peer review co-ordination, copy-editing, formatting, (if relevant) pagination and online enrichment.
Policies for sharing publishing journal articles differ for subscription and gold open access articles:

Subscription Articles: If you are an author, please share a link to your article rather than the full-text. Millions of researchers have access to the formal publications on ScienceDirect, and so links will help your users to find, access, cite, and use the best available version.
Theses and dissertations which contain embedded PJAs as part of the formal submission can be posted publicly by the awarding institution with DOI links back to the formal publications on ScienceDirect.
If you are affiliated with a library that subscribes to ScienceDirect you have additional private sharing rights for others' research accessed under that agreement. This includes use for classroom teaching and internal training at the institution (including use in course packs and courseware programs), and inclusion of the article for grant funding purposes.
Gold Open Access Articles: May be shared according to the author-selected end-user license and should contain a CrossMark logo, the end user license, and a DOI link to the formal publication on ScienceDirect.
Please refer to Elsevier's posting policy for further information.
18. **For book authors** the following clauses are applicable in addition to the above: Authors are permitted to place a brief summary of their work online only. You are not allowed to download and post the published electronic version of your chapter, nor may you scan the printed edition to create an electronic version. **Posting to a repository:** Authors are permitted to post a summary of their chapter only in their institution's repository.
19. **Thesis/Dissertation**: If your license is for use in a thesis/dissertation your thesis may be submitted to your institution in either print or electronic form. Should your thesis be published commercially, please reapply for permission. These requirements include permission for the Library and Archives of Canada to supply single copies, on demand, of the complete thesis and include permission for Proquest/UMI to supply single copies, on demand, of the complete thesis. Should your thesis be published commercially, please reapply for permission. Theses and dissertations which contain embedded PJAs as part of the formal submission can be posted publicly by the awarding institution with DOI links back to the formal publications on ScienceDirect.

Elsevier Open Access Terms and Conditions
You can publish open access with Elsevier in hundreds of open access journals or in nearly 2000 established subscription journals that support open access publishing. Permitted third party re-use of these open access articles is defined by the author's choice of Creative Commons user license. See our open access license policy for more information.
Terms & Conditions applicable to all Open Access articles published with Elsevier:
Any reuse of the article must not represent the author as endorsing the adaptation of the article nor should the article be modified in such a way as to damage the author's honour or reputation. If any changes have been made, such changes must be clearly indicated.
The author(s) must be appropriately credited and we ask that you include the end user license and a DOI link to the formal publication on ScienceDirect.
If any part of the material to be used (for example, figures) has appeared in our publication with credit or acknowledgement to another source it is the responsibility of the user to ensure their reuse complies with the terms and conditions determined by the rights holder.
Additional Terms & Conditions applicable to each Creative Commons user license:
CC BY: The CC-BY license allows users to copy, to create extracts, abstracts and new works from the Article, to alter and revise the Article and to make commercial use of the Article (including reuse and/or resale of the Article by commercial entities), provided the user gives appropriate credit (with a link to the formal publication through the relevant DOI), provides a link to the license, indicates if changes were made and the licensor is not represented as endorsing the use made of the work. The full details of the license are available

Licence for Figure 1.3

OXFORD UNIVERSITY PRESS LICENSE TERMS AND CONDITIONS

Sep 10, 2018

This Agreement between Ms. Yan Jing Yee ("You") and Oxford University Press ("Oxford University Press") consists of your license details and the terms and conditions provided by Oxford University Press and Copyright Clearance Center.

The publisher has provided special terms related to this request that can be found at the end of the Publisher's Terms and Conditions.

License Number	4374121270895
License date	Jun 22, 2018
Licensed Content Publisher	Oxford University Press
Licensed Content Publication	Advances in Nutrition
Licensed Content Title	Resveratrol: How Much Wine Do You Have to Drink to Stay Healthy?
Licensed Content Author	Weiskirchen, Sabine; Weiskirchen, Ralf
Licensed Content Date	Jul 11, 2016
Licensed Content Volume	7
Licensed Content Issue	4
Type of Use	I don't see my intended use
Requestor type	Educational Institution/Non-commercial/ Not for-profit
Circulation/distribution	50
Portions	Figure 2 to be used in an institutional repository
Requestor Location	Ms. Yan Jing Yee 76 Selway Road Brentwood Perth, Western Australia 6153 Australia Attn: Ms. Yan Jing Yee
Publisher Tax ID	GB125506730
Billing Type	Invoice
Billing Address	Ms. Yan Jing Yee 76 Selway Road Brentwood Perth, Australia 6153 Attn: Ms. Yan Jing Yee
Total	0.00 AUD
Terms and Conditions	

STANDARD TERMS AND CONDITIONS FOR REPRODUCTION OF

MATERIAL FROM AN OXFORD UNIVERSITY PRESS JOURNAL

1. Use of the material is restricted to the type of use specified in your order details.
2. This permission covers the use of the material in the English language in the following territory: world. If you have requested additional permission to translate this material, the terms and conditions of this reuse will be set out in clause 12.
3. This permission is limited to the particular use authorized in (1) above and does not allow you to sanction its use elsewhere in any other format other than specified above, nor does it apply to quotations, images, artistic works etc that have been reproduced from other sources which may be part of the material to be used.
4. No alteration, omission or addition is made to the material without our written consent. Permission must be re-cleared with Oxford University Press if/when you decide to reprint.
5. The following credit line appears wherever the material is used: author, title, journal, year, volume, issue number, pagination, by permission of Oxford University Press or the sponsoring society if the journal is a society journal. Where a journal is being published on behalf of a learned society, the details of that society must be included in the credit line.
6. For the reproduction of a full article from an Oxford University Press journal for whatever purpose, the corresponding author of the material concerned should be informed of the proposed use. Contact details for the corresponding authors of all Oxford University Press journal contact can be found alongside either the abstract or full text of the article concerned, accessible from www.oxfordjournals.org Should there be a problem clearing these rights, please contact journals.permissions@oup.com
7. If the credit line or acknowledgement in our publication indicates that any of the figures, images or photos was reproduced, drawn or modified from an earlier source it will be necessary for you to clear this permission with the original publisher as well. If this permission has not been obtained, please note that this material cannot be included in your publication/photocopies.
8. While you may exercise the rights licensed immediately upon issuance of the license at the end of the licensing process for the transaction, provided that you have disclosed complete and accurate details of your proposed use, no license is finally effective unless and until full payment is received from you (either by Oxford University Press or by Copyright Clearance Center (CCC)) as provided in CCC's Billing and Payment terms and conditions. If full payment is not received on a timely basis, then any license preliminarily granted shall be deemed automatically revoked and shall be void as if never granted. Further, in the event that you breach any of these terms and conditions or any of CCC's Billing and Payment terms and conditions, the license is automatically revoked and shall be void as if never granted. Use of materials as described in a revoked license, as well as any use of the materials beyond the scope of an unrevoked license, may constitute copyright infringement and Oxford University Press reserves the right to take any and all action to protect its copyright in the materials.
9. This license is personal to you and may not be sublicensed, assigned or transferred by you to any other person without Oxford University Press's written permission.
10. Oxford University Press reserves all rights not specifically granted in the combination of (i) the license details provided by you and accepted in the course of this licensing transaction, (ii) these terms and conditions and (iii) CCC's Billing and Payment terms and conditions.
11. You hereby indemnify and agree to hold harmless Oxford University Press and CCC, and their respective officers, directors, employs and agents, from and against any and all claims arising out of your use of the licensed material other than as specifically authorized pursuant to this license.
12. Other Terms and Conditions: ¬ In addition to the rights granted above, permission is

License for Figure 2.8

JOHN WILEY AND SONS LICENSE TERMS AND CONDITIONS

Sep 10, 2018

This Agreement between Ms. Yan Jing Yee ("You") and John Wiley and Sons ("John Wiley and Sons") consists of your license details and the terms and conditions provided by John Wiley and Sons and Copyright Clearance Center.

License Number	4364190251791
License date	Jun 08, 2018
Licensed Content Publisher	John Wiley and Sons
Licensed Content Publication	Wiley Books
Licensed Content Title	Polymer Molecular Weight Measurement
Licensed Content Date	Feb 22, 2013
Licensed Content Pages	12
Type of use	Institutional Repository
Requestor type	Author of this Wiley chapter/book
Is the reuse sponsored by or associated with a pharmaceutical or medical products company?	no
Format	Electronic
Circulation	50
Homepage URL	https://espace.curtin.edu.au/
Intranet owner	Curtin University
Expected publication date	Oct 2018
Requestor Location	Ms. Yan Jing Yee 76 Selway Road Brentwood Perth, Western Australia 6153 Australia Attn: Ms. Yan Jing Yee
Publisher Tax ID	EU826007151
Billing Type	Invoice
Billing Address	Ms. Yan Jing Yee 76 Selway Road Brentwood Perth, Australia 6153 Attn: Ms. Yan Jing Yee
Total	0.00 USD
Terms and Conditions	

- The Wiley Materials and all of the intellectual property rights therein shall at all times remain the exclusive property of John Wiley & Sons Inc, the Wiley Companies, or their respective licensors, and your interest therein is only that of having possession of and the right to reproduce the Wiley Materials pursuant to Section 2 herein during the continuance of this Agreement. You agree that you own no right, title or interest in or to the Wiley Materials or any of the intellectual property rights therein. You shall have no rights hereunder other than the license as provided for above in Section 2. No right, license or interest to any trademark, trade name, service mark or other branding ("Marks") of WILEY or its licensors is granted hereunder, and you agree that you shall not assert any such right, license or interest with respect thereto

- NEITHER WILEY NOR ITS LICENSORS MAKES ANY WARRANTY OR REPRESENTATION OF ANY KIND TO YOU OR ANY THIRD PARTY, EXPRESS, IMPLIED OR STATUTORY, WITH RESPECT TO THE MATERIALS OR THE ACCURACY OF ANY INFORMATION CONTAINED IN THE MATERIALS, INCLUDING, WITHOUT LIMITATION, ANY IMPLIED WARRANTY OF MERCHANTABILITY, ACCURACY, SATISFACTORY QUALITY, FITNESS FOR A PARTICULAR PURPOSE, USABILITY, INTEGRATION OR NON-INFRINGEMENT AND ALL SUCH WARRANTIES ARE HEREBY EXCLUDED BY WILEY AND ITS LICENSORS AND WAIVED BY YOU.

- WILEY shall have the right to terminate this Agreement immediately upon breach of this Agreement by you.

- You shall indemnify, defend and hold harmless WILEY, its Licensors and their respective directors, officers, agents and employees, from and against any actual or threatened claims, demands, causes of action or proceedings arising from any breach of this Agreement by you.

- IN NO EVENT SHALL WILEY OR ITS LICENSORS BE LIABLE TO YOU OR ANY OTHER PARTY OR ANY OTHER PERSON OR ENTITY FOR ANY SPECIAL, CONSEQUENTIAL, INCIDENTAL, INDIRECT, EXEMPLARY OR PUNITIVE DAMAGES, HOWEVER CAUSED, ARISING OUT OF OR IN CONNECTION WITH THE DOWNLOADING, PROVISIONING, VIEWING OR USE OF THE MATERIALS REGARDLESS OF THE FORM OF ACTION, WHETHER FOR BREACH OF CONTRACT, BREACH OF WARRANTY, TORT, NEGLIGENCE, INFRINGEMENT OR OTHERWISE (INCLUDING, WITHOUT LIMITATION, DAMAGES BASED ON LOSS OF PROFITS, DATA, FILES, USE, BUSINESS OPPORTUNITY OR CLAIMS OF THIRD PARTIES), AND WHETHER OR NOT THE PARTY HAS BEEN ADVISED OF THE POSSIBILITY OF SUCH DAMAGES. THIS LIMITATION SHALL APPLY NOTWITHSTANDING ANY FAILURE OF ESSENTIAL PURPOSE OF ANY LIMITED REMEDY PROVIDED HEREIN.

- Should any provision of this Agreement be held by a court of competent jurisdiction to be illegal, invalid, or unenforceable, that provision shall be deemed amended to achieve as nearly as possible the same economic effect as the original

provision, and the legality, validity and enforceability of the remaining provisions of this Agreement shall not be affected or impaired thereby.

- The failure of either party to enforce any term or condition of this Agreement shall not constitute a waiver of either party's right to enforce each and every term and condition of this Agreement. No breach under this agreement shall be deemed waived or excused by either party unless such waiver or consent is in writing signed by the party granting such waiver or consent. The waiver by or consent of a party to a breach of any provision of this Agreement shall not operate or be construed as a waiver of or consent to any other or subsequent breach by such other party.

- This Agreement may not be assigned (including by operation of law or otherwise) by you without WILEY's prior written consent.

- Any fee required for this permission shall be non-refundable after thirty (30) days from receipt by the CCC.

- These terms and conditions together with CCC's Billing and Payment terms and conditions (which are incorporated herein) form the entire agreement between you and WILEY concerning this licensing transaction and (in the absence of fraud) supersedes all prior agreements and representations of the parties, oral or written. This Agreement may not be amended except in writing signed by both parties. This Agreement shall be binding upon and inure to the benefit of the parties' successors, legal representatives, and authorized assigns.

- In the event of any conflict between your obligations established by these terms and conditions and those established by CCC's Billing and Payment terms and conditions, these terms and conditions shall prevail.

- WILEY expressly reserves all rights not specifically granted in the combination of (i) the license details provided by you and accepted in the course of this licensing transaction, (ii) these terms and conditions and (iii) CCC's Billing and Payment terms and conditions.

- This Agreement will be void if the Type of Use, Format, Circulation, or Requestor Type was misrepresented during the licensing process.

- This Agreement shall be governed by and construed in accordance with the laws of the State of New York, USA, without regards to such state's conflict of law rules. Any legal action, suit or proceeding arising out of or relating to these Terms and Conditions or the breach thereof shall be instituted in a court of competent jurisdiction in New York County in the State of New York in the United States of America and each party hereby consents and submits to the personal jurisdiction of such court, waives any objection to venue in such court and consents to service of process by registered or certified mail, return receipt requested, at the last known address of such party.

WILEY OPEN ACCESS TERMS AND CONDITIONS

Wiley Publishes Open Access Articles in fully Open Access Journals and in Subscription journals offering Online Open. Although most of the fully Open Access journals publish

open access articles under the terms of the Creative Commons Attribution (CC BY) License only, the subscription journals and a few of the Open Access Journals offer a choice of Creative Commons Licenses. The license type is clearly identified on the article.

The Creative Commons Attribution License

The Creative Commons Attribution License (CC-BY) allows users to copy, distribute and transmit an article, adapt the article and make commercial use of the article. The CC-BY license permits commercial and non-

Creative Commons Attribution Non-Commercial License

The Creative Commons Attribution Non-Commercial (CC-BY-NC)License permits use, distribution and reproduction in any medium, provided the original work is properly cited and is not used for commercial purposes.(see below)

Creative Commons Attribution-Non-Commercial-NoDerivs License

The Creative Commons Attribution Non-Commercial-NoDerivs License (CC-BY-NC-ND) permits use, distribution and reproduction in any medium, provided the original work is properly cited, is not used for commercial purposes and no modifications or adaptations are made. (see below)

Use by commercial "for-profit" organizations

Use of Wiley Open Access articles for commercial, promotional, or marketing purposes requires further explicit permission from Wiley and will be subject to a fee.

Further details can be found on Wiley Online Library http://olabout.wiley.com/WileyCDA/Section/id-410895.html

Other Terms and Conditions:

v1.10 Last updated September 2015

Questions? customercare@copyright.com or +1-855-239-3415 (toll free in the US) or +1-978-646-2777.